

# 3<sup>rd</sup> International Rotating Equipment Conference

10<sup>th</sup> EFRC Conference

14 and 15 September 2016  
Congress Center Düsseldorf, Germany



**Pump Users**  
International Forum 2016



**Compressor Users**  
International Forum 2016



**EFRC**

EUROPEAN FORUM  
for RECIPROCATING  
COMPRESSORS  
EFRC Conference 2016

PROCEEDINGS



Sponsored by







# Content

## Session 36 Controls

36-1	Reciprocating compressor capacity control – simple reliable solutions William C. Wirz	5
36-2	Stepless capacity control maintains efficiency of French natural gas compressor as production declines Justin McDonald, Arnaud Dubos, Tanguy Bosson	19

## Session 37 Root cause analysis

37-1	Barking dog noise in a natural gas compressor station: Analysis and mitigation Leonard van Lier, Pieter van Beek, Werner Temmink, Jürgen Brenner	29
37-2	Root cause analysis and solution of recurring fatigue failures in the cooler pipe bends of a high pressure LDPE compressor Cosimo Carcasci, Marco Sacco, Fabio La Monica, Emanuele Cintolo	43

## Session 38 Sealing / Wear

38-1	Low-friction buffer seals for reciprocating compressor rod packing Craig Martin	57
38-2	Novel oil wiper system Dr. Marc Langela	63

## Session 39 Pulsation / Vibration 1

39-1	The impact of reciprocating compressor pulsations on the surge margin of centrifugal compressors Klaus Brun, Rainer Kurz, Sarah Simons	73
39-2	In-field vibration assessment of the piping of a reciprocating compressor plant Dr. Richard Fawcett, Dr. Erik Jan Lingen	91
39-3	Cylinder manifold automation Marco Passeri, Riccardo Bagagli	103

## **Session 40      New concept**

- |      |  |     |
|------|--|-----|
| 40-1 | Experimental and numerical investigation of the heat transfer inside a hollow piston rod<br>Konrad Klotsche, Christiane Thomas, Prof. Ullrich Hesse    | 117 |
| 40-2 | A new piston rod design to improve packing lifetime for non-lubricated reciprocating compressor applications<br>Klaus Hoff, Gerhard Knop, Marc Langela | 131 |
| 40-3 | Vibration analysis and investigation of crack failure of reciprocating compressor<br>Jaroslav Kraml, Martin Lamrich                                    | 143 |

## **Session 41      Operations**

- |      |   |     |
|------|---|-----|
| 41-1 | Redesign and manufacture of two shrink-fit 25-ton crankshafts for a hydrogen compressor<br>Guido Kluth, Markus Weber                      | 157 |
| 41-2 | Hard particle contamination in reciprocating compressors<br>Dr. Ricardo Cruz, Dr. Norbert Feistel   | 171 |
| 41-3 | Failure analysis and rectification of connecting rod bearing failure against modified compressor operation<br>Usman Sharif, Mohsin Imtiaz | 183 |

## **Session 42      EFRC**

- |      |  |     |
|------|--|-----|
| 42-1 | The impact of reciprocating compressor pulsations on the surge margin of centrifugal compressors<br>Cyril Wentzel, Gerard Groenewegen, André Eijk, Dr. Otto Bergsma    | 191 |
| 42-2 | A novel valve design for combined reciprocating piston expansion and compression machines<br>Christian Stöckel, Dr. Jörg Nickl, Christiane Thomas, Prof. Ullrich Hesse | 211 |
| 42-3 | Internal flow in reciprocating compressors<br>Thomas Müllner, Bernhard Streibl, Prof. Herbert Steinrück  | 225 |



## Session 43      Monitoring

43-1	Electric motors for reciprocating compressors and condition monitoring Dr. Michael Ade, Dr. Artur Jungiewicz	237
43-2	Challenges in establishing predictive maintenance for high speed reciprocating compressors on a north sea FPSO using online condition monitoring William Miller, Jörg Koch	247
43-3	Advanced online condition monitoring and diagnostics support operational and maintenance decisions in an offshore gas compression and export system unit Andy Caie, Thorsten Bickmann	259

## Session 44      Valve

44-1	Next-generation compressor valve technology Matthias Kornfeld, Bernhard Spiegl, Tino Lindner-Silwester, Markus Testori, Marian Janko	279
44-2	The innovative use of nanofillers in thermoplastic materials for valve sealing elements Massimo Schiavone, Andrea Raggi, Alessandro Vollonnino	291

## Session 45      Foundation

45-1	Recip foundations – practical issues related to inspection and repair Theo de Kok, Tom K. Hoekstra, Erik Barkmeyer	307
45-2	Dynamic analysis of a compressor foundation and validation with respect to experimental data Alberto Callerio, Alfio Bisighini	323

## Session 46      Pulsation / Vibration 2

46-1	Non-traditional vibration mitigation methods for reciprocating compressor systems André Eijk, Dorus de Lange, Jan de Vreugd, Erik Slis	335
46-2	Development of a new adaptive pulsation damping device without external energy supply Patrick Tetenborg, Prof. Andreas Brümmer	353
46-3	Design change in the motor's bearing pedestal and baseplate in order to solve vibration problem in reciprocating compressor Nikolaos C. Kesimoglou, Konstantinos G. Adamakis	367

## **Session 47      Calculation 1**

- |      |   |     |
|------|---|-----|
| 47-1 | Field performance assessments using enhanced simulation modeling for reciprocating compressors<br>H. J. M. Baan   | 385 |
| 47-2 | Large size reciprocating compressor analysis with a finite volume 1D model<br>Isacco Stiaccini, Niccolò Fiorini, Francesco Balduzzi, Giovanni Ferrara, Alberto Babbini, Gianni Orsi | 397 |
| 47-3 | Vibration analysis in reciprocating compressors<br>Vasillaq Kacani, Ernst Huttar  | 411 |

## **Session 48      Pulsation / Vibration 3**

- |      |   |     |
|------|---|-----|
| 48-1 | How to evaluate the dynamic behaviour of a gas system without all the technical documentation of a compressor?<br>Urszula Warzyńska, née Radziwanowska, Piotr Harnatkiewicz | 423 |
| 48-2 | Vibration assurance of vertical scrubbers for reciprocating compressor packages<br>Kelly Eberle   | 435 |

## **Session 49      Calculation 2**

- |      |   |     |
|------|---|-----|
| 49-1 | Using OEM performance software to assist with troubleshooting a crosshead failure<br>Benjamin F. Williams, Jillian T. Toussaint | 457 |
| 49-2 | Interactions between valve flow characteristics, valve pocket geometry and compressor performance<br>Dr. Reiner Schulz          | 467 |



## **ART, SOCCER AND ROYALTY MEET RECIPS**

The 11th EFRC Conference will take place from September 20 to 21, 2018 in Madrid at IFEMA Convention and Congress Centres, in the heart of one of Europe's most vibrant metropolises.

Get inspiration from the leading brains in compression technology to create real application benefits. Experience the future of compressors at the best-known conference for recip, in an environment that combines regal tradition with modern Spanish flair.

**11<sup>th</sup> EFRC Conference**  
**September 20 / 21, 2018**  
**Madrid, Spain**

**[www.recip.org](http://www.recip.org)**



**EFRC**  
EUROPEAN FORUM  
for RECIPROCATING  
COMPRESSORS

**SAVE THE DATE**



COMMITMENT FOR LIFE

# BORSIG ZM COMPRESSION ZM

**BORSIG ZM Compression GmbH** offers flexible, innovative and high-quality solutions for compressors. Our products stand for high quality, competence and reliability. We develop and manufacture modular machine concepts to meet each individual customer's requirements. Entire concepts from planning and design to manufacturing and assembly are our philosophy.

## Reciprocating Compressors for Process Gases, API 618

Our modular designed compressor series for process gases comprises machines with both vertical and horizontal cylinder arrangements with up to a maximum of 6 axes. The series has been developed for the heaviest continuous operation.

Discharge pressure: ... 1,000 bara  
Capacity/flow: ... 115,000 m<sup>3</sup>/h  
Power: ... 16,000 kW

## Centrifugal Compressors for Process Gases, API 617, chapter 3 up to 150 bara, 300,000 m<sup>3</sup>/h, 25,000 kW

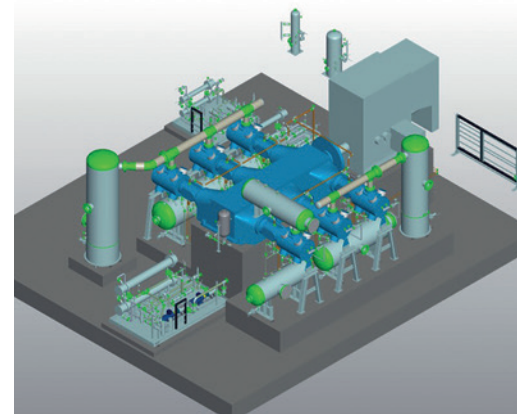
## Compressor Valves

## BORSIG BlueLine

combines control system, emergency shutdown, machine protection and condition monitoring for reciprocating and centrifugal compressor units

## Services

Installation, overhauling, engineering, maintenance, spare parts management, training



## BORSIG ZM Compression GmbH

Seiferitzer Allee 26  
D-08393 Meerane / Germany

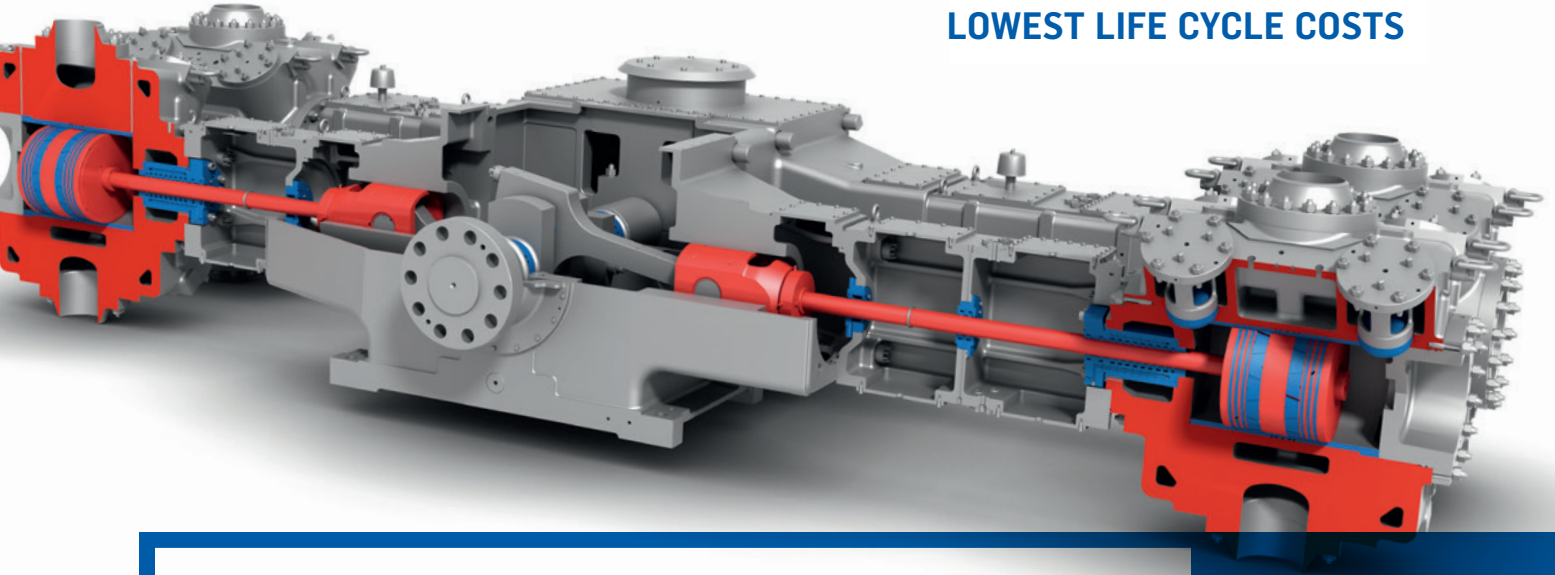
Phone: +49 (0) 3764 / 5390-0  
E-mail: [info@zm.borsig.de](mailto:info@zm.borsig.de)

Fax: +49 (0) 3764 / 5390-5092

[www.borsig.de/zm](http://www.borsig.de/zm)



**YOUR BENEFIT:  
LOWEST LIFE CYCLE COSTS**



# API 618

## HIGHEST AVAILABILITY

**COMBINED WITH BEST  
MAINTAINABILITY; FAST  
ACCESS TO ALL WEAR PARTS**

Full range:  
Rod load up to 1'500 kN / 335'000 lbs  
Power up to 31'000 kW / 42'100 hp

Lubricated up to 1'000 bara,  
non-lubricated up to 300 bara

Advanced solutions for demanding  
and sour gas applications

Over 120 years of experience in valve  
design and manufacturing

Outstanding durability of Redura®  
sealing elements for longest mean  
time between overhaul (MTBO)

Worldwide Burckhardt Compression  
quality, engineered in Switzerland

Your solution partner – From bare  
shaft compressors to turnkey  
solutions

Full range of services and top  
performing components through  
global organization and local service  
centers

→ [www.recip.com/api618](http://www.recip.com/api618)



Compressors for a Lifetime™

 **Burckhardt  
Compression**





IF YOUR COMPRESSOR IS DOWN,  
EVERY SECOND COUNTS



### It's time you consider CPI

Like a finely-tuned watch, each component in an oil and gas operation relies on every other component for the whole to function properly. When even the smallest components can interrupt uptime and productivity, you need experienced and reliable partners who can respond at a moment's notice anywhere in the world to minimize unscheduled downtime. You need partners who understand your business and have the expertise to keep you running efficiently and profitably. You need CPI.



Proven Solutions for the Global Compression Industry™

Visit us at booth A7



[www.CPIcompression.com](http://www.CPIcompression.com)



# This could be your profiled picture.

Profiled valve plates made of **PowerPEEK™**:  
the **XP valve** combines the efficiency of profiled valve rings  
with the reliability and simplicity of conventional valve plates.



[www.hoerbiger.com](http://www.hoerbiger.com)



**HOERBIGER**  
*because performance counts*





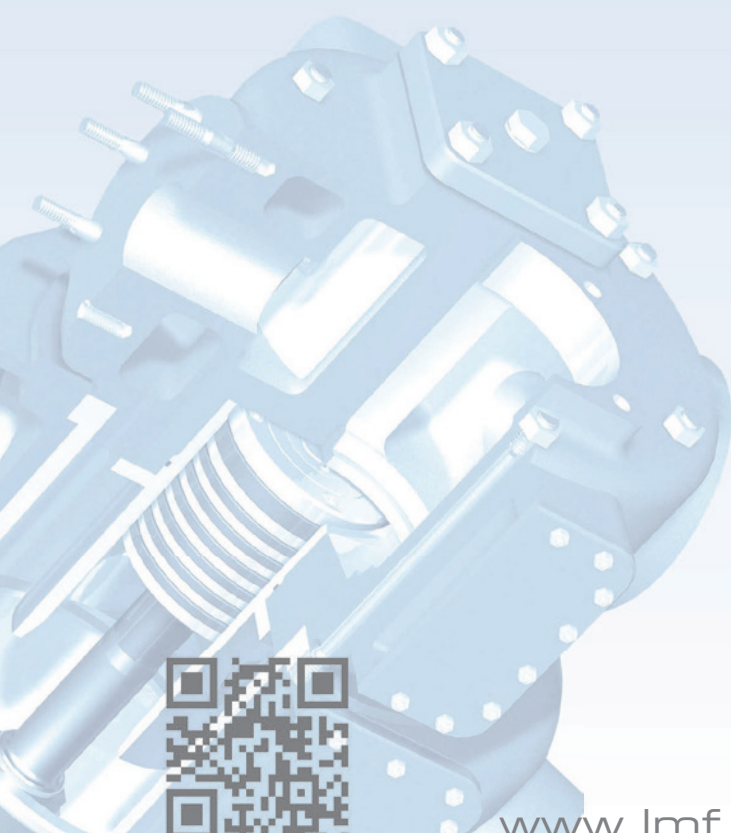
# worldwide compressor technology made in austria

LMF, the leading Austrian manufacturer with over 60 years experience in the compressor business, produces high pressure piston compressor systems for air, natural gases, technical and industrial gases (process gases) with power rates of up to 6,200 kW (8,300 hp) and pressure rates of up to 700 bar (10,150 psi).

LMF's high pressure systems are designed according to international standards, using standard design principles. As a single source LMF offers design, engineering, production, testing under full load, erection, start-up and related services.



LMF Balanced-opposed compressor type BS 604



MOBILE SYSTEMS



INDUSTRIAL COMPRESSOR SYSTEMS



RECIPROCATING COMPRESSORS AC. TO API618, API 11P



[www.lmf.at](http://www.lmf.at)



your high pressure solution

# THINK GERMAN, ACT LOCAL.

## SOLUTION NEEDED TO COMPLY WITH ZERO EMISSION?

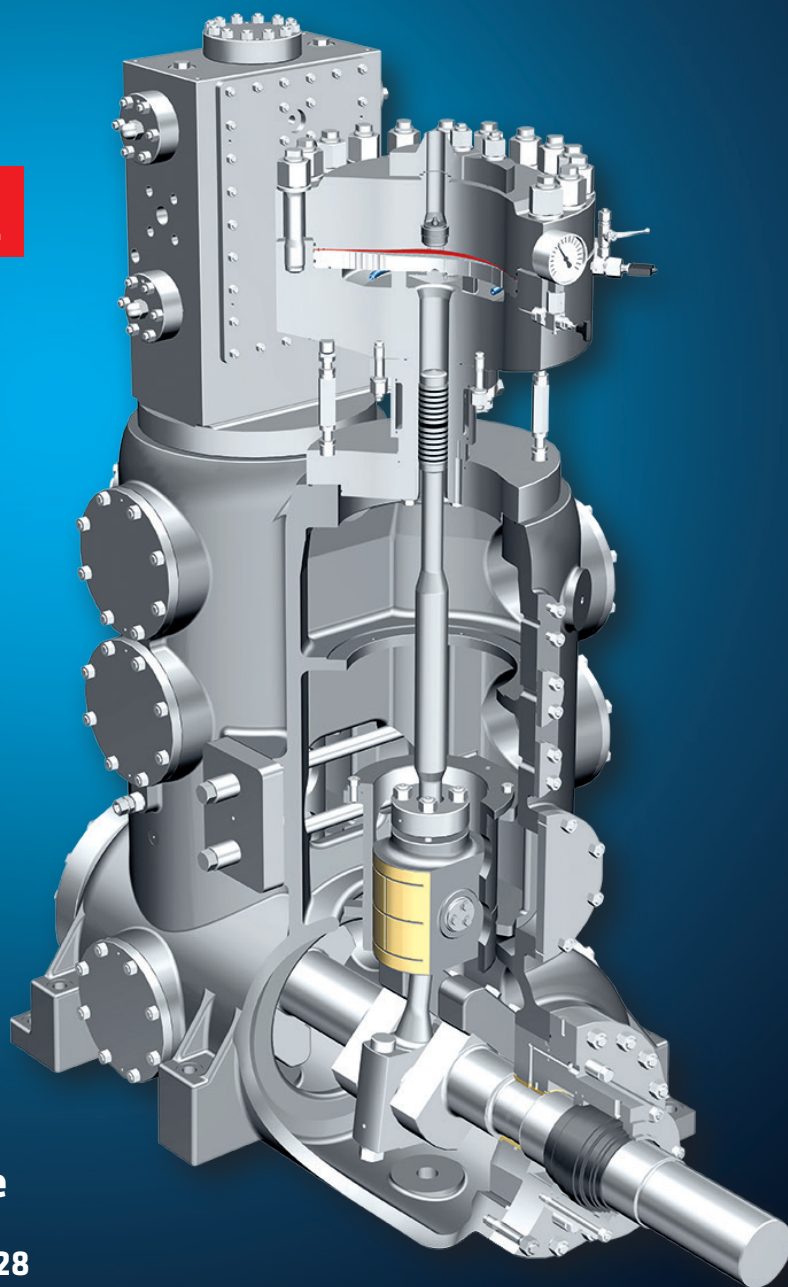


COMPRESSOR  
SYSTEMS

### COMBINE GAS-TIGHT RECIP CRANKCASE WITH LEAKAGE-FREE DIAPHRAGM HEADS.

The NEA hybrid is the answer to the technically highly demanding emission- and oilfree compression. This innovative concept combines NEA's gas-tight crankcase with HOFER's diaphragm head. The multi-stage, one crank drive system offers a leakage-free solution for low suction and high discharge pressure ratio at higher mass flows.

Once installed, NEAC Compressor Service, the service provider of the GROUP, cares for the fully sustainable lifetime of all compression systems. And even more. NEA GROUP also proves its OEM in-depth know-how when it comes to revamp & modernization of diaphragm compressors from HOFER as well as from other brands. A new fit for innovative compression.

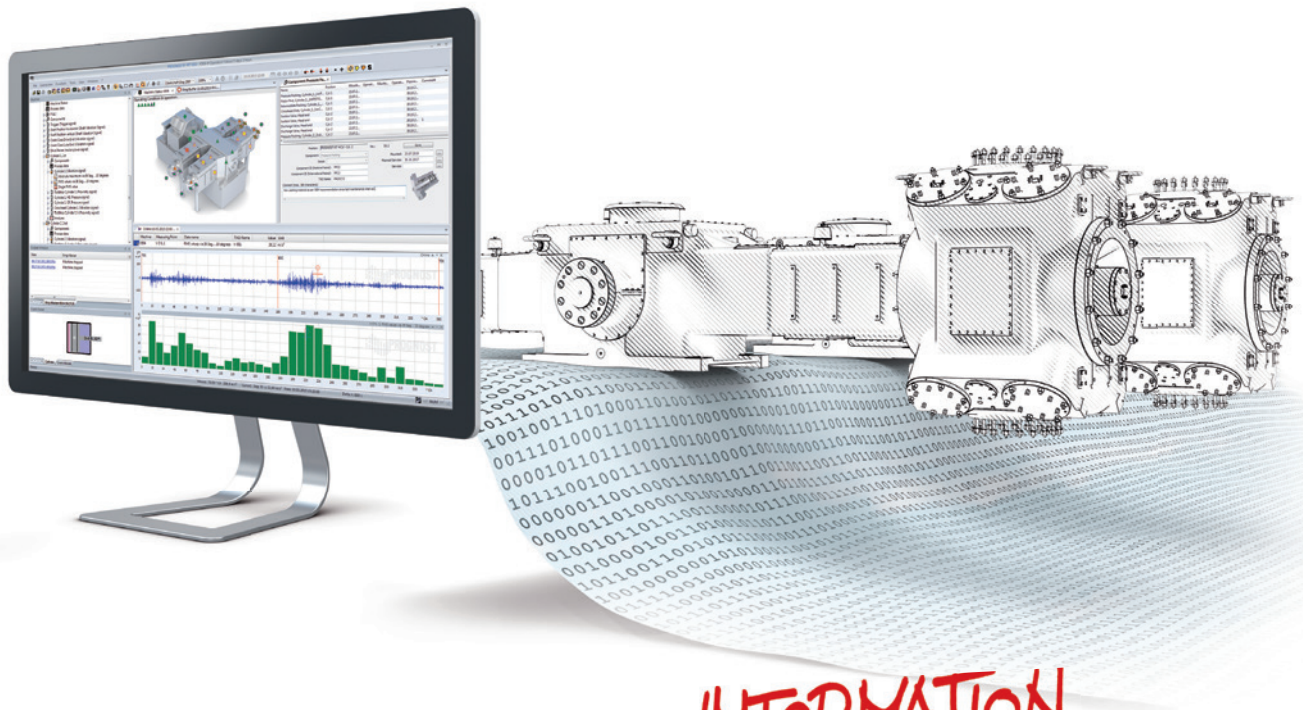


**Hofer** [www.andreas-hofer.de](http://www.andreas-hofer.de)  
[sales@andreas-hofer.de](mailto:sales@andreas-hofer.de)  
Phone: +49 (0) 208 / 4 69 96-28



[www.neuman-esser.com](http://www.neuman-esser.com)  
[sales@neuman-esser.de](mailto:sales@neuman-esser.de)  
Phone: +49 (0) 2451 / 481-147





**INFORMATION**

## Get The Power of Big ~~Data~~

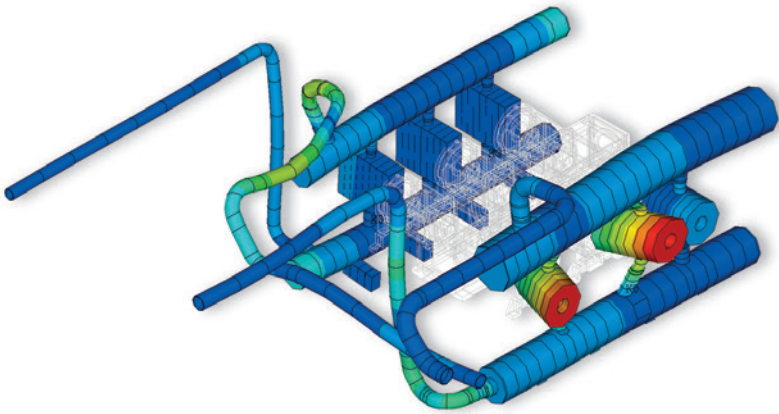
A PROGNOST® diagnostic system acquires and diagnoses 65 terabytes of sensor data every day. Impressed?

### **Data itself means nothing**

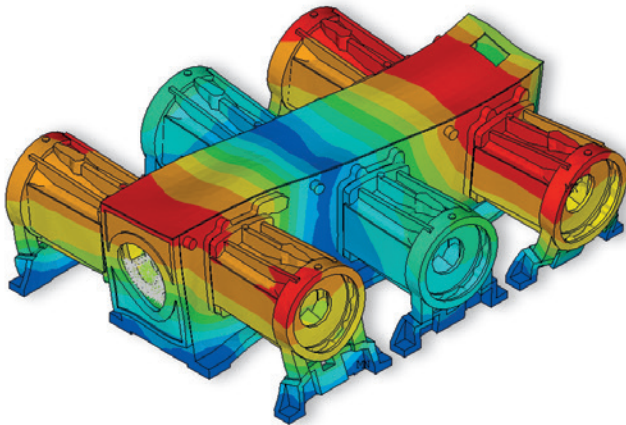
The challenge is to convert data into meaningful information. Our intelligent machine and component diagnostics retrieve the knowledge operators need, to boost uptime while reducing costs. PROGNOST® keeps operators informed. Non-stop and in real-time.

That's impressive.

# GOODBYE VIBRATIONS



Mode shape of a reciprocating compressor manifold system



FE model of a reciprocating compressor

## CONSULTANCY PROJECTS

- Pulsation and vibration analysis according to API 618, API 674 and API 619
- Flow-induced, anti-surge control and transient analysis for turbo compressors

## ROOT CAUSE ANALYSIS

Trouble shooting of flow dynamic, noise and vibration problems

## INNOVATIVE RESEARCH PROJECTS

Active surge control, high frequency dynamics and fluid structure interaction analysis for turbo compressors

## SOFTWARE DEVELOPMENT

PulsimSuite® software which integrates the different steps in an API analysis

**TNO** innovation  
for life

**Please meet us at  
EFRC 2016 at booth B5**

## CONTACT

André Eijk  
Senior Mechanical Consultant Oil & Gas  
E [andre.eijk@tno.nl](mailto:andre.eijk@tno.nl)  
P +31 88 866 63 54  
M +31 6 519 830 52

**TNO.NL/HTFD**





**EFRC**  
EUROPEAN FORUM  
for RECIPROCATING  
COMPRESSORS  
10<sup>th</sup> EFRC Conference 2016





# Technical Paper

**Session: 36-1**

**Session Name: Controls**

## **Reciprocating compressor capacity control – simple reliable solutions**

**Author:**

**William C. Wirz**  
**Business Development Manager**  
**Dresser-Rand Company – A Siemens Business**  
**14830 Painted Post, USA**

## Summary

More and more operators of compression equipment require the ability to adjust or trim the gas flow, depending on process conditions, from a remote and safe location. Manual adjustment of clearance pockets by the operator, in many cases while the compressor is running, has been the normal and successful practice for many years. However, this requires the operator to be standing next to the machine and in the same room with process gas. Operation of the manual pocket requires some physical strength to operate the clearance pocket and may pose some risk to the operator.

As an alternate to this Manual Clearance Pocket, several designs have existed for years which allows clearance to be added to the cylinder which has the effect of reducing the volumetric efficiency and therefore changing the cylinder capacity or flow. These methods are proven and take the form of pneumatic clearance pockets, pneumatic finger unloaders over the inlet compressor valves, and pneumatic plug or port unloaders. These are all reliable systems which allow for remote capacity control operation. However, if the operator needs to “fine tune” or trim the capacity even further, they cannot do it with these systems since the devices are for discrete unloading steps. For example 100%, 75%, 50% load steps. A unique solution would be to allow for a combination of the benefits of a manual control clearance pocket and a means of being able to remotely adjust the pocket.

This paper will describe the current technologies as well as their application, features and benefits. An alternate, simple, field proven solution to the need for capacity control will also be presented which allows for the operator to trim the flow based on process conditions while allowing for remote and safe operation.



## Cylinder Capacity – Definition of Terms

The capacity of a Reciprocating Compressor is determined by the piston displacement, which is defined as the total volume in the compressor cylinder which is “swept” by the piston per unit of time. In a simple formula<sup>(1)</sup> the piston displacement of a double acting reciprocating compressor cylinder is determined by the following equation:

$$PD \left[ (2d_c^2 - d_r^2) \times S \times N \right] / 2.12E+07$$

*Equation 1 – Piston Displacement – Metric Units<sup>(1)</sup>*

Where units of measure are:

- PD = Piston displacement - Cubic Meters per hour
- $d_c$  = Cylinder bore diameter , mm.
- $d_r$  = Piston rod diameter, mm.
- S = Compressor stroke, mm.
- N = Compressor speed – revolutions per minute

But, there are losses within the compressor cylinder that affect the total volume of gas that the cylinder can displace. These losses are accounted for in the term called Volumetric Efficiency. Volumetric Efficiency<sup>(2)</sup> is defined as the actual volume capacity of a cylinder compared to the piston displacement. The governing equation for volumetric efficiency is below:

$$E_v = 96 - R - C[(R^{1/k})(Z_s^2/Z_d^2 - 1)] - L ,$$

*Equation 2 – Volumetric Efficiency – Metric Units<sup>(2)</sup>*

Where units of measure are:

- $E_v$  = volumetric efficiency
- R = compression ratio
- C = cylinder clearance, % of piston swept volume
- $Z_s$  = inlet compressibility factor - accounts for gas behavior differences from an „Ideal“ gas.
- $Z_d$  = discharge compressibility factor-accounts for gas behavior differences from an „Ideal“ gas
- k = ratio of specific heats,  $C_p/C_v$
- L = slippage of gas past piston rings, %, (1% for high-speed separable, 5% for non-lubricated compressors and 4% for propane service)
- 96 = Allowance for losses because of pressure drop in the compressor valves

We can say that the net capacity for a compressor cylinder is by the simple relationship below:

$$\text{Net Capacity} \approx PD \times E_v$$

*Equation 3 – Net Capacity*

Upon review of the above equations, one can very easily see the factors that determine the capacity and how to vary the capacity of the cylinder. For example increasing the cylinder clearance, „C“, or increasing/decreasing the compressor speed, „N“, has a direct effect on Net Capacity of the cylinder and compressor.

## Cylinder Capacity – Effect of Clearance Change and Method

Referring to Equations 1 and 2, increasing the percent of clearance, reduces the Volumetric Efficiency ( $V_e$  or  $E_v$ ). This is represented by the typical *PV Diagram* below:

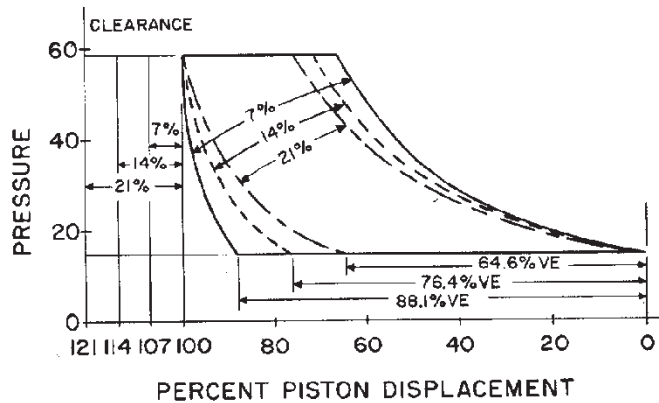


Figure 1. – Typical *PV Diagram*, Effect of % clearance on Volumetric Efficiency

In the above Figure 1, for a fixed compression ratio, if the base clearance in the compressor cylinder is 7% the cylinder has a corresponding  $E_v$  of 88.1%. When the cylinder clearance is increased to 21%, the  $E_v$  reduces to 64.6%.

What are the methods of adding clearance to a cylinder or unloading cylinders to change the net capacity? There are many specific devices to accomplish this. What will be focused on in this paper are means of adding clearance during operation with devices commonly called „Clearance Pockets“ and „Valve Unloaders“ used for pneumatically unloading ends of cylinders.

A very common means of adjusting or adding clearance to a compressor cylinder is by a „Variable Volume Clearance Pocket“ (VVCP) as per Figure 2. These devices are commonly used on high speed (>900 RPM) compressors in „Gas Gathering“ applications. Most can be adjusted while the compressor is in operation (consult operating manual for details). The operator approaches the compressor, unlocks a handwheel, and begins to turn the wheel clockwise or counter clockwise to reduce or add clearance to the cylinder. Normally, these are found on the 1st stage cylinders and serve also as the „outer head“ of the compressor cylinder.

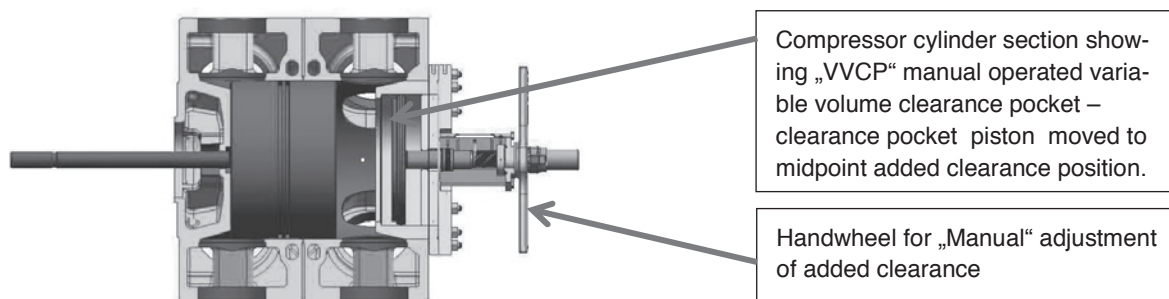
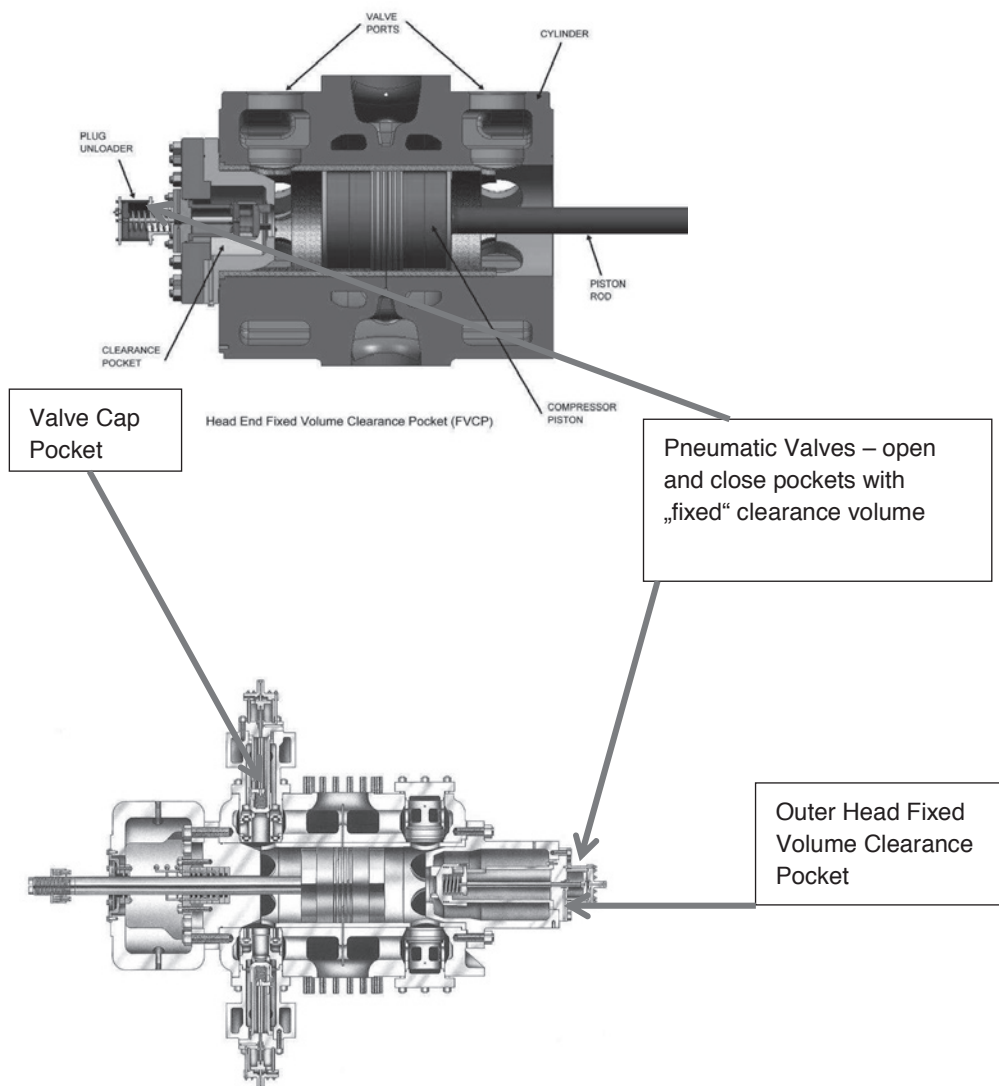


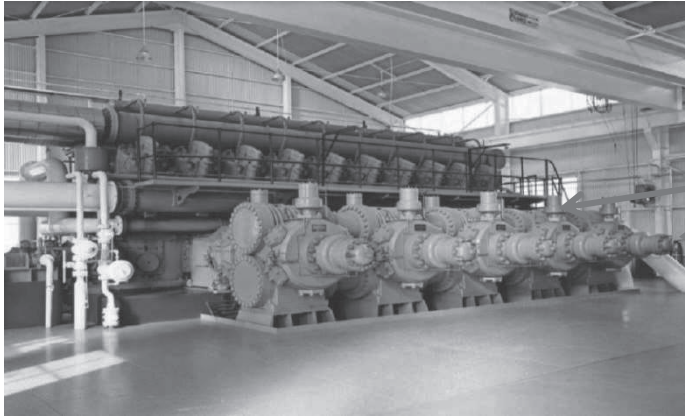
Figure 2. – Typical „Variable Volume Clearance Pocket“, VVCP, Manually Operated

Adding a „fixed“ amount of clearance to a compressor cylinder is accomplished by either a „clearance pocket“ or a „valve cap pocket“. In both cases, a pneumatic valve is provided with an air signal to open or close a pocket which controls the addition of clearance volume added to the cylinder. These devices are shown above in Figure 3.



*Figure 3. – Compressor Cylinder as shown equipped with both Valve Cap and Outer Head Clearance Pockets – Note: Pockets “Open” – no air signal applied to the pneumatic valve*

This combination of clearance devices (valve cap pockets and clearance pockets) and using them on many compressor cylinders as shown in Fig. 3, is common on Integral Engine type compressors used in Natural Gas Transmission Service. This type of compressor has the added flexibility of speed control (e.g. engine RPM) which maximizes the capacity control. See below Figure. 4:



Valve Cap and  
Outer Head  
Pockets. Note  
the quantity!

Figure 4. – Integral Engine Compressor – Used for Natural Gas Transmission Service.

When comparing unloading methods, there are associated pressure drops that occur which translate into power loss. If power is a concern particularly to electric motor drive, controlling capacity by adding clearance is preferred over „end unloading“ because of inherent lower throttling losses and therefore lower power consumption.

It should be noted that these „clearance pockets“ can be found on any reciprocating compressor type found in Gas Gathering, Gas Transmission, or Refinery type services.

### Cylinder Capacity – Effect of Cylinder End Unloading and Method

End unloading of a compressor cylinder will cause that end not to pump gas. This is accomplished by use of a device which when activated allows incoming gas to recirculate back to suction on the compressor cylinder.

The effect of „End Unloading“ can be seen on the *PV Diagram* below Fig. 5:

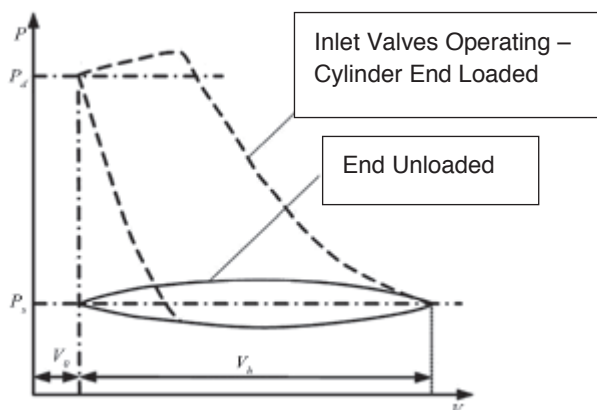


Figure 5. – Effect of “End Unloading” on a PV Diagram



End Unloading is accomplished in one of four ways:

- Valve Removal – physically removing the inlet / suction valves from one end of the cylinder
- Valve unloading via „Finger Type“ Unloaders – holding the valve element(s) in the „open“ position by „fingers“ throughout the entire pumping cycle of the compressor. The unloader is pneumatically operated. Unloaders are used on each Inlet Valve of the unloaded end of the cylinder.
- End Unloading via „Plug Unloaders“ – center portion of the valve and elements is replaced by an „open/closed“ valve which is pneumatically operated. Plug Unloaders are used on each Inlet Valve of the unloaded end of the cylinder.
- End Unloading via „Port Unloader“ – On larger cylinders with multiple inlet valves per end, one valve is completely removed and replaced by a metal seat insert and an „open/closed“ valve which is pneumatically operated.

Valve removal from an end of a cylinder is well understood and will not be shown. Other means of unloading are shown in the figures below:

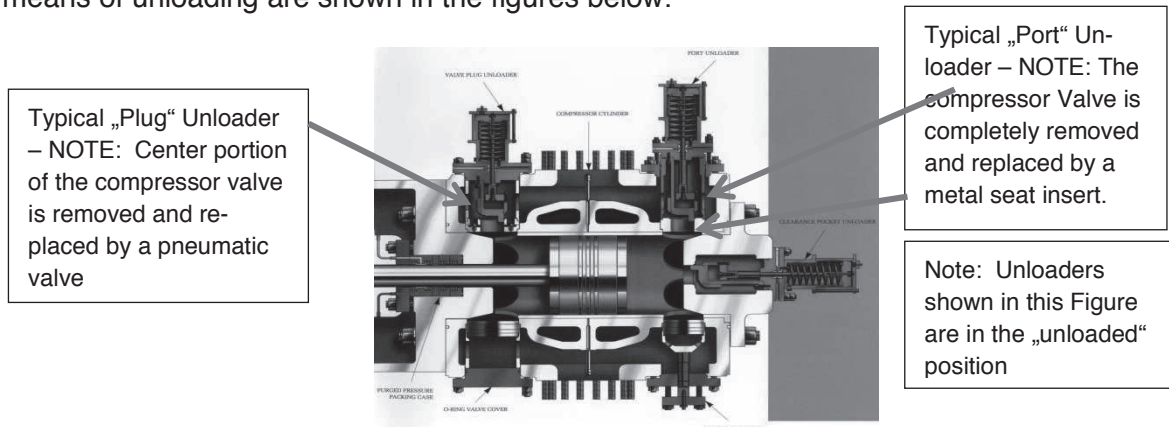


Figure 6. – “Plug” and “Port” Unloaders installed on a typical Compressor Cylinder.

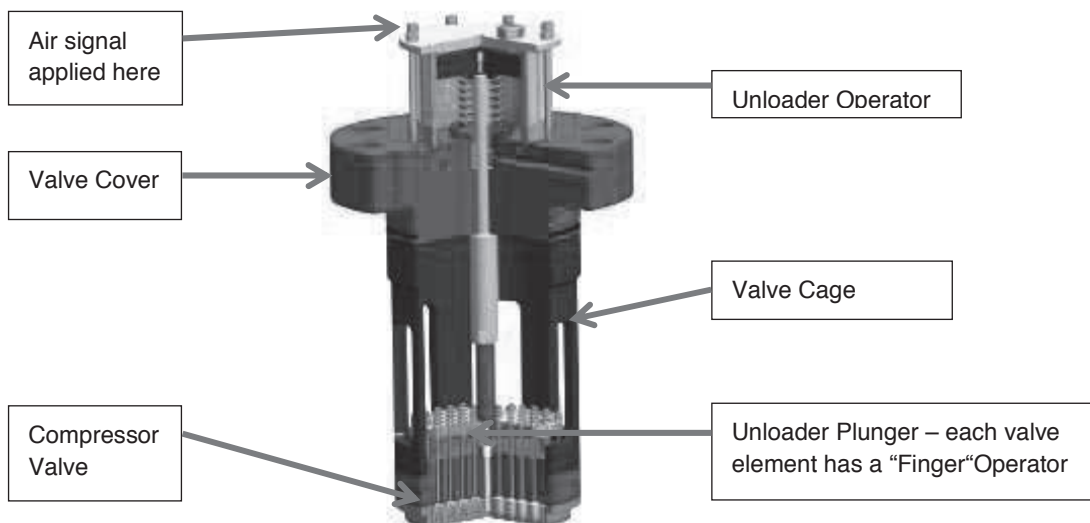


Figure 7. – Typical “Finger Type” Unloader – removed from the cylinder for clarity – Note: Unloader is in “loaded” position



Each of the Capacity Control devices described previously with the exception of the „VVCP“ , Fig. 2., require an Air Signal to activate the pneumatic valve. A typical Air Signal can range from 65 – 125 psi (approximately 4 – 8 bar). These devices provide the operator with discrete load steps. Depending on the number of cylinders on the compressor, these discrete load steps, with or without a means of varying the compressor speed (see Figure 4.), likely provide all the flexibility in capacity control that is desired by the end user. The pneumatically operated devices also allow for remote adjustment to accomplish capacity control.

### Cylinder Capacity – Further Addressing the Needs of the Customer

It is for certain that the fewer parts (by part number) in a machine, the lower the maintenance, the fewer parts the client needs to stock, is a plus for any customer . This coupled with proven designs, simplicity, and meeting clients needs can be a „winning combination“.

Albert Einstein once said „Everything should be made as simple as possible but not simpler“. Let us examine a design which combines fewer parts, simplicity, safety of operation, and the ability to vary clearance and therefore capacity while the compressor is in operation.

As mentioned previously, by adding clearance has a benefit of lower throttling losses/power consumption, compared to other means of unloading. Consider having a „Clearance Pocket“ that would allow for varying clearance adjustment remote from the machine?. Consider a Hydraulic means of actuating the clearance pocket as per Figure 8.

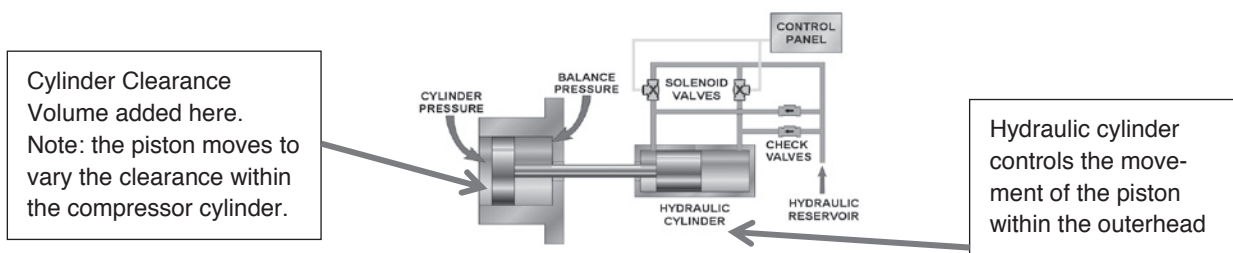


Figure 8. – Diagram of Hydraulic Variable Volume Clearance Pocket

As previously described, adding clearance volume reduces  $E_v$  of the compressor cylinder at a given compression ratio. So as the clearance volume added increases, the percent clearance (unswept volume) in the compressor cylinder increases thereby reducing the  $E_v$ . This is shown below in sequential movements of the Hydraulic Pocket (see Figure 9). Note how the area of the *PV Diagram*, becomes smaller in area as the pocket is opening. Recall from Thermodynamics that the area of the *PV Diagram* indicates the “work”(FT-lbs. / min.) which is power consumption. The power consumption decreases as the pocket opens.

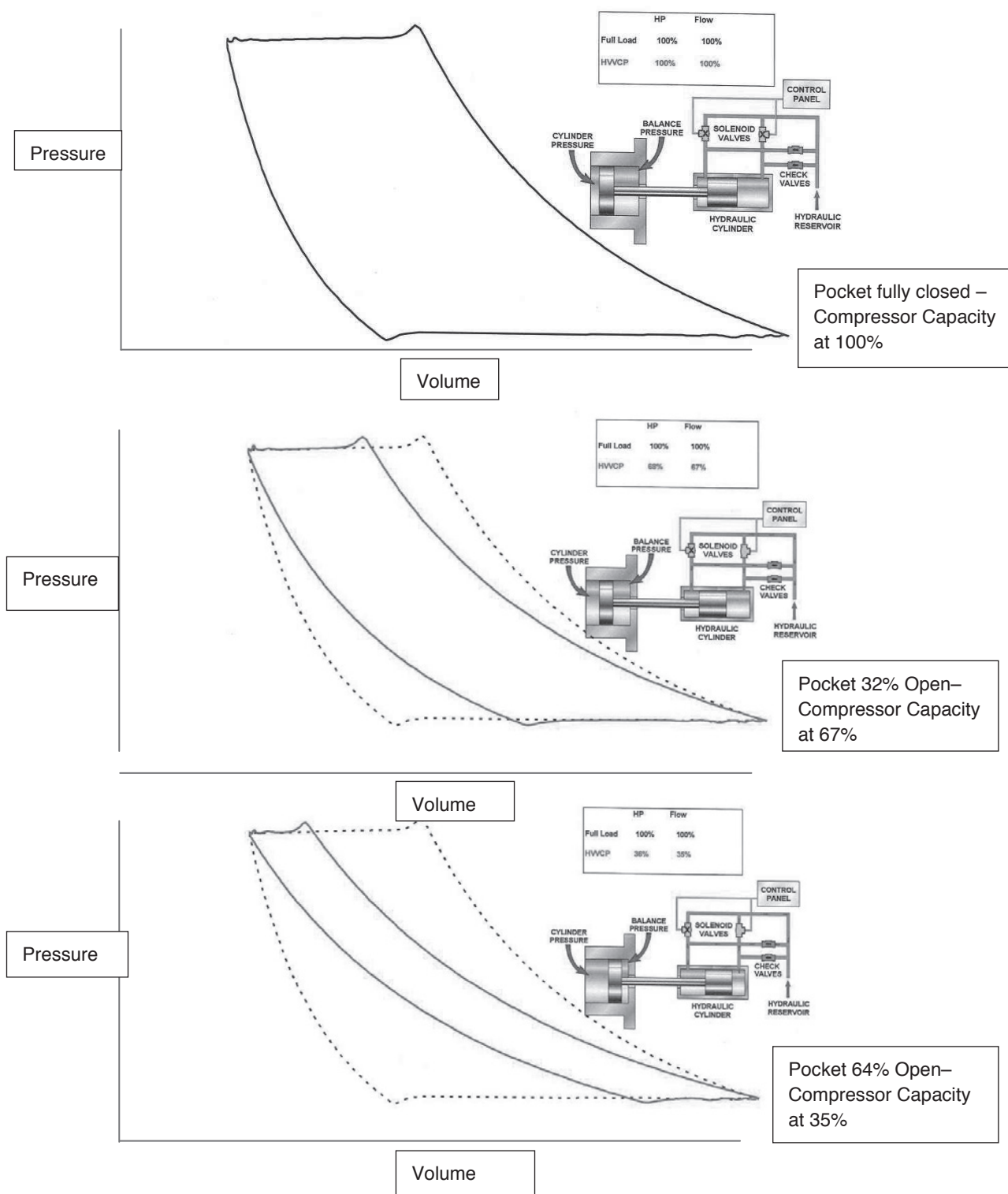
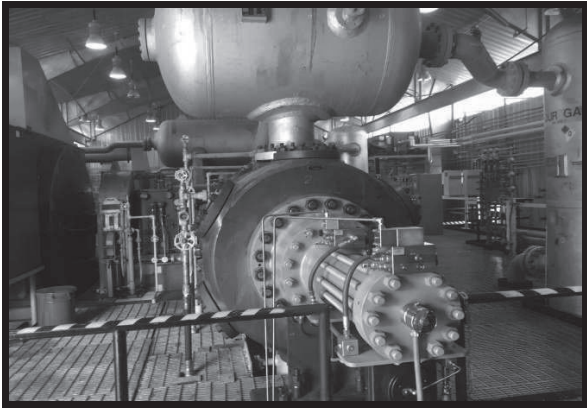
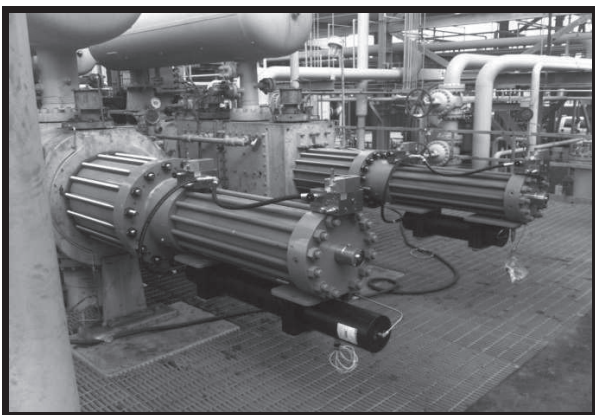


Figure 9. – Hydraulic Variable Volume Clearance Pocket Position - Sequential Pocket Piston Movement– Effect on  $E_v$  and Load as shown in the PV Diagram

The Hydraulic Variable Volume Clearance Pocket (HVVCP) addresses the need of clients to adjust the capacity of the compressor remotely, without discrete capacity steps, fewer moving parts, simple, and safe. A brief installation summary is below:



*Natural Gas Application with H2S*



*Hydrogen Service – Note application to 1<sup>st</sup> and 2<sup>nd</sup> stage cylinders*



*Hydrogen Service*



The benefits of the Hydraulic Variable Volume Clearance Pocket are:

- Allows direct replacement for “handwheel” or fixed volume pockets
- No modifications to the compressor cylinders
- Provides safe and reliable capacity adjustment while the compressor is operating under load
- Fully adjustable within limits set by the pocket volume
- Remote adjustment

A disadvantage is that the pocket can only be applied to the outer end of a compressor cylinder.

### **Cylinder Capacity Control Methods- Application**

Many more compressors are installed than compressor manufacturers will build as new equipment. Fortunately, all of the devices described in this paper can be applied to existing equipment. This can be part of an „upgrade“ or compressor „modernization“ program. It is important to the client to continue to keep the Reciprocating Compressors running to take full advantage of the initial capital investment. In addition, Compressor manufacturers can offer modern design compressor valves, wearing parts (e.g. piston rings, guide rings), ignition systems (lean burn for engines, etc.) and other upgrades to improve the life and Mean Time Between Failure (MTBF) of components that historically have increased maintenance costs.

When applying these Capacity Control Devices the same considerations are applicable as if they were applied to a new unit. For instance:

- Effect on Cylinder Pressure ratio – Are these devices needed on only the 1st stage cylinders or on other subsequent stage so as not to cause an overload (over maximum rod load) condition?
- Effect on Cylinder base clearance – How much may the base clearance change without affecting the full load capacity of the machine?
- Adequate „Rod Reversal“ at all operating conditions? – this is related to unloading sequence.
- Power –or- BHP limitation considered?
- Capacity Prediction

What needs to be known then is the range at which these Capacity Control devices can be operated not only to achieve the desired capacity but within the operating range (e.g. speed, ratio, rod load, BHP) of the compressor. This is typically shown in a „Performance Curve“ as shown in Figure 10:







## Conclusion

The Capacity Control Systems presented in this Technical Paper are by no means all that are offered by Compressor manufacturers or other Controls companies. This paper is meant as a „primer“ to acquaint the reader with some definition of Capacity Control types as well as the basic understanding of these mechanical devices and how they function and are operated.

The Capacity Control systems offered today by various manufacturers have an overall record of reliability and safety in operation. Capacity Control Mechanisms and systems can be offered on reciprocating compressors which in effect improve the reliability and flexibility of the compressor. In effect, „modernizing“ the operation of the compression equipment. However, the Capacity Control devices have design limitations and if improperly applied or operated can have an effect not only on the reliability of the device but also the compressor as well as safety of the operating personnel.

## Closing Remarks

I wish to thank my company, Dresser-Rand Company, a Siemens Business, for allowing and providing support in the preparation and presentation of this subject material. I wish also to thank my colleagues, Steve Chaykosky, David Decker, Joel Sanford, Gary Templar, Dale George, for their assistance in developing the presentation material contained within this Technical Paper. Finally, I wish to thank the EFRC committee for accepting this paper as well as allotting time during the conference for the presentation of this subject material.

## References

- 1) Rollins, John P. Editor (1989), *Compressed Air and Gas Handbook – Compressed Air and Gas Institute*, Englewood Cliffs, N.J. USA: Prentice Hall, Inc.
- 2) Woollatt, Derek. “Stepless Capacity Control for Reciprocating Compressors” – presented GMRC 2002
- 3) “Pneumatic Variable Clearance System For Natural Gas Compressor Applications”. CompressorTech<sup>TWO</sup>, November-December 1999
- 4) Chaykosky, S. and Sanford, J. “Stepless Capacity Control Systems for Reciprocating Compressors”  
9<sup>o</sup> Fórum de Turbomáquinas Petrobras. August 2013
- 5) Dresser-Rand Co. , Form 85237, *Variable Capacity Control Suite*







# Technical Paper

**Session: 36-2**

**Session Name: Controls**

## **Stepless capacity control maintains efficiency of French natural gas compressor as production declines**

**Author:**

**Justin McDonald**  
**Sr. Facilities Engineer/Ingénieur Installations Surfaces – France**  
**Vermilion Energy Inc**  
**Calgary, Alberta T2P 0R3, Canada**

**Co-Author 1:**

**Arnaud Dubos**  
**Project Coordinator - France**  
**Vermilion REP SAS**  
**40161 Parentis-en-Born, France**

**Co-Author 2:**

**Tanguy Bosson**  
**Maintenance Supervisor – Vic-Bilh**  
**Vermilion REP SAS**  
**64330 Saint Jean Poudge, France**

## Summary

Vermilion Energy operates around two dozen oil and gas wells at Vic-Bilh in the Aquitaine region of south-west France. Several dedicated gas cap wells produce gas at a pressure high enough for direct export, but lower-pressure associated gas from the remaining wells must be compressed for sale. For this duty Vermilion Energy uses a four-stage 600 kW reciprocating compressor (KB310) that dates from the 1980s.

Previously, gas throughput was controlled by a bypass valve around the compressor. With average compressor utilization only around 20%, this wasted more than 1,400 MWh of electricity every year.

To reduce the compressor capacity, the company looked at replacing some of the existing cylinders with smaller ones, or replacing the entire compressor. The final decision, however, was to retrofit a stepless capacity control system based on suction valve unloaders.

A technical analysis showed that the reverse-flow capacity control system would restore full efficiency. In addition, it would avoid the need to make big modifications to the compressors, with the consequent requirements for re-certification, and would cost significantly less. It would also improve the dynamic control of both flow rate and discharge pressure.

Vermilion chose a new all-electric stepless capacity control system. Following commissioning in spring 2015, the system has performed as designed and without problems. The payback period is around one year.



## 1. Vermilion Energy

Vermilion Energy is a Canadian oil and gas producer with particular expertise in managing declining fields. The company has been present in France since 1997, with operations in the Paris Basin south-east of the capital and in Aquitaine in south-west France. The company is currently the largest oil producer in France.

Vermilion Energy has 13 concessions in Aquitaine. Together they yield a total of around 5,000 bbl/d of oil, accounting for 40% of Vermilion's production in France.

## 2. Oil and gas in and around Vic-Bilh

One of Vermilion Energy's concessions in Aquitaine is Vic-Bilh, named for a small town in the French département of Pyrénées-Atlantiques, 125 km west of Toulouse and 150 km south of Bordeaux. Covering the landscape of rolling hills is a mixture of woodland, fields and vineyards. To the south is a view of the Pyrenees, some 75 km away.

The oil and gas fields of this part of France have been exploited since the 1950s, and production from many fields is now declining. Vic-Bilh is essentially an oilfield, but falling reservoir pressure has allowed free gas to become trapped under domes of impermeable rock. Three to four gas cap wells tap into these domes to yield natural gas at moderately high pressures. The remaining wells, which number around 20, produce oil and low-pressure associated gas.

Gas from Vic-Bilh travels by pipeline to Lacq, 40 km to the south-west. Until late 2013 Lacq was home to a large gas processing plant operated by French oil company Total. As the Lacq gas field reached the end of its economic life, however, the main processing plant was shut down. A new, smaller, processing plant will continue to supply energy and sulfur-based raw materials to nearby chemical manufacturers under the project name Lacq Cluster Chimie 2030.

The mention of sulfur is key. Gas from Lacq is very sour, typically containing 15% H<sub>2</sub>S and 9% CO<sub>2</sub>. The discovery of gas here in 1951 laid the foundations for future sour gas production worldwide, including corrosion-resistant steels and amine-based sweetening processes.

The Vic-Bilh gas, though much less sour, still contains around 2% H<sub>2</sub>S. This is high enough to make disposal difficult. In cases where flaring would normally be the economic option, only a full-scale incinerator can properly meet modern standards for environmental protection. This increased the incentive for Vermilion Energy to collect all the associated gas and send it to the customer in Lacq.

## 3. The Vic-Bilh gathering station

The 300-m wide compound at the Vic-Bilh gathering station contains pipeline valves, separator drums, and two reciprocating compressors. The latter are key pieces of equipment. After initial separation and screening to remove oil, water and sand, gas from the Vic-Bilh gas cap wells is at a high enough pressure to be sent directly to the pipeline to Lacq. The pressure of the associated gas from the remaining wells, however, is only 1.3 bar by the time it leaves the low-pressure separator. As a result, this gas must be compressed up to a maximum pipeline pressure of 34 bar (15-20 bar normal operation) for transport.

The gathering station handles a total of 25–75 kNm<sup>3</sup>/day of gas in total. Of this, 10–30 kNm<sup>3</sup>/day is associated gas that needs to be compressed for onward transport.

The 450 kW three-stage compressor (KB210) and 600 kW four-stage machine (KB310) were both installed in 1984 and later inherited by Vermilion Energy when the company took over op-

erations at Vic-Bilh. In the past, depending on the required flowrate, they have operated either in parallel or in a backup configuration. At the current production rate, the KB310 compressor handles 100% of the compression duty, leaving the KB210 machine to act purely as a standby.

Gas enters the suction side of the duty compressor via two streams at different pressures. One of these comes from the high-pressure separator and is injected between the first and second compressor stages. The other stream, from the low-pressure separator, enters the suction side of the first compressor stage (Figure 1).

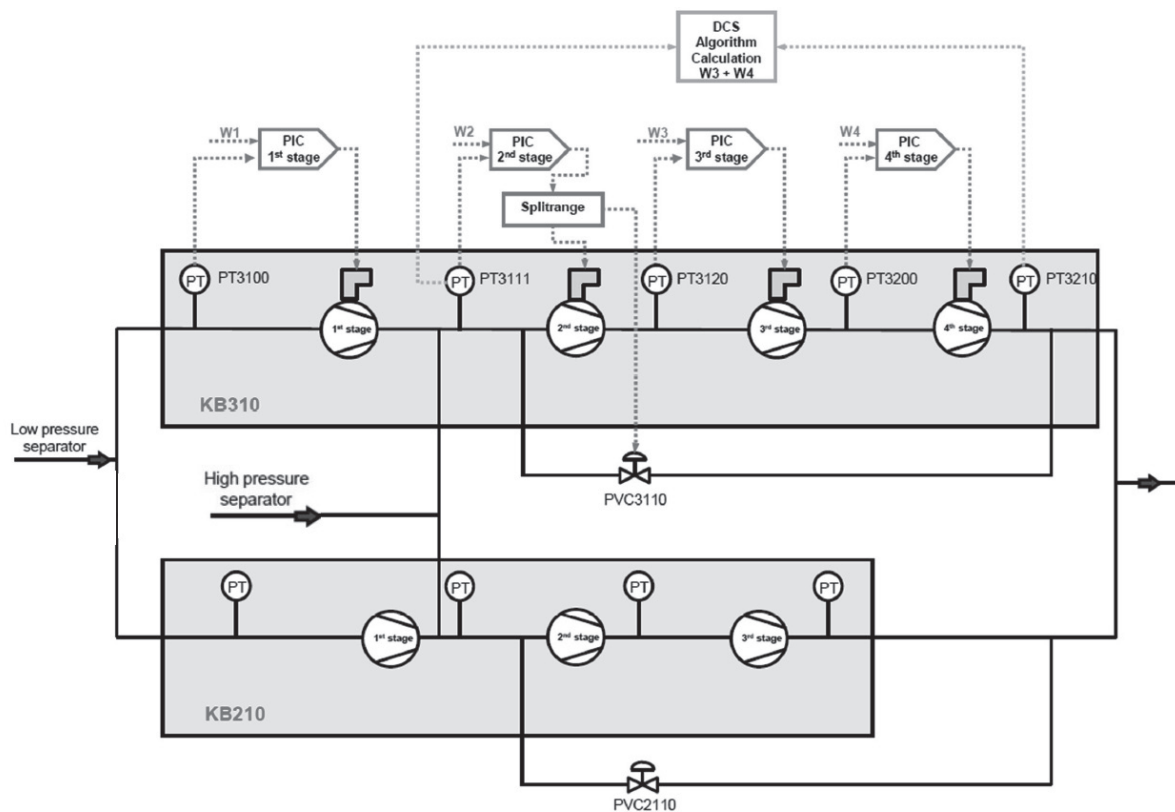


Figure 1: Block P&ID for the two Vic-Bilh compressors. The four-cylinder KB310 machine is at the top.

#### 4. The need for capacity control

The KB310 compressor previously controlled gas throughput via a combination of on-off control, which provided capacity steps of 0/50%/100%, and a recycle valve. As gas volumes have fallen, however, this method has become increasingly uneconomic. Today the compressor operates at around 20% capacity. With a rated power of 600 kW and running at the 50% capacity step, recycle control down to 20% means that the compressor was wasting an average of 180 kW, or more than 1,400 MWh every year. Even though France has some of the cheapest electricity in Europe, Vermilion Energy decided that this loss was too costly.

To maintain efficiency in the face of falling gas volumes, the company originally explored two ideas. The first was to replace some of the existing compressor cylinders with smaller ones. The second was simply to replace one or more entire compressors with smaller ones.

However, a feasibility study showed that a better choice would be to retrofit a stepless capacity control system based on reverse flow principle. This would maintain efficiency under the new



operating conditions, the study showed. In addition, it would avoid the need to make big modifications to the compressors, with the consequent requirements for re-certification, and would cost significantly less. It would also improve the dynamic control of both flowrate and discharge pressure.

Variable-speed drives are another control option sometimes used for reciprocating compressors. On this unit, the existence of two semi-independent feed streams means that to some extent the first stage can function independently of the other three stages. By allowing each stage to perform at its optimum level, suction valve unloading brings a degree of flexibility that would not have been possible with variable-speed control.

### **5. Stepless capacity control via suction valve unloading**

Vermilion chose a new all-electric stepless capacity control system for the KB310 compressor. This stepless capacity control uses actuators and unloaders to hold the suction valves open for a precise fraction of each cycle. Instead of being compressed, with the consequent waste of energy, any gas that is not needed to meet current demand is simply pushed back into the suction plenum during the first part of the compression stroke.

Barring small energy losses as the gas flows back and forth through the suction valve, the system has a high efficiency that – unlike traditional stepwise control regimes – it maintains across a wide turndown range.

The same supplier also offers a long-established technology using hydraulic actuators to generate the forces needed to hold the suction valves open. Vermilion Energy was able to take advantage of the smaller footprint, lower cost, easier installation and simplified maintenance requirements that the new electric system offers.

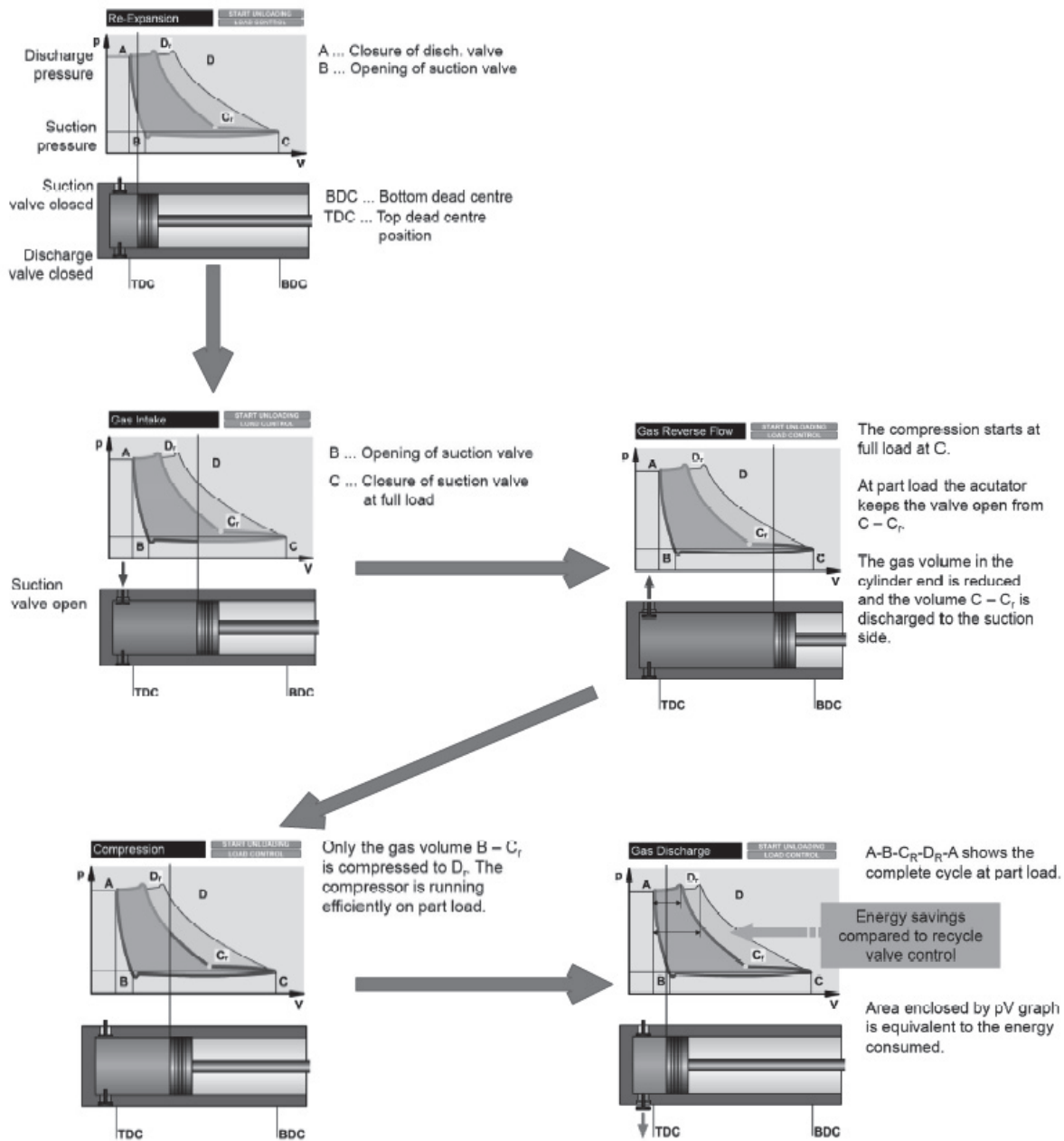


Figure 2: The local power and control units for the system are very compact

## 6. Project start and control decisions

Vermilion Energy ordered the new system from the supplier's French subsidiary. The first meeting with the supplier to discuss in detail how the system would be implemented took place in March 2014.

At this point, the main decisions concerned the control logic. Depending on the process requirements, the key control variable for stepless suction valve unloading can be the suction pressure, the discharge pressure, or the flowrate. In this case, Vermilion Energy decided to retain the existing control logic, setting the suction pressure as the primary control variable for the first stage. The second, third, and fourth stages follow the supplier's usual procedure, which is





to control them based on the respective interstage pressures. The setpoint pressures for these cylinders are calculated from the suction and discharge pressures (Figure 1).

The supplier specified an overall control narrative, which Vermilion Energy then integrated into the main plant control system. For instance, this included providing the all-electric system with pressure and crank angle signals for each compression stage, including scaling functions and start/stop information.

## 7. Installation and commissioning

The four-stage KB310 compressor has 14 suction valves: four each on the first three stages and two on the fourth stage. Each suction valve is fitted with an unloader and actuator. The supplier's French subsidiary delivered and installed the new system, plus new valves and other parts to improve energy efficiency and reliability. Each actuator is self-contained (Figure 3 and Figure 4), requiring only one connection to a local power and control unit (Figure 5). Installation of the new valves, unloaders, actuators and valve covers was therefore straightforward. A single multi-core cable connects the compressor to a control cabinet (Figure 6), from where the system links to the main operator room. The supplier also has remote access to the system for monitoring and troubleshooting.

Payback for the system is estimated at less than a year.

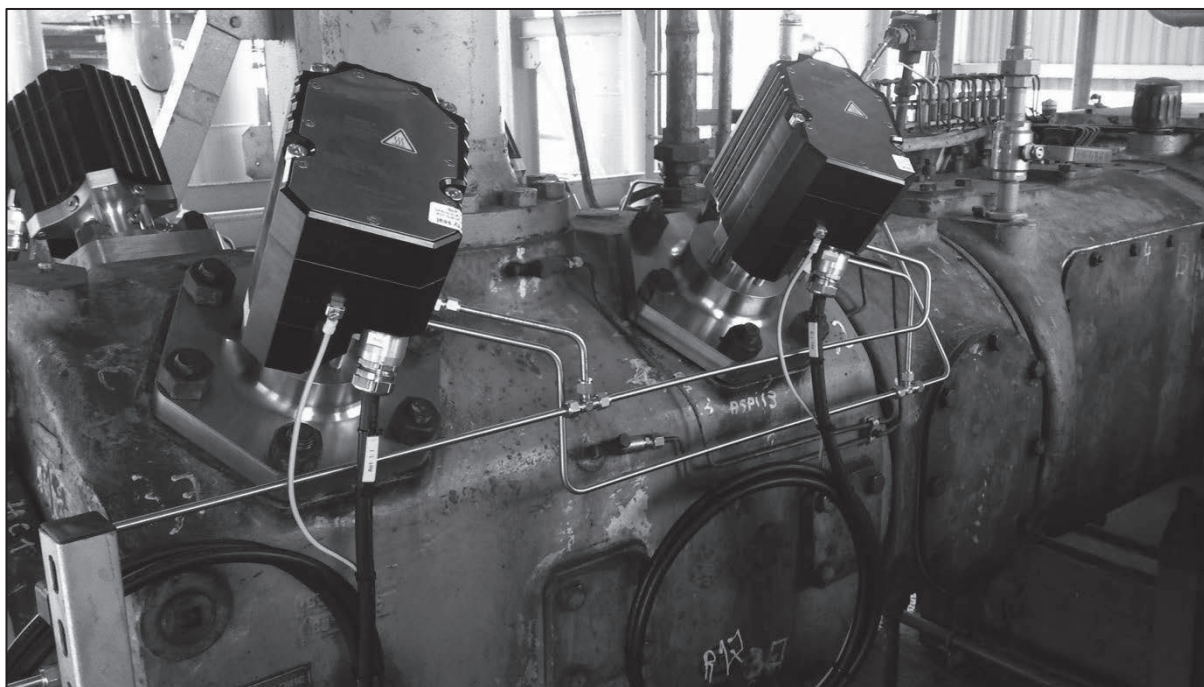


Figure 3: Valve covers and actuators as installed



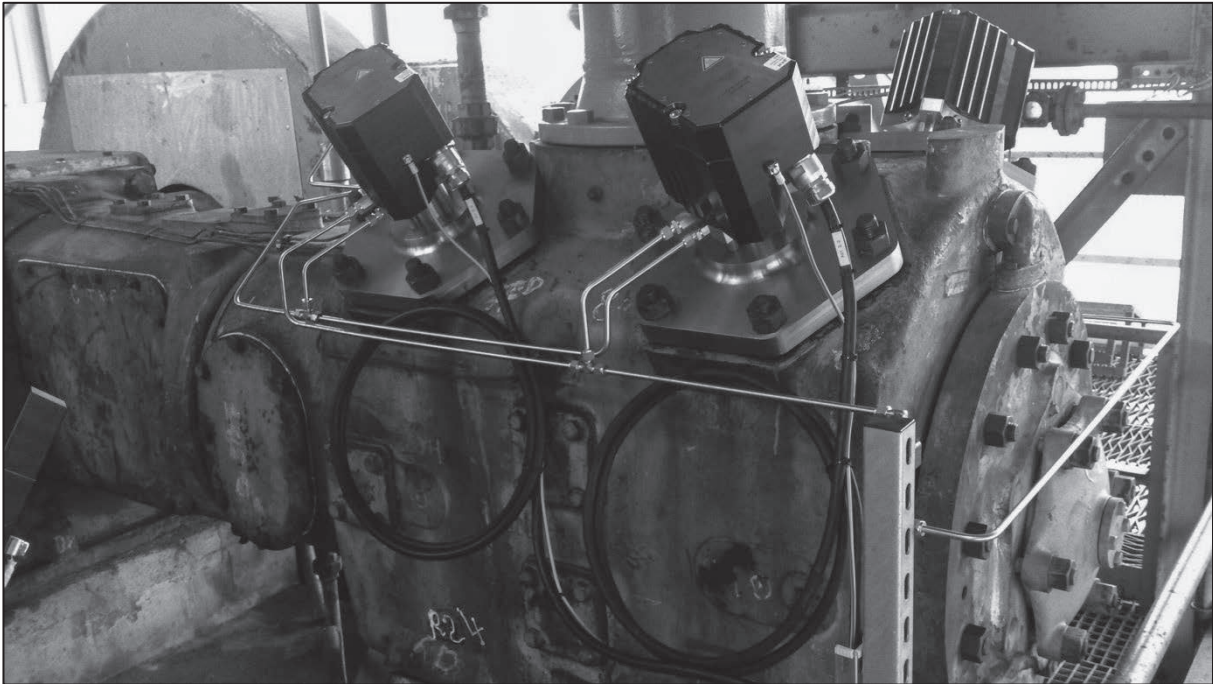


Figure 4: Another view of the electric actuators (14 in total)

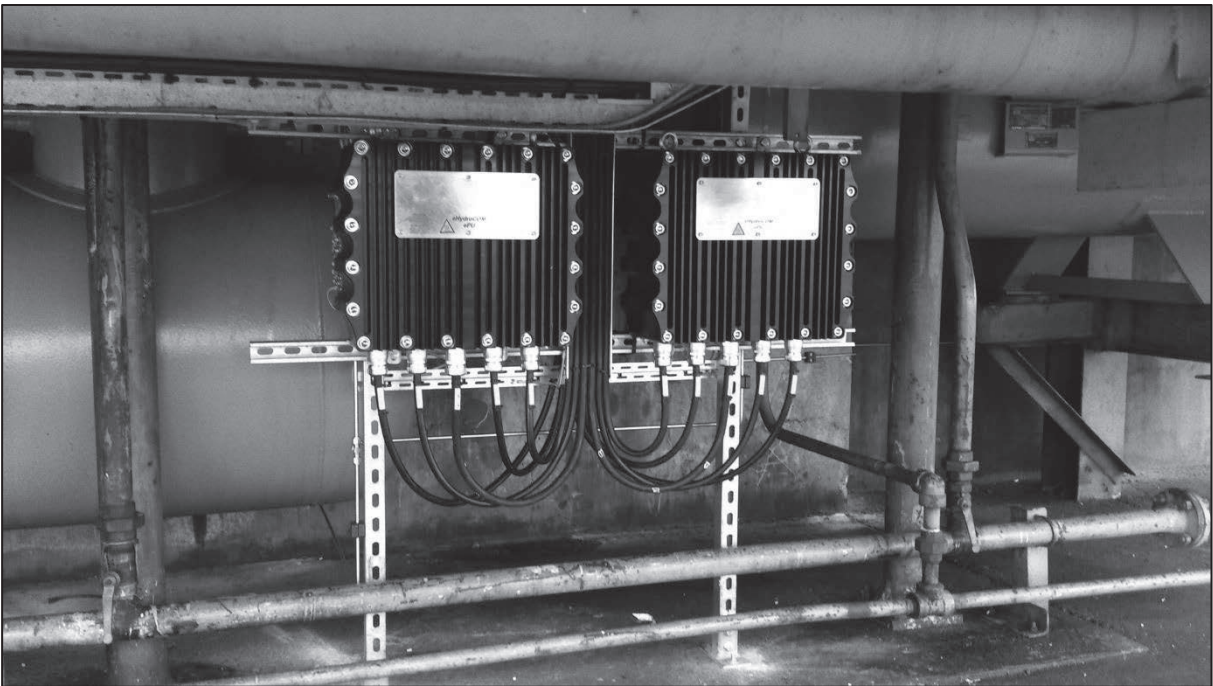
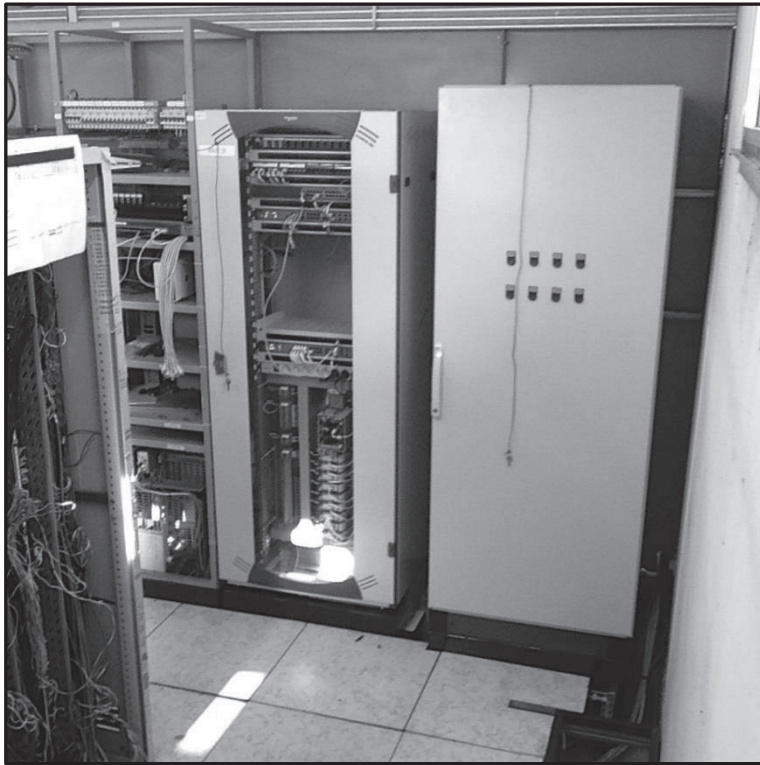


Figure 5: The local power and control units for the system are very compact



*Figure 6: The main cabinet for the capacity control system*

## **8. Conclusions**

Although adequate information for a full quantitative evaluation of operational parameters (OpEx, efficiency, & maintenance) is not yet available, the lower capital costs, shorter project timing, less complex installation and increased operating envelope have proven to be a value-add for Vermilion Energy.





# Technical Paper

**Session: 37-1**

**Session Name: Root cause analysis**

## **Barking dog noise in a natural gas compressor station: Analysis and mitigation**

**Author:**

**Leonard van Lier**  
TNO, technical Sciences  
2628CK Delft, The Netherlands

**Co-Author 1:**

Pieter van Beek  
TNO, technical Sciences  
2628CK Delft, The Netherlands

**Co-Author 2:**

Werner Temmink  
Nederlandse Aardolie Maatschappij B.V.  
9400 Assen, The Netherlands

**Co-Author 3:**

Juergen Brenner  
HOERBIGER  
1220 Vienna, Austria

## Abstract

In a compressor installation of NAM (Dutch Petroleum Association) at Coevorden, natural gas is produced and injected into the national gas grid. Three reciprocating compressors are used to compress the gas to grid pressure. To mitigate the declining suction pressure of the depleting wells, larger cylinders and new pulsation dampers have been installed. Upon startup noise issues and integrity issues with the compressor valves were observed. The noise emission was an atypical intermittent barking sound, apparently radiated from the piping and the pulsation dampers. The noise raised questions on the integrity of the installation as a whole and caused an environmental concern to the neighbors. The issues with barking noise could not be easily identified. Also a high failure rate of the compressor valves was observed. During the design phase, the pulsation study indicated significant over- and under-compression in the cylinders, limiting the compressor's capacity and increasing the power consumption. An extensive field survey was done to identify the barking noise, the issues with compressor valves and the compressor performance. The survey included various measurement techniques, such as pulsation measurements, vibration measurements, PV chart registration, power measurements, flow measurement, torque measurements and noise recording for a variety of process conditions. The analysis of the data and the subsequent RCA confined the area for generation of noise inside the cylinder. It appeared that the barking noise was caused by a defect in the suction valves, which was resolved satisfactorily by refitting of the compressor valves with an improved design. This resolved both the valve integrity issues and the barking noise. The compressor capacity appeared to be in agreement with the original datasheets. The power consumption was high in comparison to the specification, but within the agreed tolerance between NAM and the Vendor. An improved layout of the cylinder internals could result in a significant reduction of the power consumption. However, such a retrofit appeared difficult in the installation, due to practical restrictions. For future projects, it is recommended to investigate the power consumption during the early design of the cylinders, considering the valve losses, ventilation losses and the unsteady effects of the pulsating flow.





## 1 Introduction

The reciprocating compressor system of NAM in Coevorden consists of two locations COV-17 and COV-24, separated by an 8 km pipeline. The identical compressors K-170 are the '1<sup>st</sup> stage' of the compression process. The 2<sup>nd</sup> stage K-270 and 3<sup>rd</sup> stage K-370 compressors are located on COV-17. Compressor K-370 is manufactured by a different vendor, than K-170 and K-270.

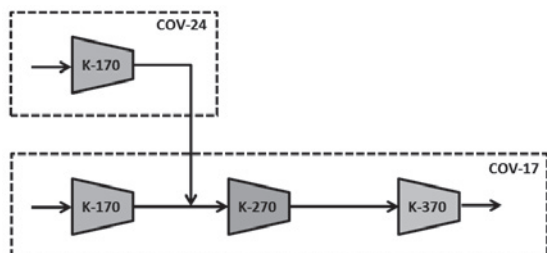


Figure 1. Schematic representation of compressor system NAM Coevorden.

Most relevant for this paper are the 1<sup>st</sup> stage compressors K-170. These are 4-throw natural gas compressors, operated at a fixed speed of approximately 370 rpm. The design range for the suction pressure is from 1.5 to 6 bar. The design range for the discharge pressure is from 4 to 15.5 bar. The gas is natural gas (MW=18 g/mol). The capacity is controlled with suction valve unloading, with automatic regulation from 100% down to 50% in steps of 12.5%. The maximum power consumption of K-170 running at 100% load is approximately 2 MW.

## 2 Re-vamp of the compressor station

In case of a new reciprocating compressor system, the API 618 standard stipulates that during the design stage, a pulsation study shall be carried out. The same requirement for a pulsation study applies for a compressor system subject to a re-vamp. Examples of re-vamps that affect the behavior of pulsations are: changing process conditions (for example depleting gas wells), changing gas composition (for example upgrades in refinery compressor systems), increased cylinder sizes, modified clearance, modified compressor valves, alternative capacity control strategy (such as step-less reverse flow capacity control), modified compressor speed, re-staging of an existing compressor and adding compressors to an existing system.

For the installation of NAM in Coevorden, enlarged cylinders were applied on compressors K-170 (COV-17 and COV-24) and K-270 (only COV-17). Also, the pulsation dampers were modified on K-170 and K-270. The discharge conditions for the '3<sup>rd</sup> stage' compressor K-370 remained nearly the same as in the original system. One of the main challenges was the spatial restriction between the compressor cylinders and the existing foundation. This spatial restriction had to be met in the design of the new cylinders, dismantling area for the discharge valves and the new discharge dampers.

## 3 Pulsation study

During the design phase for the re-vamp, a pulsation study was carried out in accordance with the API 618 standard, 5<sup>th</sup> edition, which included the following tasks:

- Analysis of the pulsation dampers ('damper check')
- Pulsation analysis of the field piping
- Mechanical response analysis
- Dynamic compressor valve analysis

The damper check is a very important preliminary assessment of the 'heart-beat area' of the pulsations. This step is typically performed in an early stage of the project when the details of the field piping have not yet been addressed in the design. The simulation model for the damper check is shown in figure 2, and includes all 4 cylinders of compressor K-170. Even though the



two sides of the compressor have a symmetric line-up of the cylinders, pulsation dampers and interconnecting piping, this model allows to investigate the acoustic interaction between all the cylinders and between the dampers and inlet KO drum.

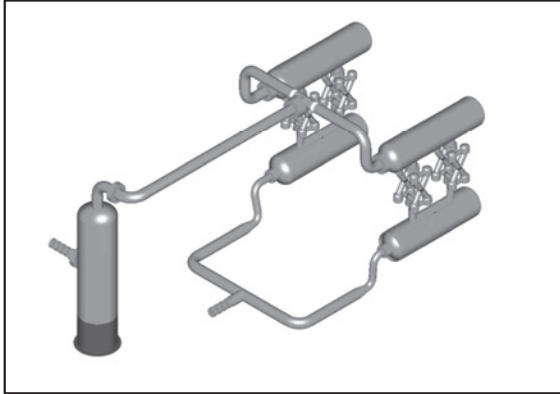


Figure 2. PULSIM model for damper check.

During the damper check, PV diagrams of the cylinders are normally presented and analysed, for various operating cases defined in the compressor datasheets. In this particular project, considerable losses were noticed, associated with the flow in the cylinder gas passages. The gas passages (connecting the working chambers on Head End (HE) and Crank End (CE) side to the cylinder flanges are shown in figure 3.

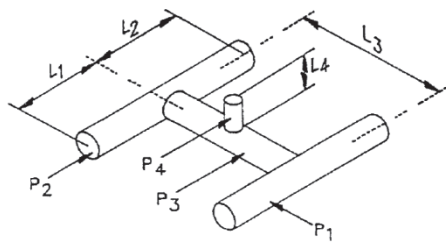


Figure 3. Schematic representation of cylinder gas passages, supplied by compressor vendor.

The calculated pressure overshoot inside the cylinder's working chamber and the excess power consumption (compared to the ideal, adiabatic PV diagram) was judged as remarkable. Closer inspection indicated high mean gas velocities in the cylinder channels, up to 60 m/s. Considering the unsteady effects of the flow due to the pulsating action of the compressor pistons and valves, the instantaneous gas velocities reached values of 200 m/s.

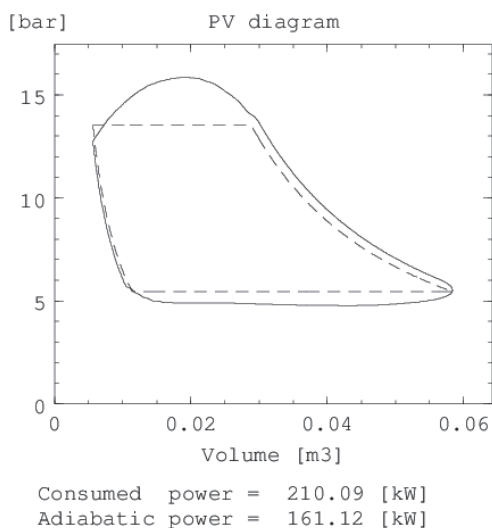


Figure 4. Typical PV diagram, calculated during the early design of the pulsation dampers.

The pressure overshoot and the excess power consumption is determined by the losses in the cylinder gas passages, the compressor valves and the pulsation effects.

#### 4 Noise issues upon start-up

Upon start-up, strange noises were observed. During an initial site visit, it became apparent that two separate noise mechanisms were causing nuisance to the disturbed neighbours:

- High frequency tonal noise with a continuous character (whistling);
- Intermittent noise, originating from the compressor assembly (barking).

The high-pitch whistling noise (approximately 2 kHz) was identified as originating from the temporary inlet strainer. The identification was rather straightforward by inspecting the noise emission from the piping. The inlet strainer was located outside the compressor building. By removing this temporary filter, the noise disappeared.

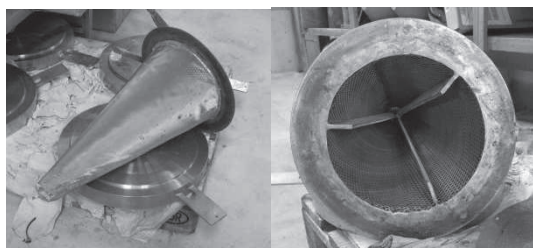


Figure 5. Inlet strainer.

The other phenomenon caused strong noise emission inside the compressor building. The noise resembled the barking of a dog and was inter-mittent, on an irregular basis. Up to 60 barking effects per minute were recorded.

The barking noise could be described as ‘violent bursts’, containing high-pitch noise. The bursts occurred on an irregular basis. The noise appears to be originating from all cylinders.

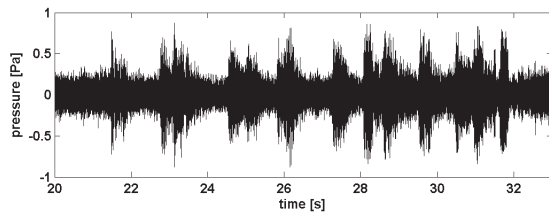


Figure 6. Barking noise events

Rotating equipment engineers were initially puzzled by the noise. No experience with similar noise phenomena was available. The issue was soon labelled the 'barking dog', or more specific 'the Keeshond'<sup>1</sup>.



Figure 7. Noise resembled barking of the Keeshond

The location of the origin of the noise could not be found easily. Based on aural inspection, the noise was radiated from the area of the cylinders and suction dampers.

The noise caused a concern to neighbours and to the operators of NAM. It was suspected that the noise corresponded to in-line noise of high amplitude and frequency. Hence, the dynamic loading on the internals of the pulsation dampers, due to the mysterious barking noise, may be considerable. The integrity of the internals of the pulsation dampers due to high-frequency loading had not been evaluated during the design phase, in contrast to the normal low-frequency loading due to the compressor pulsations.

To identify the origin of the barking noise, a root-cause analysis effort was initiated. TNO was asked to participate and propose appropriate actions to identify and resolve the issues.

## 5 Issues with compressor valves

In addition to the noise issues, an excessively high failure rate of the compressor valves was observed, in particular on the compressors K-170.

Mainly suction valves have failed, discharge valves failures have been considered as consequential damages of the suction valve failures due to loose parts such as valve ring pieces and broken valve springs.

Out of a high number of inspected broken suction valves, the following failure sequence was determined:

---

<sup>1</sup> Formerly called the Dutch barge dog; a very alert dog race, known for their loud, distinctive bark.



- Valve springs have been compressed by shock loading.
- Consequently free length of the valve springs was reduced by 2mm resulting into the loss of pretension.
- Valve springs have been able to move free in the spring pocket, leading to excessive wear on the outer diameter and consequently valve spring breakages.
- After the valve springs have failed, some individual valve rings were not properly spring loaded and their uncontrolled movement lead to valve ring breakages.

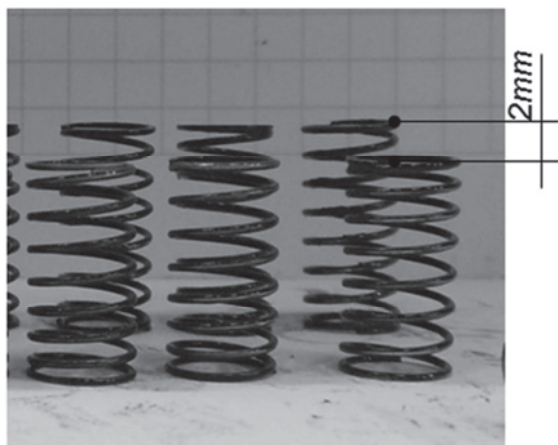


Figure 8. Consequence of shock loading valve springs: Free length of springs reduced by 2mm, therefore loss of pre-loading.

Detailed investigations showed that shock loading of this specific valve springs starts to appear at impact speeds of more than 13m/s while the valve dynamic report returns for the suction valves opening speeds only less than 3m/s. The deviation of real impact speeds and calculated impact speeds lead to the assumption that the real process condition in the compressor differed from the design process condition.



Figure 9. Valve ring damages observed on individual rings of the multi-ring valve.

## 6 Concerns with compressor capacity and power consumption

When the noise issues and the issues with the compressor valves were observed, as a first step the results of the pulsation study were closely inspected. Again triggered by the remarkable PV diagrams, the performance of the compressor was evaluated in a generic way. This was done by comparing the measured compressor capacity with the value in the datasheets (location COV-24). The measured flow was low by approximately 15%. These observations aroused suspicion on the performance of the compressor. Therefore, it was decided to do an extensive in-situ performance test for the compressor installation on COV-17.

## 7 Root Cause Analysis and field testing

During project meetings, additional analysis was presented by several partners in the project, including NAM, TNO, Hoerbiger and the engineering contractor of the re-vamp. Preliminary acoustic registration of the noise was used to analyze the intensity of the intermittent noise and the frequency content.

Various candidate mechanisms for the noise generation were raised by the project team. This included anomalous flow inside the cylinder passages, choking flow and shock waves, inadequate separator performance, condensation of liquid in the cylinder passages, accumulation and ingestion of liquid into the cylinders. It was suspected that the observed noise, valve failures and high gas velocities in the cylinder were related mechanisms, but this was hard to conclude firmly.

The performance of the separators was double-checked and found to be according to the design standards. The heat tracing and acoustic insulation were verified and in accordance to design specifications. Draining connections were added to the suction dampers, and the amount of liquid drained appeared to be small. Based on thermodynamic analysis, it was excluded that inside the cylinders excessive expansion was responsible for condensation. Also the inspection of the failed valves did not show typical signs of failure due to liquid ingestion. In short, the hypothesis that the issues were caused by liquid ingestion was classified as 'unlikely' and discarded.

Based on the reports by the operators and the preliminary noise measurements in the compressor building, no clear relation between the barking noise and process conditions could be established. The barking appeared on an irregular basis, originating apparently from all cylinders. In the absence of a key phasor registration, the exact timing of the barking event could not be related in time to the operation of the compressor valves.

The field survey focused on the barking noise, to identify the origin of the noise. In addition to unsteady pressure measurements inside the working chambers of various cylinders, pulsations were recorded at the cylinder nozzles and in the field piping. Vibrations were recorded on the suction dampers and radiated noise was recorded with a microphone.

Furthermore, during the survey, the performance of the compressor was critically investigated. This was done with various independent measurement techniques:

- Electric power measurement with a Watt meter, performed by a specialized sub-contractor.
- Thermodynamic power extracted from PV diagrams, performed by TNO [3].
- Shaft power measurements, performed by a specialized sub-contractor.
- Enthalpy rise method, using pressure, temperature and flow readings from instruments in the field, in combination with an Equation Of State (EOS) to compute the enthalpy rise [3,4].



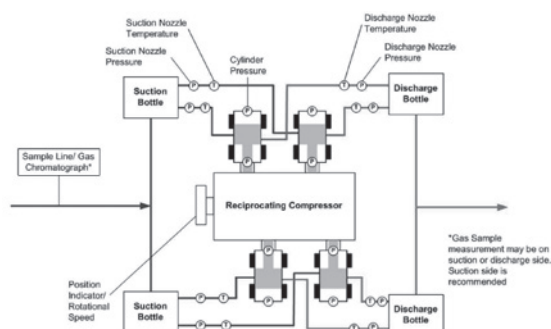


Figure 10. Typical line-up of measurement locations for performance testing [3].

To localize exactly the position where the barking noise is generated, the choice for the pressure sensor locations is critical. Since not only the effect of pulsations was evaluated during the tests, but also locations of flow losses had to be verified, special pressure sensors, recording both the static pressure and the dynamic pressure fluctuations, were used. Prior to the performance testing, the measurement method, sensor locations and proposed analysis were discussed and agreed upon with all parties. For all measurement equipment used for the performance testing, calibration certificates were shared in advance of the measurements.

Prior to the field survey and performance testing on location COV-17, a ‘dry-run’ was done on the same compressor K-170 system on location COV-24. It was concluded that the initial observation of low capacity of the compressor may be due to a leaking recycle valve. Therefore, the performance tests on COV-17 were performed with the recycle valve of K-170 removed.



Figure 11. Recycle valve removed for the testing.

The actual field survey on location COV-17 was witnessed by NAM and the compressor vendor.

Pulsations were recorded inside the working chambers of all 4 cylinders, both on Head End (HE) and Crank End (CE) side. In addition, pulsations were recorded on all cylinder connections. This enabled an assessment of the losses between the pulsation dampers and working chamber. Finally, pulsation measurements were taken on two points in the suction line, upstream of the dampers and on one location on the discharge damper drain. The pulsation measurements in the field piping were done with dynamic pressure sensors.

The measurement program for the performance testing focused on the compressor running at 100% load, without valve unloading. The program included a variation in suction pressure from 3.1 to 5.5 barg and in discharge pressure from 9.3 to 12.8 barg. For the barking noise testing, various load conditions from 100% down to 50% load were recorded. Since the barking phe-

nomenon was highly irregular, a continuous measurement approach was used, recording large traces of data.

With respect to the various recordings of the compressor power, it must be clearly understood that the methods represent different power definitions. For example, the measured electric power is the overall power: the accumulation of energy transferred to increasing the pressure and temperature of the gas, thermal loss, flow losses, mechanical losses in the drive train and electric losses in the E-motor. The electric power is measured using a Watt meter, using a direct measurement of the voltage and current. Also the phase relation between voltage and power is required, in addition to information from the E-motor vendor.

On the other hand the power derived from the PV charts (by integrating the enclosed area) includes only the thermodynamic power. The difference of the measured PV diagram with the theoretical (adiabatic) curve is an indication of losses generated by flow losses and unsteady effects occurring between the working chamber of the cylinder and the points where the line pressures have been recorded. To relate the thermodynamic power to the overall power, all other losses need to be estimated (mechanical losses in the cylinders and the drive train and the limited efficiency of the E-motor). For this specific compressor and motor, the mechanical losses were estimated at 120 kW and the E-motor efficiency was specified by the vendor at 95.7%.

The enthalpy rise method uses high-level performance parameters derived from field instruments and is relatively straightforward to use. However, no detailed information on the root cause of any losses can be obtained. Only in case of a substantial discrepancy between consumed power and predicted power based on enthalpy rise, a potential issue is identified and additional analysis is required. If the consumed power is much larger than the power estimated based on enthalpy rise, this may be an indication of excessive losses inside the cylinder. Also in case of this method, other losses (mechanical losses, E-motor efficiency) have to be estimated with sufficient accuracy. Moreover, the requirements on the reliability and accuracy of the field equipment are considerable.

Finally, the shaft power, determined from a strain gauge measurement on the rotating shaft includes the effects of mechanical losses of the drive train and the flow losses but excludes the efficiency of the E-motor. Normally it is expected that the shaft power will have an intermediate value between the electric power and the thermodynamic power.

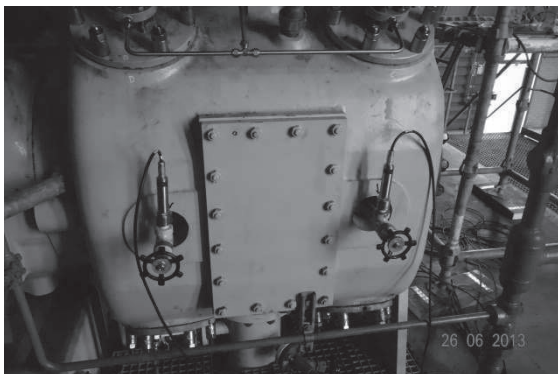


Figure 12. Pulsation measurements inside the cylinder (CE/HE).

To study the effect of the barking noise more conveniently, the lower frequencies (compressor pulsations) have been filtered out. The frequencies of the barking effect are collapsing with the acoustic resonances in the measurement branches for the pulsations. Therefore, a *quantitative*



assessment of the noise levels is difficult. In any case, no industrial guidelines are available, to assess the urgency of the barking noise

Prior to the field survey, all compressor valves on K-170 were replaced by new valves. During the testing, it appeared that the rate of barking was substantially lower than prior to valve replacements. This suggested a relation between the barking noise and the condition of the compressor valves.

The barking was most prominent at the cylinder connections, at the suction side of the cylinders.

In the suction piping upstream of the dampers, the noise was perceivable, but much weaker. From the amplitude and the time delay between the cylinders, it can be clearly identified from which cylinder the barking noise originates.

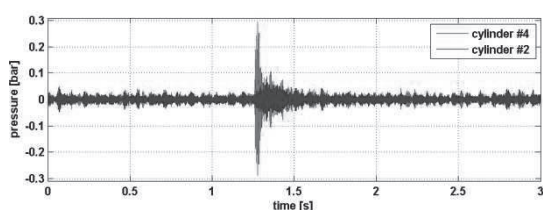


Figure 13. barking effect on cylinders 2 and 4.

From this picture, it is also concluded that the noise is generated in the cylinder connections (between the suction damper and the working chamber of the cylinder) and not in the suction damper volume, nor in the piping upstream of the pulsation dampers.

The barking appeared at all load conditions, but appeared most regularly during part-load conditions. This suggested that the barking originates from the channels leading to HE or CE side (*inside* the cylinder) and not in the 'common' channels where the flow is significantly lower during unloaded conditions.

Finally, the pulsation signals in the working chamber of the cylinders were analyzed.

The barking noise is present also inside the working chambers. In all barking cases, the noise is generated at the Crank End side.

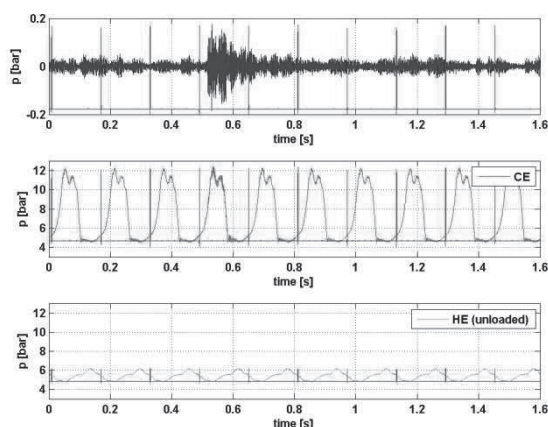


Figure 14. Barking noise, at  $t=0.5s$  on suction side, and in CE/HE working chambers.

A detailed analysis of the synchronization of the barking noise in the working chamber and the cylinder connection indicated that the barking is observed in the working chamber of the cylinder and on the suction side, *on time intervals when the suction valves are supposed to be fully closed*. The barking noise is hardly perceived at the discharge side. Based on this observation, it was concluded that the noise is associated with intermittent opening of the suction valve, during the exhaust phase in the PV diagram.

Upon barking, there appeared to be an temporary connection between the high-pressure working chamber and the suction side. The pressure ratio is considerable ( $>2$ ) and the jet is expected to be a strong noise source, containing high-frequency broadband noise.

A considerable amount of higher-order acoustic modes may be triggered inside the suction dampers. Due to efficient coupling with mechanical resonances (shell) modes, break-out noise radiation from the suction dampers is expected.

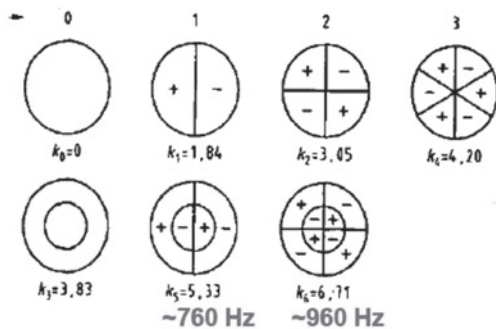


Figure 15. Acoustic modes, that may be excited in the suction damper.

With respect to the performance testing, the compressor flow was in accordance to the specification in the datasheets. The power consumption was higher than the values in the datasheets, but remained within the margin agreed between NAM and the Vendor.

The pressure signals inside the working chambers of the cylinders were compared with the pressure signals at the suction and discharge cylinder connections, and with the line pressures:

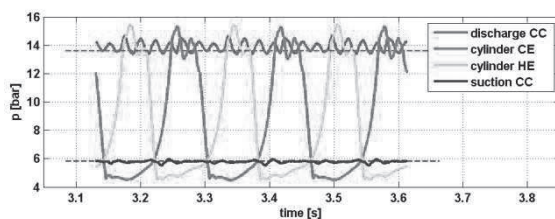


Figure 16. Pressure signals in working chamber (HE/CE), at suction and discharge cylinder connections, compared with suction and discharge line pressures (dashed lines).

The overshoot at the discharge side and the undershoot at the suction side are apparent, and in line with the preliminary conclusions made during the pulsation study. The pulsation levels at the discharge cylinder connection contain an acoustic resonance effect at a multiple order of the compressor speed. The pulsation levels are 9% peak-to-peak, which is relatively high, compared to the limits in API 618. The high pulsations are caused by the relatively long pipe length between the compressor valves and the discharge damper volume (the discharge damper contains a prolonged half-pipe toward the middle of the vessel).

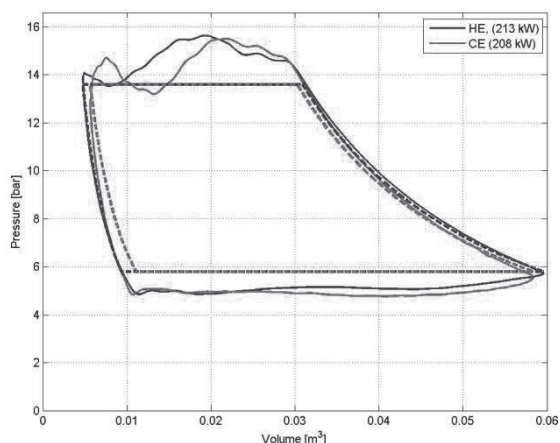


Figure 17. Theoretical and measured PV diagram.

## 8 Conclusions and proposed solutions

The performance tests indicated that the performance of the compressor was in line with the specification in the datasheets, within the agreed tolerance.

After the detailed analysis of the results of the field survey, it was concluded that the barking noise was associated with the observed issues (refer to chapter 5) in the suction valves. Therefore, the project team focussed on an improved design of the compressor valves.

The initially supplied ring type valves have not been developed to handle impact speeds as high as 13m/s, as observed during the RCA. It was therefore decided to change the valve design from ring type to profiled valve plate type.

Viewing seat and guard geometry and especially valve plate geometry as a whole, this design minimizes sticktion and improves on the impact situation of the profiled plate and guard (Figure 18).

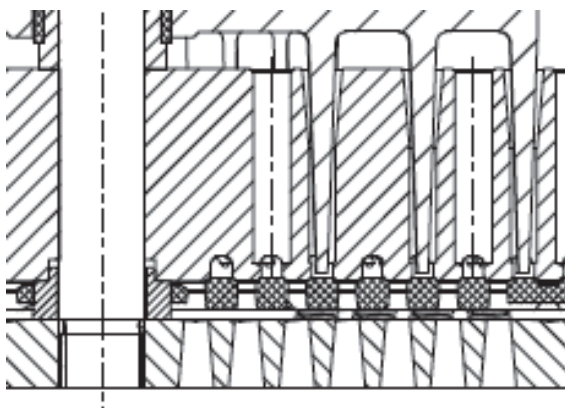


Figure 18. Cross section of seat, valve plate and guard of a profiled plate valve.

Although this suggests a straightforward modification of the valve's aerodynamics, improved construction material of the valve plate has a positive effect on valve life as well.

The profiled plate design with its contoured single sealing element (Figure 19) behaves differently than the original ring valves. Less load generation on specific valve internal components, such as valve springs, make it more resilient to impact forces and material fatigue. Furthermore this design enables reduction of valve losses, even at a lower valve lift than the original valve.





Figure 19. Profiled valve plate.

With the applied modification the compressor has been operated now for more than 13500 hours without any valve failures reported so far.

## 9 Lessons learned and recommendations for future projects

- The observed barking noise appeared to be related to intermittent erroneous operation of the suction compressor valves.
- Identifying and locating the area where the noise was generated required a substantial effort, with detailed measurements in the field.
- The issue was satisfactorily resolved with an upgrade of the compressor valves to profiled valve plate type.
- To evaluate the capacity of a reciprocating compressor in detail, is not a straightforward exercise. Various methods are available to assess the capacity in the field.
- In case of the enthalpy-rise method, using the readings of non-custody measurement equipment (flow meters and pressure transmitters) is liable to significant uncertainty and erroneous conclusions.
- Performance testing requires a careful agreement on the approach, by all parties. If independent measurement techniques are used, measuring related (but not identical) quantities, such as electric power, shaft power and thermodynamic power may display significant differences. An independent party may be preferred to supervise the testing activities, and to judge and interpret the independent measurements.
- The flow losses in the cylinders in this specific project were considerable. In theory, an alternative design may have significantly reduced the power consumption and may have increased the capacity. However, due to the specific spatial and operational requirements in this case, an easy re-fit was not feasible for this project.
- It is recommended to perform an independent verification of the flow losses inside the cylinders and the associated power consumption, during the early design phase.
- For such an evaluation during the design phase, it is essential that the geometrical representation of the cylinder internal channels is adequately described by the compressor vendor.

## 10 References

- [1] API 618 5<sup>th</sup> edition, "Reciprocating Compressors for Petroleum, Chemical, and Gas Industry Services", December 2007.
- [2] ANSI/ASME PTC 9 - Performance Test Code, Displacement Compressors, Vacuum Pumps and Blowers, 1970.
- [3] GMRC guideline for field testing of reciprocating compressor performance, 1<sup>st</sup> edition, November 2009.
- [4] Compressor Handbook, Paul. C. Hanlon, editor.



# Technical Paper

**Session: 37-2**

**Session Name: Root cause analysis**

## **Root cause analysis and solution of recurring fatigue failures in the cooler pipe bends of a high pressure LDPE compressor**

**Author:**

**Cosimo Carcasci**  
Compression Service Technology  
Maintenance Engineering Manager  
50127 Florence, Italy

**Co-Author 1:**

Marco Sacco  
Compression Service Technology  
Package Engineering Manager  
50127 Florence, Italy

**Co-Author 2:**

Fabio La Monica  
Versalis (Eni)  
Maintenance Manager  
97100 Ragusa, Italy

**Co-Author 3:**

Emanuele Cintolo  
Versalis (Eni)  
Maintenance Engineer  
97100 Ragusa, Italy

## **ABSTRACT**

Machinery vibration is one of the main causes of damage and failures in industrial plants, and reciprocating compressors are particularly subject to vibration-related phenomena as alternating forces and pressure pulsations are inherent in their design.

Vibration problems may also arise after a machine is installed and is set in operation due to inadequate attention to interaction between the compressor and plant as a whole during the design stage.

This paper will examine a case that occurred in a polyethylene plant located in Ragusa, Italy, where high vibration issues resulted in broken pipes and welding failures. In particular, the area that was most affected by vibration was the inter-stage cooler and the piping in the immediate vicinity.

New, more effective supports were studied and the exact positioning of the supports was based on the results of a dynamic forced-response FEM analysis; the vibration measurements were also used to tune the FEM model, and subsequently to identify, through the model, the key points where a stiffer structure was required. As a result, many of the existing supports were reinforced and additional supports were positioned where they would be more effective according to the FEM analysis. High damping rubber pads were also added between the supports and the piping in order to further lessen the impact of the vibration. Finally, also the cooler structure and foundations were reinforced.



## 1 INTRODUCTION

The production of Low Density Polyethylene requires compressors capable of bringing the gas, ethylene or an ethylene-based mixture, to the polymerization pressure, ranging from 160 to 350 MPa depending on the type of process utilized [1]. Due to the very high pressure, safety and plant operation are key factors. [2]

The compression of the gas is normally made in two steps:

- the first step, up to about 30 MPa, is normally performed with a heavy-duty balanced-opposed reciprocating compressor, called Primary Compressor;
- the second step, to reach polymerization pressure, is fulfilled with very special compressors, still reciprocating type but with many high-technology features to withstand the extreme working conditions, widely called Hyper Compressors or Secondary Compressors

The reactors where the polymerization occurs are normally of the tubular type for the highest pressure processes and of the autoclave vessel type for the lower pressure ones.

Due to the fact that the piping, valves and other devices of LDPE plants have to operate under very high and variable pressures an accurate acoustic calculation of the pressure pulsations is necessary to avoid problems in operation also in consideration that, volume bottles cannot be used in this environment. The basic law governing pressure pulsation is the following:

$$\Delta P/P = \Delta Q K/S c$$

where  $\Delta P$  is the pressure pulsation,  $P$  is the average pressure,  $\Delta Q$  is the flow pulsation,  $K$  is the ratio of the specific heats,  $S$  is the pipe section and  $c$  is the speed of sound.

In the case of Hyper compressors there are very special conditions of the parameters influencing pressure pulsations: the speed of sound is very high (f. i. in second stage discharge it is about five times that of air at atmospheric pressure) but also the  $K$  is very high so that pressure pulsations are largely dependent on the pipe diameters. However a deep knowledge of the thermodynamics of the gas is essential.

As it is known, pipes can originate acoustic resonance in the following conditions:

- Quarter-Wave ( $\lambda/4$ ) when the acoustic circuit is closed at one end and open at the other, with resonant frequency  $F_R = [2N-1] c / 4 L$
- Half-Wave ( $\lambda/2$ ) in two configurations when the acoustic circuit is closed or open at both ends, with resonant frequency  $F_R = N c / 2 L$

Where:  $\lambda$  = Wave length,  $N$  = Harmonic number,  $L$  = Resonant pipe length,  $c$  = speed of sound

In both cases, high harmonic numbers are expected because of the high speed of sound of ethylene at high pressures.

Pressure and flow pulsation must be kept at low level as they are linked with acoustic energy which interacts with the mechanical system of the plant generating mechanical vibrations which require special attention.[3]

The dynamic forces that are the source of the vibration phenomena are due to:

- unbalanced inertia forces and moments of the compressor;
- forces induced on the gas pipes by displacement of the cylinders;
- pressure pulsations;

High vibrations generated by acoustic resonance conditions which, as stated above, can be of rather high frequency. Moreover, if this frequency is close to the mechanical natural frequency of the piping, vibrations can result extremely high and cause fatigue failure phenomena.

In order not to fall into this kind of problems an accurate acoustic analysis followed by a mechanical analysis is necessary taking care of a correct simulation of both the thermodynamic of the gas and the piping arrangement with the relevant supporting system.

The paper will discuss a problem that occurred at a polyethylene plant, where there were high vibration issues which resulted in piping failure recurring almost every 3-4 months over some years. High vibration velocity occurred on the interstage lines and on the intercooler structure (as shown on Tables 1 and 2).

During the survey on site, the piping system was analysed, data collected and the history of failures reconstructed to overcome the encountered problems.

## **2 ISSUES EXPERIENCED ON A HYPERCOMPRESSOR**

The compressor was an old machine, installed in the seventies. About ten years ago it was re-ramped, and the frame and the driver were replaced, increasing the average piston speed. After these modifications, the customer started to experience frequent piping issues, generally in the form of cracks on the flanges or pipe segments in the intercooler area.

Despite the installation of restriction orifices following an acoustical study in the new conditions, the problems persisted. At that time, it was also suggested that some supports be modified but this was only partially implemented. The compressor is equipped with four 1st stage and four 2nd stage cylinders, and the intercooler has four sections.

The historical failures of the last 8 years were studied and it was found that not all the sections experienced the same behaviour: the area where the failures were most frequent was line B, especially on the pipes at the cooler exit. Subsequently, also lines A and D experienced a comparable number of failures while line C was the most reliable.

A detailed vibration measurement campaign had revealed 17 points with high vibrations on the interstage piping, with displacement values exceeding both the EFRC vibration amplitude limits and the South West Research Institute danger curve (in the frequency spectrum), above which corrections are urgently needed as failures are likely to happen even in a short time. Figure 1 and

*Table 1* shows some of these points with high vibrations.



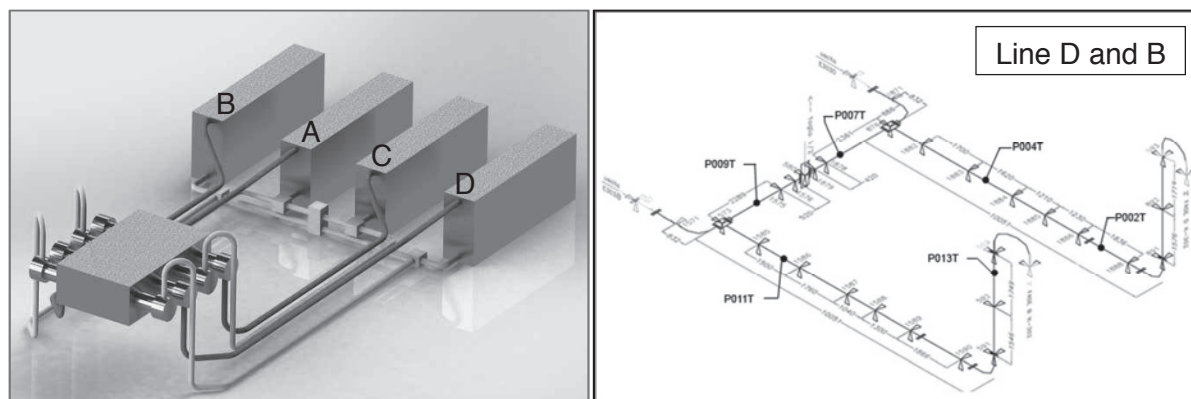


Figure 1: Interstage piping layout and Points with high vibrations on 2nd stage suction lines D and B

	Direction	Overall displacement	overall velocity	Frequency of the max Peak
		[ $\mu\text{m RMS}$ ]	[mm/s RMS]	[Hz]
P002T	X	165	41	37.3
P004T	X	76	38	78.8
P007T	Y	177	55	49.8
P009T	Y	350	95	41.5
P011T	Z	116	56	62.3
P013T	Y	116	56	70.5

Table 1: Points with high vibrations on 2nd stage suction pipelines D and B

In addition, also the cooler was analysed and the vibration amplitudes were found to be in some cases even 10 times over the danger limit. To give an idea of the magnitude of those vibrations, some of the horizontal pipes of the cooler vibrated at more than 300 mm/s rms while the EFRC unacceptable limit (keyzone C/D) is 28.5 mm/s!

Despite the technical measures that were undertaken over the last few years to avoid high levels of vibration (i.e. acoustical and mechanical analysis, restriction orifices and new piping supports) vibration continued to be a problem. In this case, the vibrations were not the result of a poor detailed design of the compressor piping system but were due to the fact that acoustical interaction between the compressor and the plant had not been taken into account with all due attention.

In particular, some of the circumstances that led to this situation were:

- the modifications to the piping supports suggested by the compressor manufacturer were assigned by the end user to another contractor and resulted in a poor and weak design (see Figure 2);
- the coolers structure was not originally supplied by the compressor manufacturer, who therefore did not have the fabrication drawings and related engineering details. When the new acoustical and mechanical analyses were performed, only the acoustical aspect was considered while the cooler was assumed to be a rigid body; however, it was in very bad condition due to rust, repeated repairs and invasive maintenance activity (for example, some beams had been cut several times and re-welded to change the pipes). See Figure 3;
- the vibrations on the cooler foundations were also high above cooler B, and a borescope inspection revealed underground voids due probably to subterranean water erosion

(cooling pipe joints were continuously leaking a large amount of water). As a result, the foundations, where the shaking forces are transferred in order to limit the vibrations, were not acting properly.

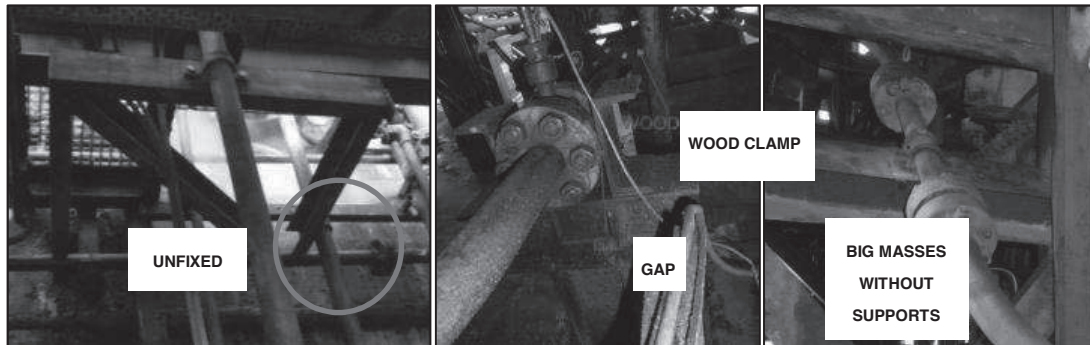


Figure 2: Examples of the ineffective supports

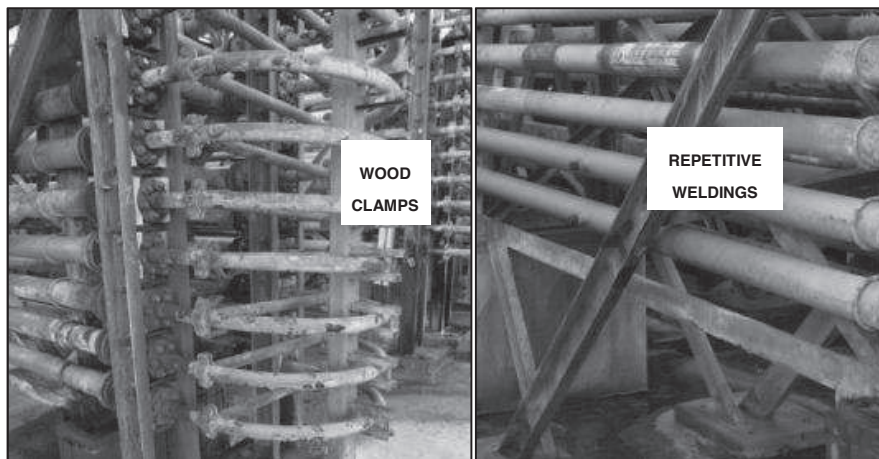


Figure 3: Cooler structure

The two main areas with high vibrations were identified and a different approach was used for each one, due to the dissimilar nature of the vibration.

In the interstage piping area, between the compressor and the cooler, like the area shown in Figure 2, most of the highest vibration harmonics (peaks) were between 60 and 70 Hz, therefore at a very high frequency, considering that the first exciting harmonic was at just 4.1 Hz. The pulsation amplitudes at this high frequency were very low, especially after introduction of the restriction orifices, therefore a simplified analysis of the piping segment mechanical frequency was performed, according to API 618.

The result was that most of the pipe segments with a length between 1.5 and 1.7m had a mechanical natural frequency in the range of 60-70Hz. In particular, this was due to the fact that these supports should have acted as fixed constrains, whereas in the actual situation, they were simply mono-directional supports.

In the intercoolers section, instead the main criticalities were that:

- the bends shown in Figure 3 had a small bend angle, thus the exiting supporting beams were not suitable to sustain the resulting shaking forces;



- the inlet and outlet connections were considered in the mechanical analysis as fixed supports but were instead just fixed with wooden clamps (see Figure 2), so they had a very low stiffness;
- the side pipes were more than 7 m long and were just clamped in the middle with simple U bolts;
- on cooler B also the baseplate vibrations were above the limit, due to voids in the foundation.

### 3 PROBLEM SOLVING: MODIFICATIONS INTRODUCED

In consideration of the short time available for the intervention (10-day outage), a simplified support design (Figure 4), was studied to minimize the time required for order processing and delivery of materials:

- a uniform clamp design was developed, using a variable support plate to adapt it to each pipe height
- a layer of fabric reinforced, elastomeric pad, 4mm thick, was placed between the clamp and the gas pipe (rolled all-round the pipe) .
- the clamp was made from a bent plate and the anchoring was made using U-bolts welded around the outer diameter.

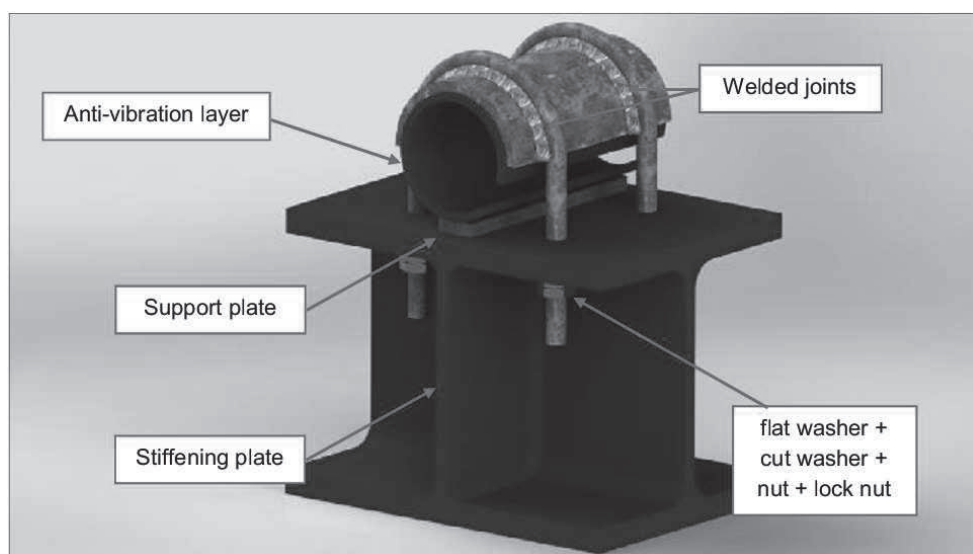


Figure 4: Typical support design

This type of clamp was adopted to substitute all the weak supports of the interstage piping, together with a reinforcement of the beams with the addition of stiffening plates.

A total of 83 weak supports were selected for substitution and for each one a criticality value was given to indicate the priority to be given to the substitution, considering that only a certain number of supports could be replaced within the scheduled outage.

In order to identify the most efficient and effective upgrades to significantly reduce the vibrations on the cooler structure, it was decided to perform a dynamic FEM (Vibration Analysis). Not having the construction drawings, the cooler structure (both front, bay and cylinder rear side) was

modelled based on dimensional measurements carried out in the field. Once modelled, the analysis of linear dynamic vibration was set, paying particular attention to extrapolation of the forcing factors to be imposed on the existing structure.

Using the results obtained from the acoustic calculation, the pressure pulsation values related to each loop were extracted. After that, the shaking forces were calculated using the API RP 688 [4] formula:

$$F_{Result} = 2P_{dyn} \frac{\pi}{4} D^2 \cos \frac{(\varphi)}{2}$$

Where:

- F** is the shaking force
- P<sub>dyn</sub>** is the dynamic pressure
- D** is the internal diameter
- F<sub>Result</sub>** is the resultant shaking force
- φ** is the elbow angle

The shaking force values indicated in Figure 5 were calculated for each harmonic (Shaking Force harmonic cut-off frequency ~139.7 Hz). Subsequently, these values (Harmonic Loading) of Shaking Force amplitude [N] were imposed in the FEM model using the principle of superposition.

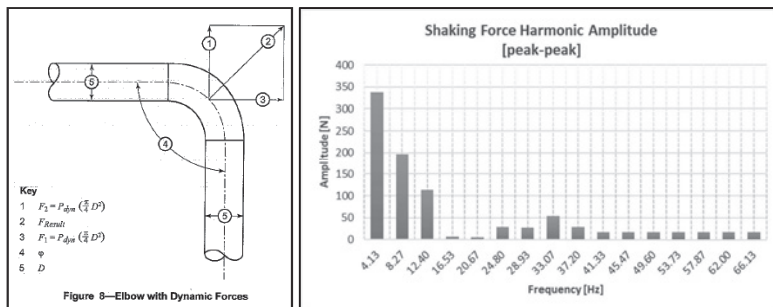


Figure 5: Shaking force harmonic amplitude

The modal superposition method represents the vibration response of a structure by using the superposition of responses that characterize Single Degree of Freedom systems (SDOF). The natural frequencies and directions of vibration of these systems correspond to the natural frequencies of the analysed structure. The number of SDOFs contributing to a dynamic response is equal to the number of modes calculated by a pre-requisite modal analysis or frequency analysis.

A harmonic analysis assumes that the load is a function of frequencies rather than being directly dependent on time as is in the case of a time response analysis [5].

$$[M]\ddot{d} + [C]\dot{d} + [K]d = F(A \sin \omega t + B \cos \omega t)$$

Where:

- [M]** Mass matrix
- [C]** Damping matrix
- [K]** Stiffness matrix
- F(t)** Vector of nodal loads (this vector is a function of frequency)
- d,  $\dot{d}$ ,  $\ddot{d}$**  Unknown vector of nodal displacements, speed, acceleration





In this case the analysis shall be performed in the range between 0 to 70 Hz, because the higher frequencies will have a negligible value of shaking force amplitude.

After defining the frequency range on which the vibration dynamic response shall be analysed, a modal Global Damping of 3% was defined. Assigning the same damping ratio to all modes represents a simplified and conservative approach. In most cases damping for higher modes will be higher than that for lower modes.

The results of the vibration analysis confirmed that the model has values very close to those obtained by the measurements in the field: 220 mm/sec rms measured on the front surface of the cooler vs a calculated value of 218 mm/sec rms as a mean of various points.

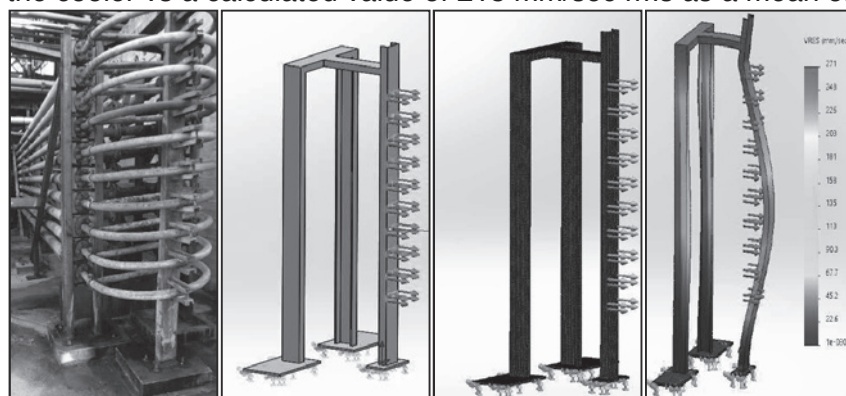


Figure 6: Cooler model

After creating a reliable model (Figure 6), four different options were studied, proceeding to check the vibrational response of each of them applying the same excitations (Figure 7):

- solution n°1: lateral “L” profile supports and boxing reinforcement of the vertical support.
- solution n°2: bottom lateral support in lower position.
- solution n°3: bottom lateral support in higher position.
- solution n°4: reinforcing gusset added on the top of vertical support.

On the basis of the structural response obtained through dynamic analysis, (carried out at the front of the cooler subjected to variable loads in the frequency domain), it was decided to select and engineer solution n°4 as it offered the best compromise between the vibration reduction and the activities required in the field:

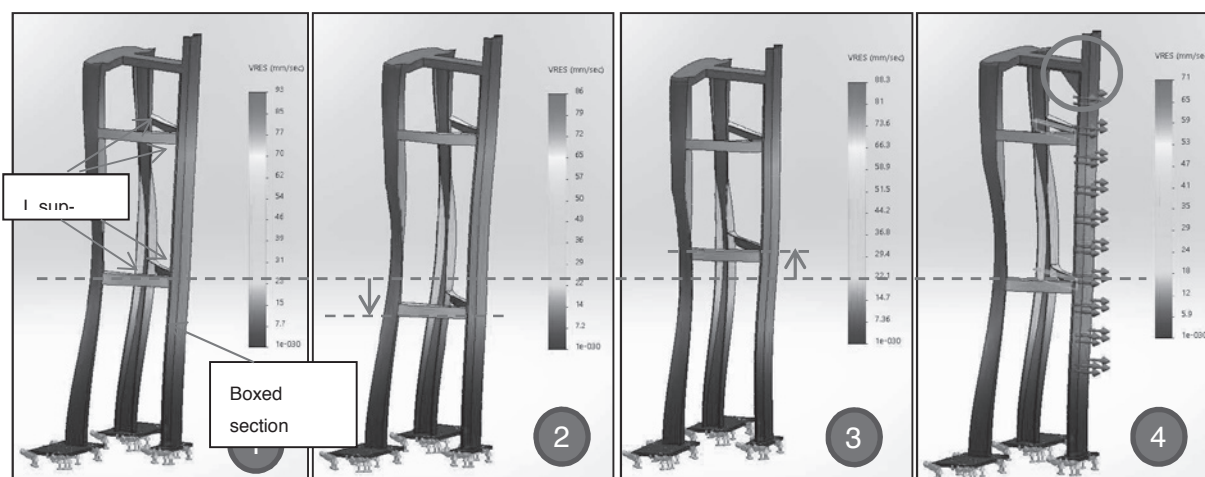


Figure 7: Dynamic analysis structural response



During a planned shutdown, it was decided to implement the changes both on the line clamps (about 60 of them) and on the two most critical coolers. In Figure 8 there are two examples of clamps installed in the field.

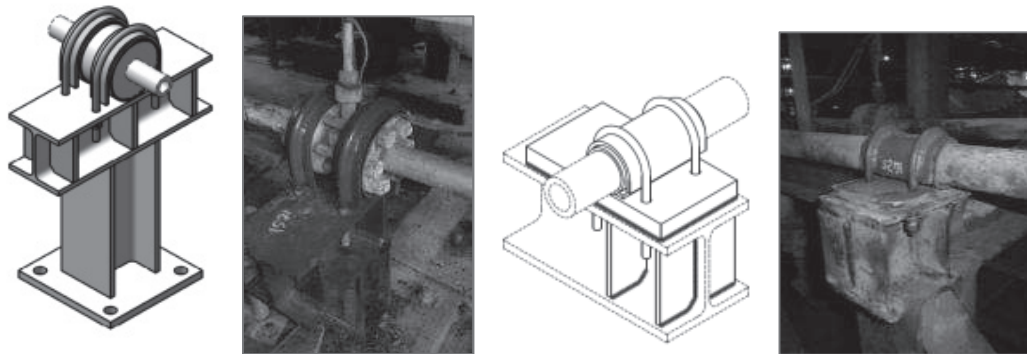


Figure 8: New clamp design

The structural stiffening of the cooler realized and installed during the plant shutdown is shown, highlighted in green, in Figure 9.

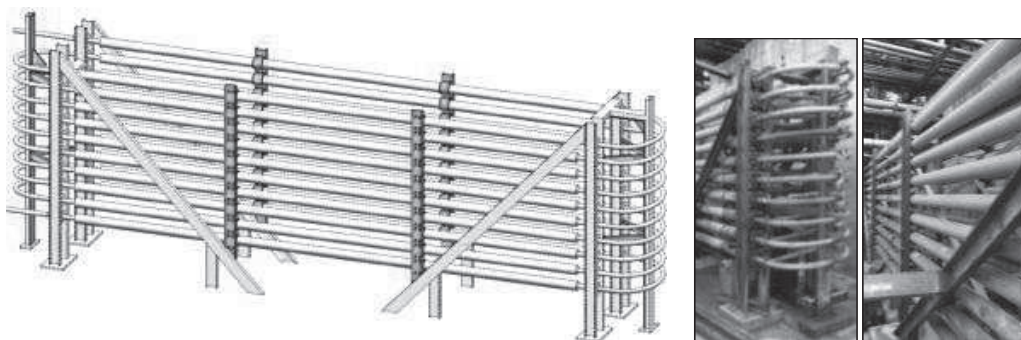


Figure 9: New cooler stiffening structure

The tightening torque for the bolts of the new clamps and support were chosen as the best compromise between the damping efficiency of the fabric pad and the support stiffness, using proprietary software developed specifically for this purpose. In fact, the manufacturer of the material recommends a specific maximum pressure to be applied in order not to excessively reduce the thickness of the material, with a consequent reduction in its damping effect. The optimum torque to be applied to the bolts was obtained from this value.

INPUT		OUTPUT	
Ø external piping	54 mm	material deformation	1.25E-06 m
Ø internal piping	31 mm	material stiffness	2.64E+10 N/m
piping lenght	800 mm	floor residual deformation	2.88E-09 m
piping falling speed	78 mm/s	KE Kinetic energy piping	0.0293 J
piping weighth	9.64 Kg	F1 Force floor without damp.	46819 N
Floor thickness	10 mm	F2 residual force floor	108 N
l floor	120 mm	Es Absorbed energy floor	1.55E-07 J
material density	7850 kg/m <sup>3</sup>	EF Absorbed energy Fabreeka	2.93E-02 J
material Young module	220000 MPa	Af Area Fabreeka	6.33E-06 m <sup>2</sup>
Allowable Sigma (Fabreeka)	17 MPa	Tf thickness Fabreeka	4.06 mm
Damping (Fabreeka)	99.77%	Df deformation Fabreeka	0.66 mm
		σ only preload on Fabreeka	16.925 MPa
		σ preload+F2 on Fabreeka	17.0 MPa
Pre load (sigma vibr)	24.160 kN		
Error (sigma vibr)	0.0		

KE=Es+EF

0.001% of KE

100.00% of KE

Figure 10: Screenshot of the software used to evaluate the appropriate tightening torque



#### 4 VIBRATION MEASUREMENTS AFTER MODIFICATION

A few months after the modifications, a diagnostic survey was performed at the plant to evaluate the effectiveness of the new supports by making new measurements and comparing them to the old ones taken before the modifications.

Displacement and velocity were measured and a real-time frequency analysis was conducted.

The survey covered all the 4 interstage lines, each with the related cooler. The measurement points were the same as those of the preliminary survey before the optimization.

The frequency peak of each measured point was compared with "Piping Allowable Vibration Limit Correction Curve" and "Piping Allowable Vibration Limit – Danger Curves" of the SwRI [6] [7]. These curves define the acceptable limits of the vibrations on the pipes associating a maximum displacement value with each frequency.

Regarding the interstage pipeline, Figure 11 shows an example of comparison between frequencies recorded on one point, before and after the optimization. The peak frequency is the most relevant to be considered in the current analysis, because it is the one that, without intervention, will cause pipe failure in the long term.

All the measured points were no longer above the “danger curve”, but close to or below the “correction curve” so that one can say that the piping vibration issue may be considered solved.

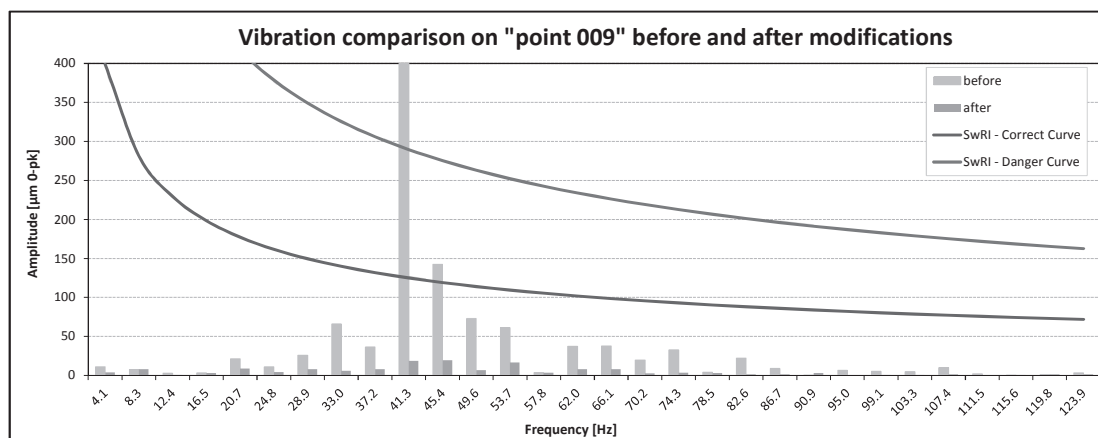


Figure 11 Amplitudes of the harmonics at the most relevant point, before and after modifications

Regarding the coolers, the ones considered most critical due to high vibrations and history failures are those related to lines A and B: on both, the measurements show a clear improvement with respect to the previous situation. Table 2 shows the vibrations in terms of velocity (mm/s rms) "before" and "after" the intervention. The main vibration frequencies of all coolers are the same as the compressor speed (4.3 Hz).

Cooler (mm/s rms)	E303B	X		Y		Z	
		before	after	before	after	before	after
inlet pipe		26	27	14	17	25	33
mid curves		255	29	200	36	15	27
outlet pipe		40	18	24	8	26	24
lower lateral pipe		170	30	-	9	150	16
upper lateral pipe		16	28	-	-	22	10

Table 2: Cooler B vibration (mm/s rms): comparison before and after the optimization

It was noticed that on two parallel sections of the suction line (line A and B) there was a significant difference in vibrations on certain sections of the piping. These lines are symmetrical to the compressor and cooler and have identical supports. The difference in vibration was explained by a different tightening torque being applied to the new clamps during the mounting stage: a test was carried out, observing the shift in the spectrum frequency in real time as tightening of the bolts was decreasing. The effect was the lowering of peak frequencies, moving within the acceptance area of SwRI curve.

### ***Piping supports***

The supports optimization produced a general improvement in the vibrations throughout the whole interstage system.

According to the frequency analysis, all points with vibration above the "danger curve" of SwRI dropped below it; moreover, the peaks of vibration and the relative frequency peak of each point, are now all below, or in a few cases near the "correction curve" of SwRI. At the moment, no point is believed to be in the danger zone. Regarding the few points that are still next to the "correction curve", all of them had an increment of the vibration frequency, which is more likely due to an over-tightening, which has altered the damping power of the rubber installed between the pipe and support.

### ***Coolers***

Observing the vibrations measured as velocity rms, a strong improvement was noted for all the coolers, including the items C and D where no structures had been stiffened.

This is probably due to the combination of the following actions:

- Reduction of vibrations in the interstage piping, which now transmits less excitation to the cooler.
- Intervention on the cooler B foundation and skid
- Replacement of the wooden blocks of the cooling jackets on the cooler C and D themselves.

Observing the peak displacement, coolers B and C have still some isolated vibrations peaks on the lower side pipes, still below the "danger curve".

Further improvement may be obtained adjusting tightening of the clamps, measuring in real time the effect on vibration, to optimize the clamping to the value that generates a lower vibration. However, in order to be sure of bringing all points below the "Correction curve" it is necessary to completely revise the cooler structure.

It was also recommended that a new measurement campaign be carried out after the winter period to assess whether the vibrations on cooler C and D returned to high values: in which case, the cause should be sought in the loss of damping power of the new wooden dowels.

After 5-6 months of operation a couple of other failures occurred on cooler B, which was the most critical. These failures occurred at points where vibrations and supports were not considered critical at the time of the first survey. Analysis and recommendations are still in progress but the conclusion has been that the cooler structure and its foundations were not responding "ideally" as per the FEM analysis due to the state of preservation of the foundations, the presence of holes in the cooler structure caused by rust and the repeated welding and fixing on the old clamps and beams. An injection of concrete in the foundations and a general replacement of the ruined cooler parts has been scheduled for the next shutdown to better replicate the structure that has been simulated in the FEM analysis.



## 5 CONCLUSIONS

This case history is a typical one. An old compressor that was revamped with most of the auxiliary equipment remaining the same as at the beginning of its operation. During its life the various parts of the machine and the associated system have gone progressively deteriorating even if in a not evident and dramatic manner. Nevertheless that machine is a part of a plant that can continue to be productive, provided that it is submitted to an expert maintenance to take care of the modified operation, of the deterioration occurred and of the steps made by the technology in the meantime.

In the case of the high pressure LDPE plant reported in this article all of this was present with the addition of the non-availability of original drawings of the cooler. Nevertheless an accurate survey of the real actual situation, an assessment of the performance for the identification of the critical points and the application of new more powerful investigation technologies allowed to strongly improve a vibratory situation that exceeded by far the values considered acceptable. All of that was done also considering the constraint due to the production schedule of the plant which is not a research center but an economic activity and has to fulfil its engagements.

## ACKNOWLEDGMENTS

The authors want to thank the company Versalis (Eni) to have allowed the publication of one experience developed in one of their High Pressure LDPE plants.

## REFERENCES

- [1] B. Crossland, K.E. Bett, Sir H. Ford, "Review of Some of the Major Engineering Developments in the High Pressure Polyethylene Process", 1933-1933, Institute of Mechanical Engineering, 1986, Vol. 200, Ne A4.
- [2] M. Agostini, C. Carcasci, A. Cristofani, "Managing start-up conditions of hyper compressors" 9th Conference of the EFRC, 2014 Vienna.
- [3] E. Giacomelli, M. Agostini "Safety, operation and maintenance of LDPE secondary compressors" PVP-Vol.238 Codes and Standards Applications for High Pressure Equipment ASME 1992.
- [4] API RP 688, Pulsation and Vibration Control in Positive Displacement Machinery Systems for Petroleum, Petrochemical, and Natural Gas Industry Services - Ed. 1 (2012) – par. 3.2.7.2.1.
- [5] E. Funaioli, A. Maggiore, U. Meneghetti, "Meccanica applicata alle macchine", vol.2, chapter 6 – Vibrazioni di sistemi a due e a molti gradi di libertà, Patron Editore, Bologna 1988.
- [6] J. C. Wachel, "Piping Vibration and Stress" Vibration Institute, Machinery Vibration Monitoring and Analysis Seminar, New Orleans, April 1981, pp. 1-20.
- [7] EP1764602 B1, developed by Walter Von Nimitz, J C Wachel, C L Bates and South West Research Institute (SWRI).







# **Technical Paper**

**Session: 38-1**

**Session Name: Sealing / Wear**

## **Low-friction buffer seals for reciprocating compressor rod packing**

**Author:**

**Craig Martin**  
**Applications Engineering Manager**  
**Cook Compression**  
**47130 Jeffersonville, USA**

## 1. Introduction

Piston rod packing in reciprocating compressors often utilizes side-loaded seal rings in vent seals and buffer seals. Traditionally these seals have a side-loading mechanism that uses angled wedge rings and/or overhung springs to push two ring components apart and load them against the side faces of the packing cups. This design tends to generate excessive frictional heat which ultimately can lead to early packing failure. Historically this has been a major limiting factor in the service life of packing using buffer systems.

There are alternative side-loading technologies existing, but most of these have small loose parts and can be difficult to maintain and install, which makes them unpopular to users. New technology has been developed that achieves a Low-Friction side-loaded seal without contributing added frictional heat to the piston rod. These seals have been shown to run at lower piston rod temperatures when compared to traditional side-loaded seals, which can lead to extended service life.

## 2. Side-Loaded Packing Rings

Piston rod packing in reciprocating compressors often utilizes side-loaded packing rings in vent seals and buffer seals. A “Side-Loaded Ring” is any packing ring that is designed to expand in the axial direction of the piston rod when installed, such that they seal against one or both faces of the adjacent packing cups. Typically the side-loading mechanism does not require gas pressure to activate. This allows side-loaded rings to seal effectively at packing vents or in buffer seals where there is insufficient pressure to activate a typical packing ring.

Most traditional side-loading is achieved by the use of angled wedge rings and/or overhung springs. Either type typically uses spring pressure to push two rings apart or to push a ring away from a cup face. Figures 1 and 2 below show the most common types of side-loaded rings used in rod packing.

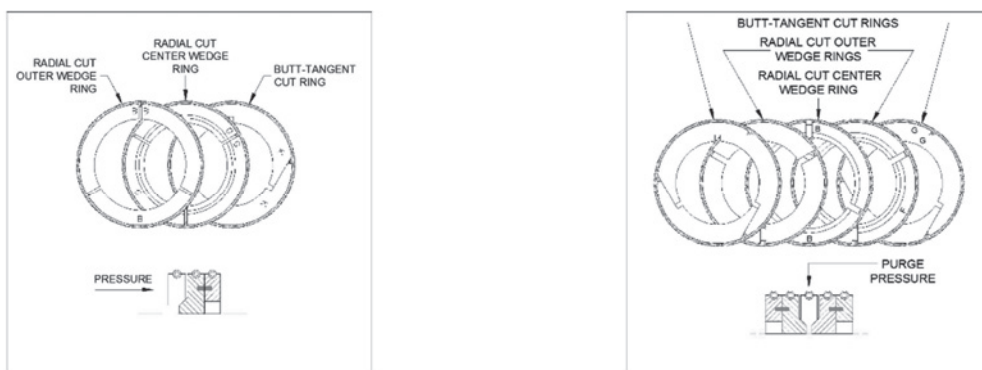


Figure 1—Single-Acting Side-Loaded Ring “WAT” Figure 2—Double-Acting Side-Loaded Ring “AL”

The WAT is a single-acting ring commonly used as a vent ring. This is typically used as an upgrade to the standard double-tangent ring. Since there is little to no pressure between the packing case vent and the distance piece, there is not enough pressure to keep a double-tangent ring sealed against the cup face. Thus the ring moves back and forth in the cup with the motion of the rod, allowing some leakage. The WAT ring, however, stays loaded against the cup face regardless of pressure and thus gives a tighter seal.

The AL is double-acting and is typically used for buffer seals. This ring seals against both sides of the packing cup and contains a purge or buffer gas within that cup, creating a barrier against process gas leakage. Buffer seals may be included as part of the main pressure packing but



can also be used as intermediate seals in double distance pieces and can even be added to oil wiper packing assemblies.

Both of these ring assemblies feature a wedge ring with a 45° angle that uses the downward load from the garter spring to push against the adjacent ring(s). The primary drawback to this design is that the springing that achieves the side load also imparts an added radial load. This load can be significant, depending on the geometry of the ring.

For example, consider an AL ring for a 1.125" piston rod. The garter spring used here has a spring rate of 4 lb-f/in [0.7 N/mm] and an initial tension of 0.5 lb-f [2.2 N]. The contact area between the ring and the rod is 0.64 in<sup>2</sup>. The center diameter of the spring when installed on the ring is 1.717" [43.7 mm].

$$\begin{aligned} \text{Deflected Length} &= 1.717" \times \pi = 5.39" \\ \text{Initial Length} &= \text{Deflected Length} - 2 \times \frac{\text{Radial Load}}{\text{Spring Rate}} = 5.39 - 2 \times \frac{1.5}{4} = 4.64" \end{aligned}$$

The spring length is rounded down to 4.50" for manufacturing, giving a final installed deflection of 0.89" [22.6 mm]. The calculation for contact pressure is then as follows.

$$\text{Contact Pressure} = \frac{\left( \frac{2 \times \text{Rate} \times \text{Deflection}}{\text{Spring Length}} + \text{Initial Tension} \right)}{\text{Rod Diameter} \times \text{Contact Width}} = \frac{\left( \frac{2 \times 4 \times 0.89}{4.50} + 0.5 \right)}{1.125 \times 0.182} = 10.16 \text{ psi}$$

Meanwhile, the assumed radial spring load was 1.5 lb-f [6.7 N]. When translated to an axial force along a 45° wedge, this results in

$$1.5 \times \cos 45^\circ = 1.06$$

So, in order to achieve just 1.06 lb-f [4.7 N] of axial force, a contact pressure of 10.16 psi [70 kPa] is applied to the ring.

For many years, users have complained of heat generated by these rings, particularly AL rings. Occasional packing failures result from overheated AL rings, especially in high-speed and/or non-lube service. This is especially true for intermediate packings where there is no gas movement or any active cooling mechanism to help remove heat.

One recent incident in the field demonstrated the potential for heat-related failures with AL rings. A packing set installed on a 1.125" piston rod, running at 1200 RPM, failed on two separate occasions within hours of startup. Extrusion of the PTFE (Polytetrafluoroethylene) material was so severe that all five rings of the AL set fused together into a single unit. The other rings in the set failed in a similar fashion. See figures 3 and 4 below for the failed AL ring. As shown in the above calculations, the contact pressure on the AL rings due to spring load was approximately 10 psi [70 kPa]. Simply increasing the spring lengths by 0.25" [6.35] mm reduced the contact pressure of that ring down to 7.7 psi [53 kPa], a reduction of 24%, after which multiple sets of the packing ran successfully and the problem has not repeated.

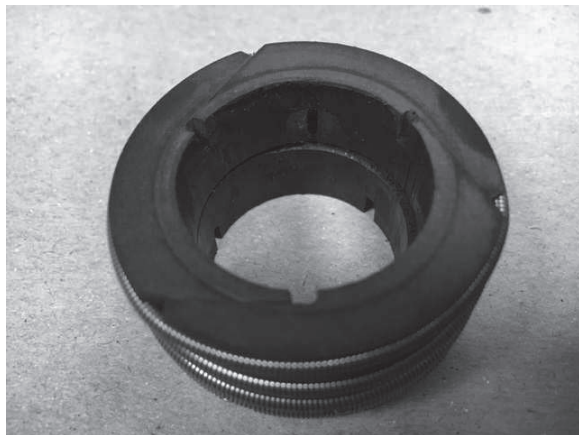


Figure 4 – Overheated AL Ring



Figure 5 – Overheated AL Ring

The tendency for these rings to run hot is obviously a liability for operation since a heavy spring can lead to failure. This forces the designer to keep the spring loads relatively low. Unfortunately, since the garter spring load also drives the axial loading, this limits the available axial load we can apply. Ultimately this limits the overall sealing effectiveness of the AL ring.

### 3. Available Alternatives to Traditional Side-Loaded Rings

There are, in the industry, some alternative rod ring types that achieve side-loading without an added garter spring. The most common of these, the XRBD, uses a standard double-tangent ring but adds a third backup ring with a series of compression springs to achieve the required axial load. This successfully loads the ring in the groove without adding unneeded and problematic frictional heat.

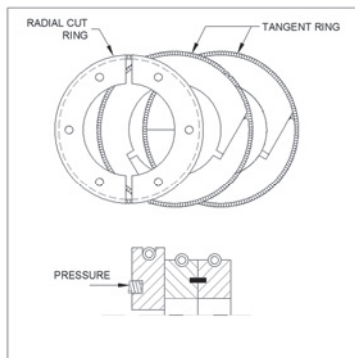


Figure 6 – XRBD Ring

This ring has two variations, one which has spring holes in the backup ring and the other which relies on spring holes in the cup. In either case, these small springs are not fully captured, and when the packing is disassembled they are loose and can easily be dropped and lost. Installation can be difficult because the springs must be carefully lined up by hand before the next cup is laid down, which can be tedious and problematic. Many compressor mechanics prefer to avoid using these rings, and their popularity is limited.



#### 4. Solution – The Cartridge Assembly

We have found that the methodology of the XRBD ring can be applied to achieve side-loading but in a more user-friendly manner. This is accomplished with a cartridge-style assembly that includes a series of side-loading compression springs, but captures these springs such that they are held in place throughout assembly, installation and removal.

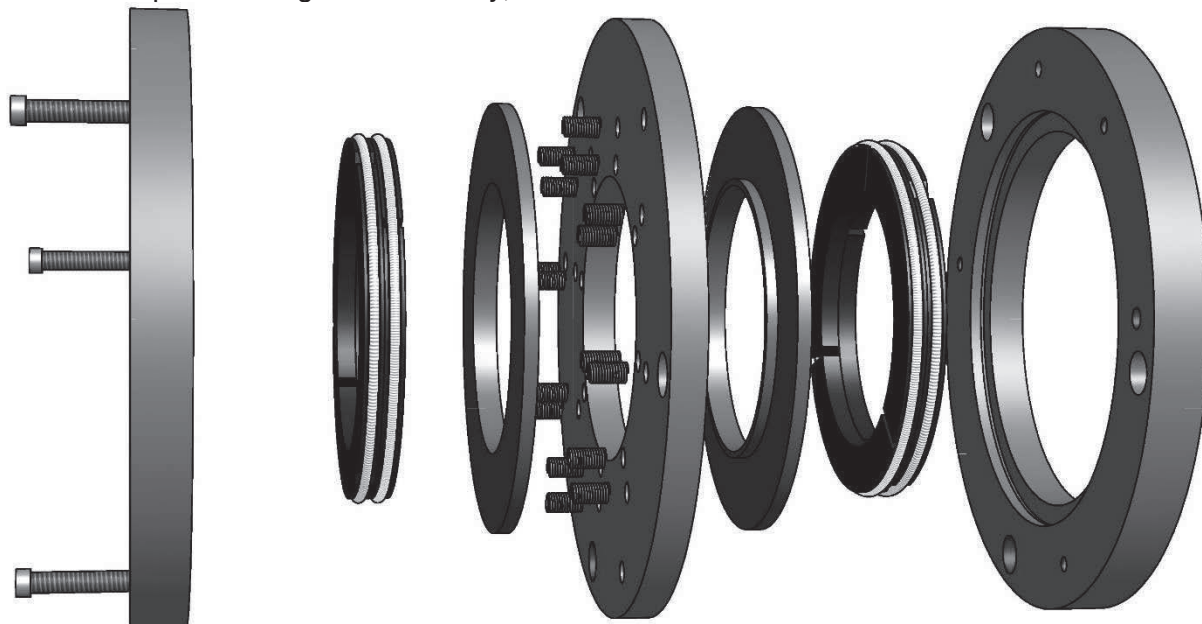


Figure 7 – Cartridge Assembly Exploded

The cartridge assembly consists of 3 metallic plates (cast iron or steel, similar to the other packing cups), along with two PEEK (Polyether ether ketone) pressure plates and a series of 16 compression springs. The compression springs are captured in drilled holes in the center plate, and are held on either side by the PEEK pressure plates. A counter bore in the left-hand and right-hand plates holds the PEEK plates in place, allowing some side movement but keeping them contained within the assembly. The entire assembly is then bolted together with three socket-head screws.

What results is an assembly that can be treated as a single cup. The cup then has counter bores on either side in which to install two simple double-tangent seal rings. When installed in a packing case, the spring-loaded pressure plates push these two rings outward against the neighboring cup faces to seal. Buffer gas is injected into the assembly through the center plate.

The compression springs provide a substantial outward load but do so with zero added radial loading, so no additional frictional heat is produced. Because the internals of the cartridge are captured, assembly of the packing case and installation are relatively simple.

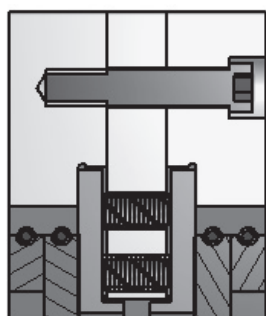


Figure 8 – Cartridge Assembly with Rings



Figure 9 – Cartridge Assembly in Packing Case



The compression springs in the cartridge assembly do not cycle once the packing is assembled, so there is no concern for spring failure. Also, none of the components should experience any impact wear, so the cartridge requires very little maintenance and should not need to be disassembled in the field. Packing changes require only that the two seal rings be replaced and the cup assembly be reinstalled to the packing case.

The cartridge assembly can be designed to fit any new packing case design or can be retrofitted to most existing packing cases. Since 2008, 152 unique cartridge assemblies have been built. Since that time several have been brought in for packing case repair. The cartridges have held up well, and we have found that only a minimal amount of debris is collected in the assembly, due to the “L” shaped design of the pressure plates and the resulting difficult path for particulates to penetrate. There has been minimal need to disassemble these cartridges, even for cleaning.

The primary benefit of this technology is the minimal frictional load on the rod as compared to traditional AL rings. Comparative laboratory testing was conducted in a pressure packing case on a 2” rod, operating at 1200 RPM and 1160 psi [80 bar]. The packing case was first set up with an AL ring with typical purge pressure of 15-20 psi [1.0 – 1.4 bar]. A temperature contact probe was mounted just behind the flange of the packing case to continuously measure rod temperature at the back of the packing case. Five repetitions were conducted, each consisting of an 8-hour run. The test was then repeated five times with the identical packing setup but with a side-loading cartridge assembly in place of the AL ring. Purge pressure was again 15-20 psi [1.0 – 1.4 bar]. Over each of the five runs, the average rod temperature with the AL rings was 214°F [101°C], while with the cartridge assemblies the average was 181°F [83°C].

This result has been replicated in the field as well. An AL ring in an intermediate packing on a 2.5” rod running at 1200 RPM was consistently overheating and failing within a matter of days, despite several attempts to troubleshoot and through material changes. The cartridge assembly was applied, reducing the rod temperature by nearly 54°F [30°C] and extending the intermediate packing life to better than 8000 hours.

## **5. Conclusion**

Traditional buffer seals using side-loaded rod rings are quite effective at helping to reduce emissions, but the frictional heat that they often generate raises rod temperatures and often leads to early packing failures.

The cartridge assembly presented here achieves the same side-loading but does so without the added frictional burden. Piston rod temperatures are significantly lower and packing life is extended in many cases. This is especially useful in high speed and/or non-lube packing, and also in intermediate packing seals where there is no gas movement nor any other method of managing heat.

This technology has been proven in laboratory trials and more importantly has proven itself in several field applications, where some troublesome packing problems have been dealt with successfully.



# Technical Paper

**Session: 38-2**

**Session Name: Sealing / Wear**

**Novel oil wiper system**

**Author:**

**Dr. Marc Langela**  
**Head of Research & Development**  
**Stasskol**  
**39418 Staßfurt, Germany**

## Summary

Reciprocating compressors are using a piston rod that is connected to the drive train at the crosshead section. A large amount of oil is lubricating the drive train as well as the cross head section in order to ensure a proper operation by avoiding fretting between moving parts that are in contact to each other. Especially at dry-running compressor applications lube oil can cause tremendous problems if a leakage from the crosshead section into the piston rod packing occurs. Mixed friction conditions will increase the wear of the sealing elements and therefore decrease the life-time of the piston rod packing. Oil wiper systems are used in order to avoid this problem, but the common systems are sometimes not efficient enough especially at high speed or if the moving crosshead is creating a differential pressure due to its movement.

For these high duty applications a novel oil wiper system was invented that maximizes the scraping efficiency due to small scraping edges and a high tightness by its unique design. Two scraper rings are combined to one scraping unit and oil is being sealed also at harsh conditions due to the fact that the rings are covering each other's gap. This enables a high sealing performance and even differential pressures caused by a reciprocating cross-head can be sealed off by using this novel oil wiper system.



## 1. Introduction

Reciprocating compressors are often used in dry-running applications where the packing rings as well as the piston and guide rings are operating without any oil lubrication. The wear resistance of the sealing elements at these applications is improved by adding so-called dry lubricants like carbon black or molybdenum disulfide to the material mix. Every drop of a liquid oil-based lubricant might spoil the application as the gases are for example used for refinery processes with catalyzers that will be blocked by even small traces of oil.

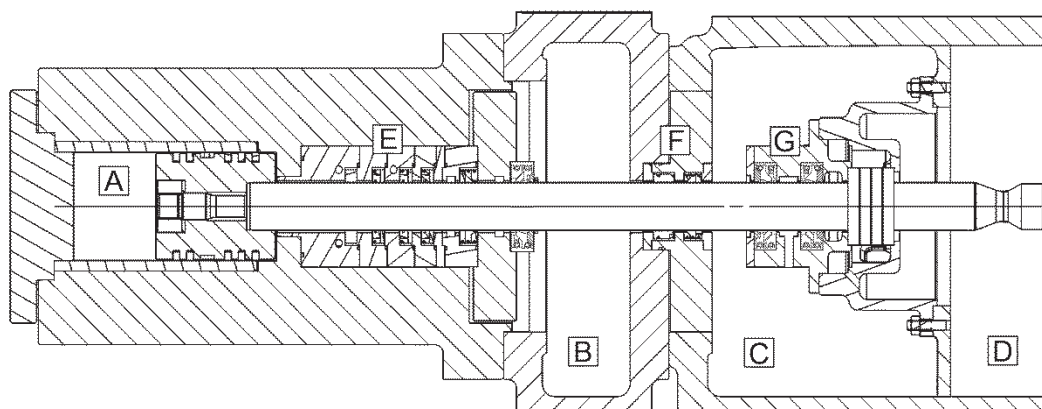


**Figure 1** Typical compressor system with compression chamber (A), 1<sup>st</sup> distance piece (B), 2<sup>nd</sup> distance piece (C), drive train (D), stuffing box (E), intermediate packing (F) and oil wiper packing (G)

However, reciprocating compressors are systems that convert a rotating movement into a linear reciprocating movement by a cross head connection and all moving parts at the drive train have to be lubricated by the use of oil in order to achieve the maximum life-time of the compressor system (see **Figure 1**). This lubrication oil has to be prevented from entering the stuffing box area and the cylinder.

Oil wiper systems are used (see position G in **Figure 1**) for separating the lubrication oil of the drive train from the stuffing box and compression chamber. We will go into more detail about these oil wiper systems at the next section.

## 2. Traditional Oil wiper systems

Traditional oil wiper systems are consisting of scraping rings with one or more sharp scraping edges (see **Figure 2**). They are mostly made out of weak white metal compounds to ensure the sharpness of the scraping edges and to provide some flexible behavior for a good alignment of the oil scrapers with the surface of the piston rod. However, some material combinations with polymer compounds are known in the field (<sup>i,ii</sup>), which are addressing this downside of pure metallic scraper rings.

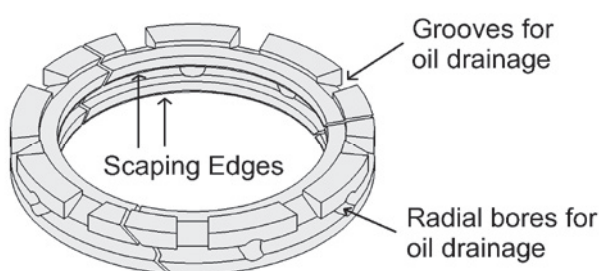


**Figure 2** Typical oil scraper ring design with 2 scraping edges and bores/grooves for oil drainage

All of the oil that is scraped off by the oil scrapers will be collected within the oil wiper housing. Therefore a drain line has to be established that allows a continuous reflux of the collected oil back to the drive train. Standard oil wiper designs as shown in **Figure 2** are including design features like grooves and radial bores to ensure efficient oil drainage from the inner diameter where the scraping edges are located to the outer diameter of the oil wipers.

So far, so good, the described oil wiper elements are working very efficient in standard process machines where the speeds are low and the intermediate distance pieces are ensuring a stroke-free operation of the oil wiper systems. The term “stroke-free” in this context means that after the oil wiper system there is a free running part of the piston rod that is at least as long as the compression stroke. Background of this requirement is the fact that even the best metallic oil scraper leaves a thin oil layer at the piston rod that has only a few micrometers in its film thickness. This oil film lubricates the oil scraper, reduces the wear of the scraping edges and prevents the rod from being scratched by the sharp oil wiper elements. Thus, this oil film is necessary for efficient operation and it re-enters the oil wiper system at every back-stroke of the compressor.

### 3. Combination of oil wipers with other systems

If there's no stroke-free operation and the area with the small oil layer is entering another system like for example the intermediate packing (Element F in **Figure 1**), then the risk is given that this layer will be destroyed and the oil will not re-enter the oil wiper area. Most likely the oil will instead enter the disturbing system like the intermediate packing in this example.

One difficult application is an oil wiper packing with a combined buffer gas system like it is shown at **Figure 3**. These combinations are often used at compressors with flammable or explosive gases in order to ensure that no process gas will be able to enter the crank case from the distance piece side. The downside of this solution is that the buffer gas sealing rings out of PTFE are partially scraping off the oil film that remains on the rod after passing the oil scraper rings.

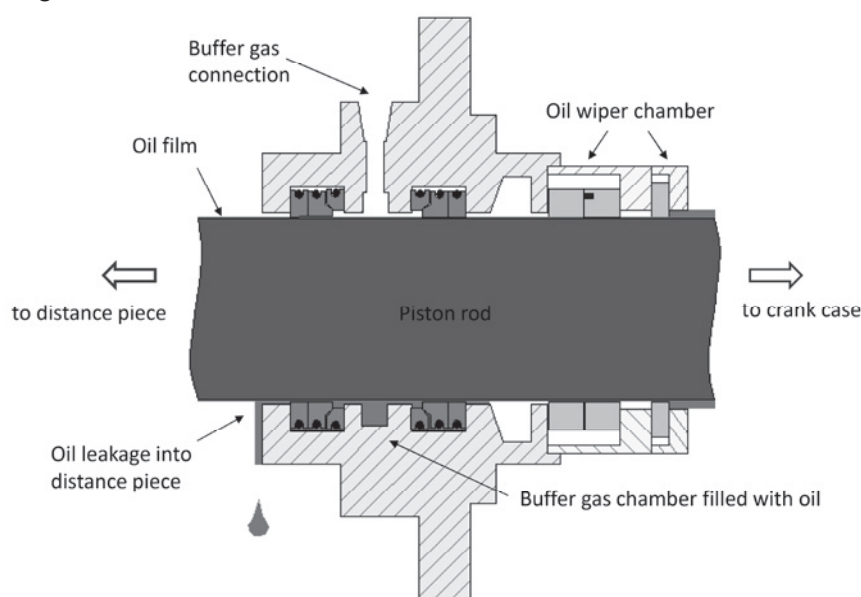


**Figure 3** Combination of an oil wiper packing with a buffer gas system

It could be assumed that the scraping efficiency of the buffer gas sealing rings is superior over the scraping efficiency of the designated oil scraper rings. However, as the buffer gas sealing rings are made out of PTFE, their contact area to the piston rod will be deformed during the stroke causing a so-called elasto-hydrodynamic effect (EHD). This effect leads to a pressure





buildup between the sealing ring and the piston rod and the oil will be squeezed into the direction of the intermediate distance piece.

Consequently, the next logical step is to use this elasto-hydrodynamic effect in order to increase the scraping efficiency of standard oil wiper systems. A novel oil wiper system can be created by combining the gas tightness of the buffer gas system with the scraping efficiency of oil wiper rings and by using sealing elements out of plastic materials like PTFE and PEEK in order to benefit from the elasto-hydrodynamic pressure buildup during the stroke of the compressor. Another benefit of using non-metallic scraper rings is the fact, that the piston rod cannot be damaged by the oil wiper system due to scratching. In principle non-metallic scraper rings are well-known in the field but their working principle is mostly comparable to their metallic counterparts, thus, they are not gas-tight and they don't take advantage out of hydrodynamic effects.

#### 4. Introducing the Novel Oil Wiper system

To realize a new and improved oil wiper system, the elasto-hydrodynamic effect of PEEK and PTFE sealing rings was combined with the scraping efficiency of an oil wiper system. This was achieved by modifying a conventional twin ring design in such way, that both sealing elements are showing an oil scraping edge (see **Figure 4**). With two scraping edges out of a non-metallic material (PEEK or PTFE), the scraper ring combination utilizes a double elasto-hydrodynamic effect in order to maximize the oil tightness and to maximize the oil reflux into the drive train.

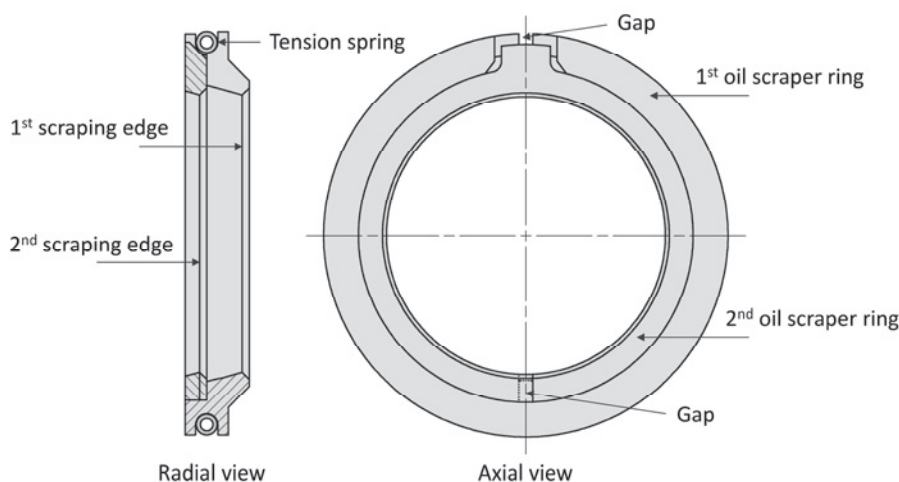


**Figure 4** Novel gas-tight oil seal combination out of two scraper rings and a tension spring

Both scraping rings have different angles at both sides of their scraping edges. These different angles are producing different oil pressures at the scraping edge during the upstroke of the piston rod compared to its backstroke due to hydrodynamic as well as elasto-hydrodynamic theory. The oil pressures are causing corresponding volume flows at the scraping edge resulting in a 'back-pumping effect' at the scraping edge geometry. Thereby, the resulting oil flow at the upstroke in the direction towards the crank side is higher as the oil flow at the downstroke towards the cylinder side. The net flow is called the 'balanced residual flow' across one revolution of the crank and it shows an excess of oil transport from the cylinder side to the crank end side, causing the already mentioned 'back pumping effect'. The flows during up- and downstroke are shown schematically at **Figure 5**.

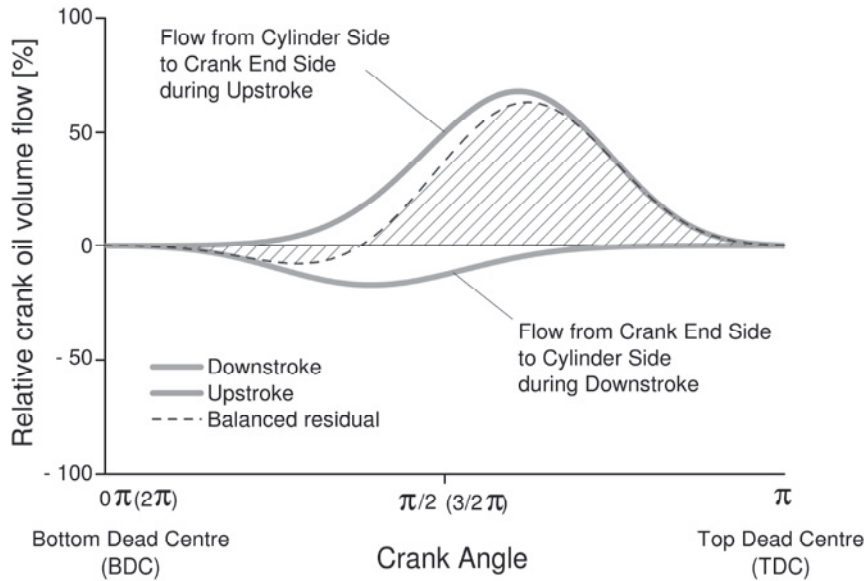


**Figure 5** Volume flow at the scraping edges during one revolution at up- and backstroke of the rod.

For wear compensation, the 1<sup>st</sup> scraper ring shows a gap to adjust its inner diameter to the piston rod diameter. At this gap there is also space for taking an anti-rotating nose of the 2<sup>nd</sup> scraper ring. This ensures that the gap of the 2<sup>nd</sup> scraper ring for adjusting to the piston rod is on the opposite side of gap of the 1<sup>st</sup> scraper ring and both scraper rings are covering the gap of each other. A circumferential tension spring keeps both elements together and presses the elements against the surface of the piston rod.

The combination of the two rings leads to a gas tight system where no leakage path exists for oil creeping through the ring package in the direction towards the distance piece. Beside the two scraping edges this furthermore increases the tightness of the novel oil wiper design. The design is used together with a clamping ring (see **Figure 6**) that clamps the ring system axially against the wall of the oil wiper housing in order to avoid leakage in radial direction between the housing and the front surface of the ring package which is formed by the common surface of the 1<sup>st</sup> and 2<sup>nd</sup> scraper ring.

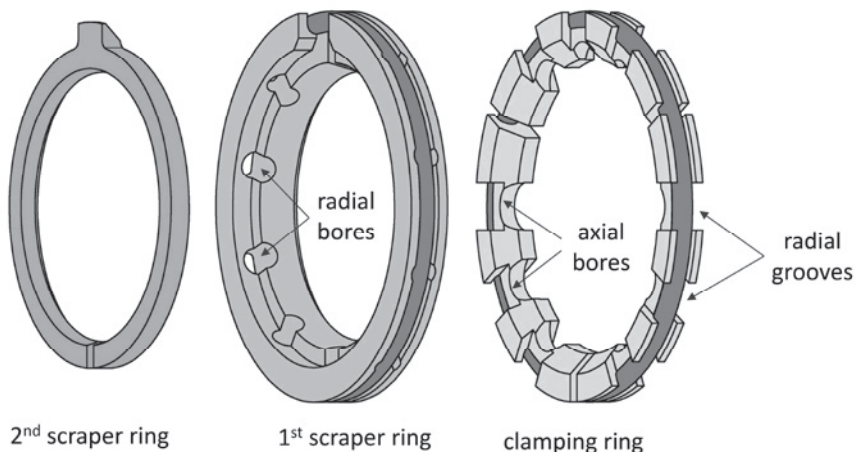


**Figure 6** Novel gas-tight oil wiper with clamping ring and with bores and grooves for improved oil reflux; drain passages are mainly the radial bores of the 1<sup>st</sup> scraper ring as well the radial grooves and axial bores of the clamping ring



For improved oil reflux back to the drive train of the oil that has been scraped off, the 1<sup>st</sup> scraper ring and the clamping ring are showing bores and/or grooves in radial and/or axial direction. As shown at **Figure 6** the 1<sup>st</sup> scraper ring has radial bores for oil getting from the inner diameter of the ring combination to the outer diameter, where the bores of the housing for oil drainage are located. The clamping ring has bores in axial direction and grooves in radial direction for the same purpose. Thus, the oil drainage from the scraping area back to the drive train can be maximized by these design features.

## 5. First experimental results

The novel oil wiper system was tested at the test compressor as well in a first field test. We will describe our experiences below.

### 5.1 Experiences at the test compressor system

In the first step the novel oil wiper design was tested at the test compressor system (see **Figure 7**). The oil wiper system was installed at the horizontal axle of the test compressor and the machine was running at the following conditions:

- Speed: 623 rpm
- Stroke: 130 mm
- Average piston velocity: 2.7 m/sec
- Rod diameter: 70 mm

A tube with a milliliter scale was installed at the distance piece after the oil wiper system to measure the amount of leak oil that passes the oil wiper system and that will be collected by the tube.

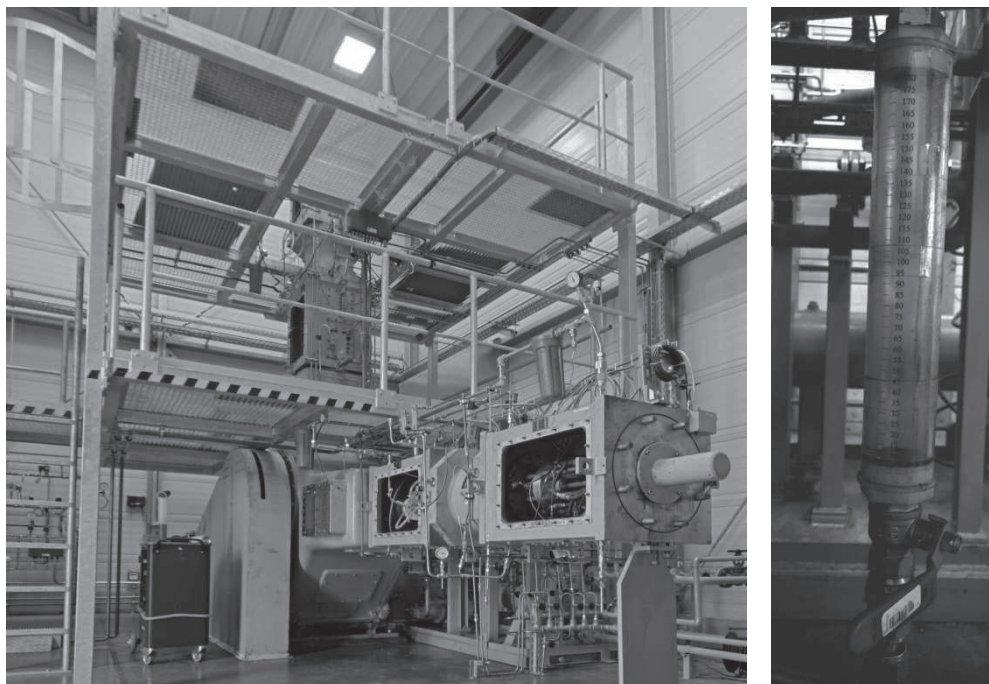


**Figure 7** Test compressor system (left) and mean to collect the oil leakage (right)

With the standard oil wiper rings a leakage of approximately 10 ml per day could be observed during continuous operation. After installing the new oil wiper system there was no oil leakage detectable at the test compressor system.

Thus, the novel oil wiper system provides increased oil tightness, but the test compressor system is operating relatively slow. The higher the speed of the reciprocating compressor system, the more demanding is the application in respect to the sealing efficiency of the oil wiper system. Higher speed means that the cross-head is pushing an increased amount of lube oil against the oil wiper packing. Therefore a field test with a high speed system was needed to verify the good result at the test compressor system.

## **5.2 Field Experiences**

At a biogas compressor application a customer did have problems with high leakage rates of the oil wiper packing. The leak oil was entering the stuffing box and was finally reaching the compression chamber leading to mixed friction conditions at the sealing elements. As a result the sealing elements only did only survive for a few thousand hours. 'Mixed friction' means that it's not a dry-running operation anymore because of the leak oil, but the amount of oil is too low to enable a sufficient lubrication. Sealing rings designed for dry-running service are showing a very low life-time at these mixed friction conditions.

The compressor system of the customer was running with the following parameters:

- Speed: 1080 rpm
- Stroke: 100 mm
- Average piston velocity: 3.6 m/sec
- Rod diameter: 40 mm

So, it was clear, that the standard oil wiper systems are not working sufficiently at this application. With the high leak rate the oil is collected within the oil wiper system, because the amount of leak oil is too high for returning to the drive train through the drain connections. The drain connections are blocked and the oil will continue its way in the direction towards the compression chamber.

After installing the novel oil wiper system at the customer compressor the leakage rate was reduced by 70 %. Thus, the amount of the remaining lube oil was less than one third of the former leakage rate and the drain channels were able to allow the reflux of this remaining leak oil into the drive train. This shows the increased sealing efficiency of the new system which was then chosen by the customer to be the standard oil wiper system at this type of compressor applications.

## **6. Summary**

A novel oil wiper was introduced which consists of two oil scraping rings that are combined to a gas tight oil sealing system. This system is been completed by a clamping ring for axial contact pressure of the sealing surfaces against the chamber wall. The two scraper rings are manufactured out of PEEK or PTFE and the choice of non-metallic materials enables the appearance of elasto-hydrodynamic effects. The contact areas of the scraper rings will be deformed during the stroke of the compressor and this leads to a pressure buildup at the scraping edges. This pressure buildup is one characteristic aspect of the elasto-hydrodynamic effect and it supports the high sealing efficiency of the oil wiper system.



The on-site test compressor is equipped with a tube for collecting leak oil after passing the oil wiper system. By the installation of the new oil wiper system the amount of leak oil was reduced to Zero as no leak oil was collected within the first 2000 hours of operation.

The new oil wiper system was also installed at a biogas field application. This specific biogas compressor did suffer from high oil leakage through the oil wiper system equipped with conventional oil scrapers. The leak oil was passing the distance piece causing increased wear by mixed friction conditions within the stuffing box of this dry-running machine. After installation of the new oil wiper system the leakage rate was reduced by 70 % which did solve the increased wear of the packing internals. The customer (OEM manufacturer of recip) now uses the new oil wiper system as a standard for his biogas applications and more results of field testing are expected in the near future.

## 7. References

---

<sup>i</sup> Radcliffe, C. *Development of a New „Oil Tight“ – OT, Oil Wiper* 1st EFRC conf., Dresden, Germany, **1999**

<sup>ii</sup> Bäuerlein, C.; Radcliffe, C.; Wustlich, M. *The OT Oil Wiper – 5 Years Field Experience* 4<sup>th</sup> EFRC conf., Antwerp, Belgium, **2005**







# Technical Paper

**Session: 39-1**

**Session Name: Pulsation / Vibration 1**

## **The impact of reciprocating compressor pulsations on the surge margin of centrifugal compressors**

**Author:**

**Klaus Brun, Ph.D.**  
**Program Director**  
**Southwest Research Institute San Antonio**  
**78238 San Antonio, Texas, USA**

**Co-Author 1:**

**Rainer Kurz, Ph.D.**  
**Manager**  
**Solar Turbines, Inc. San Diego**  
**92123 San Diego, California, USA**

**Co-Author 2:**

**Sarah Simons**  
**Research Scientist**  
**Southwest Research Institute San Antonio**  
**78238 San Antonio, Texas, USA**

## Summary

An increasing number of centrifugal compressors are being installed in older reciprocating compressor stations to increase flow capacity or to retrofit existing pipeline infrastructure. In these mixed compressor stations this has often resulted in spurious interactions between the reciprocating and centrifugal compressors. The primary reason for this phenomenon are common header pulsations from the reciprocating compressor severely affecting the operating range of the centrifugal compressor, restricting the operability of the reciprocating compressor, and requiring the retrofitting of additional pulsation control into the compressor station. An improved knowledge of these mixed compressor station pulsation interactions during the station design phase could have avoided this. But unfortunately the industry knowledge and state-of-the-art of design tools are limited in analyzing this phenomenon.

Mixed compression has been a topic of concern raised and discussed in theory by multiple authors. For example, Sparks (1983), Kurz et al., (2006), and Brun et al., (2014) provided analysis and numerical predictions on the impact of discrete and periodic pressure pulsation on the behavior of a centrifugal compressor. This interaction came to be known as the “Compressor Dynamic Response (CDR) theory.” CDR theory explains how pulsations are amplified or attenuated by a compression system’s acoustic response characteristic superimposed on the compressor head-flow map. Although the CDR Theory describes the impact of the nearby piping system on the compressor surge and pulsation amplification, it provides only limited usefulness as a quantitative analysis tool, primarily due to the lack of numerical prediction tools and test data for comparison. Recently, Brun et al., (2014) utilized an efficient 1-D transient Navier-Stokes flow solver to predict CDR in real life compression systems. Numerical results showed that acoustic resonances in the piping system can have a profound impact on a centrifugal compressor’s surge margin. However, although interesting, the fundamental problem with both Spark’s and Brun’s approach was that no experimental data was available to validate the analytical and numerical predictions.

In 2014, laboratory testing of reciprocating and centrifugal compressor mixed operation was performed in an air loop at Southwest Research Institute’s (SwRI) compressor laboratory. The specific goal was to quantify the impact of periodic pressure and flow pulsation originating from a reciprocating compressor on the surge margin and performance of a centrifugal compressor in a series arrangement. This data was to be utilized to validate predictions from Sparks’ CDR theory and Brun’s numerical approach. For this testing, a 50 hp single-stage, double-acting reciprocating compressor provided inlet pulsations into a two-stage 700 hp centrifugal compressor operating inside a semi-open recycle loop which uses near atmospheric air as the process gas. Tests were performed over a range of pulsation excitation amplitudes, frequencies, and pipe geometry variations to determine the impact of piping impedance and resonance response. Detailed transient velocity and pressure measurements were taken by a hot wire anemometer and dynamic pressure transducers installed near the compressor’s suction and discharge flanges. Steady-state flow, pressure, and temperature data were also recorded with ASME PTC-10 compliant instrumentation. This paper describes the test facility and procedure, reports the reduced test results, and discusses comparisons to predictions. Results provided clear evidence that suction pulsations can significantly reduce the surge margin of a centrifugal compressors and that the geometry of the piping system immediately upstream and downstream of a centrifugal compressor will have an impact on the surge margin reduction. In severe cases, surge margin reductions of over 30% were observed for high centrifugal compressor inlet suction pulsation. Pulsation impact results are presented as both flow versus surge margin and operating map ellipses. Basic design rules were developed to relate predicted flow pulsation amplitudes to corresponding reductions in surge margin.



## Background

Over the last 20 years it has become a common design practice to combine the operation of centrifugal and reciprocating compressors in a single compression plant for several reasons. This arrangement can provide benefits for highly cyclical process profiles. Also the market trend on older pipelines is to add new centrifugal compressors into existing reciprocating compressor stations for capacity addition or horsepower replacement. Thus, many compressor stations now operate a mix of reciprocating and centrifugal compressors either in parallel or in series arrangement. For example, on pipeline applications, the compressors are placed in parallel operation such that a large gas turbine driven centrifugal compressor provides the base-load compression while a smaller reciprocating compressor follows cyclical or peaking demand compression demands. Other applications such as gas gathering, gas reinjection, or gas storage often have reciprocating compressors placed in series with centrifugal compressors to achieve high-pressure ratios while taking advantage of the operational flexibility of centrifugal compressors. For example, a centrifugal compressor may be placed upstream of a reciprocating compressor in gas reinjection applications to handle the higher flow volumes at low pressure while the reciprocating compressors are better equipped for high pressures and pressure ratios.

Conventional thinking was that a centrifugal compressor may experience some pulsations from the reciprocating compressor when in series or from both the common suction and discharge headers, but good reciprocating compressor bottle and manifold designs would result in minimal impact on the operational stability of the centrifugal compressor. This assumption held true for small horsepower and low speed applications and with older, high-pressure drop and often significantly oversized pulsation control systems. However, recent experience with mixed compressor stations utilizing large power and high speed modern separable reciprocating compressors with modern efficient pulsation control systems shows that the centrifugal compressor can be moved into pulsation-induced operational instability for both parallel or series arrangements. This clearly presents a station design challenge, operational range limitation, and a basic safety concern.

Interfacing a centrifugal and a reciprocating compressor within the same piping system, introduces two transient fluid mechanisms that have the potential to create damaging inlet/outlet conditions on the centrifugal compressor. These mechanisms are: (i) pulsations generated by the reciprocating compressor and (ii) pulsations generated by the reciprocating compressor that are amplified by an acoustic resonance within the piping system. Both mechanisms can move the centrifugal compressor operating point into a surge or choke (stonewall) condition and, thus, should be avoided or at least controlled. Whereas the first pulsation mechanism can be mostly analyzed using a classic acoustic pulsation analysis, for, the second mechanism the model is more complex and must include the physical and thermodynamic functions of the compressors.

The surge and stall regions on a head vs. flow map of a compressor typically define its performance. This map is critical to assess the operating range of a compressor for both steady-state and transient system scenarios. However, the compressor map is generic to any piping arrangement and does not provide a complete picture of how the compressor will respond to rapid transient inputs and how its surge behavior is affected by these events. Specifically, the response of the compressor to rapid transient events such as single or multiple (periodic) pressure pulses is also a function of the compressor's upstream and downstream piping system's acoustic response and impedance characteristics. This unique response phenomenon was first described in the 1970s and is known as the "Compressor Dynamic Response (CDR) theory." CDR theory explains how pulsations are amplified or attenuated by a compression system's acoustic response characteristic superimposed on the compressor head-flow map. Although the CDR theory explains the impact of the nearby piping system on the compressor surge and pulsation amplification, it provides only limited usefulness as a quantitative analysis tool, mainly due to the lack of computational numerical tools and benchmark test data available at the time.

## Introduction

Detailed descriptions of centrifugal compressor surge can be found in numerous papers. A summary of the findings of these papers can be found in Kurz and Brun (2006) and in Brun and Nored (2008). On the other hand, the impact of the piping system on surge from both the impedance and acoustic response has received very little attention. The principle reference paper on the topic is over thirty years old and was published by Sparks (1983). Sparks discussed the theory of piping acoustics and resonances and how they can affect the surge line of a centrifugal compressor. At that time, numerical modeling capabilities did not exist to properly simulate this phenomenon. Recently, Brun et al., (2014) utilized an efficient 1-D transient Navier-Stokes flow solver to predict CDR in real life compression systems. Numerical results showed that acoustic resonances in the piping system can have a profound impact on a centrifugal compressor's surge margin. However, although interesting, the fundamental problem with both Spark's and Brun's approach was that no experimental data was available to validate the analytical and numerical predictions.

## Centrifugal Compressor Performance and Surge

Most researchers have agreed that the actual location of a surge line is a function of the compression system and not solely a function of the compressor itself. The system is impacted by the impedance and acoustics of the piping system to which the compressor is connected. This interaction between the centrifugal machine and its surrounding piping and valves is explained by CDR theory.

When CDR theory was first understood, engineering analysis tools were inadequate to properly predict pulsating flows in complex geometries, although, from a surge control and safe compressor system operating design standpoint, it is imperative to be able to accurately predict the interaction phenomenon. For example, if a compressor's discharge piping impedance design amplifies suction pulsations, the result could restrict the operating range and cause unacceptable discharge piping vibrations. The typical centrifugal compressor performance map (head or pressure ratio versus flow rate) with the corresponding speed lines indicates there are two limits on the operating range of the compressor. Global aerodynamic flow instability, known as surge, sets the limit for low-flow (or high-pressure ratio) operation while choke or "stonewall" sets the high flow limit. The exact location of the surge line on the map can vary depending on the operating condition and, as a result, a typical surge margin is established at 10% to 15% above the stated flow for the theoretical surge line. This should not be confused with turn-down, which is the flow difference between the operating point and surge line for the same head produced by the compressor. Throughout this paper, we will only use surge margin since all testing was done at a constant compressor speed. Most centrifugal compressor manufacturers design the machine to have at least 15% surge margin during normal operation and set a recycle valve control line at approximately 10% surge margin. That is, once surge margin falls below 10%, the recycle valve is opened to keep the compressor operating above the 10% surge margin line.

This classic compressor performance map is appropriate for the characterization of steady-state and slowly changing operating conditions, but it is not fully applicable for rapidly transient or high frequency periodic compressor flow inputs. It is acceptable to assume that the relatively fast flow transients (above 1-2 Hz) experienced by the centrifugal compressor do not affect the compressor's operational speed (Brun and Kurz, 2010). The centrifugal compressor continues to operate at a constant speed as the rotational inertia of the compressor (and its driver) will torsionally dampen any fluid induced by the rapid blade loading changes. Thus, the compressor will operate on a fixed head-flow speed line. However, when the compressor experiences suction or discharge flow fluctuations are superimposed on the mean-flow, these fluctuations can often be enough to momentarily move the compressor operating point on the map's speed line across the surge limit and affect the forward flow stability of the compressor. Although this flow-reversal event may be very short-lived (depending on the frequency of the flow fluctuation), it is





usually sufficient to drive the compressor into a full surge cycle. Thus, even if a compressor is operating with an adequate surge margin based on the mean-flow, high inlet or discharge side pulsations have the potential to cause the compressor to operate in periodic unsteady surge cycles.

Therefore, it is clear that surge or choke can be induced in a centrifugal compressor by strong pulsations in pressure and flow. Brun and Kurz (2010) showed the velocity fluctuations in time at the inlet to a centrifugal compressor (Brun and Kurz (2010)). In their case inlet pulsations (velocity fluctuations shown on the y-axis) became periodically negative given the acoustic and impedance system effects. This corresponds to short duration surge cycles at a frequency equal to that of the inlet pulsations. As previously noted, the dynamic behavior of the compressor system near the surge line was outlined by Sparks (1983), further discussed by Kurz et al., (2006), and then implemented into a numerical analysis tool by Brun et al., (2014). They explained how pulsations are amplified or attenuated by a compression system's acoustic and piping response characteristic superimposed on the compressor head-flow map. Kurz et al., (2006) also noted that centrifugal compressor stability is sensitive to highly pulsating flows, especially in cases where operating at piping acoustic resonance frequencies cannot be avoided. Choke should be avoided, as it is an inefficient operating regime and may result in damage to the compressor. On the other hand, it is critical to avoid any kind of surge event, as these can cause bearing or seal damage, blade rubbing, or even catastrophic compressor failures.

### Compressor Dynamic Response Theory

A piping system's acoustic impedance,  $Z$ , is given by (Equation 2):

$$Z = \frac{p}{U} = \frac{p}{uA} = \frac{z}{A} = \frac{\rho c}{A} \sim \frac{\rho u}{A} \quad (2)$$

where  $Z$  is the acoustic impedance,  $A$  is the pipe cross section area,  $p$  is the sound pressure,  $U$  is acoustic volume flow,  $z$  is the specific acoustic impedance,  $\rho$  is the fluid density,  $u$  is the molecular particle bulk velocity, and  $c$  is the local speed of sound. This impedance relates pressure to acoustic volume flow for pressure waves traveling at the speed of sound. One should note that acoustic impedance  $Z$ , which is an extensive property, is affected by local pipe flow conditions, while the specific acoustic impedance  $z$ , which is an intensive property, is a fluid physical property for a given temperature and pressure in both incompressible and compressible flows. In pipe flow pressure pulse modulation and reflection occurs whenever there is a change of impedance  $Z$ .

A centrifugal compressor has a piping system that either attenuates or amplifies pulsations at its discharge or suction side as demonstrated by its reaction to any fluctuation in flow with a fluctuation in head. This can be easily seen from its performance characteristics (Sparks, 1983). Sparks (1983) explains the process as the interaction of a piping system with given acoustic impedance and a compressor that reacts to a change in flow with a change in head (or pressure ratio). The piping impedance is usually a combination of resistive impedance (i.e., due to frictional losses) and acoustic inertia (due to the mass of the gas in the pipe) and stiffness (due to the compressibility of the mass in the pipe). The compressor head-flow characteristic will differ widely from the steady-state characteristic for higher fluctuation frequencies. Sparks (1983) also discusses practical piping system design approaches to reduce pulsation levels using acoustic elements such as bottles, nozzles, choke-tubes, and resonators.

Brun et al., (2014) further explains that for fast transient pressure pulses in the acoustic range, the pipe flow resistance curve is not applicable, and the impedance curve must be utilized to analyze the compressor operating point on the compressor performance map. Based on this analysis, the surge line can be crossed when short pressure pulses result in flow variation due

to low gradient (“flat”) impedance curves as shown in *Figure 1*. Here, a short suction pressure pulse interacts with the pipe’s flat impedance line to cause a large flow fluctuation that crosses the surge line momentarily and results in an onset of a surge event.

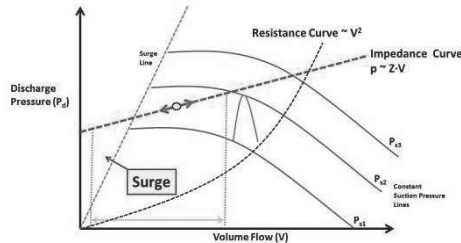


*Figure 1. Flat Impedance Line Results in Suction Pressure Pulse Causing Surge*

Brun et al., (2014) also validate CDR, numerically showing that pulse amplification or attenuation for centrifugal compressors is primarily a function of the piping upstream and downstream impedance. Piping impedance can be controlled by varying pipe diameter and pressure drop elements in the flow path as shown in *Figure 2*.

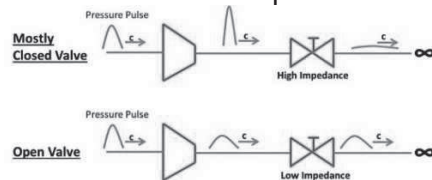


*Figure 2. Downstream Pipe Impedance Determines Pressure Pulse Amplification*

A number of other studies are available in the public domain that discuss centrifugal compressor surge and the impact of flow pulsations on turbomachines. A detailed literature review on this topic was provided by Kurz, et al., (2006), Brun and Nored (2008), and an overview of the state-of-the-art of pulsation analysis technologies was included in Brun et al., (2007).

### Testing Objectives

Due to the lack of numerical prediction tools and test data, CDR theory can only describe the impact of the nearby piping system on the compressor surge and pulsation amplification. Therefore, it provides only limited usefulness as a quantitative analysis tool. As discussed above, more recently Brun et al., (2014) utilized an efficient 1-D transient Navier-Stokes flow solver to predict CDR in real life compression systems. However, although interesting, the fundamental problem with both Sparks’s and Brun’s approach was that no experimental data was available to validate the analytical and numerical predictions. Thus, while many compressor stations have both reciprocating and centrifugal compressors installed, there is still a limited understanding of how pulsations, piping resonance, and impedance impact centrifugal compressor performance and surge.

Laboratory testing of reciprocating and centrifugal compressor mixed operation was performed in a full scale laboratory setting to overcome these technology gaps and a deficiency of fundamental physical understanding. The specific goal was to develop benchmark data that quantifies the impact of periodic pressure and flow pulsation originating from a reciprocating compressor on the surge margin and performance of a centrifugal compressor. This data was then utilized to validate predictions from Sparks’ CDR theory and Brun’s numerical approach. For this testing, a single-stage reciprocating compressor provides inlet pulsations to a two-stage centrifugal compressor operating inside a semi-open recycle loop and utilizing atmospheric air as the process gas. Tests were performed over a range of pulsation excitation amplitudes, frequencies, and pipe geometry variations to determine the impact of piping impedance and resonance response. Although the testing was performed for a series arrangement, the results are equally applicable to mixed station parallel arrangements. Detailed transient velocity and pressure



measurements were taken with a hot wire anemometer and dynamic pressure transducers installed near the compressor's suction and discharge flanges. Steady-state flow, pressure, and temperature data was also recorded with ASME PTC-10 compliant instrumentation. This paper describes the test facility and procedure, reports the reduced test results, and discusses the comparison to predictions. From the test results, some basic design rules were developed to relate surge margin reduction to flow pulsation amplitudes.

### Mixed Compression Test Loop

Laboratory testing of reciprocating and centrifugal compressor mixed operation was performed in an air loop at the SwRI compressor laboratory. *Figure 3* shows a schematic of the test arrangement and photos of the compressors. The facility allows for open, semi-open, and closed loop operation with either or both reciprocating and centrifugal air compressors arranged in series or parallel operation. Semi-open loop operation was chosen for the subject testing to best control flow and pressures at low loop process pressures. The testing was performed using a 50 hp single-stage, double-acting reciprocating compressor mounted upstream of a two-stage 700 hp centrifugal compressor. The reciprocating compressor suction was open to atmosphere with an operating range of 300 to 1,000 rpm (5-17 Hz) using a variable frequency driver. Similarly, the centrifugal compressor was operating in a semi-open recycle loop with the loop's discharge throttled back to atmospheric pressure, a speed range of 2,000 to 14,000 rpm, and maximum pressure ratio of 3:1. However, for safety reasons, the centrifugal compressor's speed and discharge pressure were limited to 7,000 rpm and 2 bar (30 psi), respectively, for the subject test series.

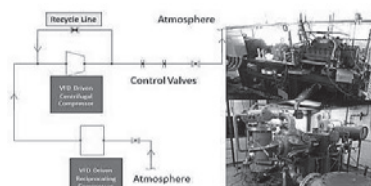


*Figure 3. Schematic of the Test Loop Arrangement*

To reduce overall measurement uncertainty, flow, pressure, and temperature measurements were installed in the test loop per ASME PTC-10 requirements. Instrumentation included four (4) static pressure and temperature measurements on each of the compressor's suction and discharge sides, six (6) dynamic pressure transducers mounted throughout the loop, steady-state flow measurement from an orifice plate meter in the main and recycle loop, reciprocating compressor flow and power from a PV card measurement, centrifugal compressor power from a shaft torque meter and enthalpy rise analysis, and transient inlet flow measurement using a high speed hot wire anemometer near the compressor's suction flange. All individual instruments were calibrated prior to the test to manufacturer's accuracy requirements. End-to-end calibrations with all data acquisition system included were also performed. Total measurement and data acquisition uncertainties were predicted using the perturbation method and validated versus data scatter.

### Results

Since the primary objective of the project was to determine the impact of pulsation on the surge margin of the compressor, accurately identifying the onset of surge is imperative. On most centrifugal compressors, surge symptoms include high axial rotor vibrations and suction/discharge cyclic pressure fluctuations at low frequencies. Previous experiments on the subject compressor had demonstrated that the compressor surges at a frequency of approximately 4 Hz. Thus, a series of tests were performed to validate the surge line of the compressor and to establish clear instrument measurement output criteria indicating that the machine is operating in surge.

### Compressor Map Validation

All surge tests were performed with the centrifugal compressor operating at 7,000 rpm and near ambient suction pressure to minimize the risk of damage to the compressor during the anticipated surge events. For example, *Figure 4* shows 4 Hz axial rotor vibration measured by proximity probes for no-surge versus surge operating conditions of the compressor. Clearly, a significant rise in 4 Hz vibration amplitudes is observed. Similar results showing significantly elevated surge pressure pulsations at the characteristic 4 Hz were seen from the suction and discharge dynamic pressure transducers. Thus, for all test series, the onset of surge criteria was established to be a rapid increase in 4 Hz compressor axial vibrations and suction/discharge flange dynamic pressure pulsations.

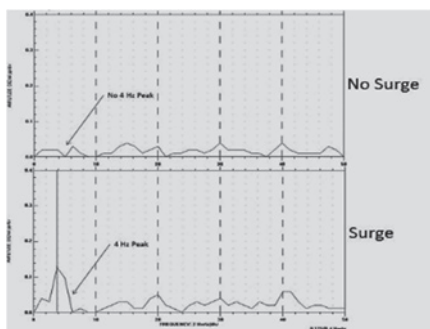


Figure 4. Axial Compressor Vibrations Before and in Surge Conditions

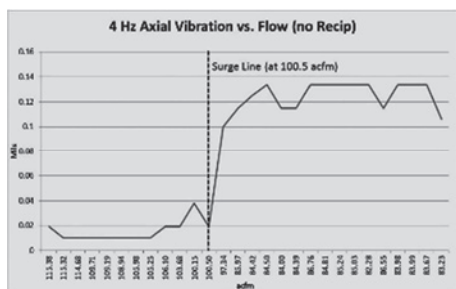


Figure 5. Axial Vibrations versus Flow at the 7,000 Rpm Speed Line

Figure 5 shows axial vibrations as a function of flow measured by the hot-wire anemometer upstream of the compressor. The centrifugal compressor is seen to surge when the flow reaches approximately 100.5 acfm. Based on the surge vibration and pulsation criteria, the compressor map and surge line were thus established. However, one should note that based on changing ambient conditions, the steady-state surge line varied throughout the testing and had to be re-measured for every single test series.

### Effect of Pulsating Flow on Centrifugal Compressor Performance

To determine the impact of externally induced pulsations on the surge margin of the centrifugal compressor, the reciprocating compressor is operated upstream in series with the centrifugal compressor. The pulsations from the reciprocating compressor thus travels through 55 ft of varying diameter pipe as shown on the P&ID before they enter the centrifugal compressor suction flange. Some pulsation attenuation or acoustic amplification will occur in this pipe segment and must be quantified for the analysis. Time domain pulsations were measured at the reciprocating compressor discharge, the centrifugal compressor suction, and the centrifugal compressor discharge.

For the testing, the centrifugal compressor was initially operated at a stable point with approximately 15% surge margin to the right of the surge line. The reciprocating compressor was then started, brought to a fixed speed, and its pressure and flow pulsation amplitudes were recorded





at the centrifugal compressor suction flange using dynamic pressure transducers and the hot wire anemometer, respectively. The centrifugal compressor loop recycle valve was then slowly closed until surge was clearly indicated by axial vibrations and suction/discharge pulsations. Only when the previously established surge criteria were fully met, was the pulsation-induced surge point recorded. The difference between the previously recorded steady-state surge point (from the performance map) and the pulsation-induced surge point was used to calculate the difference in surge margin.

Figure 6 shows a typical test run with the reciprocating compressor running. Pressure fluctuations and compressor inlet flow are plotted versus test recording time. In this case, the 4 Hz discharge pulsations are used as an indicator for the onset of surge. The test started at 1:55:44 pm with the recycle valve being slowly closed, decreasing the flow into the centrifugal compressor (red line). At the time of 2:00:53 pm, the 4 Hz discharge volute pulsations are seen to increase which corresponds to a flow of 106.5 acfm, about 6 acfm away from the steady-state surge line. As the recycle valve is further closed, and the flow is further decreased, the pulsations are seen to increase, approximately linearly with flow reduction. A drastic 4 Hz pulsation increase can then be observed when the flow reaches the steady-state surge line at 100.5 acfm. In this particular case, a gradual onset of surge can be observed well before the machine is operating near the surge line. This provides evidence that periodically unsteady flow can induce surge in a centrifugal compressor when the compressor is seemingly still operating to the right of the surge line.

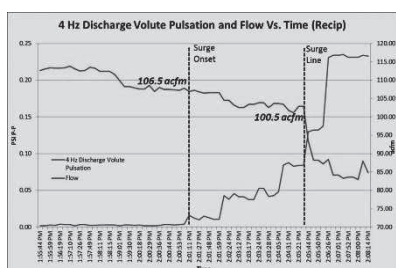


Figure 6. Test Results of 4 Hz Pulsations and Flow versus Test Time

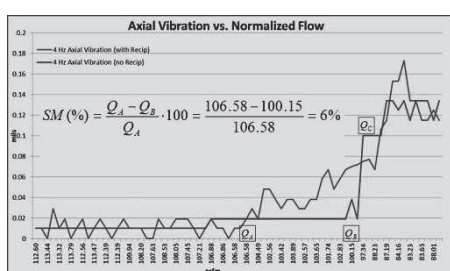


Figure 7. Axial Vibration versus Flow Showing Difference in Surge Onset for Cases with and Without Suction Pulsations

A direct comparison of the onset of surge and surge margin for cases with and without the reciprocating compressor running can thus be made. For example, Figure 7 shows the axial vibrations versus flow for cases with and without the reciprocating compressor running. The axial vibrations in the case with the reciprocating compressor running start rising at a much higher flow (106.6 acfm) than the case without the reciprocating compressor running (100.2 acfm). The difference in surge margin is thus approximately 6% between the two cases. This difference between steady-state and pulsating flow surge margin is the pulsation-induced surge margin differential. The surge margin differential corresponds to an actual reduction of compressor operating range and can severely impact a mixed compressor stations operability and safety.



## Operating Map Ellipse

For the 106 acfm surge onset case (with the reciprocating compressor running), the pulsations entering the centrifugal compressor just before the onset of surge were measured to be 44 acfm peak-to-peak in flow and 0.058 psi peak-to-peak in pressure. One can thus plot an ellipse of the actual operating point of the centrifugal compressor based on its fluctuating suction flow and pressure conditions as shown in *Figure 8*. This operating map ellipse defines the cyclically unsteady operating point of the compressor on its performance map. Specifically, the ellipse closely represents the true operating range of the compressor on the compressor map, since with periodically transient cyclic suction/discharge operating pressures, the compressor operating point will never be on its time-averaged or steady-state operating point. One should note that pulsations from a reciprocating compressor are not perfectly sinusoidal. The actual shape of the periodic operating cycle will typically not be a perfect ellipse but more irregular, depending on the higher order frequency content of the pulsations. Nonetheless, the assumption of an elliptical shape significantly simplifies further analysis and was found to not introduce significant error when used as a design tool.

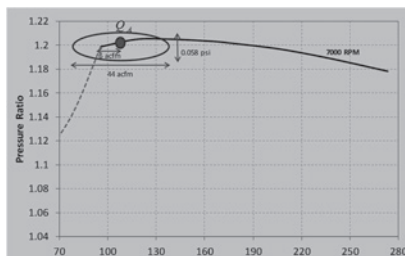


*Figure 8. Pulsation-Induced Operating Cycle Ellipse versus Actual Surge Margin Reduction*

From *Figure 8*, one can clearly see that, although pulsation amplitudes in flow (44 acfm) indicates that the compressor should have surged at the much higher flow of approximately 122 acfm, truly measurable surge occurred only around 106 acfm. Specifically, the surge margin reduction caused by the flow pulsation is significantly lower than the flow fluctuation magnitude. Similar trends were found for all cases measured. The cause for this is still under investigation but may be attributable to higher order frequency induced pulsations not having sufficient transient time to affect the low frequency surge cycle. Further discussion of this phenomenon is provided below. The operating map ellipse can be further refined by showing the different pulsation frequency orders as shown in *Figure 9*. In this example, the reciprocating compressor running speed was 615 rpm, the excitation frequency was 10.25 Hz, and a surge margin differential of 41.2% was found. Clearly, the compressor surged before it had reached its peak pressure ratio on the 7000 rpm speed line. The 1<sup>st</sup> order ellipse shows the induced pulsation only from the pulsations at the 10.25 Hz operating frequency (running speed), the 1<sup>st</sup> and 2<sup>nd</sup> order ellipse show energy from both 1<sup>st</sup> and 2<sup>nd</sup> orders (up to 20.5 Hz), and the 1<sup>st</sup>, 2<sup>nd</sup>, and 3<sup>rd</sup> order ellipse show energy up to 30.75 Hz for all three orders. Pulsations from reciprocating compressors have significantly higher order frequency content when the cylinders are double-acting since the pulse wave form is not sinusoidal. Thus, in this case, most pulsation energy was in the 2<sup>nd</sup> order as can be seen by the much larger 1<sup>st</sup> and 2<sup>nd</sup> order operating map ellipse. The energy from the 3<sup>rd</sup> order does not significantly increase the radius of the operating map ellipse (1<sup>st</sup>, 2<sup>nd</sup>, and 3<sup>rd</sup>) as it does not contain significant pulsation energy. Fourth and higher order frequency energy content was also found to be negligible. In most cases, for reciprocating compressors operating below 1,500 rpm, almost all surge-relevant pulsation energy is contained in the frequency orders below 90 Hz. One should also note that the local impedance line can be directly determined from the operating map ellipse as shown in *Figure 9* (red line). The fundamental definition of acoustic impedance, as shown in Equation 2, relates bulk acoustic flow to pressure rise for pulsations at acoustic frequencies (i.e., at the speed of sound). Thus, the slope of the impedance line must be equal to the aspect ratio of the operating map ellipse.

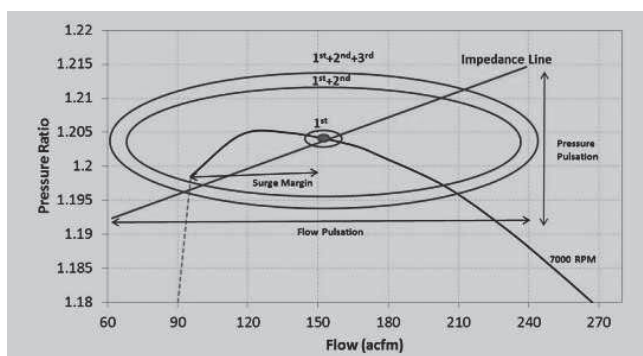


Figure 9. Operating Map Ellipses for Different Pulsation Frequency Orders

### Results and Analysis

The above described tests were performed to determine the impact of pulsation on the surge margin (surge margin differential) of the centrifugal compressor for a number of operating conditions, pulsation amplitudes, pulsation frequencies, and piping suction/discharge geometry changes. For most of the tests, the compressor suction conditions were held at near ambient conditions with inlet temperatures varying between 70 and 90 degrees Fahrenheit. Because of the changing inlet temperatures and associated air density variations, the surge line had to be retested and validated for every test series. To test varying pulsation amplitudes on the centrifugal compressor and to determine the impact of piping acoustic resonances, measurements for surge margin and operating map ellipses were performed at four (4) different reciprocating compressor speeds. Also, to increase and vary the pulsation amplitudes into the centrifugal compressor, three (3) of these operating points corresponded to piping acoustic resonance frequencies. Suction piping resonances were found at the 405 rpm (6.75 Hz), 480 rpm (8 Hz), and 615 rpm (10.25 Hz) reciprocating compressor operating speeds. An additional test point at 310 rpm (5.17 Hz), corresponding to a non-resonant operating condition, was also tested as a low amplitude pulsation test case.

Table 1 and Table 2 summarize the results from the four (4) different cases that were tested and include the flow and pressure pulsation levels at both the reciprocating compressor exit and centrifugal compressor inlet. For these cases the centrifugal compressor was running at 7,000 rpm and the reciprocating compressor speeds are indicated in the tables.

Condition		1	2	3	4
Recip Speed (RPM)		310 (5.17 Hz)	405 (6.75 Hz)	480 (8 Hz)	615 (10.25 Hz)
At Recip Discharge	Excitation pulsations (psi pk-pk)	0.37	0.65	0.55	0.88
	Excitation Pulsations (psi pk-pk) [normalized]	0.15 [0.0298]	0.11 [0.0158]	0.13 [0.02252]	0.38 [0.10699]
At Centrifugal Suction	Flow fluctuations (p-p acfm) [normalized]	44.9 [0.0014]	90 [0.0028]	110 [0.0034]	250 [0.0078]

Table 1. Impact of Acoustic Resonance: Pulsations and Flow Fluctuations

In Table 2 the pressure and flow results are converted into surge margin differential and percent area across the surge line.

Recip Speed (RPM)	405 (6.75 Hz)	480 (8 Hz)	615 (10.25 Hz)
Excitation Pulsations (psi pk-pk) [Pressure ratio fluctuations]	0.11 [0.0091]	0.13 [0.0108]	0.38 [0.0315]
Flow fluctuations (p-p acfm) [normalized]	90 [0.0028]	110 [0.0034]	250 [0.0078]
Flow at Surge (acfm)	102.5	121.0	150.8
Pressure Ratio at Surge	1.201	1.204	1.204
Surge Margin Differential %	7.9	24.3	41.2
% Area Across Surge Line	31	29	31

Table 2. Effect of Pressure and Flow Fluctuations on Surge

To evaluate the impact of suction/discharge piping impedance changes, for each of the four (4) running speed cases (5.17 Hz, 6.75 Hz, 8 Hz, and 10.25 Hz), six (6) different piping system geometries were tested. The piping geometry changes involved replacing 1.2 m (4 ft) segments of suction or discharge pipe with different diameter pipes of 7.6 cm, 10.2 cm, 15.2 cm (3 inch, 4 inch, and 6 inch) spool pieces. For the 5.17 Hz case, only the 6 inch suction and discharge piping case was tested. Thus a total of 16 operating conditions were tested.

### Experimental Test Data

The raw data from tests 1 through 16 was reduced to determine pulsating flow, pulsating flow coefficient, pulsating pressure, pulsating pressure ratio, pulsating head coefficient, operating map ellipse, surge margin differential, area of operating map crossing the surge line, pulsation amplification/attenuation, steady head and flow coefficient, compressor power, compressor efficiency, impedance slope, etc. It is beyond the scope of this paper to present all this data. However, since the raw test data and reduced results produced herein are intended to be open to the industry for benchmarking, code validation, and design comparison, *Table 3* shows test results for the most critical parameters: Pulsation pressure amplitude, pulsation flow amplitude, surge margin differential, and pulsation amplification/attenuation. As shown by the data in the table, for very high pulsation amplitudes, surge margin reductions above 40% were seen. However, for more moderate pulsation levels, similar in range to pulsation to mean line pressure ratios found in industrial compressor station applications, surge margin reductions were closer to 15-25%. The flow and pressure pulsation data in *Table 3* can be utilized to determine the operating map ellipse and the area of the ellipse that crosses the surge line. For all test cases, this area was found to be approximately 30-35% of the total operating map ellipse's area.



Test No	Recip Speed (RPM)	Excitation Pulsations (psi pk-pk) at Recip Discharge	Excitation Pulsations (psi pk-pk) at Centrifugal Suction (0-90 Hz)	Flow fluctuations at Centrifugal Suction (p-p acfm)	Surge Margin Differential %	Compressor Pulsation Amplification or Attenuation Factor	
66 Suction/ Discharge	1	310 (5.17 Hz)	0.37	0.154	44.9	6.1	0.56644
	2	405 (6.75 Hz)	0.65	0.167	209	7.9	0.93785
	3	480 (8 Hz)	0.55	0.186	153	24.3	1.40769
	4	615 (10.25 Hz)	0.88	0.326	376	41.2	3.69318
	5	405 (6.75 Hz)	1	0.171	213	6.8	0.69388
	6	480 (8 Hz)	0.66	0.176	174	17.8	1.75000
	7	615 (10.25 Hz)	2.04	0.417	407	39.8	5.12346
63 Suction/ Discharge	8	405 (6.75 Hz)	1.1	0.196	203	8.2	1.30000
	9	480 (8 Hz)	0.55	0.196	182	8.2	1.95000
	10	615 (10.25 Hz)	2.25	0.407	391	27.3	2.48466
46 Suction Discharge	11	405 (6.75 Hz)	1.03	0.152	297	19.6	0.61633
	12	480 (8 Hz)	0.575	0.21	294	26.2	1.11702
	13	615 (10.25 Hz)	2.2	0.72	394	40.1	1.07692
36 Suction/ Discharge	14	405 (6.75 Hz)	1.13	0.159	336	35.7	0.74528
	15	480 (8 Hz)	1.03	0.22	371	42.9	0.80769
	16	615 (10.25 Hz)	2.35	0.34	396	42.9	2.55814

Table 3. Results from Tests 1 Through 16

### Impact of Pulsation Amplitude on Surge Margin

The impact of pulsation amplitudes on compressor stability can be illustrated by comparing the pulsation flow coefficient,  $\Delta\varphi$ , as defined in Equation 3, to the reduction of surge margin (surge margin differential) of the centrifugal compressor.

$$\Delta\varphi = \frac{\Delta Q}{N \cdot D_{tip}^3} \quad (3)$$

Here,  $\Delta Q$  is the pulsation flow amplitude, N is the running speed of the compressor and  $D_{tip}$  is the tip diameter of the compressor impeller. Similarly, a pulsation head coefficient,  $\Delta\psi$ , can be defined as:

$$\Delta\psi = \frac{\Delta H_s}{D_{tip}^2 N^2} \quad (4)$$

where  $\Delta H_s$  is the pulsation head amplitude. Results recording the pulsation flow coefficient versus surge margin differential for tests 1 through 4 are shown in Figure 10. As anticipated, the surge margin reduction appears to be a near linear function versus pulsation amplitude. Increasing pulsations will increase the radius of the operating map ellipse and thus, decrease the distance between transient operating points and the surge line. Tests 5 through 16 showed very similar results and trends.

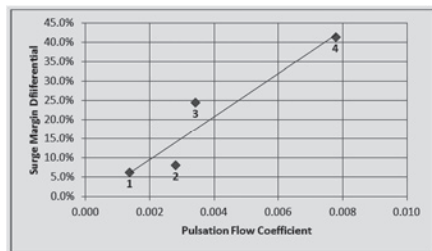


Figure 10. Pulsation Flow Coefficient versus Surge Margin Reduction

One should note that pulsation pressure amplitude or pulsation head coefficient could also be plotted versus surge margin reduction and the trends would look identical. The reason for this is that pulsation pressure and flow are directly related by impedance as shown in Equation 2. The piping impedance in this test series (1 through 4) was not changed, so the relationship between pulsation pressure and volume flow stays constant. *Figure 10* also demonstrates that when the reciprocating compressor is running on or near acoustic piping resonance frequencies, the pulsation amplitudes into the centrifugal compressor will be changed and thus, the surge margin differential will be affected. Specifically, test cases 1 through 4 correspond to reciprocating compressor running speeds on three (3) piping acoustic resonance frequency (405 rpm/6.75 Hz, 480 rpm/8 Hz, 615 rpm/10.25 Hz) and one non-resonant frequency (615 rpm/10.75 Hz). Clearly, each one produces a different amplitude pulsation and different surge margin reduction. When designing a mixed compressor station, it is important to keep this in mind, as the worst case surge margin reduction scenarios will likely occur for cases where the reciprocating compressor is running on an amplifying acoustic piping resonance.

Finally, the pulsation flow coefficients versus surge margin curve as shown in *Figure 10* was compared to numerical results presented by Brun et al., (2014). They modeled the impact of various levels of periodic pulsations on the surge margin of an industrial centrifugal compressor operation at 14,400 rpm and 52.4 bara suction pressure inside a 20 m recycle loop. Although speed, pressures, temperatures, and gas compositions of the compressor modeled by Brun et al., (2014) were significantly different than the cases tested herein, the predicted impact on surge margin differential versus pulsation flow coefficient are similar. Specifically, for their modeled case, Brun et al., (2014) predicted a surge margin differential of 17% for an equivalent pulsation flow coefficient of 0.0039. This is within 15% of the curve shown in *Figure 10*. However, one should not assume that this one good correlation between test data and numerical predictions (for these very different operating cases) allows for a broad generalization of the test results from *Figure 10*. They are specific for the geometry and operating conditions described herein only.

### Impact of Piping Impedance on Surge Margin and Pulsation Amplification

CDR theory (Sparks (1983)) and numerical results from Brun et al., (2014) predict that changing the acoustic suction or discharge impedance of the pipe will affect the level of modulation of a pulse as it travels through the centrifugal compressor. That is, based on CDR, one can predict whether a compressor and piping system will either amplify or attenuate an externally induced pulse. Tests 5 through 16 were primarily intended to validate or disprove this theory.

An easy method to alter the piping impedance is to change its internal flow area. Tests 5 through 10 changed the discharge piping diameter area of the centrifugal compressor and its impedance by replacing the original 6 inch pipe with smaller 4 and 3 inch spool pieces. Similarly, tests 11 through 16 changed the suction piping impedance by replacing the 6 inch suction piping with 4 and 3 inch spool pieces. Since pipe acoustic impedance increases linearly with decreasing through flow area, it has a square functional relationship with decreasing pipe diameter.





The primary effect of a compressor’s associated piping system impedance is on the amplification or attenuation of periodic pulses through a centrifugal compressor. This indirectly impacts the surge margin, as larger pulses tend to decrease the surge margin differential. *Figure 11* shows pulsation amplification through the centrifugal compressor versus discharge piping impedance slope for the 405 rpm (6.75 Hz) running case. For the 0.0001 and 0.0002 impedance slope cases, the pulsations are attenuated by factors of 0.7 and 0.9, respectively. For the highest impedance slope case (0.0005) the pulsations are amplified by a factor of 1.2. Thus, consistent with CDR and numerical predictions, an increase in the discharge pipe impedance line slope will result in higher discharge pulsations out of the centrifugal compressor. Similar trends were observed for the other running speed cases.

The above finding can provide some compressor station design guidance: To minimize the risk of pulsation amplification through a centrifugal compressor, the downstream piping should be designed with the flattest possible impedance slope. However, a flat impedance slope can also result in the highest conversion of pressure to flow fluctuations and thus the greatest risk for pulsation-induced surge. Furthermore, low impedance piping often corresponds to large downstream compressor volumes which are undesirable from a transient ESD surge perspective. A careful compressor station piping design must balance these opposing requirements for mixed flow applications.

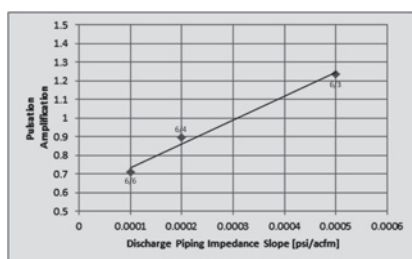


Figure 11. Pulsation Amplification versus Discharge Impedance Slope

The impact of suction piping impedance changes on the surge margin differential is shown in *Figure 12* for the 480 rpm (8.00 Hz) running case. Here the surge margin differential is decreasing with increasing impedance slope. The cause for this is that with a flat impedance slope, more pulse pressure is converted to pulse flow fluctuations which decreases the distance between the operating point and the surge line. Thus, the steeper the impedance slope on the compressor suction side, the lower the surge margin differential. This trend was consistent for all running cases with suction piping changes.

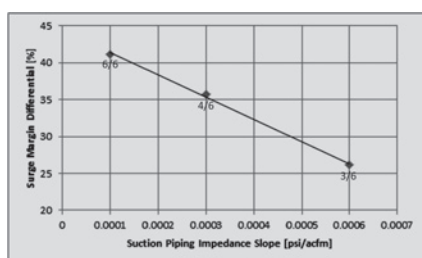


Figure 12. Surge Margin Differential versus Suction Impedance Slope

The above test findings can be summarized into trends as shown in *Table 4*. Here ↑ is for increasing, ↓ is for decreasing. The number of arrows corresponds to weak, medium, and strong effects.

	Increasing (“Steeper”) Impedance Slope	Decreasing (“Flatter”) Impedance Slope
<b>Suction Piping</b>	↓↓↓ Surge Margin Differential ↑ Pulse Amplification	↑↑↑ Surge Margin Differential ↓ Pulse Amplification
<b>Discharge Piping</b>	↓↓ Surge Margin Differential ↑↑↑ Pulse Amplification	↑↑ Surge Margin Differential ↓↓↓ Pulse Amplification

Table 4. Impact of Suction/Discharge Piping Impedance on Pulse Amplification and Surge Margin

Although the information in the above table can be used to guide the design process, it does not replace the need to perform a proper pulsation analysis for mixed compressor stations.

### Design Recommendations

To avoid centrifugal compressor surge or operating range reduction due to pulsations from a reciprocating compressor in a mixed compressor station, it is worthwhile to establish some basic engineering guidelines for station design. The most conservative design rule is simply to require that the centrifugal compressor’s operating map ellipse does not cross the surge line for all operating conditions of the compressor station. However, this rule may be excessively conservative and could result in a significantly reduced operating range of the centrifugal compressor. Specifically, for high pulsation amplitudes and low piping impedance cases, an operating map ellipse with a large radius may force the compressor manufacturer to set the recycle valve control line well beyond the industry typical standard of 10%.

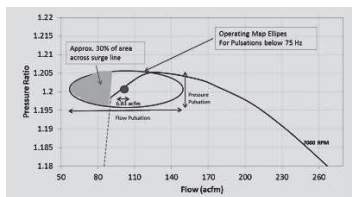


Figure 13. Operating Map Ellipse With 30% of the Ellipse’s Area Left of the Surge Line

A more pragmatic approach is to set a threshold interference level between the operating map ellipse and the surge that results in measurable surge. From the results of the above testing, it was found that surge was consistently identified when approximately 30% of the area of the operating map ellipse had crossed the surge lines for all suction/discharge pulsation frequency orders under 90 Hz. This basic design guideline is graphically illustrated in Figure 13. Figure 13 shows the operating map with 30% of the ellipse’s area crossing surge.

It was found that when the operating map ellipse for pulsation orders below 90 Hz and the surge line overlap area was less than 30%, surge was not measurable and assumed to not have occurred. The reason for this consistent finding requires further investigation, but it is likely a result of the higher order frequencies not having sufficient transient time and amplitude across the surge line to initiate the onset of a surge cycle. Specifically, the wavelengths of higher order pulsations are likely to be too short to cause flow-reversal throughout the internal gas passage of a centrifugal compressor. For example, the half-wavelength of 100 Hz pulsations is less than 1.6 m (5 ft), which is shorter than the internal through-flow passage length of most industrial centrifugal compressors. Intuitively, one would not expect a surge cycle to be initiated unless the induced pulse half-wavelength can alter the pressure and flow of the full length of a compressor’s meridional internal flow path. Thus, the above design guidance could be expanded beyond the proposed 90 Hz frequency limit and include all orders whose half-wavelength is greater than the centrifugal compressor’s internal flow-path. However, to determine whether this assumption can be generalized to all operating conditions of a mixed compressor station or is



simply limited to the test conditions and compressor geometry tested, requires further testing and analysis.

### **Summary, Recommendations, and Basic Design Rules**

An increasing number of centrifugal compressors are being installed in older reciprocating compressor stations to increase flow capacity or to retrofit existing pipeline infrastructure. In these mixed compressor stations this has often resulted in spurious interactions between the reciprocating and centrifugal compressors. The primary reason for this phenomenon are common header pulsations from the reciprocating compressor severely affecting the operating range of the centrifugal compressor, restricting the operability of the reciprocating compressor, and requiring the retrofitting of additional pulsation control into the compressor station. An improved knowledge of these mixed compressor station pulsation interactions during the station design phase could have avoided this. But unfortunately the industry knowledge and state-of-the-art of design tools are limited in analyzing this phenomenon.

External pulsations applied to the suction or discharge flange of a centrifugal compressor can reduce its surge margin significantly, going so far as to move the compressor into surge conditions. In mixed pipeline compressor stations where centrifugal compressors operate in series or parallel with reciprocating compressors, this is of special concern for operational range and safety reasons and must be considered during the design process. CDR theory, first developed in 1983, describes how a centrifugal compressor and its associated piping system interact with pulsations from external sources such as a reciprocating compressor. Unfortunately, CDR provides only limited usefulness as a quantitative analysis tool, primarily due to the lack of validated numerical prediction tools and benchmark test data for comparison. The lack of experimental data for the validation of engineering analysis tools posed a fundamental problem.

Testing of reciprocating and centrifugal compressor mixed operation was performed in an air loop at the SwRI compressor laboratory. The specific goal was to quantify the impact of periodic pressure and flow pulsation originating from a reciprocating compressor on the surge margin and performance of a centrifugal compressor in a series arrangement and to utilize this data to validate predictions from CDR and numerical approaches. For this testing, a 50 hp single-stage double-acting reciprocating compressor provides inlet pulsations into a two-stage 700 hp centrifugal compressor operating inside a semi-open recycle loop and utilizing atmospheric air as the process gas. Although the testing was performed for a series arrangement, the results are equally applicable to mixed station parallel arrangements were performed over a range of pulsation excitation amplitudes, frequencies, and pipe geometry variations to determine the impact of piping impedance and resonance response. From the test and analysis results, the following conclusions can be made as summarized below:

Surge was consistently identified when approximately 30% of the area of the operating map ellipse had crossed the surge lines for all suction/discharge pulsation frequencies orders under 90 Hz.

Test result and trends were consistent with predictions from CDR (Spark, 1983) and numerical predictions (Brun, 2014) for pulsation amplification and attenuation across a centrifugal compressor.

Utilizing the transient operating map ellipse of the centrifugal compressor to identify whether induced pulsations can result in the operating point temporarily crossing the surge line is a useful tool to identify the potential onset of surge. From the operating map ellipse surge margin differential can be calculated for various orders of pulsations.

If the upstream piping system impedance curve is flat, pressure pulses are converted to high volume flow pulses which increase the centrifugal compressor pulsation-induced surge margin differential. On the other hand, steep piping impedance curves of the downstream piping reduce the surge margin differentials.

The geometry of the piping system immediately upstream and downstream of a centrifugal compressor can have significant impact on the surge margin reduction (surge margin differential).

The reduction of surge margin due to external pulsations is a function of the pulsation's amplitudes and frequencies at the compressor suction and discharge flange. High suction flange amplitudes at low frequencies significantly increase the risk of surge.

A transient time domain 1-D Navier-Stokes pipe network analysis model was able to accurately predict suction/discharge pulsations into a centrifugal compressor and thus, its operating map ellipse.

A critically important step in designing a compressor station is to evaluate the impact of the station's piping system on the compressor dynamic behavior. Both acoustic resonance and system impedance are functions of the entire piping system connected to the compressor. Thus, a careful acoustic and impedance design review of a compressor station design should be performed to avoid impacting the operating range of the machine and to properly balance these needs against the surge control system design requirements.

### **Acknowledgment**

The authors would like to thank the Southern Gas Association and Gas Machinery Research Council for the financial support of this project and the technical guidance they provided.

### **References**

- Brun, K. and Kurz, R., 2010, "Analysis of the Effects of Pulsations on the Operational Stability of Centrifugal Compressors in Mixed Reciprocating and Centrifugal Compressor Stations", *Journal of Engineering for Gas Turbines and Power*, vol.132, 7.
- Brun, K., Nored, M., and Kurz, R., 2014, "Impact of the Piping Impedance and Acoustic Characteristics on Centrifugal Compressor Surge and Operating Range," ASME Paper No. 2014-2504.
- Brun, K. and Nored, M., 2008, "Application Guidelines for Surge Control System," GMRC Publication.
- Brun, K., Deffenbaugh, D. M., and Bowles, E. B., Jr., 2007, "Development of a Transient Fluid Dynamics Solver for Compression System Pulsation Analysis," Gas Machinery Conference, Dallas, Texas.
- Kurz, R., McKee, R., and Brun, K., 2006, "Pulsations in Centrifugal Compressor Installations," ASME GT2006-90700.
- Sparks, C. R., 1983, "On the Transient Interaction of Centrifugal Compressors and Their Piping Systems," ASME 83-GT-236.
- Iwasaki, M., Ikeya, N., Marutani, Y., and Kitazawa, T., 1994, "Comparison of Turbocharger Performance between Steady Flow and Pulsating Flow on Engines," Proc. SAE International Congress and Exposition, Detroit, Michigan.
- Morini, M., Pinelli, M., Venturini, M., 2006, "Development of a One-Dimensional Modular Dynamic Model for the Simulation of Surge in Compression Systems," ASME Transactions, *Journal of Turbomachinery*, 129 (3), pp. 437-447



# Technical Paper

**Session: 39-2**

**Session Name: Pulsation / Vibration 1**

## **In-field vibration assessment of the piping of a reciprocating compressor plant**

**Author:**

**Dr Richard Fawcett  
Dynaflow Research Group  
2719 EB Zoetermeer, The Netherlands**

**Co-Author:**

**Dr Erik Jan Lingen  
Dynaflow Research Group  
2719 EB Zoetermeer, The Netherlands**



## Executive Summary

For a number of years visible vibrations were noticeable in the process piping connected to a reciprocating compressor at a refinery, this was despite a pulsation analysis having been conducted at the design stage. The effects of these vibrations were also visible in the small-bore instrumentation pipes, even though they were braced back to the main run pipe. The operator of the plant was worried that fatigue cracks could occur, especially in the small bore lines, and therefore a study was conducted to determine how the vibration levels could be reduced and whether they were leading to stress levels exceeding the endurance limit.

To calculate the stress magnitudes arising in the piping, including those in the small bore connections, a forced mechanical response analysis was performed using a numerical computer model. As well as using the as-built technical drawings the behaviour of the model was tuned to replicate the findings of in-field vibration measurements taken upon both the piping and the bracing. Tuning a piping model to replicate the dynamic behaviour of an operating piping system is not a trivial undertaking. Within this paper the effect of various factors that were given special attention in tuning (matching) the computational model will be discussed.

Attention was given on how to ensure that the correct mechanical mode shapes were present in the model and that they were excited to the same level as in the field. These mode shapes were identified from the vibration measurements taken using a three-axis accelerometer. Factors such as equipment weights within the piping, and gaps and stiffnesses in the supporting deviate to varying degrees from those envisaged at the design stage in any piping system. Consequently the mechanical resonance modes predicted by the numerical model, initially based on the as-built technical drawings, exhibited some differences from those measured in the field. This was in terms of their shapes but also their response at a given excitation frequency.

In tuning the model the stiffness of the spring loaded guide supports, both laterally and axially had to be varied, as well as the stiffness of the bracing of the small bore branches. Only by modifying these values was it possible to match the vibration amplitudes seen in the field with the computational simulation of the piping system. It is impossible to include these factors at the design stage and they are addressed by the requirement that all mechanical resonance modes should be above 2.4 times the compressor rotational speed. However unintentional installation factors could result in this margin not being met in the field, and thus this additional modelling step with a tuned model is required for determining the stress level and the margin of safety.

The output of the study was a robust set of conclusions to the operator of what changes should be made to ensure there was sufficient margin to prevent cracking in the line. The vibrations in the header lines were reduced using rigid supports where possible, given thermal expansion of the system, which have far fewer unknowns in their installation in the field than supports with pre-loaded springs. Additionally recommendations were given for the bracing and gussets on the small bore instrumentation lines so they were less sensitive to vibrations in the header.

In sharing this study though the intention is to increase the awareness of the factors that need to be considered when tuning a numerical piping model to replicate the field experience under a dynamic loading such as pressure pulsations. Thus improving the robustness of numerical simulations used for assessing potentially critical situations in the field. It is noted that the presented method is not as detailed as an Operating Deflection Shape (ODS) analysis of the system or an analysis in which the mechanical natural frequency and damping were determined directly. The method presented here though is easier to apply and is suitable for indicating relative improvements to the system.



## Introduction

During operation noticeable vibrations were observed by the operator of a reciprocating compressor plant. The vibrations had been noted over a significant period of time and there was a concern that they may ultimately lead to fatigue. The vibrations were observed in both the main large bore run piping as well as in a number of the small bore instrumentation branches. Vibrations are always a potential risk in reciprocating compressor piping [4] [5]. The request from the operator was to assess if the observed vibration levels and resulting stress levels were within allowable design limits. The outcome from the study for the operator was a series of recommendations, where necessary, for mitigating the fatigue failure risk.

The aim of this paper is however not to discuss the project and conclusions for the operator, but instead the focus will be on the complexities of tuning a dynamic computational simulation to match the measured vibrations in the field. Here three of the part models used for conducting the study are presented, with the intention of introducing the reader to different factors to consider, and the impact of these uncertainties on the results. It is noted that the presented method is not as detailed as an Operating Deflection Shape (ODS) analysis of the system [6] [7] or an analysis in which the mechanical natural frequency and damping were determined directly. The method presented here though is easier to apply and is suitable for indicating relative improvements to the system. The paper closes with an overview that will helpfully assist an engineer in conducting a robust analysis.

## System Overview

The system under investigation had three double acting compressors arranged in series of which two were in use at any one time. Each compressor provided two stage compression with an air cooler located in the inter-stage loop. The reciprocating compressors had a running speed of 298RPM or 4.96Hz. As the compressors were always running at 100% part load the largest pulsation amplitudes were arising at a frequency of 9.9Hz. At the time of installation a pulsation analysis had been performed which showed that all of the piping mechanical natural frequencies were above 15Hz (3 x the running speed), which was predominantly achieved through the use of spring loaded guide supports.

During the site visits, visual inspection revealed observable piping movements especially immediately downstream and upstream of the pulsation bottles, and in the small branch connections. Vibration measurements were made in these regions. The measurements were made using a tri-axial accelerometer, with a sampling frequency of 48 kHz, which was connected by a magnet to either the piping or a pipe support. Given the highly-explosive nature of the process gas and that the isolation had to be removed to permit the measurements it was desired by the operator to keep the number of measurement points to a minimum.

The systems that will be discussed in this paper are as follows:

- Discharge side of the interconnecting line immediately downstream of the compressor
- The second stage discharge line
- A small bore branch located in the interconnecting line

Each of these systems will be introduced and discussed separately and the salient features in matching the vibration measurements will be explained.

### **Computation Modelling Approach**

The dynamic computation simulation has been conducted using the piping stress analysis software CAESAR II [3]. CAESAR II is a FEA package using beam elements, which is appropriate given that the resonance modes at the frequencies of interest are all beam type modes (and not shell modes). The piping model was split into small elements, 3 to 4 pipe diameters in length, to ensure that there was sufficient resolution to capture the shape of the mechanical eigenmodes.

The model of the compressor piping was built according to the received piping isometrics, and the routing and supporting were verified during the site visits to conduct the vibration measurements. The insulation weight was included and the weights of the valves and flanges were taken from typical design data given their nominal diameter and pressure class. Only the structural steel supporting frames were included in the models which in the experience of the authors could not be considered be rigid (for instance insufficient stiffness in the plane of the applied load) and thereby they could have a significant impact on the calculated mechanical eigenmodes.

For this study the modal and harmonic solvers in CAESAR II were used. The former determines the natural frequencies of the piping system whilst in the latter the response of the system to a (series of) sinusoidal load(s), or displacement(s), of a given frequency and phase angle is evaluated. A harmonic solver calculates the stress level at every phase angle of an applied sinusoidal load, from which the most critical phase angle based on the maximum stress amplitude was automatically selected. When this automatic selection was found not be sufficient then the phase angle at the location of interest was selected manually. The mechanical damping coefficient for the harmonic simulations was 0.03, a value in accordance with the range recommended in piping design practice, for example the design code EN13480.

### **System 1: Interconnecting line**

The system is shown in *Figure 1* and runs from the discharge side of the compressor to the inlet of the air cooler. During the site visit it was seen that there were noticeable vibrations in the piping close to the discharge bottle and near the support frame, as highlighted in *Figure 1*. Measurements were taken at these two locations, where Location 12 was on the support frame just below the pipe show and Location 11 was on the rest support underneath the flange connection with the bottle exit nozzle. The measured vibration amplitudes are shown in *Table 1*. It is seen that the rms velocity exceeds the Energy Institute [1] T7.2.2 guidelines. It is noted the compressor bottle is not included in the model as the focus of the study at the request of the operator was the piping, and the directional anchor immediately downstream of the bottle nozzle meant that the bottle flexibility had no impact on the mode shape at measurement location 12.

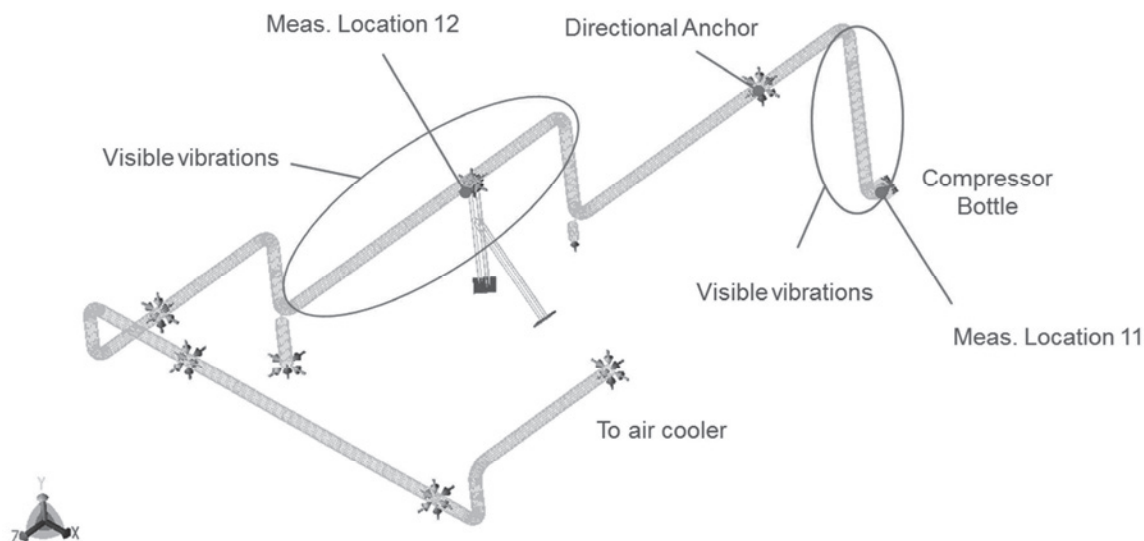


Figure 1: Overview of System 1 with measurement locations.

Table 1: Vibration amplitudes in System 1, peak at 10Hz is shown.

Location	Axes	p-p disp. Measured (mm)	rms velocity (mm/s)	EI 'problem' rms velocity* (mm/s) [2]
Meas. Loc. 11	X	1.8	38.7	23.8
Meas. Loc. 11	Y	1.6	35.3	23.8
Meas. Loc. 11	Z	1.7	36.2	23.8
Meas. Loc. 12	X	0.5	10.7	23.8
Meas. Loc. 12	Y	0.5	10.7	23.8
Meas. Loc. 12	Z	1.0	21.8	23.8

\*allowable at 10Hz.

### Applying the displacements to the model

The first stage in trying to match measured vibrations was to apply the displacements shown in Table 1 with all the spring loaded guide supports as stiff rigid supports which fully restraint dynamic motion. On running the model it was seen that the stress levels remained within the fatigue design limit at all locations, however measurements were only possible for two discrete points and it is needed to extrapolate these results to other locations for example downstream of the support at location 12.

To extrapolate the results it was required to determine the magnitude of the underlying unbalanced forces that are causing the vibration. Here the unbalanced forces were calculated using the worst case pulsation amplitudes at 10Hz per straight pipe section (between elbow pairs) from the earlier third party pulsation analysis of the system. The unbalanced force was then modified if the length between elbow pairs was shorter than the wavelength of a 10Hz pulsation.

Running the model with these pulsation amplitudes did not result in any significant vibrations at location 12, with those in the axial direction (Z) being an order of magnitude smaller than those in *Table 1*. It could be that the compressor pulsation amplitudes were higher than calculated, but as displacement is linear with applied force it is unlikely to provide the full explanation as they were unlikely to be ten times larger than the calculated pulsation amplitude at the design stage.

Investigation therefore moved to the spring loaded supports and the stiffness of the support at measurement location 12. As the vibration measurement at location 12 was taken on the structure (and not on the pipe) the spring support at this location must be providing a reasonable degree of axial restraint. It was found however that if the spring support further downstream was made free then a resonance mode existed in that section with a frequency of 9.5Hz. This mode shape is shown in *Figure 2*. When the pulsation loads were applied for this case the observed displacement at 10Hz matched the displacement in the Z direction at location 12 from the measurements.

It can be seen in *Figure 2* that the compressor bottle has not been modelled, and has instead been replaced by an anchor for the modal analysis. This was done as the directional anchor (rather than spring support) located between the compressor bottle exit and measurement location 12 (see *Figure 1*) meant that the mode shape at measurement location 12 was independent of flexibilities in the compressor bottle.

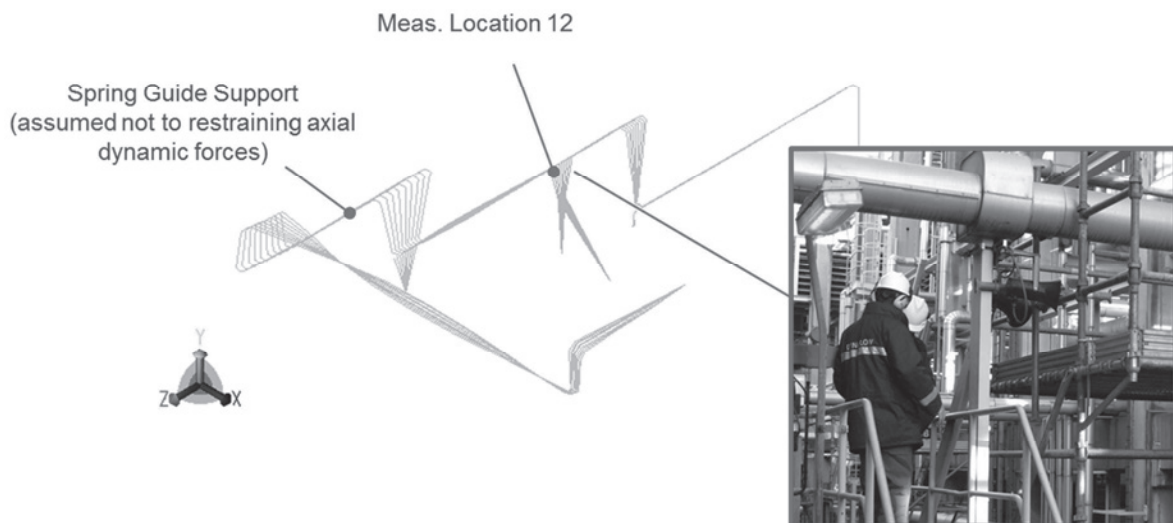


*Figure 2: Mode arising at 9.5Hz if spring guide support assumed not to be restraining dynamic axial forces, photograph shows the structural frame at measurement location 12 (note angle of photograph is mirrored).*

### **Conclusions from Model 1**

This example has shown that the spring guide support cannot necessarily be presumed to be providing full restraint against dynamical axial loads. It is unlikely that this was providing no restraint to the axial forces and given the large displacements seen at the compressor bottle discharge (location 11) it was suspected that the pulsation amplitudes were also higher than those simulated at the design stage. Thus the measured vibration appeared to be a combination of larger than designed pulsation amplitudes and a non-ideal spring guide support. This concept will be taken further in the following model.





## System 2: Compressor Discharge Line

This model is the discharge line downstream of the compressor bottle up until the connection with the general discharge header between the three compressors. An overview is shown in *Figure 3*, with the three locations at which the vibration levels were measured. The vibration amplitudes are listed in *Table 2* and these are compared to the ‘problem’ rms velocity limit from the Energy Institute guideline.

As for model 1 the displacements shown in *Table 2* were applied as harmonic displacements at the measurement locations. In this case though it was found that the stress amplitudes near measurement locations 22 and 23 exceed the allowable value for the fatigue design curve. Additionally the displacements at measurement location 21 lead to significant stresses (which would have caused fatigue failure) in the compressor nozzles. The harmonic displacements from measurement 21 were thus applied as a boundary condition as the vibrations arose partially across the entire compressor skid and not only the bottle and piping. It is reminded here that the operator wanted to keep the focus of this study on the piping only.

*Table 2: Vibration amplitudes in System 2, peak at 10Hz is shown.*

Location	Axes	p-p disp. Measured (mm)	rms velocity (mm/s)	EI 'problem' rms velocity* (mm/s) [2]
Meas. Loc. 21	X	1.5	32.6	23.8
Meas. Loc. 21	Y	2.3	49.5	23.8
Meas. Loc. 21	Z	2.8	60.7	23.8
Meas. Loc. 22	X	0.8	16.3	23.8
Meas. Loc. 22	Y	0.8	16.7	23.8
Meas. Loc. 22	Z	1.5	32.6	23.8
Meas. Loc. 23	X	2.1	46.7	23.8
Meas. Loc. 23	Y	0.6	12.6	23.8
Meas. Loc. 23	Z	0.8	17.5	23.8

\*allowable at 10Hz

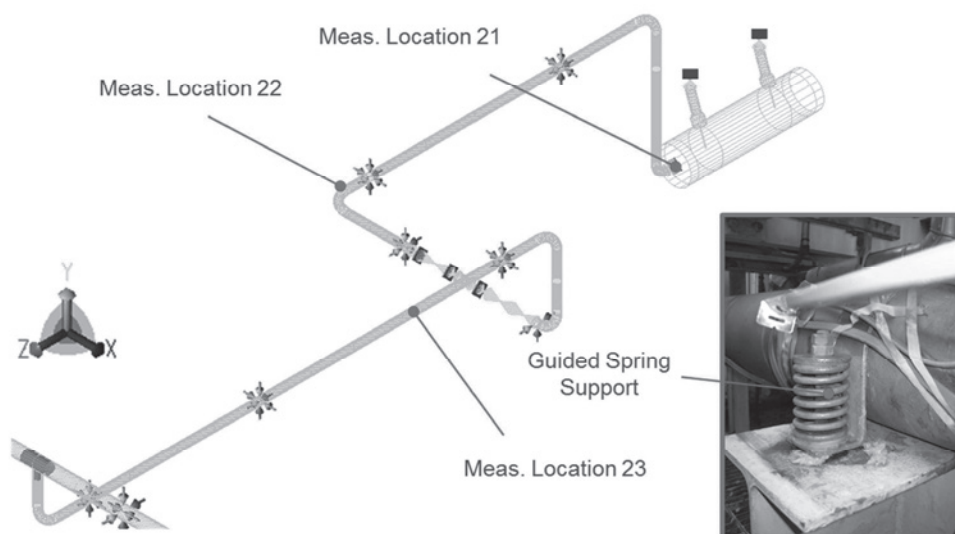


*Figure 3: Overview of System 2 with measurement locations, photograph shows the design of the guided spring supports.*

### Matching the displacements

To tune the model, the design stage pulsation amplitudes, as in System 1, were used to provide the unbalanced forces acting between all elbow pairs. By doing so the vibration amplitudes at points other than the measurement location could be estimated. The unbalanced forces were all taken to act in phase, as detailed phase information was not available from the earlier third party pulsation study.

The simulated displacements at measurement locations 22 and 23 were compared to the measurements considering the spring guide supports as perfectly stiff or flexible. However in both cases the calculated displacement was lower than that from the measurements. Reviewing the mechanical resonance modes when the spring loaded support was assumed to provide no axial restraint it was seen that there was a mode at 8Hz (shown in *Figure 4*) that could be causing the measured vibration amplitudes.

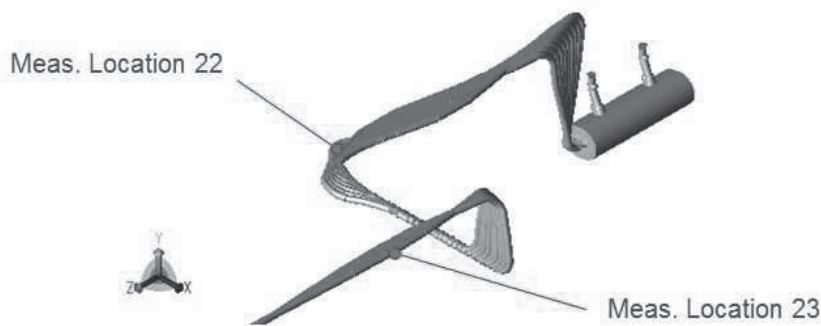


*Figure 4: Mode arising at 8 Hz if spring guide support assumed not to be restraining dynamic axial forces.*

In *Figure 5* the impact of varying the stiffness and the axial restraining capacity is shown, here it is seen how the frequency of maximum response varies as the axial stiffness is increased. In the computational model this was done by introducing the stiffness friction factor (FF). This is an arbitrary calibration factor for a dynamic system used in the following formula to create the dynamic frictional stiffness ( $K_{fric,dyna}$ ) [3]. Where  $\mu$  is the static friction coefficient at the applicable support location,  $F_{vert}$  is the vertical static load and  $\delta_{static}$  is the calculated static displacement at the support location.

$$K_{fric,dyna} = FF \cdot K_{fric,static} = FF \cdot \frac{\mu \cdot F_{vert}}{\delta_{static}}$$

The effect of varying the friction factor is to stiffen the system and the resonance frequency increases. This can be seen in the two graphs below for measurement locations 22 and 23. Here it is seen that frequency increases as the friction factor is increased. Here it is seen that increasing the friction factor (FF) to 10 means that the displacement measured at location 22 is the same as that measured. At location 23 however the situation is more complicated as increasing the resistance of the spring support to a FF of 5 provides the best match in frequency response but the displacement is lower than measured.

A further option was to review the stiffness of the guide supports. Initially as for the limit stops these were also modelled to be stiff, however calculating the stiffness of these using a shell FE model this was found to be 1.6kN/mm. As shown in *Figure 5*, applying this value at all of the guide supports means that the resonance frequency changes and now the displacement at location 23 exceeds that measured.

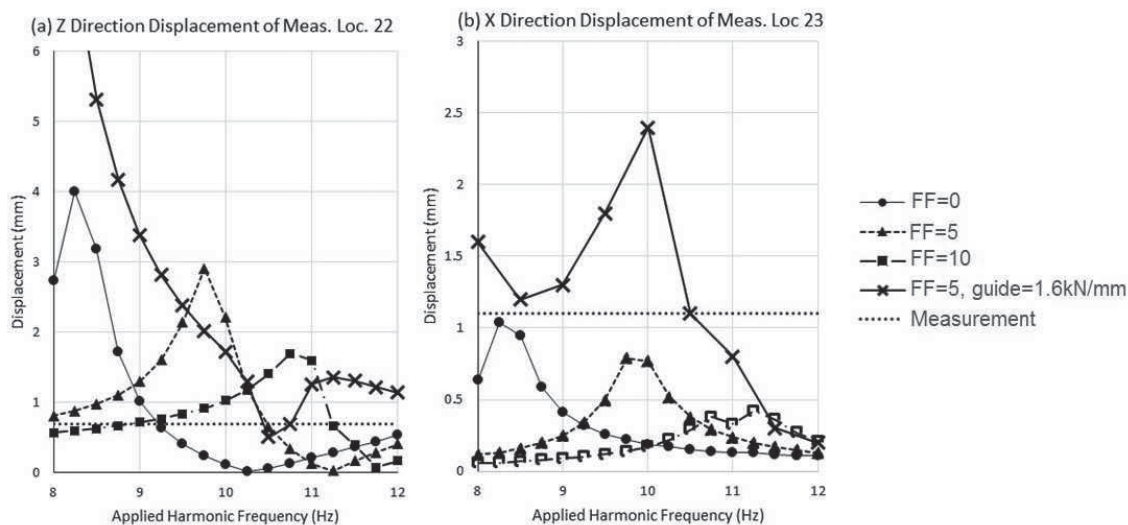


Figure 5: Displacement at measurement locations 22 and 23 for varying stiffnesses in the limit stop and guide.

### Conclusions from model 2

Here it has been shown that it is necessary to modify the support stiffnesses (rather than take them to be rigid) to obtain a best fit with the measured vibration levels. However, as for system 1 this is complicated by the fact that the unbalanced forces in the system are based on design pulsation levels. The solution offered to the client for both model 1 and model 2 was to increase the stiffness by ensuring the stiffness of the spring supports and where possible, given thermal expansion, to introduce directional anchors. The sensitivity of the system in this approach clearly justifies the criteria of API 618 to ensure that all resonance modes are above 2.4 times the compressor running speed.

### System 3: Small bore connection

Subsequent to the measurements on the header the vibration levels in the small bore lines were checked. A typical example of one of these small bore lines is shown in Figure 6(a). The small bore connection has a ND of 1/2", is gusseted to the header and has two 1500lb valves. Between the two valves it is restrained to the steel bracing by means of a U-bolt, which was taken to restrain lateral movement only. The measurement locations are shown in Figure 6. Here it is seen that the location 31 is found on the header and 32 and 33 are on the steel frame.

The amplitudes of the measured vibration for this small bore connection are shown in Table 3 for both the compressors that were in service at that time (B and S). These are the displacements recorded at 10Hz, there is also amplification between the header and the branch which indicates that a resonance mode within the branch is being excited.

### Calibrating the model

When calibrating the models for the measured vibrations what is important is the combination of the absolute amplitude and the amplification compared to the header. For instance a large amplitude on its own does not mean a large stress in the small bore connection as if it is moving in-phase with the header then no bending stress is generated. Similarly a large amplification is irrelevant if the displacement amplitudes are small. By reviewing the mechanical response when

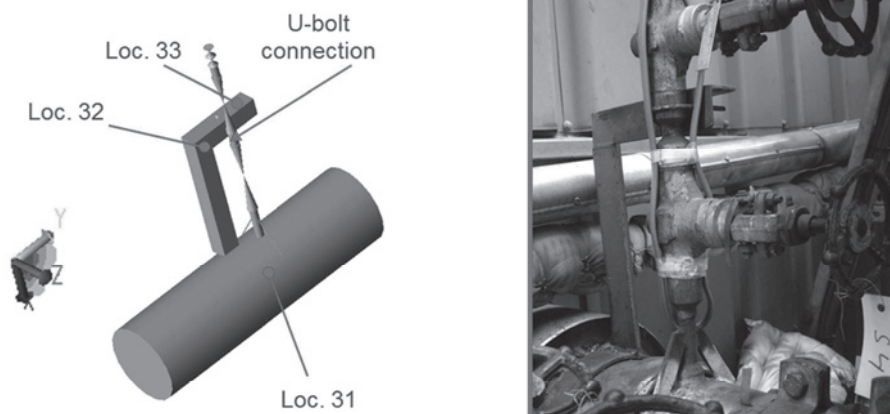
applying different frequencies in the computational analysis it was concluded that the header and branch excitations were in-phase unless the mechanical resonance frequency was exactly matched.

To determine which mechanical resonance mode was being excited the modal solver was used to determine the in-plane and out-of-plane resonance modes. These are shown in *Figure 6* (b) and (c), and both have a frequency of 31Hz, which is significantly above the response at 10Hz seen in the vibration measurements.

The resonance frequency of a branch connection is a function of  $\sqrt{k/m}$  where  $k$  is the stiffness of the branch and the mounting of the bracing on the pipe, and  $m$  is the mass of the components such as the valves in addition to the bracing and piping. To establish the effect of different parameters on the resonance frequency a number of these parameters were varied as listed here:

- Case 1: Baseline, all valve weights are as per typical information.
- Case 2: As Case 1, but with branch U-bolt assumed to work as a three way stop (also restrains axial movement).
- Case 3: As Case 1, but doubling of the weight of the valve (for example due to uncertainties such as the control equipment).
- Case 4: As Case 3 but with increased flexibility of the connection between the bracing and the run pipe, (for example due to a loose buckle).
- Case 5: As Case 4 but with the flexibility of the gusset/weld connection reduced.

(a) Measurement locations and photograph of the small bore connection



(b) Out and in-plane resonance modes

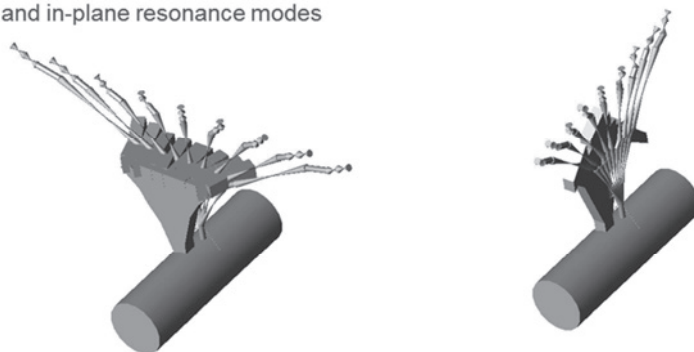


*Figure 6: Overview of System 3 with (a) measurement locations and (b) showing the resonance modes.*



Table 3: Vibration amplitudes in System 3 at 10Hz

	Frame displacement amplitude (mm)*	Increase compared to header (-)
Comp B – in plane	0.18	2.7
Comp S – in plane	0.04	11
Comp B – out of plane	0.13	1.4
Comp S – out of plane	0.28	2.0

\*Mean of points 32 and 33

The effect on the system response for a given excitation frequency is shown in *Figure 7*. In *Figure 7(a)* the response of the branch connection to in-plane amplification is shown whilst in *Figure 7(b)* the response to out-of-plane amplification is shown. The location of the maximum amplification indicates the resonance frequency. It can be seen from *Figure 7* that introducing flexibility into the branch and frame connections leads to a large reduction in the resonance frequency. The amplification for Case 5 (and for Case 4 out of plane) is now similar to that shown in Table 3 for 10Hz as it shows approximately a two-fold increase.

### Conclusions from model 3

It has been shown here how to the response at 10Hz could be matched, however it cannot be certain that this accurately models the branch at all frequencies. Given the uncertainties the choice was taken to provide a robust solution as the current vibration levels in the gusset weld toe were close to the design fatigue limit. The solution was to introduce additional in-plane bracing and additional out of plane bracing. This had the effect of increasing the resonance frequency (for Case 5) to 30Hz for both modes and thereby significantly far away from the excitation frequency.

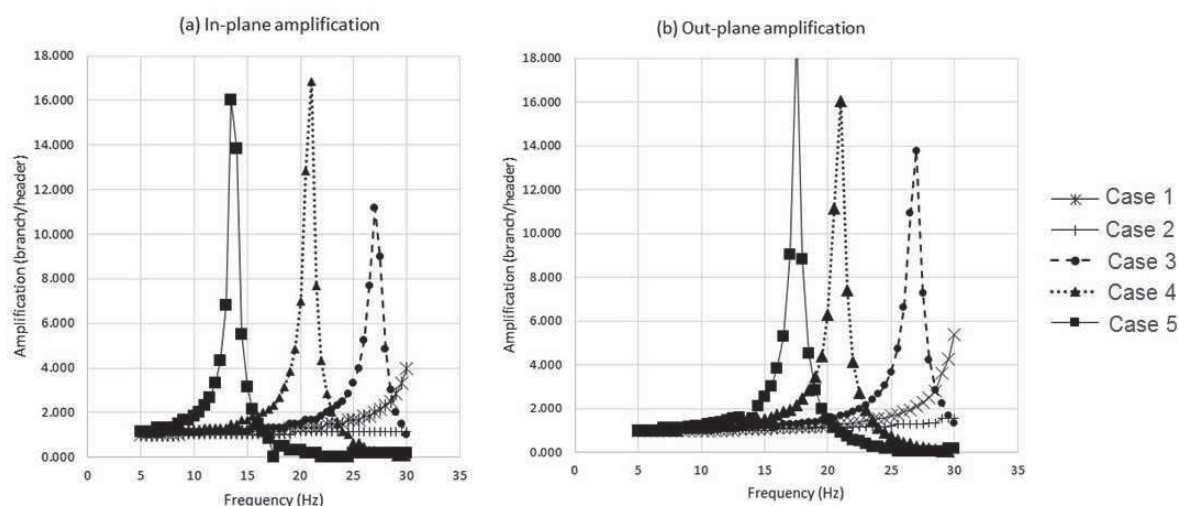


Figure 7: Effect of different factors on the resonance modes.



## Conclusions and Recommendations

As stated at the beginning of this paper the aim here is not to explain the solutions for this specific reciprocating compressor plant, but more to demonstrate and explain the factors involved in trying to match vibration measurements in the field to a computational model of the system. Of course in a perfect computational model the vibration amplitudes would match perfectly, but a perfect model relies on exact knowledge of the system, which given uncertainties including corrosion, support stiffnesses, small clearances and equipment weights is not readily available for a practical study.

A possible method to avoid this uncertainty is to take sufficient measurement points through the system. The arising modes shapes and associated stresses can then be calculated and if they are within the fatigue allowable then no further analysis is required. In this the stiffness of the supports (including the spring guide supports) are all rigid and that the measurement needs to be made at the location of maximum vibration amplitude. However as shown in this study this could lead to large stresses as the flexibility of the modelled system is significantly reduced compared to the case with some flexibility in the supports.

If the stresses are excessive or if intermediate points need to be calculated then the forces acting on the piping (due to the pulsations) should be estimated. Even if a computational pulsation study is available there is no certainty that this is an accurate representation of what is occurring in reality, as appeared partially to be the case in the analysis presented here. The measured vibration is a function of the product of the applied force and the DAF (Dynamic Amplification Factor). If the applied force is unknown then calculating the DAF and the precise mode that is being excited is not possible. This difficulty is implicitly addressed by the requirement in API 618 [2] that the mechanical resonance frequencies should be greater than 2.4 times the rotational speed of the compressor, as the DAF is minimal if there are no resonance frequencies to excite.

The question then arises how do vibration measurements assist in solving a vibration issue? In the cases shown here the DAF was not minimal as the vibration amplitudes could only be achieved if a mechanical eigenmode was excited. The methods shown here, where uncertainties in support and connection stiffnesses have been varied, provides a simple method to identify the resonance mode that has been excited. The authors note that more detailed analysis, such as Operating Deflection Shape or Mechanical Mode Shape analysis could have been possible if significantly more vibration measurements and post processing had been performed. The current method though is easier to apply and was more desirable to the operator in this instance given the explosive nature of the process fluid. The method was able to provide targeted recommendations for the operator to reduce the relative vibration levels.

## References

1. Energy Institute, "Guidelines for Avoidance of Vibration Induced Failure in Process Pipework", 2<sup>nd</sup> ed. 2008.
2. API 618 5<sup>th</sup> ed. "Reciprocating Compressors for Petroleum, Chemical and Gas Industry Service," 2007.
3. CAESAR II v 7.0 and v 4.5, Pipe Stress Analysis Software, Intergraph.
4. "Vibrations in Reciprocating Machinery and Piping Systems," Wachel J.C. and Tisen J.D. Proceedings of the 23<sup>rd</sup> Turbomachinery Symposium, 1994.
5. "Integrity Evaluation of Small Bore Connections (Branch Connections)" Harper C.B. Proceedings of the 9<sup>th</sup> EFRC Conference, Sept 2014.
6. "Is it a Mode Shape, or an Operating Deflection Shape?" Richardson, M.H. Sound & Vibration Magazine 30<sup>th</sup> Anniversary Issue, March 1997.
7. "Vibration Analysis of a Piping System Attached with Pumps and Subjected to Resonance," Shetty S.K. and Raghunandana, K. Int. J. Emerging Technology and Advanced Engineering, Vol. 4 Special Issue 9, Sept 2014.



# Technical Paper

**Session: 39-3**

**Session Name: Pulsation / Vibration 2**

## Cylinder manifold automation

**Author:**

**Marco Passeri**  
Reciprocating Compressor Consulting Engineer/Technologist  
GE Oil & Gas  
50127 Firenze, Italy

**Co-Author:**

**Riccardo Bagagli**  
Reciprocating Compressor Engineering Manager  
GE Oil & Gas  
50127 Firenze, Italy

## Summary

Machinery today must have ever-increasing performance capabilities, which also means greater compression system vibration risks.

A thorough knowledge of dampener pulsation force phenomena and related best practices is essential to significantly reduce system vibrations. While loads acting on the foundation are defined early in the process to allow a proper design, “cylinder gas loads” depend on compressor data sheet specifications and cannot be adjusted without changing requirements. Due to their high amplitudes and frequency spectrums, some exciting frequencies are more likely to coincide with the natural frequencies of the mechanical system: this can generate mechanical resonance phenomena.

For these reasons, extensive efforts are required during preliminary cylinder manifold response studies to guide compressor general arrangement (GA) design. Specific software that includes Compressor standard elements selection and that allow building dampers by parametric inputs is cost effective in model creation.

In addition to significant cost benefits, this software helps the designer to simulate multiple configurations by a quick rebuilding of the model, in order to explore several solutions and find the most suitable for vibration control.

A finite element method (FEM) specialist is not required for the model build-up, as the software allows the designer to automatically apply cylinder gas loads at the model and run the analysis. The design of the dampers must be done balancing the pulsation shaking forces so that to minimize their impact on the vibration behaviour. The software can apply also the pulsation induced forces on the dampers if they are available at the first run, otherwise these must be applied in a new run immediately after the dampers check execution.

The software then compares the results (in terms of vibrations) to the limits. If the limits are exceeded, the GA designer can easily change the inputs and run the new solution, iterating this loop until satisfactory results are achieved.

Obviously, the preliminary CMS analysis has to be repeated each time a significant mechanical modification is made at system or an operating parameter adjustment is required.

These software iterations can be quickly performed and repeated, to design dampers and supports with reduced vibration risk enhancing quality and safety.

This paper explains how the compression system layout can be optimized during the design process using this specific software, in order to avoid excessive vibrations of reciprocating compressor system.

## Nomenclature

Parameter	Symbol
Computer Aided Design	CAD
Cylinder Manifold System	CMS
Finite Element Method	FEM
General Arrangement	GA
Mechanical Natural Frequency	MNF
Revolutions per Minute	RPM



## 1. Introduction

Chemical and petrochemical applications often rely on highly efficient and flexible reciprocating compressors. Large-scale plants require equipment with greater capacities (a larger acoustic damping system) or step-less capacity control to improve system performance. Variable flow compressors, such as Reciprocating compressors, generate pulsations and vibrations that can lead to elements fatigue failure, capacity loss, and associated increased maintenance costs [3]. The cylinder manifold system is made up of the compression system and related dampers. This system represents the heart of the application, but also can be a source of severe vibrations. The preliminary cylinder manifold study must be made using the most advanced simulation methods to assure safety and reliability prior compression system and dampers manufacturing. Finally, after the final acoustic study inclusive of the whole plant system involved by the pressure pulsations, a complete CMS forced response analysis is again conducted. This study includes cylinder gas loads and pulsation induced forces on the dampers and piping around the compressor, so that any problems with the piping supports could also be adjusted. This paper describes a cost-effective procedure that can guide compressor and dampener design from the beginning of a project to avoid excessive CMS system vibrations, assure safe and smooth plant operation, and meet contract project delivery requirements. This is a fundamental target for very complex applications with several stages and many dampeners such as booster-primary low density polyethylene (LDPE) applications.

## 2. Description of the Problem

Standard compressor components are dimensioned with a stress analysis that is performed during the machine's design. This analysis defines loads and vibration limits to assure safety and operability. However, the same process cannot be used for dampeners, whose characteristics vary, depending on the specific application [3]. Additionally, dampener design requires information relevant to the piping plant system, which is usually available only in later project stages. For this reason all parts have to cooperate in order to meet the contractual delivery date, scheduling in advance the design of critical compression system components (API 618 5th Edition) [1] such as pulsation suppression devices. Theoretically, these long-term delivery components must be procured after the results of the acoustic and mechanical dynamic analysis that considers the entire scope of supply of the customer's piping plant. Because application schedules are often tight, when customers are unable to provide the necessary information quickly the project contract delivery is jeopardized. In these cases, design risks are sometimes taken in the attempt to stay on schedule. The following new design procedure significantly reduces vibration risks and limits final study CMS requirements only to the piping supports that are directly connected, without negatively impacting project schedule.

## 3. Exciting Forces

Reciprocating compressors generate different types of exciting dynamic forces that may induce high vibration levels, poor performance, noise and high risk of fatigue failures. The most significant dynamic forces are described below.

### Pressure Pulsation

Pressure pulsation harmonic components, generated by the compressor pulsating gas flow, may produce plant resonance effects when interacting with plant piping and equipment. Pressure pulsation analysis recommendations can protect plant operation by limiting their effect through a proper damping/filtering system. This study aims to determine a method that limits pulsation amplitude and consequently reduces the relevant induced forces in the compression system, connected piping, and equipment [3, 4, 5]. Shaking forces are generated by geometrical discontinuities in the dampener (e.g. a change of direction or closed end). Because it is impossible to avoid such occurrences, the only way to limit their effect is to balance the opposite forces placing the cylinder connection at the center of the dampener. For multiple cylinders, connections should be placed at the center of the chambers by the internal pipes or deviators

welded in the shell (see Fig.1). When this type of balancing approach is used, the pulsation induced forces are not critical for the project's vibration design (i.e. they can be neglected in the initial CMS verification). The same results can be achieved by baffles that divide the equipment into chambers of equal size or by internal pipe that reach the centre.

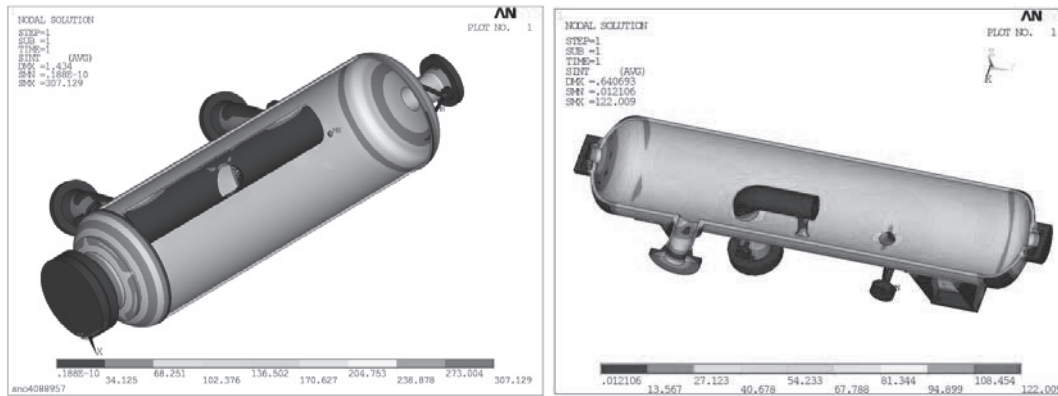


Figure 1 - Dampener of two cylinders with deviator

### Foundation Loads

Reciprocating compressors induce dynamic forces on the foundations mainly due to centrifugal forces of the rotating masses, inertia forces due to masses reciprocating motion and torque transmitted by the motor to the compressor. Compressor design strongly influences the forces and moments amplitude, so the design parameters must be carefully adjusted in order to reduce their effects. Full balance is generally not feasible – excluding special arrangements – for various reasons (such as type of crank-gear, pistons weights, etc.). As a result, unbalanced couples and forces acting on the foundations are always present. After balancing, the remaining forces and moments define foundation design. Therefore, loads acting on the foundation are known from the beginning, so the foundations can be properly designed without significant vibration risk.

### Gas Forces Due to Compression

Significant gas forces are generated by compression on cylinder internals. They depend on bore and operating pressures in the cylinder ends under various operating conditions. Being strictly dependent on the data sheet and capacity control system, they cannot be adjusted unless the requirements are changed. In theory, if the system was rigid, these forces would be balanced/reclosed on the compressor frame. In actual operation, these gas forces cause “cylinder stretch”, which can result in vibration problems. Cylinder stretch occurs as the cylinder assembly lengthens and shortens at the compressor RPM frequency. Because of cylinder gas loads’ high frequencies spectrum (5th to 10th harmonic components) and relatively large amplitudes, their frequencies may easily coincide with the MNF of the compression system, resulting in mechanical resonance phenomena. For this reason, a detailed dynamic investigation of the effects of cylinder gas loads vibration is an important early project step in guiding compressor general arrangement design. This effort involves a costly preliminary CMS analysis because study has to be repeated each time a significant system modification is made.

## 4. Project execution

To properly design the compressor GA, at the project start, it is essential to perform a preliminary dynamic analysis of compression system vibrations due to cylinder gas loads and pulsation induced forces.





### Influence of Capacity Control and Variable Speed on cylinder Gas Loads

- Step-less capacity control can produce several high exciting frequency harmonic components, in respect to standard system such as suction valve unloading.
  - Compressor variable speed results in variable exciting frequencies that can easily fall in the range of mechanical natural frequencies of the CMS.
  - Wide operating range may produce resonances conditions due to exciting forces amount.
- All above factors should be considered to limit capacity control range to the actual needs.

Knowledge of operating conditions allows identification of the “worst-case” cylinder gas loads harmonics distribution (Figure 2). By analysing the maximum loads spectrum and the conditions that produce high harmonics peaks, the designer can evaluate possible parameter adjustments (such as capacity control steps and compressor ratio distribution among the stages). This is done in an attempt to optimize harmonics distribution (by limiting the harmonic peaks). Figure 2 shows the differences in terms of frequency spectrum between two capacity control systems. Moreover this activity makes the designer aware of the forces amplitudes and frequencies.

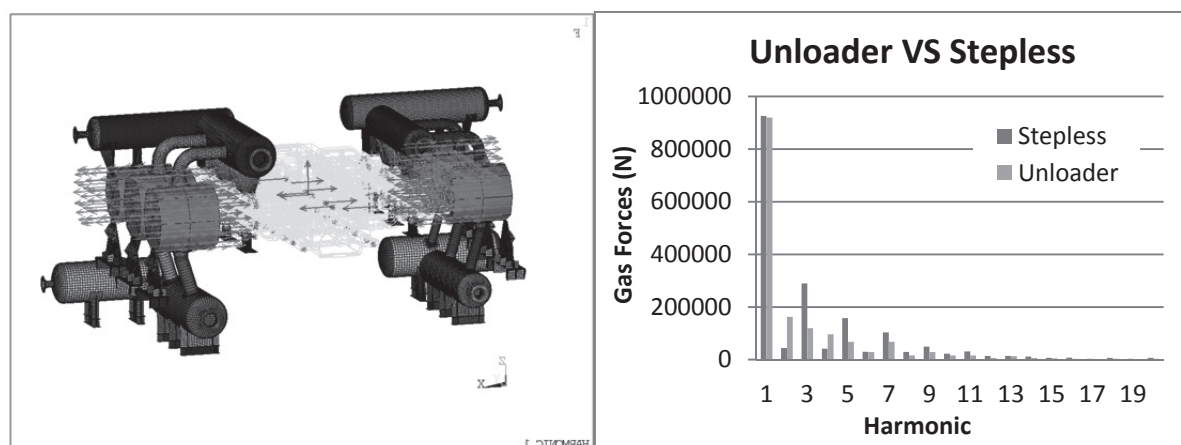


Figure 2 - Cylinder gas forces distribution depending capacity control used

### Dampener Selection

One fundamental action is the selection of the type (empty volume or filter) and size (volume and piping connections) of pulsation devices. A preliminary sizing dedicated program [6] that takes data directly from compressor simulation software calculates the volume, diameters, and length of chokes as well as the relevant pressure drop, optimizing the results for all operating conditions. These basic elements (without dampener geometry) are sized to meet API618 STD Approach 3 pulsations limits with a sufficient margin (70-80 percent of the limits according to API 618 5th edition section 7.9.4.2.3.4 “pre-study”) [1].

### Preliminary General Arrangement Design

The initial compression system and dampeners layout design (as shown in Figure 3) can be completed with sufficient accuracy to prepare a very detailed FEM by selecting compressor frame, cross-heads, cylinders, cylinder supports and dampener characteristics.

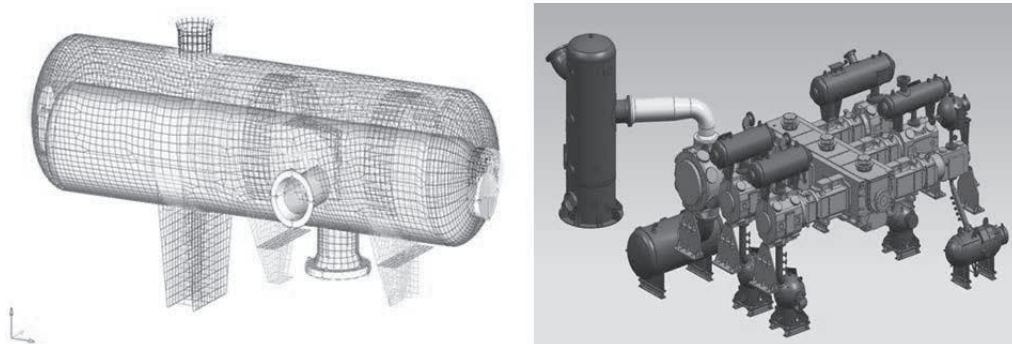


Figure 3 – Selection of damper shape and CAD of model Booster-Primary GA

To ensure that the vessel's manufacturing schedule can be met, CMS forced dynamic response studies should be performed as the project start. These analyses are necessary to verify that the vibration levels of the CMS are within the limits. The scope of preliminary studies is to drastically reduce the chances of discovering CMS problems later in the project when the schedule impact can be significantly larger. Studies must be repeated when significant changes are applied to the system during project execution. The use of specific software allows the GA designer to comply with the schedule without to be vibration or FEM expert.

The software helps the designer by:

- Perform CMS FEM build up by selecting compressor standard elements (frame, cross-heads, cylinders, cylinders supports and so on) and dampener elements by parametric input;
- Automatically apply the cylinder gas loads (resulting from compressor sizing) and pulsation induced forces (after dampers check) to the FEM model;
- Run the CMS forced response analysis (initially without the connecting piping);
- Compare the results with the vibration limits;
- Change the input data (such as the dampener shape type or related support data) when the results are above the limits and repeat the study till satisfactory results are found.

To achieve satisfactory results, GA designers should work together with vibration specialists to enhance their sensitivity to dynamic aspects for a 360° design approach.

### Finite Element Model Building

The main step in building a FEM model able to simulate the real dynamic behaviour of a CMS is to carry out an accurate structural evaluation of the system, paying special attention to components that affect dynamic behaviour. Applying suitable simplifications, it is possible to achieve an appropriate balance between accurate and quick calculations. The decision on how to best model the CMS system must be driven by these goals, so for each part of the model a specific structure element type have been selected.

The dampers are different each time, thus they need to be verified each time (usually they are the most sensitive dynamic elements). The dampers are modelled as shell elements, which are appropriate on simulating components with small thickness (e.g. parts made from plate metal). The standard parts of the compressor (frame, sliding body and distance piece) have been cyclic stresses designed in advance, in order to define loads and compressor vibration limits to assure safety and operability. These thicker elements are modelled using the super-element (see Figure 4) derived from solid elements so that to have equivalent static and dynamic behaviour. This technique allows a simplification of the frame- sliding body-distance piece model, using only a minimum set of degrees of freedom, to provide proper stiffness and mass properties at the concrete anchoring and connecting bolts (i.e. connection points between the compressor and the other parts of the system). This simplified elements structure needs minor computational effort maintaining high model accuracy, like a solid element model.



Compared to other compressor components, cylinders behave like a rigid body that is sensitive only to its mass distribution; therefore they can be treated as solid bodies. Modelling of the bolted junctions between the cylinders, distant pieces, crosshead guides, and compressor frame is fundamental to estimating the elasticity response related to connecting different components. A standardized software procedure using manufacturing drawings data (such as  $n^\circ$ , diameters, length, distribution of the bolts, and flange dimensions) can translate these junctions into the equivalent spring elements needed for a proper FEM simulation. In conclusion the chosen approach attempts to balance the required complexity to assure FEM accuracy with a model that includes all significant parts of the CMS. By limiting the computation time, the GA designer can quickly test different configurations to verify which one is the best.

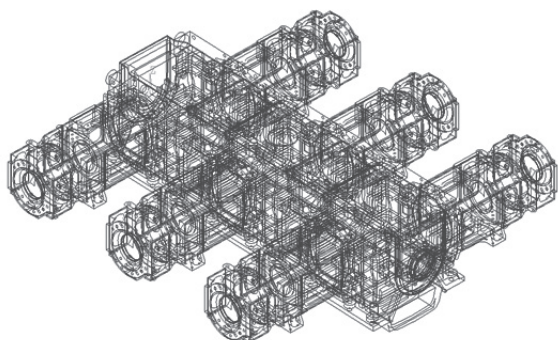


*Figure 4 – Frame Super-element simulation technique applied*

#### **Finite Element Parametric Input Selection**

The input and selection interface must allow for simple parametric input so that the user can build an accurate FEM model without to be a FEM software specialist. The creation of the FEM model is a complex task, so the software interface is divided into several parts that allow the user to select and define compressor parts, cylinder support, and dampener type (see Fig. 5).

#### **Compressor Parts Standardized Selection**

The software must include a library containing the compressor super-element models of the CMS standard parts (such as the frame, slide-body and distance piece). The user has only to select these components and insert the related dimensions using a parametric input interface.

#### **Cylinder and Support Selection**

The interface must allow the user to set the type and size dimensions of the cylinders along with the type and dimensions of the relevant supports.

#### **Dampener Type Selection**

The dimensions and support arrangement of dampeners varies by application. Standardization, based on experience, allows the selection of a limited set of shapes whose parametric models must be included in the software library. Then the user has only to select the types of dampeners used in each cylinder compressor stage.

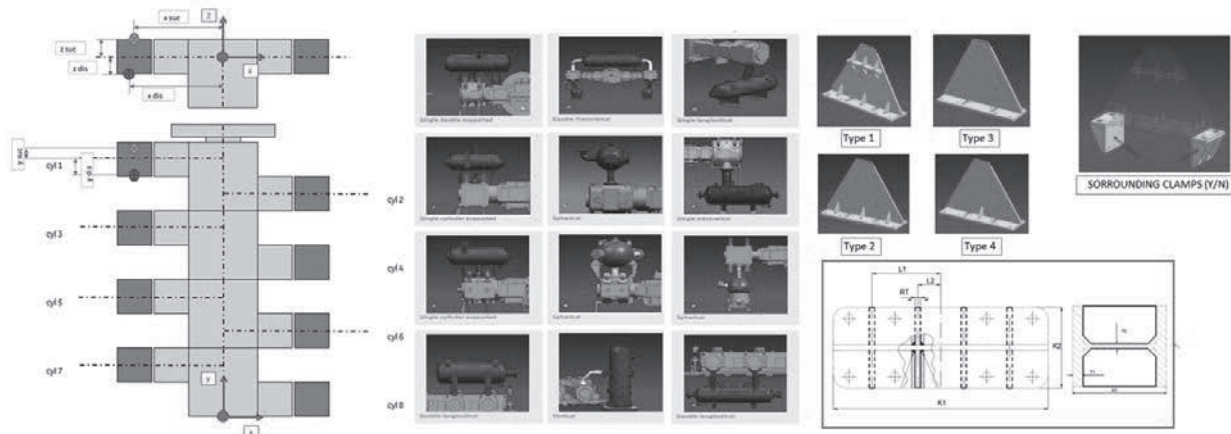


Figure 5 - Interface for general parameters

In the second part of the interface, the user inputs the dimensions of each dampener of the system. Because the dampeners are the most sensitive elements, their definitions are critical for CMS mechanical natural frequencies modal shapes and dynamic forced response. Due to the large amount of detail needed, the input of this part is the most time-consuming. For each dampener type, a specific interface allows the user to set the specific parameters. In conclusion using specific libraries that contain parametric models and super-element models, the proper simulation of each CMS component can be completed.

### Model Generation

After the parameters have been entered, the user can run the batch process to generate the FEM model (see Figure 6). The software creates several images of the model that help the user to easily verify inserted input parameters and in case apply adjustments.

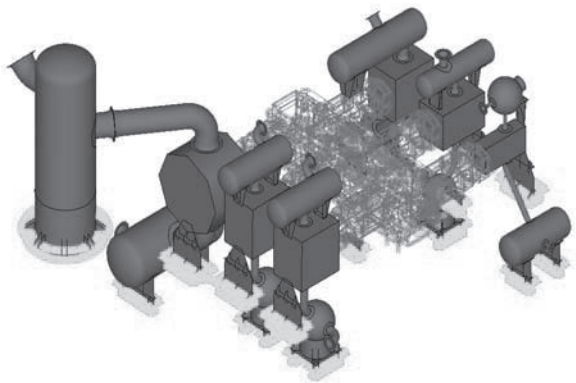


Figure 6 - FEM model built by parametric software

## 5. Software Dynamic Analysis

### Forced Response

Before performing the forced response, the software batch procedure must extract the cylinder gas loads directly from the compressor sizing program archive and automatically apply such forces on the CMS FEM model through the interface. The same can be done for the pulsation induced forces when available (i.e. the preliminary study has to be repeated after the dampers check execution). The software creates some images of the model with red arrows to indicate the applied forces. The designer can easily control the model to verify that forces have been properly applied.





Next, the forced response [3] of the system is performed for each harmonic component using the relevant cylinder gas loads (such as the pressure and phase acting on each cylinder axis) as input to calculate the relevant vibration amplitude.

The forced harmonic response is performed for each possible mechanical resonance condition. Through the Campbell diagram (which shows the correlation between mechanical natural frequencies and exciting forces harmonic frequencies) it is possible to define resonances that may occur. Usually the analysis is carried out for each harmonic, within a certain percentage variation (for instance, plus or minus 20 percent) of the nominal frequency (RPM).

An important aspect in performing a forced mechanical analysis is the evaluation of the damping coefficient, which is influenced by typical structural material and the connection between components (such as joints and gasket). Standards, piping, and compressor systems typically have damping ratios between 1 and 5 percent, and therefore have amplification factors of 10 to 50. Field experiences indicate that it is conservative to include only the structural damping of the material in the standard forced response analysis. Therefore, when possible (for instance, when measurements are available for an existing application), a damping value derived from field measurements can be used. The model used to evaluate the forced response of the system at a specific frequency is based on the uniform structural damping model; the user can either set this value or leave the 2 percent default value.

CMS forced response results produced by the batch procedure are:

- An amplitude-frequency chart (Fig.7), which shows harmonics vibrations amplitude vs limits
- Several CMS vibrations images to identify vibration locations that are outside the limits

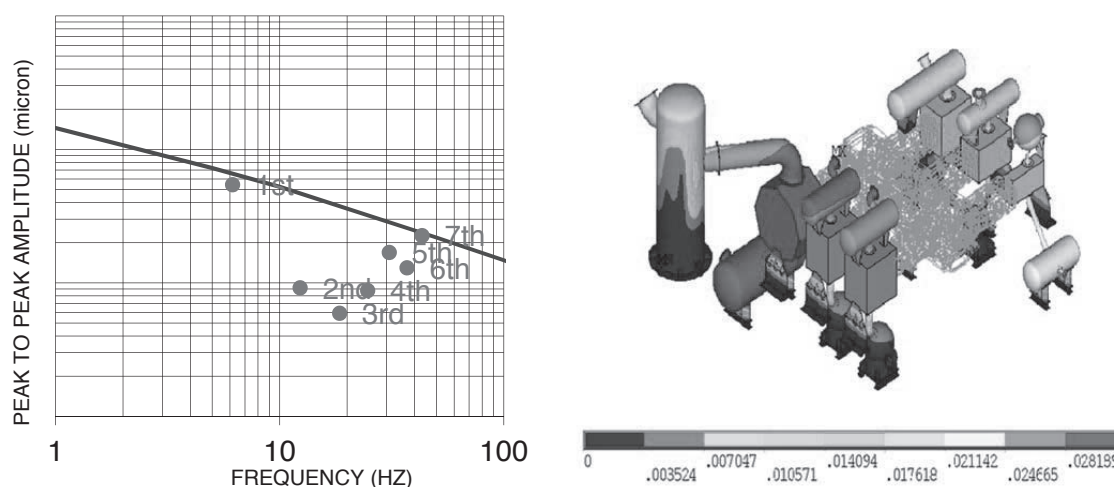


Figure 7 - Calculated vibrations vs. limits and Vibrations displacements picture

When the amplitude-frequency chart vibration identifies an exceeding of the limit, the GA designer must view all stored vibration amplitude pictures (usually 21 steps are made +/-20%) relevant to the harmonic components, to define the necessary modifications. Usually, during this phase, vibration specialist cooperation is necessary, especially for complex cases.

### Typical Modifications

The CMS vibration images highlight which components can be critically affected by vibrations. Several modifications can be applied to the system to reduce vibration levels: for example, stiffening the cylinder supports or changing the volume bottle type from single support to double supports (as shown in Figure 8).



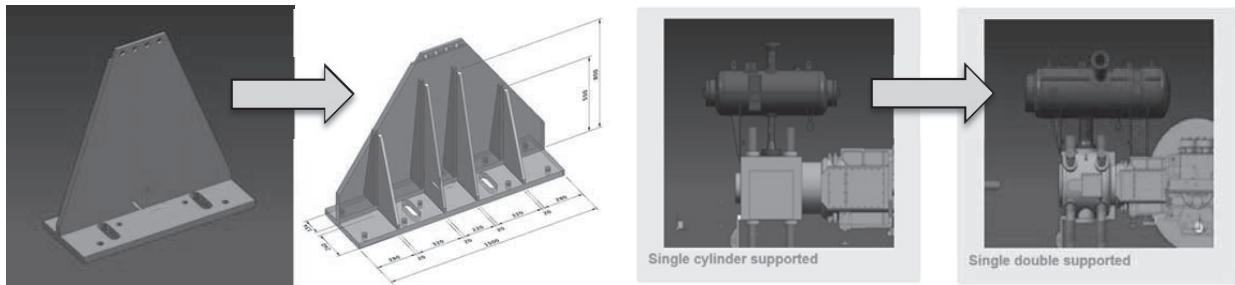


Figure 8 – typical modifications

Once the modifications are defined, the parametric input of FEM must be updated and the calculation repeated until satisfactory results are achieved. When the vibration levels are within the limits, the preliminary vibration design is completed. After the acoustical analysis is completed, the final CMS study has to include the piping immediately connected to the compression system to solve any possible issues related to piping supports.

### Dampers Check Prior to Manufacturing

Once upon the best dampers shape is selected achieving acceptable vibration levels, the next step on vibration design validation process is the damper Check. This check calculates the pulsation induced forces on the cylinders and dampers so that these forces can be applied to the FEM model and the CMS forced response verification can be repeated. Usually dampers shaking forces are not critical, if properly balanced, however this have to be confirmed by the analysis prior their fabrication.

The dampeners (including nozzle orientation and necessary internals to balance shaking forces) are subjected to a pre-study (or “bottle check”) with the piping system replaced by an infinite length (acoustically non-reflective line) to verify that the pulsation requirements are achieved with a sufficient margin (such as 70 to 80 percent of the limits as per API 618 5th ed. para 7.9.4.2.3.4). This approach usually allows satisfactory control of the acoustic resonance conditions that may be discovered during the final pulsation study. In theory, the procurement of dampeners must be done after the results of the acoustic and mechanical dynamic analysis, including analysis of the customer plant. However, because the customer may not be able to provide the necessary information in a timely manner, the described procedure is the best approach to use prior to dampener manufacturing to avoid vibration risk and keep the project on schedule.

## 6. Final acoustic and Mechanical piping Studies

### Acoustic Analysis

Verifications will take place again after the entire plant system with the final acoustic and mechanical analysis is available, and will be performed considering all possible compressor operating conditions and the capacity control range. All significant components (such as piping, cylinders, valves, orifices, dampeners, equipment) are analysed to the proper boundary points. Pressure pulsations and shaking forces acting on the components are calculated at all significant points, reduced to acceptable levels, and used as input for the mechanical studies.

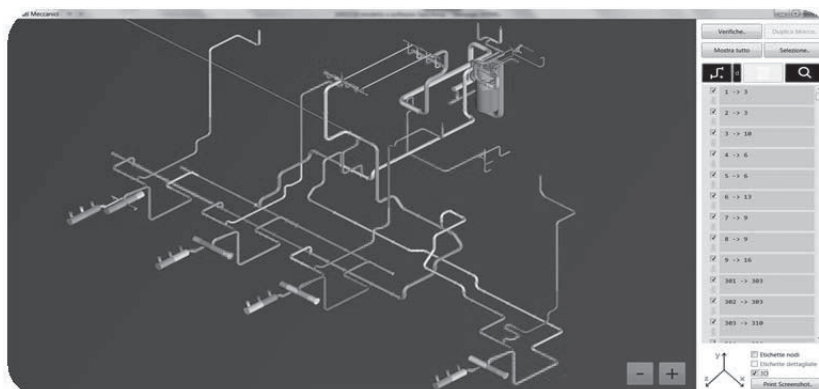


Figure 9 – Acoustic plant model 3D view

### Piping Vibrations and Cyclic Stress

The piping-induced forces (shaking forces) calculated by pressure pulsation analysis are introduced automatically as input data for the plant's final mechanical study. This study is performed by a FEM program that provides the mechanical natural frequencies, total vibration amplitudes, and relevant stresses, along with the reactions at support location.

Then, the overall forced response of the piping system is calculated using the “modal superimposition” technique as the sum of the response of each mode to the exciting harmonics, each with its module and phase [7]. Finally, the piping maximum alternate stress is calculated using the procedure explained in ASME VIII-2 appendix 5 [2]. The calculated stress is compared with the cyclic stress limit and, if needed, a combination of additional orifices and/or supports can be adopted to maintain cyclic stress within the limit.

### Final CMS Forced Response

Finally, the CMS model must be updated considering manufacturing drawings and inserting directly connected piping (generally up to the second support upstream and downstream of the dampeners). Then the forced response [3] of the CMS is repeated using as input the exciting forces resulting from the pulsation study, cylinder gas loads and foundations dynamical loads. This allows the calculation of vibration amplitudes and cyclic stresses, along with the dynamic reaction forces at the constraints.

### Results and Considerations

The forced analysis is made to determine the vibration amplitude and cyclic stress. The vibration amplitude (Figure 9) should be compared to the manufacturer vibration limit levels for the cylinder-frame-spacer block (such as alarm limits with an adequate margin). For the dampener and piping, the relevant limits are based on experience and field measurements. The cyclic stress (Figure 10) should be compared with the limits (API cyclic stress limit 180 N/mm<sup>2</sup>) [1], reduced to consider the stress concentration factors and safety factor.

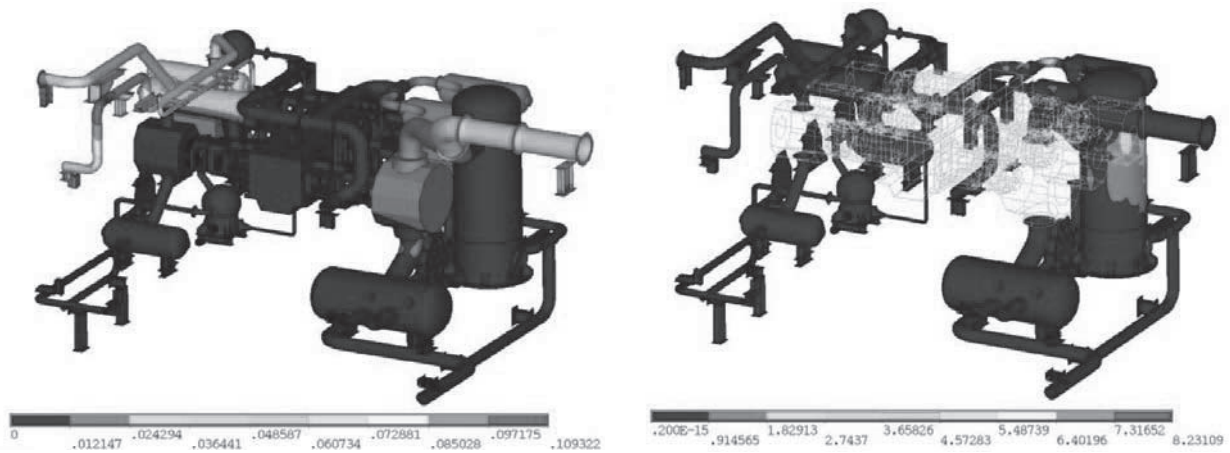


Figure 10 - Vibration displacements and relevant cyclic stress

### Typical Modifications

Several modifications can be applied to the system to reduce CMS vibration levels. However, when the described procedure is applied, the final CMS analysis made after the addition of customer piping can only identify minor piping support adjustments (such as additional piping constraints) and structures (e.g. to increase the stiffness of the bearing support structure).

## 7. Reciprocating Compressor uprating/revamping

The same tool can be used in case of compressor revamping or change of capacity step control (e.g. from suction valve unloaded to step-less). In these cases, being existing plants, it is important to define the field vibrating baseline (to be sure of the initial vibration levels and evaluate possible need of maintenance, see figure 11) so that to tune (e.g. adjust constrains) the model and properly predict the future plant vibrations once upon the plant is uprated.

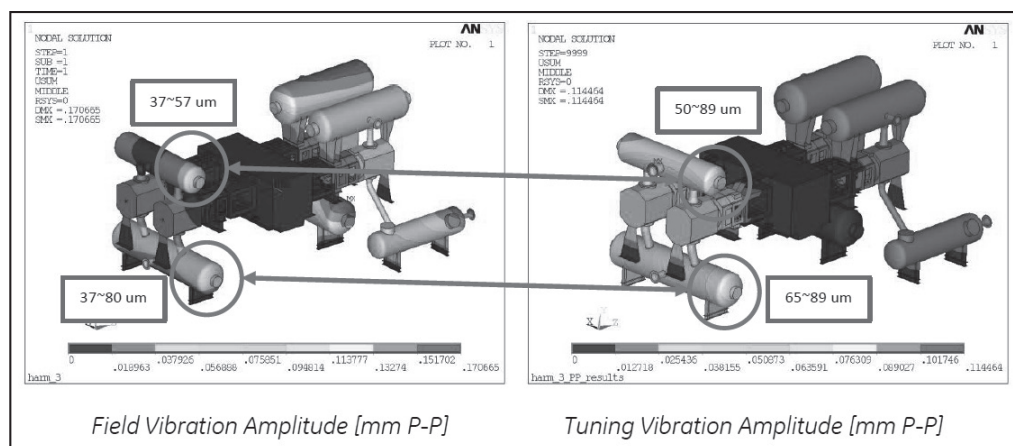


Figure 11 – Field vibrations Vibration vs model calculated values

This kind of analysis is fundamental, like the feasibility compressor checks, to verify if the compression system can properly run once the uprating is applied, can identify possible adjustments to avoid big issue are discovered on field with negative impact on production. The same tool, by an additional dedicated section, can model the skid baseplate and compressor base (see figure 12) that in case of high speed compressor are essential elements to properly predict the real vibration levels.

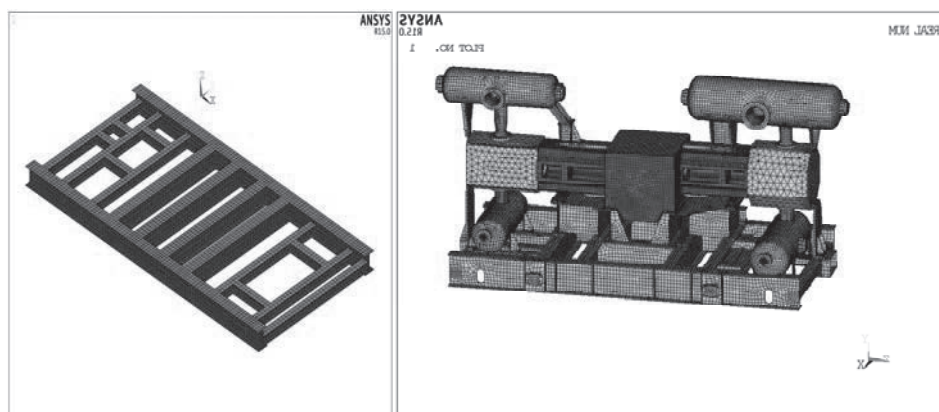


Figure 12 – Compressor baseplate - Complete model mounted on skid

## 8. Conclusions

Reciprocating compressors and systems that include associated dampeners (CMS) may be the source and location of severe vibrations. For safe and reliable operation, specific analyses are necessary to properly design CMS components from the beginning of the project to avoid major modifications that could jeopardize the delivery date or be discovered when the system is manufactured. By using best practices related to pulsation-induced force phenomena, the system vibrations can be reduced significantly.

Loads acting on the foundation are known from the beginning; therefore adequate foundations can be easily designed.

Depending on compressor data sheet and capacity control specifications, cylinder gas loads may not be able to be significantly modified unless changes are made to the requirements. Considering their amplitudes and frequencies spectrum, they easily can generate mechanical resonance phenomena.

For this reason, it is essential to use specific software based on an FEM archive of compressor standard elements. The software can complete the CMS FEM by a parametric input of standardized dampener types. To be effectively used by a GA designer who is not a vibration specialist, the software input and selection interface must allow for a straight-forward input procedure to create the FEM model. Finally, the software must automatically apply the cylinder gas loads resulting from compressor sizing (after dampers check also the pulsation induced forces can be applied), quickly run the CMS forced response, and then compare the results to the limits. This procedure must be repeated if changes are applied at the CMS prior to manufacturing.

Later in the project, after the acoustic study is complete, an analysis of the CMS (including the piping around the compressor and pressure pulsation induced forces) must be repeated.

By applying the process as described, the final studies will only require minor modifications on piping supports and their bearing structures, without impacting the project delivery schedule. In addition, the process allows for controllable project costs, reduced vibration risks, and safe, smooth compressor operation.

If, instead, the CMS response study is used only for final verification, the project may be exposed to significant vibration risks. While this latter approach is less costly, the associated risks should be carefully evaluated.



## References

- [1] API 618 STD 5th edition, Reciprocating Compressor for Petroleum, Chemical and gas Industry services American Petroleum Institute.
- [2] ASME - Boiler and Pressure Vessel code, sect. VIII DIV. 2 2001, The American Society of Mechanical Engineers.
- [3] Passeri M., Generosi S.: Cylinder Manifold forced, 7th Conference of the EFRC October 21th / 22th, 2010, Florence, Italy
- [4] Giacomelli E., Passeri M., Giusti S., Zagli F., Generosi S.: Modeling of Pressure Pulsations for Reciprocating Compressors and Interaction with Mechanical System, Proceedings of ESDA, Eng. System Design and Analysis, 19-22 July, 2004, Manchester, UK, The American Society of Mechanical Engineers.
- [5] Giacomelli E., Passeri M., Romiti M., Generosi S.: Forced Response of cylinder manifold for Reciprocating Compressors applications, proceedings of ESDA 2006: Eng. Sys. Design Analysis 4-7 July 2006
- [6] Giacomelli E., Passeri M., Battagli P., Euzzor M.: Pressure Vessel Design For Reciprocating Compressors Applied in Refinery and Petrochemical Plants - PVP2005-71292, Proceedings of PVP conference 2005, Pressure Vessel and Piping July 17-21, 2005, Denver, Colorado, USA The American Society of Mechanical Engineers.
- [7] Passeri M., Generosi S., Bagagli R., Carmelo M.: Preliminary piping sizing and pressure pulsation evaluation, Proceedings of ASME PVP 2014 Pressure Vessels & Piping Conference PVP 2014 July 20-24, 2014, Anaheim, California, USA
- [8] Passeri M, Bagagli R, Carmelo M.: Compressor general arrangement design guided by cylinder manifold forced response, Proceedings of ASME PVP 2015 Pressure Vessels & Piping Conference PVP 2015 July 19-23, 2015, Boston, Massachusetts, USA
- [9] A. Eijk: Cost-effective and detailed Modelling of Compressor Manifold Vibrations, ASME Pressure Vessels and Piping Conference 21-26 July, 1996, Montreal, Canada
- [10] A. Eijk: Economic benefits of CAD models for compressor manifold vibration analysis according to API 618, 3rd EFRC Conference 27-28 March, 2003, Vienna





# Technical Paper

**Session: 40-1**

**Session Name: New Concept**

## **Experimental and numerical investigation of the heat transfer inside a hollow piston rod**

**Author:**

**Konrad Klotsche**  
**TU Dresden**

**Research associate, Bitzer-Professur für Kälte-, Kryo- und Kompressorentechnik**  
**01062 Dresden, Germany**

**Co-Author 1:**

**Christiane Thomas**

**Postdoctoral researcher, Bitzer-Professur für Kälte-, Kryo- und Kompressorentechnik**  
**TU Dresden**  
**01062 Dresden, Germany**

**Co-Author 2:**

**Ullrich Hesse**

**Professor, Bitzer-Professur für Kälte-, Kryo- und Kompressorentechnik**  
**TU Dresden**  
**01062 Dresden, Germany**

## Summary

The temperature inside the working chamber of a reciprocating piston compressor and its temporal behavior influences the efficiency of the compression process. In addition, for non-lubricated compressors it has been shown that there is also a relation between the temperature in the sliding zone and the wear of the piston rod sealing elements. Thus, the lifetime of the sealing elements and their sealing performance are affected. For all three effects the behavior can be improved if the prevailing temperatures are reduced. One opportunity to positively influence the mentioned aspects is to reduce the temperatures of the adjacent components, for instance the piston and the piston rod, by an enhanced component cooling.

Here, the approach for this is that the piston rod and / or the piston are designed with an internal cavity to contain a fluid. The oscillating translational motion of these components can be used to accelerate the fluid and thus to transfer heat by the fluid movement from hot regions in the area of the cylinder to the colder usually oil-lubricated crosshead. Due to the high operating frequency of such compressors the heat transfer capability of the piston rod and the piston can be increased significantly with respect to conventional solid material designs of these components.

Among other factors the heat transfer of the cooling technology depends on the filling fluid and the volume ratio of the liquid and gas phases. To improve the heat transfer inside the piston rod both influencing factors are investigated experimentally on a test rig. The test rig comprises a vertically oscillating hollow rod which is heated at its upper end and cooled at the lower end. Additionally, both the heat input and the temperature of the cold end can be varied. Using temperature measurements at relevant points of the test rig the quasi-stationary thermal behavior of the test rig and in particular of the fluid can be investigated at various speeds.

The results are presented and the influences of the two varied parameters regarding the filling fluid are discussed. In order to compare different test rig configurations by means of a generalized parameter the results can be reduced to the axial heat flux of the internal cavity. For this purpose the temperature field of the test rig is reproduced using a numerical simulation based on the finite element method and the achieved axial heat fluxes can be shown. Based on the resulting values the heat transfer capability of the prescribed cooling technology can be predicted and the benefits for the compression process can be derived.



## Introduction

When there is a demand for oil-free compression typically dry-running reciprocating piston compressors are used. The applied sealing elements are usually made of polymer composite materials which do not require an additional lubricant, offering economic and environmental benefits. In this field not only a growing research but also an increasing utilization can be observed over the last decades<sup>1,2,3,4</sup>.

Especially for higher flow rates the advantages of crosshead-based compressor designs are typically preferred, requiring a sealing at the piston rod – the so-called packing – in order to minimize the leakage to the environment. Due to the lack of lubrication the mechanical and thermal stress of the sealing elements are significantly higher compared to oil-lubricated designs. Hence, on the one hand friction increases and on the other hand the omitted lubricant reduces the heat rejection. This leads to higher temperatures and to an increased wear of the sealing elements. As a result the service life of the sealing elements is reduced and the operating costs of the compressor increase.

According to Kriegel<sup>1</sup> the temperature in the contact zone between the non-lubricated sealing and the counter surface is crucial to the wear rate of the polymer sealing elements. Their attrition increases with increasing temperature hence their cooling is expedient.

Up to the present a coolant circuit provided in the housing of the packing is often applied for the rejection of heat<sup>3</sup>. However, such an external packing cooling shows several drawbacks in terms of additional constructional and operating means giving rise to higher investment and operating costs. In addition, the risk of blockage of the coolant ducts as well as leakage of coolant is well-known.

Based on these circumstances a different cooling approach was created for which a coolant is poured into an internal cavity of the piston rod. The hereafter presented investigations and related results firstly show the influence of the filling fluid on the heat transfer of a reciprocating cooling cavity. Subsequently, the impact of the quantity is examined for the most suitable fluid.

## Internal Cooling Concept for Reciprocating Compressors

The idea of an internal cooling of the piston rod for reciprocating piston compressors was firstly delineated and patented by Quack and Nickl<sup>5</sup> in 2007. The following section gives an overview of the principle of operation and the latest state of the internal cooling concept as well as the consequential motivation for this publication.

### *Principle of Operation*

The aim of the internal cooling concept is to extract heat from areas that need to be cooled, for instance the packing and the cylinder area, by a filling coolant, transport it through a hollow piston rod and transfer it to the oil-lubricated crosshead (see Figure 1).

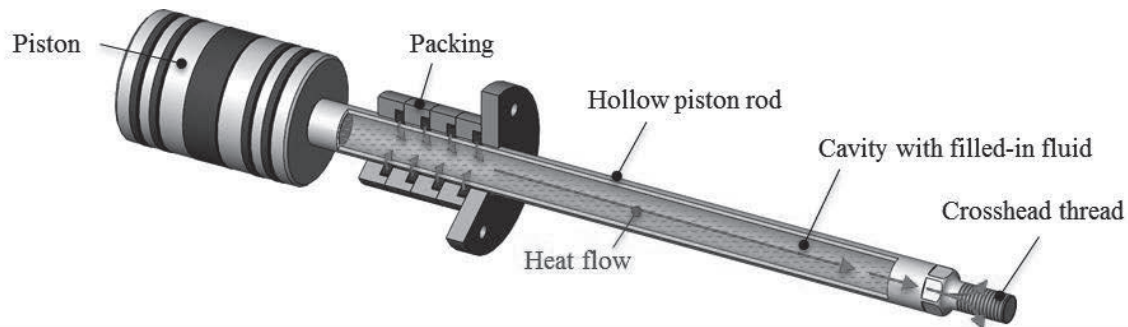


Figure 1: Design and principle of operation of the internal piston rod cooling concept

Although the thermodynamic drive is given by the temperature gradient, the main idea and benefit of this cooling technology is to utilize the reciprocating motion of the piston rod causing an enhanced fluid flow inside the piston rod cavity. In this way the fluid absorbs heat by flowing through warmer regions and carries it to colder areas where it is finally released. Here the typical high working frequency of the compressor enables an enhanced heat transfer through the piston rod and an increased cooling of high temperature compressor parts compared to conventional solid piston rods.

### Previous Work and Results

Since the first reference of the described idea several experimental and theoretical studies were conducted focusing on its feasibility and general applicability. Hammer et al.<sup>6</sup> measured a significant cooling effect at a test rig with a vertical oriented oscillating hollow rod induced by internal cooling of the rod. In addition, results were presented indicating the possibility to model the heat transfer processes inside the rod's cavity by means of a Finite Element (FE) simulation. In 2013 Thomas<sup>4</sup> presented extensive results from both experimental and theoretical investigations which show the effectiveness of the internal cooling at three different test rigs, including a single-stage double-acting balanced-opposed compressor. Making use of the internal piston rod cooling the measured gas and solid body temperatures inside the packing of this compressor could be reduced by up to 70 K. In addition, the sealing quality could be improved by reducing the temperatures in the sealing gap.

Comparable approaches in terms of an enclosed internal cooling cavity supported by a reciprocating motion can be found in the sector of combustion engines, for instance the cooling of engine valves<sup>7</sup> and the heat transfer from the piston to the crankcase oil via heat pipes molded into the piston<sup>8</sup>. Unfortunately, different scales impede the transfer of these results to dry-running compressor piston rods.



## **Open Tasks**

Since the feasibility and effectiveness of the internal piston rod cooling has been demonstrated the next target is to optimize the heat transfer. A variety of parameters, influencing the heat transfer of the discussed cooling technology, allow for more detailed investigations. The results of these investigations are the basis to enhance the heat transfer capability. These parameters are

- the fluid itself and its charge,
- the cross section (shape, size) of the cavity,
- the kinematics of the crank drive (speed, stroke),
- the orientation relative to gravity,
- the temperature difference between the heat source and sink, and
- the heat quantity to be transferred

as well as other thermal resistances.

Two of the most significant influences are the kind of the filling fluid that transfers the heat and its quantity which leads to the volume ratio of the liquid and gas phases. In order to find the optimum filling for a maximized heat transfer experimental investigations are conducted with a variety of fluids and with different charges.

## **Test Rig and Experimental Investigations**

At present the theoretical examination of the fluid flow by CFD seems not expedient since the transient and turbulent processes in the shaken-up cavity can't be simulated by reasonable effort. In contrast, an experimental approach is less complicated and more appropriate at the moment. Hence, the general construction of the used test rig and the obtained results are shown in this section.

### **Test Rig Setup**

For the experimental investigation of the heat transfer inside a reciprocating hollow rod a test rig is available at the Technische Universität Dresden (see Figure 2). It comprises a vertically reciprocating hollow rod actuated by a crank drive that is driven by an electric motor. The stroke is 100 mm and the length of the connecting rod is 250 mm. The rod is mounted onto a temperature-controlled crosshead. It comprises a cooling duct connected to an external cooling circuit providing the entire heat to be completely rejected at the rod's lower end, i. e. the temperature at this location can be held constant for all operation points. At the upper end of the rod a cylindrically shaped electrical heater is installed to provide a defined heat input and the rod is closed by an end cap. All relevant components except the crosshead are insulated against the ambient environment to guide the majority of the heat input through the rod and the filling fluid. In order to connect any electrical signals to the measurement system and to guide the crosshead coolant from the test rig to the cooling unit of the laboratory an energy chain is attached to the rod's cap.



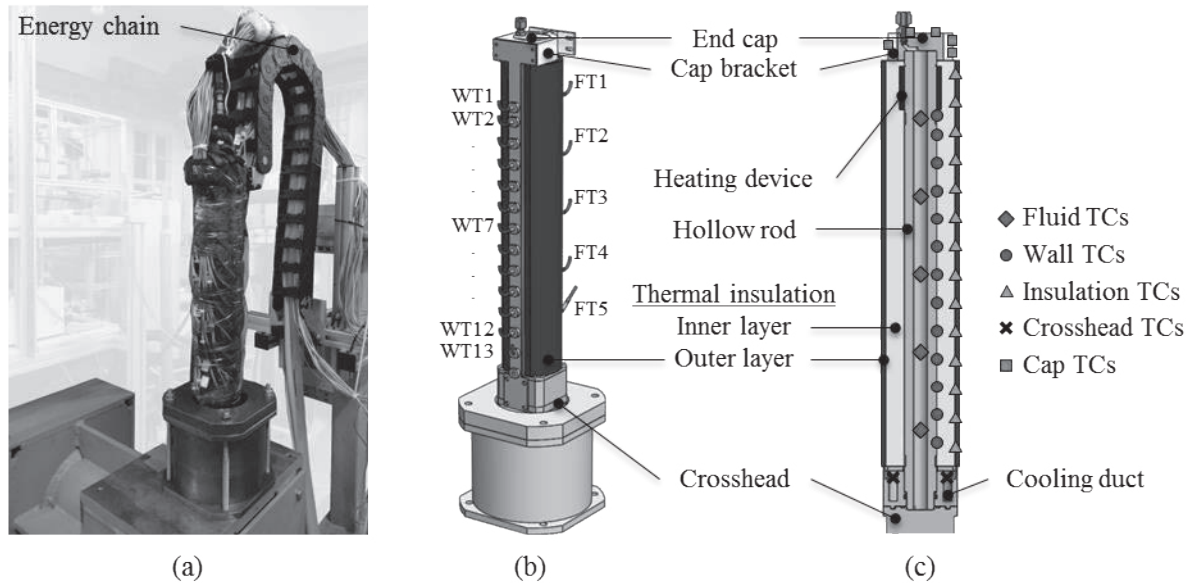


Figure 2: Setup of the test rig (a), CAD representation (b) and sectional view with installed thermocouples (c)

To accurately record the temperature fields of the relevant components 39 type K thermocouples (TCs) are installed whose signals are sampled by 1 Hz. Their locations can be seen in Figure 2 (c). Five TCs (FT1...FT5), positioned inside the cavity are distributed along the rod's axis measuring the fluid temperature. Thirteen temperature sensors are positioned 2 mm below the rod's external radial surface capturing the wall temperature (WT1...WT13). They are distributed along the rod's length similar to the fluid TCs. For the benefit of the thermal simulation of the experiments and therefore required boundary conditions two TCs are located at the rod's cap and 3 TCs at the lateral surface of the cap bracket as well as 2 TCs inside the cooling duct of the crosshead. The rod is equipped with two insulation layers. Fourteen TCs within the insulation layers measure the temperature along the rod's axis. A first setup of the facility exhibited only one layer and the boundary condition at its outer surface was a convective heat transfer which is rather difficult to specify<sup>6</sup>. The TCs at the insulation are now utilized to provide the temperatures as boundary condition for the numerical simulation which is more accurate than the previous setup.

### Measurement Procedure

At first the fluid to be investigated is poured into the cavity and the hollow rod is closed. This results in a coolant-air mixture at ambient conditions. Then the rotational speed (in this study only  $600 \text{ min}^{-1}$  are presented) is adjusted and the flow through the crosshead's cooling circuit as well as the power supply of the heater is switched on. After a transient period in which the temperatures are converging towards a steady state the following interval is used to record the final temperatures which are averaged over 5 minutes. In this way long term transient phenomena are excluded. All measurements are carried out under laboratory conditions ensuring the ambient temperature to be sufficiently constant over time.

The power input of the heating device ( $P = 70 \text{ W}$ ) and the temperature of the crosshead coolant ( $t_c = 10.3 \text{ }^\circ\text{C}$ ) were held constant for all measurements. Hence, the boundary conditions are consistent in terms of the heat sink and source. For all experiments the same rod was used which has a rod's length to inner diameter ratio of 20. Thus, all measurements are sufficiently comparable.



### Measurement Series I – “Fluids”

Since information on reciprocating heat transfer devices and on related fluids is scarce the thermodynamic suitability of the fluid is derived from the heat pipe and thermosiphon literature. In this area the so called merit numbers for heat pipes as well as for thermosiphons (see<sup>9</sup> for details) are used to determine the general heat transfer ability of different fluids in the assumed application range of 40 °C to 80 °C. Some fluids that actually appeared appropriate with respect to the merit numbers had to be excluded due to pressure or safety restrictions or because of their unsuitable critical point. One advantage in terms of filling and handling is that the normal boiling point is above the ambient temperature. Finally, for a first test series five different fluids were chosen according to aforementioned considerations (see table 1 for fluid classification). For the experimental comparison of the fluids a volume ratio of liquid to gas of 11.1 % was used for all test cases.

	Test case				
	A	B	C	D	E
Fluid classification	Natural coolant	Alcohol	Alcohol	Aromatic hydrocarbon	Saturated hydrocarbon

Table 1: Classification of fluids used within the measurement series

Since this paper aims at determining the heat transfer capability of the fluid, only the temporal behavior of the fluid temperature of the measurement’s last six minutes is shown (see Figure 3).

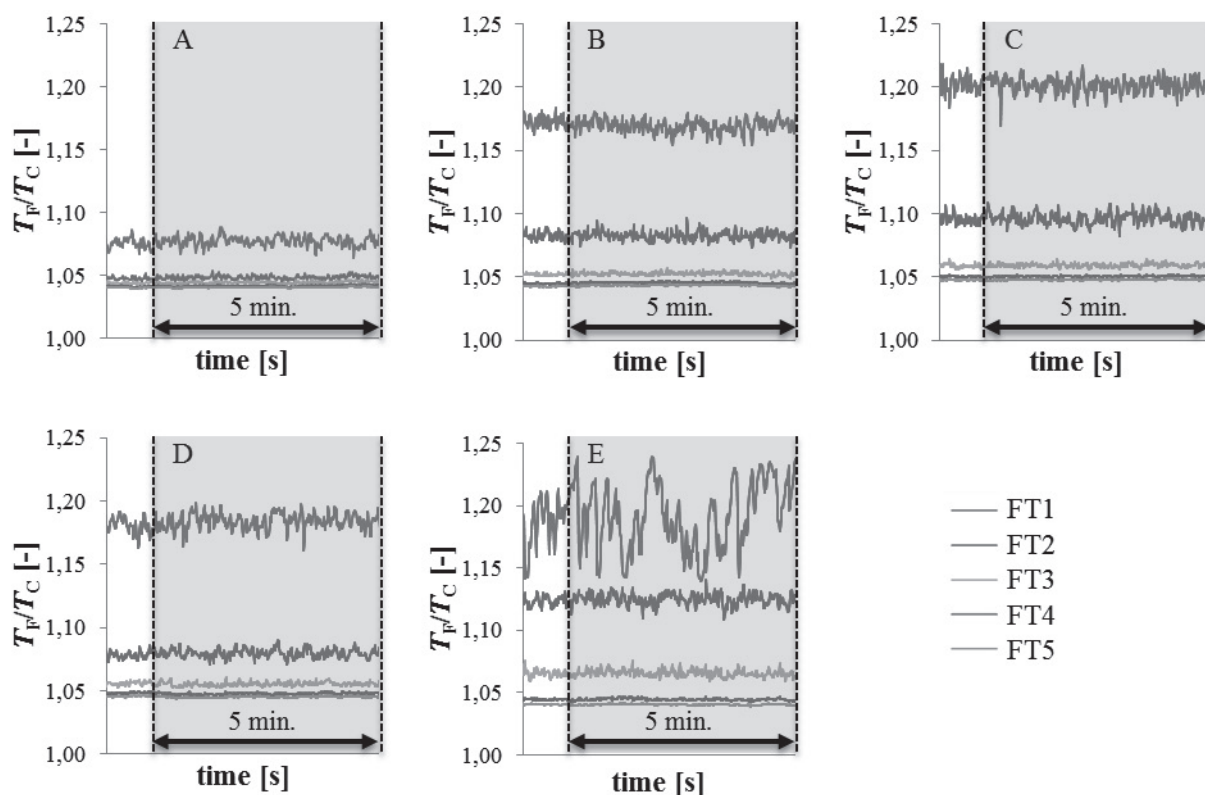


Figure 3: Fluid temperatures from the evaluation period (highlighted gray) for all five test cases

It can be seen that the temperature distribution along the rod differs from one fluid to another. So the chosen heat input for the measurements are appropriate to distinguish the thermal behavior. In particular, the upper fluid thermocouples allow for confirming the best heat transfer as it can be seen for test case A with the lowest temperatures. This test case also shows the most stable conditions in the upper part of the cavity affirming a better cooling. The temperatures of the alcohols and of the aromatic hydrocarbon show a similar performance and appear clearly higher than in test case A for the upper thermocouples. Furthermore, the fluctuations of their FT1 and FT2 signals are a little bit more significant than for test case A. Therefore, the heat transfer in these cases is inferior to test case A. Test case E shows even worse cooling conditions. Here, the temperature distribution along the rod is the highest indicating the lowest heat transfer with this configuration. Additionally, the sensor FT1 is subjected to the highest fluctuations by far.

The measured values of both the fluid and the wall temperatures can be averaged over the steady-state period (highlighted gray in Figure 3). Thereby, the thermal gradient along the rod represents the heat transfer capability according to one-dimensional Fourier's law:

$$\hat{q}_z = -\lambda \frac{dt}{dz}$$

The mean values of the fluid and wall temperatures for the five test cases are presented in Figure 4.

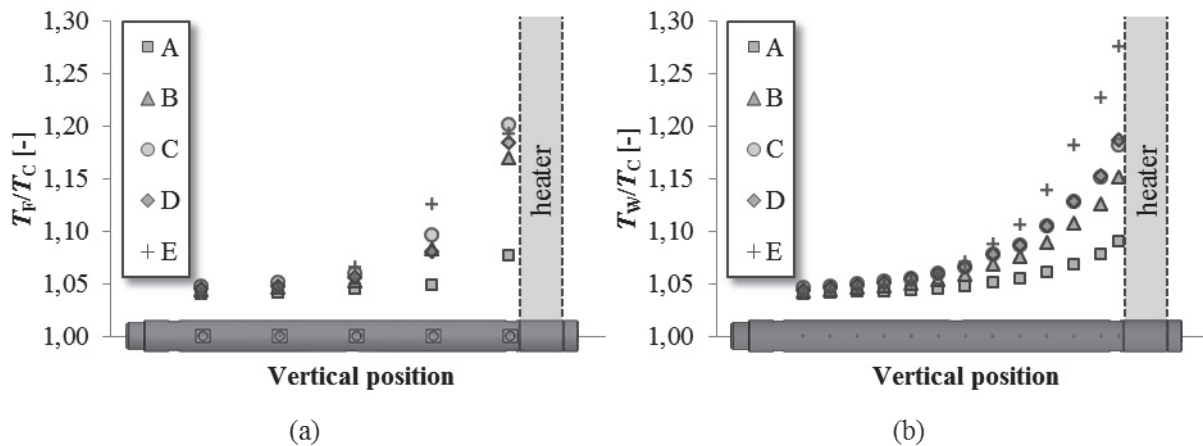


Figure 4: Averaged fluid (a) and wall temperatures (b) from the evaluation period of the measurement series I

As it is indicated in Figure 4 the fluid of test case A exhibits the best heat transfer between the upper and lower end of the rod and therefore leads to the most advantageous cooling. The temperatures exponentially ascend with increasing height. Since the TCs are equally spaced along the rod the influence of gravity cannot be neglected for the heat transfer in a vertical moving internally cooled reciprocating piston rod even at  $600 \text{ min}^{-1}$ . Interestingly, comparable fluid temperatures of the uppermost thermocouple for the test cases C, D, and E do not lead to comparable temperatures at the rod's wall in this region. Here, the upper wall TCs of test case E show higher values than C and D. Hence, the heat transfer between the fluid and the wall at this height appears significantly lower for test case E in comparison to C and D.



### Measurement Series II – “Liquid Filling Volume”

Based on the results of the test series for different fluids the most promising fluid (test case A) was chosen for the second measurement series to find the optimal liquid to gas volume ratio for an optimal axial heat transfer. The measurements were conducted in the same way as the first measurement series and with the same boundary conditions.

To achieve a good coverage of the possible range of liquid to gas volume ratios 5 measurements were taken with different liquid volume fractions. Table 2 summarizes the used volume fractions of the liquid normalized by the volume fraction of test case V.

Parameter	Symbol	Unit	Test case				
			V	W	X	Y	Z
Normalized liquid volume fraction	$\lambda_{liq}/\lambda_{liq, \text{test case V}}$	[-]	1.0	2.0	3.0	4.0	5.0

Table 2: Normalized liquid to gas volume fractions for the test cases of measurement series II

As shown for the measurement series I the recorded temperatures for different liquid volume fractions are averaged over 5 minutes at the end of a measurement when the test rig is in a thermodynamic steady-state condition. These mean values for the fluid and for the wall TCs are shown in Figure 5. It can be seen that test case X offers the best heat transfer leading to both the lowest fluid and wall temperatures. Moreover, this test case seems to represent the global maximum of axial heat transfer since the increase of quantity of liquid from test case V to W and further from W to X improves the cooling indicated in particular for the upper wall TCs. However, a further increase of liquid volume – as can be grasped by comparison of test case X, Y, and Z – is detrimental to the heat transfer.

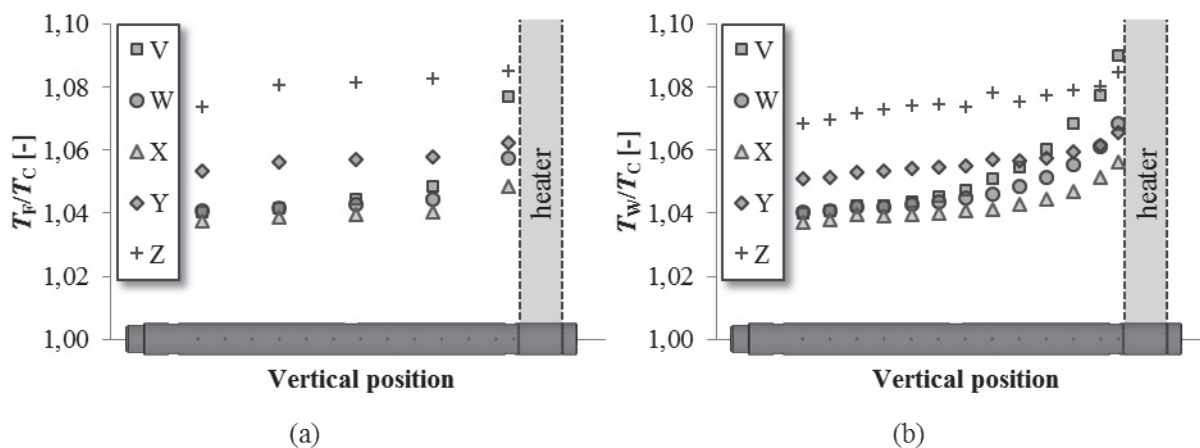


Figure 5: Averaged fluid (a) and wall temperatures (b) from the evaluation period of the measurement series II

Presumably two contrary effects occur: if the quantity of liquid is too small, not enough heat can be absorbed at the upper part of the rod (test cases V and W). However, if the liquid amount is too high, the lower end of the rod is blocked by liquid and the mixing in this area is reduced (test cases Y and Z).

## Test Rig Temperature Field Simulation

The experimental results presented in the previous sections allow a qualitative evaluation of the axial heat transfer capability of reciprocating hollow rods depending on the kind of the filling fluid and its quantity. To estimate the axial heat flux inside the cavity, the recorded temperatures can be used to simulate the temperature distribution of the relevant parts. Therefore, the following section introduces the developed simulation model and the related assumptions as well as the resulting axial heat fluxes.

### Structure and Conception of the Simulation Model

For calculating the thermal distribution of the test rig a steady-state thermal simulation is used which is based on the finite element method. This simulation model consists only of solid elements. By this, the fluid's thermal behavior (and not its flow characteristics) is represented by an equivalent thermal conductivity. Since most of the test rig components are nearly axially rotationally symmetric, the three-dimensional construction is transferred into a two-dimensional model (see Figure 6). Moreover, the domain to be calculated is demarcated to an essential extension. This means, that some parts of the insulation as well as the lower part of the crosshead were not adopted to the simulation model.

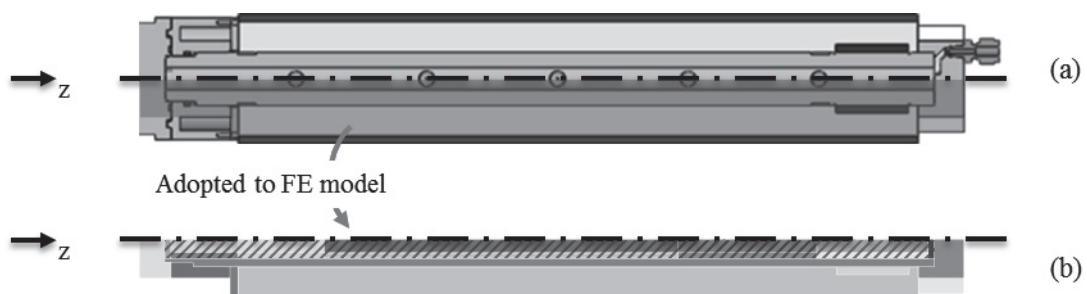


Figure 6: 2D CAD model (a) and derived simplifying FE model (b) with striped areas representing the cavity

As shown in Figure 6 (b) the area of the filled cavity (highlighted striped) is divided into several parts taking into account different behaviors of the heat transfer. According to different temperature gradients and corresponding to the design of the test rig this area is separated in axial direction. Additionally, these sub-areas are segmented into one part close to the rod's wall and a second internal part, resulting in 12 areas representing the filling.

After meshing the model with reasonable accuracy (for details see<sup>10</sup>) all boundary conditions (temperature specifications and rotational symmetry) provided by the measurements (see Figure 2) and the thermal conductivity of all parts of the model except the fluid's one were predefined. Additionally, the heat input is specified as heat generation rate for the cross sectional area of the heating device. Then, the only unknown influence is the thermal behavior, i. e. the thermal conductivities of the filling areas. The idea here is to find a thermal behavior of the modelled filling that corresponds to the fluid's one in the experiments and is done by an iterative procedure. In order to check this correspondence the calculated temperature field is compared to the measured fluid and wall temperatures shown in Figure 4 and 5. The result of such a comparison for test case A is presented in Figure 7.



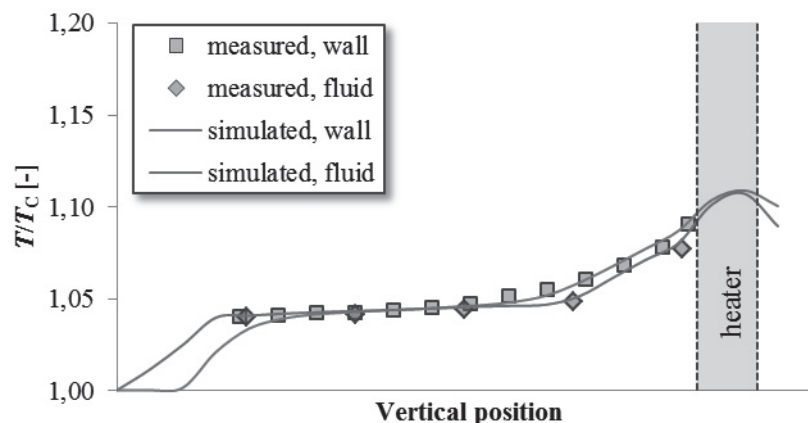


Figure 7: Measured and simulated steady-state temperatures of test case A

A sufficiently good correspondence between the measured and simulated fluid and wall temperatures can be seen in Figure 7. Hence, the assumed equivalent thermal conductivities of the simulated filling areas represent the thermal behavior of the fluid in the experiment with sufficient accuracy. With this finding the temperature field is used to deduce the heat flux of the filling in axial direction at a significant height. For logical reasons this position is chosen to be at the middle of the rod's length. To determine this value the axial heat fluxes for all simulation elements associated with the fluid at this height are averaged. This reduction to only one generalized parameter enables the simplifying comparison of different measurements. The procedure of adjusting the simulation model to the experiment was done for all measurements resulting in the values summarized in table 3 and table 4.

Parameter	Symbol	Unit	Test case				
			A	B	C	D	E
Axial heat flux	$ \hat{q}_z $	W/mm <sup>2</sup>	0.140	0.099	0.092	0.116	0.096

Table 3: Axial heat fluxes of the test cases A, B, C, D, and E

Parameter	Symbol	Unit	Test case				
			V	W	X	Y	Z
Axial heat flux	$ \hat{q}_z $	W/mm <sup>2</sup>	0.140	0.141	0.143	0.136	0.123

Table 4: Axial heat fluxes of the test cases V, W, X, Y, and Z

## Conclusion

Experimental and theoretical investigations have been carried out in order to verify the impact of different fluids used as coolant in a vertically oriented hollow rod with regard to the axial heat transfer. The comparison of the resultant temperature distributions and a subsequent FE simulation yield the most effective fluid offering the highest axial heat transfer capability. In a second measurement series a similar approach shows the effect of different liquid to gas filling ratios for the most suitable fluid identified in the above-mentioned study. The best proportion was found resulting in the highest axial heat transfer that was quantified by a simulation.

These results constitute the basis for the selection of the two addressed parameters for future configurations and lead to an enhanced performance of the internal piston rod cooling. From a

scientific perspective the attained findings allow for an improved insight into the thermal mechanisms of an internally cooled reciprocating device.

## Acknowledgements

Sincere thanks I express to Prof. G. Will for his inspiring and motivating help.

## References

- 1 Kriegel, G.:  
Beitrag zur Berechnung des Radialverschleißes von Trockenlaufkolbenringen  
Dissertation, Technische Universität Dresden, 1977
- 2 Tomschi, U.:  
Verschleißverhalten von Trockenlaufwerkstoffen für Abdichtelemente in  
Kolbenkompressoren  
Dissertation, Universität Erlangen-Nürnberg, 1995
- 3 Feistel, N., Samland, G. Fejzuli, B., Spindler, R.:  
Unterschiedliche Konzepte zur Wärmeabfuhr aus Kolbenstangen-Dichtsystemen unter  
Berücksichtigung der API618  
7. Workshop Kolbenverdichter, 2003
- 4 Thomas (née Hammer), C.:  
Innenkühlung der Kolbenstange von trockenlaufenden Kolbenverdichtern  
Dissertation, Technische Universität Dresden, 2013
- 5 Patent DE 10 2007 000 652 A1
- 6 Hammer, C., Will, G. Hesse, U.:  
Temperature Reduction of the Piston Rod in non-lubricated Piston Compressors by  
Internal Cooling  
8<sup>th</sup> EFRC Conference, 2012
- 7 Bush, J. E., London, A. L.:  
Design data for “cocktail shaker” cooled pistons and valves  
SAE Technical Paper No. 650727, 1965
- 8 Cao, Y., Wang, Q.:  
Thermal analysis of a piston cooling system with reciprocating heat pipes  
Heat transfer engineering, 16(2), 50-57, 1995
- 9 Reay, D., McGlen, R., Kew, P.:  
Heat pipes: theory, design and applications  
Elsevier Science, 2013
- 10 Klotsche, K.:  
Simulation von stationärer und instationärer Wärmeleitung und Wärmeübergang in der  
Kolbenstange zur Bestimmung der Kolbenstangentemperatur mit ANSYS  
Großer Beleg, Technische Universität Dresden, 2012



## Nomenclature

Parameter	Symbol	Unit
Rotational speed	$N$	$\text{min}^{-1}$
Power input of heater	$P$	W
Heat flux	$\hat{q}$	$\text{W}/\text{mm}^2$
Temperature	$t$	$^{\circ}\text{C}$
Temperature	$T$	K
z axis	$z$	m
Thermal conductivity	$\lambda$	$\text{W}/\text{m}/\text{K}$
Volume fraction	$\varphi$	$\text{m}^3/\text{m}^3$

## Subscripts

liq	liquid
C	Crosshead
W	Wall
F	Fluid
z	z axis





# Technical Paper

**Session: 40-2**

**Session Name: New Concept**

**A new piston rod design to improve packing lifetime for non-lubricated reciprocating compressor applications**

**Author:**

**Klaus Hoff**  
Head of Central Division of Technology  
Neuman & Esser  
52531 Übach-Palenberg, Germany

Co-Author 1:

Gerhard Knop  
Head of R&D  
Neuman & Esser  
52531 Übach-Palenberg, Germany

Co-Author 2:

Marc Langela  
Head of R&D  
STASSKOL  
39418 Staßfurt, Germany



## Summary

There is a tendency that more and more reciprocating compressor installations are designed without lubrication of the piston rings/rider bands and packings. The lubrication of the contacting sealing elements has the advantage that the lifetime of those wearing parts is typically more than acceptable. At least three years of uninterrupted operation can be expected for lubricated service. But, there is the disadvantage that typically oil is not desired in the process gas. Therefore, it needs to be removed from the gas by the installation of separators. For some applications, it is even forbidden to lubricate the compressor since any oil residual in the gas can harm the underlying process. Non-lubrication of the wear parts overcomes these difficulties. A development process of the plastic materials used for the wear parts of non-lubricated services has been observed during the last years. An even warranted lifetime of 8,000 hours is usual in many applications nowadays. But, three or more years of uninterrupted operations is hardly feasible for non-lubricated services with contacting sealing elements. The lifetime of the compressor concerning the wearing parts is restricted by the packings for most applications. The reason for that is the worse cooling of the tribological contact area of piston rod to sealing elements compared to the contact area between the piston rings and cylinder liner. The contact area between piston ring and liner is directly cooled by the water cooling system of the cylinder whereas the contact area between piston rod and packing internals is just indirectly cooled by the water cooling of the packing chambers. A better frictional heat removal by the piston rod is essential to improve the life time of the packing. The concept described in this paper to improve the frictional heat removal is based on a much better thermal conduction from the contact area of the packing along the piston rod to the well cooled part of the piston rod at the crosshead end. This is accomplished by drilling a bore into the piston rod and filling it with copper. The heat conductivity of copper is about ten times higher than the one of steel. This physical fact is used to improve the frictional heat removal. This effect has been verified by tests on a reciprocating compressor test bed. In addition, the improvement of the wear rates was shown by comparative run tests with and without the copper-filled piston rod. The paper covers the theoretical heat examinations and the comparison with the test bed measurements. The wear rate results of the comparative packing run tests are given. Since the piston rod is one of the highest loaded part in a reciprocating compressor the necessary strength verifications are also included.



## 1. Introduction

The tribological system of the contact area between piston ring/rider band and liner and packing elements and piston rod respectively in a lubricated reciprocating compressor service is rather complex. A comprehensive attempt to understand the hydrodynamic and mixed-frictional mechanisms was done by A. Voncken<sup>i</sup>. This work revealed that the complexity of the combination of mechanics, thermodynamics and hydrodynamics taking place in parallel for this tribological system needs a tremendous calculation effort even with modern multi-body-simulation software. A practical design approach to determine the minimum necessary oil amount is not possible at the moment. Nevertheless, the experience of lubricated compressors shows that an absolutely reliable design of a lubricated compressor is feasible with very simple design rules for the number of rings and the oil amount.

The tribological system of a non-lubricated ring/liner or ring/piston rod contact is even more complex. Experiences show that a stable transfer layer is necessary to create acceptable wear rates for a non-lubricated contact. This transfer layer is created by tribo-chemical reactions in the contact zone. These tribo-chemical reactions depend on material and fillers of the sealing elements, on the material, hardness and surface roughness of the counter surface (liner, piston rod), on the compressed gas, on the contact pressure and contact temperature.

It is readily acceptable that any attempt to describe and predict this tribological behavior with a comprehensive analytical approach will not be successful. Therefore, the experimental approach has been used by various authors. There are two options to experimentally describe the tribo-system.

1. The tribo-system is approximated by a so-called tribometer. With this system, the real reciprocating tribo-system is replaced by a simplified tribo-system which includes some major influencing factors like contact pressure, materials of contacting partners, gas and humidity of gas. These tribometers can either incorporate the reciprocating movement of the real contact or just replace the reciprocating movement by a fixed-speed rotational movement.
2. The tribo-system is analyzed by a real test compressor installation. Such a test installation is very close to the reality but has the disadvantage of higher effort in terms of space, time, power and gas consumption. In the end, this is an expensive approach.

Both approaches should be followed in a development process. A pre-selection should be done with a tribometer to select promising tribo-systems. These promising systems need to be verified on a test compressor installation before going into real field installations. Experiences have shown that promising systems identified by tribometer tests failed completely on the test compressor. Simplifications introduced by the tribometer test can sometimes exclude important factors for the tribo-chemical reactions.

A pioneering work in experimentally analyzing the tribo-contact of non-lubricated reciprocating compressor contacts with a tribometer was fulfilled by U. Tomschi<sup>ii</sup>. A remarkable extension of this work was done by N. Feistel<sup>iii</sup>. His studies were done on a nitrogen packing test rig and on a hydrogen compressor test installation. Both works revealed that temperature at the contact and, therefore, a good cooling of the tribo-contact is essential for a low-wear sealing contact. Feistel explicitly stated that the indirect packing cooling via the packing chambers is necessary for demanding applications in terms of sealing pressure. This result was experimentally verified although the frictional heat flux through the sealing elements into the packing chambers is poor compared to the heat flux through the piston rod. He anticipated that a direct cooling through the piston rod would improve the overall cooling and the wear behavior.

Based on those fundamental works, C. Thomas<sup>iv</sup> researched a hollow piston rod filled with an air-water mixture. The intention of this work was to effectively remove frictional heat from the packing contact area in order to improve the lifetime of the packing elements. The analyses revealed that such a system effectively removes the heat only at a certain amount of acceleration (piston speed). Another disadvantage of this system is that the hollow piston rod needs a bore to fill the water and is manufactured by a welding procedure. This has a dramatic impact on the rod load capability of the rod. That means one could make use of the advantage only at reduced rod loads. Another point, maybe only psychological, is that in the reciprocating compressor world a great rejection needs to be assumed with having water close to the compression chamber. Any chance of liquid loss into the compression chamber could create a liquid slug with catastrophic consequences.

## 2. The new piston rod heat removal concept

The API 618<sup>v</sup> states that reciprocating compressors need to be constructed for at least 3 years of uninterrupted operation. Even though the standard accepts that interruptions to the continuous operation may occur due to exceeding the lifetime of wearing parts the intention of the petroleum, chemical and gas industry is to run the compressor for at least 3 years of uninterrupted operation.

Typically, only the valves, rings and packings are responsible for not reaching that goal. The valves can be designed more conservative in terms of the impact velocity which makes it feasible to reach the goal. For the rings and packings, the typical approach is to lubricate them. For lubricated service, the 3 years of uninterrupted operation is not demanding at all. But, the oil needs to be removed and the oil is negatively influencing the lifetime of the valves by the oil sticking effect.

Target should be to reach similar lifetime of the wear parts and higher working pressure limits at the packing than the typical limit of 80 to 100 bar also for non-lubricated service.

The new concept contrary to the concept of C. Thomas<sup>vi</sup> is to fill the hollow piston rod with another solid material of a much better heat conductivity, e.g. copper. The frictional heat removal mechanism is heat conduction instead of heat convection. A possible contact temperature reduction at the contact area of the packing is visualized in figure 1.

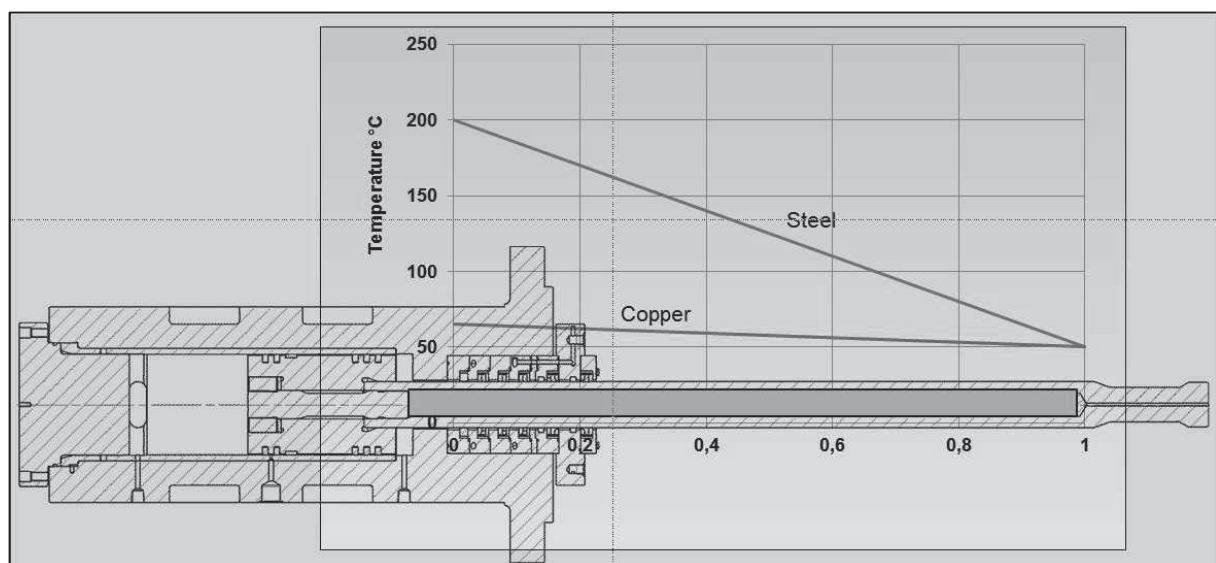


Figure 1: Comparison of temperature profile along the piston rod with/without copper filling



The temperature profiles of figure 1 are the result of a calculation under the following assumptions:

- The same amount of frictional heat is introduced at the piston end of the piston rod.
- The crosshead end of the piston rod is cooled down to the oil temperature.
- The convective heat flux along the piston rod to the ambience is neglected.
- No heat flux from the compression chamber into the piston rod.

Figure 1 clearly demonstrates that a dramatic reduction of the contact surface temperature is possible by introducing a material of excellent heat conductivity like copper. Of course, the real behavior will be different since the piston rod will also remove compression heat through the piston rod. So, the temperature in the packing area cannot fall below the mean piston temperature. Nevertheless, at tribologically critical application a contact temperature of 200°C is possible which obviously will not result in good wear rates. A reduction of the temperature down to e.g. 120°C could dramatically improve the situation.

### 3. Strength considerations

At conventional piston rod designs, the weak location in terms of fatigue is always at the connection to the crosshead due to the unavoidable stress concentration. The piston rod in the area of the main diameter is never critical because of no stress concentration and a large cross-sectional area. The use of a copper core piston rod however requires looking at this location, too. The definition of an admissible copper core diameter requires a detailed knowledge of the piston rod strength, especially the influences caused by fretting fatigue which is described in this section.

The rod load due to gas and inertial forces as well as a certain amount of bending creates a cyclic elongation of the hollow piston rod which the copper core is not completely following at every location. Consequently, there is a resulting axial micro-slip between the copper core outer diameter and the piston rod bore diameter. This slip gives rise to tribological effects which can reduce the material fatigue strength significantly. The mechanisms of such fretting have been investigated in many publications<sup>vii viii ix x xi xii xiii xiv</sup>. The slip creates local mechanical (adhesion and abrasion) and chemical (oxidation, micro-welding) loads on the surface, creating micro cracks which may propagate into macro cracks at the presence of respectively high bulk stress levels.

The amount of loss in fatigue strength can be very high as indicated in the following diagram (Fig. 2).

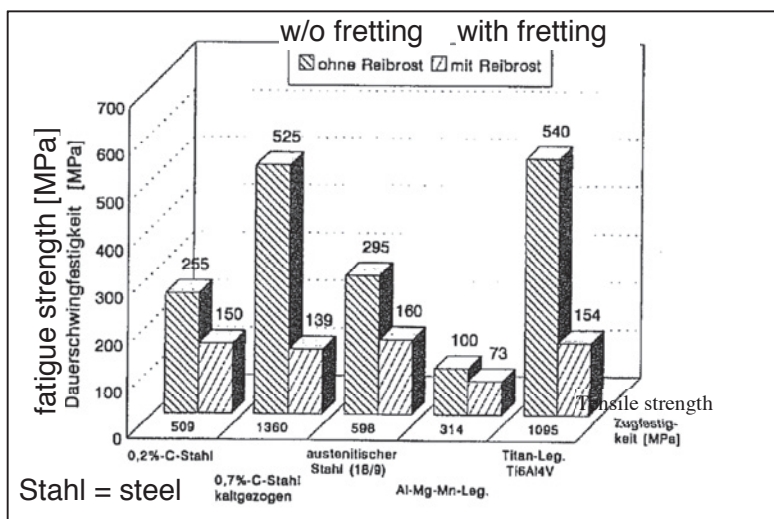


Fig. 2: Fatigue limits of different materials with and without fretting<sup>13</sup>

It turns out that high-strength steels can lose fatigue strength by a factor of 2 or 3, whereas low-strength steels lose only little strength. Exposed to fretting, both material groups seem to approach about the same fatigue level!

It must be noted that the diagram above can only give an exemplary idea in quality about the expected loss in fatigue strength. For the individual case, the quantification is more complex and includes load parameters like slip, contact pressure, friction factors and load cycle frequency. An important parameter to be considered is the amplitude of the cyclic slip. Fig. 3 shows the dependence of the slip (U-shaped curve), which was already described by Vingsbo and Söderberg<sup>7</sup> in 1988 and confirmed by many others<sup>e.g.8</sup> later.

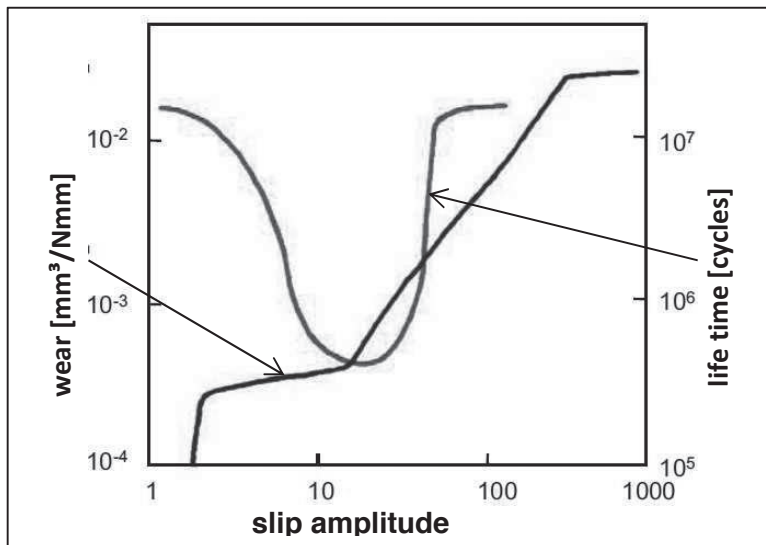


Fig. 3: Life time vs. slip (U-shaped curve) and wear of a surface exposed to fretting (Vingsbo and Söderberg<sup>7</sup>). Note that the numbers given here are not generic and give only a representation in quality.

The life time (and also the fatigue strength limit) has a minimum at a certain slip level. Below this level, strength increases which is explained by the creation of shorter micro-cracks. Above this slip level, strength also increases which is explained by the prevention of crack propagation because of continuously wearing away every newly initiated crack. More recent investigations show the strength minimum of the U-shaped curve at much lower slip numbers<sup>10,11</sup>.

The effect of the material strength on the strength loss of parts exposed to fretting is shown in Fig. 4

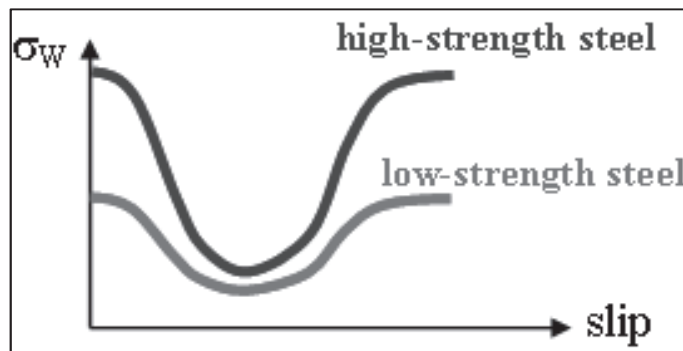


Fig. 4: Comparison of the Söderberg U-curve (Fig. 3) for different material grades<sup>14</sup>





The obvious problem in the quantification of fretting fatigue limits is the uncertainty of the slip amplitudes at the different locations. A pragmatic approach is to use the fatigue strength minimum that has been experimentally found for the most critical slip and contact pressure. Using this approach, the design is always conservative.

#### 4. Packing test rig results

The influence of the copper core on the temperature development as well as on the packing ring wear was tested on the horizontal axle of a reciprocating test compressor (see Fig. 5). The compressor is operating at a speed of 623 rpm with a stroke of 130 mm which gives an average piston speed of 2.7 m/s. The cylinder was pressurized with 80 bar static Nitrogen pressure and a piston rod packing with 4 sealing elements was installed to seal the static pressure against the atmosphere. All testing was performed by using a white PTFE material in dry-running service under Nitrogen atmosphere in order to generate a fast wearing material combination together with a high amount of frictional energy generated by the sealing elements. This ensures a quantification of the influence of the copper core at short test durations.

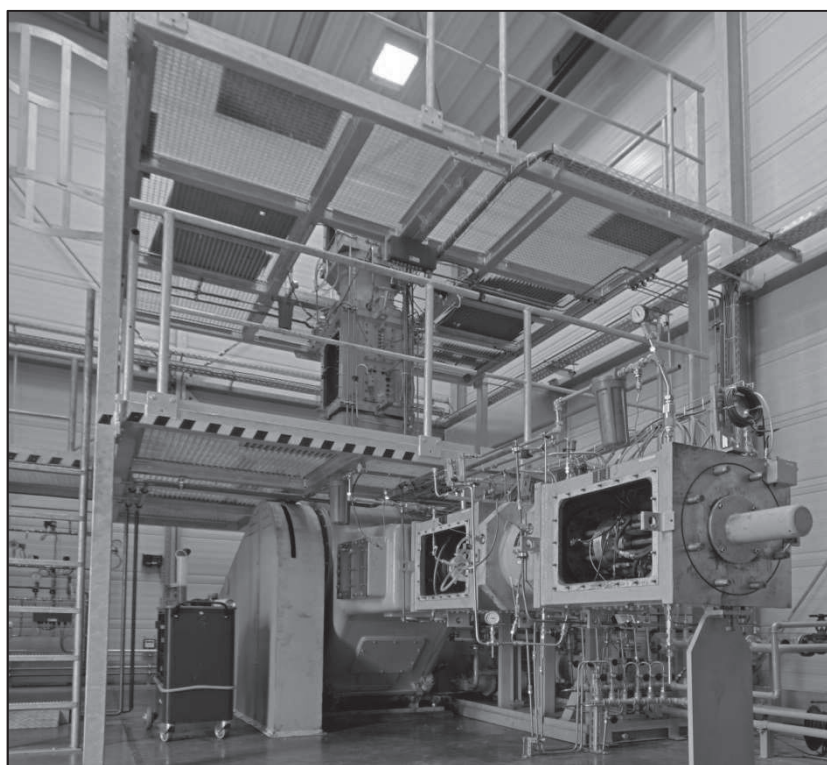


*Fig. 5: Reciprocating test compressor, horizontal axle was used for the test*

In the first step, the temperature development of the piston rod between the packing area and the cross head was characterized with and without the use of the copper core. Additionally, the rod temperature at chamber 3, which is located in the middle of the pressure packing, was measured. The goal of this pre-test was the quantification of the cooling effect caused by the copper core.

After a run-in time of 24 hours the compressor was stopped and the rod temperatures between the piston rod packing and the crosshead connection were measured every 50 mm as well as the piston rod temperature at chamber 3. Fig. 6 illustrates the positions of the temperature

measurement. This procedure was repeated after additional 24 hour of running time and the average values of the measurement with and without copper core were calculated.

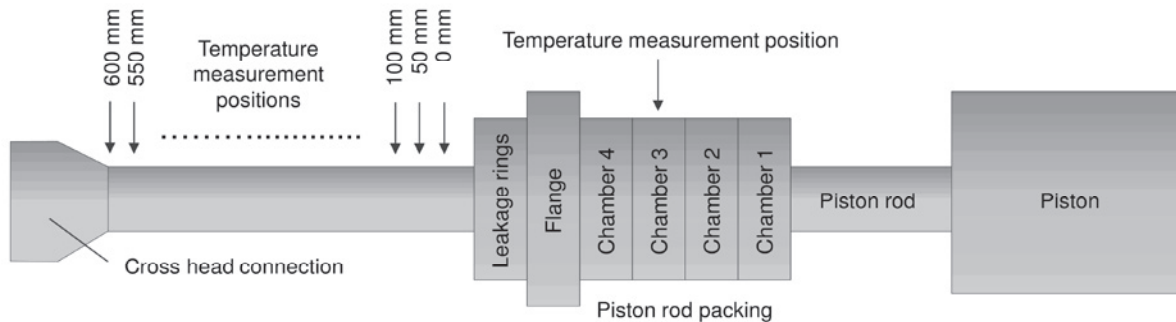


Fig. 6: Sketch for illustrating the temperature measurement positions along the piston rod

The results are summarized in Table 1 and they are graphically shown at Fig. 7.

Table 1: Results of the temperature measurements without and with copper core

Position [mm]	0	50	100	150	200	250	300	350
Temperature w/o copper [°C]	109.5	105.5	91.0	83.5	75.0	70.0	66.0	63.5
Temperature with copper [°C]	95.5	93.5	89.0	87.5	82.0	79.5	74.0	74.5
Position [mm]	400	450	500	550	600	@ chamber no. 3		
Temperature w/o copper [°C]	64.5	61.5	60.0	54.5	51.0	104.6		
Temperature with copper [°C]	75.5	68.5	70.5	62.0	56.0	93.4		

The red curve at Fig. 7 shows the temperature development along the piston rod with the use of a piston rod with a copper core. Starting from the end of the pressure packing the temperature decreases linearly towards the crosshead connection. This temperature development indicates a good heat transfer along the rod and it proves the working principle of the copper core by increasing the thermal conductivity of the rod in the axial direction. Without the use of a copper core an asymptotic temperature decrease can be observed due to the significant lower thermal conductivity of the rod. This result clearly shows the improved heat transfer by the use of the copper core. Additionally, the temperature at chamber 3 is reduced by more than 10 °C because of the increased thermal conductivity which creates the desired cooling effect within the piston rod packing.

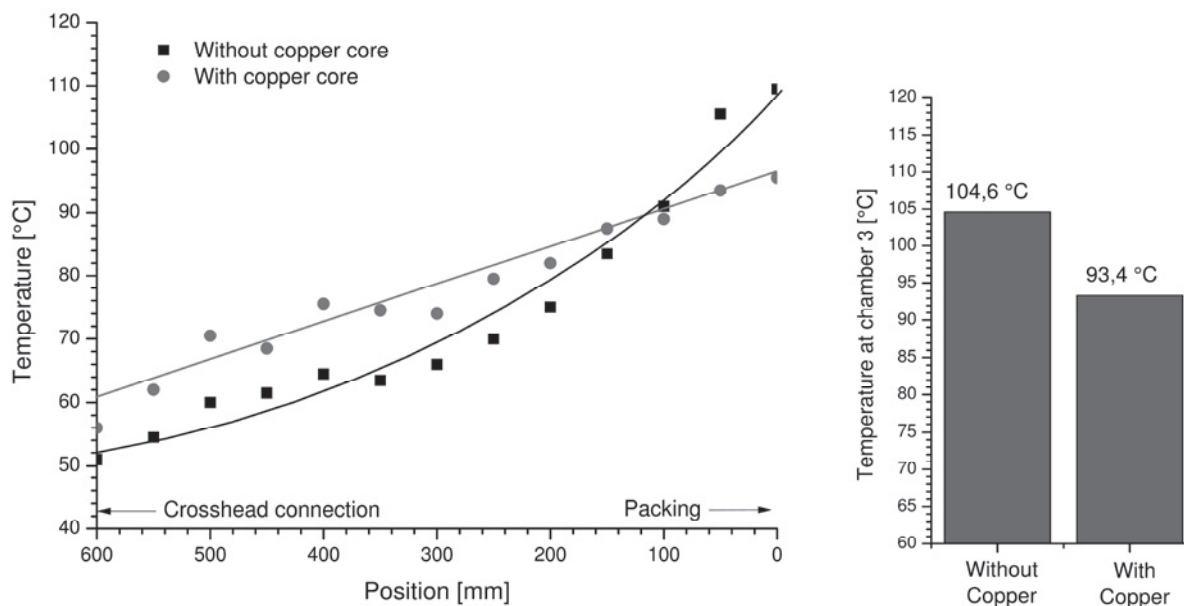


Fig. 7: Graphical results of the temperature measurement along the rod (left) and at chamber 3 (right)

In the second step the compressor was operating for additional 192 hours after the temperature tests in order to achieve a total running time of 240 hours for both cases, with and without copper core. As already explained above, a white PTFE material was used at this dry running nitrogen application to get significant wear in this relatively short operational time. After the test, the remaining gaps of all 4 sealing rings were measured, which did have an original gap of 12 mm per sealing ring at the beginning of the operation. From the remaining gaps the maximum life-time of the ring sets could be calculated.

The results of the ring life tests are summarized in Table 2. The conditions at both 240 hours test runs were identical except the presence/absence of the copper core. At test no. "A46-5" the rod was used with the copper filling and after test duration of 240 hours all 4 sealing rings were showing significant gap to adjust the sealing segments to the piston rod. The total gap of all 4 sealing rings was 41.0 mm compared to the total manufactured gap of 48 mm at the beginning of the operation. Thus, more than 85 % of the original gap was left, which in turn means that the wear at the sealing elements was below 15 %. Thus, an expected service life-time of approximately 1,646 hours for this system can be calculated by combining the low wear with the duration of this test.

Test no. "A46-6" was performed without the copper core and here we get a complete different picture. After the 240 hours test run the last three sealing rings didn't have any remaining gap to adjust to the piston rod which means that they were fully worn. The 1<sup>st</sup> ring did have a small remaining gap of 4.0 mm, which was the total remaining gap of the whole sealing system. By setting the remaining gap into relation with the 240 hours test duration an expected service life-time of only 262 hours can be calculated for this application.

Table 2: Comparison of ring wear at the piston rod packing with/without copper filling

Test run no.	A46-5	A46-6
Rod	<b>With copper core</b>	<b>Without copper core</b>
Original gap	4 x 12 mm = 48 mm	4 x 12 mm = 48 mm
Remaining gap ring no. 1	10.5 mm	4.0 mm
Remaining gap ring no. 2	11.1 mm	0.0 mm
Remaining gap ring no. 3	10.7 mm	0.0 mm
Remaining gap ring no. 4	8.7 mm	0.0 mm
Total remaining gap	41.0 mm	4.0 mm
Actual run-time	240 hours	240 hours
Predicted maximum run-time	<b>1,646 hours</b>	<b>262 hours</b>

With the copper core a predicted life-time of 1,646 hours was estimated whereas this number is reduced to 262 hours without copper filling of the piston rod. This clearly indicates that the measured temperature drop by the improved thermal conductivity has a significant influence on the life-time of the sealing elements. The reason for this has not yet been investigated but it is most likely, that the Tribofilm stability increases by lowering the temperature at the piston rod which in turn reduces the wear of the sealing elements.

## 5. Summary

There is a clear tendency to get rid of the lubrication for reciprocating compressor applications. For lubricated service, more or less infinite lifetime of the sealing elements can be achieved. This is explained by the dominating hydrodynamic tribology. The tribology in the contact zone for non-lube is rather complex. Tribo-chemical reactions are responsible for a stable or unstable transfer layer. Only when a stable transfer film is created good lifetimes will be reached. The tribo-chemical reactions are very complex and depend on several influencing parameters. One of these parameters is the temperature in the contact zone. Studying the literature revealed that reducing this contact zone temperature will probably increase the lifetime of a non-lubricated tribo-system.

This paper proved that the temperature in the packing contact area can be reduced by increasing the thermal conductivity of the piston rod by filling it with a copper core. The thermal conductivity of copper is much higher than the one of steel.

In addition, it was demonstrated by tests on a compressor test rig that a reduction of the wear can be achieved by reducing the contact temperature. Since the piston rod load capability is influenced by filling it with copper a detailed fatigue analysis is necessary to assess this effect. The necessary theory to comprehensively check the fatigue was summarized.



## Bibliographic details

- 
- <sup>i</sup> A. Voncken, Study on cylinder lubrication, Final Report, 2014, EFRC R&D work group
- <sup>ii</sup> U. Tomschi, Verschleißverhalten von Trockenlaufwerkstoffen für Abdichtelemente in Kolbenkompressoren, Dissertation Universität Erlangen-Nürnberg, 1995
- <sup>iii</sup> N. Feistel, Beitrag zum Betriebsverhalten trocken laufender Dichtsysteme zur Abdichtung der Arbeitsräume von Kreuzkopfkompressoren, Dissertation Universität Erlangen-Nürnberg, 2002
- <sup>iv</sup> C. Thomas, Temperature Reduction of the Piston Rod, Final Report, 2013, EFRC R&D work group
- <sup>v</sup> API 618, 5th edition, 2007
- <sup>vi</sup> C. Thomas, Temperature Reduction of the Piston Rod, Final Report, 2013, EFRC R&D work group
- <sup>vii</sup> Vingsbo, Söderberg: On fretting maps. Wear, 1988, 126 (2), 131-147
- <sup>viii</sup> Rabb, Hautala, Lehtovaara, Fretting Fatigue in Diesel Engineering, Paper No. 76, CIMAC Congress 2007, Vienna
- <sup>ix</sup> Merrit, Zhu, The Prediction of Connecting Rod Fretting and Fretting Initiated Fatigue Fractures, SAE International 2004
- <sup>x</sup> Madge, Leen, McColl, Shipway, Contact-evolution based prediction of fretting fatigue life: Effect of slip amplitude, Wear 262 (2007) 1159-1170
- <sup>xi</sup> Forschungsvereinigung Verbrennungskraftmaschinen FVV, Auslegungsrichtlinie Reibkorrosion, Heft 984 -2013
- <sup>xii</sup> Forschungsvereinigung Verbrennungskraftmaschinen FVV, Reibkorrosion, Heft 1097 -2016
- <sup>xiii</sup> Issler, Ruoff, Häfele, Festigkeitslehre – Grundlagen, Springer Verlag 1997
- <sup>xiv</sup> Knop, Hoff, A closer Look at Rod Load Definitions and Rod Load Limitations of Reciprocating Compressors, Gas Machinery Conference (GMC) 2015







# Technical Paper

**Session: 40-3**

**Session Name: New concept**

## **Vibration analysis and investigation of crack failure of reciprocating compressor**

**Author:**

**Jaroslav Kraml**  
Senior Designer, FEA Engineer  
Howden ČKD Compressors  
19000 Prague, Czech Republic

**Co-Author:**

**Martin Lamrich**  
Senior Designer, FEA Engineer  
Howden ČKD Compressors  
19000 Prague, Czech Republic

## Summary

There are 2 units of reciprocating compressors in severe operation at a petrochemical plant in Russia. Those units have been delivered by our company. They are two-stage, six-cylinder, moderate speed, and horizontal-opposed types (boxer type) reciprocating compressors. The assembly is shown in fig.1. Cylinders of the compressors are not lubricated and work with hazardous explosive gas with rich percentage of hydrogen at quite high pressure.

A fatigue cracking has been observed in the supports of 1st stage damper .Detailed measurement of vibration levels has been performed by our company for the purpose to identify an operating deflection shape and to improve the structural design.

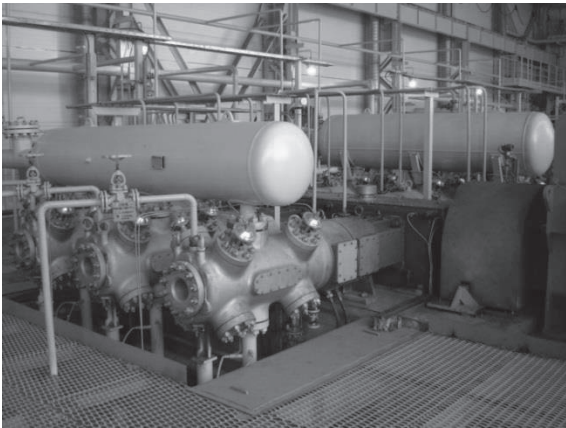
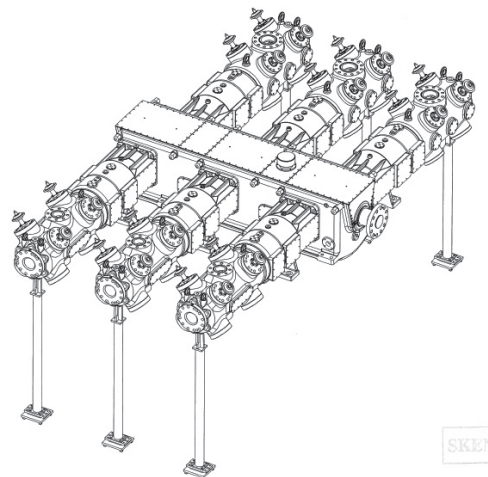


Figure 1: Assembly of the compressor at the customer site

### Technical data of compressor:

Speed	1000 rpm
Compressed medium	rich hydrogen gas
Suction pressure	2.3 MPa
Discharge pressure	8.6 MPa
Suction temperature	40 °C
Discharge temperature	110 °C
Stroke	150 mm
Number of cylinders	6
Number of stages	2
Bore (1st stage/2nd stage)	280/210 mm



The compressor is provided by a step capacity control from 100 to 0 % using suction valve depressors.

It is powered by electric motor via flexible couplings. The compressors are anchored directly to concrete foundation.



## Introduction

Reciprocating compressors are widely utilized in the natural gas transmission and natural gas industries because they are flexible in throughput capacity and discharge pressure range.

Compression process in these machines is intermittent (stepper), respectively done in steps. Gas is drawn into a cylinder, trapped, compressed by the moving action of a piston and finally discharged. Pressure forces increase and decrease on the piston during the cycle. In addition, even non-steady state inertial forces are created as the piston accelerates and decelerates. The combination of pressure and inertial forces create varying forces during each revolution of the compressor. These forces are transmitted to the main crankshaft bearings, then through the casing to the base frame. In a “boxer” type (i.e. horizontal opposed cylinders) reciprocating compressors, these forces are balanced by an opposing piston and optimization of the weight of all rotating parts [4].

This optimization and the balancing cannot be done perfectly and there will always be some unbalance. The unbalance, naturally, creates moments and unbalanced forces that are the cause of vibrations of reciprocating compressors. The vibrations could be damped and become insignificant but could be the reason of a bearing damage and even cracking in the construction as well [1].

A typical resonant frequency generally occurs at 1<sup>st</sup> and 2<sup>nd</sup> harmonic frequency of running speed. A standard running speed is around 1000 RPM, which means 16, 6 Hz (almost 17 cycles per second). It is around one and a half million cycles per a day so we are definitely talking about high cycle fatigue stress. This means that even if the vibrations are under an allowable limit, stress of the most part of the construction has to be under the material fatigue endurance limit. It is hard to determine the vibration and stress of the construction in the design phase. Hence it is not always easy to determine correct design of all parts such as supports and mountings. The best way to determine the cause of a problem is to do a vibration measurement which provides inputs for simulations and reveals what is actually happening in operation.

### ***Description of the failure***

The compressors had shown some high level of vibrations (200 mm/s) since the very beginning that had not been within acceptable limits (28 mm/s)[5]. Discharge pressure dampers were provided with adjustable vibration-isolation elements that decreased vibrations. Totally different situation occurred in the suction pressure dampers that are installed on the top surface of the cylinders through flange connections and vibration-isolation elements could not be used in here. There were not any supports of the suction damper; each suction damper had three flanges connected to the individual cylinders of the same stage (shown in fig.1).

The high level vibrations had to be reduced by some reinforcing. The situation was consulted with the damper manufacturer and we both recommended a partial change in damper design.

These changes consisted in reinforcing of flange connections to the damper shell using U-beams supports welded to the shell of damper. These improvements reduce the vibration to 15 mm/s, but U-beams supports cracked after a few days. A big crack at both connecting sides was found after 3 days of running. (It is shown below in Fig. 2).

Detailed measurement of vibration levels has been performed by our company for the purpose to identify an operating deflection shape and improve the structural design.

Finally we designed new system of supports in 3D CAD software and analysed by Finite Element Method solver. These supports were applied on dampers and performed well.

Then we decided to do a detailed measurement of all vibration levels to confirm our solution and identify a possible root cause of the failure.



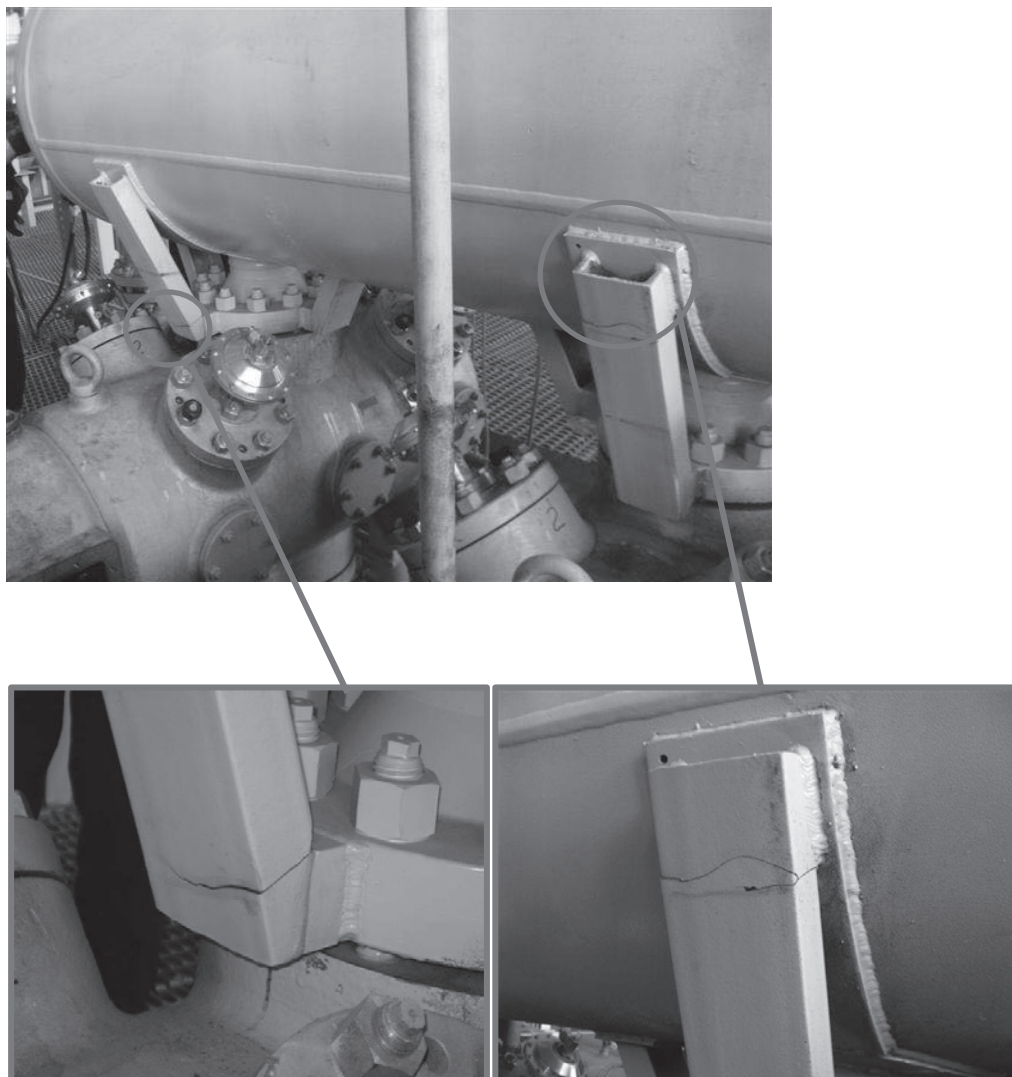


Figure 2: The final crack propagation in the supports after 3 days of running

### **Experimental measurement**

An experimental measurement was done to identify mode shapes of oscillation (vibrations), frequency of the oscillations, amplitude and natural frequencies of the machine. There were selected about 200 points distributed on surface of cylinders, dampers and piping at suction side. Wire-frame model based on measured points is shown in fig 3. Marking system is shown in fig.4.

Usage of sophisticated instrumentation was limited by explosion hazard environment due to hydrogen service in the machine room. At least one of the machines was in operation. Due to this fact the results of bump test (experimental modal analysis) have been influenced by the operation of another machine that was operating next to the measured one. [2].

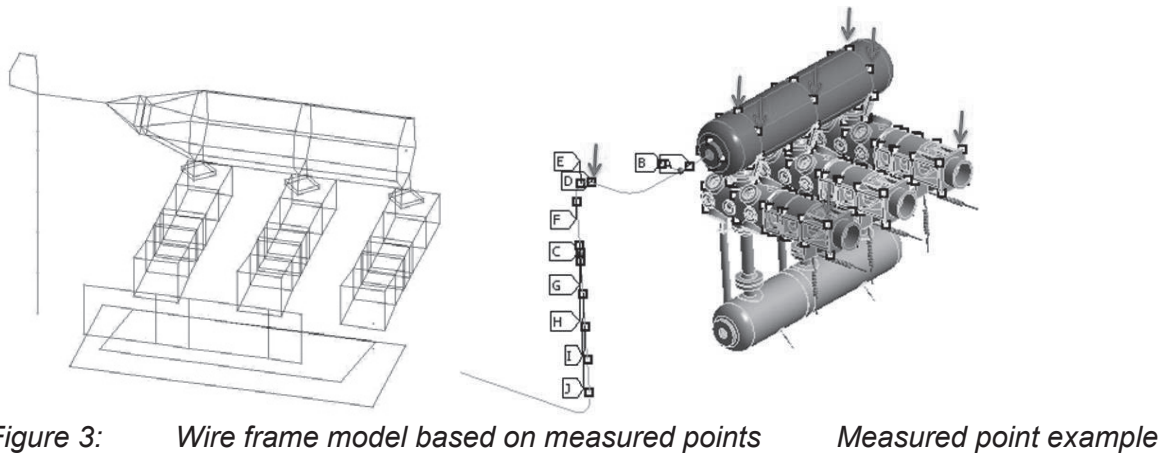


Figure 3: Wire frame model based on measured points Measured point example

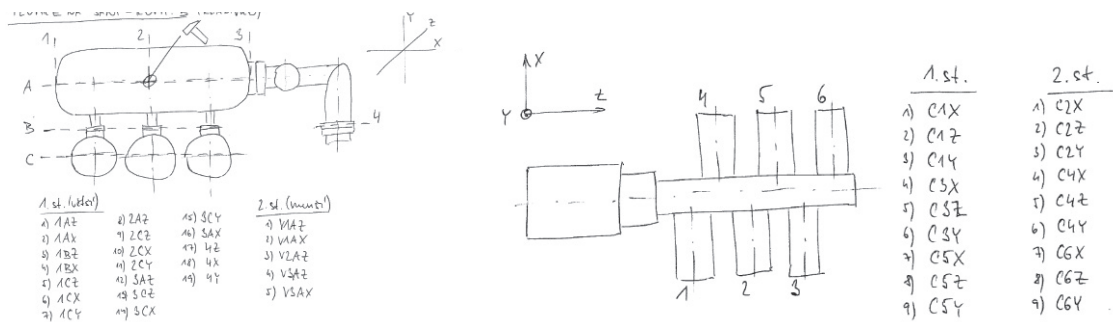


Figure 4: Marking system of the measured points

Measured data provide us with information in 3 areas:

- bump test
- frequency spectrum
- operating displacement shape
- natural frequencies
- qualification of system behavior under operation
- quantification of structure displacement / deformation

### Bump Test results

The bump-test has been performed on the machine out of operation. However, the data are affected by the second machine operated nearby and the nominal speed is clearly visible in figures below (Fig.5) [2]. Some of the results of the bump test are shown below, there are visible a lot of peaks out there, many of them are caused by the other operated machine, but still there can be seen some natural frequencies at or very near to operation speed. It is hard to say which of the measured frequencies are really natural frequencies of the machine and which of them are just caused by operation of the other machine, so the results of the bump test have been more or less just a huge pile of useless data.

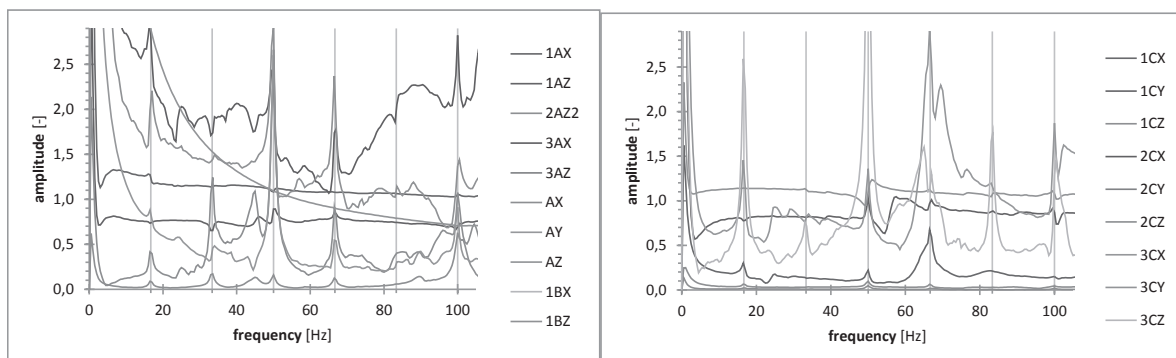


Figure 5: Suction damper of the 1st stage

Cylinders of the 1st stage

### Frequency Spectrum

Frequency spectrum measured on the 1st stage cylinders is shown below (Fig.6)[2].

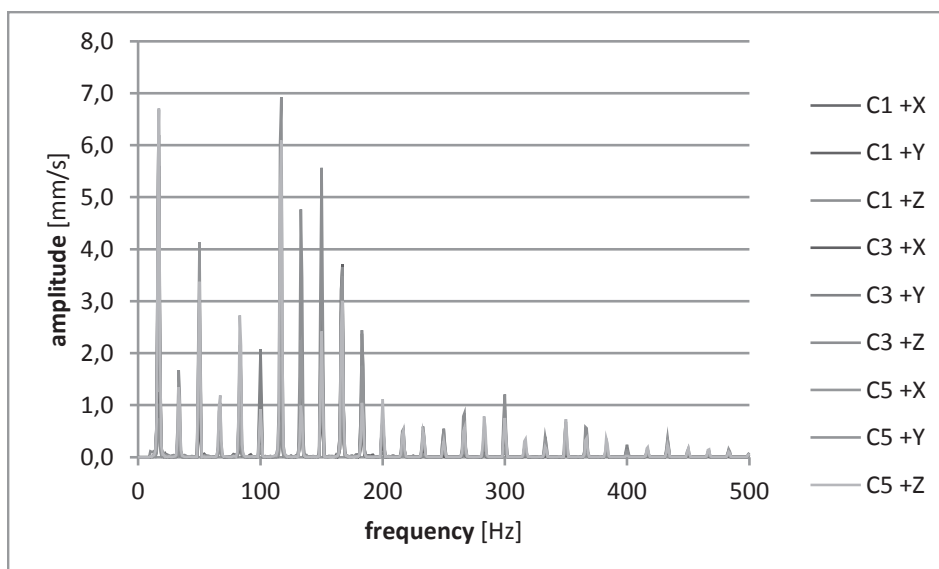
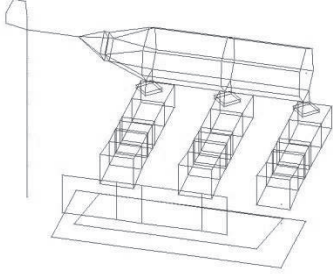
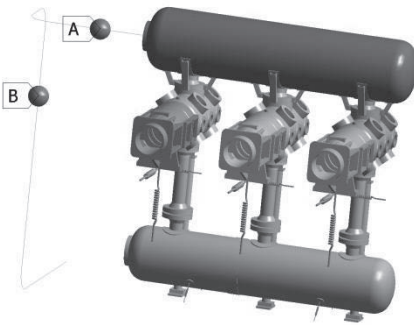
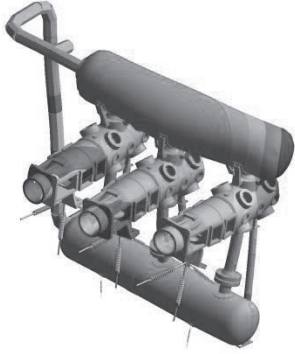


Figure 6: Frequency spectrum measured on the 1st stage cylinders

### FEA Simulation and Fatigue Analysis

Measured data have been cleaned and applied into finite element model. A pseudo-static analysis has been run. The analysis simulates modal shapes of oscillation for individual frequencies of the operation.

Measured points	Finite Element Model	Modal shapes
		

*Workflow of the FEA simulation*

The results from measurement (directional displacements, frequency spectrum) were imported to FEA software. All simulations have been done for the first compressor stage (the damaged one). FE model has been loaded by directional displacements for individual harmonic mode. Due to FE model it is possible to simulate modal shapes in operation across whole frequency spectrum. Dependency of total amplitude on frequency is shown in Fig.7 and dependency of directional amplitudes on frequency is shown in fig.8.

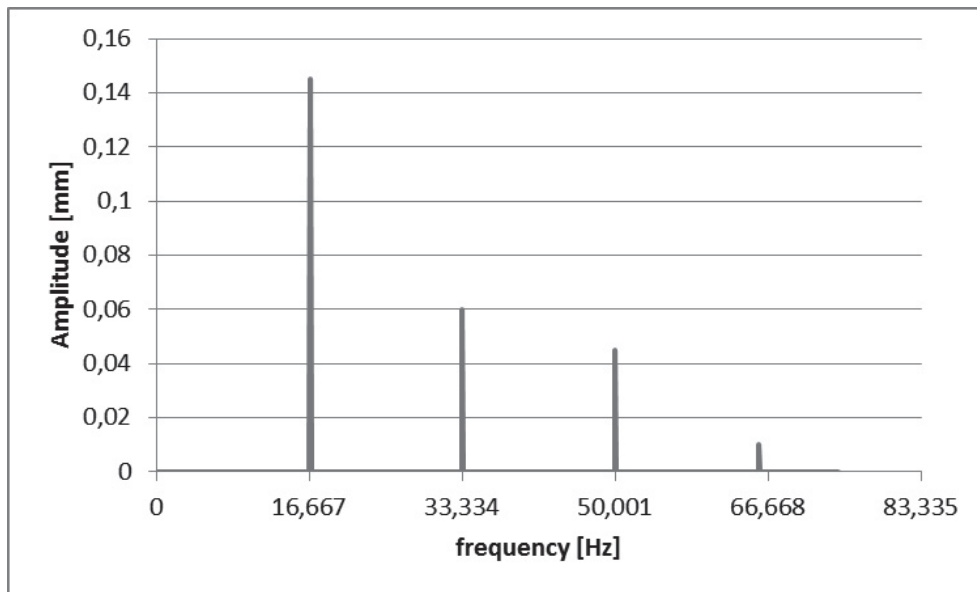


Figure 7: dependence of the total amplitude at oscillation frequency

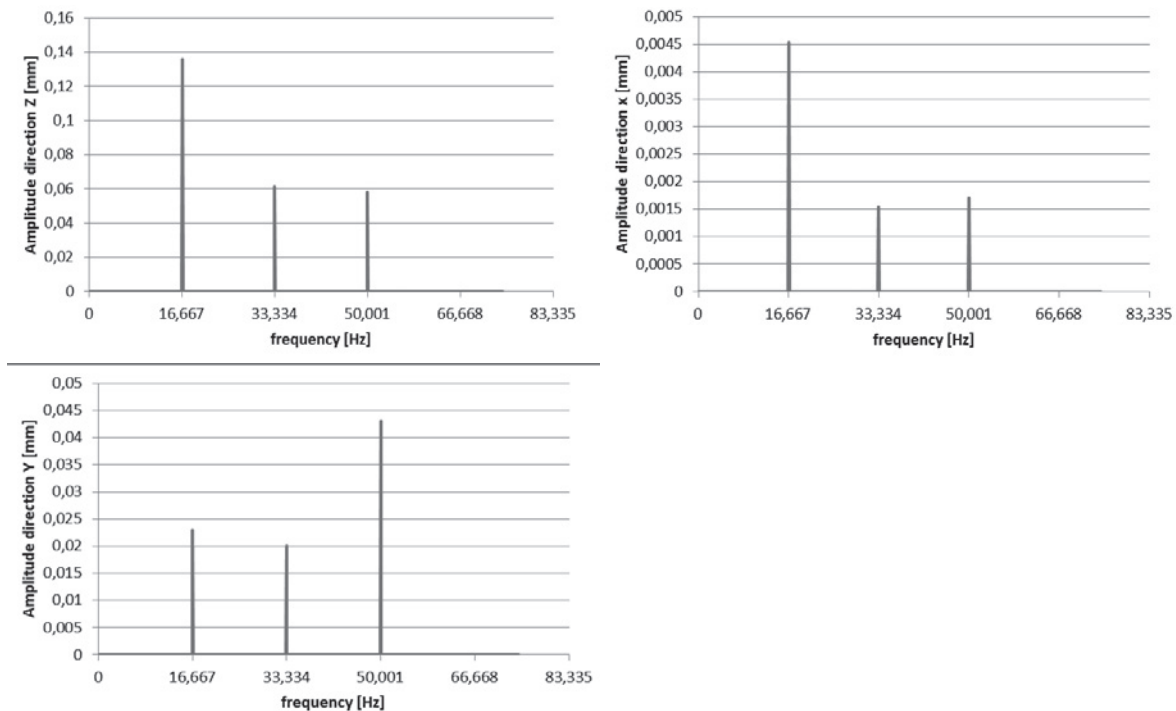


Figure 8: Dependence of the directional amplitude at oscillation frequency

Maximum value of total amplitude was measured at around 16, 6 Hz which is 1<sup>st</sup> harmonic mode (operation speed is 1000 RPM), and it is almost 150  $\mu\text{m}$ . Modal shape at the first harmonic mode is shown in fig.9. This modal shape is characterized by dominant oscillating of suction damper and suction pipe system.

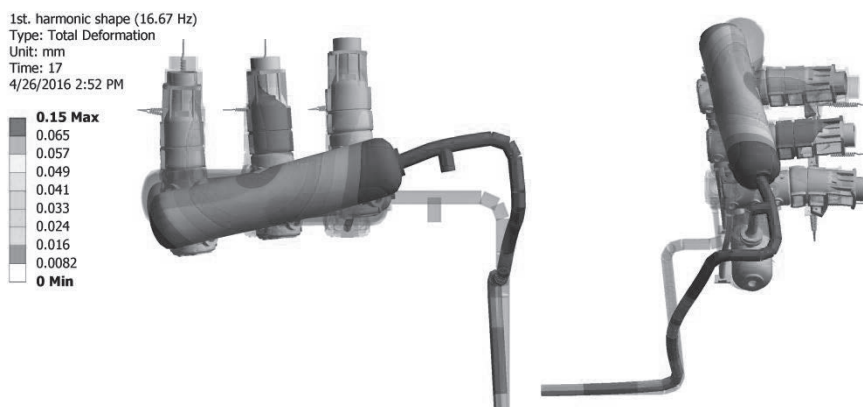


Figure 9: 1st harmonic modal shape (frequency 16, 66 Hz)

Second high pick (fig.10) is at second harmonic mode (around 33, 3 Hz). Oscillation of the suction pipe is dominant in this mode shape. Max. Total amplitude at this shape is 60  $\mu\text{m}$ . Modal shape for 2<sup>nd</sup> harmonic frequency is shown in Fig.10.



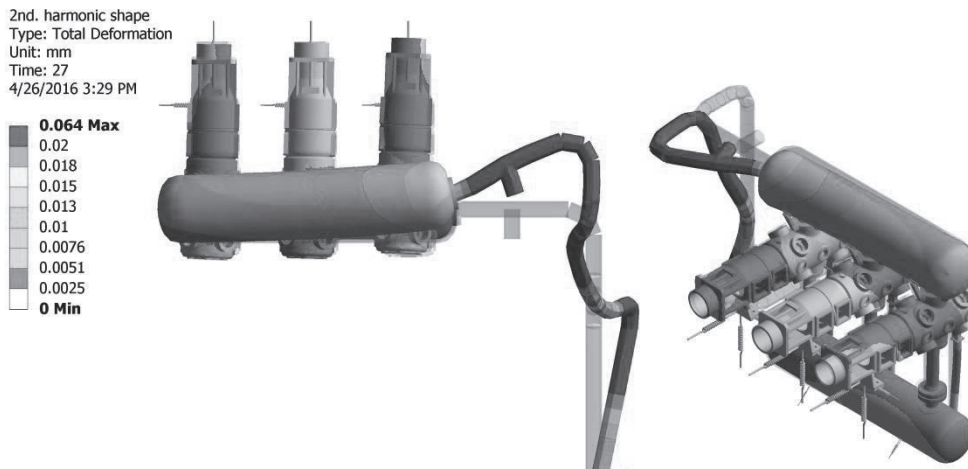


Figure 10: 2nd harmonic modal shape (frequency 33, 3 Hz)

The last high pick is at third harmonic mode (around 50 Hz). Oscillation of the suction pipe is dominant in this mode shape as well. Max. Total amplitude at this shape is 45  $\mu\text{m}$ . Modal shape for 3<sup>rd</sup> harmonic frequency is shown in Fig.11.

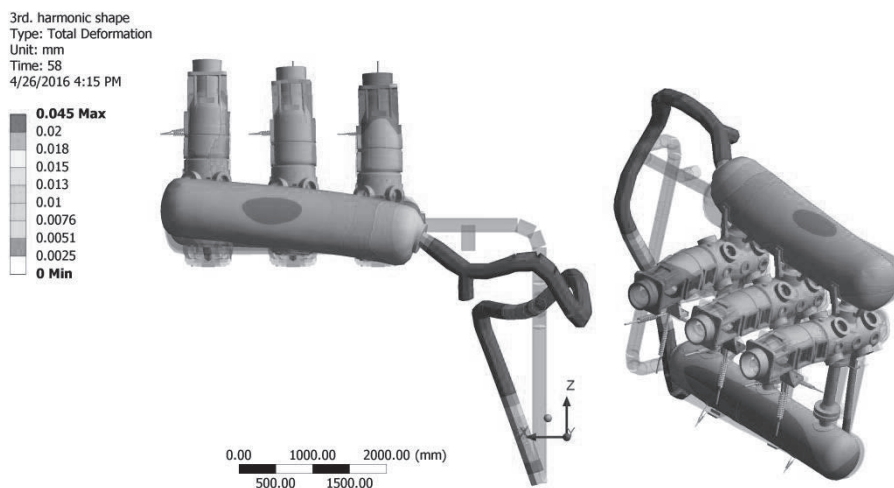


Figure 11: 3rd harmonic modal shape (frequency 50 Hz)

### Fatigue Analysis of Damper Supports

A sub-model of supports of a suction damper has been created; the sub-model was loaded by displacements from global model at cut boundary conditions. This simulation provides mechanical stress due to oscillation in operation. The results of simulations are shown in fig 12. It is inappropriate and incorrect to evaluate fatigue endurance limit based on this results. The real stress could be very different due to structural errors of model such as:

- stress singularity
- poor mesh quality (at critical spots)
- interpolation of cut boundary conditions
- stress concentration of sharp edges
- unknown geometry of welds
- omission of residual stress after welding
- omission of static stress



All these fact more or less significantly influence the final value of the mechanical stress. Nevertheless the simulation can identify critical spots subsequently critical modal shape and try to suggest some design change to eliminate fatigue stress.

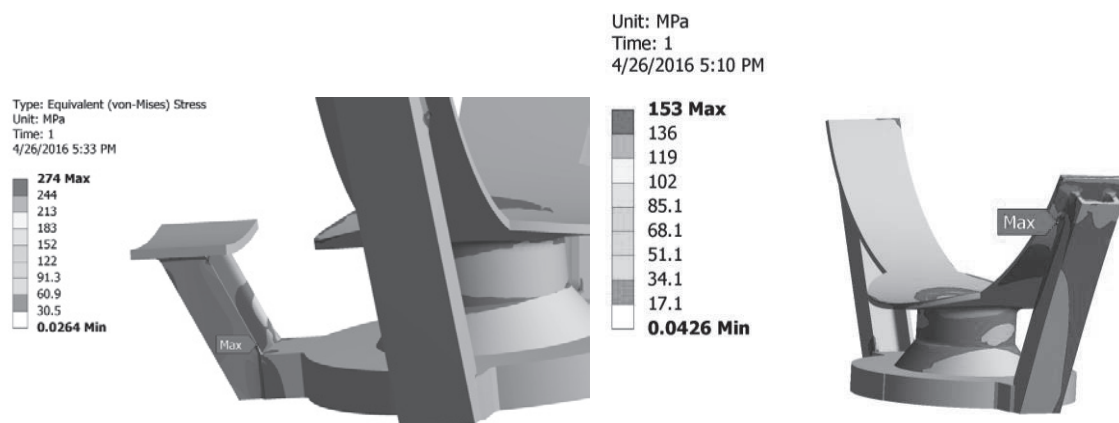


Figure 12: Stress distribution of supports at 1<sup>st</sup> harmonic shape oscillation

As is seen in fig. 12, critical spots from Finite Element simulation are the same as the cracked ones. Main stress is produced by 1<sup>st</sup> harmonic shape. Stresses of all other harmonic shapes are negligible compared with the 1<sup>st</sup> harmonic [3].

### Solution

The simulations from previous chapter show that the problem is caused by oscillating on 1<sup>st</sup> harmonic shape (1<sup>st</sup> natural frequency 16, 6 Hz). This oscillation causes displacement of suction damper and cylinders as well. These are connected by supports which are too stiff and therefore don't adapt to the deformation. Hence stress concentrations on connection spots occur. The fastest and most effective way to solve the issue is to redesign the supports. The new design was focused on better adaptability to the operation condition, mainly the oscillation at 1<sup>st</sup> harmonic shape. The new design was loaded by the displacements from the measurement to find the most optimal geometry. The final design is shown below (Fig.13) [3]. This design change has decreased the vibration of the suction dumper to 17 mm/s (ISO 10816-6 allows 28 mm/s) [5].

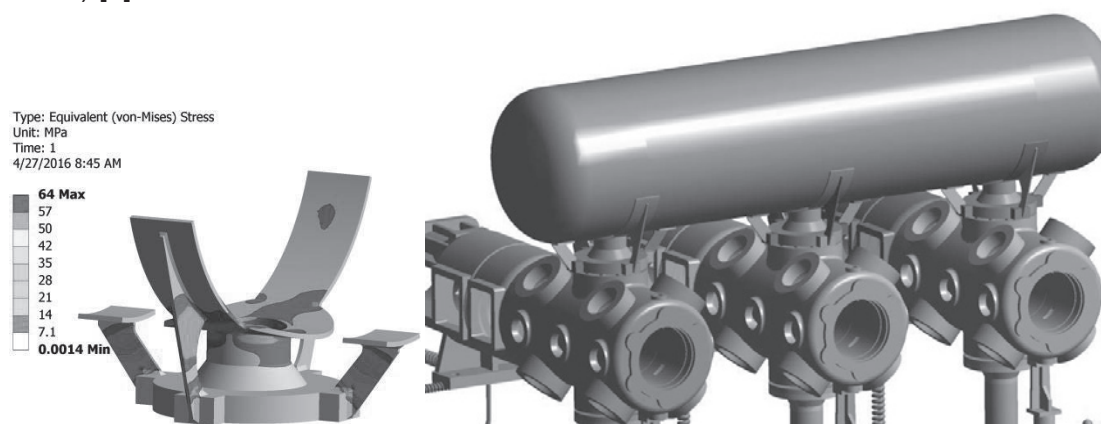


Figure 13: Stress distribution of the new design of supports and execution of the new design

The design has been installed at site in November 2013 and still works. Pictures of the installation and the embodiment are shown in Fig.14. The cause of the cracking of supports is inappropriate design of the supports.



Figure 14: Pictures of the installation and the embodiment

### Conclusion

Some high levels of vibration (200 mm/s) have been observed at the very beginning of start-up of the machine. The highest amplitude was measured at suction dumper of the machine. This problem was eliminated by reinforcing of flanges of the suction dumper by U-beam supports. This change decreased the level of the vibration to 15 mm/s (ISO 10816-6 allows 28 mm/s, for this type of machine)[5], but a fatigue cracking has been observed in the supports of 1st stage damper. Detailed measurement of vibration levels has been performed for purpose to identify natural frequencies, frequency spectrum and vibration level in the operation. The results of the measurement have been compiled and imported to FEA simulation software to simulate an operating deflection shape and improve the structural design.

Individual modal shapes of operation and even the problematic modal shape were determined due to simulations. A sub-model of supports has been loaded by deflection from the simulated shapes. The cause of the cracking is a response to 1<sup>st</sup> harmonic shape. The supports are too stiff to resist and adapt to this oscillation and that's the reason of the fatigue cracking.

A new design of supports was made and optimized based on FEA simulations and the results of measurements. The redesign has been installed in November 2013 and it is still working so the cause of the failure seems to be incorrect design of the supports and its oscillating in the operation and even the vibration level of the redesigned construction have dropped to 17 mm/s, which undoubtedly meets the required standards [5].



## References

[1] Patrick J. Smith. Reciprocating compressor vibration problem. *energy tech.* [online]. 1.12.2014 [cit. 2016-05-05].

[http://m.energy-tech.com/mobile/columns/machine\\_doctor/article\\_d9cfde0a-907c-592c-8078-edeb6b0a169b.html](http://m.energy-tech.com/mobile/columns/machine_doctor/article_d9cfde0a-907c-592c-8078-edeb6b0a169b.html)

[2] J. Behal. Reciprocating compressor vibration problem. *Intern technical analysis report: TAR-0060*. 10.4.2013 [cit. 2016-05-05]

[3] M.Lamrich. FEA simulation of reciprocating compressor measured data. *Intern technical analysis report: TAR-0205*. 12.7.2015 [cit. 2016-05-05].

[4] Ing. Vladimír Chlumský: . Pístové kompresory, druhé rozšířené vydání,. SNTL, Praha 1958

[5] ČSN ISO 10816-6. *Mechanical vibration — Evaluation of machine vibration by measurements on non-rotating parts. Part 6: Reciprocating machines with power ratings above 100 kW*. Prague: Czech Standards Institute, 1997.







# Technical Paper

**Session: 41-1**

**Session Name: Operations**

## **Redesign and manufacture of two shrink-fit 25-ton crankshafts for a hydrogen compressor**

**Author:**

**Guido Kluth**  
**Snr. Rotating Equipment Engineer**  
**Shell Deutschland Oil, Rheinlandraffinerie**  
**50387 Wesseling, Germany**

**Co-Author:**  
**Markus Weber**  
**Rotating Equipment Engineer**  
**BASF**  
**67056 Ludwigshafen, Germany**

## Summary

Designing and manufacturing a new crankshaft for an *Einheitsverdichter* compressor dating back to the late 1930s poses considerable challenges. The aim was to avoid the cracking of the crank pins that had plagued the original design. Without a clear understanding of the failure mode and a full set of documentation, however, a previous manufacturing attempt could not even replicate the service life of the original crankshaft.

Study of this failed attempt showed that fretting fatigue in the shrink-fit joints of the crankshaft was probably to blame. An innovative mathematical model taking into account the effect of friction work was backed up by experimental studies. The latter revealed the stress/slippage regimes under which fretting fatigue is likely, and the number of cycles to failure under different conditions.

This understanding led to a revised design with larger-diameter crank pins. By reducing the necessary compressive stresses in the crank web, this should reduce the likelihood of fretting fatigue. This primary finding was backed up by other design details to reduce stress concentrations, shot peening to introduce compressive stress, and a re-think of how the shrink-fit joints are assembled. As a result, two new crankshafts were manufactured and installed successfully.



## 1 Introduction

The compression system on the fresh gas stream of the hydrocracker at the Wesseling refinery dates from the late 1930s. It comprises five compressors with a total of nine compression trains (cranks). The compressors are of the type known as *Einheitsverdichter* (“integral compressors”). This design of each has just two parallel (non-opposed) throws, with five cylinders on each crank (stages 3, 4, 4 auxiliary, 5, and 6). Each *Einheitsverdichter* is driven by a 4 MW electric motor and compresses hydrogen from 15 to 320 barg.

The *Einheitsverdichter* crankshaft is a large assembly weighing around 25 t. It is of the “fully built” type, in which the crank pins are manufactured separately from the webs, rather than being forged in one piece. Both the crank pins and the main journals are attached to the webs by shrink-fit joints. As far back as the early 1960s, the crankshaft always cracked after extended operation (~700 million cycles or app. 15 years of operation). The cracking usually occurred within the shrink-fit joint between the web and the crank pin, approximately 30 mm from the end of the pin.

Earlier occurrences of this problem had necessitated extensive manual repairs. In the absence of replacement crankshafts, it became necessary to manufacture two new crankshafts. Because of the age of the equipment, however, no detailed information was available describing how this type of crankshaft should be built. It was not possible to manufacture a new crankshaft as a single forging, nor could the crank pins be repaired on a crankshaft grinding machine. As far as is known, Shell Rheinland and BASF SE, Ludwigshafen, are the last two operators of this type of reciprocating compressor. As a result, the two companies established a joint research team to study the problem.

## 2 Previous manufacturing attempt proved unsuccessful

The first attempt to manufacture a new crankshaft based on the available part drawings failed. The new crankshaft ran for just 16,000 hours before showing the same signs of cracking that were usually expected after many years of operation (*Figure 1*).

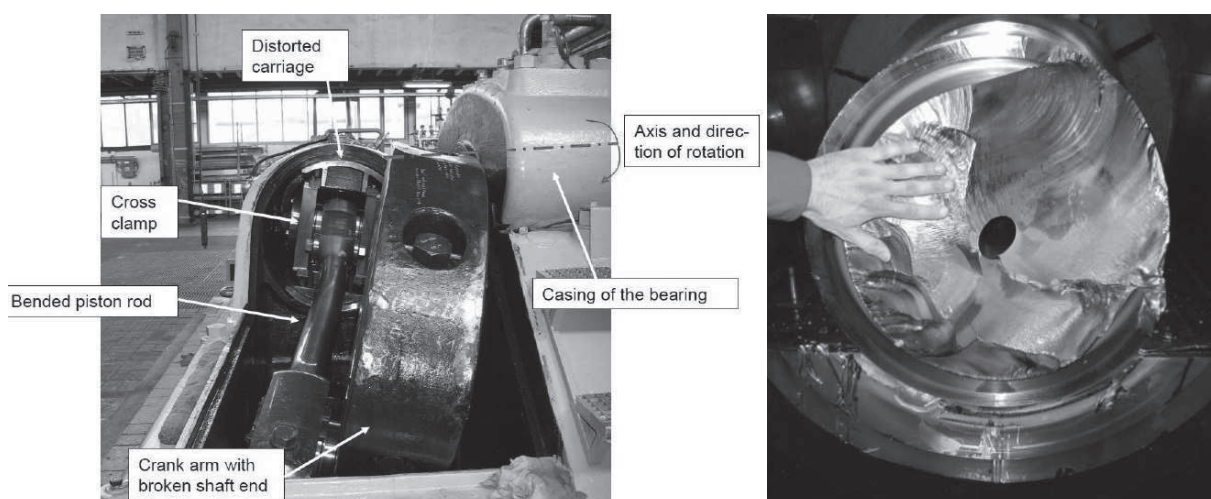


*Figure 1: Damage following crankshaft cracking [1]*

The unexpectedly short operating life prompted the engagement of an independent expert from AZT, Munich, to conduct a comprehensive root cause analysis. A study of past incidents, includ-

ing laboratory analysis of steel samples, yielded the hypothesis that the problem was due to fretting fatigue.

A detailed calculation was also carried out at TU Dresden. The result of load variation during each rotation (*Figure 2*) was taken into further investigation of the relief undercut at the crank pin shoulder and the shrink-fit.

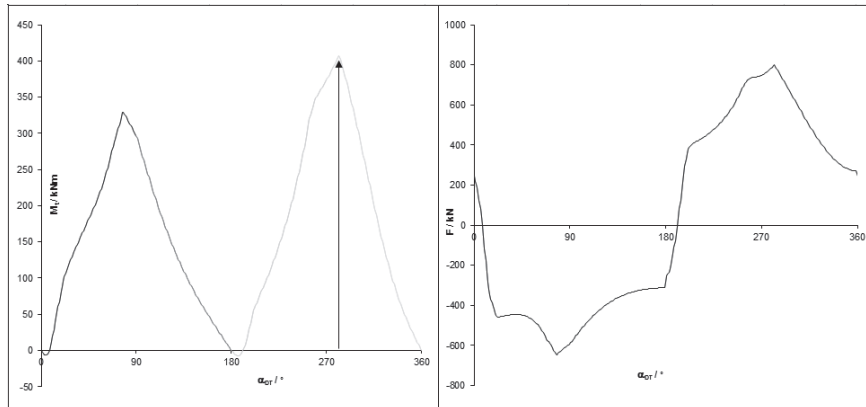


*Figure 2: Torque and force development calculation [2]*

Mathematical modeling in the form of finite element analysis (FEA) was decided on to explore the detailed engineering of the shrink-fit in the existing crankshafts. The aim was to confirm the hypothesis of fretting fatigue, learn more about how the damage occurred, and study design variants that might lead to a more durable crankshaft. Another question was why the service life of the most recent crankshaft was negligible compared to the old crankshafts.

### 3 Limited historical information available

Reports available from archives as well as other literature on fretting fatigue formed the basis for the present investigation. For instance, crankshaft damage that occurred in the 1960s was analyzed at the time in the refinery's Construction Design Department with the help of acrylic samples and polarized light (*Figure 3*).

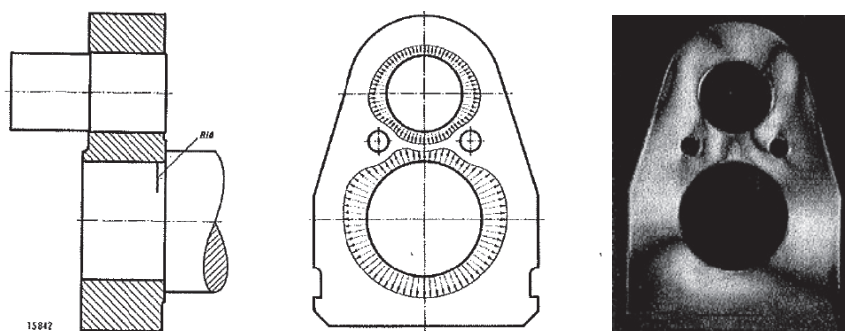


*Figure 3: Analyses of load distribution in 1967 [3]*

The findings from these studies were reflected in a number of design optimizations, such as the relief bores in the crank web.



Figure 4 shows some of the variations. Other suggestions to optimize the axial undercut or crank pin shoulder, however, could not be found in any existing design drawing. Consequently, no comparisons existed of the performance of these hypothetical variants.

A further problem was that the available sources did not describe how to create the shrink-fit in such a way as to reduce the likelihood of potential failures.

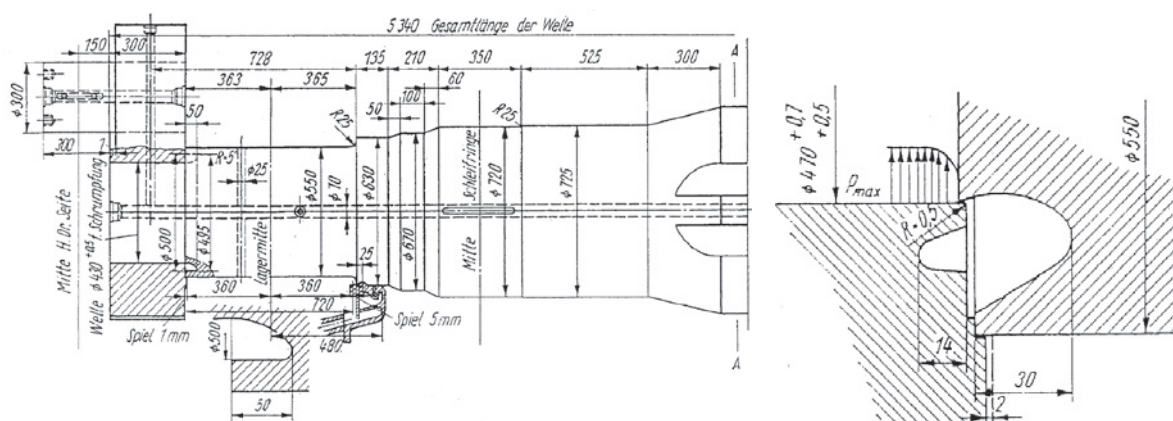


Figure 4: Some design variations appear in contemporary drawings, while other suggestions apparently were not implemented [8]

#### 4 Root cause analysis based on the previous failure

Macro- and microscopic investigation suggested that the fracture could be related to fatigue overloading stemming from the benchmarks and the smooth surface structures. The stress mode responsible was a combination of bending and torsion (the inclination of the fracture surface relative to the shaft axis can create significant torsion).

The crank pin surface showed fretting marks from where the observed crack obviously propagated. Both axial and circumferential movements, clearly identified by scanning electron microscopy (SEM), caused fretting marks and wear even on the inner side of the crank (Figure 5) [1].

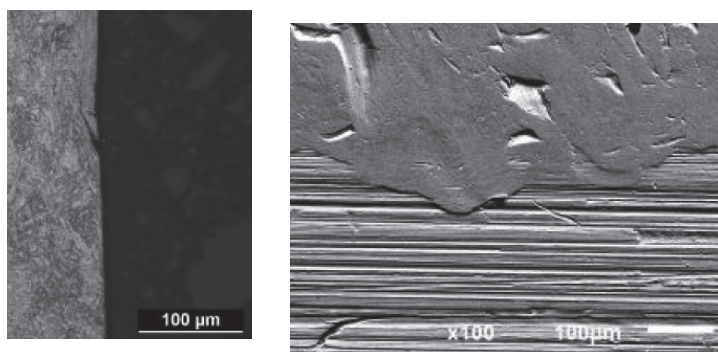


Figure 5: Deformed surface in the transition region [1]



## 5 FEA and experiment combine to explain fretting

### 5.1 Understanding fretting fatigue

Generally speaking, there is a particular risk of fretting fatigue when components are braced under high surface pressures and experience reciprocal relative movements (slippage) as a result of dynamic loads. This causes progressive cracking, and ultimately failure. Fretting fatigue occurs in both bolted joints and shrink-fit assemblies. In reciprocating compressors, typical highest risk areas are the crosshead/piston rod joint, the fit in the crosshead body for the crosshead pin, the surfaces where the cylinder attaches to the engine frame, and the seats in the bearing blocks that accommodate the sliding bearings, or fitted bolts in the case of rigid clutches. These areas should receive special attention when metal surfaces in the compressor are being examined.

Empirical tests show that fretting does not always result in surface cracking followed by crack propagation and eventual component failure. Statistical evaluations of experiments reveal various different damage profiles based on the degree of relative movement. They also indicate a relationship (qualitative if not quantitative) between the amplitude of the slip and the applied surface pressure. Figure 6 shows results from many experiments in which an alternating flexural load was applied to a shaft/hub shrink-fit joint.

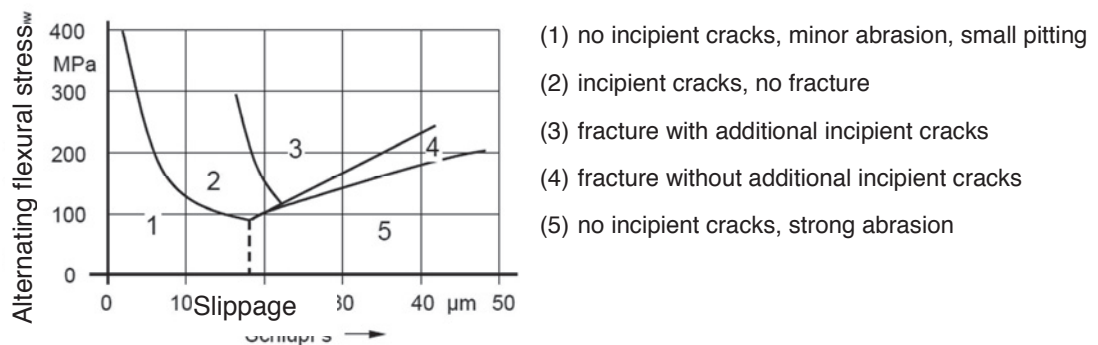


Figure 6: Experiments show five different damage regimes based on the stress and the degree of slippage [4]

More tests were conducted with flat specimens that were moved with small amplitudes between bridges pressed together with defined forces. This yielded a qualitative understanding of the relationship between slippage, surface pressure, and the number of cycles until fracture (Figure 7)

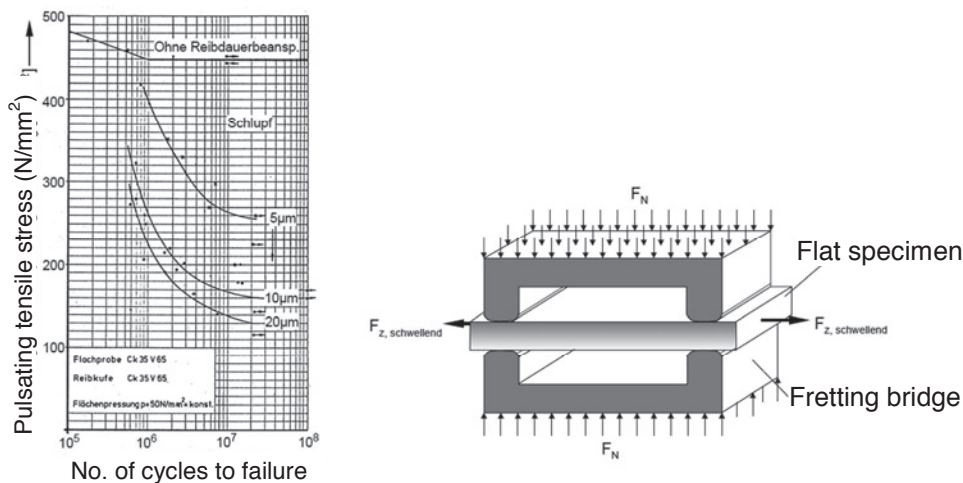


Figure 7: Fretting experiments with a flat specimen showed how time to failure relates to the applied stress and the amplitude of the slippage [5]

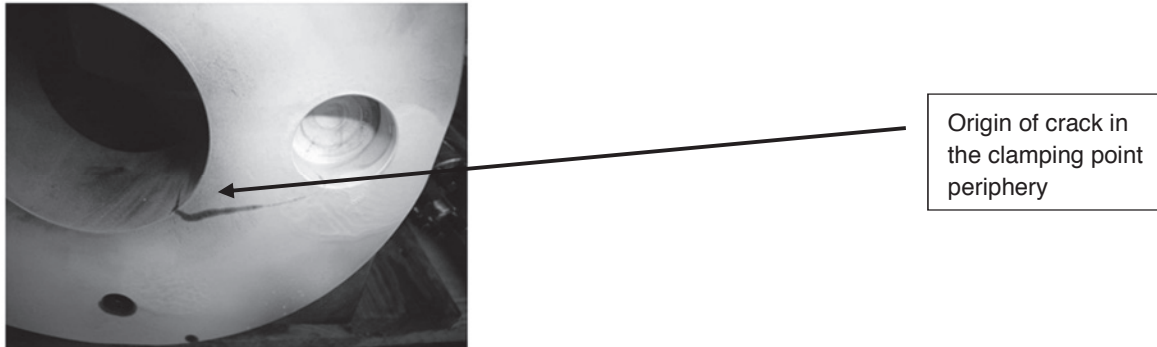
It appears that fretting fatigue is not always considered – or at least not predicted – in the design of reciprocating compressor components that are subject to dynamic loads. To complicate the situation, the root cause of fretting fatigue is frequently either improper assembly or component quality with respect to wear pattern, geometric dimensioning and tolerancing that is no longer ideal.

## 5.2 Fretting fatigue in a crosshead

Computer aided design of mechanical components frequently takes into account equivalent stresses, along with the corresponding notch effects and safety factors, when evaluating strength and fatigue strength. If relative movement and surface pressure are ignored, however, components may still fail through fatigue despite having been designed with adequate strength. With this in mind, we will look briefly at a case in which fretting fatigue damaged a compressor crosshead. The experience gained in solving this problem proved very useful when the time came to create a mathematical model to aid the optimal design of the shrink-fit joint between the crank pin and the web.

In the case of the crosshead, the crosshead body cracked at the piston rod joint (*Figure 8*). This happened repeatedly, at almost identical time intervals, and the cracks always originated from the same spot. The origin of the crack was clearly localized at the periphery of the clamping point. The first step was to establish that the compressor was not operated outside its intended range, that the permitted load was not exceeded, and that assembly errors could be ruled out. Next, a strength analysis was carried out using the finite element method, but this did not reveal the damage mechanism. On the contrary, the model showed that the equivalent stresses at the spot where the crack originated were anything but excessive. As a result, the mathematical model was initially useless in explaining the cracking.

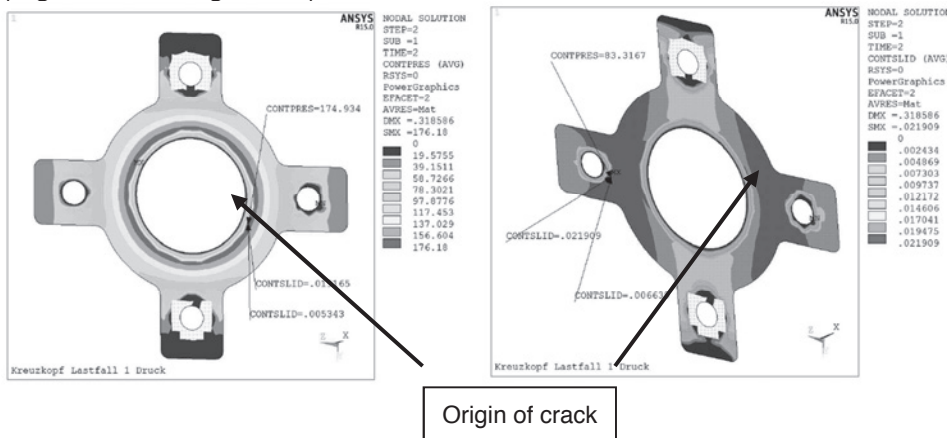
A theoretical understanding only became possible when microstructure replicas revealed surface distress and a multitude of microcracks in the surface. The calculation of friction work ( $WR = \mu F_N s$ ) based on the finite element model was found to be extremely useful in assessing the local criticality of crack formation as a result of fretting fatigue. This method allowed the origin of the crack and the location of the most advanced surface distress to be recreated precisely. It was then possible to use the mathematical model to compare design modifications with a view to minimizing friction work and hence prevent cracks caused by fretting.



Origin of crack in the clamping point periphery

Figure 8: Surface damage due to fretting led to cracking of the crosshead body, even though the equivalent stresses at this point were comparatively low

The model was initially framed in terms of two load cases, corresponding respectively to the maximum piston rod axial force in each direction. The model took into account the local surface pressure, the elastic deformation of the components, and the resulting relative movements (Figure 9 and Figure 10).



Origin of crack

Figure 9: (left) Surface pressure map of the crosshead joint, and Figure 10: (right) Slippage [10]

Comparison with the real crosshead, which showed the same damage time and again, revealed that the crack always originated at the point where the product of compression and slippage is greatest. The ability to use the mathematical model to minimize local friction work allowed the crosshead to be redesigned to prevent cracking, and this knowledge was even incorporated into the FE-Analysis of the *Einheitsverdichter* crankshaft.

### 5.3 Adapting knowledge to the crank pin joint

In the case of the failure of the shrink joint between the crank pin and the web, the clear finding is that slippage occurred between shaft and hub. The combination of slippage with high compression forces caused by the shrinkage overlap that surface distress and microcrack formation were accompanied by additional crack propagation. Ultimately this caused the newly manufactured crankshaft to fail prematurely due to fatigue. As expected, the crack originated on the side of the shrink-fit facing the periodically reversing forces (Figure 11). The crack appeared in particular in areas of low partial slip regime.

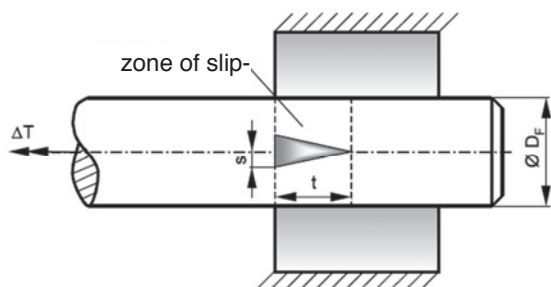


Figure 11: Slippage at a shaft/hub connection subject to torsion caused by elastic deformation [5]

In addition to fretting fatigue, alternating flexural bending loads must not be overlooked in the crank pin/web shrink joint, since these can play a decisive role in the propagation of microcracks from the distressed surface.

As with the crosshead discussed in section 0 above, a solid model of the crank pin joint was created. As well as calculating the expected equivalent stresses, the model also provides information about the compression of the component surfaces and their relative movement. The model was then used to evaluate variations in fretting fatigue, equivalent stresses, fatigue strength, and alternating flexural loads caused by the changing operating load. The ultimate aim was to produce a detailed design for a new crankshaft.

To begin with, press fits with differing shrinkage overlap and the resulting slippage were analyzed. This investigation was accompanied by a thermal analysis for creating the press fit. This showed that, with growing shrinkage overlap, slippage also increased by virtue of the press fit and operating force.

For the purpose of comparison and rating, the product of joint pressure (determined by shrink-fit and operating load) and slippage was used.

In addition, differing material versions were analyzed since the earlier crankshafts were made of Ck35 (1.1181) and the more recent crankshafts of 34CrNiMo6 (1.6582). The material 34CrNiMo6 +QT was selected due to its better behaviour in terms of mean stress sensitivity. As expected, the newer material produced higher strength characteristics, and the equivalent alternating stress was also significantly below the permissible values, resulting again in greater reliability.

As a result, design variants that might reduce the maximum amplitude of friction work by better distributing the slippage along the length of the shrink-fit joint. One idea was to chamfer the edge of the bore at a small angle (*Figure 12*).

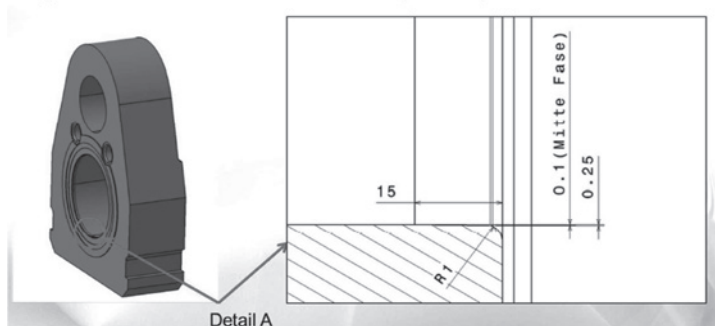


Figure 12: Chamfering the bore of the crank web might be expected to distribute slippage more evenly [9]



However, this “softer” transition did not significantly reduce the maximum friction work amplitude. Instead, it merely caused a small shift in the location of the maximum friction work, accompanied by a slight but undesirable increase in flexural stresses.

Another variant was the introduction of a relief groove extending around the bore (Figure 13). This did not usefully decrease the slippage amplitude, though its effect on flexural stresses in the shaft was less than in the case of the chamfer.

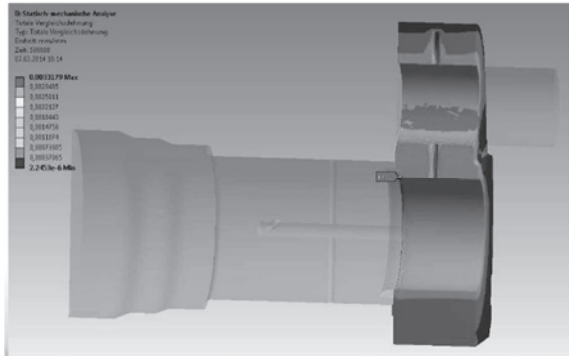


Figure 13: A relief groove surrounding the bore of the crank web had little effect on slippage [9] Several variants of relief grooves and chamfers were checked with the mathematical model, primarily by evaluating the maximum equivalent stresses in the shaft caused by operation loads, bending, torsion and transient loads. As expected, the type of relief did not have any great influence on the friction work that occurs in the area of slippage.

On the other hand, it was found that varying the diameter of the shrink-fit joint does influence the maximum friction work essentially. Increasing the joint diameter from its starting figure of 431 mm initially to 480mm causes a minor increase in slippage. However, the increased area of the joint makes it possible to reduce the amount of compression, resulting in a “softer” web. The model showed that reducing the compression also reduces the maximum friction work (Figure 14 and Figure 15).

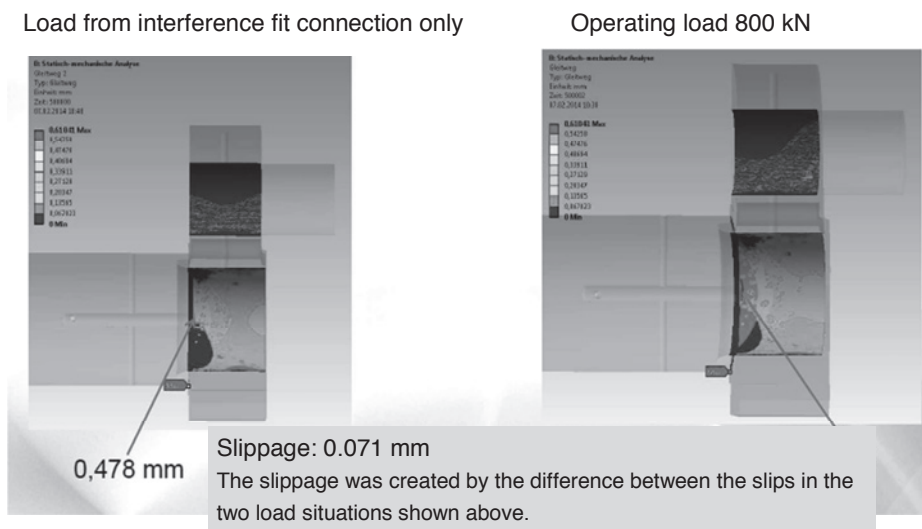


Figure 14: Slippage with a shaft diameter of 431 mm [9]



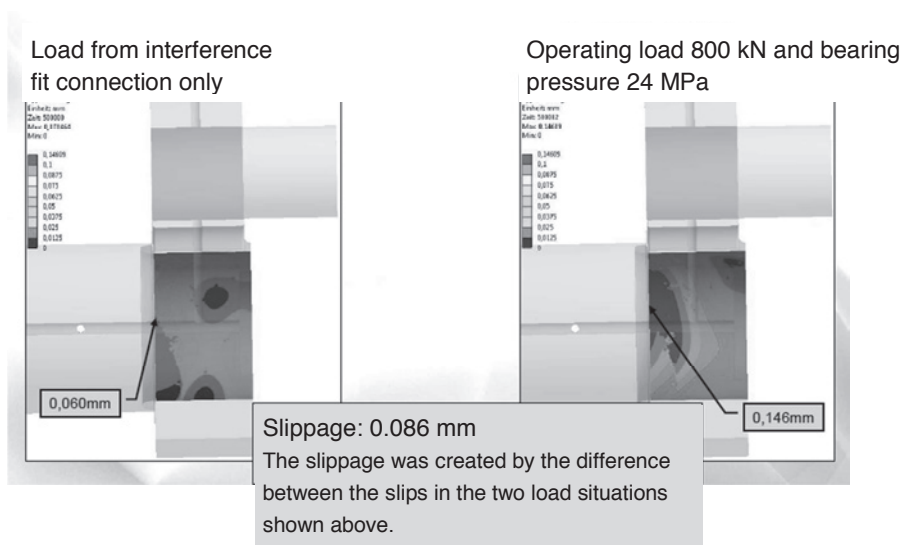


Figure 15: Increasing the shaft diameter to 480 mm reduces slippage [9]

The minimum friction work amplitude was found to occur at a shaft diameter of 480 mm (

Figure 15). Any further increase in diameter makes the crank web increasingly “softer”, the slippage amplitude rises, and so does the friction work. Depending on the value of the friction coefficient, sliding may also occur.

In addition to minimizing the friction work, increasing the shaft diameter also has the advantage of reducing the equivalent stresses in the shaft (

Figure 16 and

Figure 17). This increases the safety factor to 4.8, from an already high value of 3.5 with the original diameter.

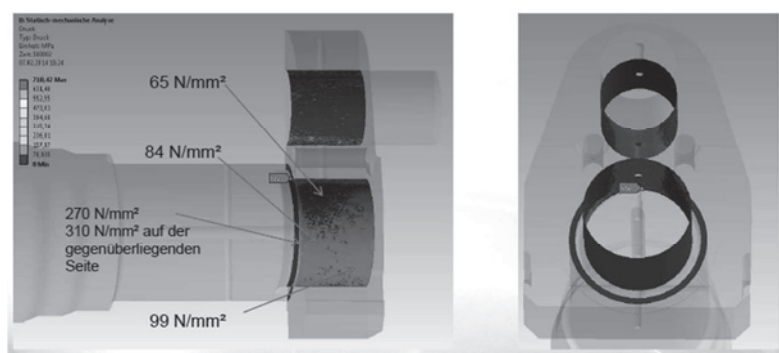


Figure 16: Distribution of surface pressure for a shaft diameter of 431 mm [9]

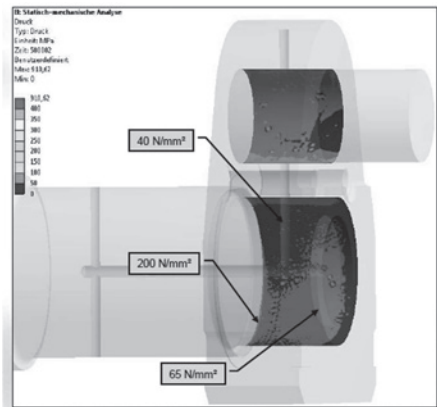


Figure 17: Distribution of surface pressure for a shaft diameter of 480 mm [9]

The mathematical model is valuable in analyzing failures that have already occurred, but cannot make predictions about components where real failure data is not available. This is because no limit values are yet known for the amount of friction work that will cause fretting failure. Each joint requires its own dedicated model.

## 6 Other important features in manufacturing and assembly

Besides increasing the shaft diameter as discussed above, the literature on fretting fatigue in shrink-fits [6] revealed two other critical points required to increase the fatigue strength of a new crankshaft. First, the design requirements of the axial shaft undercut must be optimized (Figure 18). Second, the surface must be work-hardened, for instance by shot peening (Figure 19). The latter is intended to decrease susceptibility to cracking by inducing residual stress into the shaft in the transition area of the joint, between the solid support and the part of the crank web in which slippage occurs. The literature describes decreased susceptibility to cracking compared to untreated surfaces of 20% for such shrink-fits.

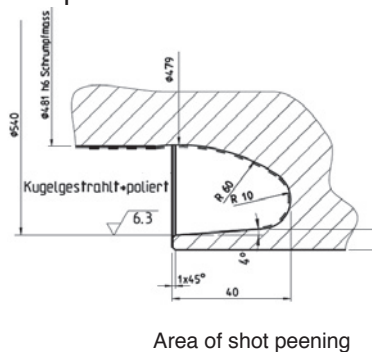


Figure 18: Optimized undercut design

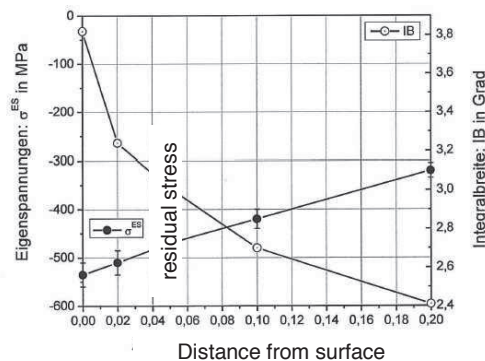


Figure 19: Residual stress from shot peening [7]

The crankshaft components were manufactured as forgings (Figure 20). After the shoulders had been machined and the respective fit dimensions created, the critical areas were work-hardened by shot peening (Figure 21). Since this increases the dimensions slightly, the surfaces were then polished down to the desired size.

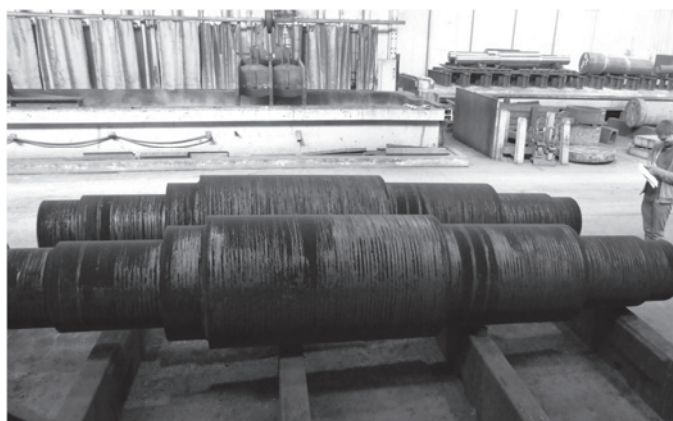


Figure 20: Forged crankshaft components

The most critical dimensional accuracy is required in the area of the shrink-fit. This was achieved by final honing of the bores in the crank web (Figure 22).

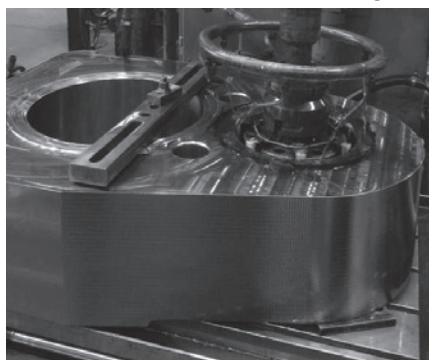
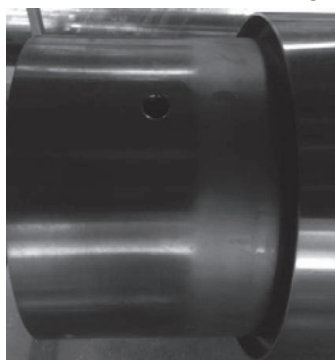


Figure 21: Shot-peened shoulder      Figure 22: Honing the bores of the crank web

The shrink-fit process itself is also critical to success. In previous attempts, the crank pins were first joined to the web, with the main journals attached as a separate step. This approach was abandoned, however, when it was discovered that the process of fitting the crank pins distorted the main journal bores. Instead, it was decided to create both shrink-fit joints during the same operation, so as to create a homogeneous distribution of stresses in the crank web.

Each web was therefore heated uniformly while the crank pin and the main journal were cooled with dry ice. Figure 23 shows the insertion of the crank pin, and Figure 24 shows both joints after assembly.

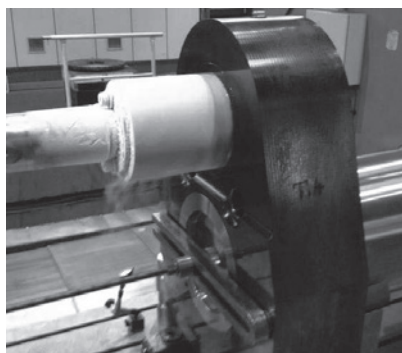


Figure 23: Joining the crank pin

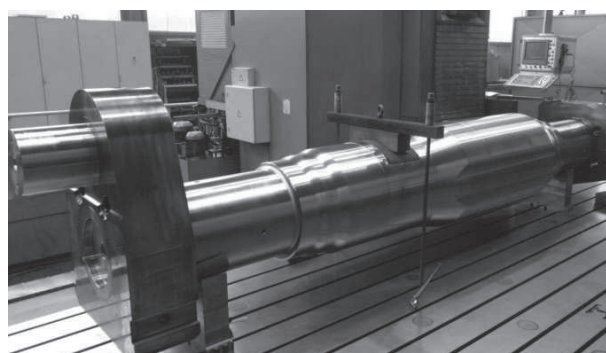


Figure 24: Position test of the crankshaft

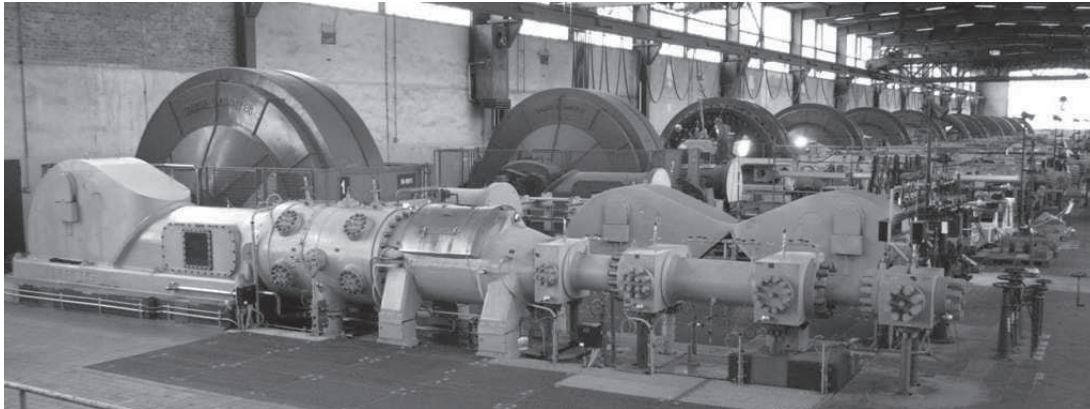


Figure 25: H2 compressor station for hydrocracking service

## 7 Summary

The failed first attempt to manufacture a crankshaft based on individual production drawings, without any in-depth analysis, highlighted the potential risks inherent in this type of assembly.

A successful design was possible only through a combination of studies: careful analysis of previous failure modes, finite element modeling, an appreciation of the role of friction work, and laboratory experiments to identify the different regimes of stress and slippage that influence fretting fatigue. This work was backed up by investigations of various previously suggested design variants, and a good understanding of the processes of shot peening and shrink fitting.

With reliable partners at all stages of the work – from investigation, through forging and machining, to assembly and testing – it was possible to develop an effective solution in this case.

## 8 References

- [1] B. Persigehl, Dr.-Ing., Root cause analysis of crankshaft fracture, AZT Investigation report, Munich, 06/2013
- [2] J. Nickl, Dr.-Ing., Berechnungen zum Einheitsverdichter (Calculations regarding the Einheitsverdichter), TU Dresden, Dresden, 2012
- [3] F. Anders, Dipl.-Ing. Allianz – Der Maschinen-Schaden (Allianz – Machine Damage), issue 6/67, Allianz, Munich 1967
- [4] „Neue Erkenntnisse zur Simulation der Reibkorrosionsvorgänge in torsionsbeanspruchten Wellen – Naben – Verbindungen“, Autor Hr. Dipl. Ing. Ulrich Hartmann von der Fakultät V –TU-Berlin, Date: 2005
- [5] „Untersuchungen an spannungshomogenisierten und zylindrischen Pressverbindungen unter Torsionsbelastung“, Dipl. Ing. Christian Göggl der Fakultät Maschinenbau der Univ. Stuttgart, Date: 2003
- [6] Jaap Schijve, Fatigue of structures and materials, 2nd edition, Springer, Netherlands, 2009.
- [7] Untersuchungen zu Eigenspannungen durch Kugelstrahlen (Examinations regarding residual stress as a result of shot peening), MIC Unna, 2014
- [8] M.I.Frenkel / Dr.-Ing.W.Christian, „Kolbenverdichter“ Schrumpfverbindung (shrink-fits), VEB, 1969
- [9] “FE-Analyse Schrumpfverbindung Kurbelwelle (FE analysis of crankshaft shrink-fit)”, ENTECH, 25/02/2014
- [10] Bericht EN.RV.FE.024.BASF-001 (Fa. ENTECH), Date: 20/02/2015



# Technical Paper

**Session: 41-2**

**Session Name: Operations**

## Hard particle contamination in reciprocating compressors

**Author:**

**Dr. Ricardo Cruz**  
**Burckhardt Compression**  
**8404 Winterthur, Switzerland**

**Co-Author:**

**Dr. Norbert Feistel**  
**Burckhardt Compression**  
**8404 Winterthur, Switzerland**



## 1. Summary

The reliability of process gas compressors has never been more in the focus of plant managers and process equipment engineers. Often, the presence of gas contaminants in the form of abrasive particles is not taken into consideration during the design stage. The sign of accelerated wear due to hard particle contamination is only usually observed after an unscheduled process gas compressor shutdown. In many cases, condition based monitoring is a valuable aid in detecting early signs of accelerated wear. During operation, problems due to hard particle contamination are most often indicated indirectly by valve failure. Once the process gas compressor is shutdown, in order to understand the failure root cause and bring the process gas compressor reliability to acceptable levels, in a first step, it is required that a detailed forensic investigation to be conducted on sealing rings, guide rings, packings and cylinder liners. As a second step, corrective actions are required to be implemented. In such cases, the investigation brings the entire process gas compressor and process under scrutiny. The relation between the compressor OEM and End User/Operator becomes extremely strained. The potential corrective actions are in many instances limited as the plant has already completed the engineering stage and plant managers want to focus on production. The cost of such gas contamination, both in compressor downtime and material costs can in many instances exceed several thousands of euros. The origin of such gas contamination can be various, such as materials used as adsorbents in pressure swing adsorption (PSA), which is a technique used as gas dryer and purifier. The lack of piping cleanliness after welding and fitting, the absence of rust inhibitors during hydro testing are potential sources for contamination. The material selection on the gas compressor can be made in order to counteract the accelerated wear created by the foreign particle ingress. The cause/effect understanding of hard particle contamination is critical for a reliable compressor operation and for drafting of maintenance schedules. Thermally sprayed tungsten carbide coatings or other ceramic based materials have seen successfully used in mitigating the consequences of abrasive particle ingress. This paper will provide an overview of such investigated cases; it will disclose effects of two body and three body abrasion found on cylinder liners and piston rings. The paper will disclose potential repair and protection measures required for trouble free compressor operation.



## 2. Introduction

Process gas compressors under API 618 are designed to a minimum of 20 years lifetime and a minimum of three years of continuous operation [1]. Most operators have their own maintenance schedule and their mean time between overhaul (MTBO) varies greatly. Upon the occurrence of a major breakdown it is inevitable that maintenance and repairs are immediately required. The cost of such failures remains difficult to quantify, but it can incur in to the 6 digits sums. Also cylinder liners are critical compressor parts with long leads times. It has been reported in literature [2] that 8.8% of failures can be related to process related problems. In the same survey, the top causes for unscheduled reciprocating compressor shutdown were compressor valves (36%), pressure packings (17.8%). Within the failures related to process related problems, it is not possible to find exactly the ratio between process-related liquids in the gas stream and debris entering the compressor cylinders, or its impact to valves and piston rod packings. It is well accepted as one of the main parameters for reciprocating compressor reliability is the cleanness of the gas [2]. Possible parts affected by gas contaminations in a reciprocating process gas compressor, to name a few, and represented in Figure 1:

- Cylinder Liners
- Piston rings & Rider bands
- Packings
- Compressor Valves

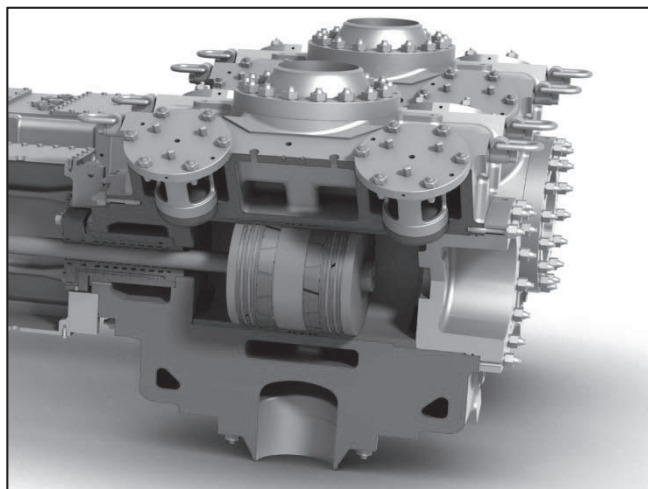


*Figure 1 – Process gas compressor cylinder cross section*

Considering the parts affected, the occurrence of such event can have disastrous effects. The time of which these occur is usually within the first year of operation (8000 hours). Some failures have occurred in periods less than 500 hours. Critical equipment can be delivered with online monitoring system and the information required is collected and evaluated. Process operation conditions, vibration, dynamic pressures, temperature and rod position are typical monitored parameters. The performance of piston rings and valves can be monitored by dynamic pressure curve measurement, pressure/volume diagram, (pV diagram). Rod position can give a very good insight on the condition of the rider band wear condition, as they carry the piston weight. The location of the wear band should be in a position which is protected from direct contact with the process gas, i.e between the two piston ring packs – for a double acting piston. This translates to an increased reliance on the pV diagrams to detect blow-by, by a shift in the pV diagrams, crossing the theoretical curve for both chambers. If compressor valves begin to leak, one of the immediate reactions is the increase of the gas temperature.

In some cases crankshaft bearings can modify the effective load angle of the piston resulting in increased surface pressure in the cylinder, hence the frame vibration is also important to monitor.

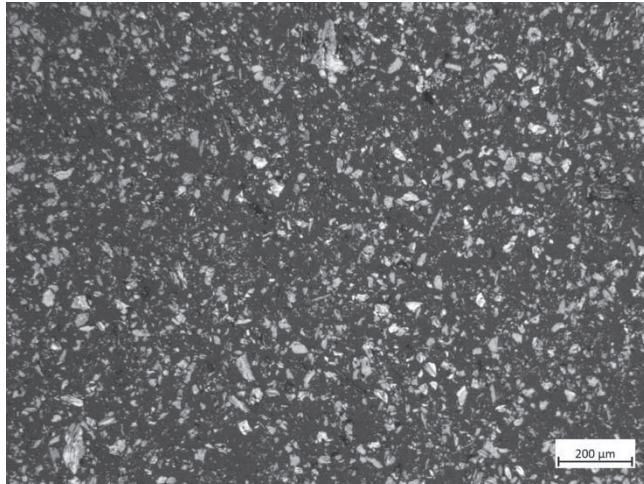
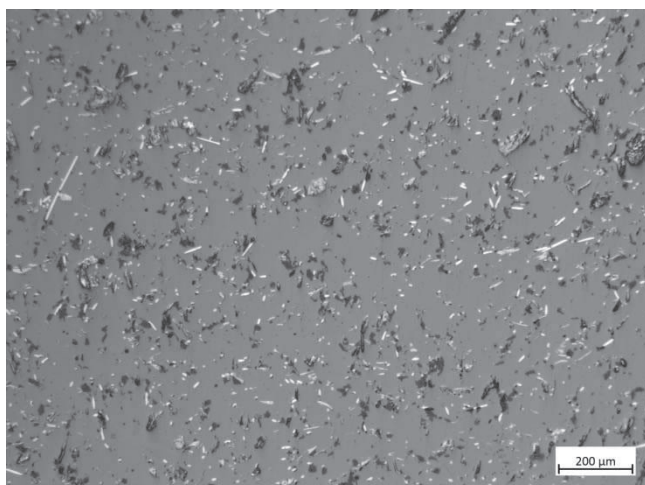


Figure 2 –Microstructure of carbon/ graphite-filled PTFE.

### 3. Compressor parts – Piston rings and Cylinder liners

For many years Polytetrafluoroethylene (PTFE) based materials are used for both sealing rings and rider bands in the compressor industry. The most commonly used fillers are carbon/graphite which are known to be soft and ductile. PTFE, Figure 2, is known for poor abrasion resistance due to the lack of mechanical resistance in an unfilled state. Graphite and carbon fillers are added in defined quantities to improve wear resistance. The cold flow/creep limit of filled PTFE depends of a number of factors, intrinsic to the operational window and depending on material properties and piston ring design. During the design stages, some operational parameters have to be known, such as, temperature, pressure difference, piston ring geometry and joint sealing to name a few. This is linked with the operational performance of filled PTFE based materials which begin to creep, therefore reducing the sealing efficiency and lifetime of piston rings. With proprietary PTFE processing and careful piston ring pack design, in some cases the pressure limit can be extended further than 250 bar. High temperature polymers, e.g. Polyether ether ketone (PEEK), in combination with PTFE, graphite and carbon fiber is known to have low scuffing resistance and sliding and micro abrasive wear resistance when compared to its pure state [3]. PEEK is recommended to be used at heavy duty applications.

Figure 3 shows a bearing grade PEEK microstructure. The cylinder liner material can be made out of 34CrAlNi7, in Gas nitrided condition. Gas Nitriding is a ferritic thermochemical treatment in which nitrogen is diffused into a steel surface at a temperature between 480-570 °C. After nitriding, a thin compound layer known as white layer is formed at the surface, which is composed of iron nitrides. The thickness of the white layer is typically between 5-30 μm. This formation of this layer is actively controlled by heat treatment process. To prevent the white layer from spalling during operation, the white layer needs to be mechanically removed [4]. The motivation to nitride cylinder liners is mainly to improve the surface hardness and wear resistance, with a reduced risk of scuffing and galling. A typical micrograph of nitride surface is shown in Figure 4.



*Figure 3 –Microstructure of bearing grade PEEK*

For all cylinder liners the white layer is removed by a further honing operation, using diamond impregnated honing stones. This results in typical surface hardness values between 900-1100 HV [4]. Soft cylinder liner materials such as Cast iron and Ni resist can also be used in compressors but their matrix is recommended to be run against PTFE based materials and in cases of particle free process gas. The expected wear rate of a good performing lubricated process gas compressor cylinder liner wear rates tends to be lower than 0.1 mm/1000 hours operation. Piston rings and rider bands which are considered being a consumable, have wear rates ranging between 0.1-0.3 mm/1000 hours, for lubricated service, further depending on other process conditions and after careful selection of the material type for the specific service.

#### 4. Cases

The situation of external particle contamination remains a “taboo” subject within the compressor industry. Many processing plants receive the process gas from other gas providers; hence the contamination origin cannot always be ascertained. The occurrence of such events is rare but extreme troublesome. In some cases cylinder wear rates could be extremely high, as 6 mm/1000 hours of operation and piston ring wear rates higher than 15 mm/1000 hours. Occasionally, it has occurred that operators have several older process gas compressors machines in operation and use increased capacity of the most recently engineered process gas compressor, as the base load equipment and the older equipment becomes peak load equipment. In some cases even though for the other machines it had ordered more than 30 cylinder liners in the last 25 years. One aspect that remains unanswered is the fact that lower stages of process gas compressors are not affected. This can be attributed several factors: a) lower pressure difference, b) softer polymer ring, PTFE (60-70Shore A) vs PEEK (80-85ShoreA) and c) tribology pairing between a soft cylinder liner, e.g cast iron, which has a graphite open structure being capable of embedding particles.

Figure 5 shows a piston ring from a hydrocarbon compressor, which suffered from extreme cylinder liner wear with clear metal particles embedded. Using scanning electron microscopy with energy dispersive X-ray spectroscopy (SEM/EDX) it was possible to determine the chemical composition of the particles embedded on the ring surface (Figure 6) which was  $Al_2O_3$ .



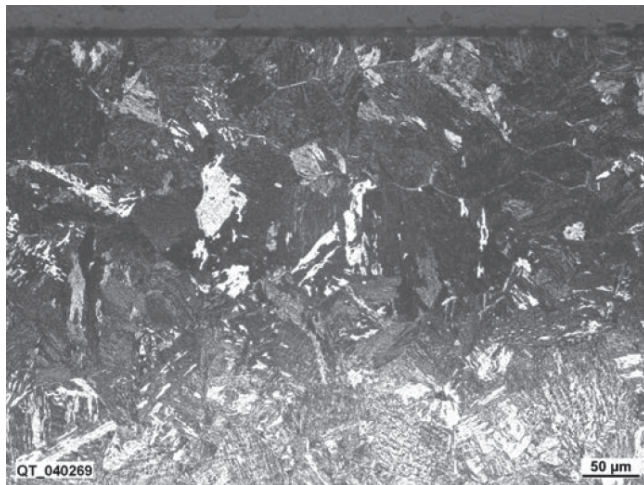


*Figure 4 – Typical microstructure of 34CrAlN7 – etched condition.*

The piston ring during operation is a very dynamic component. During the compression stroke the ring flank is compressed against the piston ring groove. As the rings are relatively soft, metal particles coming from the process gas or even wear particles from the cylinder liner wall can be embedded on the piston ring flank, creating wear on the piston ring groove as seen in Figure 7. The cylinder liner can present heavy scoring marks, as shown in Figure 8. These marks will be in the sliding direction and with ploughing, only visible under SEM. The wear mechanisms will be further detailed in section 6. There are cases where fine filtration systems are fitted in upstream of compressor.

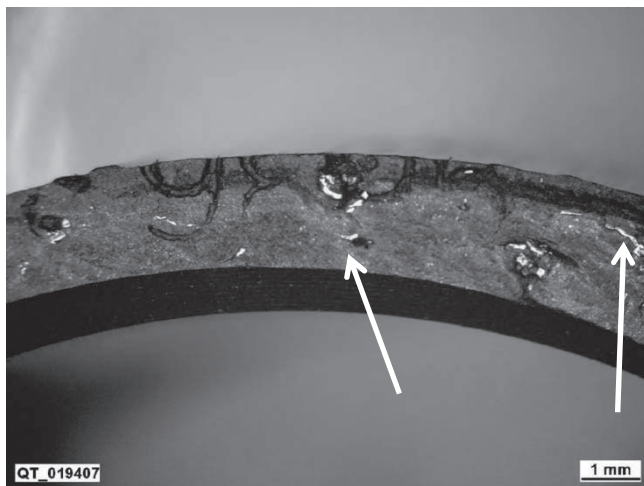


*Figure 5 – Piston ring with embedded metal particles.*

However, some operator startup procedures include operation with the filter in bypass mode, due to their experience of fast filter clogging. This means that particles could ingress the compressor until the filter is put into operation. Once the filter is in operation the cylinder liner wear rate is expected to decrease to acceptable levels.



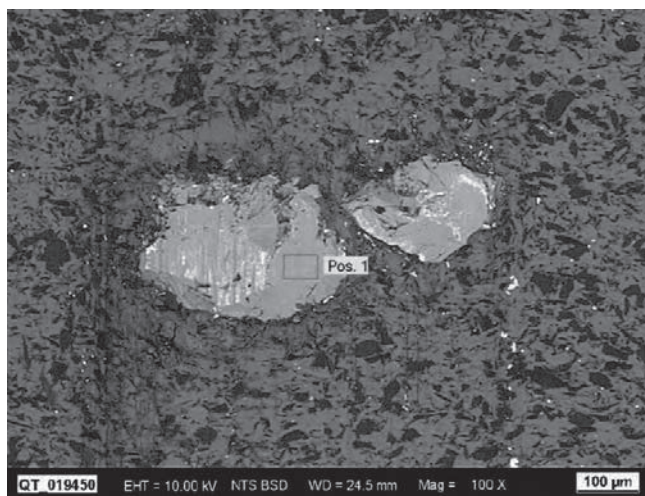


Figure 6 – SEM micrograph of  $Al_2O_3$  particles embedded in piston ring.

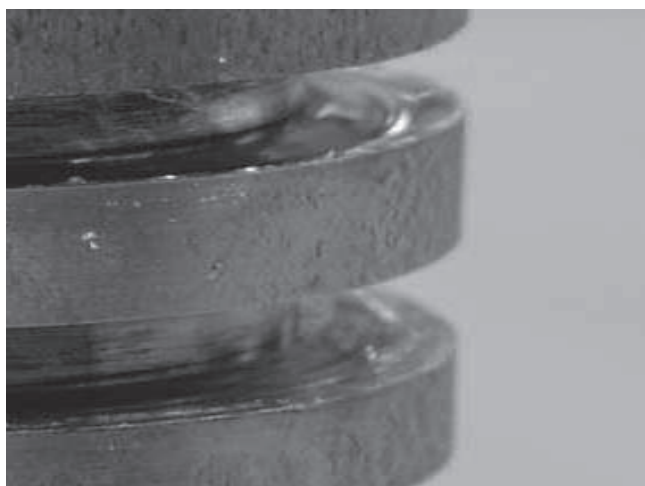


Figure 7 – Piston ring groove wear

## 5. Contamination Origin

The source of contamination can arise from multiple sources. Outside of the compressor OEM battery limits, there is usually little or no information is exchanged. Some factors have to be taken into consideration depending whether the plant is new or already for some years in operation, i.e new process gas compressor in old pipes. In some occasions during welding/fitting some debris can remain, after the hydro testing the absence of rust inhibitors in some cases combination with aggressive process gases might lead to pipe corrosion. Iron oxide based particles are the most prolific in this case. Table 1 summarizes the hardness values of possible contaminants. Certainly these types of contamination would create limited compressor damage. However, if the process gas contamination level remains high and constant immediate measures have to be taken. Such measures include gas treatment/conditioning, by means of filtration systems and a careful revision of the materials used. In order to obtain purified process gas, pressure swing adsorption (PSA) is a well-established gas separation, gas drying and hydrogen purification technique. In general it is used to separate some gas species from a mixture of gases, according to their characteristics and affinity for an adsorbent material. Typical

adsorbents can be activated carbon, silica gel and zeolites. The PSA process is based on a physical method to cage the bigger water molecules by holding them in porous material.

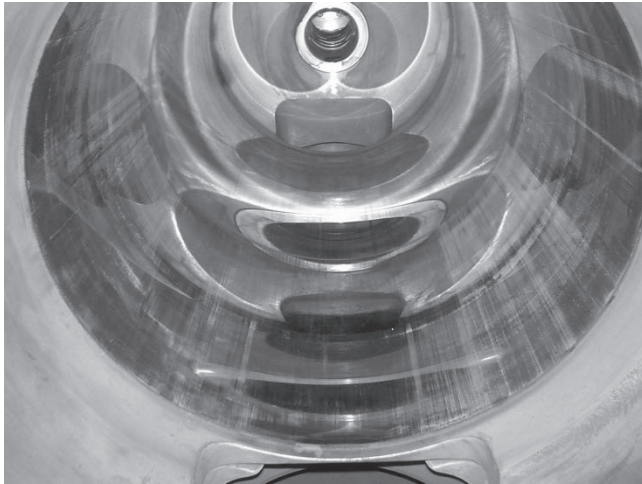


Figure 8 – Dry running  $H_2$  Compressor

Therefore huge columns are built and filled with corresponding material, in order to provide good flow distribution across the adsorbent bed. Some of these materials are based aluminosilicate minerals,  $Ca_x$ ,  $Na_x$ ,  $Al_xO_x$  and  $SiO_x$ . The hardness values of such materials are summarized in Table 1. The composition of such materials can vary widely depending on the application.

	Hardness Scale	
	Vickers (HV)	Mohs scale
Aluminosilicate minerals		3.5 - 4.5
Iron oxides ( $Fe_xO_x$ )	~600	4.5 – 5.5
Silicon Oxide ( $SiO_2$ )	~1200	7-8
Aluminum oxide ( $Al_2O_3$ )	~2000	9

Table 1 – Hardness values of possible compressor contaminants.

The cleaning process of such columns is based on the back flow process. By introducing dry and hot gas, to the cleaning process this can cause damage to the adsorbent material. Small broken parts of ceramic nature will then travel with the process gas flow into the compressor equipment. The backflow process is assured by a network of valves; in the case of PSA dusting, the valves are subjected to excessive wear. During the first few hours of operation, it is also practiced to bypass the filter to prevent excessive fouling and clogging the filter within the first few hours of operation. Some other cases due to economic constraints the filter bypass line does not have any filtration. Also, improper filter design can result in the same effect as no filtration at all. In addition it is also possible that remains from the construction period are still in the system. Due to the fact that dirt will reduce over the time assuming that the process gas is fairly clean, the effect of rapid wearing cylinder liners will decrease. In any case it's of the utmost importance a properly designed filter

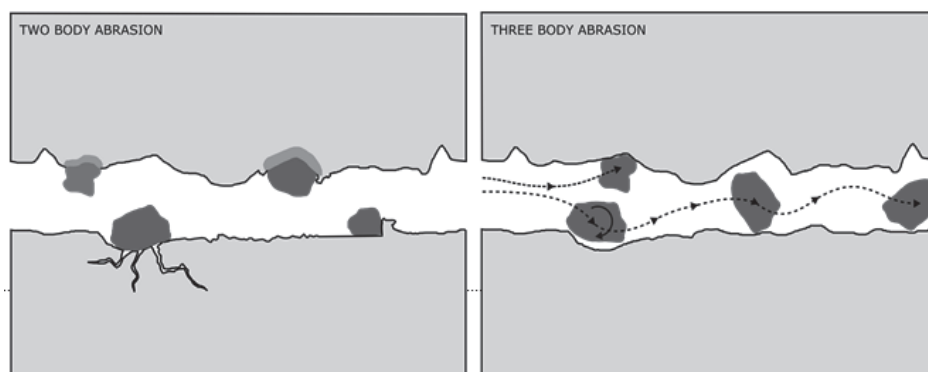


Figure 9 – Two and Three-body abrasion wear.

## 6. Wear Mechanisms

Abrasive wear is a general term which requires to be analyzed with great care. For an in depth comprehension of the abrasive wear mechanism a few insights into abrasion theory are given. In order to wear occur by abrasion, relative contact between two surfaces with a given load is required and obviously knowledge of the material properties in question. Some abrasive wear mechanisms are [5]: micro-cutting, fracture, fatigue and grain pull-out.

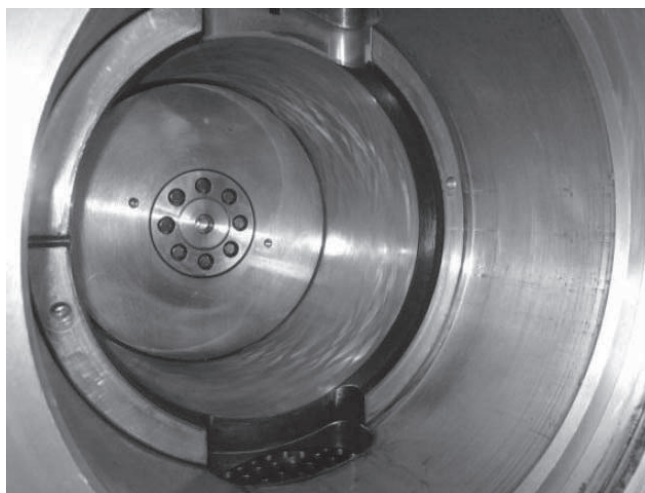


Figure 10 –WC coated liner after 6000hrs of operation

The nature of abrasive wear is given by the interaction between the external particle and the surface, i.e two-body and three-body abrasive wear. In simple terms for the case of polymer based piston ring vs a metal cylinder liner. The rigid external particles are held by the soft polymeric matrix acting in a similar manner as a cutting tool, as shown in Figure 9, left side. In a three-body the external particles are not held on the polymeric matrix and are free to roll and slide over the surface, Figure 9, right side. The abrasion is mainly dependent of the hardness ratio between the particle and the surface. If the ratio is higher than 1.2, then plastic indentations are produced on the surface, hence hard, fast abrasion. If the hardness ratio is below 1.2 there is no plastic indentation on the surface [5]. The shape and size of abrasive particles is also of great importance. Angular particles cause much more severe wear then rounded particles. Furthermore, particles with sharp edges cause more abrasion than round particles. Large particles can produce high values of abrasive wear. For high wear rates, a constant flow of hard particles needs to be introduced in order to create such amount of wear in

a short time frame. In the case of hydrodynamic lubricated parts such as piston rings, abrasive damage only occurs if the particle size overcomes the fluid film thickness, and the highest amount of wear concentrates on the mixed lubrication areas (TDC and BDC). Hence the appearance of such cylinder liners is close to a double trumpet shape – in case of a double acting compressor. From experience it has shown the critical size for particle damage ranges between 10-100  $\mu\text{m}$ . This is within the expected range for the fluid film thickness.

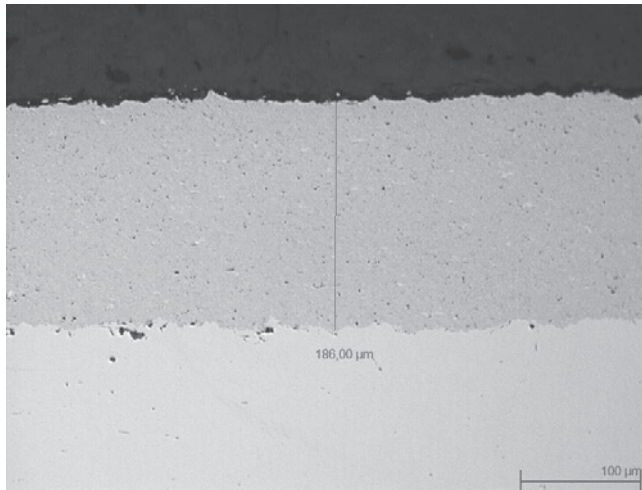


Figure 11 – Micrograph from WC coating.  
Courtesy of RHEIN-RUHR Beschichtungs-Service GmbH.

## 7. Solutions – Path Forward

If a process gas compressor is being fitted to a new or existing plant good working practice would be to evaluate the equipment upstream of the compressor and evaluate the risk of hard particles ingress. Also special attention should be taken to the piping. During the upstream piping fabrication and hydro test, appropriate cleaning and passivation should always be practiced. If particles are detected during or after commissioning it may be required to bite the bullet and chemically clean, flush and passivate the system. Additional measures to protect the compressor cylinder liner can be taken even after the commissioning. A revision of the cylinder liner materials is the most common approach. Cermet's comprising of 88% Tungsten Carbide (WC) and 12% Cobalt (Co) present hardness values between 1200 HV and 1400 HV. The heterogeneous structure sintered composites of hard carbides (WC-Co – 2300 HV) in a soft metal matrix has proven to be wear resistance even in the presence of very hard gas impurities such as  $\text{SiO}_2$  and  $\text{Al}_2\text{O}_3$ . The microstructure of such coating is shown in Figure 11.

Figure 10 shows a cylinder liner coated with WC-Co after 6000 hours in operation. Other sprayed coatings can be used such as  $\text{Cr}_x\text{O}_x$  and other ceramic ternary alloys [6]. The state of the art solution considered is proprietary bi-metal hot isostatic process of the cylinder liner with diameters smaller than 200 mm. This implies a solid base body encapsulated (outer surface) and inner body (powder form) to be processed by hot isostatic press. This combines the benefit of different material properties with a high quality uniform microstructure with a diffusion type bonding without segregations. In the case of suspicion of a particle contamination has occurred proactive and open communication between OEM and End user/operator is required. In such cases focus on well documented information is crucial. The material investigations should be properly structured using experienced certified laboratories according to ISO/IEC 17025.



## 8. Conclusions

The subject of gas contaminations is far from over. These situations will continue to occur in the future. Hence it is of vital importance to understand the equipment upstream of the process gas compressor and evaluate the risk of occurrence for each project. It remains a critical issue to be addressed as early as possible, ideally during the contracting stages. The OEM should be prepared with guidelines for maximum contamination values and with appropriate countermeasures. In the event of high occurrence risk, the OEM should take the lead, with the support of the end user in an open and fair manner in order to understand and resolve the situation as swiftly as possible. From the end user side, the system cleanliness and filtration should be taken seriously. From the OEM perspective, the process gas compressor materials should be appropriately selected in order to assure smooth compressor operation.

## References

- [1] American Petroleum Institute: API STD 618, Reciprocating Compressors for Petroleum, Chemical, and Gas Industry Services, Fifth Edition, Washington DC, 2007.
- [2] Leonard, S.: Increasing the Reliability of Reciprocating Compressors on Hydrogen Services Dresser-Rand, Painted Post, NY, USA.
- [3] Schroeder, R et al, Failure mode in sliding wear of PEEK based composites, Wear Vol 301, p 717–726, 2013.
- [4] George Totten, Steel heat treatment: metallurgy and technologies, CRC Press, ISBN - 13:978-0-8493-8455-4, 2006.
- [5] Bharat Bhushan, Modern Tribology Handbook, Vol 1, CRC Press, ISBN 9780849384035, 2000.
- [6] N. Feistel, Friction surface coatings in dry running piston compressors – benefits and risks, 8th EFRC conference, September 27-28, Dusseldorf, 2012







# Technical Paper

**Session: 41-3**

**Session Name: Operations**

## **Failure analysis and rectification of connecting rod bearing failure against modified compressor operation**

**Author:**

**Usman Sharif  
Fauji Fertilizer Company  
Rahimyar Khan, Pakistan**

**Co-Author:**

**Mohsin Imtiaz  
Machinery Maintenance Engineer  
Fauji Fertilizer Company  
Rahimyar Khan, Pakistan**

## Summary

This paper deals with the achieving goal along with additional benefit of power saving and how by applying engineering techniques the reliability can be improved. Ammonia booster compressor is installed to boost ammonia vapors and deliver to the main centrifugal refrigeration compressor. 02 compressors are installed, one as a stand by and other in operation. The compressor operation required at 50 percent of loading due to plant load conditions. Different solutions were discussed and worked upon, however modification of valves was finalized. The modification in operating of number of suction and discharge valve not only results in achieving the objective of reduced load operation but also decrease in the power consumption manifold. However, the problem of connecting rod bearing failure started to appear after this modification. Detailed analysis of problem along with rod loads and bearing design was carried out. In light of the findings different modifications in system were carried out to avoid the bearing failure. Oil system and bearing babbiting technique were also implemented.

Currently the system is operating as per expectations and delivering more than expected



## INTRODUCTION

Ammonia Booster Compressors are installed to compress ammonia vapors recovered in V-507 and send to Ammonia Compressor K-441 suction line.

This is reciprocating compressor with balanced opposed cylinders. Gas is compressed in one stage, adopting two double acting type cylinders. Pulsation dampers are placed at the suction and delivery to make gas speed and pressure constant inside the piping. Refer Fig 1

The cooling system is obtained as under;

- Cooling of crank gear oil coolers, gearbox oil and stuffing box by means of tower water circulation
- Cylinders and cylinder heads cooling is obtained by a forced circulation of ethylene glycol solution in closed loop

The compressor is driven by 3 phase induction motor of 300KW with speed reducer and coupling.

The compressor takes suction at 1 ATA and discharges at 3.1 ATA with capacity of 5980 Nm<sup>3</sup>/hr

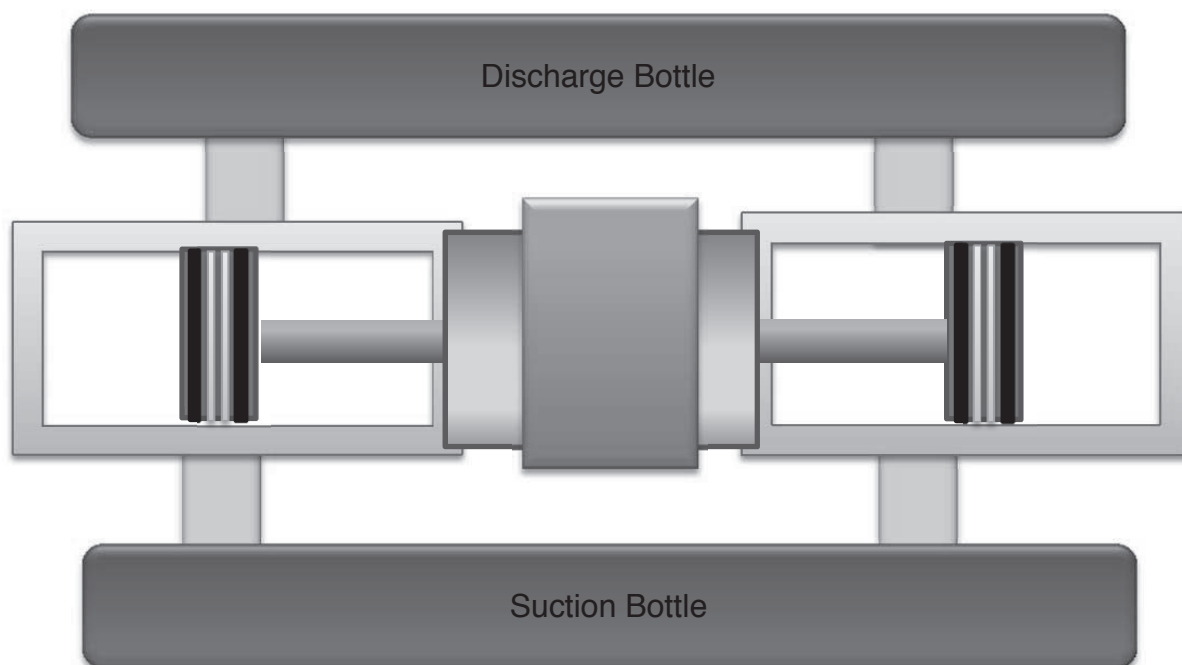


Fig: 1 Layout

## BACKGROUND

The flow through one compressor is higher as required by plant parameters. There are different standard options for capacity control;

1. Opening recycle valve: *not available*
2. Variable speed drive: *not available*
3. Capacity pocket: *can only reduce the load by 5%*
4. Offloading by valve loaders: *takes 22 Amp*

As the volume of vapors recovered during normal operation is not enough to run the compressor at full capacity. Therefore one of the compressors i.e.K-451A was reduced to 50% capacity permanently since the commissioning of plant. During normal plant operation, only compressor "A" remains in service at 50 % load capacity.

But in case of Urea Plant shutdown both the compressors have to run in parallel to full fill the process requirement. Although capacity can be reduced by using bypass line, but it requires about 4 times more energy. Therefore during plant commissioning, compressor was unloaded by removing valves of the compressor permanently.

- At 50% load one compressor requires 22 Amps
- At 100% load it requires 56 Amps.
- When one side valves are removed it requires: 14 Amps

So to save energy and making the compressor more efficient as per plant requirement the option to remove suction valves and blinding discharge valves was opted.

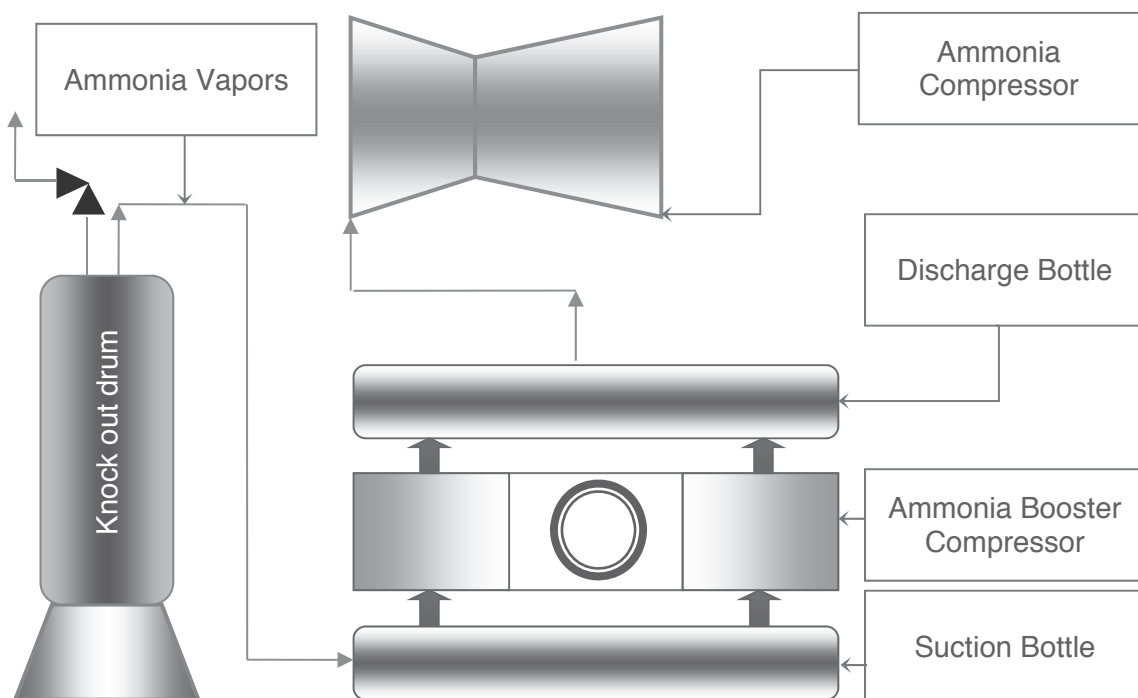


**Fig: 2 Process Flow Diagram of K-451A**





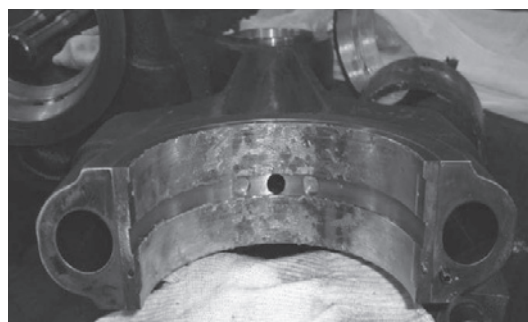
## BEARING FAILURE

Failure of connecting rod big end and small end bearings remains a chronic problem since the commissioning of the compressor A. Meantime between failures (MTBF) of the compressor bearings was 03 to 04 months only.

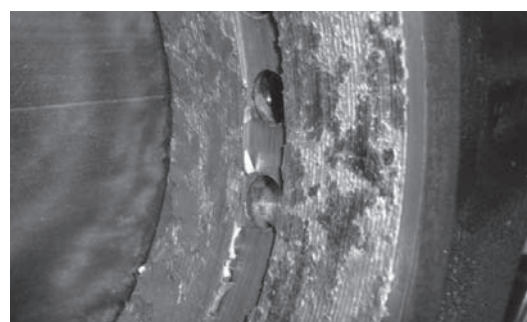
White metal of the bearings always found chipped off from the bearing shells. Refer picture 1 and 2. Lot of work was performed on the machine to rectify the problem including the improved babbiting techniques, changing the thickness of white metal on bearing shells, removal of bearing journals ovality and replacement of connecting rods.

All these works did improve the situation but could not last longer.

Therefore finally a preventive maintenance plan with 03 months of frequency was set for the compressor.



**Pic 1: Damaged big end bearing**

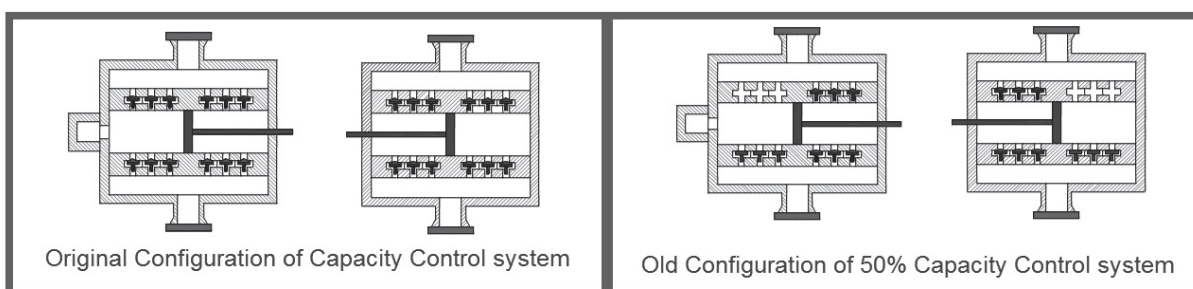


**Pic 2: Close up big end bearing**

## FAILURE ANALYSIS

Bearing Failure problem was persistent with K-451A only and not with K-451B. The only difference between K-451A and K-451B was capacity control configuration. Capacity control system of the compressor was analyzed focusing on the rod load reversals.

*“Rod Load Reversal is the reversal of rod load on small end bush during one complete stroke of reciprocating compressor”*



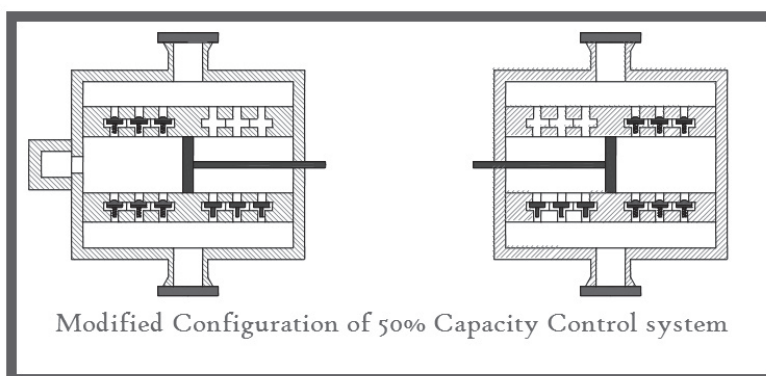
Capacity control system was analyzed as under:

Since commissioning, all the suction valves of both head end sides of compressor K-451A were removed and discharge valves were blinded off. According to this configuration only crank end were loaded while head ends were completely off loaded. However, vendor had loaded head end valves at 50 % capacity in its “Capacity Control Diagram”.

Rod loading diagram shows the uneven distribution of load reversals during one complete revolution of the crank.

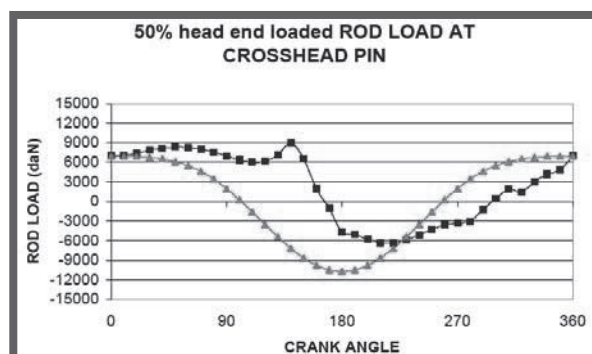
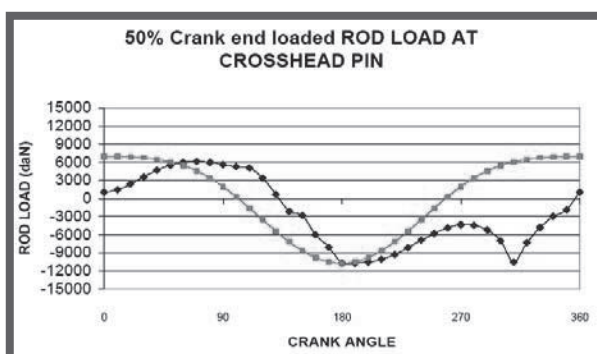
Considering this uneven rod reversal loads, impacts and machine manual's recommendation, head ends were loaded and crank ends were unloaded. This was done by blinding off all discharge valves and removing suction valves of both crank ends.

After Changing the capacity control configuration compressor was taken into service. Compressor MTBF increased significantly.



### ROD LOAD DIAGRAMS:

To carry out troubleshooting the API was referred. In view of API standard rod loading during each step as shown below is within limits but if we further refine our study, we can see that the rod loading is equally balanced (Crank angle during compression 180 degree, crank angle during tension 180 degree) at 100% capacity and 50% capacity with head end loaded only, while rod reversal at 50% capacity is not equally balanced (Compression 120 degrees, Tension 240 degree). This may cause uneven impact loading and lubrication/oil starvation in the bearings. Therefore taking in account the rod reversal loading it is better to operate the compressor at 50% with head end loaded than crank end loaded. This arrangement will improve the lubrication of bearings and reduce shock loading





## LUBRICATION OF BEARINGS

A force feed lubrication system is provided on this compressor Refer Fig 3. Following are the oil system specifications:

- Oil Grade: XX 68
- Oil pressure: 2.5 to 03 Kg/cm<sup>2</sup>
- Oil Temperature: 40 to 50 C
- Auxiliary oil Pump: Yes (Motor Driven)

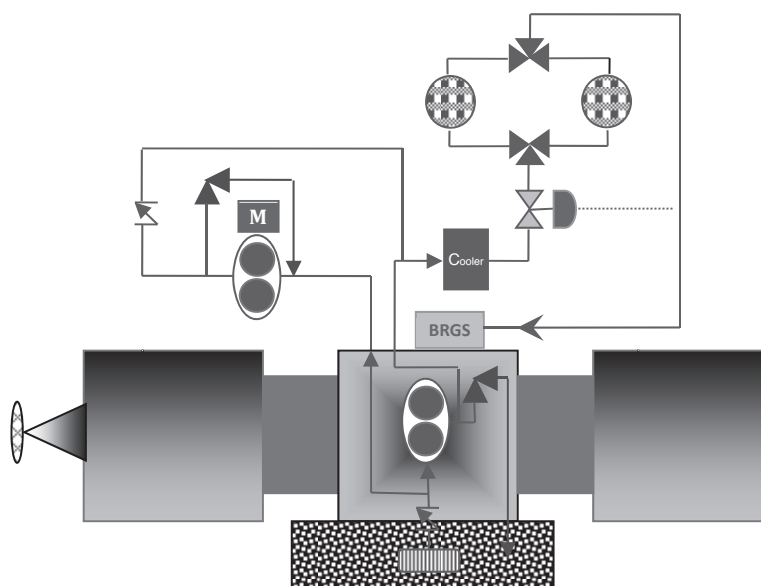


**Fig 3: Compressor Lube oil System**

## OIL VISCOSITY

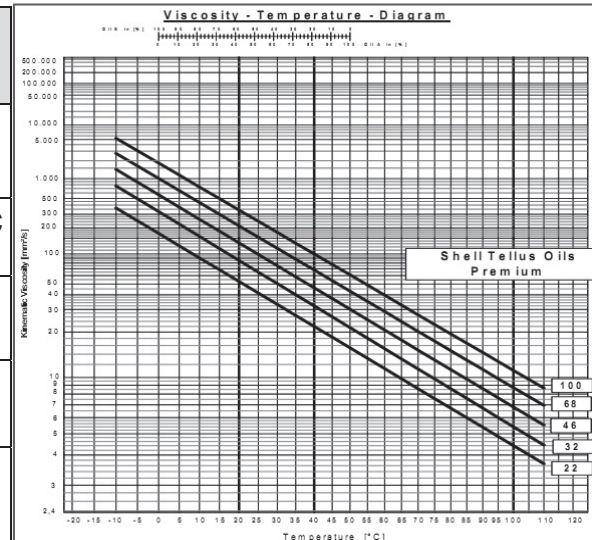
Oil viscosity has major contribution on lubrication quality. The oil film forms between stationary and rotating parts greatly affects by viscosity of the oil being used. Oil being utilized in Compressor crank case since inception was XX-68 which was recommended by the OEM. Study of the bearing failure pattern shows instability of oil film between crank pin and connecting rod bearing. It was decided to replace the XX- 68 with higher viscosity grade oil. XX -100 was selected as the new oil which has viscosity of 100 cSt in comparison with 68 cSt of the existing oil. Compatibility of XX- 100 was checked with respect to service and operating parameters and found suitable. Therefore Oil grade was changed from XX-68 to XX-100. After this change significant improvement has been observed in reliability of the compressor. During the past few years, the crankcase has attended with MTBF of 10 months as compared to 03 months in the past.

## VISCOSITY GRADE COMPARISON:

When Kinematic viscosity of oil in use (XX- 68) was compared with OEM recommended oil (AGIP F1 SIC 75) viscosity at the same temperature (running oil temperature). It is found less than the recommended value.

It may be summed up as this low viscosity oil is not adequate to handle such an impacting load and therefore causing premature bearing failures.

Description	In Use since 1982	OEM Recommended	New Charge
Oil Type	XX 68	AGIP F1 SIC 75	XX 100
Viscosity cSt	68 @ 40C	57-64 @50C	100 @40C
Viscosity Index	97	95	96
Flash Point °C	218	230	234
Pour Point °C	-30	-16	-24



## CONCLUSION:

During plant operations we operate machines at different conditions. We carry out modifications and retrofiting. Although we get desired result but sometimes there are few hidden problems generated due to the modifications. These problems require proper engineering study and control measures are taken to avoid these problems. We had successfully operated our machine as per our requirement and suppress the problem which was generated as a consequence of the mode of operation. This was all possible due to technical knowhow, comparison with related machines, effectiveness of proper grade of oil and understanding the system.



# Technical Paper

**Session: 42-1**

**Session Name: EFRC**

## **The impact of reciprocating compressor pulsations on the surge margin of centrifugal compressors**

**Author:**

**Ir. Cyril Wentzel**  
**Inventor**  
**Wentzel Dynamics**  
**2498 Den Haag, Netherlands**

**Co-Author 1:**

**Ing. Gerard Groenewegen MSc MBA**  
**Owner**  
**Novi Vendi Marketing and Innovation**  
**2628 Delft, Netherlands**

**Co-Author 2:**

**Ing. Andre Eijk**  
**Senior Consultant**  
**Department Fluid Dynamics, TNO**  
**2628 Delft, Netherlands**

**Co-Author 3:**

**Dr. Ir. Otto Bergsma**  
**Associate Professor**  
**Delft University of Technology**  
**2628 Delft, Netherlands**



## Summary

What started out as an exercise in exploring the weight reduction potential of those allegedly “heavy recip crossheads”, turned out to be a fast leap towards implementation of a new hybrid material concept for very lightweight pistons. This was enabled by a next phase in the EFRC R&D group research project which has been subject of this conference before.

The 2014 paper was technical in nature, addressing the context and requirements and defining the solid polymer concept (SPP) as an exciting solution, as well as the characterization of polymer composite materials in fatigue. Building on these foundations, the current paper focuses on the challenge of turning the obvious good idea into a readily available technology under the restrictions of pre-competitive research. Therefore it identifies the things that should be done, how to do it and also which things are best left until later.

Bypassing the extensive volume of technical work that had to be done to demonstrate feasibility and develop key materials and testing technology, the results of the full scale validation experiments are presented as well. Following an earlier 1:10 scale piston fatigue test, a full scale test demonstrated a residual strength – after accelerated fatigue – of 400 kN.

Comparing against commonly encountered designs based on steel and aluminium, a 30 – 70% mass reduction is found for typical larger size pistons.

Enabled by the full scale validation of the concept, the technology readiness is enhanced to a level that by 2016, the technology seems ready for validation in an actual compressor. As a matter of fact, the results of the R&D project are industrially applied, witnessed by the emergence of a spin-off company and plans by major compressor manufacturers to design and/or launch new and significantly improved machines.

The authors argue that the EFRC R&D project may be seen as a model case in efficacious creative innovation, where the time between idea generation and industrial application is less than 3 years. A brief discussion of why we believe this was possible is included. It explains what is required to achieve success – in spite of a rather odd idea introducing an unknown ‘plastic’ material into a self-declared conservative industry – to get a disruptive innovation like the solid polymer piston accepted so quickly.



## 1. Introduction

Lowering the reciprocating mass has been a continuous activity over the past decades because of the associated improvements in machine capacity, durability, efficiency and vibration behavior. While the application of conventional metals has supported the current state of the art in recip machinery, the returns of these efforts have been diminishing. A previous paper introduced and explained an initiative by the R&D group to explore the potential offered by other materials than have normally been applied in the recip world. The present paper describes how over the two years since then the feasibility of one candidate material and structural concept has been investigated and technology has been developed. In doing so, the master plan as outlined in [1] has been essentially followed and implemented.

### Focus on the piston

To summarise, in [1] it was argued that there was good reason to put emphasis on mass reduction of the piston rather than of the crosshead because of two major reasons: First, the piston is typically significantly heavier than the crosshead (and piston rod); this applies especially to the low pressure stages where the piston mass may even limit the machine capacity directly. Second, the crosshead is structurally more complex, limiting the potential mass reduction from the outset.

Most manufacturers have obtained some experience with investigating the potential of other materials for pistons. For example, ceramic pistons and fiber composite materials have been investigated to some extent in scattered research efforts. Whereas no major applications have resulted from such studies, it may be argued that the effort spent, scope and expertise was insufficient to result in a breakthrough. This was the background and rationale for the joint research in the EFRC R&D group. In doing so, the master plan as outlined in [1] has been essentially followed and implemented in a three phase project.

### From requirements versus the state of the art to a new design concept

In the early study phases, a careful compilation of requirements was made and an exploration study was done against a background of data from materials science and similar developments in other industries. For example, it was seen that automotive suspension springs were successfully made much lighter under severe fatigue requirements using fiber composite materials. In general however, it seemed that high manufacturing cost, design complexity and even more severe (very high cycle) fatigue (VHCF) requirements would jeopardise the competitive potential of CFRP<sup>1</sup>.

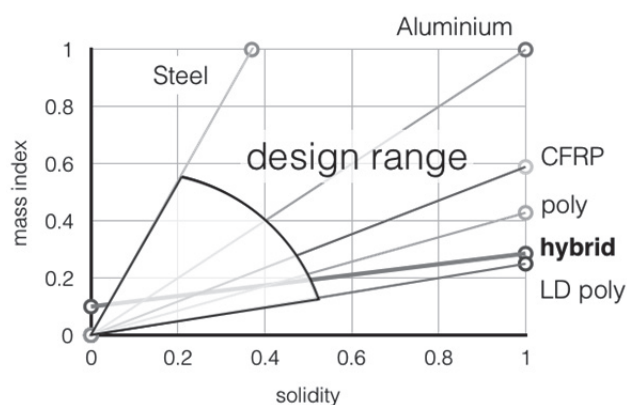


Figure 1 Basic mass-solidity-density (MSD) diagram

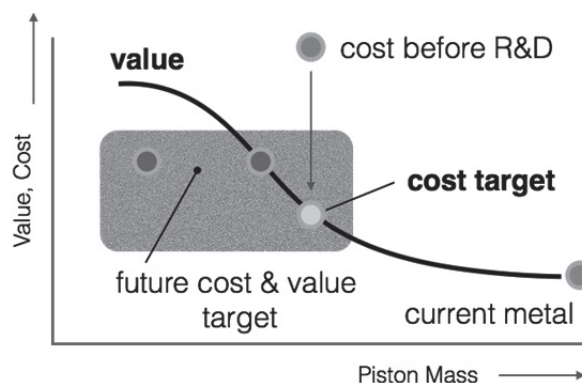


Figure 2 Tentative saturation sketch for mass reduction

<sup>1</sup> CFRP: Carbon Fiber Reinforced Polymer

It was concluded that a radically new approach had to be taken to the design and material selection. Thus, the so-called *Solid Polymer Piston* (SPP) concept was conceived and presented in [1], a hybrid combination of metal and composite polymer (CCPC: Controlled Cavity Polymer Compound) which derives its potential competitiveness from three key factors:

- low density core material allows efficient transfer of gas pressure loads to piston rod using a solid or pseudo-solid core;
- relative ease of consistent manufacture from one-offs to series production;
- an affordable engineering development sufficient to guarantee infinite fatigue life.

With a mass reduction potential of typically 50% or more relative to both steel and aluminium baseline, it was apparent that efforts had to be focused on this concept during the remainder of the project. The SPP is discussed under the corresponding header, allowing the reader to become familiar with its basic tenets which already allow dramatic mass savings (Figure 1). Moreover, it was felt that the drive for even further weight reduction would disappear as mass contributions of crosshead and piston rod would become of comparable magnitude and an S-curve saturation would be approached (Figure 2).

#### ***From precompetitive research to innovation***

A vital aspect that was considered from the outset is what can be called the valorisation of the idea/invention. This is a challenge for the pre-competitive EFRC research group. An idea may be good in itself, but in practice many obstacles can and do prevent its implementation. This is true especially in an industry where any perceived risk may be too much and which has relied extensively on metals technology for structural components. Therefore the transfer of the idea of using a hybrid polymer concept toward actual application was built into the project using concepts of disruptive innovation theory. This means that the conditions were to be promoted for implementing the new technology if and when the specified success criteria had been met. This involves aspects of pre-competitive development and follow-up competitive activities, which were formulated and concretised during the project, as will be discussed under the heading *Innovation Concept*. Members of the R&D group would then have a choice, to embrace and extend the technology either as their own proprietary development from a common background, or to adopt the technology more passively by involving a supplier – be it from a knowledgeable perspective enabling a truly *smart-buyer* position.

On a technological level, it was essential to demonstrate the feasibility by experimentally validating the concept, again going as far as the precompetitive nature would allow to do so. Under the heading *Validation*, some results are presented of materials and scaled and upscaled experiments which cover manufacturing feasibility and structural integrity.



requirement item	requirement	SPP compliance
mass	significant saving	from ~30% to ~70% depending on size and allowable cost
structural integrity	resistant to environmental attack (lubrication oil and process gas)	polymer inherent resistance very good; elimination of metal surface as a factor in fatigue life.
	infinite fatigue life	low stress and good testability and predictability
	thermal boundary conditions satisfied	proper polymer selection allows elevated temperature operations
	condition monitoring	can be built-in,
economic value	affordable	price comparable to metal for very small series
development feasibility	3 years, < 1M€ investment	qualitative compliance; 2 years pre-development with core technologies
industrial requirement	no mandatory single source dependence	SPP as open-ended concept allows multiple implementations
	limited industrial risk	by retaining metal hub and sleeve, many aspects remain unchanged and success is promoted

Table 1 Evolved requirement overview for the lightweight piston.

### Requirements

In the original article [1], the set of requirements was presented and discussed, which should guarantee that the developed idea would be both techno-economically feasible and near-optimum. Such a set of requirements is subject to gradual evolution in a process called requirement discovery. Some of the most important evolved requirements, together with an assessment for the SPP concept, are listed in Table 1.

## 2. The Solid Polymer Piston (SPP) concept

### Anatomy of the SPP

In its most basic form, the SPP consists of three elements as illustrated in Figure 3. By being solid, the low density core offers a simple load path from pressurised faces to the piston rod. Corresponding shear stresses (discussed below) are relatively low because the load transfer area (via the shaft or hub) is large.

The sleeve, being well-supported by the core, can be shaped as desired from considerations of weight and manufacturing. A choice for metal such as stainless steel or aluminium would be obvious for several reasons, but not required in itself.

For lower values of the piston length-to-diameter ratio of the desired piston design, a fourth element may be introduced, namely a piston pressure face liner which could be metal and could be integrated with the sleeve.

As a solid element, the core would be subject to the square cube law, implying that its mass contribution would become large for the larger size pistons. For such cases, there exists an obvious possibility to design a core with cavities which would counteract this trend. We may designate such a concept with the abbreviation CSPP (Cavity-SPP).

Variations could be applied throughout. For example, one could be in the assembly on the interfaces: these could be smooth and adhesively bonded or with a form-fit in combination with adhesive bonding. In all cases, the common feature is the low density core of the CCPC type. The possibilities to conceive such a core is discussed next.

### Low density materials

Typical polymer densities are in the range of 0.95 to 1.25 kg/dm<sup>3</sup>. In order to transfer these into CCPC materials of even lower density, they should be mixed (compounded) with low density fillers, but this is not a straightforward issue. The reason is that many desirable polymer properties lead to high viscosity which inhibits proper mixing. To promote easier processing, the polymer is best chosen to be of a thermosetting type. Then, in combination with the fillers and depending on the compound composition, a density in the range of 0.4 to 0.8 kg/dm<sup>3</sup> can be achieved.

In the previous article [1] it was argued that the mechanical performance (e.g. fatigue strength) does decrease due to the fillers, but if done properly will maintain a sufficient level to sustain the applied stress typical for piston application. It was also remarked that comparison of our project data and literature suggests that achieving an outstanding manufacturing quality is essential for good fatigue performance. The ideal would be to produce defect-free cured compound, as VHCF performance is especially susceptible to minor flaws.

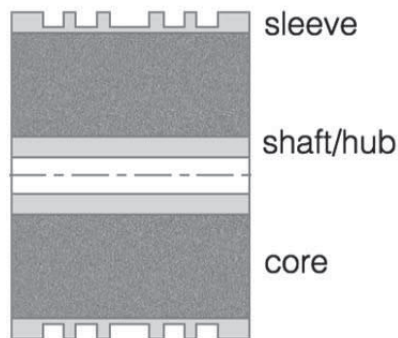


Figure 3 The generic SPP

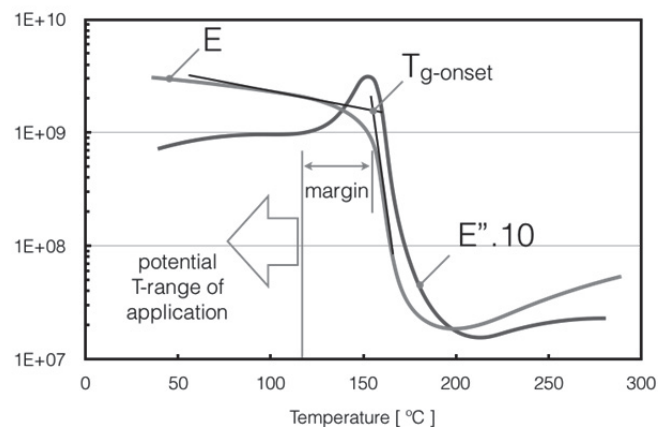


Figure 4 Stiffness and damping as a function of temperature for a medium temperature thermosetting polymer.

For any elevated temperature application of polymers, temperature is a driving requirement. For the present project, a high temperature curing epoxy was selected to support also intermediate temperatures. A tentative equilibrium temperature requirement range was formulated pending a full measurement or validated computation of the temperature distribution through the piston. On the low end, a 90°C requirement was considered to be on the safe side. On the upper side, a value of 140°C seems to be representative. Figure 4 shows how stiffness of a typical thermosetting polymer is a function of temperature. Also, the internal damping of the material is seen to increase as the glass-to-rubber transition ( $T_g$ ) is approached in this so-called DMTA test diagram. While it is typically good practice to maintain a 30°C margin between the  $T_g$  onset and an operational temperature under load, it is probably even more important to consider the





fatigue performance under elevated temperature. The corresponding fatigue limit is a property which cannot be computed, but is only accessible through empirical research. As discussed in the next section, this was beyond the scope of the precompetitive work and only room temperature data were generated for the VHCF range, although [1] also presents data up to 120°C in the HCF range.

### Stress levels and fatigue performance prediction

The core material will be loaded in a three-dimensional state of stress, especially near the critical areas. Therefore we have stress concentration (reduction) and multi-axial fatigue performance as our main challenges. Moreover, stress will arise due to imposed strain (from the pre-load on the shaft) as well as from alternating (gas and inertia) loads. In addition, residual stress from manufacturing will be present depending on the processing that has been applied. Figure 5 shows typical computed stress components for the shaft to core interface. We may consider the situation as an average shear stress ( $P/(\pi \cdot D_s \cdot L)$ ) with stress concentrations, superimposed on a compressive stress distribution. The average cyclic shear stress will for low pressure stages be of the order of 1 or 2 [MPa], according to:

$$\tau = \Delta p \pi / 4 D^2 / (L \cdot D_s) = \Delta p \pi / 4 (D/L) \cdot (D/D_s)$$

, where  $\Delta p$  is gas pressure difference,  $P$  is maximum piston rod force,  $D$  and  $L$  are piston diameter and length and  $D_s$  is shaft diameter. The imposed (axial) compressive stress in the polymer will depend on the shaft stiffness, i.e. modulus and cross sectional area. It will also be of this order of magnitude especially if aluminium alloy is chosen. Even in this case, there is an option to reduce this stress field if desired by performing the bonding operation under load. In addition, elevated temperature curing may be used to tune the core stress levels at the operational temperature to a desired value.

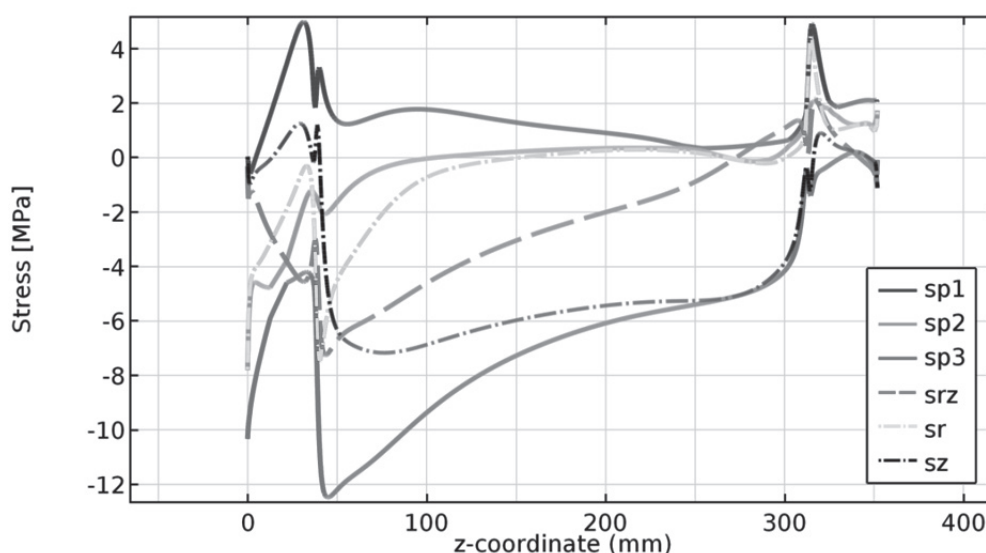


Figure 5 Representative stress components along a simple (straight) shaft-to-core interface;  $sp1$ ,  $sp2$ ,  $sp3$  are principal stresses;  $sr$  and  $sz$  are radial and longitudinal stress,  $srz$  is shear stress.

When designing the piston using the SPP concept, a fatigue evaluation for the core material should be enabled by a database obtained from experimental work. In [1], results from a uniaxial test into the High Cycle Fatigue (HCF) domain of 10 Mcycles was presented. The uniaxial stress condition was obtained by using a 3 point bending test. In order to better represent the three-axial stress condition from Figure 5, a unique shear strength test for the VHCF domain

(Very High Cycle Fatigue, 1 up to 10 Gcycles) was developed especially for the SPP application. This biaxial test could be combined with an axial load to achieve the desired tri-axial state of stress. Table 2 shows the possibilities using this technology, together with the limitations of scope as applied in the present project. The last column contains the “Final” requirement which would apply to an actual application where such a material characterisation would be part of a risk reduction effort as required. The 100°C test temperature used in the table would cover many applications such as API-618 machines, but would have to be increased for cases where the piston local equilibrium temperature is expected to be higher. To clarify this, the section about *critical aspects* contains a discussion of the thermal behavior.

test method	stress type			temperature		* test - frequency	N <sub>max</sub>	EFRC R&D	Final
	uni-axial	bi-axial	tri-axial	RT	~100°C	[Hz]	[ - ]		
3P bending	x			x	x	< 25	2. 10 <sup>6</sup>	phase 2	
torsional shear		x		x		< 300	3. 10 <sup>9</sup>	phase 3	
torsional shear		x			x	< t.b.d.	1. 10 <sup>9</sup>	–	✓
residual strength		x		x			n/a	–	✓
pre-stressed torsional shear			x	x			0.1 10 <sup>9</sup>	–	✓

*Table 2 Overview of applicable material test methods related to fatigue performance (RT = Room Temperature), to be applied to CCPC materials (\* indicates achieved or allowable frequency). N<sub>max</sub> is the maximum number of load cycles.*

### Hybrid Elements

From the outset, the SPP is conceived as a hybrid structure, allowing for the best materials to be applied locally to achieve the best compromise for performance and cost. In particular, metal is initially retained in the inner and outer zones so that the best of both worlds may be combined and transition would be easier and risk severely reduced. Table 2 presents a brief overview of options and design considerations.

	materials options	optional features	baseline SPP
shaft	aluminium alloy; stainless steel; fiber composites	straight or form-fit; interface to torque-nut; recess for collar	straight where sufficient, Al 7075-T6
sleeve	stainless steel; aluminium alloy; filled polymers	full castellation contour	straight, modestly staggered
face	metal sheet; filled polymer gelcoat	-	no face cladding
core	thermoset polymer and controlled cavity filler compound	stress concentration reducing features, gradient zones, macro cavities	

*Table 3 Specification of basic SPP components*



### **Critical aspects for the SPP and research efforts**

General concerns about potential shortcomings of polymer composites and several specific to the SPP concept and CCPC (Controlled Cavity Polymer Compounds) are listed in Table 4 below, together with a brief discussion on the relevance and criticality. The major aspects have been addressed in the current project and are discussed more extensively below.

The most important design driver which is decisive for the feasibility of the SPP concept is the fatigue strength. It was argued in [1] that for a polymer one cannot simply assume the existence of a fatigue limit, one will have to test it into the VHCF domain of 1 Gigacycles. However, at the normally allowable testing rates (below 10 Hz), such an effort would take much too long. The first concern then is to find or design a material that will allow accelerated testing without introducing failure due to non-representative internal heating. On this subject, the section on *Validation* presents some results that have been generated with the testing methods mentioned in Table 2, as an essential start of the materials data. Given a dataset for any particular CCPC compound, a design can be based on these data and appropriate design margins (on stress, not on life<sup>2</sup>) and this should be sufficient if: (a) product quality is reproducible on every level, and (b) if the behavior on a product level has been successfully related to material level test data. The latter condition is also discussed in the *Validation* section where both scaled and full scale SPP testing is presented.

A second critical factor is the thermal behavior and the thermal load itself. Because of its importance, work was done to predict the temperature. This is not a trivial task however, since it involves complex heat transfer phenomena of a non-steady flow – which is at present beyond the state of the art (see for example the discussion in [2]). Nevertheless, one can apply an empirical combination of heat transfer coefficient and average temperature to result in an educated guess through a stationary computation. It should be noted that the value obtained from experience or direct measurement as such on a steel or aluminium piston cannot be used as a requirement, because the SPP's much lower thermal conductivity will cause a quite different and inhomogeneous temperature distribution. Therefore, the code "Compressor 3D" as developed for the EFRC R&D group [3], which enables to compute estimated heat transfer coefficients, was used. An example of a temperature distribution calculated from these heat transfer values and also others, is given in Figure 6.

It is seen that for this particular estimation, temperatures of 90°C to 110°C are representative. Because of the insulating property of the CCPC material, the result is highly dependent on heat transfer through the piston rod; this effect may be cooling, especially for a rod which is specifically designed to cool (see for example, the EFRC project described in [4]). One contributing factor has yet to be implemented: the heat generation due to hysteretic heating by the stressed polymer itself. A computational procedure has been devised and work is ongoing to assess the total effect of this phenomenon and heat transfer from the gas. This is done in conjunction with efforts to experimentally measure the temperature transient on the piston itself, but this is beyond the scope of the original EFRC project.

---

<sup>2</sup> The mistake is sometimes made to use a design margin on life; for brittle materials especially, the low slope in the S-N diagram makes this an inappropriate approach which is too sensitive for scatter, outliers and manufacturing error.

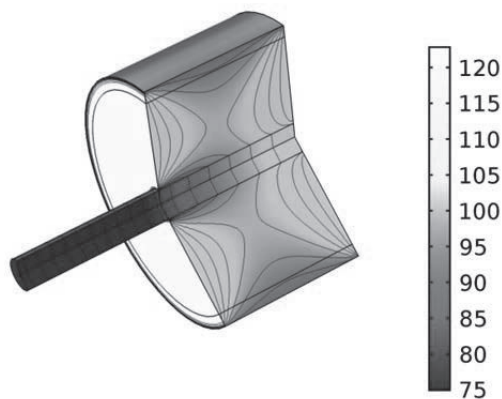


Figure 6 Stationary temperature distribution within the SPP based on estimated heat transfer coefficients.

Thermal expansion of a hybrid piston and its components is a factor that should be well recognised. In itself, thermal expansion behavior of the piston as a whole is sometimes of concern, but in general it can be said that it is only necessary to know the final geometry, so therefore the main criterion is predictability. More relevant and also more subtle is the structural integrity issue that is related to differences in thermal expansion, both during manufacture and in operational life. With steels having expansion ratios in the order of 10, aluminium alloy 25 and polymers in the range of 30 to 60 [ $\mu\text{strain/K}$ ], the effect can only be assessed with consideration of stiffness, i.e. modulus and geometry. In general, the consequence is:

- incorporate the thermal state relative to the stress-free condition (from manufacturing) as a load case in stress computation;
- there may be resulting constraints on heating rates as applied during manufacture and also heating rates during operation should be checked; this can result in detail design changes to guarantee structural integrity.

The material class (CCPC) which has been presently explored, is a brittle material. Lacking ductility, construction needs to be done with care since design mistakes will certainly result in unexpected premature failure. Such care starts in the conceptual design phase, where architecture should be such that load paths and deformations may utilise the material's load bearing capability under compressive loading. Under tension it will be more prone to fracture. This principle implies that, when the material is contained, it can transfer high shear loads while even impact loading can be absorbed, for example due to liquid slug<sup>3</sup> ingestion. The highest regular design loading occurs near the interface to the shaft and is in shear. As argued before, compressive stress will dominate in the axial direction. What will happen in the radial direction depends on detail design features and also the temperature distribution relative to its as-manufactured state, which can be considered a design variable besides being a manufacturing issue. In general, the desired containment is an implicit property of the SPP with metal shaft and sleeve at the extremities.

A final major concern that was addressed/screened in the project was the corrosive effect or other susceptibility to either gaseous components or lubrication oils. In general, the resistance of thermoset polymers to corrosive gases is good and similarly to oil as well. In the aerospace

<sup>3</sup> it is interesting to tentatively consider the behavior under slug loading: rather than overloading the piston rod (with large scale damage as a consequence), the surface may be *indented* at relatively low repeated local loads, supporting a 'graceful degradation' failure mode allowing a regular shut down and repair to be done.



world, the most challenging test for polymers is to expose them to hydraulic fluid (e.g. Skydrol) and observe residual properties. For one particular candidate polymer (pdcpd), there was concern about potential absorption of a-polar oil types. Subsequent exposure to various oil types at 90°C however, did not result in any significant uptake, so the concern was dropped. Even so, it will be prudent to apply oil exposure before or during fatigue testing as part of any qualification effort.

#	aspect	assessment	#	aspect	assessment
1	fatigue prediction	solved in project	8	corrosive gas	good resistance
2	temperature re-sistance	solved by proper material selection	9	static charge build-up	t.b.d. (avoid by design)
3	brittleness	requires good engineering	10	UV resistance	not applicable to enclosure
4	stiffness	sufficient in SPP concept	11	condition monitoring of core	candidate technologies exist if desired
5	bonding to metal	solved industrially by surface treatment	12	development time	potentially fast, as demonstrated in current project
6	creep	in control for thermosetting polymers	13	marginal benefits	high mass reduction demonstrated
7	decompression damage	not-susceptible; Helium used	14	economical competitiveness	moderately expensive materials, favorable processing; but expensive engineering effort for generating data

Table 4 Overview of 14 compiled potential aspects of concern and their assessment for piston application.

### **The SPP as an open ended concept**

Combining a product improvement challenge with philosophy, we may refer to the groundbreaking theory about cognition, concerning concept formation from Ayn Rand [5]. Concepts are viewed as an abstraction based on essential properties using measurement emission. We may recognise this in the current SPP concept where the elements, material classes and topology have been specified, but the dimensions and specific materials are omitted. The concept is open ended in that variations can be conceived which involve a specialised application. Such extensions of the concept are valuable for the R&D partners involved as these allow a proprietary, competitive edge to be achieved.

The idea of the precompetitive research effort becomes clearer when one considers these opportunities. They build on a common technology level among the R&D members, which itself would cover TRL<sup>4</sup> at the most. A number of potential variations of the concept have been listed in Table 5. Both the missing technology to achieve (TRL9) application of the SPP and these variations are discussed next under the header *Innovation Concept*.

<sup>4</sup> TRL: Technology Readiness Level, refer to next section



variation	feature	application
large pistons	size up to t.b.d. with special core features	Large API-618 machines
disk type pistons	with L/D < 0.4; introduce integrated facing	certain types of compressors
trunk type pistons	different type of structural concept	even combustion engines
high temperature pistons	For example for T > 130°C	high pressure ratio and T <sub>suction</sub>
graded density core SPP	one way to achieve a lighter core for large pistons	large very lightweight pistons
integrated piston rod piston	eliminating the pre-stressed joint	t.b.d.
high pressure piston	high strength and pressure resistance	specialties
aggressive environment piston	special inert polymer compounds	t.b.d.
flexible revamp	fully flexible manufacturing for arbitrary size and high mass reduction, e.g. increasing piston diameter.	revamping existing machinery, solving an acute problem
unlubricated, ringless piston	close tolerance piston with thermal control	e.g. laby-seals
pressurised cavity piston	extra light weight reinforced piston with floating piston potential	e.g. floating pistons

Table 5 Open ended lightweight SPP concept offspring examples

### 3. Innovation Concept

#### **Precompetitive versus competitive elements in the SPP invention**

This section is concerned with the demarcation line between the competitive area and the common ground of precompetitive research. This line was continuously explored as the project progressed and further phases were defined within the overall master plan. For the sake of discussion, the degree of technology maturity towards an actual application will be indicated by a measure of *technology readiness level* (TRL) as defined by NASA [6].

Competitive development elements	reasons	status*
high temperature fatigue properties database	high investment required; proprietary knowledge of materials	pending
multiple CCPC material screening	optimum material formulation is application specific and is beyond generic demonstration	ongoing
extensive building block testing	beyond generic demonstration	partially ongoing
in-machine demonstration of piston	high investment required	imminent
advanced shaft to core integration	beyond generic demonstration	–

Table 6 Competitive elements of SPP technology development towards TRL 9; \* status refers to known follow-up initiatives.

Obviously, the precompetitive parts addressed those questions which involved the feasibility evaluation as such. Clearly, a minimum level of demonstration was necessary of the fatigue performance as well as the means for testing them in an economical way. Also, some of the concerns listed in Table 5 were addressed such as the potential mechanical capabilities at ele-



vated temperatures and the resistance to oils. Also, the manufacture of the demonstrator hardware (at the level of a mock-up) was essential in illustrating the feasibility of the SPP concept. Finally, both the scaled and the full scale (room temperature) fatigue test into the HCF domain were considered suitable technology demonstration stepping stones to TRL6 status.

The parts that were agreed to be outside of the precompetitive domain were agreed on the basis of a few common sense criteria, refer to Table 6. In general, the precompetitive elements are concerned with essential feasibility demonstration and the remainder supports some degree of optimisation towards specific applications as well as risk reduction.

### ***Radical innovation theory applied to the piston project***

There is a question how good new ideas can be brought to the market. Looking at the academic literature on this subject, this is ultimately done by so-called ‘*First-movers*’. Schilling [7] describes these as the first market players that bring a product or service to the marketplace. As such, they typically experience additional disadvantages, the so-called ‘*First-mover disadvantages*’. These involve high costs for Research en Development with a long break-even period, patenting concerns, absence of a distribution channel and all the factors listed in Table 7 up to the absence of applicable standards. The development of own proprietary standards may even worsen the risks when these standards are not adopted by the industry at a later stage (examples: Philips with the V2000 video standard, Microsoft with the .doc standard). Also in general, standards which are too far ahead of the industry contribute to problems due to the difficulty of communicating with the ‘*external world*’.

An analysis of so-called success factors is presented in [9]; here the definition of disruptive – and radical – innovation was enhanced from Abetti [8], resulting in the following:

*A radical innovation is an innovation with a unique and original product , system or business model, that will make other already existing ones unnecessary or obsolete and has a high uncertainty of success because of the level of newness and obscurity of the needed design effort, technology, knowledge and market.*

This definition takes into account that radicalism is accompanied by a high level of uncertainty, newness, risk, differentness and market impact. More literature background can be found in the original article of Groenewegen [9]. We proceed with considering some related questions and making a link to the hard core technology and market context of the present case. We do this because studying these issues makes us better able to make a success of the idea.

*Why is it so hard to be successful with a radical innovation?*

A shortlist of the problems when dealing with radical innovations was found in the literature [9], see Table 7.

Financial	Organisational / Market	Technological
<b>High costs of R&amp;D and long payback period;</b>	<b>Resistance, fear and uncertainty of potential customers;</b>	Non existing ‘ <b>enabling</b> ’ technologies and supporting products;
Defensive behavior of the established order;	Uncertainty how to manage a radical innovation ( R&D and businesswise);	Not matching existing legislation and current <b>quality norms</b> ;
Largely unknown size of market and <b>customer needs</b> ;	Difficulty of getting feedback from potential interested parties due to secrecy because of competition threats	Struggle about the use of <b>standards</b> and agreements upon them
	Non existing distribution channel	

Table 7 Innovation obstacles inventory (categorised, from [9]).

Some of these factors can be influenced by properly incorporating these considerations in the development work; these have been printed in bold. For example, the “fear and uncertainty” will be mitigated by performing and presenting technological work meeting the highest standards and making use of world class expertise. The high cost issue has in our case been tackled by first joining forces/funds and then choosing a technology with cost as a main driver. Enabling technologies could mean for example the existence of test methods for extremely long durability, which were developed here as a necessity.

#### What are the success factors of a radical innovation?

After the extensive literature study [9] a conceptual model was designed in which three main factors determine the success of growth: the uniqueness of the advantages of the innovation, the startup organisation characteristics and the person of the entrepreneur.

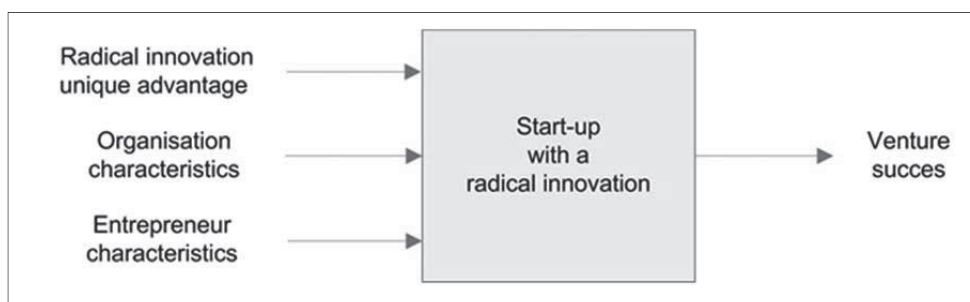


Figure 7 Conceptual model for the First Mover, towards success in the start-up scenario [9].

Abetti [8] concluded first and foremost that a radical innovation should have unique advantage to existing other solutions which is sufficiently big, so that it helps potential customers and companies to overcome their resistance and fear for the unknown because of the attractiveness of the new solution.



Variable	Mean	Std. Dev.	1	2	3	4	5	6	7	8	9	10	11	12	13	14	15	16	17	18	19	20	21
1. Thoroughness Business plan	3,75	1,96	1,00																				
2. Member of formal networks	0,56	0,50	0,35	1,00																			
3. Intensity external advice	3,69	2,37	0,26	0,25	1,00																		
4. Customer Proactiveness	12,23	4,02	0,20	-0,04	0,25	1,00																	
5. Degree of structure innovation process	3,51	1,49	0,31	0,12	0,21	0,43	1,00																
6. Degree of expertise	4,79	1,73	0,04	0,00	0,10	0,12	0,15	1,00															
7. Application of investors money	0,35	0,48	0,33	0,25	0,15	0,04	0,11	-0,04	1,00														
8. More then 75000 seed capital	0,25	0,44	0,12	0,08	0,06	0,31	0,09	0,04	0,09	1,00													
9. Multiple owners	0,51	0,50	0,08	0,09	0,03	0,08	0,14	-0,06	0,16	0,02	1,00												
10. Uniqueness advantage of the innovation	9,77	2,44	0,17	0,02	0,16	0,32	0,34	0,25	0,15	-0,07	0,17	1,00											
11. Willingness to take risk	11,55	1,79	0,29	0,15	0,10	0,23	0,17	0,21	0,11	0,11	-0,06	0,14	1,00										
12. Years of industry-experience	5,52	6,60	-0,14	0,01	0,18	0,12	0,22	0,32	-0,14	-0,03	-0,16	-0,08	0,10	1,00									
13. Years of management experience	5,40	6,56	0,05	0,11	0,05	0,25	0,25	-0,20	-0,03	0,39	-0,15	-0,14	0,03	0,24	1,00								
14. Relevant social network	5,23	1,62	0,05	0,23	0,19	0,25	-0,02	0,11	-0,03	0,13	0,11	-0,01	0,13	0,08	0,06	1,00							
15. Higher education (BSc or higher)	0,83	0,38	0,07	0,09	0,03	0,11	0,01	0,31	0,04	-0,06	0,18	-0,01	0,12	-0,07	-0,27	0,28	1,00						
16. Previous jobs	3,20	2,09	-0,19	-0,07	-0,04	-0,09	-0,07	0,15	0,00	-0,03	-0,14	-0,29	0,04	0,23	0,01	0,14	0,13	1,00					
17. Years of previous working experience	11,47	8,39	-0,08	0,23	-0,03	0,17	0,19	-0,05	-0,18	0,14	-0,24	-0,18	0,19	0,50	0,51	0,13	-0,12	0,51	1,00				
18. Years of earlier entrepreneur experience	2,35	4,77	-0,01	0,02	0,14	0,28	0,12	0,07	0,21	0,18	-0,10	0,11	0,07	0,12	0,39	0,16	-0,19	-0,12	-0,01	1,00			
19. Degree of radicalness	25,12	5,09	-0,02	0,12	0,07	0,36	0,22	0,33	-0,06	0,10	0,06	0,53	0,05	0,02	0,03	0,05	0,06	-0,30	0,00	0,07	1,00		
20. Turnover growth in %	493,37	879,81	0,24	0,01	0,15	0,20	0,01	-0,03	0,24	0,09	0,27	0,36	0,04	-0,21	-0,10	0,22	0,15	-0,21	-0,26	0,05	0,08	1,00	
21. Employment growth in %	132,12	332,70	0,21	0,07	0,18	0,09	0,00	0,09	0,16	0,20	0,09	0,14	0,11	-0,05	0,06	0,12	0,09	-0,02	-0,04	0,12	0,11	0,57	1,00

Table 8 Correlation matrix of success factors [7]; mean, standard deviation and correlations.

In Table 8 an overview can be found with all the variables measured to operationalise the main question. Some are related to the uniqueness of the innovation, some to market & organisational approach and others to the personal traits of the inventor/entrepreneur.

With the help of Table 8 some additional observations were done: A very high correlation (>0.5) exists between degree of radicalness and uniqueness of advantage of the innovation. This is also true between working- experience, industry-experience, management experience and previous jobs. And also true for turnover growth and personal growth. The percentage of employment growth turned out to be a factor 4 smaller than the turnover growth.

#### What are the conclusions?

The study [7] tried to expand the existing theory of the success factors of a radical starter (Table 8). In the other empirical research on success factors of starters, we have seen the importance of specific organisational and entrepreneurial traits. This we combined with the success factors of a radical innovation within an established firm, which added innovation characteristics (unique advantage), organizational traits (customer pro-activeness) and confirmed entrepreneurial traits. This was combined further with the success factors found for innovative entrepreneurs in general which added specific organisational (use of seed capital) and entrepreneurial traits (willingness to take risks). All these factors were combined in a model for starters with a radical innovation. This model states that to succeed, there are three relevant factors. The starter has to be an entrepreneur (with specific personal traits and human capital), the organization has to have certain characteristics (business plan, seed capital, etc.) and the innovation has to have some unique advantages for the (potential) customers.

Testing this model through a questionnaire, we see a statistical relevance for each measurement of success. The general findings do support the idea that growth is determined by the uniqueness of the advantage of an innovation, specific organizational characteristics and entre-

preneurial traits. The results however are clearer for turnover than for employment growth and not all the factors identified in the existing literature were found statistically significant or positive.

From the outcomes of this study an image of the radical start-up with the most turnover growth in the first 3 years can be drafted. The start-up exist of a team of founders with not too much working experience and with a relevant social network. There is a thorough business plan that is executed with at least 75,000 euro seed capital. By a pro-active customer approach the start-up is able to bring to the market, successfully, a radical innovation with enough unique advantages (compared to other existing possibilities) to overcome initial customer and market resistance.

#### *The EFRC R&D connection*

The connection with the Light Weight Piston is obvious. Because of the significant unique advantages of a lighter weight piston, many people and companies are willing to test and use this radical innovation. Obstacles such as listed in Table 7 can be removed. Companies associated with the EFRC R&D group are in a position to either choose to develop the last technology elements themselves, or to adopt a specialised supplier from a knowledgeable position, thus enabling a proper requirement set to be formulated. Because of the open-ended nature of the SPP concept, there is a multitude of possibilities to develop proprietary installments or contributions for EFRC members.

#### **4. Validation**

##### ***Test and verification philosophy***

Test and verification is an essential part of the feasibility assessment, development and implementation for two reasons:

- the properties that are decisive for the feasibility (e.g. fatigue and a favorable manufacturing concept) are accessible only through empirical work (and not by simulation);
- introducing a novel concept into an industry that relies heavily and successfully on metals requires experimental evidence.

A strong emphasis was therefore put on experimental work, after careful early theoretical analysis and synthesis. This even involved developing a new test method for VHCF life of polymers under stringent requirements of low budget and decimated testing time. Figure 8 illustrates the elements supporting the feasibility assessment and the transition to full scale verification, also including manufacturing. It must be emphasised at this point that in a good practices approach of composite materials, processing (i.e. manufacture) and materials should be an integrated whole<sup>5</sup>. This leads to the incorporation of the manufacturing concept in the materials and building block testing. In this respect, it is important to mention that it was chosen to apply pre-cured polymer blocks and investigate its particular performance level.

##### ***Scaled testing approach***

In developing the technology, it is desirable to apply an approach where for each project phase the complexity and predictability of the outcome is under control. In combination with the factors listed in Table 4, this leads to the scaled testing overview in Table 9.

##### ***SPP Full scale fatigue trials result***

---

<sup>5</sup> This is not unlike the area of cast metals where material quality is entirely dependent of the casting process. With the current CCPC materials, there is an option to choose an in-situ curing or a machined pre-cured route; this can be expected to have impact on performance which should be investigated.





Figure 8 shows the test setup used for the full scale test. This test rig was specifically designed to withstand high fatigue loads and allow the (adjustable) application of prestress on the loading rod. Full load reversal could be applied, while even simultaneous testing of two specimens is possible. Also, elevated temperature testing is foreseen while diagnostics mainly concern the evolution of the pretensioning force in the rod. This feature allows the monitoring of an anticipated failure mode along the core to shaft interface. A second technology involving continuous fiber optical strain measurement was prepared but was not applied.

	Fatigue RT	Fatigue HT	Core shaft shear	pre-stress	Manufacturing induced de-	Lube oil	T transient	Gas Attack	Gas Flow	Boundary layer	T distribution, heat flow	Full environment
Material level	x	x				x		x				
Building block								x				
Scaled SPP	x		x	x	x		x					
Full scale SPP	x		x	x	x							
Compressor piston					(x)	x	x		x	x	x	x

Table 9 Assignment of research aspects to scaled testing elements (RT, HT: Room and High Temperature respectively)

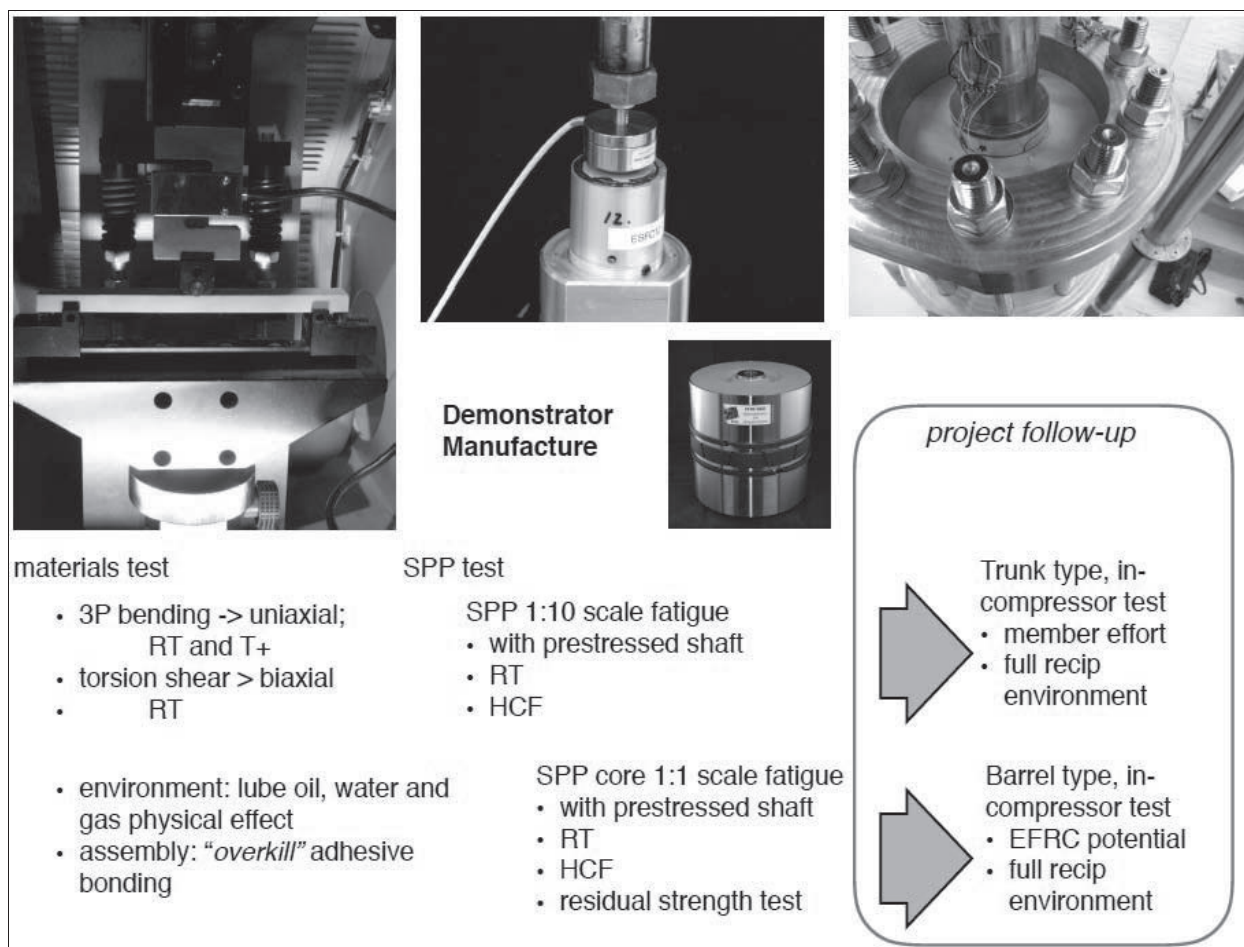


Figure 8 Illustration of the test and verification philosophy supporting the SPP concept road to

implementation.

The result of the test is presented in Table 10 together with the result of the 1:10 scaled “mini-piston” test. In terms of failure mode and residual strength, it was surprising to see that with a maximum sustained load of 400 kN (equivalent to 800 kN design), the failure behavior involved stable damage extension up to the maximum load and finally core pull-out at a load of 65 kN (LF=1). This was in contrast with the behavior usually observed for brittle materials and indicates a mechanism involving radially compressive stress in confined configuration as discussed before.

	mini piston	full scale piston core	comment
Design piston rod load $P_d$	1.3 kN	$\pm 130$ kN	130 kN scaled down to 65 kN by length reduction
Demonstrated maximum fatigue life/loadfactor	$N = 3.50 \cdot 10^6$ , LF = 4	$N = 0.82 \cdot 10^6$ , LF = 2	at shaft prestress factor 3: $F_{pre} = 3 \times 1.6 \times P_d$
Residual strength	n/a	$LF_{max} = 6.1$	after crack growth at LF=2.5

Table 10 Scaled and Full Scale test results (load factor  $LF=P/P_d$ )

### In-machine validation

While it is difficult to explicitly project what kind of “things could go wrong” after full scale fatigue testing such as described above, it is equally obvious that any application would first be preceded by a test of the actual piston in a testbed compressor. First and foremost this would involve the actual manufacture of the full piston, complete with required manufacturing tolerances for installation etcetera. Subsequent testing may take days or even weeks or even longer where on-site application is foreseen with the presence of a back-up machine. Among the variables to be monitored are the temperature (distribution) and the specimen stiffness. On-piston temperature measurement is not trivial. Periodic inspection may be labor intensive and hence costly, but its frequency could be minimised by proper instrumentation. Final tear-down inspection may be done as a last step or even destructive testing (residual strength).

While such a competitive activity will be an expensive exercise, an application to a much smaller machine might be a useful intermediate step. This would for example allow already the quantification of the actual effective thermal load, which is most difficult to access by theory as discussed above. One initiative of this kind is already being implemented based on an 11 [kW] two stage machine, 35 [bar] air compressor and a hybrid low pressure piston of the trunk type [10]. Other applications will be able to benefit significantly from the insights which will result from such an exercise.

## 5. Conclusions

This paper describes the final outcome of a successful project initiated by the EFRC R&D group with the aim to investigate the potential for weight reduction by using non-conventional materials and subsequently develop the technology for implementation. The work started with a creative phase which was well grounded in reality by studying the state of the art as well as working on the requirements. The outcome was a concept coined the Solid Polymer Piston (SPP) which stood out among any other competing concepts such as those based on CFRP material. Faced with multiple challenges in inventing a new affordable configuration as well as precompetitive considerations, three project phases were construed which each confirmed the expectations of feasibility towards a typical 50% mass reduction. Not only does this mass reduction enable a more than gradual improvement of machines (it can be considered a *disruptive innovation*), but technology readiness can be obtained in a short period of time and at a modest cost associated with the hybrid SPP concept making use of the CCPC class of materials.



Validation of the technology was obtained as far as precompetitive research could take it. Starting with an SPP demonstrator (for manufacturing), a materials database was obtained confirming good “infinite life” fatigue strength and yielding also statistical data. Finally, scaled and full-scale fatigue testing confirmed the ability to resist enhanced fatigue loading up to 1 million cycles.

Extensive effort has been spent on adopting the right approach and cooperative model to allow valorisation of the present development. Implementation by several EFRC members can be foreseen in the near future. Among the anticipated machine improvements are efficiency improvement, capacity increase and the reduction of vibrations.

## 6. Acknowledgement

The authors would like to thank all R&D members of the EFRC for sponsoring this very exciting project.

## 7. References

1. C.M. Wentzel & O.K. Bergsma, A. Eijk; Feasibility Investigation of Non-Metallic and Light Weight Metallic Materials for Light Weight Compressor Pistons, 9th Conference of the EFRC September 11th / 12th, 2014, Vienna
2. U. Lekic; Fluid Flow and Heat Transfer in a Helium Gas Spring; PhD thesis University of Twente, 2011.
3. T. Müllner: "Flow Patterns and Valve Dynamics in Multi-Valve Reciprocating Compressors"; PhD thesis TU Wien, 2015.
4. C. Thomas, Innenkühlung der Kolbenstange von trockenlaufenden Kolbenverdichtern. Dissertation TU Dresden, 2014.
5. L. Peikoff, Objectivism: The Philosophy of Ayn Rand. Penguin Books, 1991.
6. NASA: Technology Readiness Level definition.
7. Schilling (2008, 88-91); Strategic Management of Technological Innovation (2 ed.). New York: McGrawHill, 88-91.
8. Abetti, P. A. (2000). Critical Success Factors for radical Technological Innovation: A Five Case Study. Creativity and Innovation Management, 9(4), 208-220.
9. G. Groenewegen, F. de Langen (2012). Critical Success Factors of the Survival of Start-Ups with a Radical Innovation. Journal of Applied Economics and Business Research, 2, 155-171.
10. [www.panacea-piston.com/validation](http://www.panacea-piston.com/validation)





# Technical Paper

**Session: 42-2**

**Session Name: EFRC**

## **A novel valve design for combined reciprocating piston expansion and compression machines**

**Author:**

**Christian Stöckel**  
Research associate  
Institute of Power Engineering  
TU Dresden  
01062 Dresden, Germany

**Co-Author 1:**

Dr. Jörg Nickl  
Postdoctoral researcher  
Institute of Power Engineering  
TU Dresden  
01062 Dresden, Germany

**Co-Author 2:**

Christiane Thomas  
Postdoctoral researcher  
Institute of Power Engineering  
TU Dresden  
01062 Dresden, Germany

**Co-Author 3:**

Prof. Ullrich Hesse  
Professor  
Institute of Power Engineering  
TU Dresden  
01062 Dresden, Germany



### **Summary:**

Loading and unloading processes in gas storage systems are going to play a significant role in the energy sector. For example, there is the need for storage systems to compensate the fluctuating availability of renewable energies (short periods) or the use of underground storages to countervail the varying consumption of natural gas over the seasons in combination with the constant delivery (long periods). Reciprocating machines offer the possibility to cover a wide range of operating conditions. However, they are nowadays designed as a compressor or an expander where the most occurring difference in design is the valve and especially its actuation. While compressor valves are normally self-actuated, expander valves need a forced actuation. For an economic operation of the loading and unloading process in a gas storage facility an expander-compressor-unit can be used, which consists of only one reciprocating piston machine. Therefore a valve system has to be designed which could fulfil both of the functionalities: the self and the forced actuation.

The present report points out the general boundary conditions which have to be taken into account for such an expander-compressor-machine. Afterwards the design criteria for the valves are discussed and a proposal for a general design is derived. For compression mode a high, pressure induced force acting on the valve at small pressure differences is desired, therefore a large pressure working surface is needed. When working as expansion valve the requirement is just contrary. The valve movement is towards the high pressure difference but low acting forces are preferable. Hence low pressure working surfaces are desired. Poppet valves can handle those conditions when additionally to the valve open cross section the opposite surface is used to achieve a pressure balance. Three different possibilities for the valve actuation, which are the electro- magnetic, the hydraulic and the pneumatic, are examined with respect to their functionality in both compression and expansion mode. It can be shown, that the pneumatic actuation has several advantages when realized with the process gas as pneumatic fluid. Based on those previous findings a general design for the valve assembly is proposed and afterwards adapted to a specific compressor. By numerical simulation of the now achieved reversible compression-expansion-machine at different operating points an evaluation of the design concept could be performed.

Overall it is shown that the proposed valve design allows the two different operation modes for a reciprocating piston machine in only one unit. Also it is conceivable to achieve variable valve timings with the proposed design, therefore a nearly continuous control of the machine would be possible.



## 1 Introduction

Meeting the 2-degree-C-target is one of the main goals of the contemporary climate politics of the industrialized countries. To reach that objective governments stimulates the energy sector with funds and investment in research to switch from the conventional fossil-based fuel to the alternative so called renewable energy sources. However, contrary to the energy supply by conventional fuel the amount of renewable energies is fluctuating and cannot be manipulated to the demands of the customers as good. For that reason energy storages have to be built, to compensate the over and under production. Another approach for saving energy and therefore decreasing CO<sub>2</sub>-emission is the optimization of industrial processes with respect to efficiency and energy recuperation.

## 2 Energy storage systems

A great potential of energy recuperation is given by the expansion of pressurized gases like those used for reactions in the chemical industry or for the underground storage of natural gas. To compensate the fluctuation of the demand of natural gas in comparison with the nearly continuously delivery over pipelines from the gas reservoirs big underground storage sites (UGS) are used, with pressure levels varying from less than 100 bar up to more than 300 bar [1]. However, the loading process includes pressurizing and cooling of the gas, so that it can be stored. For the unloading process the pressurized gas is heated and afterwards expanded by a throttle to the pipeline pressure. Compression and heating requires a significant amount of energy, contrary the energy of the gas expansion is dissipating. Enhancing the storages overall efficiency seems possible by using the energy of the pressurized gas in an expansion machine. The power output of such an expansion machine strongly depends on the storage and pipeline pressure but can be estimated in a range of 1 GW up to 4 GW [1]. However beside ecological advantages of such a process management the economic benefit would be increased when the compressor used for pressurizing the gas also could be used reversibly as expansion unit when unloading the UGS.

Another application of such a loading/unloading cycle could be the compensation of short-term and long-term fluctuations of renewable energy sources like on-shore wind turbines or photovoltaic plants. Apart from mechanical and chemical accumulators the use of pressurized air storages or thermal retention with a reversible organic rankine cycle seems promising. With a combined compression-expansion-machine the economic benefit would increase as well.

There are many industrial plants, which offer the possibility of recuperation using a reversible machine. However replacing the existing compressors with new machines – which can handle both compression and expansion mode – seems economically not reasonable. Though a possibility for the retrofit of existing machines in such dual-usable machines could be viable. The control mechanism of the valves is the reason for the compression or expansion mode of a reciprocating machine. Hence a new concept for a valve system is required which can handle both operating modes.

### 3 Valves for combined compression-expansion-machines

#### 3.1 Basic requirements to a combined valve

To design a combined valve for both compression and expansion mode which could be installed at existing machines, the following basic requirements should be taken into account:

- Possibility for retrofit into existing machines
- Low pressure loss in compression and expansion mode
- Small leakage to achieve a good volumetric efficiency
- Low inertia leading to only small delay time during opening and closing
- Low seat impact in respect to fatigue
- Good robustness

Besides those general requirements valves for reciprocating machines have special demands in dependence of the operating mode. Therefore a more profound analysis of the valves and their behavior in compressors and expansion machines has to be set up.

#### 3.2 Working principles of compressor and expander valves

A closer look into the working cycle of reciprocating piston compressors and expanders reveals some differences between the demands of the control mechanism. Figure 1 shows the simplified indicator diagrams of single acting piston machines.

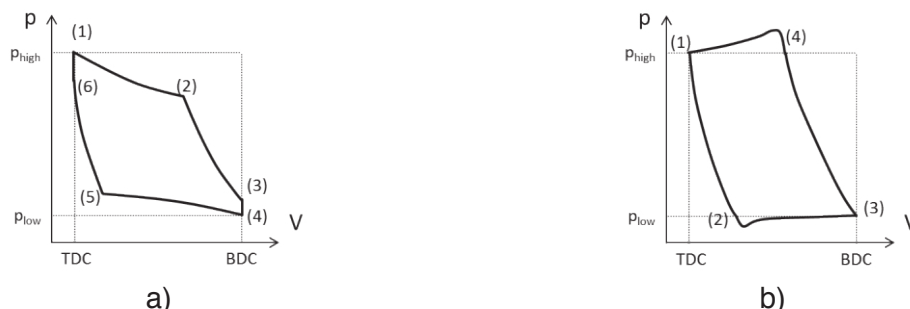


Figure 1: Simplified indicator diagrams for a) expansion and b) compression

For the expansion cycle the entrance valve has to be opened against the pressure difference at the top dead center position (6, 1). Then the pressurized working fluid fills the working chamber. The valve is closed again at point (2) and the expansion of the working fluid proceeds until the piston reaches the bottom dead center (3, 4) where the discharge valve has to be operated. The gas is leaving the working chamber until the discharge valve is closed (5) and the compression takes place up to point (6) where the entrance valve is opened again. Knowing that the enclosed area in the indicator diagram represents the technical work it is emerged that the timing of the actuation of the scavenging organs plays a significant role for the entire expansion process.

The compressor cycle runs counter-clockwise. At the pistons top dead center (1) the discharge valve closes in a self-acting manner and the remaining gas in the working chamber is expanded up to point (2) where the suction valve opens automatically driven by the pressure difference between the suction and the working chamber. The gas is aspirated as long as the cylinder pressure is lower than the suction pressure. Idealized this takes place at the bottom dead center (point (3)). Afterwards the gas is compressed until the cylinder pressure reaches the discharge pressure and the delivery valve opens self-actuated in point (4). The pressurized fluid is discharged up to point (1). Also in compressors a forced opening of the valves



can be worthwhile. To operate the compressor with partial load one option is to keep the valves open beyond the top respectively the bottom dead center.

Comparing the two working processes the following differences could be indicated. The valves of an expansion machine are force controlled and they have to be opened against a high pressure difference with a desired low force. Conversely the valves of a compressor are self-actuated during regular operation and at low pressure differences a high opening force is requested.

The indicated work is given by

$$W_i = -\oint_V p dV = \oint_p V dp, \quad (1)$$

which is represented in the p-V-diagram as the enclosed area. It can be seen, that the pressure loss over the valves decreases the obtained work of the expansion machine (reduction of enclosed area) and increases the necessary work for the compressor (enlargement of the area). A simple formulation of the pressure loss  $\Delta p$  in an orifice is

$$\Delta p = \zeta \frac{\rho}{2} c^2, \quad (2)$$

where  $\zeta$  is the pressure loss coefficient,  $\rho$  the fluid's density and  $c$  the fluids mean velocity at the valve which is indirectly proportional to the flow cross section of the valve. To achieve minimal pressure losses a high flow cross section is necessary.

The size of the valve area is limited by the geometric dimensions of the machine itself. Therefore it is necessary to use the same valves for compression as well as expansion mode. That means we need a low pressure valve which is the suction valve in compression mode and the discharge valve in expansion mode and a high pressure valve vice versa. This results in a special design for the valves justified by the requirements mentioned above.

### 3.3 General designs of scavenging organs for reciprocating piston machines

Looking at different control mechanisms for reciprocation piston machines a first classification needs to be formulated. While in expansion machines mostly sliders are used, where the movement of the slider is perpendicular to the fluid flow, valves are the mostly applied control units for compressors. The valve motion is parallel to the flow direction.

The self-acting valves used in compressors typically consist of a sealing element, which is pushed to the valve seat by a pre-stressed spring. The sealing element is usually a plate or a ring plate. Another common type is the reed valve. An increasingly popular design is the poppet valve, where multiple mushroom-shaped valve bodies are pressed to the valve seat, each supported by an own spring. This design can result in low pressure drops and has also the advantage, that if one valve body is damaged the others can work independently and the process has not to be interrupted immediately.

As already mentioned sliders are the commonly used scavenging organs for expansion machines. Three types could be distinguished:

- the flat side slider, which is a very simple design but has a very limited possibility for timing
- the rotary slider, which has some more flexibility in timing
- the piston slider, which has the advantage of a complete pressure relief and therefore only forces to compensate the friction have to be applied.

Also valve designs are known for expansion machines. Double seated pipe valves can be designed with pressure relief and valve timing could be independent [1]. Poppet valves can also be used as scavenging organ and also an independent valve timing is possible. An overview of common used control organs for piston expanders is listed in *Table 1*.

Sliders			Valves	
+ Pressure relieved designs available - Often considerable frictions forces			+ Pressure relieved designs available - Always oscillating movement	
Flat side slider	Rotary slider	Piston slider	Pipe valve	Poppet valve
+ Very simple design - No pressure relief - Difficult lubrication - Fixed timing	+ More flexibility in timing + Continuous movement - design possible Sealing effect dependent on - gap width Difficult lubrication Vulnerable against particles	+ Completely pressure relieved + Piston sealing is proven technology + Simplified rod-sealing - No inherent timing flexibility	+ Pressure relieved design + Independent valve timing - Double-seats usually not completely gas-tight	+ Simple and proven design - Independent valve timing - Usually no pressure relief

*Table 1 Overview over commonly used scavenging organs for expanders [1]*

Summarizing the demands for expander and compressor mode the requirements for a combined expander-compressor-valve are the following:

- possibility to switch between self-actuation and forced-actuation
- variable valve timing
- low valve mass in respect to valve dynamics and valve response
- low pressure loss over the valve → high flow cross section

Looking at this overview one valve stands out: the poppet valve. In the past this type has been used in expanders as well as in compressors. Furthermore there is the possibility to pilot the valve lift over the two control surfaces on the front and back side of each single poppet. The simple design allows the implementation in already existing configurations.

### 3.4 Valve actuation concepts

To enable the control of the valve lift in expansion mode, an actuation concept for each single poppet is necessary. One possibility is the use of electric magnets, as shown in *Figure 2 a)*. Actuating each single poppet, a design with no internal leakage path is possible. Disadvantages are the high effort for the integration and a high valve impact velocity through high





magnet forces. This is caused by the increase of the electromagnetic field when the magnet anchor moves towards the end position. Another design concept could be the use of a hydraulic actuation (*Figure 2 b*). Separated by a membrane, each poppet is manipulated by a hydraulic pressure provided by an additional pump. Similar concepts are already used for forced opening of suction valves in compressors, however there in combination with a gripper. The additional hydraulic cycle with a pump and sealing is a drawback. Furthermore an internal leakage could occur if the membrane fails, which would lead to a critical mixing of the process gas and the hydraulic fluid. A third possibility is the use of a pneumatic actuator which uses the process gas itself (*Figure 2 c*). The necessary pressure is provided by the compression-/expansion-process. That is why no additional pump is required. As with the hydraulic coupling a leakage could occur, but this is non-critical to the process since the pneumatic gas and the process gas is the same. Using the poppet's shaft and guidance as gap seal a good integration into the system could be realized.

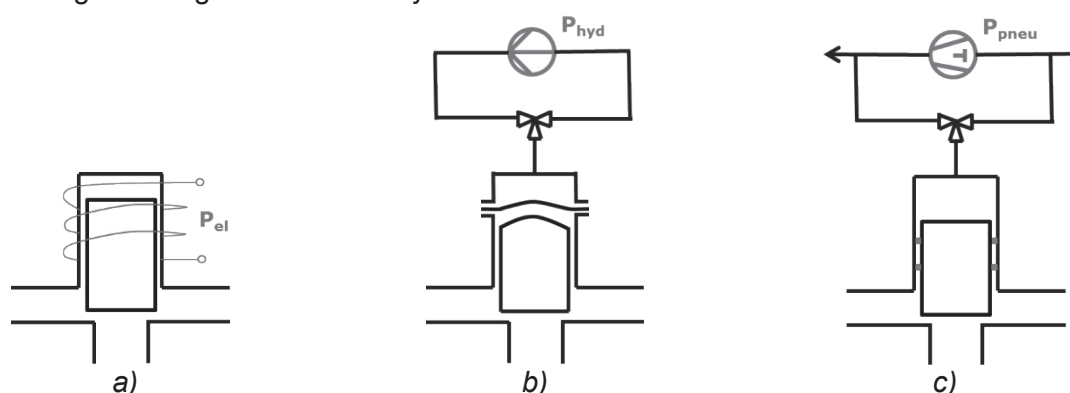


Figure 2: Forced valve actuation (a) electrical, (b) hydraulic, (c) pneumatic concept)

Comparing the three presented concepts the pneumatic actuation with process gas seems the most promising to realize the combined expansion-compression-valve.

### 3.5 Design of a combined valve

Figure 3 shows exemplarily the CAD-model for a combined expander-compressor-valve for the high pressure side which represents the discharge valve for compression and the inlet for the expansion mode. As an ordinary poppet valve the basic design consists of the valve seat plate and the single poppets mounted to the poppet guidance and each is preloaded by an own spring. There is only a small radial clearance between each poppet and its guide to allow a smooth poppet lift but only small leakage between the poppets front and back during the valve motion. Small pressure channels inside the poppet guidance are connected to a slider valve actuated by an electric magnet. In compression mode the slider is in the lower position and therefore the poppets control chamber is connected to the high pressure valve chamber; the poppets work self-actuated. To open the valve in expansion mode the electric magnet moves the slider to the upper position. The connection to the valve chamber is closed but the pneumatic connection to the low pressure side is established. The pressure difference between the poppet's front and back side forces the valve to open.

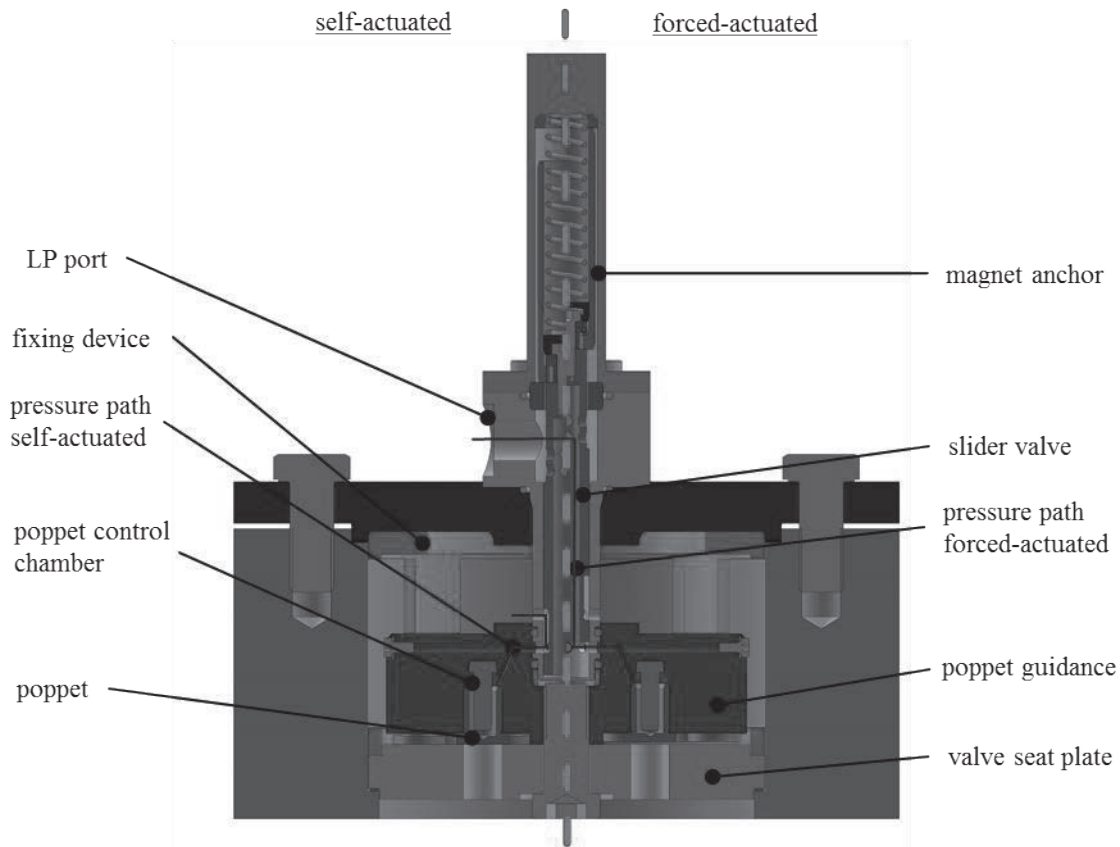


Figure 3 CAD-model of the combined valve for high pressure side (springs hidden for better clarity)

## 4 Process modeling

### 4.1 General assumptions and governing equations

The governing equations for the simulation of a reciprocating piston machine are well known and described in the appropriate literature, e.g. [2] and [3]. For the calculations the ideal gas equation was used to describe the general fluid properties:

$$p = \frac{mRT}{V} = \rho RT \quad (3)$$

The mass flow through an orifice can be described by the one-dimensional adiabatic flow through a nozzle

$$\dot{m} = A c_Q = A \Psi \sqrt{\frac{p_R Q_R}{\zeta}}, \quad (4)$$

with index "R" describing the fluid's properties upstream the restriction. The discharge function  $\Psi$  is given by



$$\Psi = \left(\frac{p}{p_R}\right)^{1/\kappa} \sqrt{\frac{\kappa}{\kappa-1} \left[1 - \left(\frac{p}{p_R}\right)^{(\kappa-1)/\kappa}\right]} \quad (5)$$

For the mass balance only the fluid flow through the valves is considered and leakage is neglected. Knowing the dependency between the crank angle and the piston stroke

$$x(\varphi) = r \left[ (1 - \cos \varphi) + \frac{1}{\lambda_s} \left(1 - \sqrt{1 - \lambda_s^2 \sin^2 \varphi}\right) \right], \quad (6)$$

the machines working chamber volume can be calculated as

$$V(\varphi) = A_p x(\varphi) + V_0. \quad (7)$$

Neglecting the heat transfer between the working fluid and the cylinder walls the fluids temperature can be calculated as either the medial temperature or from phase change during compression or expansion.

$$T = \begin{cases} \frac{m_1 T_1 + m_2 T_2}{m_1 + m_2}, & \text{if } \dot{m} \neq 0 \\ T_1 \left(\frac{V_1}{V_2}\right)^{\kappa-1}, & \text{if } \dot{m} = 0 \end{cases} \quad (8)$$

The valve motion can be calculated by balancing the forces acting on the valve as shown in *Figure 4*.

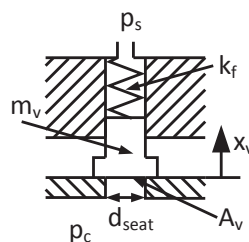


*Figure 4: Model for the valve motion of a poppet valve*

Allowing only one degree of freedom and assuming that the forces through damping, valve sticking and valve return after impact at one of the end positions are negligible, the movement of the valve can be described by the valve inertia, the spring force and the force caused by the pressure difference up- and downstream of the valve:

$$m_v \ddot{x}_v = A_v \psi_{eff} (p_s - p_c) - k_f (x_{v,0} + x_v) \quad (9)$$

## 4.2 Thermodynamic model

To understand the thermodynamic working behavior of the above described valves, a 1D-model was chosen. The basic concept is shown in *Figure 5* with the cylinder (index "c"), a high pressure (HP) and a low pressure (LP) valve and the low and high pressure ports. The

3/2-valves symbolize the possibility to switch the pressure on the backside of the compressor valves.

The cylinder volume is described by the kinematic of the reciprocating machine. Pressure and temperature can be calculated by solving the equation for ideal gas and the mass balance under consideration of the mass flow through the valves equally affected by the valve dynamics (*equation (8)*). Using the ideal gas equation and the mass flow through the nozzle, the pressure chambers for pneumatic valve actuation can be calculated simultaneously. By solving the valve dynamics equation and knowing valve lifts direct influence on the actuators chamber gives a coupling of cylinder volume and valve actuation. Although it is known, that the leakage path between poppet and poppet guidance has an effect on the poppet performance it is neglected for the first step of the study. It could also be suggested that this leakage path is influenced by thermal extension during operation.

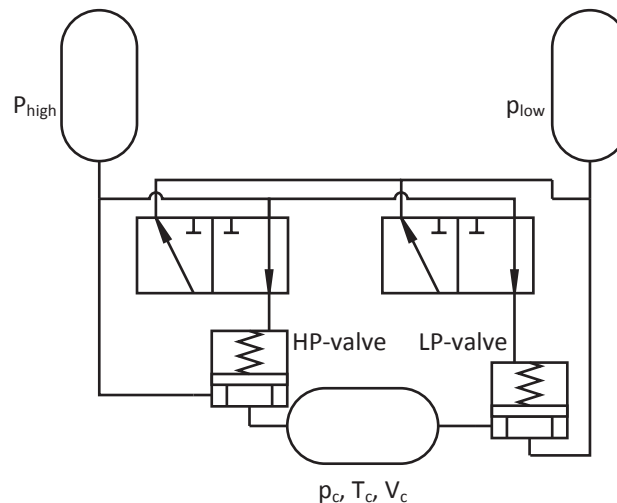


Figure 5: Model for simulation of the expander-compressor-valves

For the comparison to a real reciprocating machine working points of a preliminary chosen test compressor where used. The compressor is an Atlas Copco AR1 with two valve assemblies for the low and high pressure port at each cylinder. The machine and valve data for the first stage are given in *Table 2*.

First calculations where made using only the 1st stage of the compressor. Spring tension and preload where set to allow only a small closing delay and valve flutter in compressor mode at full load. The valve actuation was simulated by changing the inlet pressure of the valve actuation chambers.

machine data (1st stage) [4]			valve data		
n	585	min <sup>-1</sup>	i	2x18	
d <sub>p</sub>	285	mm	d <sub>seat</sub>	20.75	mm
s	150	mm	x <sub>v,max</sub>	1.5	mm
l	295	mm	x <sub>v,0</sub>	1	mm
ε <sub>0</sub>	0.03448		k <sub>f</sub>	900	N/m
p <sub>low</sub>	0.1	MPa	m <sub>v</sub>	40.96	g
p <sub>high</sub>	0.177	MPa			
T <sub>low</sub>	293	K			

Table 2: Machine and valve data for the simulation



### 4.3 Results

Figure 6 shows the p-V-diagram in compressor mode. Since no actuation is used the pressure curve is only influenced by the poppet's characteristic. The pressure loss during suction and discharge is quite high which results from high velocities in the valve flow cross section. For decreasing the mean velocity the flow cross section could be increased by enlarging the valve lift. However this will have an effect on the speed of the poppet, which has an upper limit in respect to the valve impact in the end positions. However the basic concept for compression could be demonstrated theoretically and first steps for the optimization could be made. For simulation of the expansion mode only valve timing, which means the position of the slider for controlling the poppet's pressure chamber, was changed. The resulting pressure-volume-diagram is shown in Figure 7. Like in compressor mode the pressure loss is quite big. Also due to the machine's operating point the filling and discharge time have to be chosen very large to avoid overcompression respectively underexpansion.

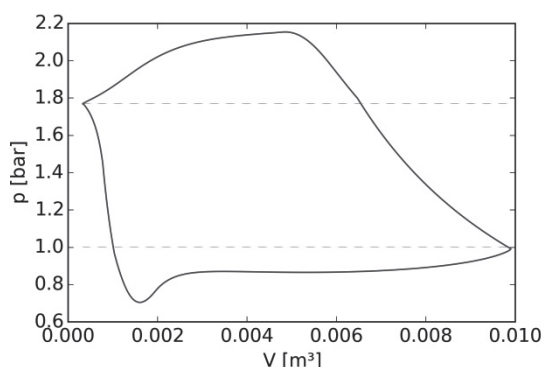


Figure 6: Indicator diagram in compression mode

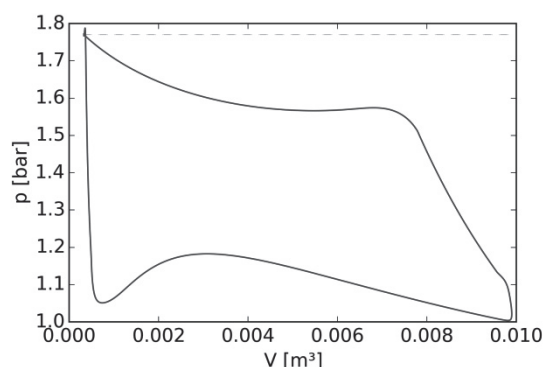


Figure 7: Indicator diagram in expansion mode

Figure 8 shows the behavior of the high and low pressure valves in expansion mode. After changing the inlet pressure to the poppets control chamber ( $p_{s,in}$ ) the control chambers pressure ( $p_s$ ) follows with some delay to the same level and simultaneously the valve moves. This behavior has to be kept in mind, since valve opening is not directly coupled to the crank angle like in mechanically controlled valves. The delay might be reduced by an optimization of the flow path between the slider and the poppet control chamber. However, since the control of the slider for the poppet control is suggested to be managed by a stored program control the valve timing can be readjusted during operation.

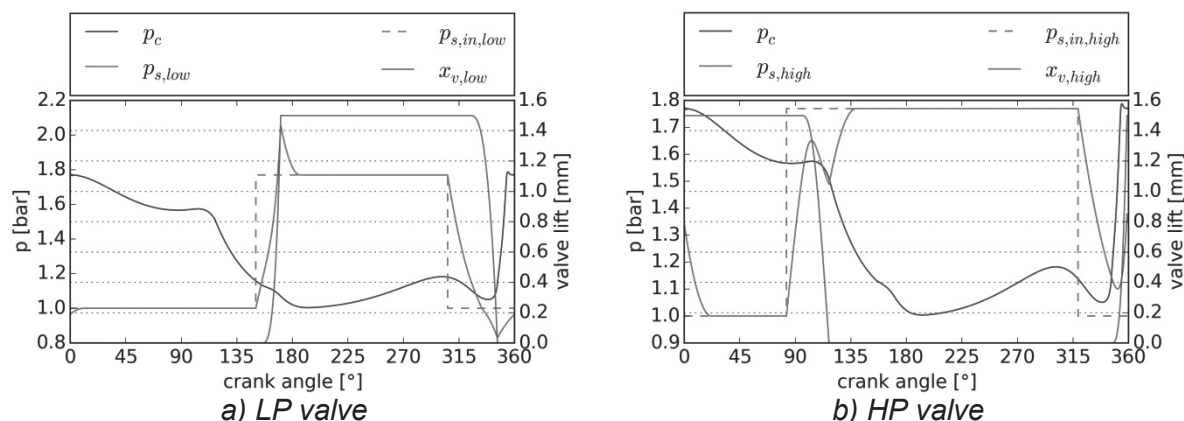


Figure 8: Pressure behavior of poppet control and valve lift in expansion mode



## 5 Summary and Outlook

A dual use valve design has been conceived which offers the possibility to retrofit actual compressors for the possibility to be reversed to work as an expander divergent from the regular compression mode. Different valve and actuator concepts were studied and it was concluded, that poppet valves with a forced actuation by the process gas can fulfil the requirements. A numerical 1D simulation of a real piston reciprocating machine was used with the proposed valve design. It could be shown that compression as well as expansion mode behave as expected from initial considerations. Another recognition is, that the valve timing needs further observation. Since the valve actuation is not fixed to the crank angle the valve movement gives a feedback to the valve control. However, this non-rigid coupling offers the possibility of a step-less change of the valve timing.

The simulation of the actual design shows large pressure drops over the valves. So one point of the future work is the optimization of the poppet design for an improved efficiency. The thermal behavior of the valves is not considered in the actual calculation. To avoid failure a small gap has to exist between the poppet and the poppet guide. This gap changes during operation caused by thermal strain and therefor the leakage over the valve changes. For a deeper understanding of the valve dynamics more operation points of the machine have to be considered. Afterwards the valves will be manufactured and experimentally analyzed in the mentioned a test compressor.

### Acknowledgement

This work was supported by the European Forum for Reciprocating Compressors (EFRC) in the project "Valve systems for Piston Reversible Compression-Expansion Machines".



## Nomenclature

### Symbols

#### Latin letters

A	area [m <sup>2</sup> ]	c	velocity [m/s]	n	rotational speed [s <sup>-1</sup> ]
P	power [W]	d	diameter [m]	p	pressure [Pa]
R	spec. gas constant [J/kgK]	i	number of poppets [-]	r	crank radius [m]
T	temperature [K]	k <sub>f</sub>	spring rate [N/m]	s	piston stroke [m]
V	volume [m <sup>3</sup> ]	m	mass [kg]	x	length [m]
W <sub>i</sub>	indicated work [J]	$\dot{m}$	mass flow [kg/s]	$\ddot{x}$	acceleration [m/s <sup>2</sup> ]

#### Greek letters

$\Delta$	difference [-]	$\epsilon_0$	dead space factor [-]	$\lambda_s$	rod ratio [-]
$\psi$	discharge function [-]	$\zeta$	pressure loss coefficient [-]	$\rho$	density [kg/m <sup>3</sup> ]
$\Psi_{\text{eff}}$	correction factor [-]	$\kappa$	isentropic exponent [-]	$\varphi$	crank angle [°]

#### Indices

0	minimum clearance	high	high pressure side	s	control side
1, 2	thermodynamic state	hyd	hydraulic	seat	valve seat
R	resting state	low	low pressure side	v	valve
c	cylinder	p	piston		
el	electric	pneu	pneumatic		

## References

- [1] U. Hesse und P. Goldmann, „Final Report Survey on Valve Systems for Piston Expansion Machines Phase 1,“ EFRC, Dresden, 2013.
- [2] W. Eifler, E. Schlücker, U. Spicher und G. Will, *Küttner Kolbenmaschinen*, Wiesbaden: Vieweg + Teubner, 2009.
- [3] M. Frenkel, *Kolbenverdichter: Theorie, Konstruktion und Projektierung*, Berlin: VEB Verlag Technik, 1969.
- [4] *Data Sheet: Atlas Copco, Machine list No. 0856*, 1969.





# Technical Paper

**Session: 42-3**

**Session Name: EFRC**

## Internal flow in reciprocating compressors

**Author:**

**Thomas Müllner**  
Research Assistant until 3/2014  
TU Wien, Institute for Fluid Mechanics and Heat Transfer  
1060 Vienna, Austria  
currently: Robert Bosch  
5400 Hallein, Austria

**Co-Author 1:**

Bernhard Streibl  
CEO  
Dr S<sup>3</sup> Simulation  
und Strömungsberechnung  
1110 Vienna, Austria

**Co-Author 2:**

Herbert Steinrück  
Associate Professor  
Institute for Fluid Mechanics and Heat Transfer  
TU Wien  
1060 Vienna, Austria

## Summary

A key factor for the performance of a reciprocating compressor is the gas change. To achieve a good design, the physics of the flow in and out of the compressor have to be understood. In principle, this can be investigated by using commercial CFD software. However, for many applications simpler models turn out to be sufficient. For the prediction of the valve dynamics of compressors of barrel design, a one or in the case of multi-valve compressors a two-dimensional flow modeling is appropriate and have been implemented in the stand-alone tools Compressor1D and Compressor2D, respectively. Concerning the heat transfer from the gas in the compressor to the surrounding walls, these models are of limited use. During in- and outflow the heat transfer could be represented reasonably well since the characteristic flow velocity is given by the in- or outgoing mass flow. During expansion and compression, there is no obvious characteristic reference velocity for the internal flow. Thus, a three-dimensional flow simulation is required. As a consequence, a solver for the three-dimensional Euler-equations has been developed in a project of the EFRC R&D working group. The basic idea is that the heat transfer does not influence the flow and thermodynamic state of the gas in the compressor significantly. Thus, the flow and heat transfer problem can be decoupled. After the inviscid flow in the compressor is determined the heat transfer problem is solved using the boundary-layer approximation along the cylinder walls. For the flow calculation, the flow domain is split into parts; the compression chamber and the valve pockets. Due to the different topology of these domains different meshing strategies have been applied. In the cylinder, a structured mesh with dynamic layering accounting for the piston motion is used. In the valve pockets, an unstructured tetrahedral mesh is employed. The connection of both meshes has been implemented in a conservative way by constructing a common partition of the interface between the compression chamber and the valve pocket. The valve model is based on Costagliola [4]. For the easy use of the program, the user has to specify the main dimensions of the compressor in a graphical user interface. To specify the geometry of the compressor, a sample mesh for a valve pocket is provided. The user has to specify the actual dimensions of the valve pocket and define the direction of the valves in the plane of the cylinder head. The internal flow patterns and valve dynamics for selected compressors will be shown.





## Introduction

In a reciprocating compressor, gas is compressed from a low pressure (suction pressure) to a high pressure (discharge pressure). Thus, a certain amount of mechanical work has to be supplied which can be easily calculated by simple quasi-static thermodynamic considerations. However, in practice losses of many different kinds (valve losses, pocket losses, inertia effects, piston masking, and others) occur, and deteriorate the theoretical limit. As a matter of fact, most of the losses can be attributed to the flow of the compressed gas through the compressor and models have been derived to estimate their effect, see e.g. E. Machu [6]. On the other hand, the availability of CFD-software makes it possible to simulate the flow and its interaction with the valves, c.f. Steinrück et al. [9]. It still takes a lot of effort to set up a simulation of a reciprocating compressor including the valve dynamics. In particular, the definition of the geometry, and the meshing of the valve pockets and the definition of the boundary conditions describing the passive valves is tedious. Moreover, the resolution and the prediction of the flow field is far from being trivial. Getting the flow structure at high Reynolds number right is even impossible. We refer to the well known driven cavity flow problem, wherein the 2D case an uncontroversial numerical solution exists only for Reynolds numbers up to about 20000. In reciprocating compressors, the Reynolds number is of the order  $10^5$  -  $10^6$ . Thus, we can only expect to get the basic flow features correctly. Another issue is the long computation time which is usually a matter of hours or days for a complete cycle. Thus, there was the demand for simple, fast and reliable compressor models. To answer this need, the EFRC R&D working group funded projects to develop the simplified simulation tools Compressor1D, Compressor2D, see Aigner [1], and Compressor3D, see Müllner [7]. Since the one- and two- dimensional models have been presented at previous EFRC conferences, Aigner et al. [2], [3], we want to present here the main features of a simplified three-dimensional compressor model.

The main goals are to predict the valve lift dynamics (valve lift as a function of time), the indicator diagram, the time-dependent forces and moments on the piston, and the heat transfer to the casing.

## Model assumptions

The main objective of the flow modeling of the gas in a reciprocating compressor is to predict the response of the gas in the compression chamber to the action of the piston and the valves. In particular, one is interested in internal waves as far as the valve dynamics and the time varying loads on the piston are concerned and in the global flow patterns to get an estimate of the heat transfer. Using a better geometrical model, say a 3D model instead of a 1D model does not necessarily improve the quality of the numerical solution. For example, consider a compressor of barrel design with only one suction and one discharge valve. The motion of the valve plate is affected by internal pressure waves running back and forth between the discharge and suction valve. It was shown that these waves could be well described by a one-dimensional wave propagation/flow model, see Aigner [1]. In a one-dimensional numerical model, the number of grid points can be chosen sufficiently large to compensate numerical diffusion and thus the numerical results are in reasonable agreement with measurements. In a 3D-dimensional approach, one is limited to a relatively large cell size to keep the computation within reasonable time limits. Thus, waves will be strongly damped by numerical diffusion. However, the benefit of a 3D-solution is that one gets the global flow pattern right. This is essential when one is interested in the heat transfer from the compressed gas to the surrounding walls. Thus, selecting the numerical model depends on the question one wants to answer. Of course, most of these problems can be overcome by using high-performance computing as done when simulating the flow and combustion process in internal combustion engines. So the definition of the problem was to develop simple tools to predict the internal flow and heat transfer in reciprocating compressors, which can assist the design of such machines.

## Flow model

The gas flow is described by balance equations for mass, momentum, and energy written in conservative form. Neglecting viscosity, these are the well-known Euler equations. As a consequence, heat conduction and thus, the heat transfer to the walls of the compression chamber is also eliminated.

But this contradiction can be easily resolved by the fact that along the solid walls thin boundary layers form. Thus, the heat transfer can be calculated after the inviscid flow calculation a boundary layer calculation. The Euler equations have to be complemented by equations of state for the gas. Here, an ideal gas with constant heat capacities is assumed. It is described by  $\gamma$ , the ratio of the specific heats and the molar mass. The numerical method for the solution is a finite volume method. Thus, the computational domain is divided into small finite volumes, and the mean values of the state variables (density, momentum, and energy) of each volume are used as computational quantities. Due to the conservative formulation, these mean values can be changed only by the flux of these quantities across the volume boundaries. Therefore, the mass, momentum, and energy conservation principle are strictly satisfied even for the discretized equations. In a numerical scheme, the fluxes across a cell boundary have to be computed as a function of the cell averages of the state quantities of the neighboring cells. Here, the Roe-method is used. It calculates the numerical flux from the cell average of the adjacent cells using an approximate Riemann solver. This is a robust, well-proven method of first order accuracy.

## Description of the geometry

The flow region inside the compressor consists of the cylinder confined on one end by the movable piston and on the other side by the cylinder head, and the valve pockets, see figure 1. In the cylinder, a structured mesh for the finite volume method is used. It is given by a two-dimensional mesh in the plane of the cylinder head, see figure 3a), and is extruded in the direction of the cylinder axis. Due to the motion of the piston, these finite volumes are stretched in the axial direction. If the aspect ratio of the cells exceeds a critical value, a re-meshing in the axial direction will be performed and the cell averaged values of the density, momentum and energy have to be interpolated in a conservative way for the new mesh, see figure 2.

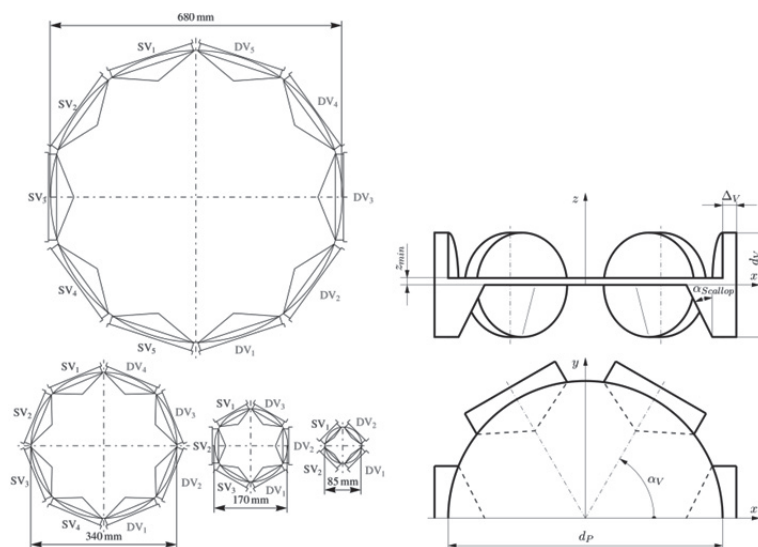


Figure 1: Compressor geometry



For the valve pockets, a reference geometry has been chosen. It consists of a cylinder of diameter  $d_v$ , which intersects the cylinder of the compression chamber, and a cone of height  $h_c$ . The axis of both, the cylinder and the cone are in the plane of the cylinder head. Due to its complex geometry, it is not possible to mesh it with a structured mesh. A prototype unstructured tetrahedral mesh was constructed for the valve pocket, see figure 3b). The prototype mesh will be mapped onto the actual valve pocket. Finally, the geometry of a compressor can be described by a few parameters: bore diameter, stroke, clearance, the number of valves, the direction of the valve pocket axis, the radius of the valve pocket, heights of valve-pocket cone and cylinder. At the interface of the valve pocket and the cylinder, the unstructured tetrahedral grid and the hexahedral grid in the cylinder have to be coupled in a conservative way. Therefore, a common partition of both grids at the common interfaces at the cylinder head and the circumference of the cylinder are constructed. In Fig 3c) the common interface with the quadrilateral surface mesh of the cylinder and triangular surface mesh of the pocket valve is shown.

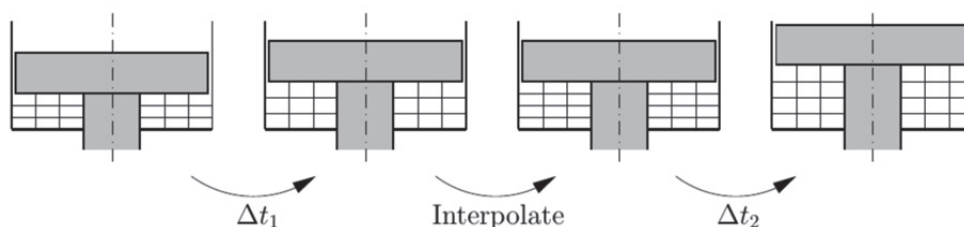


Figure 2: Dynamic mesh

Hence, in order to derive the interface facets, all the triangles of the valve pocket surface mesh and all the quadrilaterals of the cylinder surface mesh are decomposed into a priori unknown number of polygons, being the result of that intersection. Every single polygon is then part of a triangle and a quadrilateral, respectively. Recently, Fahs [5] identified five possible configurations for the intersection of triangles with convex quadrilaterals, giving polygons with either three, four, five, six or seven edges. Once the number of edges and the positions of the intersection points of every polygon is known, the area of every polygon can be computed easily by decomposing it into single triangles. It is also not difficult to determine the barycenter of the polygons, eventually required for a second order finite volume method. However, for a first order finite volume method, the numerical flux computation only requires the area and the unit normal vector, here taken in the area center.

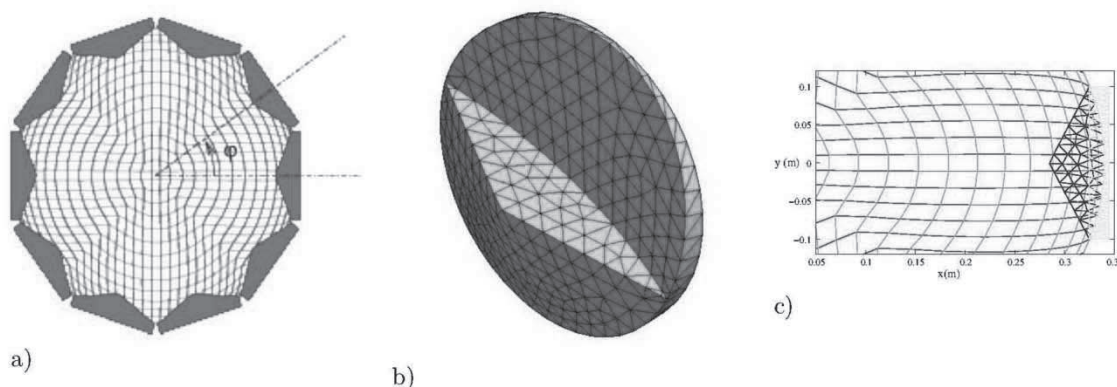


Figure 3: a) planar structured grid in plane of cylinder head, b) tetrahedral mesh in valve pocket, c) common partition of interface of structured and unstructured grid

## Valve model

The discharge and suction valves are self-acting, spring loaded plate valves. For all three compressor simulation tools, the same valve model based on the paper by Costagliola [4] is used. The gas flow through the valve is assumed to be quasi-steady. This assumption is valid if the transit time of a gas particle through the valve is short compared to the opening time of the valve, which is the case under usual operating conditions. Thus, the mass flow through can be expressed by the well-known outflow formula by Saint-Venant Wantzel, see Zierep [10], as a function of the effective flow cross-section  $\Phi_V$  which is, in turn, a function of the valve plate lift  $x_V$ .

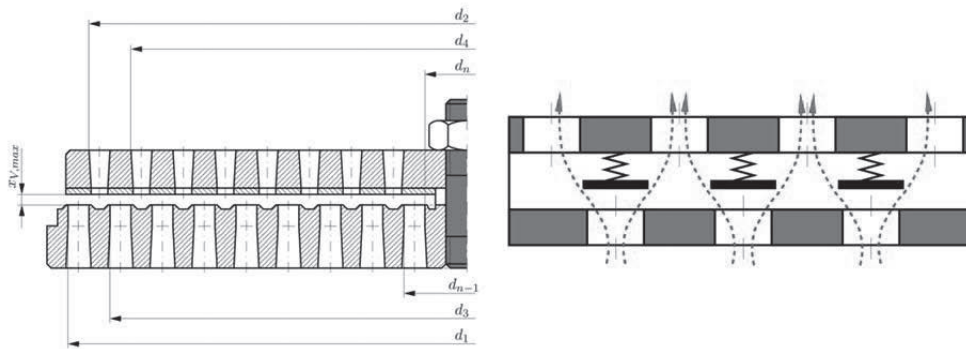


Figure 4: Flow paths through a plate valve (left), mass spring model of plate valve (right)

Moreover, a model for the state of the valve is needed. That is an equation of motion for the valve plate of mass  $m_V$ . The gas pressure acts on the so-called force areas  $A_f$  on both sides of the valve plate. Springs with spring constant  $k_V$  and initial deflection  $L_V$  press the valve plate onto the seat and thus define a closing pressure  $\Delta p_{\text{closed}}$ , see figure 4.

## Heat Transfer model

Since the Reynolds number for the gas flow in a reciprocating compressors is large, we can expect that the flow is almost inviscid in the interior, and turbulent boundary layers form along the walls. In a state of the art commercial CFD software, one would use a more or less elaborate turbulence model to describe the Reynolds stresses in the flow region. Rigid walls suppress the turbulent fluctuations and thus, special wall treatments are required. Very close to the wall viscous stresses dominate, and this region is called viscous sub-layer. In the case of an attached flow, the flow profile has to be matched to the so-called defect layer of the boundary-layer. It has been argued by Prandtl and later be confirmed by measurements that in the overlap region of the defect layer and the viscous wall layer the velocity and temperature profile is given asymptotically by a logarithmic profile.

Thus, there is the choice to resolve the viscous sub-layer or to use wall functions to describe the flow and temperature field close to the wall.

In our approach, the external flow field is given by the numerical solution of the Euler-equations. Thus, it remains to solve the boundary-layer equations to obtain the heat transfer coefficients. Since the Mach number of the gas flow near the wall is small, we can consider the boundary-layer flow as incompressible. We remark that in the passage between the valve pocket and the cylinder the flow velocity may become supersonic. But this is not the case for the flow along the walls.

For the solution of the boundary-layer equations several methods are possible: using turbulence models plus wall treatment or integral methods are among them. Since we are interested only in





an overall heat transfer coefficient for each face, we will use a very simple integral method. Following Gersten Schlichting [8], we will use logarithmic velocity and temperature profiles close to the wall. With these assumptions, we derive the relation for the average heat transfer coefficient  $\alpha$

$$\alpha = \rho c_p \bar{u} \frac{1}{Pr_t} \left( \frac{\kappa G(\Lambda, D)}{\ln Re} \right)^2,$$

where  $u$  is the mean velocity of the Euler flow along the considered face and the Reynolds number  $Re$  is formed with this velocity and the piston diameter. The value of the turbulent Prandtl number  $Pr_t$  is 0.9 and of the von Karman constant  $\kappa$  is 0.4.  $\rho$  and  $c_p$  denote the density and isobaric heat capacity of the gas, respectively. The function  $G(\Lambda, D)$  is approximated by 1.5, see Gersten Schlichting [8].

## Results

The program has been tested for four test cases shown in figure 1. The data for the 10-valve compressor is listed in table 1 and will be discussed in detail. In Figure 5 the maximal Mach number in the valve pocket is shown as a function of the crank angle for the first two cycles of the simulation. We remark that the first cycle depends weakly on the initial condition of the simulation. Time-periodic behavior is obtained after the first cycle. During outflow (at a crank angle of  $320^\circ$ ) the Mach number in the discharge pocket rises up to 0.75. The flow stays subsonic. Only when increasing the compressor speed to 1200 rpm supersonic flow conditions occur for a short period, and the present code is capable of dealing with it.

piston diameter	680mm	# suc. valves	5	valve radius	100 mm
min. gap width	1.5mm	# disch. valves	5	height of valve cone	40 mm
stroke	150 mm	$\alpha$	2.0	height of valve pocket	19 mm
speed	800 rpm	$\beta$	$1.8 \cdot 10^5 \text{ m}^{-2}$	max valve lift	2.5 mm
Molar mass	29 kg/kmol	force area	$0.0178 \text{ m}^2$	mass valve plate	0.21 kg
ratio of spec. heats	1.4	spring stiff.	3750 N/m	$fe_{1\text{mm}}$	5.938 m
kinematic vis.	$2 \cdot 10^{-5} \text{ m}^2/\text{s}$	initial deflection	0.75 mm		
suc. press.	1 bar	suct. density	$1 \text{ kg}/\text{m}^3$	disch. press.	1 bar

Table 1: data of test case

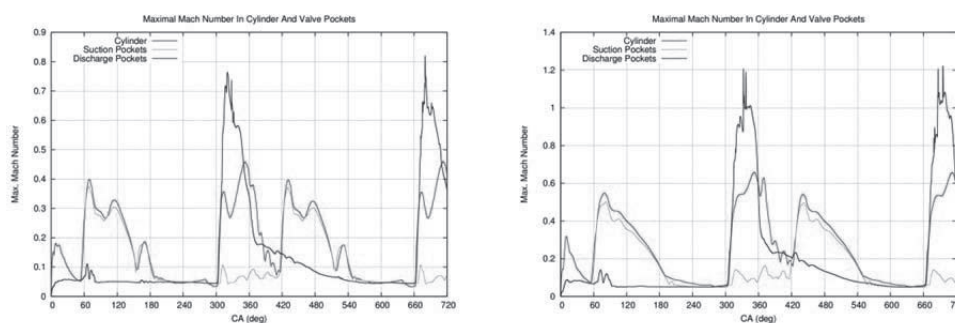


Figure 5: Maximal Mach number for 800 rpm (left) and 1200 rpm (right)



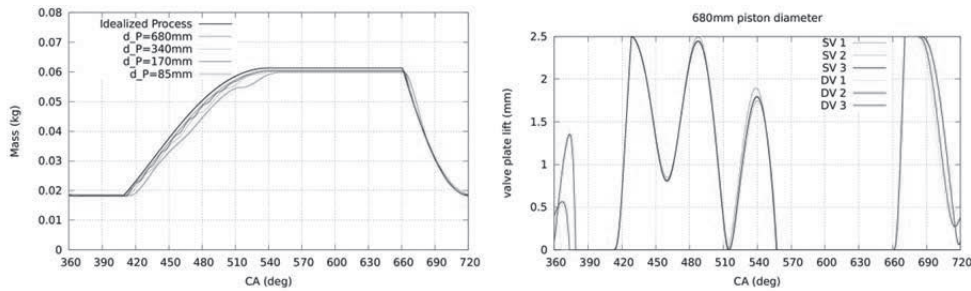


Figure 6: Valve dynamics: mass flow during discharge for all four test cases compared with the ideal compressor process (left), valve lift of the suction and discharge valves of the 10-valve compressor (right)

The operating point of the four test cases has been chosen such that they can be considered as different stages. Thus, they refer to the same idealized compressor cycle. The total mass flow through the discharge valves shown in figure 6a) is close to the idealized compressor process. However, it can be seen that the compressors with piston diameter 340 mm, 170 mm and 85 mm show oscillations in the mass flow. This is due to fluttering of the suction and discharge valves. By changing the springing, the eigenfrequency of the spring-mass system of the plate valve can be decreased to avoid fluttering, see Müllner [7].

For the 10-valve compressor, the suction valves do not stay fully open during intake. They are completely opened only for two short moments. They even close for a moment at 515 deg crank angle. The discharge valves behave well. It is interesting to note that the central discharge valve DV<sub>3</sub> opens again after the piston has reached the dead center. For the lateral valves DV<sub>2</sub> and DV<sub>1</sub>, this secondary opening is less pronounced.

Calculating the average velocity on each face of the compression chamber and using the simplified boundary-layer heat transfer model the heat transfer coefficients on the different faces of the compression chamber are estimated. As expected, the heat transfer is large during the discharge between 300 and 400 deg. During intake, it is only of moderate size while it is almost negligible during compression, see figure 7b).

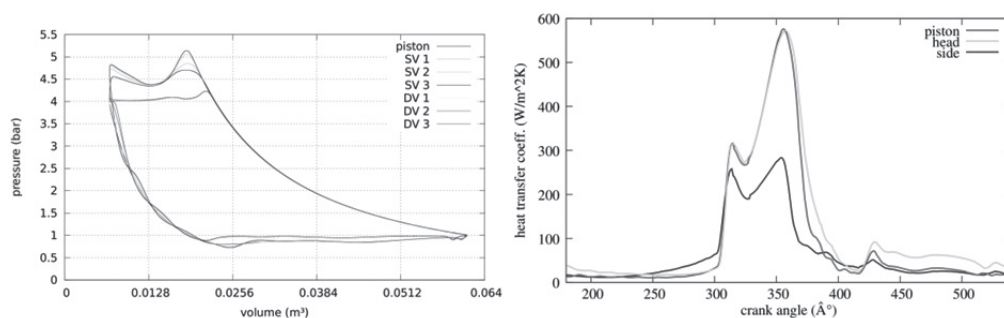


Figure 7: Indicator diagram (left), heat transfer coefficients (right)

In the indicator diagram, figure 7, the pressure at the piston, the suction valve, and the discharge valve is shown. It can be clearly seen that the pressure at the suction valves is markedly larger than the pressure at the piston. In the valve pockets of the discharge valves, the pressure is only slightly above the discharge pressure. In figure 8 a)-c), the pressure at the piston is shown shortly before and after the opening of the discharge valves. At CA=660 deg the pressure is almost uniform. At the interfaces to the valve pockets, the pressure is slightly



smaller. Shortly, after the discharge valves open at CA=662 deg, the development of a pressure wave traveling transversally through the cylinder can be observed.

During re-expansion internal waves can be observed in the indicator diagram and at the snapshots of the pressure field at the piston, figure 8 d)-f). An estimate of the time needed for traveling back and forth in the cylinder  $t = 2d/c$  gives a crank angle difference of about 20 deg. for the complete passage back and forth in the cylinder. Indeed, the pressure snapshots between 380 and 390 deg show the wave has once passed the cylinder.

The velocity field along the piston is shown in figure 9. At a crank angle of 360 deg the piston is at the dead center. At 370 deg the re-expansion has already started, and the gas flows from the valve pockets back into the cylinder. Since the pressure in the suction valve pockets has been larger than that in the discharge valve pockets the flow velocity along the piston at the suction side is considerably larger than at the discharge side. During intake (450 deg) we observe the inflow from the suction side. At the dead center (540 deg) only relics from the intake motion are visible. During compression, there is a slow redistribution of the gas into the valve pockets visible. When the discharge valves open at 670 deg the outflow motion into the discharge valve pockets sets in.

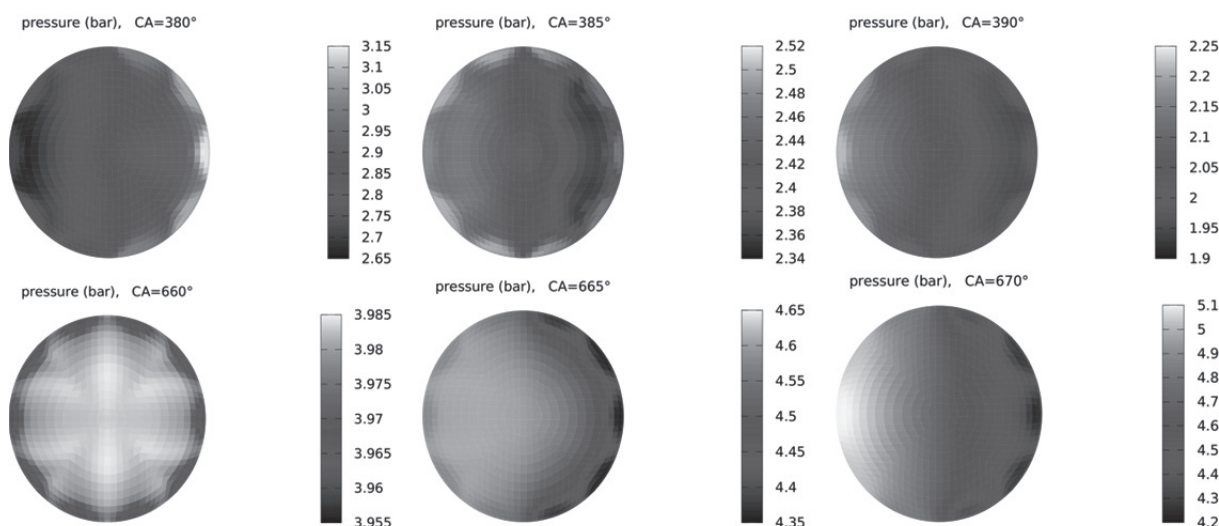


Figure 8: Pressure at the piston

### Comparison with Compressor1D

In Compressor1D, the Euler-equations are averaged over the cross section of the compressor perpendicular to the diameter between the two valves. Thus, a wave propagation problem through a channel with varying cross section has to be solved. It has been shown that the restriction to a one-dimensional flow is reasonable during the interesting phases of the compressor cycle. However, due to the nature of the one-dimensional flow model the passage of the flow from the cylinder into the valve pocket cannot be accurately described due to the discontinuous change of the flow cross-section at the interface between the cylinder and the valve pocket. In the following, we compare simulation results of Compressor1D with Compressor3D for a 2-valve compressor with a 220 mm bore. In figure 10a), the motion of the valve plate during the opening of the discharge valve is shown. The one-dimensional model predicts a higher impact velocity of the valve plate. This can be attributed to a larger pressure loss at the interface of the valve pocket to the cylinder than in the three-dimensional case.

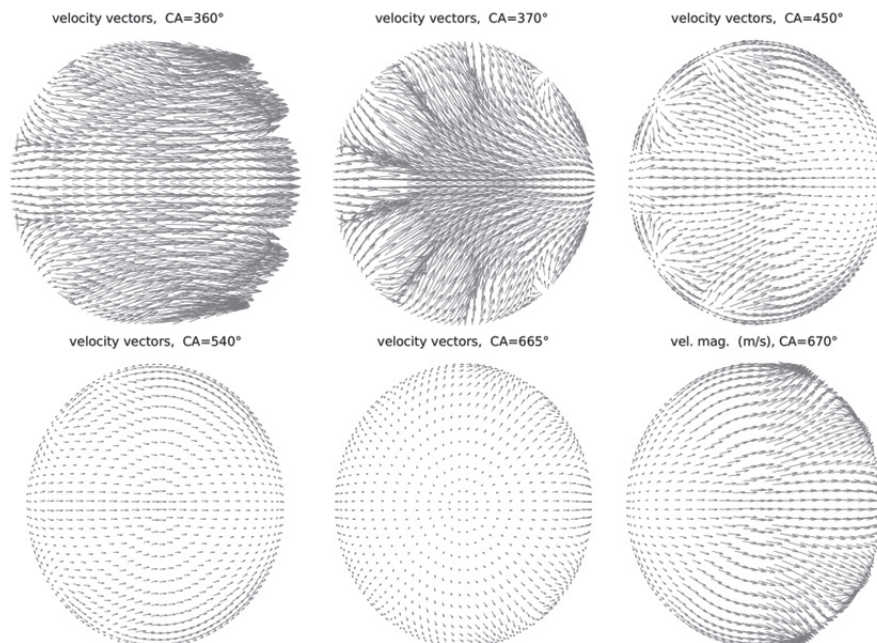


Figure 9: Velocity field along piston

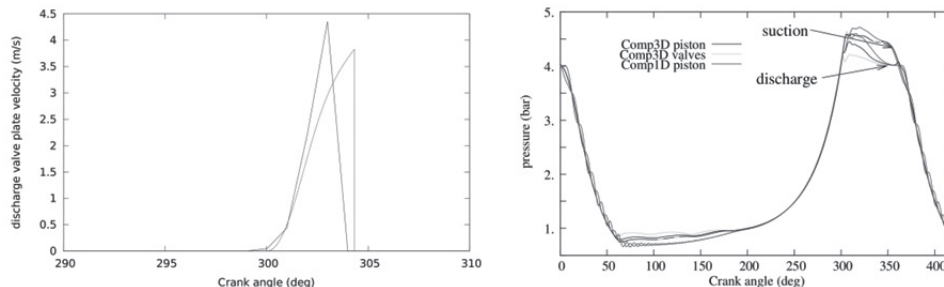


Figure 10: Comparison Compressor1d/Compressor3D for a 2-Valve compressor: plate velocity of discharge valve (left), pressure at different positions in the compressor (right)

In figure 10b), the pressure at different positions as a function of the crank angle is shown. In the three-dimensional case, the mean pressure at the suction and discharge valve is indicated with a cyan-colored line. The blue lines correspond to the pressures at the piston close to the valve pockets. At the beginning of the discharge, a pressure difference across the discharge valve pocket can be observed. This difference decreases until the end of discharge. In the one-dimensional model, this pressure difference is obviously larger. On the suction side, there is no pressure difference across the valve pocket. The one-dimensional model predicts on the suction side a larger pressure than the three-dimensional model.

During inflow, the 1D model predicts at the piston a lower pressure than the 3D model which can be again attributed to a significant pressure loss across the passage from the valve pocket into the cylinder. Moreover, the one-dimensional model predicts only slightly damped pressure waves running back and forth across the cylinder. These waves are not present in the 3D-dimensional model. On one hand there is no damping mechanism in the one-dimensional



model, except numerical diffusion, which is, however, small due to the relatively large number of grid points and on the other hand in the 3D case waves are damped geometrically and by the numerical diffusion due to the relatively small number of cells per diameter to keep the computational time within reasonable limits.

### Conclusions

A three-dimensional model for the simulation of reciprocating compressors based on the Euler-equations has been presented. The interaction of the flow with the valve dynamics and the occurrence of internal waves have been shown. Moreover, an educated guess of the heat transfer coefficients has been given, and a comparison with the existing one-dimensional model has been made.

The use of these models is to obtain an educated guess of the compressor performance with a ready-to-use-tool. To study details of the flow and heat transfer, a detailed analysis using a state of the art tool will be unavoidable.

### Acknowledgement

The work has been funded by the EFRC-R&D working group.

### References

- [1] R. Aigner, Internal Flow and Valve Dynamics in a Reciprocating Compressor, Ph.D. thesis, TU Wien, 2007.
- [2] R. Aigner, G. Meyer, and H. Steinrück, Valve dynamics and internal waves in reciprocating compressors. In 4th EFRC Conference, pages 169–178, 2005.
- [3] R. Aigner and H. Steinrück, Modeling fluid dynamics, heat transfer and valve dynamics and in reciprocating compressors. In 5th EFRC Conference, pages 169–178, 2007.
- [4] M. Costagliola, The theory of spring-loaded valves for reciprocating compressors. J. Appl. Mech., pages 415–420, 1950.
- [5] H. Fahs, High-order discontinuous Galerkin method for time-domain electromagnetics on non-conforming hybrid meshes. Mathematics and Computers in Simulation, 107:134–156, 2015.
- [6] E. Machu, Problems with high-speed short stroke reciprocating compressors: Increased power requirements due to pocket losses, piston masking and gas inertia, eccentric loads on the piston. In Proceedings of Gas Machinery Conference USA, 1998.
- [7] T. Müllner, Flow Patterns and Valve Dynamics in Multi-Valve Reciprocating Compressors. Ph.D. thesis, TU Wien, 2015.
- [8] K. Schlichting, H. Gersten, Boundary-layer theory. Springer, 8th edition, 2000.
- [9] H. Steinrück, R. Aigner, and G. Machu, Transversal waves in a reciprocating compressor. Acta Mechanica, 201(1):231–247, 2008.
- [10] J. Zierep, Grundzüge der Strömungslehre. Springer, 1997.







# Technical Paper

**Session: 43-1**

**Session Name: Monitoring**

## **Electric motors for reciprocating compressors and condition monitoring**

**Author:**

**Dr.-Ing. Michael Ade**  
Development Engineer  
Siemens  
13629 Berlin, Germany

**Co-Author:**

Dr.-Ing. Artur Jungiewicz  
Development Engineer  
Siemens  
13629 Berlin, Germany

## Summary

(Electric motors and drives are the best choice for driving the highest loads as they combine all of the essential characteristics required. These include, for instance, high torque or power density, long service life, high efficiency and reliability. Further, they are flexible when it comes to their electromechanical properties, the type of construction and the mounting arrangement, which means they can be simply adapted to address the requirements of the driven load. Synchronous and induction motors are both suitable for driving reciprocating compressors. Each type has its own specific electrical properties that define the best type for a particular application. The typical characteristics, potential and limits of each type will be highlighted in the first section of this paper.

The second section deals with specific requirements and improvements that customers are today asking motor manufacturers for, with the objective of getting the best possible motor for the specific application. Using selected examples, it will be shown how the improvements that have been requested have been incorporated as part of the redesign process for synchronous motors for reciprocating compressors. Top priorities include serviceability and a flexible design with respect to features like the type of cooling, the motor inertia, explosion protection and the mounting arrangement.

The third and last section is about advanced condition monitoring for electrical motors driving reciprocating compressors. Data acquisition and data analysis of selected physical quantities allow failures, wear and aging to be detected at an early stage. It enables users to apply corrective measures before serious damage occurs, often associated with long down times and high costs. An advanced monitoring system will be presented in this paper. The focus is on the description of the system, the physical quantities that we recommend be monitored and the customer's benefits as a result of the monitoring system.



## Electric Motors for Reciprocating Compressors and Condition Monitoring

### Introduction

Figure 1 shows a typical design of a high-rating electric motor. The rotor (1) consists of the pivot-mounted shaft, the active iron (3) and the rotor winding (4). The wide variety of shapes and arrangements of the active rotor iron and the rotor winding are determined by the type of machine and the motor characteristics required. The stator arrangement is similar for almost all high-rating electric motors. A three-phase stator winding (7) is inserted in the slots of the stator lamination (6), which is surrounded by a support structure (8).

The active motor parts are surrounded by a housing (9) with a top-mounted canopy (10) that protects personnel from severe injury and the motor against the ingress of water and dust.

Air-to-water cooling is one of the most common methods of cooling high-rated electric motors. A fan (5) blows air as primary coolant through the motor and that absorbs the heat generated in the active parts. The hot air (red arrows) is cooled down (blue arrows) using an air-to-water heat exchanger (11). The air that has been cooled down is recycled through the motor again.

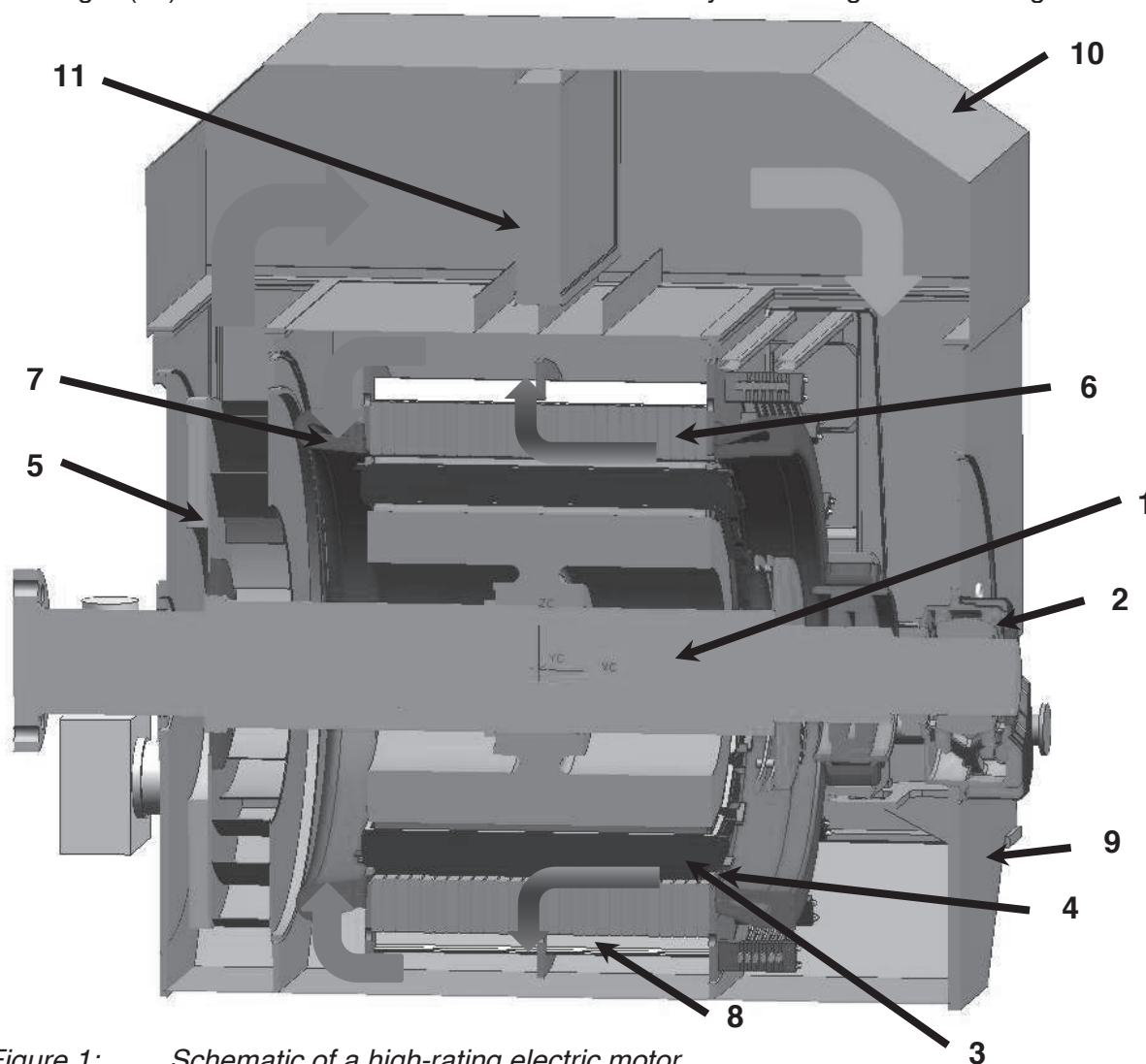


Figure 1: Schematic of a high-rating electric motor.

### Electric motors suitable for driving reciprocating compressors

Squirrel cage induction (IM) and synchronous motors (SM) are capable of driving reciprocating compressors. The stator design is similar for both, while the rotor design and the operating characteristics differ considerably.

The rotor of a squirrel cage induction motor consists of the rotor lamination and the squirrel cage winding. Massive copper bars are embedded in the slots of the rotor lamination and connected to massive copper short-circuit rings on the face sides. When the motor is operational, the rotating stator field induces a voltage in the rotor winding, thus requiring the stator field to rotate slightly faster than the rotor [1]. Due to the principle of operation, neither an exciter machine nor sliprings are required for electrically supplying the rotor. Typically, attributes of induction motors include the cost-efficient and rugged rotor design, high starting- and acceleration torques and rugged operating characteristics when disturbances occur, such as external torque peaks. They are mostly used in the power range up to approx. 12 MW.

Synchronous motors have either cylindrical or salient pole rotors (Fig. 2). In the first case, a concentric field winding is inserted in the slots of the cylindrical rotor lamination. In the second case, the field winding is wound around the salient rotor poles thus providing the machine with special characteristics. Usually both types are equipped with an additional damper winding thus preventing oscillations in case of sudden load changes. In a more rugged design, the damper winding can also serve as the starting cage for a direct online start [2]. For driving reciprocating compressors, salient pole rotors offer advantages as discussed below. The field winding is supplied with DC current via sliprings or the rectified rotor current of a separate exciter machine. Compared to an induction motor, the rotors of synchronous motors are more complex as they require a high number of subassemblies. On the other hand, synchronous motors are more suitable when it comes to higher ratings. Further, they are also more efficient and provide the option of adjusting the power factor. Induction and synchronous motors are compared based on selected criteria in Table 1.

	IM	SM
Rotor design	+	- (More complex due to higher number of subassemblies)
Ruggedness	++	+ (Higher number of subassemblies)
Torque	o	+
Maximum output	o	++
Online start performance (DOL)	++	+ (Starting performance can be improved by additional measures such as starting cage or starting resistor)
Stability during operation	++	+ (Damper winding required)
Reactive power demand	o	++ (Adjustable excitation)
Efficiency	o	+
Short-circuit torque	-	-
Suitability for inverter operation	o (Magnetizing current supplied from the stator)	+
Cost	+	o
Maintainability	++	+ (Brushes, higher number of rotor subassemblies)



Table 1: Comparison of induction and synchronous motors based on selected criteria

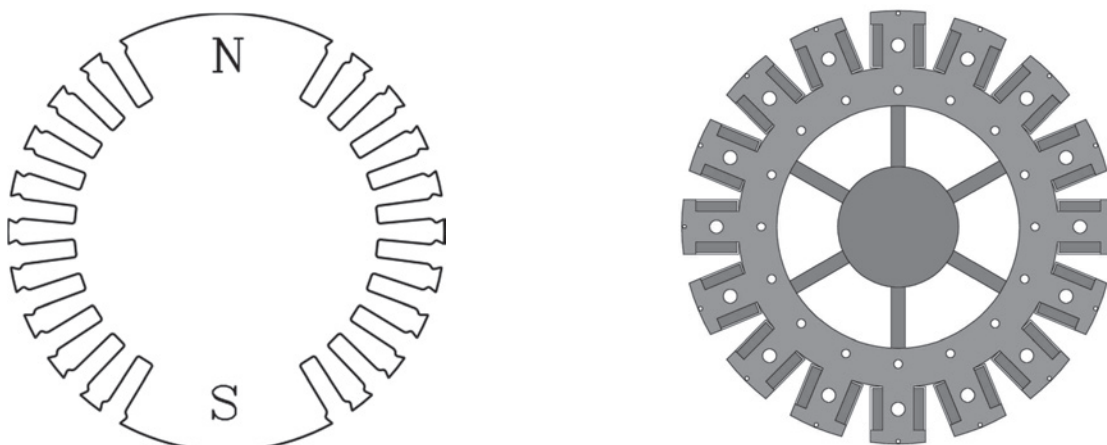


Figure 2: Left: Cylindrical rotor [1]; right: salient pole rotor

### Typical and special requirements for motors driving reciprocating compressors

Power range	... 40MW ↔ approx. ... 2000kNm (S1 operation)
Voltage level	10kV, 13.2kV (other voltage levels are possible)
Speed range	200 ... 600rpm
Cooling methods	IC616, IC81W, IC86W, WPII
Mounting arrangement	IM 1001...7, IM 1101...7, IM1201...7, IM1301...7 IM 7001...7, IM 7101...7, IM7201...7, IM7301...7
Degree of protection	IP23, IP54, IP55, IP56
Ex-protection	Ex n, Ex p

Table 2: Typical requirements for high-rating single-bearing motors driving reciprocating compressors

An overview of the typical requirements for motors driving reciprocating compressors is provided in the Table 2. The data shown focuses on high-torque single-bearing motors. Further, there are several specific requirements relating to the application and the conditions at the installation site.

- The **pulsating torque** of reciprocating compressors varies from case to case between 0.5 and 2.5 times the rated motor torque within one shaft revolution. It causes current pulsations that need to be restricted according to established standards [3]. Providing the rotor with sufficient inertia helps to limit the current pulsations. On the other hand, the inertia should not be too high in order to ensure acceptable acceleration times and energy losses in the motor windings and the active iron.
- A **direct online start** is the preferred starting method since no additional equipment is required – for example an inverter or a starting transformer. While accelerating, the armature current increases up to approximately 4 ... 7 times the rated current. This causes the line voltage and in turn the motor terminal voltage to drop. This means that the motor starting torque also decreases. In addition, the voltage reduction may cause grid loads to be undesirably shed.
- The **starting current** depends on the type of motor and its electromagnetic design. Synchronous motors have lower starting currents, however, their starting torque is also lower. The electromagnetic design offers measures for influencing the starting



current such as increasing the leakage inductances, applying a starting resistor and so on.

- The ignition of flammable gases must be avoided at all costs if the motor is installed in an **explosive atmosphere**. In particular, flammable gases must be prevented from coming into contact with hot motor parts – and sparks inside the motor must be prevented. Sparks may occur in case of partial discharge. Any gas that may have accumulated within the motor can be removed by purging the motor with air before closing the starting circuit breaker. Creating an overpressure condition inside the motor prevents flammable gases from entering the motor housing.
- **Noise** generated by electric motors predominantly have a fluid-dynamic, mechanical or magnetic background. Fluid-dynamic effects are caused by the coolant flowing through the motor, and can hardly be influenced. Mechanical effects are mostly caused by imbalance, loose parts or bearing noise and can be eliminated by measures such as balancing and resolving any loose parts. Magnetic noise is caused by periodic magnetic forces that excite mechanical structures to vibrate. During the design of the motor it has to be ensured that the periodic magnetic forces do not excite any critical natural frequencies of the mechanical structure, and that the excitations are as small as possible. However, a noise-reducing cover should be used anyway.

### Large synchronous motors for reciprocating compressors

Our synchronous motors for reciprocating compressors have gone through a redesign process in recent years. The goal was to develop a flexible design at a reasonable cost. A basic design should be able to be adapted to the wide range of different customer requirements with a minimum of modifications required.

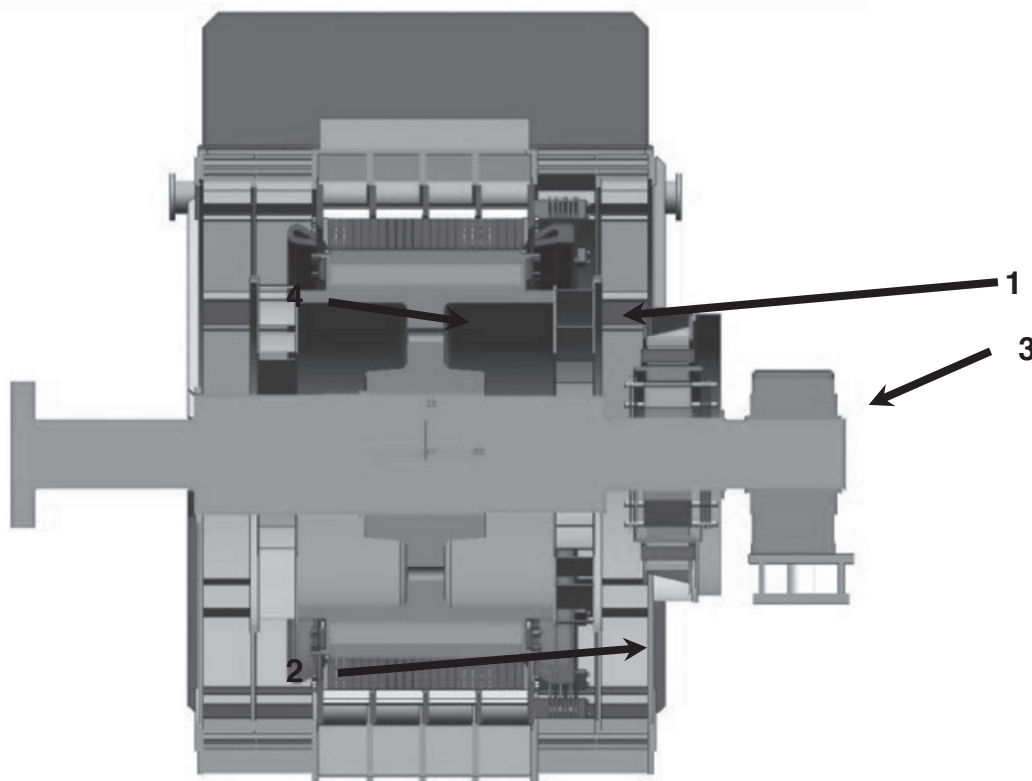


Figure 3: Schematic cross-section of a salient pole synchronous motor for a reciprocating compressor.



Figure 3 shows the schematic cross-section of a typical machine. Its core consists of the active parts of the salient pole synchronous motor with a starting cage. A magnetic wheel (1) is shrunk onto a solid shaft. The rotor poles (2) are bolted to the magnetic wheel. This design offers a couple of advantages.

- Each rotor pole can be replaced individually (serviceability).
- The rotor inertia can be adapted by varying the wall thickness of the magnetic wheel thus providing flexibility with respect to the requirements for each particular drive train.
- The magnetization, or respectively the air gap width, can be adjusted by just varying the heights of the poles.

The exciter (3) is located between the non-drive end bearing and the salient pole synchronous rotor. In the case that the shaft sag exceeds design limits, the position of the exciter and the bearing can be changed. When specified, sliprings can be provided instead of an exciter. The shaft-mounted fan (4) is positioned next to the magnetic wheel. The design of the ventilation as a one- or two-sided ventilation depends amongst others on the cooling method required - and the boundary conditions for the cooling. These include the airflow, motor speed etc. One-sided ventilation means that the active motor parts are axially supplied with cooling air from one side (Fig. 1). Accordingly, in the case of two-sided ventilation, the active parts are axially supplied from both sides. The airflow that can be realized for each ventilation type is decisive when selecting the ventilation. For maximum utilization, the solution that ensures the highest airflow is preferred. The cooling-circuit has been designed so that different cooling methods can be implemented with a minimum associated modification costs - such as air-to-water, air-to-air and open-circuit-cooling.

Two stator embodiment types are available. The first type comprises separate subassemblies for the stator, the base frame and the cover (Fig. 4, left). The base frame is first mounted on the foundation. This stator is then mounted on the base frame. Finally a canopy is placed on top of the motor. The second type comprises one assembly for the stator, the frame and the cover (Fig. 4, right).

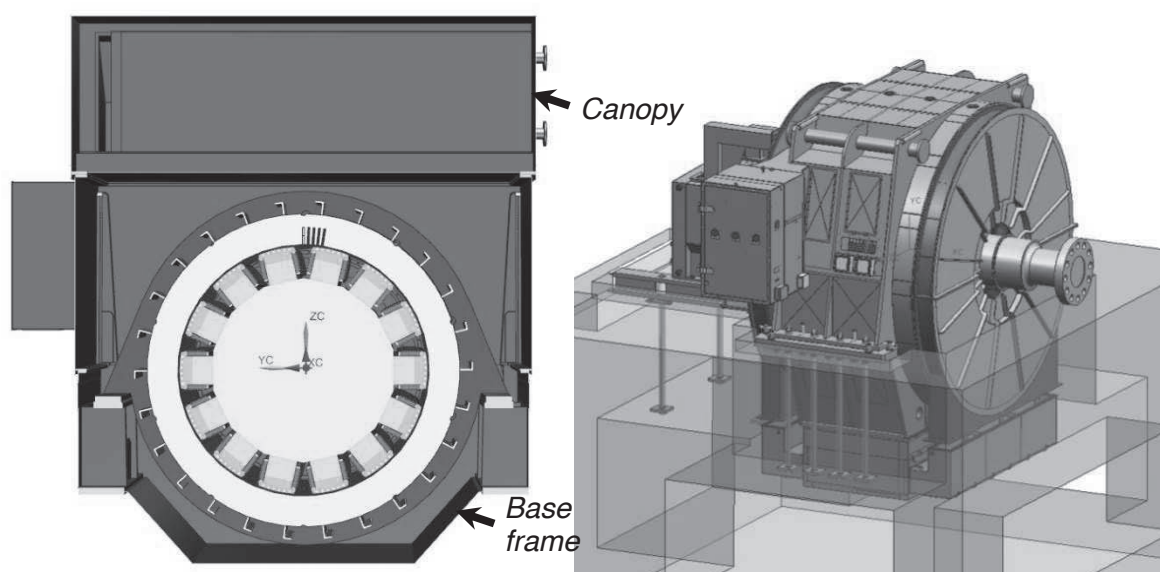


Figure 4: Left: Motor with separate subassemblies for the baseframe, the stator (dark blue/white) and the cover. Right: Motor comprising one assembly for the frame, the stator and the cover.

In addition to the design changes described above, the electrical design has also been improved. The modifications predominantly involve the rotor design and in particular the optimization of a) the rotor winding including its insulation and b) the rotor diameter. These measures have improved the heat transfer of the rotor winding, reduced the thermal gradient in the motor and enhanced motor utilization. A positive side effect of the enhanced motor utilization is the lower starting current.

### A "Drive Train Analytics" approach for electric reciprocating compressor drives *System overview*

The "Drive Train Analytics", offered on the basis of Industrial Service Backbone (ISB), are a promising enhancement of conventional condition monitoring. Deployed in industrial plants it helps to increase the availability of components, processes and plants and minimizes unplanned shutdowns. Being a higher-level system, it goes far beyond monitoring limit values or issuing alarms. The concept comprises the process of capturing the initial data and generating reports:

- Instrumentation and sensors installed on the motor and other drive train components (Figure 5, right).
- Data acquisition using protection and control devices (Figure 5, left).
- Data preparation for ISB transfer, primarily the compression and encryption of data (Figure 5, top).
- Archiving the data to the ISB server.
- Data processing for the expert- and service network as well as "Digital Twins".
- Reporting using the "Customer Dashboard".

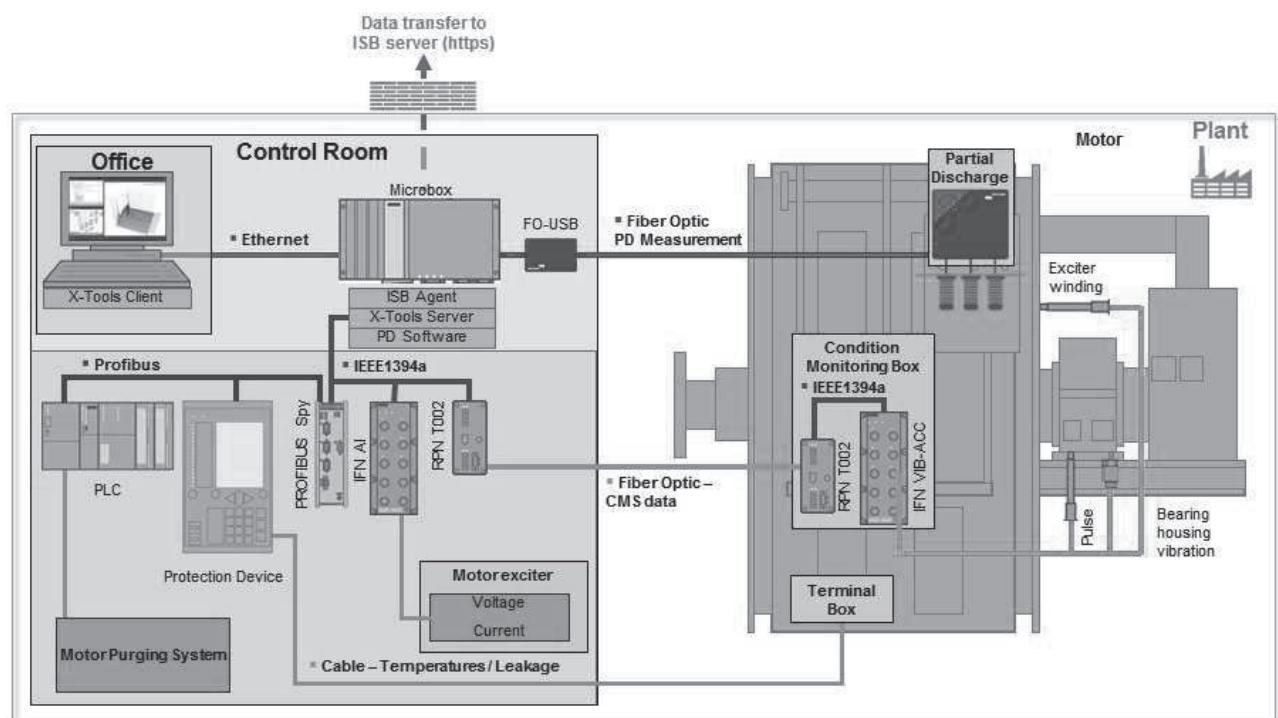


Figure 5: Schematic showing the instrumentation, data acquisition and data transfer on site.

Figure 5 shows an example of the instrumentation, data acquisition and data transfer on site, while Figure 6 shows the interface between the plant and the ISB infrastructure.

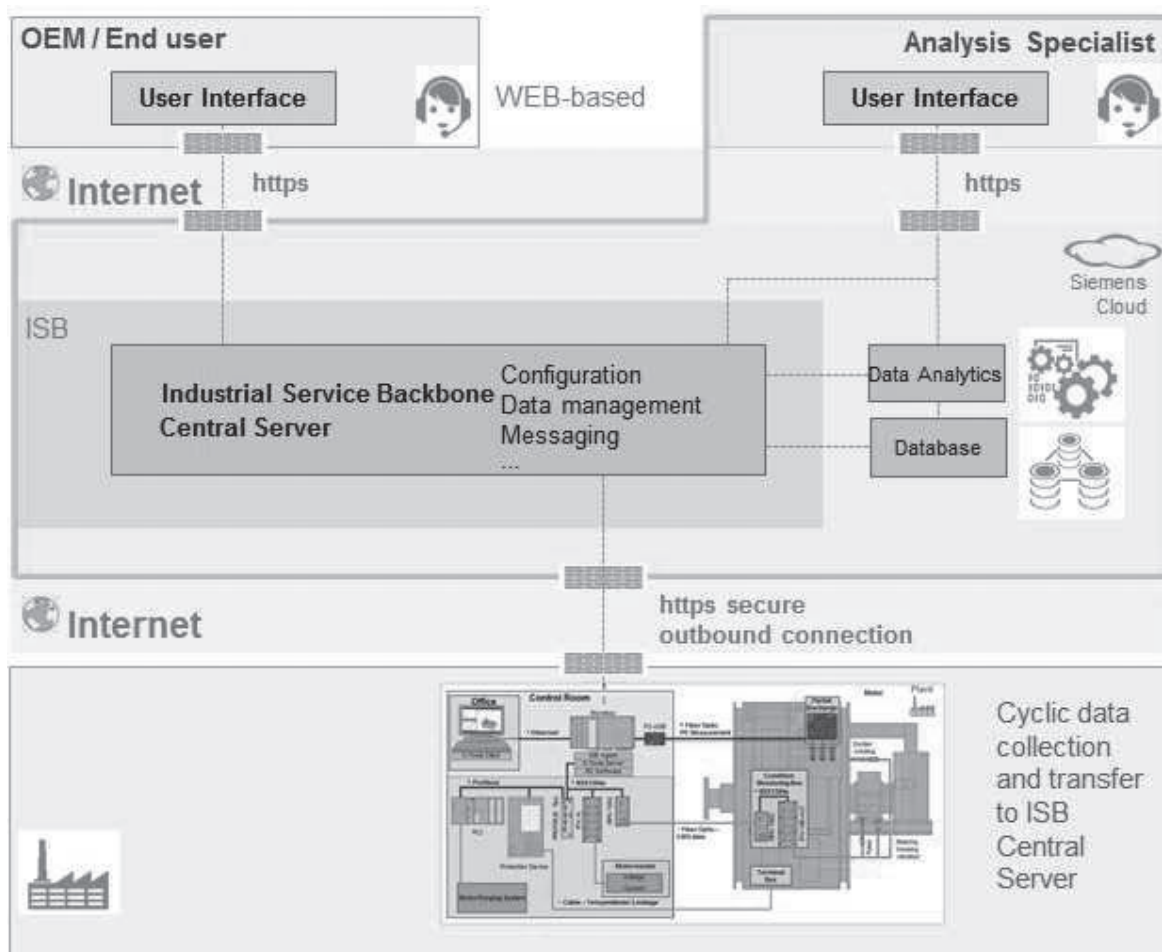


Figure 6: Interface between the plant and the ISB infrastructure

ISB key benefits are:

- All of the relevant operating data and documents are recorded at an early stage during FAT (Factory Acceptance Test).
- Direct data connection to the customer support and the factory thus supporting smooth commissioning.
- The company network is used, incorporating experts for the RCA (root cause analysis) and the service infrastructure comprising both technicians and the supply of spare parts.
- The drive or drive train is connected to servers with routines for optimizing maintenance schedules.
- Abnormal operating conditions are simulated using “Digital Twins” which reduce the time until a plant or system is released for operation.

### Condition monitoring, predictive maintenance and optimization of drive train operation

In accordance with established standards, our high-rating motors are equipped with a basic configuration of sensors to protect the motor [3], [4], [5], [6]. Precise information about the condition of motor components and causes of failures can be obtained by enhancing the basic sensor configuration and by processing and analyzing the recorded data. This enhanced approach includes condition monitoring, predictive maintenance and the potential for optimizing drive train operation. Table 3 shows selected examples for defects or abnormal behavior of motor components that can be detected using condition monitoring or predictive maintenance.

Rotor	Stator winding	Bearing
Imbalance	Aging of the stator insulation	Wear and tear
Misalignment	Excessive temperature rise	Damage
Loose or cracked parts	Ground/ interturn fault	Instability
Ground fault or interturn fault	-	-
Torque pulsations	-	-
Lubrication	Heat exchanger	Base frame and housing
Oil leakage	Temperature differences between the primary and secondary coolant	Tightness of the motor housing with respect to pressurization system
Bearing jacking system	Leakage detection	Expected service life of mechanical components (monitoring external excitations)
Contamination of the lube oil (content of oxygen, copper or iron)	Determination of cleaning and replacement intervals	Vibrational behavior (changes in the mechanical system or respectively the foundation)
Cooling equipment	-	-

*Table 3: Examples for defects or abnormal behavior of motor components that can be detected using condition monitoring or predictive maintenance.*

This data can be used to optimize drive train operation.

- The pulsating torque of a reciprocating compressor produces current pulsations that the motor draws from the line and thus influences electrical loads on the local grid. These current pulsations can be limited using design measures such as increasing the motor inertia. However, the interaction between the electrical and the mechanical system offers potential for optimization.
- Monitoring the starting procedure comprises run-up and pause times. Optionally, it can be enhanced by recording the temperature rise of the starting cage with the goal to accurately assess the thermal load of mechanical components. On the basis of this knowledge, it is feasible that the starting sequence can be optimized. In the case of an abnormal starting sequence, the remaining service life of mechanical components can be determined based on “Digital Twins”.
- The pulsating torque of a reciprocating compressor may affect mechanical components. Alterations to the mechanical system, such as changes to the foundation, cracks or ruptures influence the mechanical resonance behavior. This can be identified using the appropriate vibration sensors.

### Literature

- [1] Mueller, Gernar; Ponick, Bernd: Grundlagen elektrischer Maschinen, Band 1, Wiley-VCH-Verlag Weinheim, 2006.
- [2] Binder, Andreas: Elektrische Maschinen und Antriebe, Springer Verlag Berlin Heidelberg, 2012.
- [3] NEMA Standards Publication MG1-2006, National Electrical Manufacturers Association, 2006.
- [4] DIN EN 60034, Drehende Elektrische Maschinen.
- [5] API Standard 541, Form-wound Squirrel Cage Induction Motors-375 kW (500 Horsepower) and Larger, 5th Edition, December 2014.
- [6] API Standard 546, Brushless Synchronous Machines-500kVA and Larger, 3th Edition, 2008.





# Technical Paper

**Session: 43-2**

**Session Name: Monitoring**

## **Challenges in establishing predictive maintenance for high speed reciprocating compressors on a north sea FPSO using online condition monitoring**

**Author:**

**William Miller**  
**Maersk Oil North Sea UK Limited**  
**Aberdeen, United Kingdom**

**Co-Author:**

**Jörg Knoch**  
**Prognost Systems GmbH**  
**Rheine, Germany**

## Executive summary of the subject

Maersk Oil UK operates the Floating Production Storage and Offloading vessel (FPSO) “Gryphon Alpha” in the North Sea with 114 people on board. This 260m long FPSO was built in 1993; located north east of Aberdeen and produces 20,000 barrels of oil per day. On board are three high-speed (850 rpm) horizontal reciprocating compressors in re-ejection service of gas that came up with the crude oil. Initially the compressors had been equipped with limited condition monitoring equipment that did not provide satisfactory results for various reasons. From day one, earthquake sensors have been on the machine frames as safety protection measures. Several false alarms from these sensors as well as costly missed detects made an adjustment of the maintenance concept necessary. At a later time a kind of condition monitoring system was installed but did not have the ability for remote monitoring by specialist vendor. The system was not fully commissioned and never utilized or maintained. The only monitoring being carried out was manual valve temperature readings which gave limited fault diagnosis. After a number of significant and repeat failures it was recognized that a reliable online condition monitoring system was required for successful predictive maintenance, and to be used as a tool to prevent and or minimize damage resulting from equipment failure.



In 2013 it was agreed to install a condition monitoring system with distinct features for reciprocating compressor diagnoses. The new system shall be based on acceleration and pV measurements. Next to this, the monitoring system shall provide gapless and dynamic piston rod movement diagnoses, because it is well recognized that many machine trips, based solely on acceleration or velocity signals, lack information for subsequent root cause analyses. Having a specialized system in place, all these requirements are fulfilled. However, the marine environment is an outstanding challenge for the diagnostic capabilities as well as for the hardware and system maintenance.

Based on experience, this paper describes the special challenges presented by the introduction of a suitable online condition monitoring system for piston compressors in offshore applications. In the process, the main focus lies on problems standing in the way of the use of the system for condition-oriented servicing. The following points summarize the content with which this article deals:



- Environmental conditions
- Training efforts
- Logistics
- Servicing of measuring loops
- Signal analyses on piston compressors
- Examples of damages
- Machine protection

This article is naturally not intended to explain all detailed steps for introducing an online condition monitoring system for offline applications. Rather, it covers the special experiences and challenges since the commissioning of the system.

### Installation

After the system was running for close on a year some deficits were detected. The monitoring system was installed in dry dock during a general inspection of the ship. This resulted in considerable logistical advantages. The final commissioning by the supplier of the system took place at sea a few weeks later. At this point, measuring loop errors were identified and remedied. Some of the glued sensor sockets fell off and sensitive sensor cables were damaged due to improper fastening.



*Figure 1: Broken vibration sensor – mounting base detaches from glue*

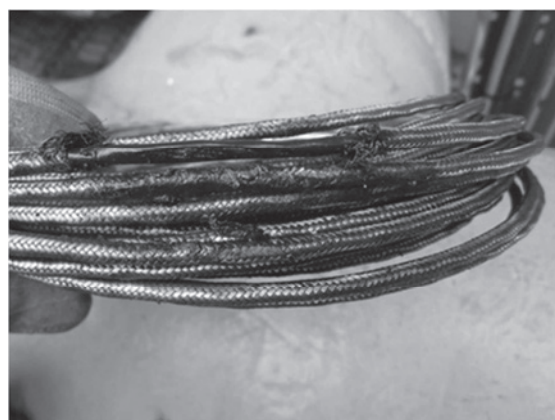


*Figure 2: Damaged sensor cable due to incorrect installation*

After about three months at sea, problems then occurred with the pressure sensors. The measuring loop was connected to the sensor with an M16 aluminum screw plug. It emerged that, on the one hand, the threaded connection of the sensor for connecting the measuring loop had been damaged by strong compressor vibrations (Figure 3a) also the connections on the sensors were found to badly corroded (Figure 3b). The cause was determined to be electrochemical corrosion in interaction with the high salt content from the ambient air and moisture.



a) b)  
*Figure 3: a) Shows the sensor cable connection socket with thread damage b) Cable connection socket with heavy corrosion*

In cooperation with the supplier and sensor manufacturer an appropriate solution was found very quickly. The sensors were dismantled during a shutdown and sent to the sensor manufacturer. The sensor manufacturer then converted the cable connection. Instead of a connecting plug, a cable integrated into the sensor with a length of 2 meters was installed. The end of this cable now possesses the connecting plug that can be seen in Figure 4. Through this measure, it was possible to install the cable in a way that the connecting plug is decoupled from the machine vibrations. The integrated cable also eliminates the problem of the corroded connections. During installation all the connections for pressure sensors and vibration sensors were also wrapped in self amalgamating tape to further eliminate the corrosive effect of the environment.

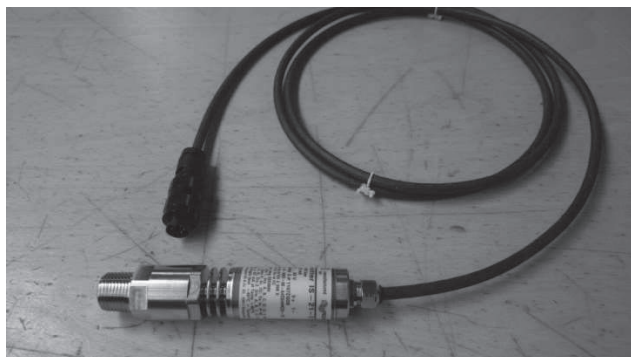


*Figure 4: Sensor with integrated cable after modification*  
*Additionally all the pressure sensors were connected to compressor using double block and bleed isolation valves with small bore tubing and fittings to orientate sensors in vertical position. This led to issues due to increased number of leak paths. The valves, small bore tubing and fittings were subsequently removed and sensors were mounted directly onto compressor cylinders in a horizontal orientation.*

#### **Further issues – after first problem solving**

After successful commission, the onshore personnel were trained in the handling of the software and the initial approaches for analyzing common machine errors. An important component of the training is the maintenance and servicing of the system/all measuring loops. This training, however, must also be provided to the three crews of the FPSO and should take place offshore live on the system since the ship's crew is responsible for performing the servicing measures. The implementation of such training requires considerable effort. The following prerequisites must be observed during planning:



- Scheduling of the training for each crew
  - Availability of the trainer on the part of the supplier
  - Offshore suitability of the supplier
  - Transport and accommodation of the supplier/availability of beds on board
  - Consideration of the crew's work load
- Costs for performing each training course

The abovementioned organizational efforts led to the first crew training being provided six months after the actual commissioning.

Due to a lack of knowledge of the offshore personnel in the handling of the measuring loops and/or the entire system, measuring loops and sensors were repeatedly installed improperly during maintenance work in this time period (and beyond). As a result, pre-alarms and main alarms occasionally occurred due to damaged measuring loops. The measuring loops of the proximity sensors were particularly frequently affected. In addition, the shutdown alarms were not triggered early enough due to incorrectly adjusted sensors. Shutdown alarms also frequently occurred during maintenance work on the compressors. The frame vibration sensors (velocity) were mainly affected in this case. Since the offshore personnel had no knowledge in handling the system, these alarms were not reset, which often led to misinterpretations in the initial phase after the start of the compressor.

For economic reasons, the downtimes of the compressors are limited to the minimum possible. The compressors were thus quickly recommissioned again after maintenance work. As a result, a function check of the measuring loops could often not be performed by the previously trained onshore personnel before the restart. Measuring loop errors were thus not discovered until the machines were running. Servicing could not be performed, however, until the next, regular shutdown of the respective compressor.

### **Facing the consequences of continuous loop issues**

Neglecting the causes of the serious measuring loop errors and the faulty alarms, the reliability of the system was initially questioned by the offshore personnel. The consequences of this were an ignoring of the alarms provided by the system on the one hand and a medium-term loss of acceptance for the system if no improvement in the described situation were to occur.

The abovementioned consequences naturally excluded the integration of the automatic shutdown function for machine protection. Frequent false alarms that would lead to a deactivation of the compressor were not acceptable for production, regardless of their cause.

The challenge was now to determine and implement the steps in the right direction to prevent the predicted consequences and utilize the full potential of the system.

There was no question that we had to accept this challenge due to the serious machine damage that had occurred in the meantime.

Two of these damage incidents that occurred after the installation of the system are introduced on the following pages. Both damage incidents were analyzed and used as an expressive example for the use of the system and significance of proper measuring loop servicing.

### ***Broken Motor Fan***

In the previously mentioned transition phases, frequent alarms occurred due to fault measuring loops. As a result, alarms were assigned to one of the compressors in the "Measuring loop error" category in case of serious damage. In this case, however, the observance and



evaluation of the alarms considerably reduced the extent of the damage. The fan of one of the drive motors suffered considerable damage while running. This resulted in a complete destruction of the fan blades. The compressor was ultimately shut down after an increase in the motor winding temperature, seven hours after the first alarm from the monitoring system. The motor had to be removed and sent onshore for internal fan replacement.

The alarm from the monitoring system was triggered by a measuring loop for the monitoring of the engine shaft vibrations. An inductive proximity sensor was used for this purpose. High peak-to-peak values were achieved in a horizontal measuring direction in particular, but also in a vertical measuring direction. Figure 7 shows the clear, sudden increase in the horizontally measured peak-to-peak values of the motor shaft vibration as a trend diagram. In addition, the alarms resulting from the increase can be seen as entries on the trend diagram (symbols in magenta at the top of the figure).

The two pictures of the damage integrated into the trend diagram clarify the extent of the damage.

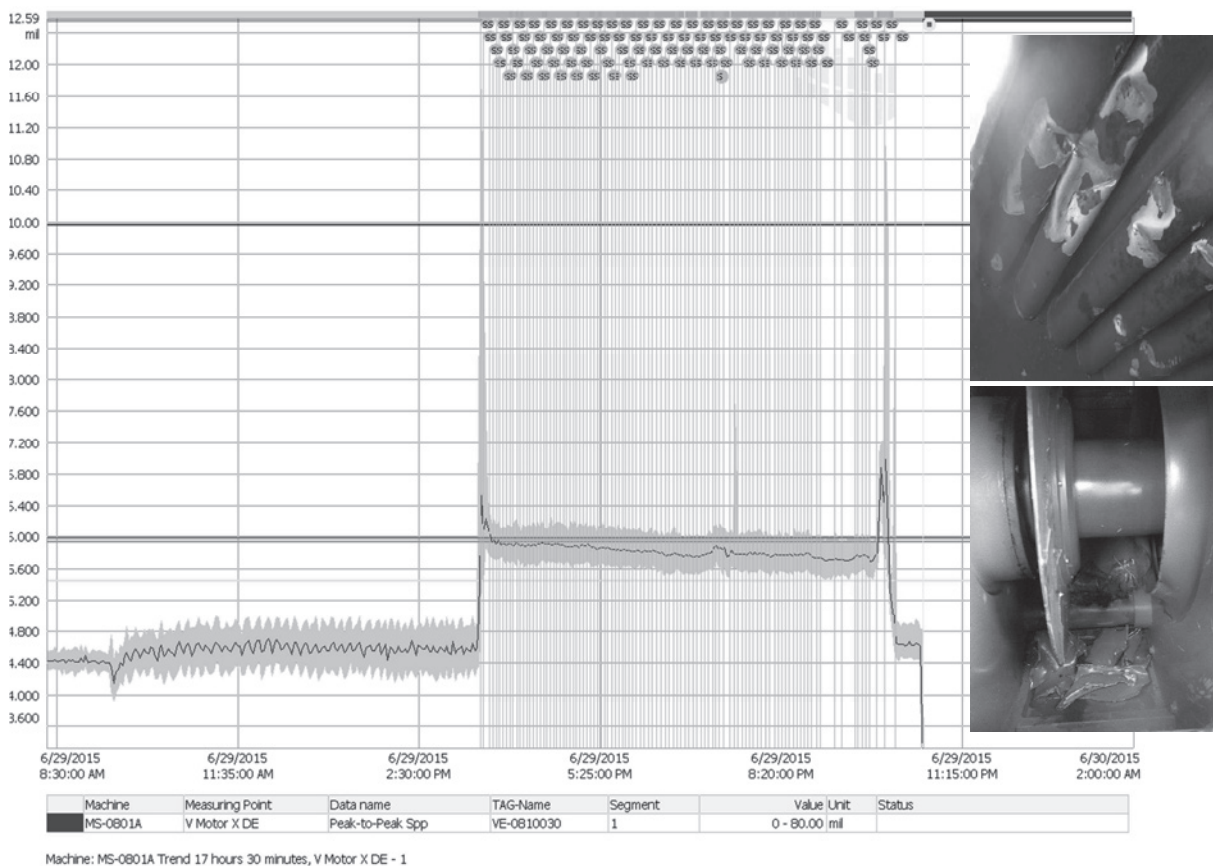


Figure 5: Trend view of „Peak-to-Peak values of motor shaft vibration“ in horizontal direction

### Broken Piston Rod:

There are also examples of how the alarms to shut down the compressor were triggered too late due to improperly installed measuring loops. One of these cases was a broken piston rod. The measuring data show clear signal changes before the actual breakage. Due to an improperly set proximity sensor, the measuring signal was very close to the upper measuring range nonetheless. It can be recognized that the piston rod completed higher, vertical deflections a few seconds before the actual breakage. A shutdown would have taken place



based on the peak-to-peak values. Since the measuring signal was “cut off” in the upper measuring range, however, the necessary peak-to-peak values for the shutdown were not reached. The described behavior can be seen in Figure 6. The shutdown alarm took place five revolutions after the breakage of the rod due to high crosshead guide vibrations. These vibrations were caused by the rod hitting the piston. Figure 7 shows the signal of the piston rod position and crosshead track vibrations in the revolution of the piston rod breakage.

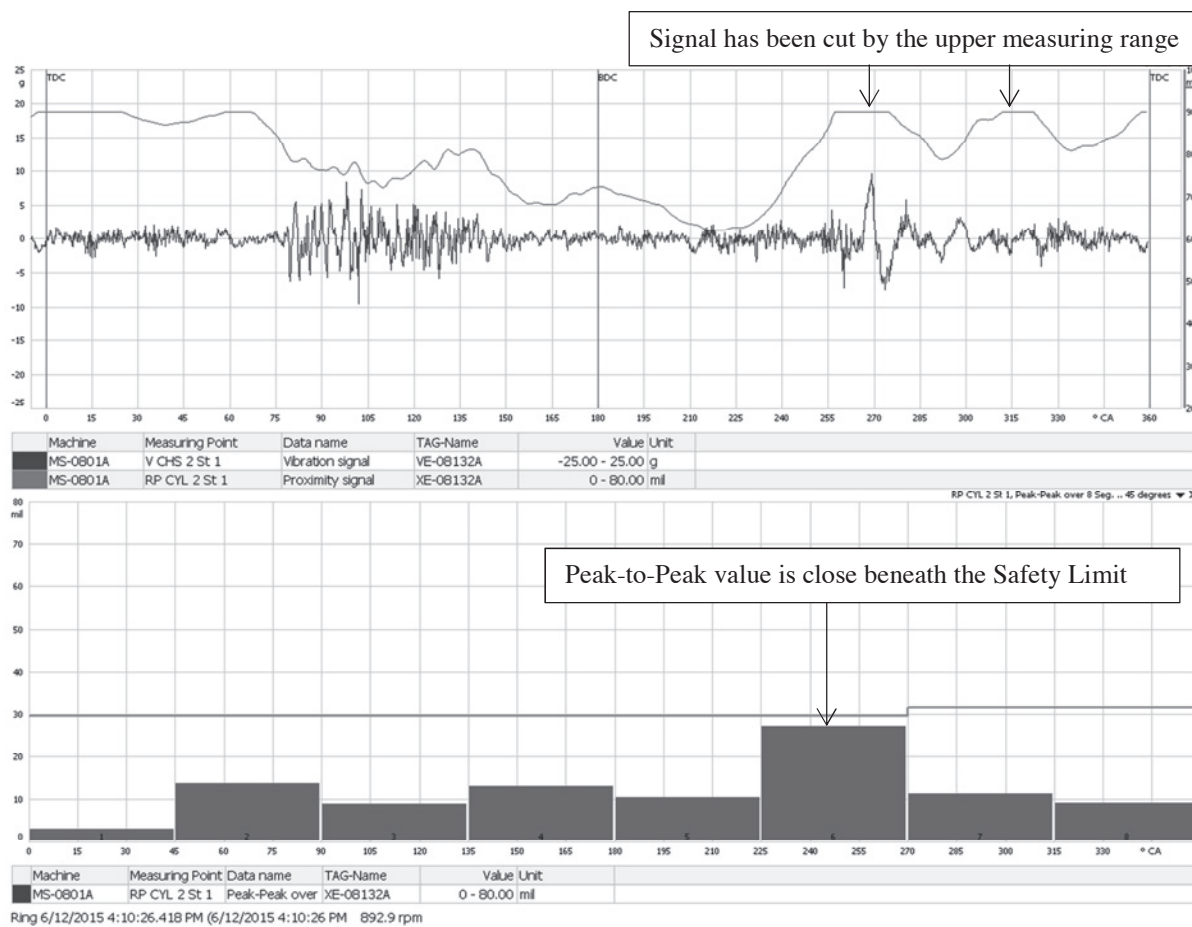


Figure 6: Trend view of „Peak-to-Peak values of motor shaft vibration“ in horizontal direction

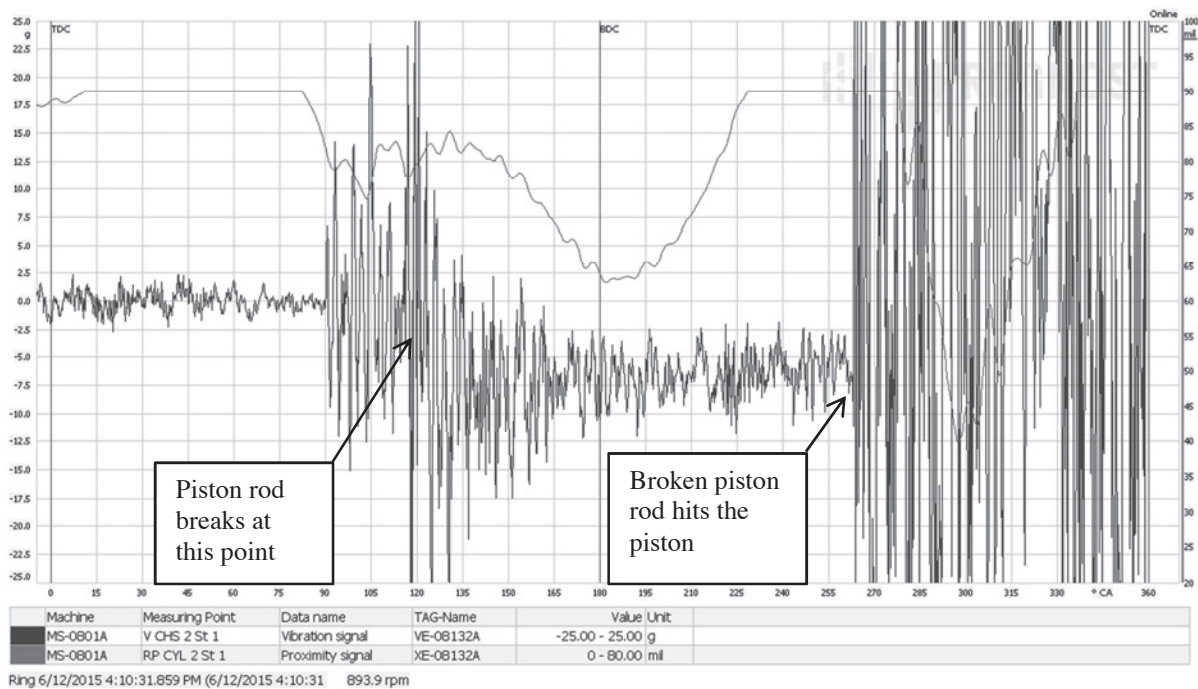


Figure 7: Vibration and rod position signal from the ring buffer „revolution of piston rod break“

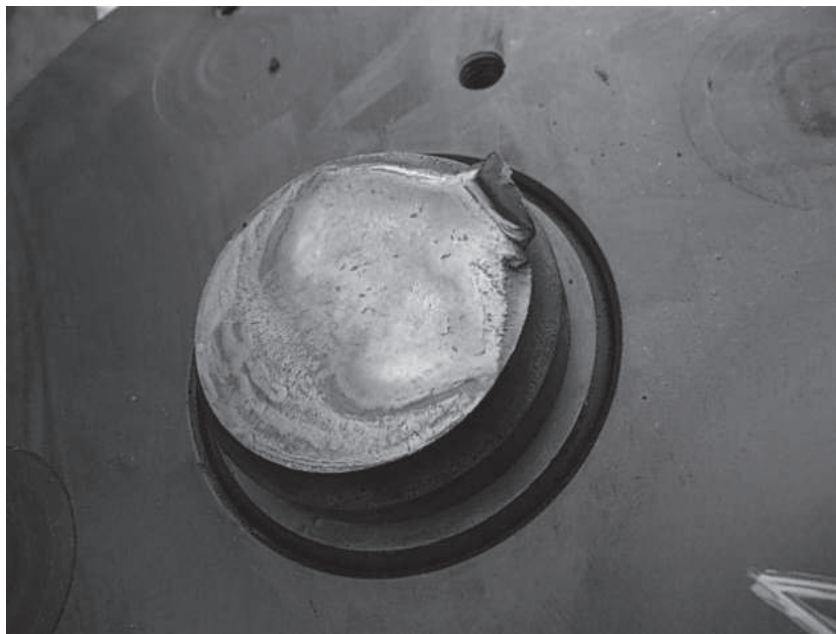


Figure 8: View from the piston side on the broken piston rod



## Steps in the right direction

To utilize the full potential of the system in future, solutions were defined internally and in cooperation with the suppliers that should make it possible in the medium term to implement the automatic shutdown function and thus automatic machine protection using the online condition monitoring system. Some of the following points are obvious, but, as experience has shown, not always easy to implement:

- 1.) Reduction of the measuring loop errors/failures due to incorrect handling
  - Check of the measuring loop changes before every start of the compressor (using onshore personnel trained in remote access, among other things)
  - Creation of clearly defined handling instructions for the ship's crew for checking the measuring loops/setting the sensors
  - Efficient, timely training measures for the ship's crew
  
- 2.) Simplified display of information from the system for the ship's crew
  - Definition of the most important information from the system for the ship's crew/machine operator for an easier handling of the system
  - Creation of a piping and instrumentation diagram (P&I) for each machine in which the most important information can be recognized at a glance
  
- 3.) Support of the ship's crew by the supplier
  - Use of the 24/7 hotline by the ship's crew
  - Clear definitions as to the cases in which the supplier's hotline must be contacted
  - Weekly status reports (statuses of both the machine and the measuring loop) from the supplier

## First achievements

The implementation of the defined measures and resulting successes were checked and evaluated at regular interval.

A clear improvement in the handling of the system by the ship's crew has already been determined. The number of measuring loop errors caused by maintenance work has been reduced considerably. Individual errors were able to be reliably identified by a regular check of the measuring loop through remote diagnosis and then subsequently remedied by the crew. The check of servicing measures performed on the individual measuring loops by remote diagnosis before each start of a compressor also lead to a considerable reduction of errors and false alarms.

Another important point was the training effort for the core crew especially for the operators. To reduce the needed training effort (roughly one day for each group of operators) Maersk Oil decided to use a simplified display (P&I) which contains the most important information with reference to previous and most common damages in one view.

Figure 9 shows an example of the simplified display of core information from the monitoring system. In addition to the alarm, this P&I diagram contains the statuses of all shutdown-relevant measuring loops, including the values of individual analyses. These analyses are calculated from the dynamically measured, internal cylinder pressures. Changes in these values due to leakage also lead to a change in color of the corresponding fields. This makes it possible for control room personnel to identify valve leakages quickly and easily.

The introduction of the simplified display of information from the online condition monitoring system, the considerable reduction of measuring loop errors and the readiness of the crew to work with the system already lead to an authorized, manual shutdown of the compressor due to a bent piston rod.

Due to alarms from the system directly after the start of the compressor, the control room personnel decided to shut it down properly first. The subsequent evaluation of the measured values by the supplier of the system resulted in clear indications of a fault in the oscillating drive train. In Figure 10, the piston rod position in the described fault scenario is compared with a reference signal before the fault scenario. In the fault scenario, a clear lift in the piston rod can be detected in the movement from the top to the bottom dead center (TDC – BDC). The movement of the piston rod from the BDC back to the TDC, on the other hand, leads to a lowering of the piston rod. An alignment error was initially assumed. As the investigation showed, however, a piston rod was clearly bent.

Maersk Oil experienced that the online condition monitoring and safety protection system provides important benefits compared to preventive or reactive maintenance philosophy if the general preconditions are met. We learnt that the integration of such a system requires more effort than a standard installation. This article summarizes the challenging events which occurred since the installation. Due to the positive achievements the activation of the automatic shutdown based on alarms from the condition monitoring system is planned presently.

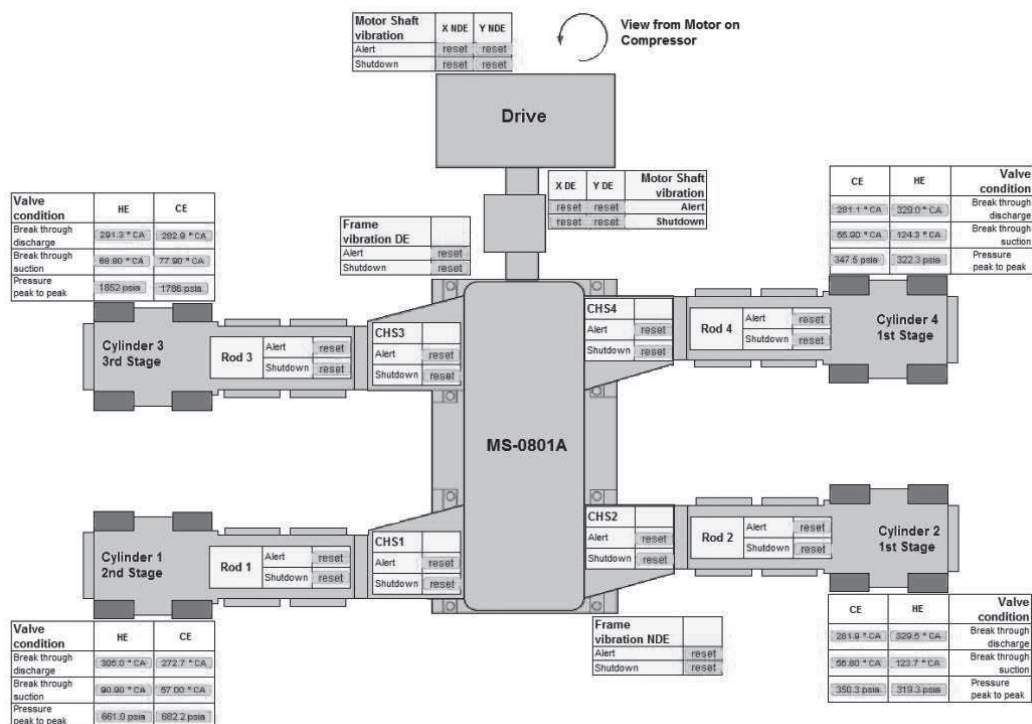


Figure 9: P&I – compressor overview with key information from the Monitoring System



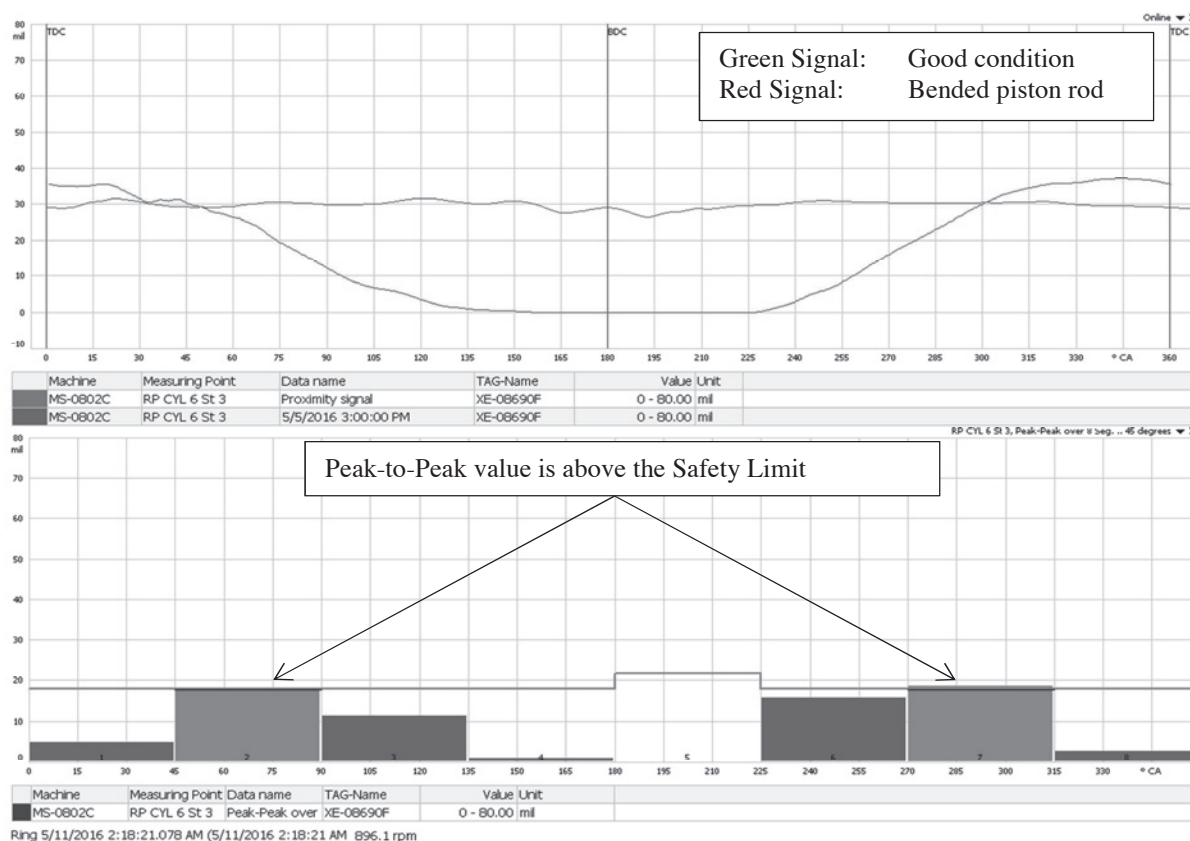


Figure 10: Upper part of the screen capture shows the piston rod position signals in “good” and failure condition. The lower part of the screen shows segmented peak-to-peak values in failure condition along with the assigned Safety Limits.

### Final conclusion / lessons learnt

The harsh offshore environment has strong influence on the functionality of some measuring loops and sensors and can lead to failures which make online condition monitoring a challenge. Suitable control measures need to be defined and communicated with all personnel involved.

A key point for the maximum efficiency and reliability of such a system is the cooperation and acceptance by the core crew of the offshore asset. Definition and training of clear maintenance procedures are very important points to achieve good results in this part of implementation.

A well maintained system together with the correct handling and usage provides key information for efficient predictive maintenance and machine protection.





# Technical Paper

**Session: 43-3**

**Session Name: Monitoring**

**Advanced online condition monitoring and diagnostics support operational and maintenance decisions in an offshore gas compression and export system unit**

**Author:**

**Andy Caie**  
**Senior Reliability Engineer**  
**Chevron Upstream Europe - Chevron North Sea Limited**  
**Aberdeen AB15, 6XL, United Kingdom**

**Co-Author:**

**Thorsten Bickmann**  
**Machinery Diagnostics Services Tech Lead Recips - Europe**  
**GE Oil & Gas - Digital Solutions – Bently Nevada**  
**60313 Frankfurt/Main, Germany**

## Summary

Chevron North Sea Limited operates two 3-stage reciprocating compressors on the offshore platform which are in service of the Gas Compression and Export System unit.

Essential information to evaluate the condition of the reciprocating compressor are a base for operation decisions, therefore Chevron North Sea Limited installed an online condition monitoring system for reciprocating compressors to increase the reliability and safety protection for their compressors.

This paper presents several case studies about malfunctions like a broken rod, loose crosshead shoes and misalignment, as well as lessons learned which helped to reduce outage time and costs.

## Introduction

### Chevron - Captain Field and Facilities

Chevron is one of the world's leading integrated energy companies being engaged in every aspect of the oil, natural gas, and geothermal energy industries, including hydrocarbon exploration and production; refining, marketing and transport; chemicals manufacturing and sales; and power generation. The upstream business combines innovation and the effective use of technology to maximize mature fields, discover new resources and meet the world's growing demand for energy.

Chevron has key operations in the world's most important oil and gas regions including the North Sea within which is the Captain Field.

The Captain Field is located in block 13/22a in the United Kingdom sector of the North Sea, approximately 130 km northeast of Aberdeen. Chevron North Sea Limited and Dana Petroleum (E&P) Limited hold licence interest shares of 85% and 15% respectively in the Field and the Field is operated by Chevron North Sea Limited.

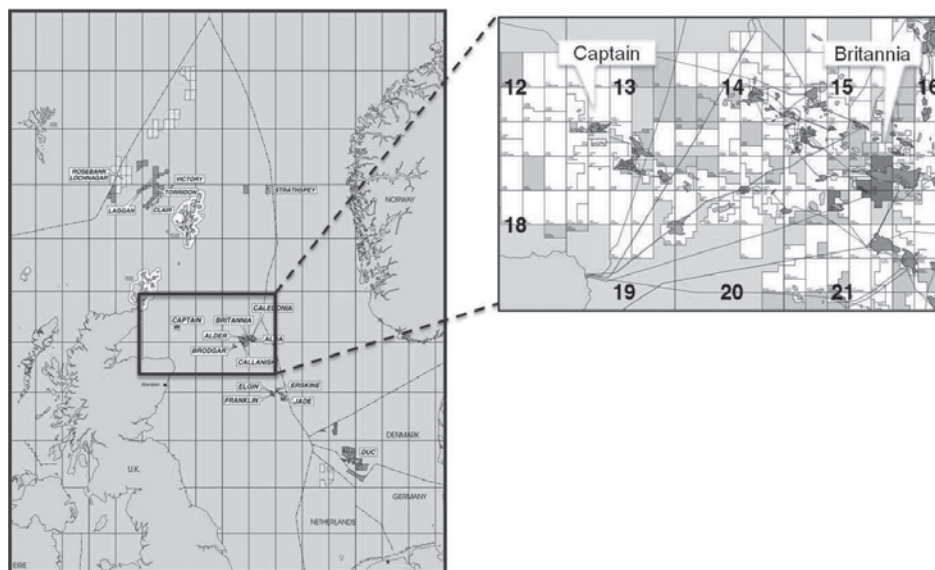


Figure 1: Captain Field Location Map



The field was discovered in 1997 and developed in three stages;

- Area A - Platform Drilling
- Area B - Subsea Drilling (east)
- Area C - Subsea Drilling (far-east)

The Captain development consists of a Floating Production Storage and Offload facility (FPSO), a Wellhead Protection Platform (WPPA) and the Bridge Linked Platform (BLP).

Produced fluids consisting of oil/gas/water from the wells are treated through a single process train on the BLP and FPSO. Gas, in excess of fuel demands, is exported to the Frigg gas pipeline system and oil is exported via shuttle tankers loaded from the FPSO.

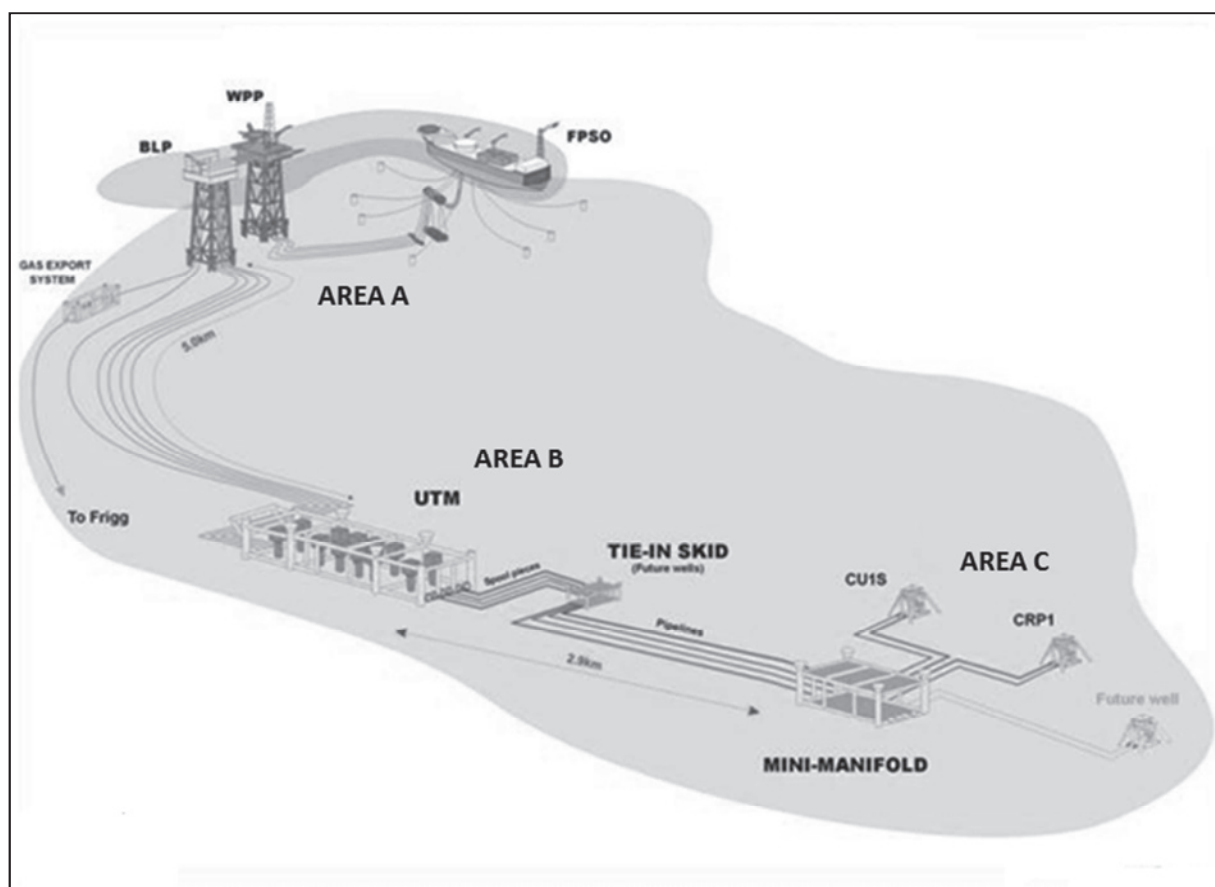


Figure 2: Captain Facilities Map

### Gas System Overview

The Captain Field gas liberated through partial stabilization of produced fluids is utilized to meet the fuel gas requirements of the platform power generation turbines. The remaining gas is compressed and dehydrated for export to the Frigg pipeline system via a 70 km 8" export flow line.

Gas in excess of fuel requirements is routed to the Gas Compression Package A-4760. The maximum A-4760 throughput is 18 mmscf (Million standard cubic feet per day).



Following removal of entrained liquids, the gas stream is split and routed to two identical Reciprocating Gas Compression Trains, A-4760A and A-4760B. Each train consists of three stages of compression with inter stage cooling and liquid knockout. Liquids removed from the gas stream in each train are routed under level control to a Gas Scrubber Vessel.

High pressure gas from Compressor After coolers is connected and routed to a Common Discharge KO Drum. From there the gas enters a Glycol Dehydration System which dehydrates the gas by contact with Tri-Ethylene Glycol (TEG) to the required export water dew point specification. The gas is then metered and delivered to the Frigg pipeline for export.

The Gas Compression and Export System is supported by lubricating oil and cooling water systems, and also interfaces with other utilities systems, Inert Gas (Nitrogen), Drains, Compressed Air and Flare Systems.

**Gas Compression Train A-4760A**

<b>Type</b>	<b>Induction</b>
<b>Power</b>	<b>1815 kW</b>
<b>Rated Speed</b>	<b>890 RPM</b>
<b>Bearing Lubrication</b>	<b>Self Lubricated (Oil Ring)</b>
<b>Coupling</b>	<b>Flexible Rubber Segmented Membrane</b>

*Table 1 Main Electric Motor KM-4760A*

The main drive motor for Compression Train A is an HV induction motor.

Motor to Compressor K-4760A coupling utilises a flexible rubber segmented membrane-type coupling designed to accommodate slight lateral, angular and axial misalignment between the two machines.

<b>Type</b>	<b>3-Stage/4-Cylinder, Horizontally Opposed, High Speed Reciprocating</b>
<b>Capacity</b>	<b>10358 Nm<sup>3</sup>/h (7670 kg/h)</b>
<b>Gas Molecular Weight</b>	<b>16.4 – 16.52</b>
<b>Driver</b>	<b>Electric</b>

*Table 2 Gas Export Compressor K-4760A*

Gas Export Compressor K-4760A is an electrically-driven, 3-stage, 4 cylinder reciprocating compressor.

Gas enters Compression Train A-4760A and the first compression stage K-4761A via a 1st Stage Suction Volume Bottle. There is a volume bottle at the suction of each stage. The purpose of these bottles is to minimize gas pulsation and starvation in the compressor suction resulting from the intermittent gas flow in and out of the reciprocating compressor cylinder.

The first stage of compression in cylinders 2 and 4 raises the pressure of the gas to 21.6 barg.



Gas then enters the 2nd compression stage via a 2nd Stage Suction Volume Bottle. The 2nd stage of compression raises the pressure of the gas from approximately 21 barg to 67.6 barg maximum. Compression is carried out in cylinder 3.

The gas is then directed to the 3rd compression stage from the last Suction Volume Bottle. The 3rd stage of compression raises the pressure of the gas to approximately 187.3 barg. Compression is carried out in cylinder 1.

Gas from V-4764 is then routed to the Glycol Dehydration System and Glycol Contactor for dehydration to Frigg export pipeline water dew point specification.

The compressor has a sister unit, K-4760B, that is the same type and specification of machine. It is currently out of service for structural redesign giving K-4760A a heightened criticality to production with high availability required for efficient operations. This provided the justification for deployment of an online condition monitoring system.

### **Reciprocating Compressor Health Monitoring**

The two reciprocating compressors are monitored by an online condition monitoring system. With the goal to establish a condition based maintenance strategy, a detailed knowledge of the machines' behavior is essential. Vibration measurements at each crosshead slide and at frame, in combination with dynamic indicated pressures and rod position are constantly collected and analyzed with hard- and software thresholds. The online condition monitoring system synchronizes the vibration signals with crankshaft rotation to associate vibration peaks to the piston position along the stroke. This provides machinery protection and detailed information of machine condition.

Main drive winding temperature is monitored by the starter motor protection relay. Motor cooling is effected via an integral air-to-air heat exchanger. On high exchanger temperature an alarm will be initiated in the Unit Control Panel (UCP) and Integrated Control System (ICS). Continuing rise in temperature will trip the motor.

Motor bearing temperature monitoring and over temperature protection is provided for the Drive End (DE) and Non-Drive End (NDE) respectively. On high temperature, an alarm will be initiated in the UCP and repeated in the ICS. Continuing rise in temperature will initiate a trip of the motor.

Also provided on this unit is DE and NDE bearing vibration monitoring and protection. Vibration of 7.1 mm/sec will trigger an alarm in the UCP and the ICS. Rise in vibration to 11mm/sec will initiate a trip of the motor.

### **Crosshead Acceleration**

The mechanical safety of each throw is monitored by accelerometers, which are mounted on the top of each crosshead slide. Placing accelerometers over each crosshead slide provides the best method to detect machinery problems due to impact-type events. Acceleration spikes in the waveform refer to the response of impulse events, occurring during normal operation

As parts wear over time, the mechanical clearances increase. The extra clearance gives the parts more distance to gain velocity and the impacts between the components become more energetic. As examples, such impacts can occur between the crosshead and its guide, as the babbitt of the crosshead shoes slowly erode. Loose rod nuts or bolts, worn pins as well as liquid ingestion can be detected in early stages of development.

The mechanical impacts produce a high frequency structural vibration, which is characterized by a high amplitude peak, followed by a “ring down”. Crosshead acceleration signals are normally in the range of about 0.7 to 2.0 g.

### Frame Velocity

Two Frame velocity transducers on the side of the frame monitor the response of the system to the main forces and moments that are occurring on the balanced-opposed compressors. If used for machinery protection, these velocity measurements provide additional safety monitoring capabilities.

Frame velocity measurements monitor malfunctions such as imbalance due to unusual pressure differential or inertial unbalance, looseness in the foundation attachment (such as deteriorating grout or shims) and high moments caused by excessive rod load.

However installing frame vibration transducers only may be insufficient, as the increase in frame vibration due to incipient failures developing at the running gear or cylinder assembly will be small and typically covered by the larger vibration contribution due to machine movement. By the time the malfunction has been detected by the frame velocity transducer and the compressor shut down, major secondary damage may have already occurred. [1]

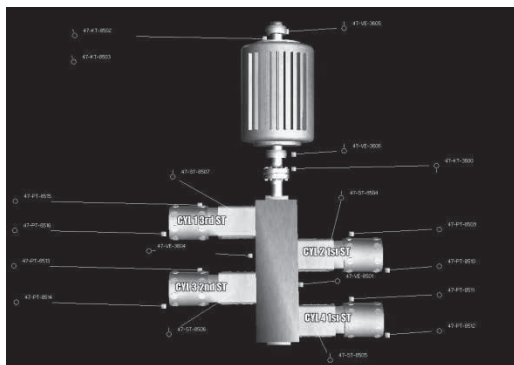


Figure 3: Overview of the compressor with installed measurements

### Cylinder Pressure and Forces Monitoring

The single most effective way of determining the overall health of a reciprocating gas compressor is by examining the cylinder pressure profile. Online access to the internal pressure for each compressor cylinder enables continuous monitoring of cylinder pressures, compression ratios, peak rod loads, and rod reversal. This provides valuable information on the condition of suction valves, discharge valves, piston rings, packing glands, and crosshead pin. In addition, the functionality of capacity control devices, such as unloaders, clearance pockets and stepless control systems can be analyzed.

From the diagnostic standpoint, the dynamic cylinder pressure measurement provides great value. The ability to correlate events in the crosshead acceleration waveform with events in the pressure, rod load curve and crosshead vertical force plots is essential. This enables to make precise maintenance decisions, to exchange the failed parts, only.

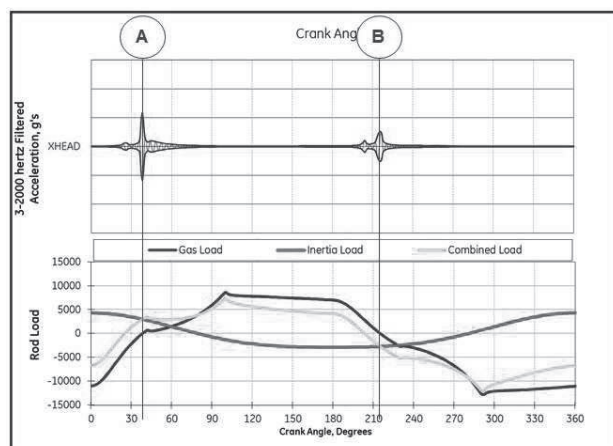


Figure 4: Crosshead acceleration overlaid with rod loads

The figure above displays the overlay of the filtered (3-2000 Hz) crosshead acceleration signal with impulse events caused by a loose piston. In addition, the rod loads over one revolution are presented. At the point A, the gas load (blue line in the rod load plot) changes from compression to tension forces and vice versa at point B. The significant impulses of the crosshead acceleration occur exactly at these points.

For most reciprocating compressors, the mass of the piston is much smaller than the total reciprocating mass. If the piston to piston rod bolted joint relaxes, the piston will begin to slide on the rod. Since the inertia of the piston is small, the impacts between the piston and rod occur near the gas reversal points.

### Vertical Crosshead Force

As the crankshaft turns, the combined rod load (inertia- and gas load) at the crosshead pin varies. As a result, the forces acting at the crosshead can be calculated directly by the monitoring system using the cylinder pressures and geometrics of the reciprocating components.

The crosshead transmits the axial acting pressure loads to the piston through the piston rod and absorbs the dynamic forces produced in a direction perpendicular to the horizontal axis of the motion.

The figure below shows a force reaction diagram with summation of all of the forces that are acting on the crosshead pin. The angle  $\Phi$  can be found from the known dimensions of the

crank-slider mechanism.

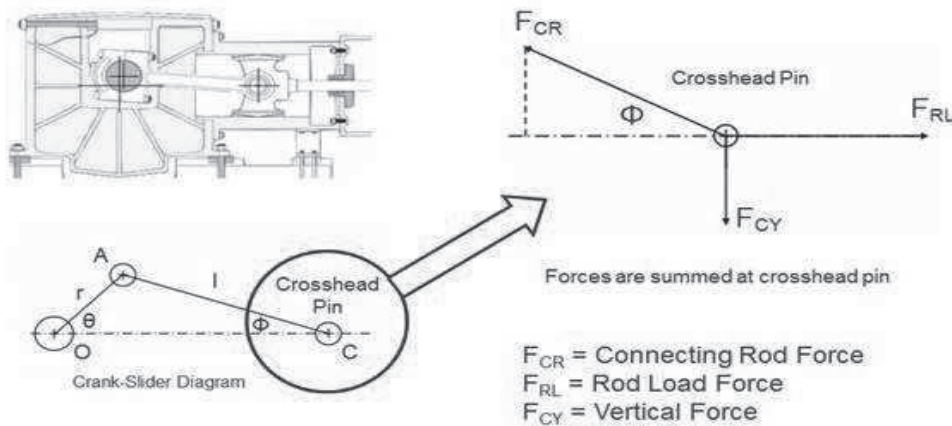


Figure 5: Balance of forces acting on the crosshead pin

Throughout the piston's stroke, the horizontal component of the connecting rod force ( $F_{CR}$ ) balances out the Rod Load Force ( $F_{RL}$ ) generated at the piston rod. With respect to crankshaft rotation, the vertical force ( $F_{CY}$ ) applied to the crosshead pin is affected.

With the exception of the dead center positions, the acting forces at the connecting rod include a horizontal force (to counter the gas and inertia forces acting on the wrist pin) and a vertical force, which is in downward or upward direction. When crank angle is 0 or 180 degrees, the connecting rod is directly in line with the cylinder bore, and it is incapable of imparting vertical forces to the crosshead. At these crank angles, the vertical force on the crosshead will be zero regardless of the combined rod load. At all other crank angles, the loaded connecting rod passes a vertical force component to the crosshead pin.

If this vertical force is in upward direction and exceeds the weight of the crosshead, the crosshead will physically lift off the lower guide and be pressed against the upper guide. The downward restraining force that is being applied to the crosshead pin is caused by the crosshead weight and the reaction between the upper crosshead shoe and the upper surface of the crosshead guide. This is the secondary motion of the crosshead motion which takes place across the clearance between crosshead and crosshead guide

Thus, the crosshead moves periodically against the inner surface of the crosshead's lower and upper guide which introduces consequently impact-induced vibration, which is one of the sources of vibration in reciprocating compressors.

At balanced opposed vertical compressors, in the case of the left crosshead (which is being pulled downward by its connecting rod), the weight of the crosshead adds to the downward vertical load component. For the right crosshead (which is being pulled upward by its connecting rod), the weight of the crosshead is subtracted from the vertical load component. . However, for a small time period in either case, the force does act opposite of the expected direction.[1]



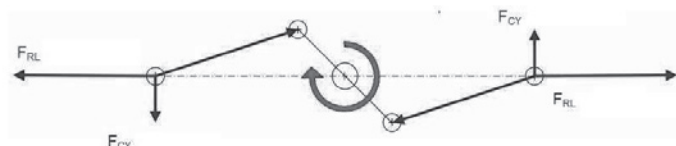
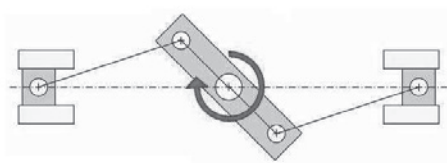


Figure 6: Up- and down- running crossheads

### Rod Position Monitoring

Horizontal and vertical proximity probes, mounted in an orthogonal arrangement, observe the piston rod movement. Continuous monitoring over time measures the rider band wear. But in addition, the peak to peak displacement along the piston stroke allows conclusions to the condition of the rod.

In the figure below, the three rod position plots (orange, blue, red) illustrate three different stages of a machine's condition. The yellow & red dashed arcs represent estimated alarm thresholds (alert & danger, respectively) from the bore clearance extrapolated back to the measurement plane. If the piston rod shifts more than 60 mils / 1520  $\mu\text{m}$  from the geometric center in any direction, then an alert condition would be raised to prevent actual piston to cylinder liner contact.

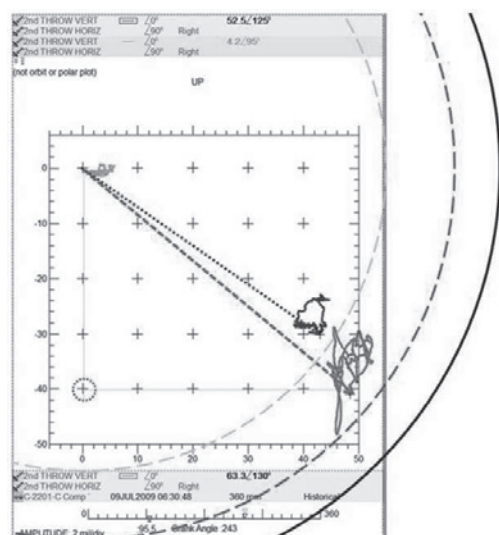


Figure 7: Example for Rod Position Monitoring displaying the rod position in three different stages of machine's health

The orange trace shows the piston rod motion in reference/baseline conditions with new rider bands. The low amplitude and proximity of the piston rod centerline to the geometric centerline

indicates that the throw is running smoothly with low peak-peak displacement and Position Magnitude values.

The blue trace shows the rod position at a later time as the condition progresses. The peak-peak displacement has increased slightly; however, the Position Magnitude is much larger and more significant.

And finally, when the machine is in an alarm condition (red sample), the peak-peak is much larger along with the rod position clearly indicating an alert condition. In this state there is greater potential for contact with the cylinder wall; however, it should be noted, that the equivalent vertical displacement reading is still indicating much less than the alarm value. This example shows the benefit of the horizontal transducer for a fully 2 dimensional measurement. [2]

### Cases - Condition Monitoring helps to define precise maintenance decisions

#### Case: Broken Rod at Throw 2, 1st stage

On July 25th the Machinery Protection System tripped the reciprocating compressor due to high frame velocity vibration. The trend showed a sudden increase from 3 mm/s RMS to above 40 mm/s. The accelerometer, mounted above the crosshead slide at throw 2, 1st stage displayed the same symptoms of rapid vibration increase. Also observed in the preceding minutes to trip was an indicated fall in throw 2 rod position.

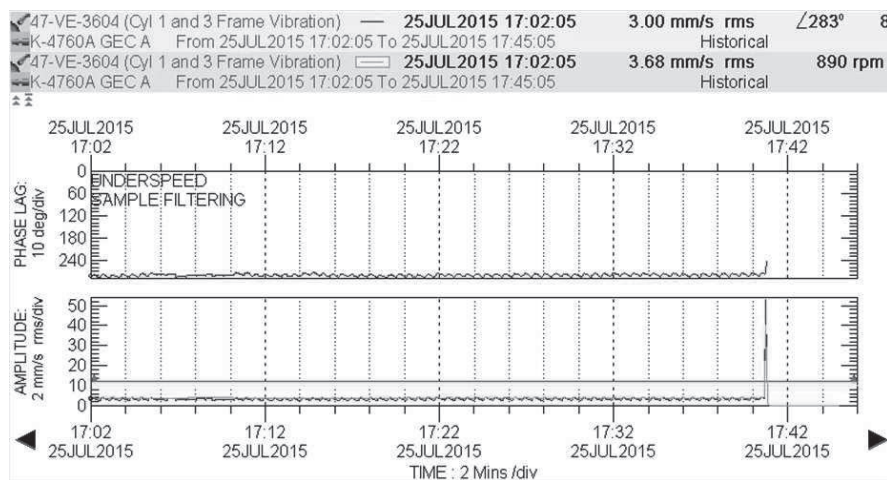


Figure 8: Trend of the two frame velocity measurements on 25 Jul 2015

Following the machine stop, the throw 2 covers were removed for internal inspection by the mechanical team and the compressor was barred over. It was reported that nothing unusual was observed in the course of these activities and that next a restart of the compressor should commence.

However, based on the initial data review, it was considered that prior to attempting a machine start a more detailed analysis of the diagnostics should be performed to fully understand the shutdown characteristics.

This encompassed a variety of in-depth dynamic assessments detailed as thus:

The following crank angle based vibration plots illustrate the sequence of events of the 1st stage, Throw 2 at K-4760 A on July 25th.



Two minutes before the failure, the crosshead acceleration waveform (upper right plot) shows no indication of a developing failure. The piston rod peak to peak movement of 500  $\mu\text{m}$  (lower right plot) indicates a typical movement. The cylinder pressures (lower left plot) and the calculated gas- inertial- and combined forces (upper left plot) are normal.

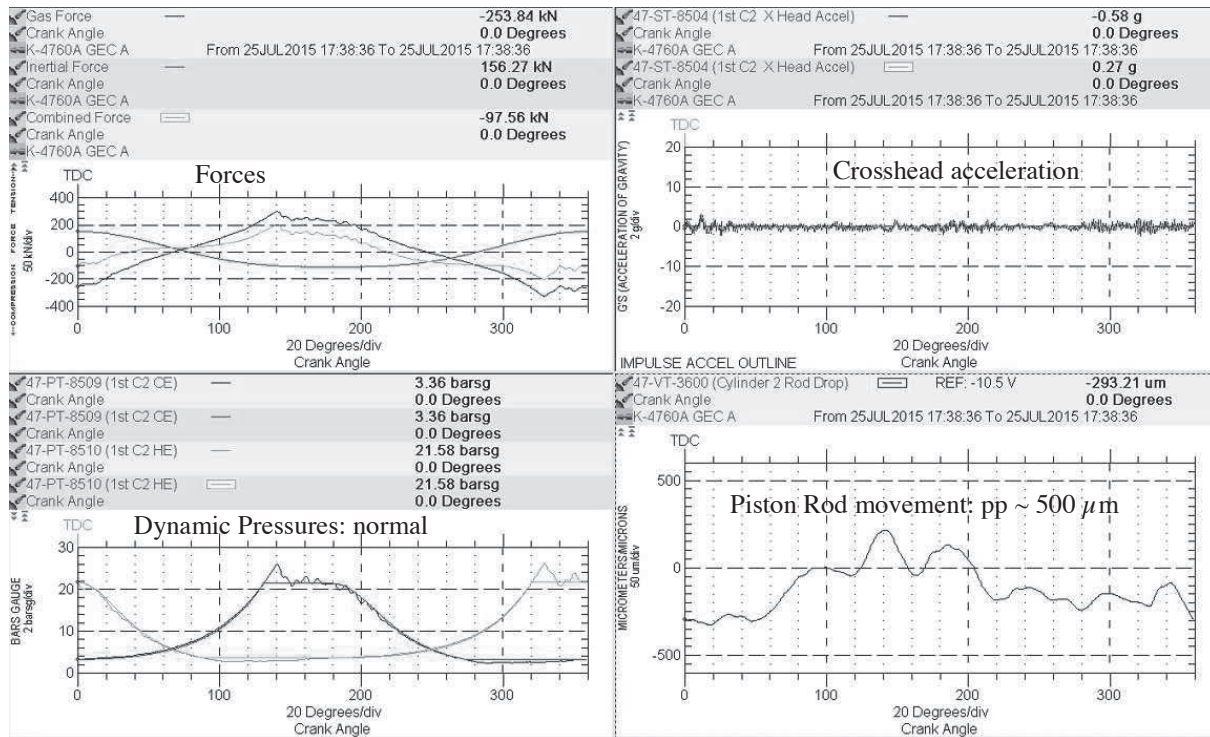


Figure 9: 25 Jul 2015 17:38:36 h – normal behavior

46 Seconds before the rod breaks, no indications are visible at the crosshead vibration, but peak to peak movement at the piston rod increases up to 950  $\mu\text{m}$ . It seems that the rod is already cracked, because the highest peak to peak movement occurs in the area of the rod load reversals.

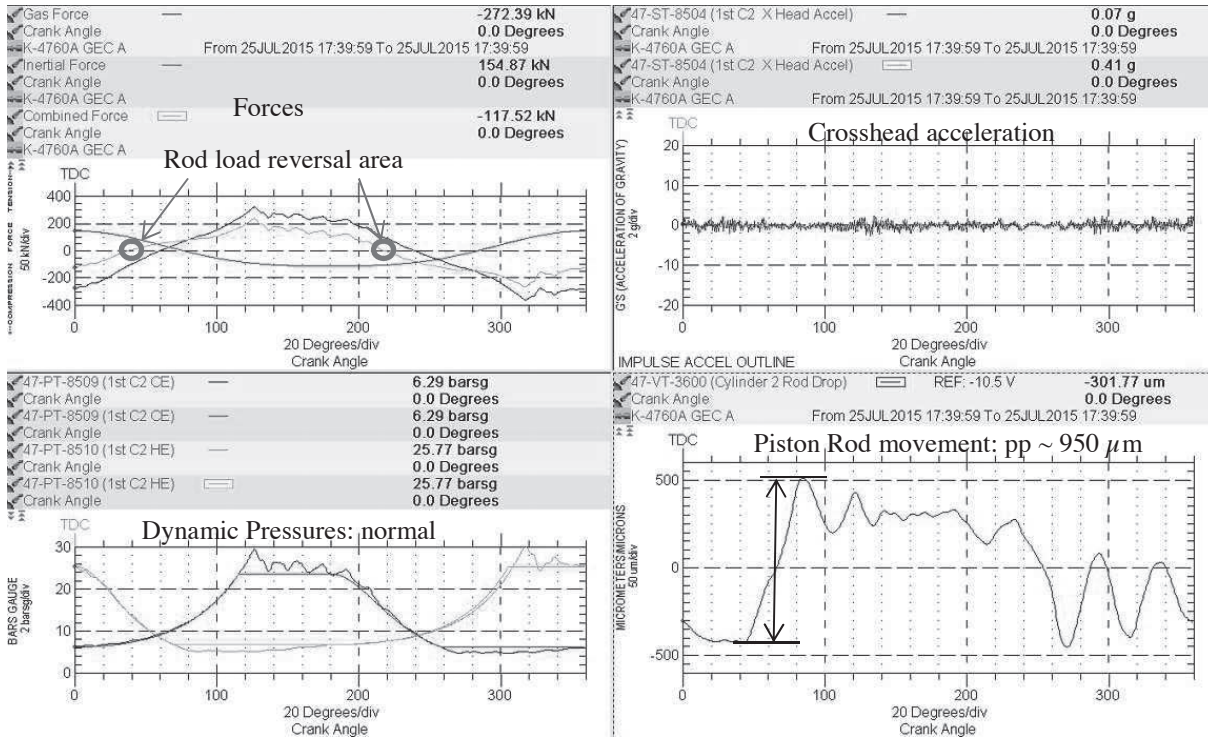


Figure 10: 25 Jul 2015 17:39:59 h – 46 seconds before the rod breaks.

As the failure develops, the piston rod peak to peak movement increases significant. The crosshead acceleration waveforms show a slightly higher acceleration in the load reversal areas – which would not provide an alarm, yet.



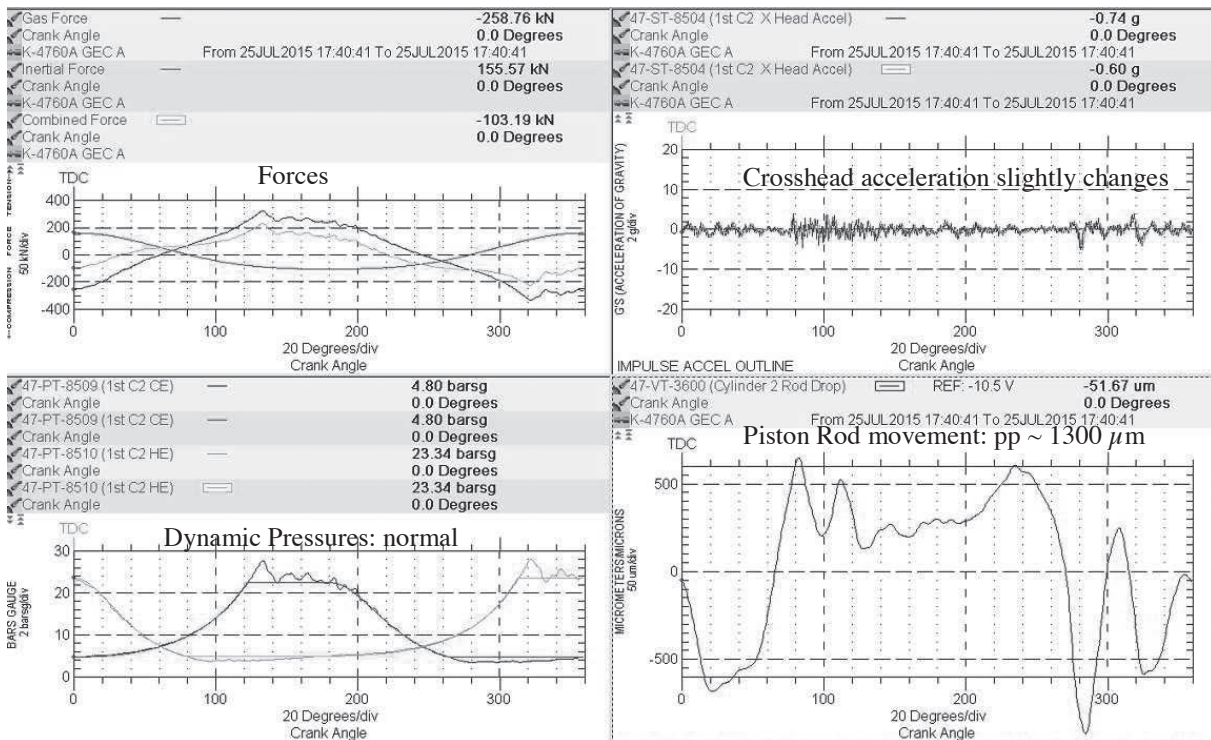


Figure 11: 25 Jul 2015 17:40:41 h – 4 seconds before the rod breaks. Crosshead vibration signature changes slightly, but peak to peak movement at the piston rod increases up to 1300  $\mu\text{m}$ .

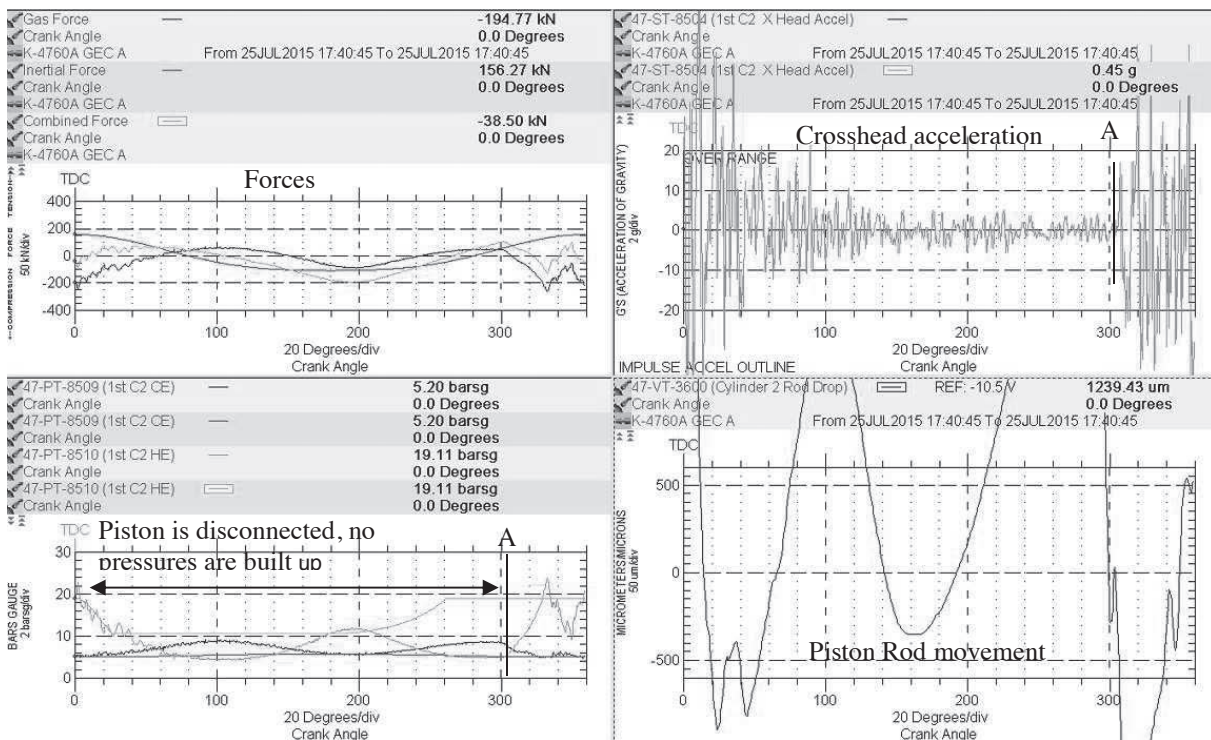


Figure 12: 25 Jul 2015 17:40:45 h – Rod is disconnected.



The figure above represents a revolution, where the rod is already broken. When the reciprocating components travel from the Bottom Dead Center (180° crank angle) in direction to the Top Dead Center (0° / 360° crank angle), they hit the disconnected piston at point A and pushed it towards Top Dead Center. Due to the acceleration of the piston, the head end cylinder pressure increases (orange line in lower left plot). The collision of the disconnected rod and disconnected piston is also visible in the high amplitude of the crosshead acceleration at point A (plot upper right). The amplitude remains in the Top Dead Center, as the piston pumped the cylinder head. During machine stop, the following revolutions displayed the sharp impulses, when the reciprocating components hit the disconnected piston.

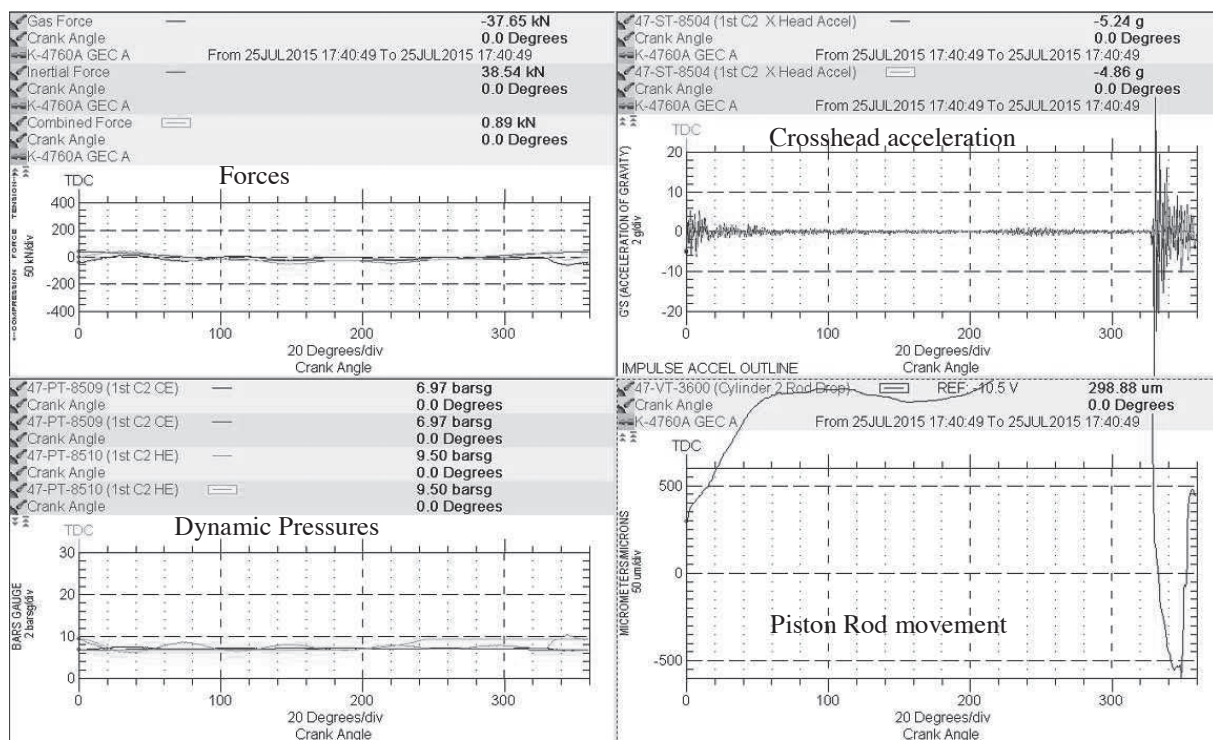
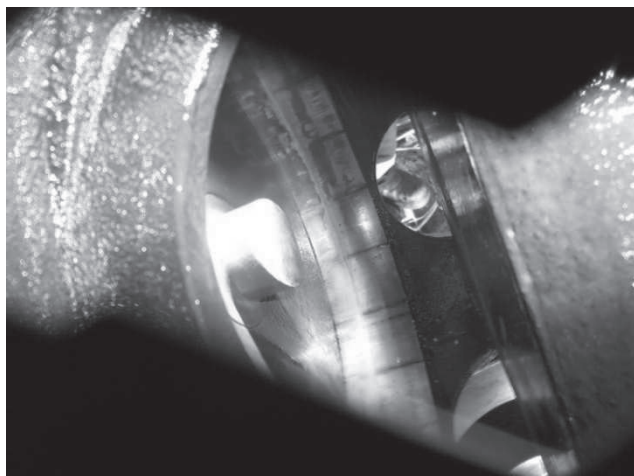


Figure 13: 25 Jul 2015 17:40:49 h – Rod is disconnected. The sharp knock is again at the point where the reciprocating components hit the disconnected piston

The detailed analysis of the reciprocating diagnostics provided the foundation for a decision not to attempt a restart of the compressor and to instead mobilize materials and Original Equipment Manufacturer (OEM) field engineers offshore for confirmation and replacement of a sheared piston rod at cylinder 2.



*Figure 14: After the crank end suction valve was removed, the disconnected rod became visible*

Lessons learned from this failure: during the course of the event investigation and data analysis a number of parameters were identified with the potential for providing early warnings as to the presence of a machine operating environment that could instigate a propagation of mechanical defects. In addition, a further layer of shutdown protection limits, to prevent significant secondary damage during failure occurrences, were defined. This enhanced machinery protection consisted of peak to peak displacement of the rod movement with Alert level at  $750 \mu\text{m}$  peak to peak and  $900 \mu\text{m}$  peak to peak for Danger and crosshead acceleration boundaries which were included into the trip logic.

From the Root Cause Analysis investigation it was highlighted that five days prior to failure, the 1st stage suction pressure upstream (red trend line in figure below) of the compressor started to become more erratic and that this was initiated by a gas scrubber pressure spike. Subsequently the gas scrubber behavior became erratic and the export compressor suction pressure started to increase in range. The cause of this was narrowed down to the gas recycle valve controlling irregularly.



*Figure 15: Trend of erratic suction pressure before the failure*

Reviewing the liquid carryover potential at the time, the levels in the vessels hadn't been any higher than normal. Deducing from all the associated data and information; fluctuating pressures and therefore changing in the compression ratio could have led to component stress and ultimately to the rod failure.

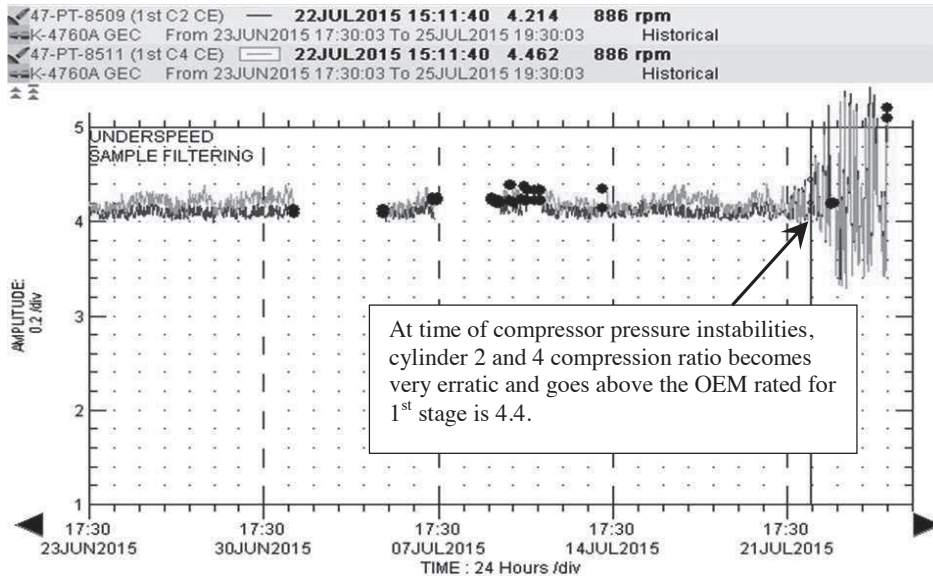


Figure 16: Trend of pressure ratio of both 1<sup>st</sup> stages before the failure

### When machines stop – problems start

Subsequent to the verification of the broken piston rod on line 2 and further assessment by the OEM field service engineers; to enable a rapid turnaround restoration to get the machine back to an operational ready state, a repair was progressed utilizing materials from the B machine. The plan was to undertake a more extensive refurbishment during the planned 12,000 hour service in November. A successful post repair start of the compressor was initiated on the 17th of August.

47-ST-8504 (1st C2 X Head Accel)	—	∠0°	21AUG2015 05:46:58	5.61 g pk	887 rpm
47-ST-8505 (1st C4 X Head Accel)	—	∠0°	21AUG2015 05:34:02	1.61 g pk	887 rpm
47-ST-8506 (2nd C3 X Head Accel)	—	∠0°	21AUG2015 03:24:49	0.89 g pk	891 rpm
47-ST-8507 (3rd C1 X Head Accel)	▬	∠0°	21AUG2015 05:47:33	1.36 g pk	887 rpm

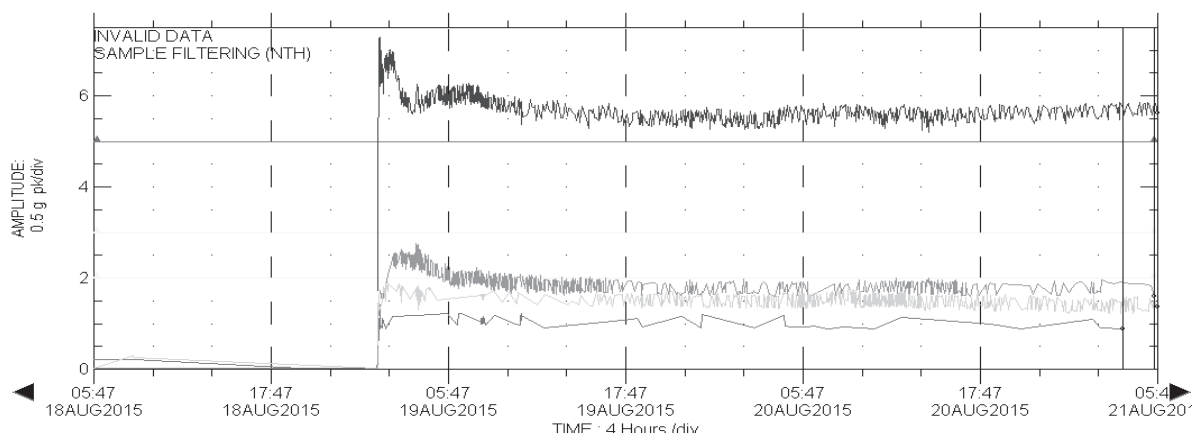


Figure 17: Overall vibration level of all four crosshead accelerometers after the repair of the broken rod



An assessment of the compressor in operation highlighted a higher than expected Throw 2 crosshead acceleration value, exactly the throw with the disconnected piston rod. The vibration level was three times higher when evaluated against the usual level and in comparison to the other throws. This prompted further analysis and investigation.

The cause for the high crosshead acceleration became visible in the crank angle domain. A large impulse with an amplitude of 6g's (Band pass-filtered: 3-2000 Hz) occurred at around 310° crank angle at the cursor position followed by a second impulse at 110° crank angle (Figure below, upper right plot).

In addition, the piston rod moved slightly during these events (lower right plot).

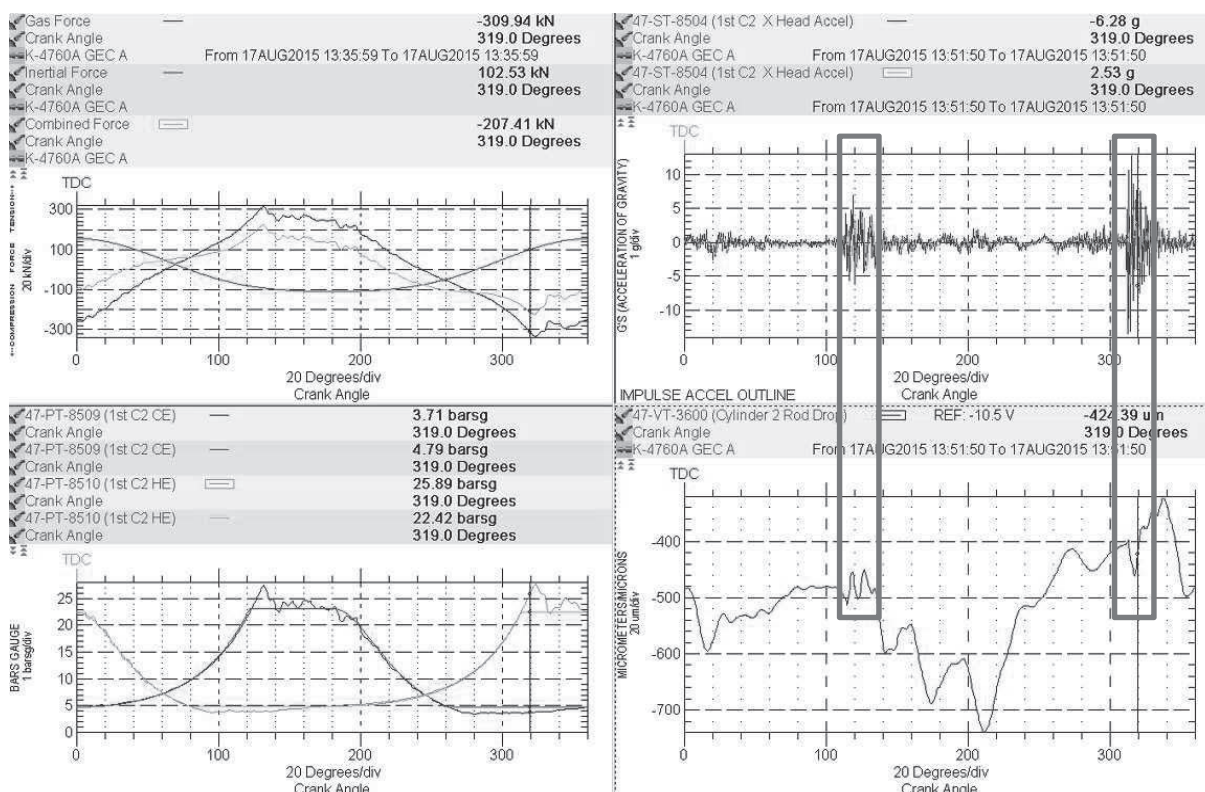


Figure 18: Crank angle based plots after the exchange of the broken rod

To determine the nature and severity of an impulse/impact event from a crosshead acceleration signal waveform, the most appropriate analytic methodology is based on signal timing. Even when peaks' position in crank angle domain is tracked, the large number of mechanical events occurring in a reciprocating compressor cylinder and running gear components present a real challenge for those attempting to determine the source of a knock. [1]

The synchronization of the vibration signal with crankshaft rotation did not associate vibration peaks to gas load or combined rod load reversal positions along the stroke (upper left plot). Thus, a loose piston to rod or crosshead to rod connection could be excluded.

As introduced in the chapter "Vertical Crosshead Force", the secondary motion of the crosshead occurs across the clearance between crosshead and crosshead guides.

If this vertical force is in upward direction and exceeds the weight of the crosshead, the crosshead will physically lift off the lower guide and be pressed against the upper guide. After reach-



ing the maximum vertical force, the crosshead will drop down and continue travelling on the bottom guide.

The overlay of crosshead vibration, piston rod position and vertical force showed that the impact-induced vibrations were related to these areas where the crosshead moves periodically against the inner surface of the crosshead's upper and lower guide. In addition, the dynamic rod position displays unusual movement in these areas. Based on this it was recommended to keep monitoring for any deterioration and to check the crosshead shoe to guide clearance at the next planned service.

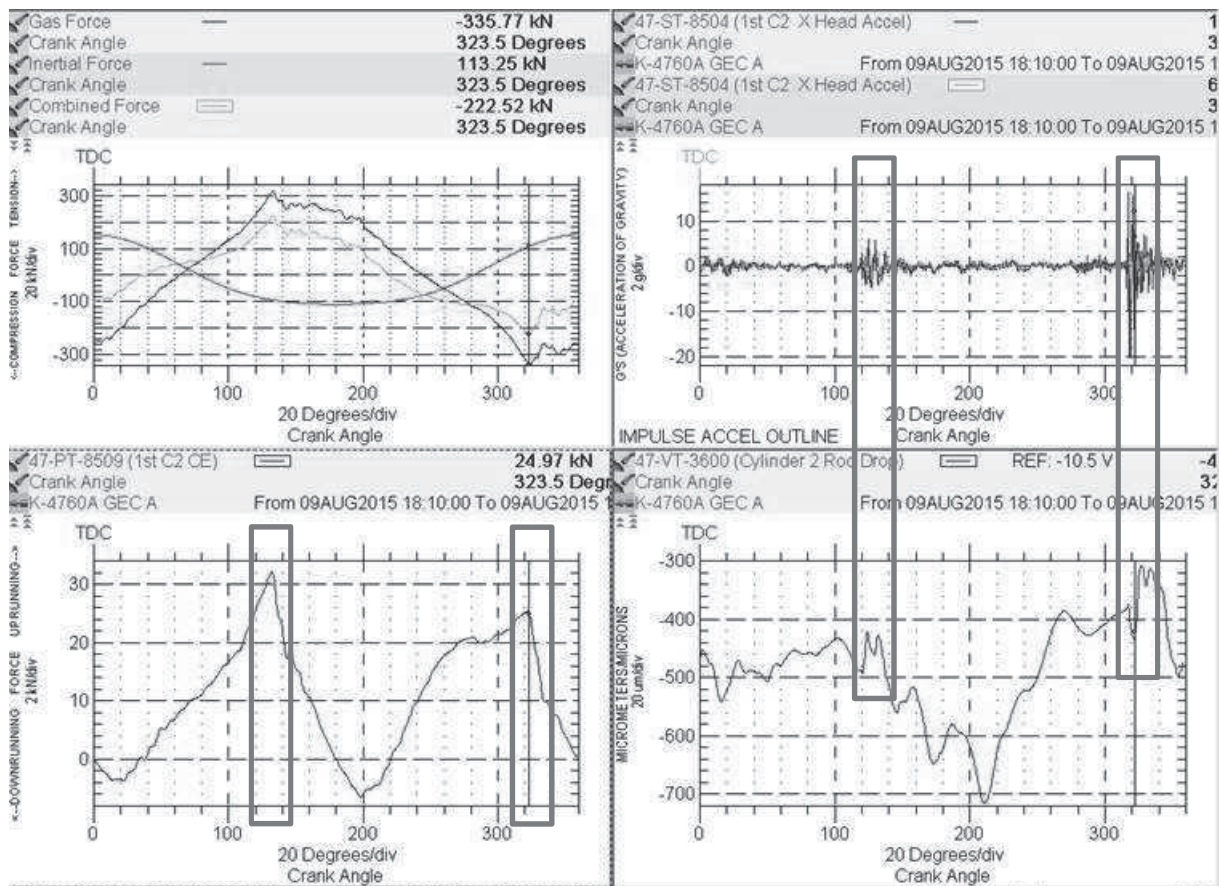


Figure 19: Overlaying of the vertical force (bottom left) with crosshead vibration and rod position

Due to the production critical function of the gas compressor and the extensive real time diagnostics and monitoring capability at the disposal of diagnostics engineers, it was decided to modify the surveillance attributes and introduce additional crosshead vibration into the trip logic of the machinery protection system.

This allowed continued operation of the compressor with added confidence that if the fault deteriorated the unit could be shut down safely without incurring additional damage.



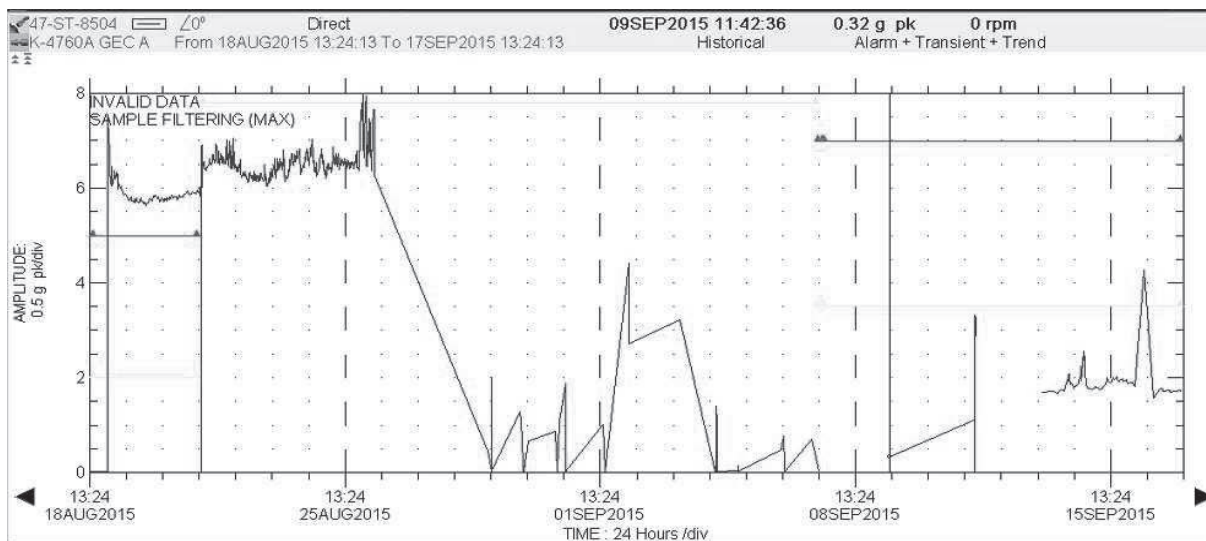


Figure 20: Trend of crosshead vibration, left: during critical operation condition, right: after repair

One week later, instability of the crosshead vibration started and resulted in the monitoring channel blipping into the new alert level of 7.5 g's. The decision was made to stop the machine for the planned overhaul.

As the connections between the crosshead/rod and rod/piston were confirmed to be tight, the technicians inspected the crosshead assembly also and found the following issues:

- When the crosshead was removed, wear was found on the body due to contact with the con rod small end bush. The small end bushing was verified and the dimensions found to be ok, but the bushing was not centered on the connecting rod and was in fact flat on the pump side and out on the motor side.
- The bottom crosshead shoe was found to be slightly loose from the crosshead body. The lock plate was open.

Findings highlighted that the crosshead was working with reduced clearances as a result of the bottom shoe being slightly loose. This was as a consequence of the small end bush not being fully centered, initiating a state of no axial clearance and friction within the crosshead body surfaces.

The abnormalities were rectified and the machine was put back in service. The resultant crosshead vibration level of 2 g's pk was normal and three times lower than before. Condition monitoring had enabled swift location of the defect and ensured reduced downtime.

## 5 Conclusion

Machinery protection and condition monitoring system data can provide supplementary functionality and vital information when running on the edge of an equipment's working envelope. Having the authority of extensive real time reciprocating diagnostics and the facility for continuous trending and modeling ; this opens up additional opportunities for machine operation under extenuating circumstances. The augmented capability derived ensures prompt and expedient diagnosis of abnormalities and confidence in running with these defects whilst minimizing and mitigating the associated threats.



## 5 References

- [1] Rossi, Gaia Localization of reciprocating compressor components faults using on-line dynamic correlation of impulsive vibration signatures with calculated forces and displacements at individual running gear components ; 8th Conference of the EFRC, 2012
- [2] Orbit article Rod Position & Rod Drop: What's the Difference?, March 9th, 2015



# Technical Paper

**Session: 44-1**

**Session Name: Valve**

## Next-generation compressor valve technology

**Author:**

**Matthias Kornfeld**  
**Research and Development**  
**HOERBIGER Ventilwerke GmbH&Co KG**  
**1220 Vienna, Austria**

**Co-Authors:**

**Bernhard Spiegl / Tino Lindner-Silwester / Markus Testori / Marian Janko**  
**Research and Development**  
**HOERBIGER Ventilwerke GmbH&Co KG**  
**1220 Vienna, Austria**

## Summary

The demand for higher compressor availability and lower investment costs for new compressors has traditionally been the key driver for advances in valve technology. In recent years, however, greater awareness of operating and capital costs, and the need to save energy, has also driven the demand for more reliable and efficient valves.

Improved sealing element materials and better simulation methods have paved the way for higher lifetimes of standard plate, poppet, and ring valves over the last decade. However, small gains in efficiency have often been bought dearly through sacrificing valve lifetime, i.e. unplanned compressor shutdowns.

Fundamental research backed by the latest FEA and CFD simulation technologies has given new insight into the reasons for the limited improvement potential of today's various valve types. It has been found that a hybrid approach, referred to as profiled valve plate technology, has the potential to overcome previous technical limitations and hence to improve both reliability and efficiency. This new valve design, featuring a sealing element made from a new impact-resistant material, helps to reduce costs for compressor OEMs through its superior efficiency, especially in medium- and high-pressure cylinders. By enabling service intervals of three to five years, depending on the specific application, valve service costs can be cut by more than 70%.

Profiled valve plate technology yields substantial improvements in reliability and efficiency, as outlined by three case studies presented in this paper. In the first case study, the run time of a trouble-prone compressor in a refining application was increased from a few hundred to several thousand hours. The second case study shows how energy savings due to increased valve efficiency reduce operating costs to an extent that leads to payback times of a few months. The third case study shows how investment costs for new compressors can be brought down by reducing the required number of valves and even cylinders.



## 1 1 Introduction

Reciprocating compressors are key elements of many processes in chemical and petrochemical plants. Since the valves determine the overall performance of the compressor more than any other component, the demand for increases in valve lifetime and reliability has been the traditional key driver for new valve technologies. However, nowadays there is also a growing awareness of operating and capital costs. Operators of reciprocating compressors demand higher power densities and fewer valve pockets, in order to reduce investment costs. They also require reliable and efficient valves, so as to reduce operating costs. With standard valve technology having more or less reached its physical limits, sufficient valve lifetime in demanding applications can only be obtained by sacrificing valve efficiency.

At the 7th EFRC conference in 2010 in Florence [1] the profiled valve plate concept was presented for valve diameters up to 100 mm. This valve type is now running very successfully in many critical applications, thereby preparing the ground for the next generation of new and larger valves for even more demanding applications.

Fundamental investigation made it clear that a comprehensive development strategy covering:

- fluid mechanics,
- structural mechanics,
- material science and composite material technology, and
- manufacturing technology

is required to push the limits of valve technology beyond current ones. It has also turned out that the findings stemming from these fundamental investigations need to be incorporated into the engineering tools used in valve design in order to fully exploit the potential of this new valve generation.

## 2 Requirements to be met by modern compressor valves

Recent developments in compressor design have tremendously strengthened the market position of reciprocating compressors. These machines can nowadays operate at pressures beyond 1,000 bar, capacities up to 250,000 SCM/h, and power consumptions of 20 MW and above.

Initial investment costs can be reduced by going to fewer but larger cylinders – which poses the challenge of keeping the valve losses within reasonable limits while significantly increasing the flowrate through each valve. Energy savings, which result in lower operating costs, can be achieved in two basic ways. On the one hand, components can be made more efficient. On the other hand, compressors then can cope efficiently with changing operating conditions will reduce energy wastage. Since the valves are the main reliability-determining components of the compressor, maintenance costs can be reduced by increasing valve reliability and lifetime.

Thus, the next-generation valve has to excel in the following areas:

- **reliability:** the valve should no longer be the component that limits the maintenance-free run time of the compressor;
- **robustness:** with sealing elements made from materials that tolerate particle-laden gases and harsh operating conditions;
- **efficiency:** 30% higher efficiency to allow for higher cylinder capacities.
- **strength:** with heavy-duty seats and sealing elements for differential pressures up to 1,000 bar, yet without sacrificing valve efficiency.



### 3 Next-generation compressor valve technology for demanding applications

Reconciling these apparently conflicting targets requires a holistic and interdisciplinary development approach. The profiled valve plate technology has already demonstrated its high potential [1]. Extending this to even more demanding applications, however, requires a deep dive into the research areas of materials, manufacturing technologies, and valve design.

#### 3.1 Materials research

The sealing element of the valve is exposed to a dynamic load collective arising from the opening and closing impacts during operation, typical failure modes being crack initiation, crack propagation and subsequent valve plate failure (Figure 1, left). Suitable sealing element materials are thus characterized by their ability to withstand this dynamic load. However, it is well known that commonly measured material properties such as tensile strength, tensile elongation, modulus, and so on are poor indicators for assessing whether a material is capable of resisting this fatigue load.

It is thus of great importance to test sealing element materials under conditions closely resembling compressor conditions. This can be done on a specially designed test rig (Figure 1, right). This is basically a serial reciprocating compressor with two cylinders, modified with a special cylinder head that carries a chamber in which the cyclic impact resistance of small-diameter sealing elements can be tested. By achieving two times higher impact speeds than in most demanding applications in real-world compressors, this setup allows for accelerated lifetime testing. Long-term field experience has provided correlations between the performance of a material on the test rig and performance in the field.

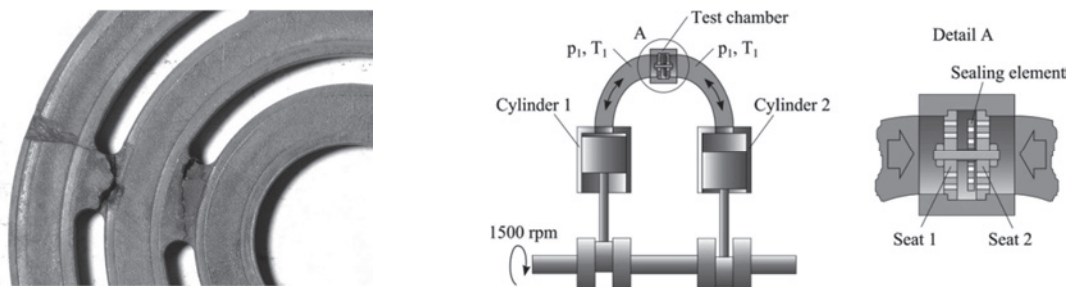


Figure 1: Valve plate failure (left) and schematic sketch of the lifetime tester (right).

By this means, the effect of different base polymers, additives, fiber types, and filler amounts can be systematically investigated. As a result, a new PEEK-based material has been developed that shows outstanding performance (Figure 2).

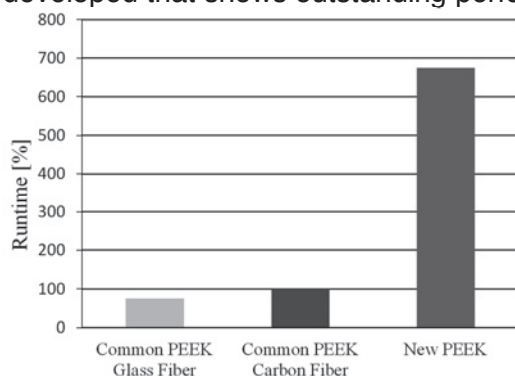


Figure 2: Lifetime test results of common fiber reinforced PEEK and the newly developed PEEK grade.



### 3.2 Manufacturing technology

Apart from resistance to cyclic impact, valve plates also have to exhibit great robustness when being kept open by an unloader in reverse-flow mode (see section 0). This robustness has been achieved by using carbon-fiber reinforcement. Since the shape of the mold affects the resulting fiber orientation, the interaction between material, mold, and injection molding process is of utmost importance. This interaction has been made use of so as to arrive at an optimum fiber alignment with respect to thermal expansion and plate stiffness.

The need to bridge the gap between the requirements to be met by the sealing element material and the design restrictions limits potential manufacturing methods and technologies. One technology satisfying all the requirements is injection molding, which offers the greatest freedom in the design of the valve plate (Figure 3). However, standard injection molding processes exhibit severe disadvantages, such as the formation of weak spots in the material – so-called weld lines – where two melt streams join during the injection process [2],[3]. Hence, these valve plates require an injection molding technology far beyond the capabilities of standard technology.



Figure 3: A profiled valve plate produced by injection molding.

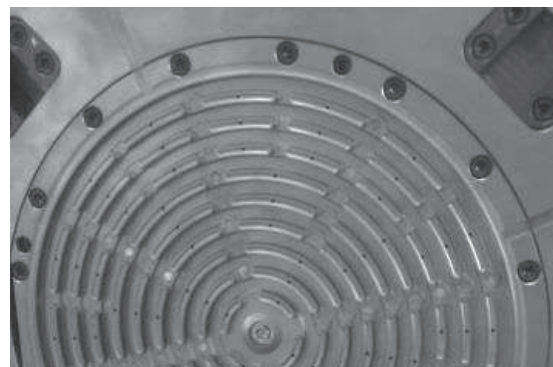


Figure 4: Ejection side of a mold for producing profiled valve plates.

At the heart of the manufacturing process is the injection mold (Figure 4). For the profiled valve plate technology a novel and patented molding technology has been developed where the fiber orientation and the weld-line formation are actively influenced during the injection process [4]. Using melt-flow simulations [5] to optimize process parameters (Figure 5), it is possible to orient the fibers in the direction of maximum stresses, resulting in plates of highest robustness and strength.

Apart from optimizing plate strength, special attention was paid to minimizing the difference in thermal expansion between the steel valve seat and the thermoplastic profiled valve plate. The aim is to ensure optimum sealing behavior of the valve over the entire operating temperature range. With the thermal elongation of steel being typically an order of magnitude lower than that of thermoplastics, leakage would increase tremendously with operating temperature if no countermeasures were taken. By deriving an optimum combination of design, material, and fiber orientation, however, it is possible to create a valve plate that exhibits a similar radial thermal expansion rate to that of the valve seat, so the valve seals well at all operating temperatures.

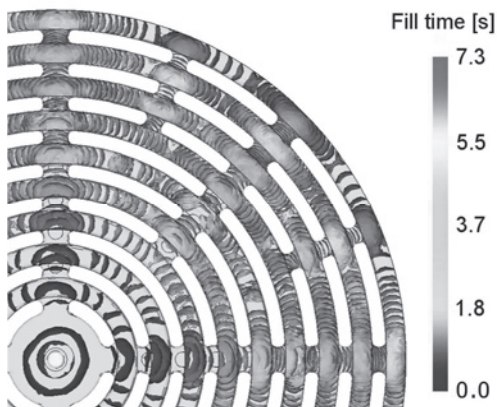


Figure 5: Melt-flow simulation of a valve plate showing locations of weld lines and fiber orientation.

### 3.3 Valve design

In the standard approach to designing valves, the valve components are optimized more or less independently of each other. In contrast, a holistic approach sets the development focus on the valve assembly as a whole. Cutting-edge simulation tools for structural mechanics and fluid dynamics have been applied. For the structural analysis of the seat, a new fatigue criterion (the FKM criterion, see [6]) has been used, taking into account not only the three-dimensional stress tensor but also stress gradients. Applying this fatigue criterion can achieve a much better match between calculated seat strength limits and physical ones, compared to standard fatigue criteria such as the equivalent von Mises stress approach (Figure 6). Computational fluid dynamics (CFD) calculations have been performed in parallel to optimize pressure losses without sacrificing seat strength (Figure 7).

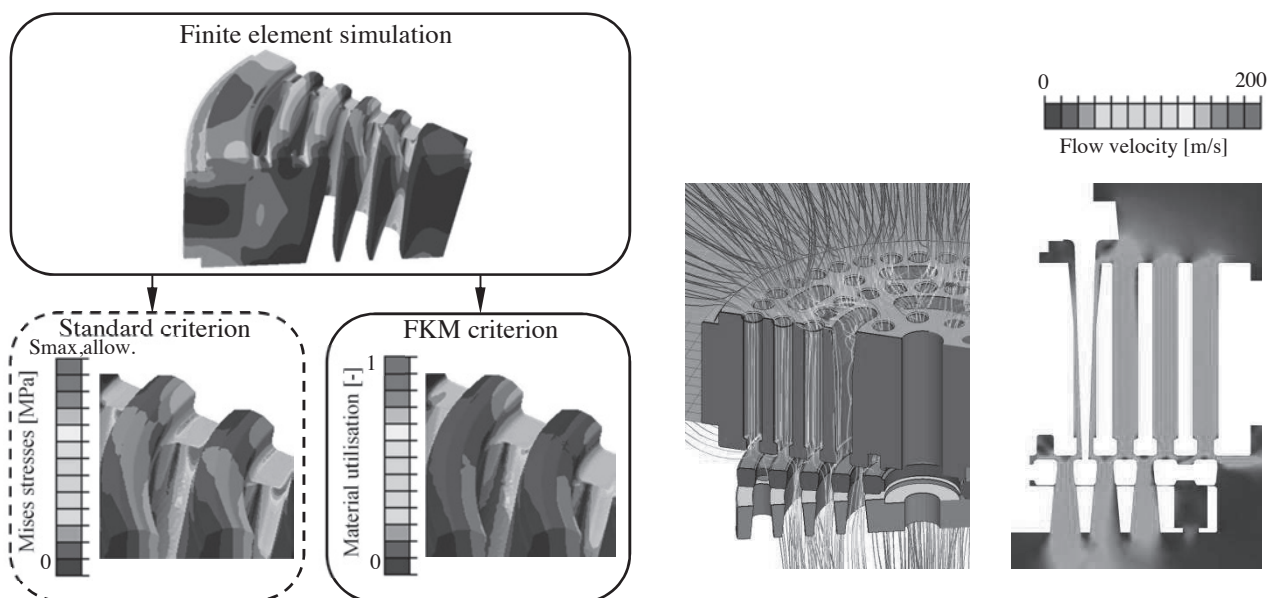


Figure 6: Finite-element seat strength analysis (top) showing the fatigue criteria limits (red regions) and the difference between a standard fatigue criterion (above left) and the improved FKM criterion (above right).

Figure 7: CFD results showing the optimized flow field for a given seat geometry, with streamlines (left) and flow velocity (right).



Applying this simulation strategy to the entire valve family has resulted in up to 30% higher maximum allowable differential pressure levels, compared to similarly sized valves designed using conventional methods, and seat clearance volumes that are up to 20% lower.

Furthermore, the valve plate and the guard have been designed to strike an optimum balance between minimizing oil stiction (less oil stiction on the guard leads to lower closing impact speeds) and maximizing gas damping (more gas damping means lower opening impact speeds). This allows the technology to be used in applications requiring the highest pressures without reducing the reliability or lifetime of the valve.

A novel spring pocket and guidance systems has also been introduced. The spring pockets are equipped with patented spring savers made from a nonmetallic tribological material. These spring savers stop the spring coils contacting the spring pocket. In combination with the unique way the valve plate is guided directly by the springs, the risk of spring failures during operation is greatly reduced.

### **3.4 Challenges arising from capacity control systems**

A capacity control system is required to adjust the amount of gas delivered by a compressor. For reasons of energy savings and process control, stepless reverse-flow regulation has become the most popular approach to controlling capacity in demanding applications. With an unloader keeping the suction valve open for a well-defined period of time during the compression stroke, only the required amount of gas is compressed; the remainder is pushed back into the suction line.

However, this approach poses significant challenges, as outlined in [7], not only to the actuator controlling the motion of the unloader but also to the sealing element of the suction valve. Owing to the valve losses, the cylinder pressure is higher than the suction pressure during the reverse-flow phase, resulting in a pressure differential  $\Delta p_{\text{reverse}}$  across the valve. This pressure differential drives the flow of gas out of the cylinder into the suction plenum while the suction valve is open. The reverse-flow force gives rise to bending stresses in the sealing element, whose resulting deflections reduce the flow area of the valve. This in turn increases  $\Delta p_{\text{reverse}}$  and hence the reverse flow force. As the suction valve closes, the valve flow area decreases further, so there is a steep rise in  $\Delta p_{\text{reverse}}$ . This is most pronounced when the suction valve closes at the point where the piston is at the mid-cylinder position, and hence travelling fastest.

For the valve to operate reliably in challenging applications for many years, and thus for billions of load cycles, the sealing element has to be of highest robustness. On the other hand, the valve has to be very efficient to keep the reverse-flow losses low. A high valve efficiency means not only lower reverse-flow forces but also less heating of the gas during part-load operation. The latter point is essential in applications requiring high turndown while keeping the discharge temperature below critical limits.

To precisely predict the loads to which the sealing element is exposed in a reverse-flow capacity-controlled application, fluid-structure interaction (FSI) simulations have been performed. It is important to take into account the fiber orientation in the valve plate. The upper part of Figure 8 shows how the gas pressure arising from reverse flow varies over the surface of the valve plate. The lower part of Figure 8 shows the corresponding stresses and deflections of the valve plate. These deflections (which are exaggerated in the diagram) mean that during the closing event, parts of the valve plate will contact the seat before the valve is fully closed. This effect is also accounted for in the simulations.



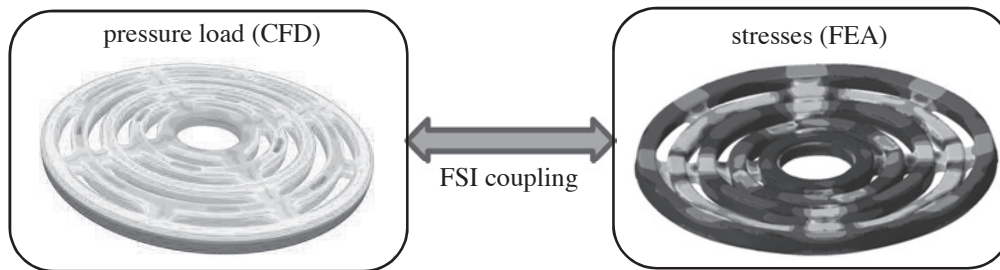


Figure 8: (Left) CFD predicts the pressure distribution across the valve, while (right) finite element analysis reveals the resulting stresses and deflections.

The fatigue limit has been determined experimentally by loading the valve plate in a way that closely resembles what happens when the suction valve closes following the reverse-flow phase (Figure 9, left). In these dynamic load cycling tests, a servo-hydraulically actuated unloader pushes against the valve plate at 20 Hz, with a force that varies sinusoidally with time. The amplitude of the force was gradually increased over several test series until the valve plate cracked. The fatigue limit was then derived by calculating the stresses in the valve plate that lead to crack initiation (Figure 9, right).

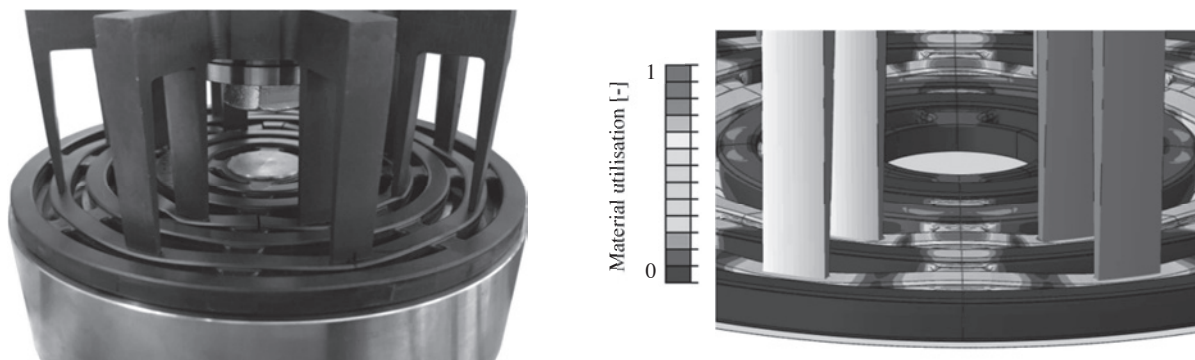


Figure 9: (Left) experimental rig for fatigue limit testing; (right) finite element analysis showing stresses / material utilisation.

For each configuration of unloader and valve plate, calculations of the interaction between reverse-flow forces, stresses, deflections, reduction in flow area, and unloader prong forces have been performed. These data sets have been incorporated into a comprehensive simulation tool that allows the engineer to choose the optimum valve and predict its behavior accurately for each application.

#### 4 Case studies: three field installations

Profiled valve plate technology has already proven its outstanding potential in many demanding field installations, as the three following case studies demonstrate.

##### 4.1 Reliable performance in a CCR regeneration loop compressor

The first case study concerns the compression of nitrogen and carbon dioxide in the regeneration loop compressor of a continuous catalytic reformer (CCR) in a Indian refinery. Since commissioning of the compressor, the original ring-type valves had been failing every 500 hours. Significant amounts of liquid were found in the cylinders. This caused corrosion and deposition of debris on the valves and inside the valve pockets, which finally affected the reliability of the valves.





The valves were upgraded to profiled plate types in April 2015 and since then have run without problems. A first valve inspection after 3,000 hours showed some debris agglomeration and corrosion on guards and seats, arising from the harsh operating conditions (Figure 10). However, the performance of the valves was not affected. The robustness of the valves has extended the valve lifetime by a factor of more than 10 so far.

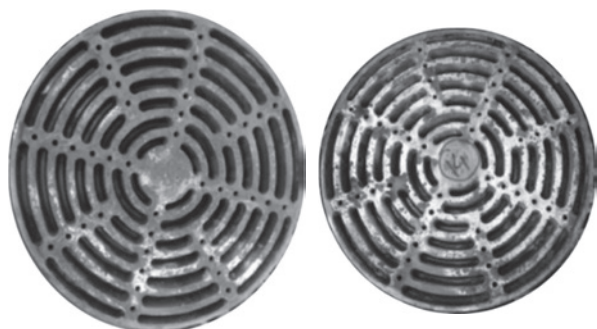


Figure 10: Inspection after 3,000 hours shows the valves in good condition, despite some surface corrosion and debris resulting from harsh operating conditions on a CCR unit.

#### 4.2 Lower operating costs and higher efficiency in natural gas storage

The second case study demonstrates the potential of profiled plate valves to save energy. This customer stores natural gas in one of the world's largest cavern fields. The 3,700 kW compressor has eight 211-mm diameter valves on the first stage and another eight 197-mm diameter valves on the second stage (Figure 11). Flow is regulated via a combination of step control and variable-speed drive.

Switching from the original plate valves to the new generation of profiled plate valves yielded measured savings in indicated power of 2.6% at 70% load, and more than 4% at full load. This gives a payback time of just a few months in energy savings alone. In addition, the extra lifetime due to the robustness of the valves will also reduce maintenance costs.

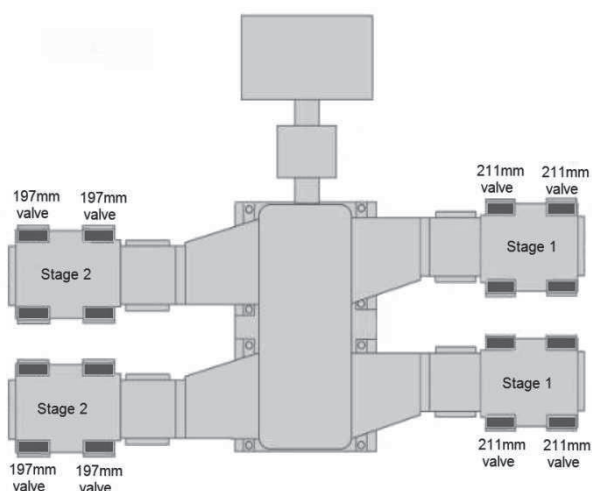


Figure 11: This large natural gas storage compressor has eight 211-mm diameter valves and eight 197-mm diameter valves. Profiled plate valves have paid for themselves in a few months through power savings alone, with increased valve life as a bonus.

### 4.3 Capital cost reduction for a refinery compressor

The last case study shows the potential of the profiled plate design to reduce the number of valves, and even cylinders, on new compressors. This gives original equipment manufacturers (OEMs) a competitive advantage. For a 1,000 kW refinery compressor with a restricted driver power rating, one OEM was able to reduce the number of cylinders and valves by utilizing profiled valve plate technology.

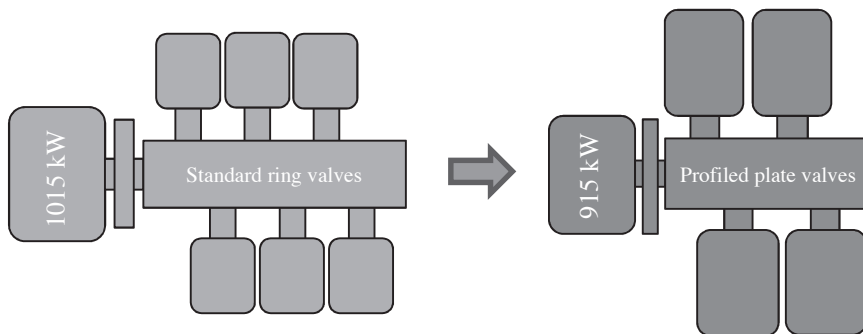


Figure 12: (Left) The standard 1-MW compressor design requires six cylinders with 48 valves. (Right) profiled plate valves enable a compact four-cylinder design with 32 valves.

The last case study shows the potential of the profiled plate design to reduce the number of valves, and even cylinders, on new compressors. This gives original equipment manufacturers (OEMs) a competitive advantage. For a 1,000 kW refinery compressor with a restricted driver power rating, one OEM was able to reduce the number of cylinders and valves by utilizing profiled valve plate technology.

The new generation of profiled plate valves with a diameter of 365 mm allowed the number of cylinders to be reduced from six to four (Figure 12) and the number of valves from 48 to 32, while maintaining the requested throughput even with the restricted driver power rating owing to significantly lower valve losses. The four-cylinder design has a significantly lower capital cost than the standard six-cylinder compressor. This helped the OEM to win the tender, and reduced investment costs for the end user.

## 5 Conclusions

Profiled plate valves are the next generation of valve technology. They match the trend towards raised awareness of operating and capital costs for reciprocating compressors by increasing valve reliability and life, especially in demanding applications. Pushing the limits of today's valve technology requires diving deeply and in an interdisciplinary manner into fluid dynamics, structural mechanics, materials science, and manufacturing technology. As the result of such a holistic approach, profiled plate technology is proven to substantially improve reliability and efficiency in demanding applications. The result is substantially lower investment, operating, and maintenance costs for reciprocating compressors.



## 6 References

- [1] B. Spiegl, M. Testori, G. Machu, Next generation valve technology for high speed compressors, 7th EFRC Conference (Florence, 2010).
- [2] P. J. Cloud, F. McDowell, and S. Gerakaris. Reinforced Thermoplastics: Understanding Weld-Line Integrity. *Plastics Technology*, 22(August):48–51, 1976.
- [3] S. Y. Hobbs. Some Observations on the Morphology and Fracture Characteristics of Knit Lines. *Polymer Engineering & Science*, 14(9):621–626, 1974.
- [4] M. Janko, B. Spiegl, A. Kaufmann, T. Lucyshyn, C. Holzer, Weld line improvement of short fiber reinforced thermoplastics with a movable flow obstacle, *Journal of Applied Polymer Science*, 132, 42025, 2015
- [5] Autodesk Inc. Moldflow 2012.
- [6] B. Hänel, E. Haibach, T. Seeger, G. Wirthgen, H. Zenner, *Rechnerischer Festigkeitsnachweis für Maschinenbauteile*, VDMA Verlag (2005).
- [7] B. Spiegl, P. Dolovai, T. Lindner-Silwester, New concept for electrical stepless compressor capacity-control system, 8th EFRC Conference (Düsseldorf, 2012).





# Technical Paper

**Session: 44-2**

**Session Name: Valve**

## **The innovative use of nanofillers in thermoplastic materials for valve sealing elements**

**Author:**

**Massimo Schiavone**  
**Technical Manager**  
**Dott. Ing. Mario Cozzani Srl**  
**19021 Arcola, Italy**

**Co-Author 1:**

**Andrea Raggi**  
**R&D Manager**  
**Dott. Ing. Mario Cozzani Srl**  
**19021 Arcola, Italy**

**Co-Author 2:**

**Alessandro Vollonnino**  
**Quality Manager**  
**Dott. Ing. Mario Cozzani Srl**  
**19021 Arcola, Italy**



## Summary

Since the 1970's plastic materials have been used in cylinder valves of reciprocating compressors in order to achieve new goals in terms of energy consumption reduction and in reliability improving. With the introduction of thermoplastic matrices such as polyamide PA66, polyetherimide (PEI) and, mostly in the 1990's, with the introduction of polyether ether ketone (PEEK), additional benefits of reliability and safety have been reached compared with solutions of steel valve sealing elements. The amorphous thermoplastic matrices, such as polyethersulfone (PES) and PEI are characterized by high deformability and toughness, while the semi-crystalline matrices (PEEK, PPS) are characterized by a better crack resistance and solvent resistance.

Several options have been analysed to increase the reliability of the valve sealing elements. For example, the use of elastomers ensure a better initial seal, but it is more sensitive to impacts and prematurely loses its initial benefits. The use of layers of carbon fibres impregnated in matrices of PEEK resin, epoxy resin, phenolic resin, provides high mechanical characteristics for the valve sealing elements but it requires a sophisticated production process in order to ensure the tightness of the valves.

Despite continuous technological improvements on the valves, they still remain among the most critical elements of the reciprocating compressor. The updated statistics ascribe to the valves malfunction most of unscheduled shutdowns of the reciprocating compressors and most of their malfunction is associable to premature failure of the valve shutters. Analysis performed on broken thermoplastic plates, glass or carbon filled, put in evidence that the fracture mechanism appears to be a combination of plastic nature triggering followed by a brittle nature propagation. Thanks to the recent evolution of the nano-composite technology, the research target has been to evaluate the application of this technology to the valve sealing elements using the nanofillers today available on the market. The purpose of this research has been to obtain new materials for valve sealing elements characterised by higher mechanical properties using a nanofiller or combining their mix into several thermoplastic matrices. This paper highlights the results of the research activities showing the benefits gained adding one or more inorganic nanofillers on the thermoplastic matrices of PEEK or PEI filled with glass and/or carbon fibres. Several nanofillers in different percentages and combinations on a semi-crystalline matrix have been taken into account to evaluate their contribution on the mechanical properties of the plate valve. Comparison between these new formulations and the currently used materials highlights new opportunities to be implemented for innovative valve sealing elements.



## Introduction

Automatic valves on reciprocating compressor cylinders are generally acknowledged as being one of the most critical components for the proper functioning of these machines.

These days, the market demands increasingly significant improvements to increase the operating time of compressors and consequently extend the Mean Time Between Maintenance.

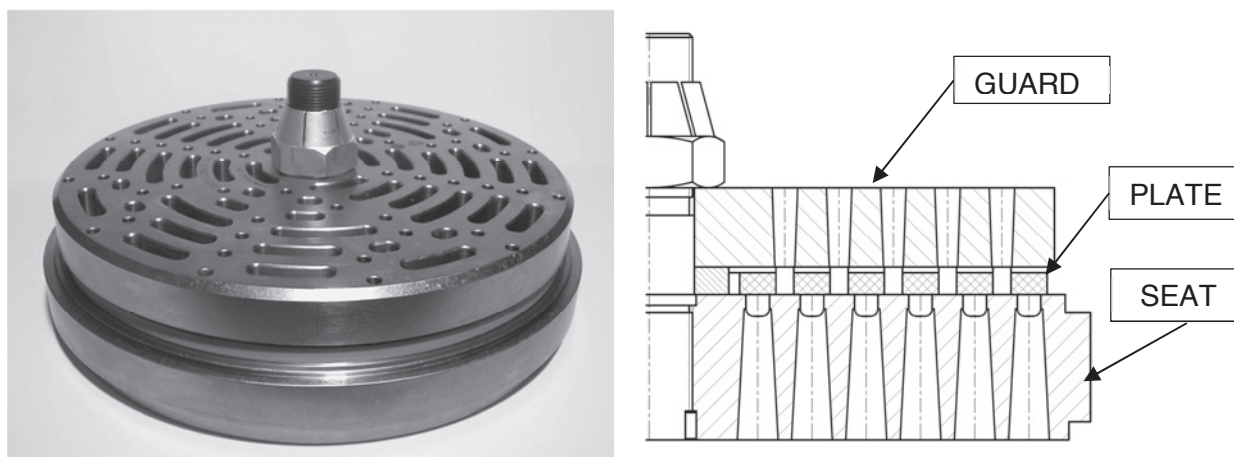


*Figure 1 – Example of discharge valve*

Every manufacturer specialising in the design and production of valves is continuously committed to implementing innovative materials and technical solutions to achieve increasingly reliable products, which are therefore capable of reducing the operating and maintenance costs of systems.

The reason for the premature breakage of a compressor valve can often be attributed to various causes, such as liquid inside the cylinder, external metal particles in the gas, corrosive elements, incorrect lubrication, or operating conditions that differ from the design specifications.



*Figure 2 – Example of damaged valve plate by external elements*

These factors may lead to a critical situation inside the valve and therefore compromise the most important internal components, such as the springs and sealing elements.

Indeed, despite constant technological improvements, according to industry statistics, shutters remain the most critical components inside valves.

Shutters affect the performance of valves according to their seal tightness.

If they are distinguished by an aerodynamic profile, they can also affect the efficiency of the valve reducing gas pressure losses.

Shutters, in the case of premature breakage, *Figure 3*, could compromise the life span of the valve, with the ensuing sudden stoppage of the compressor.

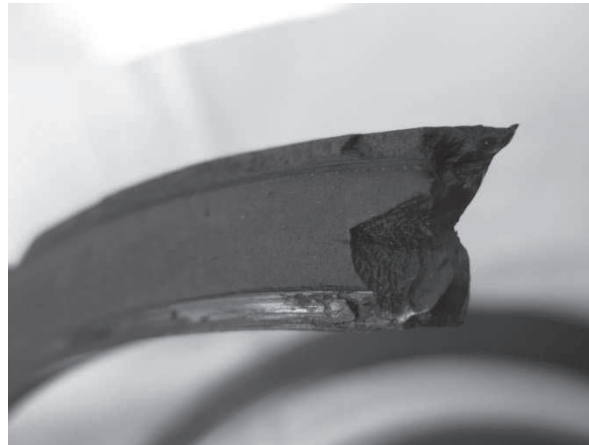


*Figure 3 – Broken valve ring*

The sealing elements open and close the gas passages on the valve seat, thanks to the difference in pressure that is created between the side downstream and the side upstream of the valve itself, as the piston moves inside the cylinder.

These continuous valve opening and closing movements during every single compression cycle are the main causes of the high levels of stress which the shutters are subjected to during repeated impact. If we consider a compressor that operates at a speed of 1,000 revolutions per minute (rpm), the shutters strike the valve seat to close the gas passages 16.6 times per second and strike the counter-seat just as many times during the respective openings.

If we consider the minimum market request to guarantee at least 8,000 hours of operation in one year, we can estimate approximately 480 million impacts to close the gas passages and just as many to open them, for a total of approximately 960 million impacts on shutters over their guaranteed operating life.

This is a low estimate of the number of shutter impacts, because the above raw calculation does not take into account the bounces which in actual fact occur (although obviously to a lesser extent) during the opening and closing phases. In addition, we should also consider the



possible dynamics and excess stresses due to oblique impacts of the shutter with the body that marks the limit of its stroke (*Figure 4*).

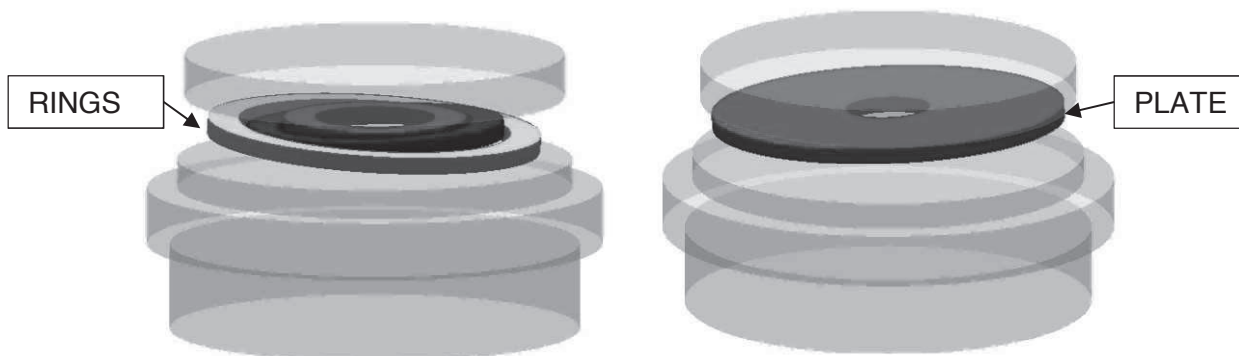


*Figure 4 – Oblique impact of the shutter in a 3D simulation*

Companies that specialise in valve design, thanks to the development and fine-tuning of proprietary calculation codes, can minimise the number of bounces or fluctuations to which the shutters are subjected.

In addition to work cycles, obviously, the design of these valves must also take into account all the operating conditions which the valve must comply with, such as pressure (in some cases in excess of 500 bar), temperature (normally between -40 and + 200°C) and gas variety, which often includes aggressive elements (the most widespread being without a doubt H<sub>2</sub>S). Last but not least, the designer must take into consideration the market expectations in terms of life span, as in some cases the expectation is to achieve 3 years of continuous operation without having to conduct any preventive maintenance work.

### **Purpose of the Research**

In thermoplastic materials, the rise in ductility generally occurs to the detriment of the mechanical properties. Considering the above information, the objective we set ourselves was to achieve new compounds with a high ductility and tenacity without compromising the physical characteristics such as tensile strength, modulus and shock resistance.

Summarizing, the valve sealing elements are subjected to local and repeated impacts against the valve bodies and stressed by temperature and pressure cycles. Considering what above mentioned, the desired material should have high modulus and strength to sustain high impact velocities and in the same time high ductility and tenacity to avoid embrittlement phenomena.

This paper describes the research activities that the Company carried out in order to increase in a selective way the desired mechanical properties, by using fillers with nanometric dimensions. The activity starts with a bibliographic investigation into the various nanofillers most commonly found on the market and continues with the identification of new formulas capable of bringing benefits to the properties of valve shutters. Tests were carried out on specimens at different temperatures to compare the results of the various combinations deemed to be most promising. The paper opens a new path towards using new nanotechnologies within the design and manufacturing processes of valve shutters for reciprocating compressors.

## General background

Before the 1970s, shutters were mostly made with special high-resistance steels. Resistance and stiffness are traditionally considered to be key factors in choosing a material, whereas fatigue fracture and deterioration of the surfaces of the component are the parameters which limit its useful life span.

The availability and overall cost of the component (not just the cost of the raw material) are also essential elements to keep in mind when choosing the material.

Thanks to the development of technologies and production equipment, designers have been able to face the constant challenges set by the market.

From the early 1970s, with the introduction of plastic materials for the production of cylinder valve sealing elements, new performance and reliability standards have been defined.

Moreover the operating speed of compressors has on average increased, whereas at the beginning of the 1970s, compressors operated on average at around 600 rpm, these days depending on the application, we have already exceeded 1,000 rpm, reaching 1,800 rpm for specific applications or even higher speeds and, despite the increase in fatigue cycles, the reliability of valves has increased considerably.

Talk of plastic materials opens up a vast universe. Indeed, plastic materials constitute a large and variegated group of organic synthetic materials whose elementary components are monomers. At particular temperature and pressure conditions, polymerisation takes place, which combines the monomers together, giving rise to polymers. Some examples of the most well-known polymers include:

Monomer	Polymer
<i>Ethylene</i>	<i>Polyethylene</i>
<i>Propylene</i>	<i>Polypropylene</i>
<i>Vinyl Chloride</i>	<i>Polyvinyl chloride</i>
<i>Styrene</i>	<i>Polystyrene</i>
<i>Tetrafluorethylene</i>	<i>Polytetrafluorethylene</i>

The combination of a growing number of monomers for the formation of increasingly longer polymer chains increases the molecular weight and profoundly changes the physical properties of the material.

Traditionally, plastic materials are split up into three families: thermoplastic, when they can be hot processed, thermosetting when they harden irreversibly with heat and elastomers when they are characterised by high deformability.

Another essential characteristic of polymers is their degree of crystallinity. Generally, no polymer is completely crystalline, and they are defined as being semi-crystalline.





Whereas amorphous materials are formed by knotted molecular chains, in semi-crystalline polymers, the chains are prevalently arranged in order.



Amorphous



Semicrystalline

This differentiation in molecular make-up generally translates into an increase in the mechanical properties, with a rise in crystallinity.

Whereas amorphous thermoplastic matrices such as PEI and PES are characterised by high deformability and tenacity, semi-crystalline matrices such as PEEK or PPS (Polyphenylene sulfide) are characterised by greater resistance, resistance to creep, modulus of elasticity, density, resistance to solvents, but also by lesser tenacity.

From the group of thermoplastic polymers, during the early 1970s, valve designers picked out those polymers whose physical properties better accommodated those required for the production of valve shutters. Some of the most well-known include polyamide PA66 and Polyether ether ketone (PEEK). Obviously, their dissemination was made possible thanks also to the introduction into the polymeric matrices of appropriate glass or carbon fibres capable of enhancing their mechanical characteristics considerably.

The greater benefits derived from the use of technopolymers in the design of valves are without a doubt the rise in reliability and efficiency of such valves, which therefore translate to a rise in reliability and efficiency for the compressor manufacturer and for the end users, exceeding in some applications a generous 24,000 hours of continuous operation.

Despite these improvements, the market has never stopped raising the stakes in terms of product quality and technological expectations have grown and become increasingly demanding in terms of efficiency and durability.

### Research activity

Analysis performed on broken PEEK plates and rings, glass or carbon fibre filled, put in evidence that the fracture mechanism appears to be a combination of plastic nature triggering followed by a brittle nature propagation (*Figure 5* and *Figure 6*).

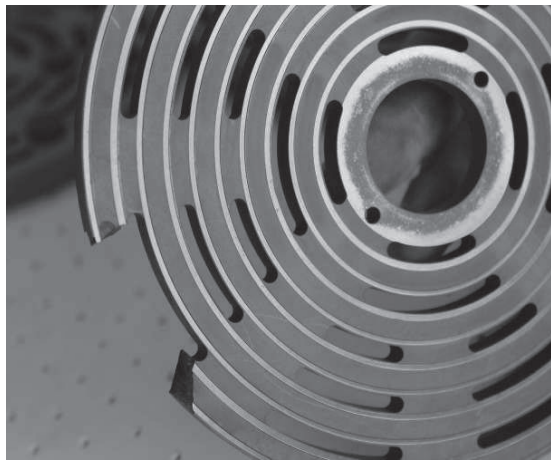


Figure 5 – Broken valve plate

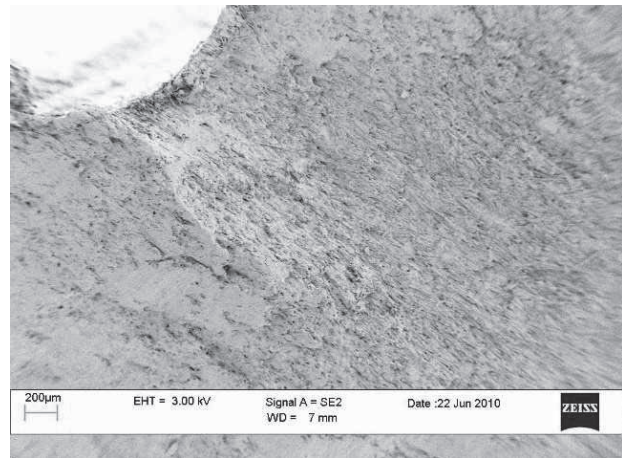


Figure 6 – Micrographic image of the fracture

This research activity analysed first and foremost the solutions found in literature to counter the above-mentioned phenomenon, investigating both in the specific field of cylinder valves but also in other sectors such as the automotive, aeronautical and biomedical industries.

Let's take elastomers for example. Elastomers are polymeric materials whose  $T_g$  (glass transition temperature) is below ambient temperature and normally they are characterised by high levels of deformability and elasticity. Consequently, the use of elastomers as valve shutters ensures a better initial seal on the valve seat. The problem with using them in the above-mentioned application is linked to the very low mechanical and thermal properties that characterise them. As a matter of fact, the above-mentioned initial benefit is quickly lost following impacts and stresses, which, in our opinion, makes them unsuitable for use as valve shutters.

If on the other hand we take for example the use of multi-layers of fibres impregnated in polymeric matrices, we have completely the opposite situation. In this case, we achieve high mechanical characteristics but also a high sealing difficulty, which can only be solved with sophisticated production processes. The use of multi-layer solutions as valve shutters obviously has its limits, tied mainly to the inability to use them with all the various types of shutter profiles.

The goal of the research activity carried out by the Company can be summed up as follows: starting with the most widely available thermoplastic matrices on the reference market, to analyse the advantages deriving from the introduction of nanotechnologies in the production of valve shutters, thereby defining new formulas of nano-compounds characterised by improved physical properties, which are suitable for valve shutters.

When we talk of a “nano-material”, we mean a material characterised by a size of less than 100nm. Comparing a nano-particle with a football is like comparing the latter with the globe. For this reason, some of the properties of nanomaterials are affected by the laws of atomic physics rather than by the behaviour of solid material. The variety of nanofillers and polymeric matrices in which to disperse them is extremely high. Thanks to the nanometric dimensions of these



fillers, we can achieve a high degree of dispersion within the polymer, thereby obtaining a compound material with a homogeneous nature (heterogeneous only at nanometric level) and with significant improvements to the physical properties such as tensile strength, thermal stability, flame delay and abrasion and solvent resistance. Nevertheless, one of the most interesting aspects is the possibility of drastically reducing the quantity of fillers to add to the polymer. For example, to guarantee comparable reinforcement performance levels, 5-6% weight of nanofiller is sufficient compared to 20% weight of classic filler with micrometric dimensions.

The difficulty in preparing polymeric nano-compounds depends on the hydrophobic nature of the polymer with respect to the hydrophilic nature of the nanofiller. The latter therefore needs to be rendered more similar to the polymer using a chemical process of “compatibilization” which increases its hydrophobicity, encouraging adhesion and dispersion in the matrix. The shape, size, surface morphology and distribution of the nanofiller in the polymeric matrix determine the base properties of the nano-compound. The filler can be a “nanofiller” on one dimension, two dimensions or even three dimensions and for each of these shapes, there are different properties. Obviously, the choice of type of nanofiller depends on the performance levels and parameters one wishes to reinforce.

Based on the above information, the production of a better performing and innovative material for the production of cylinder valve shutters has made it necessary to discretize the analysis process.

In using different nanofillers, an attempt has been made to obtain new formulas that would be able on the one hand to increase ductility and tenacity compared to the formulas currently found on the market and on the other to retain or even increase modulus of elasticity and tensile strength, as well as bending and shock resistance.

Considering the large number of variables at play and the multiple physical properties to analyse (nanofillers, polymeric matrices, physical properties, production parameters, etc.), we decided to begin with a screening activity, taking into consideration certain parameters, such as yield strength, tensile strength, Young's modulus, yield strain and breaking strain.

In order to better assess the properties of the various formulas, considering the maximum design temperature for the valves, a value which is normally around 200°C, we decided to measure the parameters both at ambient temperature as well as at the above-mentioned temperature of 200°C.

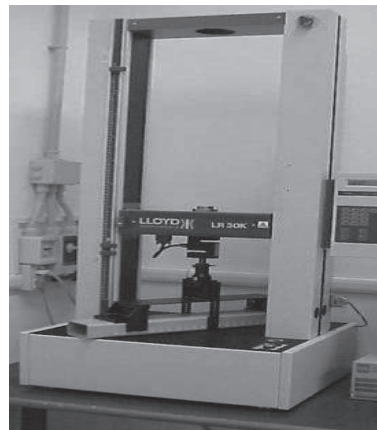


Figure 7 – Tensile test machine

As is well known for semi-crystalline materials, and more specifically for all materials which have an amorphous state, the exceeding of the glass transition temperature ( $T_g$ ), which depending on the polymeric matrix used can occur between 60 and 150°C, leads to a mobility of the polymer chains. The material becomes less fragile and more visco-elastic and its mechanical properties, such as modulus and resistance incur a sudden deterioration (*Figure 8*).

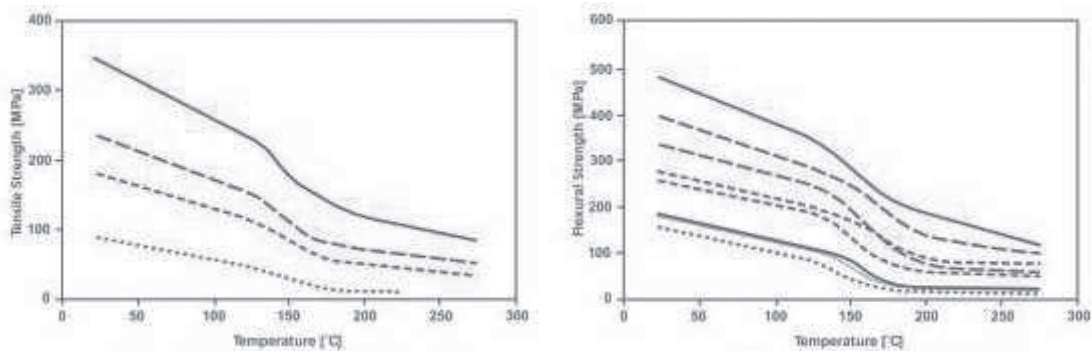


Figure 8 – Strength vs Temperature

The test specimens were created using a micro-extruder capable of exceeding the melting temperature ( $T_m$ ) necessary for the injection-molding process used.



Figure 9 – Extruder



The screening activity was particularly long and hard work. Initially, for each polymeric matrix selected (PFTE, PEEK, PEI, etc.), it was necessary to identify the best mixing time to use in order to maximise dispersion in the selected nanofiller, keeping its concentration unchanged.

The concentration of the nanofiller can vary up to 30% in weight but in this initial screening phase, we decided to use the typical concentration found in literature for each filler. The identification of the optimal concentration for the nanofillers selected was left to a subsequent refining phase.

Once the bibliographic investigation phase had been completed, we therefore moved on to the creation of a series of specimens with different formulas, with different types of nanofillers. The specimens underwent mechanical tests and thanks to the use of appropriate climatic chambers, the tests were also conducted at temperatures above the T<sub>g</sub>. For formulas with a PEEK matrix, we took the temperature of 200°C as our reference value.

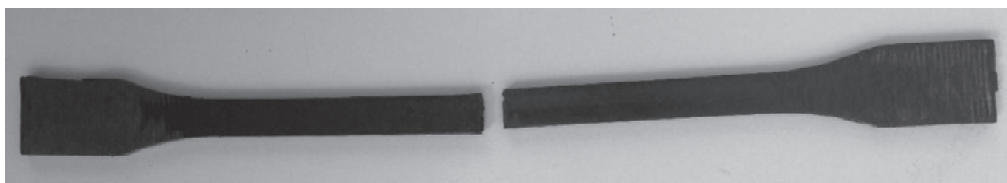


*Figure 10 – Tensile test specimen*

This activity enabled us to identify among nanofillers available on the market those capable of giving the reference matrix an increase in physical properties. Among the most significant nanofillers, we mention silicates, carbon-based nanofillers, metal oxides and ceramic nanofillers.

For the identification and refining of the various nanofiller-based formulas, we used the specimen values obtained from the respective original polymeric matrices for reference. For the PEEK polymeric matrices, we quote the PEEK polymer filled with glass and carbon fibres, which are definitely among the most well-known and popular polymers used in valve production.

As mentioned earlier, improving the properties of valve shutters by introducing nanotechnologies was our starting concept. If we consider the most common PEEK valve shutter fracture mechanisms, in other words the combination of plastic nature triggering followed by a brittle nature propagation, one of the objectives of this research was to attempt to give PEEK shutters greater ductility, in other words we tried to combine the physical properties typically found in fibres with the specific properties of nanofillers.

The activity was conducted in two directions. The first, by adding nanofillers to current compounds filled with glass and carbon fibres, in order to increase the overall filler level of the matrix. The second was instead conducted to decrease the fibre content to encourage the introduction of nanofillers. The conduction in both these directions obviously led to a drastic increase in formulas and specimens.



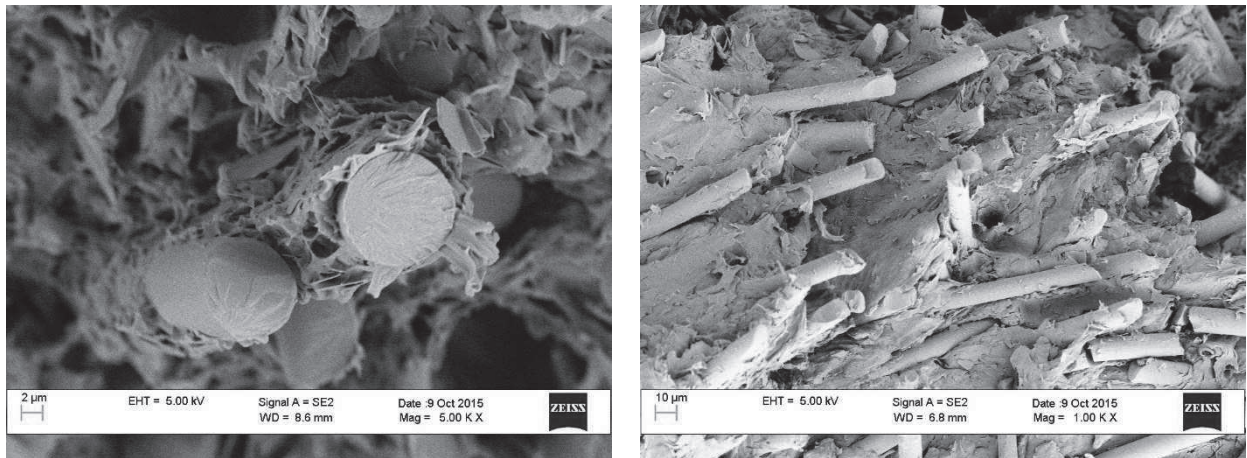


Figure 11 – Micrographic images of some of the formulas tested

Despite the considerable workload, the activity enabled us to identify certain formulas capable of achieving our target objective.

In Figure 12, Figure 13 and Figure 14 are showed some mechanical properties of various tested formulas.

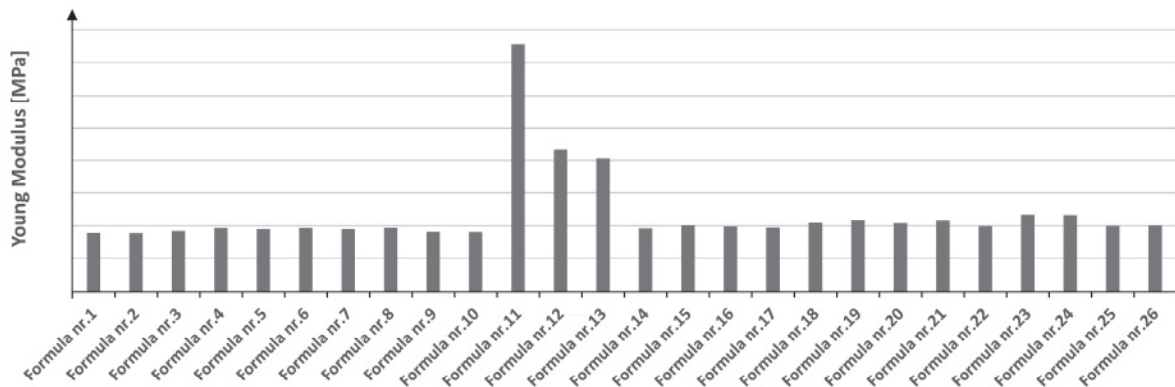


Figure 12 - YM of various nano-compound formulas

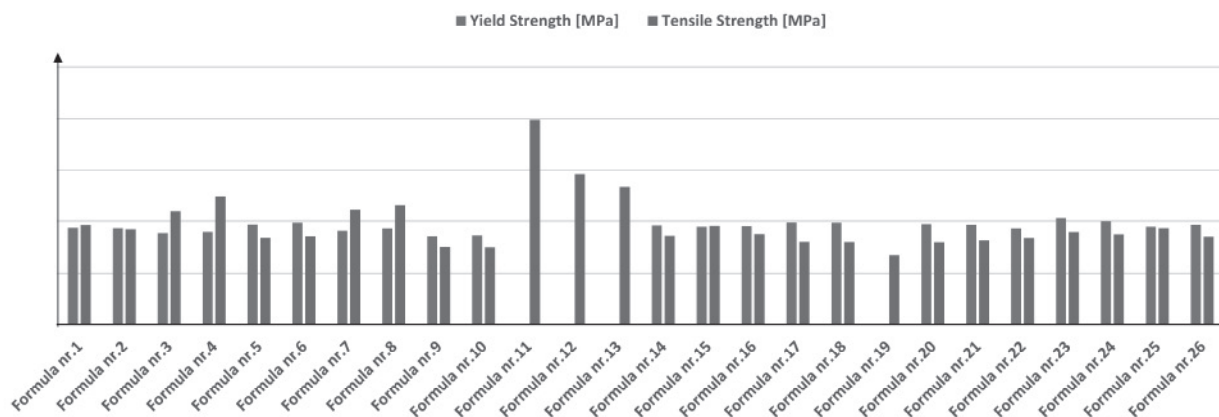


Figure 13 – Yield and Tensile Strength [MPa] of various nano-compound formulas

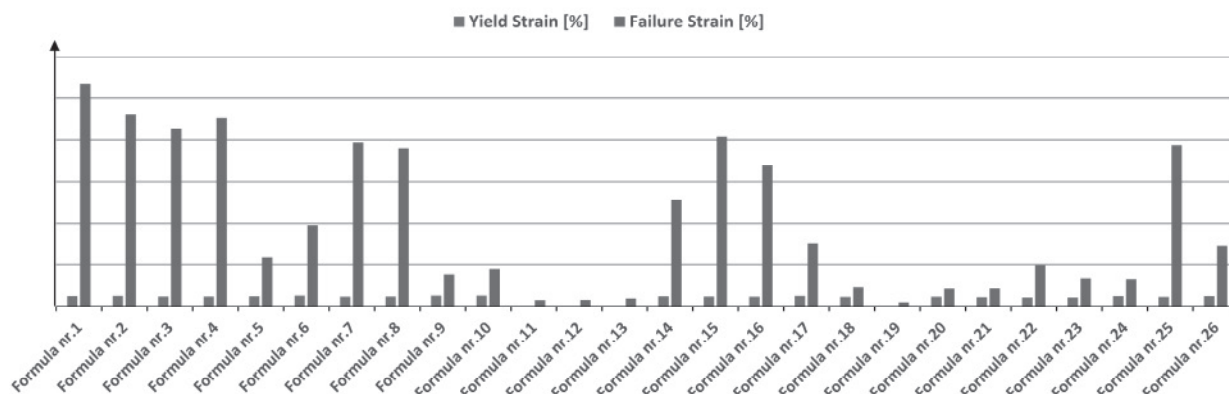


Figure 14 - Yield and Failure Strain [%] of various nano-compound formulas

In Figure 15 you can see the comparison between a PEEK reference formula with glass fibres and a PEEK formula with glass fibres and nanofiller at high temperature testing. The new hybrid formula shows significant percentage increases, +4% for Young's Modulus, +20% for the Tensile Strength and +188% for Failure Strain.

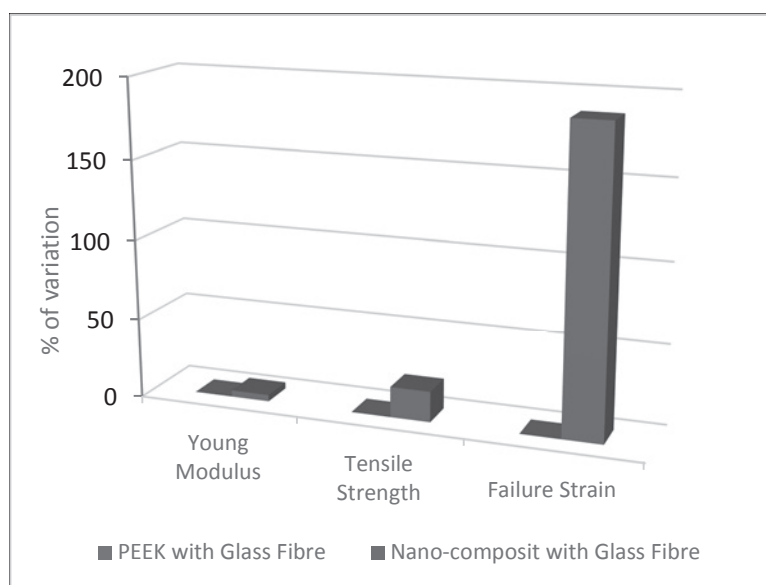


Figure 15 – Nano-composite vs PEEK GF

In Figure 16 you can see the comparison between a PEEK reference formula with carbon fibres and a PEEK formula with carbon fibres and nanofiller at high temperature testing. The new formula shows significant percentage increases for certain parameters, +6% for Young's Modulus, +53% for the Failure Strain, retaining the Tensile Strength value unchanged.

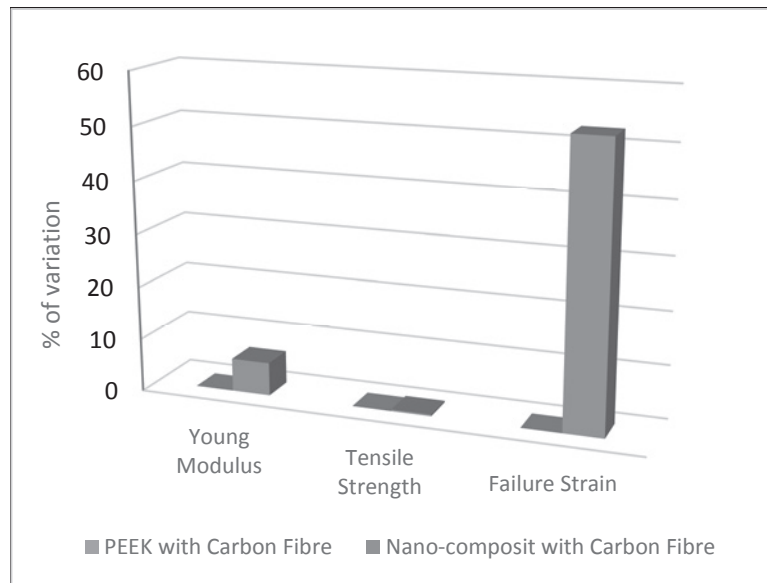


Figure 16 – Nano-composite vs PEEK CA

The results shows the benefits ensuing from the introduction of nano-compounds in the production of valve shutters and it opens up new research possibilities. Consequently, we can state that at nano level, we can move in the desired direction, acting more selectively on the characteristic we wish to increase.

Obviously, we need to select and combine nanofillers with matrices and fillers appropriately.

### Conclusion

From the early 1970s, with the introduction of plastic materials for the production of cylinder valve sealing elements, new performance and reliability standards have been defined, despite the fact that the operating speed of compressors has on average increased.

To date, from the group of thermoplastic polymers, valve designers have picked out those polymers whose physical properties better accommodate those required for the production of valve shutters. Some of the most well-known include polyamide PA66 and Polyether ether ketone (PEEK). Obviously, their dissemination was made possible thanks also to the introduction into the polymeric matrices of appropriate glass or carbon fibres capable of enhancing the mechanical characteristics considerably.

The research activity intends to set up the foundations for a new phase in the design and production of valve shutters, a phase which is represented by the use of nanotechnologies. Starting with the analysis of the most common fracture mechanisms in valve shutters, i.e. the combination of plastic nature triggering followed by a brittle nature propagation, the activity shows the ability to generate improvements on the shutters through the use of nanotechnologies.



Indeed, thanks to the properties of nanofillers, including silicates, carbon-based nanofillers, metal oxides and ceramic nanofillers, it is possible to obtain new hybrid formulas that act selectively on the properties of the compound.

The tests conducted on the countless specimens showed considerably interesting results for valve application. By mixing suitable combinations of nanofillers and fillers on polymeric matrices, we managed to achieve compounds with superior mechanical properties of resistance and considerably higher ductility and tenacity compared with thermoplastic materials commonly used for valve shutters.

## References

- [1] Yakobson BI, Brabec CJ, Bernholc J. Nanomechanics of carbon tubes: instabilities beyond linear response. *Phys Rev Lett* 1996; 76:2511–4.
- [2] Ruoff RS, Lorents DC. Mechanical and thermal properties of carbon nanotubes. *Carbon* 1995; 33:925–30.
- [3] Treacy MMJ, Ebbesen TW, Gibson TM. Exceptionally high Young's modulus observed for individual carbon nanotubes. *Nature* 1996; 381:680–7.
- [4] Wong EW, Sheehan PE, Lieber CM. Nanobeam mechanics: elasticity, strength, and toughness of nanorods and nanotubes. *Science* 1997; 277:1971–5.
- [5] Yu MF, Files BS, Arepalli S, Ruoff RS. Tensile loading of ropes of single wall carbon nanotubes and their mechanical properties. *Phys Rev Lett* 2000; 84:5552–5.
- [6] Yu MF, Lourie O, Dyer MJ, Moloni K, Kelly TF, Ruoff RS. Strength and breaking mechanism of multiwalled carbon nanotubes under tensile load. *Science* 2000; 287:637–40.
- [7] Thostenson ET, Ren Z, Chou TW. Advances in the science and technology of carbon nanotubes and their composites: a review. *Compos Sci Technol* 2001; 61:1899–912.
- [8] Iijima S. Helical microtubules of graphitic carbon. *Nature* 1991;54:56–8.
- [9] Salvetat JP, Kulik AJ, Bonard JM, Briggs GAG, Stočkli T, Métevier K, Bonnamy S, Béguin F, Burnham NA, Forró L. Elastic modulus of ordered and disordered multiwalled carbon nanotubes. *Adv Mater* 1999; 11:161–5.
- [10] Carneiro OS, Covas JA, Bernado CA, Caldeira G, Van Hattum FWJ, Ting JM, Alig RL, Lake ML. Production and assessment of polycarbonate composites reinforced with vapour-grown carbon fibres. *Compos Sci Technol* 1998; 58:401–7.
- [11] Tibbetts GG, Finegan JC, McHugh JJ, Ting JM, Glasgow DG, Lake ML. Applications research on vapor-grown carbon fibers. In: Tomaneč D, Enbody RJ, editors. *Science and application of nanotubes*. New York: Academic/Plenum Publishers; 1999. p. 35–51.
- [12] Lozano K, Barrera EV. Nanofiber-reinforced thermoplastic composites. I. Thermoanalytical and mechanical analyses. *J Appl Polym Sci* 2001;79:125–33.
- [13] Kuriger RJ, Alam MK, Anderson DP, Jacobsen RL. Processing and characterisation of aligned vapor grown carbon fiber reinforced polypropylene. *Composites, Part A* 2002;33:53–62.
- [14] Tsagaropoulos G, Eisenberg A. Dynamic–mechanical study of the factors affecting the 2 glass-transition behavior of filled polymers— similarities and differences with random ionomers. *Macromolecules* 1995;28:6067–77.
- [15] Goodwin AA, Simon GP. Dynamic mechanical relaxation behaviour of poly(ether ether ketone) / poly(etherimide) blends. *Polymer* 1997; 38:2363–70.
- [16] David L, Etienne S. Molecular mobility in para-substituted polyaryls. 1. sub-T(g) relaxation phenomena in poly(aryl ether ether ketone). *Macromolecules* 1992;25:4302–8.

- [17] Chou TW. Microstructural design of fiber composites. Cambridge:Cambridge University Press; 1992.
- [18] Blundell DJ, Osborn BN. The morphology of poly(aryl ether ether ketone). *Polymer* 1983;24:953–8.
- [19] Barlow CY, Peacock JA, Windle AH. Relationships between microstructures and fracture energies in carbon-fiber PEEK. *Composites* 1990;21:383–8.
- [20] Crick RA, Leach DC, Meakin P, Moore DR. Interlaminar fracture morphology of carbon-fiber PEEK composites. *J Mater Sci* 1987;22:2094–104.
- [21] Hull D. An introduction to composite materials. Cambridge: Cambridge University Press; 1981.
- [22] Shaffer MSP, Windle AH. Fabrication and characterization of carbon nanotube/poly(vinyl alcohol) composites. *Adv Mater* 1999;11: 937–41.
- [23] Tibbetts GG, Beetz Jr. CP. Mechanical-properties of vapor-grown carbon fibers. *J Phys D: Appl Phys* 1987;20:292–7.





# Technical Paper

**Session: 45-1**

**Session Name: Foundation**

## **Recip foundations – practical issues related to inspection and repair**

**Author:**  
**Theo de Kok**  
**EMHA BV**  
**3341 LW Hendrik Ido Ambacht, Netherlands**

Co-Author 1:

Tom K. Hoekstra  
EMHA BV  
3341 LW Hendrik Ido Ambacht, Netherlands

Co-Author 2:

Erik Barkmeyer  
ITW Engineered Polymers  
3341 LW Hendrik Ido Ambacht, Netherlands

## Summary

Originally reciprocating compressor foundations were expected to last 20 to 30 years. But many of the machines installed in the 60's or 70's are still running and are in need of repair or replacement of their foundation because of poor design, construction or maintenance. [12]

Very often, problems indicate that there is something wrong with the compressor foundation. This can be a broken anchor bolt, twisting movements of the machine frame or excessive vibrations.

Often, the machine has to be stopped to repair this - or it will even stop by itself. In many cases, unplanned shutdown could be avoided by looking at maintenance records, the original construction and the as-built situation. There are signs to let you know that the foundation is in bad condition.

Meanwhile, many updated publications of API, ASTM, GMRC, ISO, DIN, CUR, EOTA and other regulations and advises were done. Also, the machinery-performance\* (flow capacity), accuracy of alignment and environmental requirements with respect to sound and vibrations (due to stricter governmental regulations) were increased radically over the past decades. This made the need for increased attention to the foundation, anchorage and maintenance an important issue.

\* An example: Hitachi was able to deliver a 450kW unit in 1953, while nowadays they are able to supply 11.000 kW units.

Without naming all data and figures and describe all possible scenarios, this paper is intended to give some guidance on how to inspect a compressor foundation and what possibilities there are for repair. It will also cover some practical issues faced over the past 15 years.



## 1. Desk Investigation

To get a good understanding of the situation, first a desk research is required to gather all necessary information.

### 1.1 As-built construction

Especially when observing older configurations, an inspection of the foundation plan and as-built constructional drawings is required to check if the foundation and anchoring is designed and performed according to relevant guidelines such as API Recommended practices 686, GMRC Guidelines and PIP REIE 686. Also, check if there has been an update of the compressor or driver while the foundation was not updated accordingly.

The as-built construction should be reviewed on:

#### 1.1.1. Concrete mat and block design

Information on the required dimensions & minimum weight of the concrete block can be found in above mentioned guidelines. Although a detailed analyses is to be made by the design engineers, it is possible to perform a check to see if a more detailed analysis is required.

#### 1.1.2 Rebar details

In general, there should be a minimum bar size of 19,05mm (GMRC Guidelines for high speed reciprocating compressor Packages)[5]. There are also rules and practices that can be found in GMRC and API686 RP to check rebar spacing and material. Again, a simple check could be enough to determine if further action is required and/or if the original design was made according to applicable standards. Please note that other guidelines may provide different values and therefore one should determine which guideline is to be followed.

It is important to understand if possible cracks can be related to insufficient rebar. For example: 15+ years ago rebar spacing at the top of the foundation should be approximately 300mm, while nowadays 150mm is advised.

#### 1.1.3 Concrete properties

The concrete should have a minimum compressive strength of 28MPa (GMRC, API RP 686), although the design value in many cases does not reflect reality since concrete can be weakened by oil or just because the actually poured concrete was not exactly what it should be. If the properties are in doubt, it is advised to have this checked in a laboratory.

#### 1.1.4 Soil and pile setup

A foundation should never be installed without thorough characterization of the underlying soil. For this, the advice of a geotechnical consultant is required to determine important elements like mass density, different layers and stiffness of the soil. Based on this data and on the type and mass of the compressor system, the type of foundation and the necessity to use pilings should be determined.

First off all, find out if a study is made before designing the foundation. Also, look for any changes in soil properties, for example due to raising water levels.

A tool that could be helpful to check whether the design of a compressor foundation might be susceptible is the Compressor Foundation Analysis Tool (COFANTO). This program is available for R&D members of the EFRC only.

### **1.1.5 Anchor type and dimensions**

It is of major importance to gather all information on the anchor bolts. Some installations incorporate outdated anchor bolt designs which can eventually lead to problems. At least following information is to be obtained on the anchorage:

- Bolt preload and designed clamping force;
- Bolt material, size and type;
- Designed stretch length / elongation;
- Coating / surface treatment;
- Pre-installed versus post-installed;
- Pocket size and type information;
- Edge distance of the anchor pockets;
- Type of grout used for bonding;

Most standards and guidelines such as API RP 686 provide helpful guidance on the above mentioned subjects.

The information gathered during research on the as-built construction must be combined with maintenance records and a field investigation to form a judgment on the foundation's state.

## **1.2 Maintenance records**

The compressor's maintenance records are to be analyzed to see if there are any signs of:

- Inability to hold alignment or anchor bolt tension;
- Loose or broken anchor bolts;
- Increasing vibration levels (above zone B/C of the EFRC guidelines)[7];
- Crank case, crosshead or support block damage and wear;
- Excessive bearing wear;
- Piping damage (excessive repairs needed to the attached piping);

These points could indicate foundation problems. All gathered information on trending vibration measurements, repair records, oil analyses and more will also be of great help in foundation troubleshooting.

## **2. Field investigation**

After all data of the desk research is collected, it is time to examine the compressor foundation on-site. First, the foundation and compressor is examined while running. More comprehensive investigations can be done while the machine is stopped, however in general this is only done when it is already determined that there is something wrong with the foundation or anchorage.

### **2.1 Visual inspection (running compressor)**

During a systematic visual inspection, a lot of information can be found. Most common issues are quite good to notice. One should look at following points:



### 2.1.1 Loose or broken foundation bolts

Loose or cracked foundation bolts are easy to notice. Very frequently, the compressor trips on a broken anchor bolt and often, machine operators realize there is something wrong with the foundation if one of the anchor bolts failed.

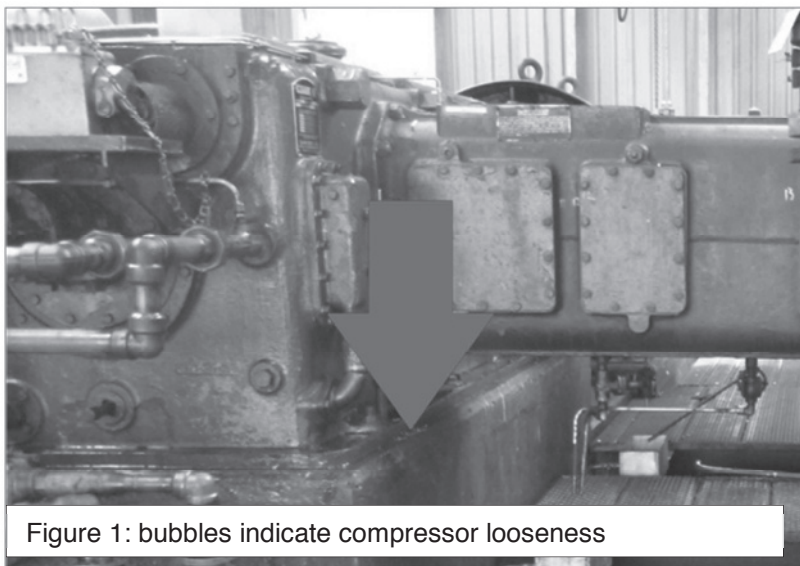


Figure 1: bubbles indicate compressor looseness

While this is indeed a strong indication, it is also possible that the cause of a bolt failure has to be found somewhere else. Sometimes it is easy to over-torque bolts with hydraulic tools for example.

### 2.1.2 Compressor looseness

Looseness of the compressor is easily noticed by air bulbs showing between frame-feet and grout in oil or water. These air bulbs indicate looseness, mean-

ing that the anchoring system is not performing as it should. Oil also considerably reduces the required friction between the frame-parts and the grout layer.

### 2.1.3 Usage of shim plates

Excessive usage of shim plates often indicates that there is a need to 'fill-up' something. This can be an indication that there is something 'moving' or a mistake is been made during the design phase. The maximum number and thickness of shim plates differ depending on the guideline, region and the local engineering standards. Different guidelines agree on not using more than 3 shims in a pack, as more shims lead to spongy (soft) pads.

Unfortunately, adjustable jacks, steel shim blocks or wedges are still frequently advised to be used for alignment of pumps, skids, base-frames or even compressors while they remain in place. These steel jacks make the equipment stand on 'high heels', forming a direct steel contact between machine-frame and concrete foundation. Instead of having the necessary constant compression on the grout layer, the machinery stands on non-compressive steel blocks, which allows oil and water to penetrate between steel and grout.

Even worse, the anchors nor the grout can function according to their design as pre-tension is lost on the steel jacks and grout is merely an aesthetic cover.

Another problem with steel shim blocks in the grout is that they intend to corrode. This is a very common condition and causes serious problems such as cracking grout and a machine that is tilted out of alignment.

### 2.1.4 Edge lifting and delamination of the grout

Edge lifting is caused by the difference in the rate of thermal contraction between epoxy grout and concrete. Generally, the main reason for edge lifting is poor or inexperienced application and the usage of bad quality concrete.



Delamination often occurs between cementitious grout and concrete. Mostly caused by the bad adhesive properties of the grout or due to poor preparation of the concrete block.

Edge lifting and delamination do not always form an immediate threat to the foundation of the machine, since the part under the machine (if well grouted) is under constant pressure and therefore in better condition. However, oil and water can intrude in the foundation, causing more problems. Also can be a sign of poor application and therefore a reason to suspect more problems.

### 2.1.5 Cracks in the grout layer

Cracks in the grout layer may have different causes such as sharp corners, fast curing or thermal expansion. In many cases these cracks do not form an immediate threat however it is important to look for their root cause and to seal it to prevent further damage.

### 2.1.6 Deterioration of the grout layer

Penetration of (crude) oil and other fluids into cementitious grout will over time weaken its compressive strength and the adhesive capacity of cementitious grout in the anchor-pockets.[10] This will continue up to a point where the grout will crumble between your fingers.

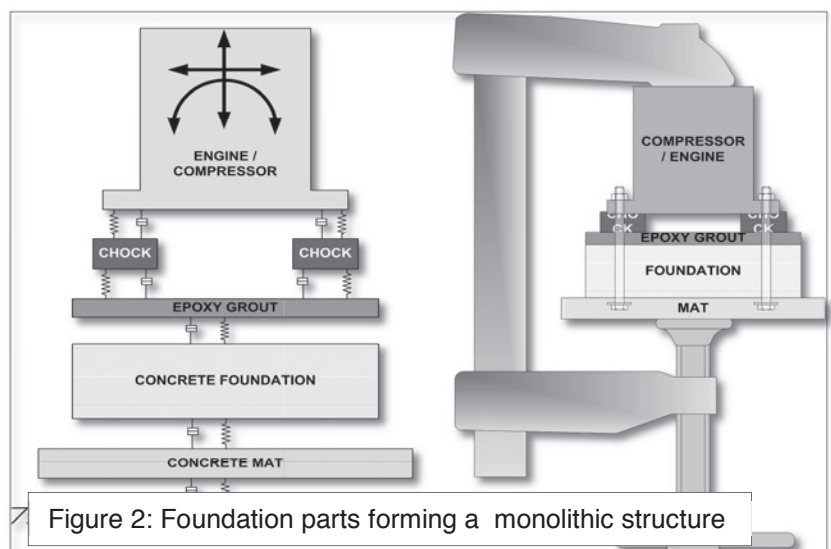
Oil penetrating along the anchors will eventually jeopardize the fixation of the machinery.

### 2.1.7 Cracks and cold joints in the concrete foundation

Cracks in the concrete foundation can be caused by various reasons such as weather conditions, thermal or aggregate expansion and can be found at re-entrant angles such as the corners where the foundation of the crosshead support is connected to the main block. But also in the sump area and of course cracks running from the anchors towards the outside of the foundation.

When observing cracks in the concrete foundation, one has to realize that vertical cracks are less 'dramatic' than horizontal cracks. Horizontal cracks can cause alignment disorders while vertical cracks do not.

The compressor and its foundation must form a tightly integrated structure. Vibration energy travels in the form of waves down and out through the foundation where the soil can absorb it. Breaks, cracks or separations in the integrated-compressor / foundation structure will prevent the vibration waves from traveling downward.[2]



Horizontal cracks create 'separated' parts in the foundation and therefore it will become unable to transfer vibrations into the soil. The monolithic structure (as shown in figure 2) is 'disconnected'.



The same problems can be caused by construction joints, also called 'cold joints'. Because concrete does not bond very well to itself, separation can occur if different parts of the foundation are not poured continuously.

### 2.1.8 Concrete carbonation and spalling

If Carbon dioxide from the air reacts with calcium hydroxide in concrete, it forms calcium carbonate. This process is called carbonation. This is a slow and continuous process progressing from the outer surface inward and has two effects: it decreases mechanical strength of concrete and it decreases alkalinity, which is essential for corrosion prevention of the reinforcement steel.

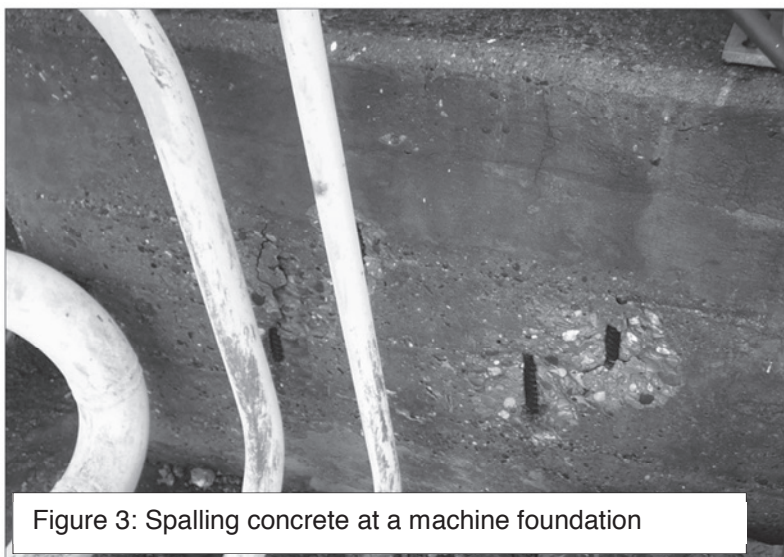


Figure 3: Spalling concrete at a machine foundation

Carbonation and rebar located too close to the concrete surface can cause rebar corrosion. The expansion of the iron oxides induce mechanical stress that can cause the formation of crack, disrupt the concrete structure or make outer parts of the foundation fall off (spalling).[8][9]

These phenomena's are easily to recognize during visual inspection of the foundation.

### 2.1.9 Displacement of foundation

Instability of the soil can cause sinking or tilting of the foundation. Therefore displacement of the foundation can indicate that the soil is not adequately supporting the foundation. This can be checked with tools such as a digital water level and tapeline or more precise by laser scanning.

Trending measurements can provide more suitable information.

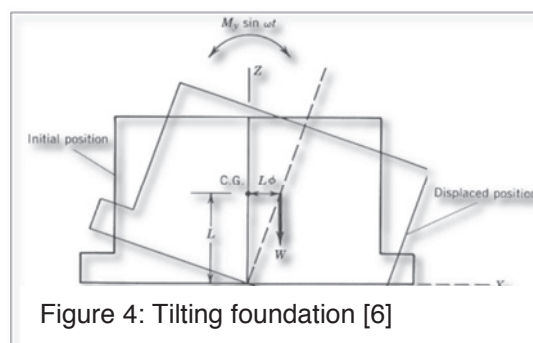


Figure 4: Tilting foundation [6]

## 2.2 More comprehensive investigations (running compressor)

Above mentioned visual inspection can be done relatively simple in a few hours. Depending on the gathered information from the desk research and the visual inspection, it may be wise to perform additional investigations.

### 2.2.1 Vibration measurements

Vibration measurements and analysis on the machine system (which includes anchoring and foundation), will provide hard data to compare with the ISO10816-8 Classification table and the EFRC Guidelines for vibrations in reciprocating compressor systems. [7][13]

Additional, an ODS (operating deflection shape) animation can offer a clear visualisation of the movements of the complete installation. This can help you to recognize things as looseness or unwanted movements.

### **2.3 More comprehensive investigations (stopped compressor)**

Some more comprehensive investigations can be done if the machine is stopped. In case of a foundation repair or re-grout, these investigations can be useful to decide if anchor bolts are to be replaced or to find out how many of the concrete has to be chipped away.

#### **2.3.1 Core drilling and investigations**

Diamond-drilling of core-samples is required to check the depth of oil-penetration into the block.

These cores may also be used for a more extensive carbonation investigation [8] and to check the quality of the concrete. Differences in homogeneity of the concrete can be identified and a compressive stress test can be performed.

Note: oil penetration and changes in concrete quality can also be noticed when new anchor-pockets are drilled or old anchor bolts are removed.

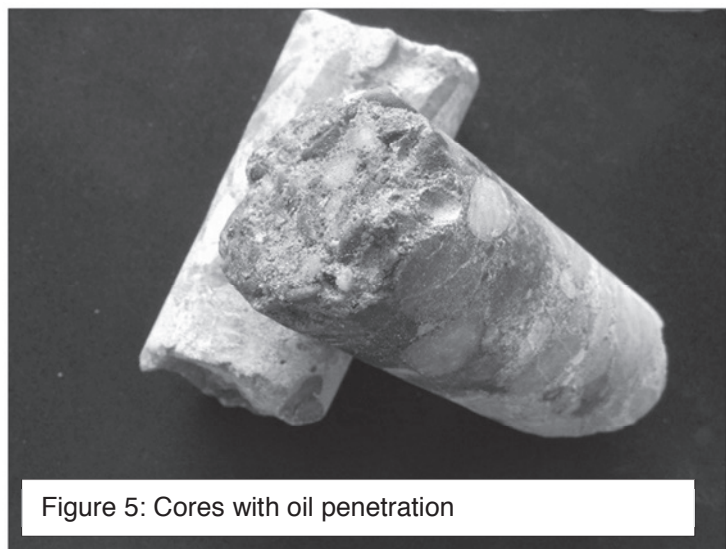


Figure 5: Cores with oil penetration

#### **2.3.2 Alignment checks**

The alignment of the compressor to the driver and the alignment of the extensions to the frame needs to be checked since foundation issues will ultimately lead to alignment issues. Also the alignment of the rotor to the magnetic centre is to be checked. Determine web deflection and rod run out.

Depending on the need for further investigation, more values can be measured such as the flatness of soleplates and the line-bore (centre line measurement).

#### **2.3.3 Inspection of the anchor bolts**

Anchor bolt stretch may be measured with an Ultrasonic Bolt Meter, provided the anchor model and data are known. Are there signs of bolt over-stretching? If the grout layer has blocked the anchor to stretch; it will stretch typically just below the nut.

If the compressor is removed, it is also possible to investigate bonding of the anchor into the concrete foundation by using a hollow plunger cylinder and a dial indicator. This can be done by placing the cylinder over the bolt and applying load with a hydraulic cylinder while the dial indicator is attached to the head of the anchor bolt. If the bolt comes up more than the stretch length after applying the design load (be careful not to apply too much load) for 24 hours, then one can be sure that the anchor is debonding from its pocket.



### 3. Analysis and correction plan

After all data of desk and field research is gathered and combined, it is time to write an analysis and correction plan. The analysis plan is an evaluation of foundation and anchoring and should also contain an indication of the urgency.

For example: a loose anchor bolt in combination with vibration levels above EFRC reference values, requires a high urgency since the anchoring of the machine cannot be guaranteed. The machine should be stopped to perform at least an emergency repair. Cracks in a grouting layer in combination with normal vibration levels require in general no special urgency. A repair can be planned during a next overhaul or when convenient.

It is hard to provide a list to indicate which problems require immediate attention and which not, since there is always a combination of problems and every situation is different. Hence, in general one can say that every problem that is an immediate threat for anchoring and load transfer of the compressor should be a reason for instant repair.

#### 3.1 Repair methods

After the urgency of a repair is determined, the repair method is to be selected. If an urgent repair is compulsory, it is also possible to perform a crisis repair on short notice while planning a more durable repair in a maintenance stop.

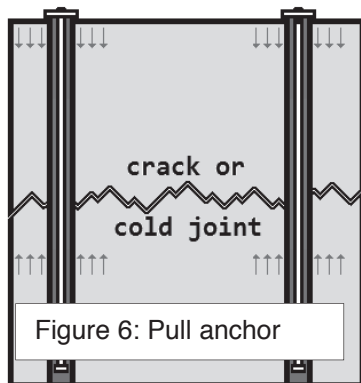
There are more factors that influence the selection of a suitable repair method. The most important (surely not the only) factors are:

- Urgency of the repair;
- Safety conditions;
- Time frame for the repair;
- Possibility to remove the machine or not;
- Time of the year (weather conditions);

Here under a brief sum-up of some common problems, their typical urgency and possible repair methods. Please note that this list is not a complete reference with required urgency indications and repair methods, but it will give you some guidance.

Problem	Typical urgency	Emergency repair	Durable repair method
Loosness of compressor	Intermediate	N/A	Machine regrout + anchor test
Broken anchor bolt	High	Replace anchor	Replace all anchors + regrout
Loose anchor bolt	High	Replace anchor	Replace all anchors + regrout
Loose anchor nut	High	Tighten and check	Anchor bolt test
Cracks in grouting	Low	N/A	Replace defect grouting
Detoriated grouting	Low	N/A	Replace defect grouting
Cracks or joints in vertical foundation plane	Low	Epoxy injection	Epoxy injection + pull anchors*
Cracks or joints in horizontal foundation plane	Intermediate	Epoxy injection	Epoxy injection + pull anchors*
Carbonation and spalling	Low	N/A	Sand blasting + coating
Displacement of foundation	Intermediate	N/A	Soil stabilization, extra piling

Table 1: Some possible foundation problems and their repair options



\* A pull anchor pulls separated parts of a foundation together. See also figure 6.

The correction plan should include a proposal for repair, specifying alignment, usage of soleplates, anchoring method, grouting, injecting and other activities with a time schedule. It is also important to make a safety and risk analysis and to provide a budget price for the repair.

#### 4. Practical Issues during repair

When repairing a compressor foundation (regularly incorporating a re-grout of the machine), some issues require special attention. New techniques, materials and insights may require a change of mind for many companies. To avoid unexpected changes in planning and budget, this subjects should be discussed in an early stage.

Following of these topics are covered below:

- 3D positioning;
- Soleplates;
- Method of alignment;
- Anchoring;
- Grouting;
- Injection of cracks.





## 4.1 3D positioning

Before an installation is removed, the exact position of the complete line shall be registered. A 3D-tracking laser is used to measure the exact position of frame, anchors, cylinders, crosshead supports, centreline of the crankshaft, expansion vessels and all flanges of the main piping. This 3D position measurement provides full data information on the position of the installation.

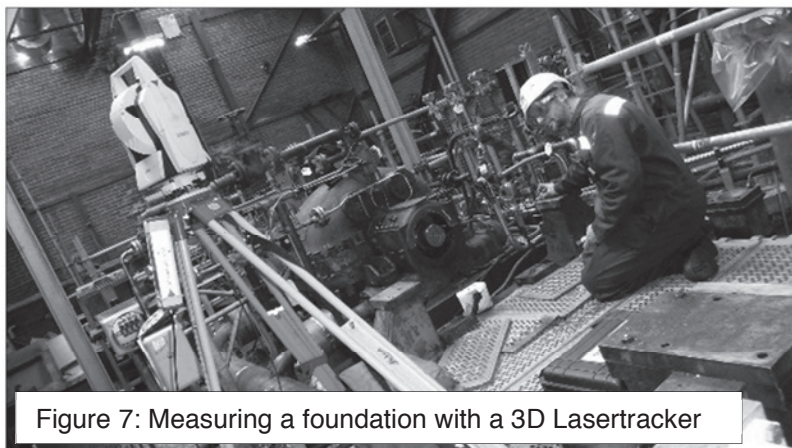


Figure 7: Measuring a foundation with a 3D Lasertracker

For example if the total installation (compressor-driver) is within tolerances in the water-level plane. This information may indicate possible tilting the total foundation. Corrections at the time of re-installation need to be

addressed as early as possible. The consequences are to be considered from case to case.

If the old anchor bolts are to be removed, the 3D measurement data is used to install the machine on the exact same (or improved) coordinates. In case of urgency it is even possible to install the anchor bolts in place before the compressor is back on-site.

## 4.2 Soleplates

Not all reciprocating compressors are installed with soleplates under e.g. the crosshead supports. Some compressor configurations require some free horizontal movement of the crosshead due to thermal expansion. This will be indicated by the compressor manufacturer. Soleplates (in these configurations called sliding plates) or bending plates allow these movements, while grouts will crack.

Another big advantage of installing soleplates, is the ease of removal of the crosshead-support without having the grout to be jacked away. Especially since nowadays high performance epoxy grouts are advised, it will save a lot of time and money if one does not have to jack away and replace the grouting. Furthermore, precision alignments are easier to perform at any later moment.

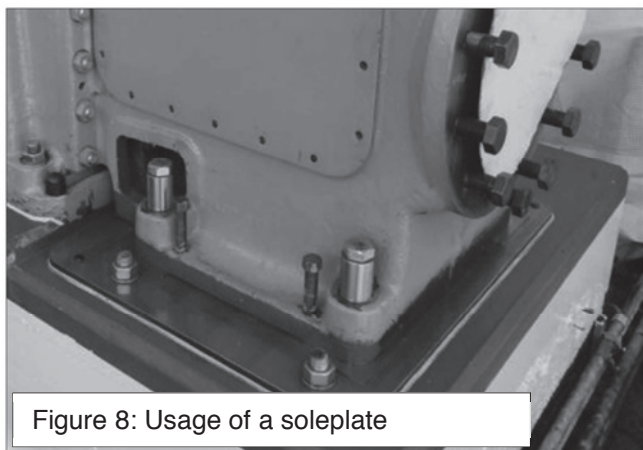


Figure 8: Usage of a soleplate

When designing soleplates it is important to avoid sharp corners (otherwise the grout will crack) and include a good jacking solution (levelling bolts) Also, the design should be stiff and there must be a possibility to conserve the soleplate on-site, depending on location and local coating specifications.

In some cases it is also required to adapt a special anchoring system with coupling, so it becomes possible to loosen the extension and slide it away. This is required for many reciprocating compressor models, otherwise it will not be possible to remove the extension.

### 4.3 Method of alignment

Unfortunately, adjustable jacks, steel shim blocks or wedges are still frequently advised to be used for alignment of pumps, skids, base-frames or even compressors.

These steel jacks make the equipment stand on 'high heels', forming a direct steel contact between machine-frame and concrete foundation. Instead of having the necessary constant compression on the grout, the machinery stands on non-compressive steel blocks, which allows oil and water to penetrate. The anchors nor the grout can function according to their design as pre-tension is lost on the steel jacks and grout is merely an aesthetic cover. Furthermore, these parts are subjected to corrosion which jeopardizes the alignment. Leaving (adjustable) alignment tools in place is strongly dis-advised. (API RP 686). [3]

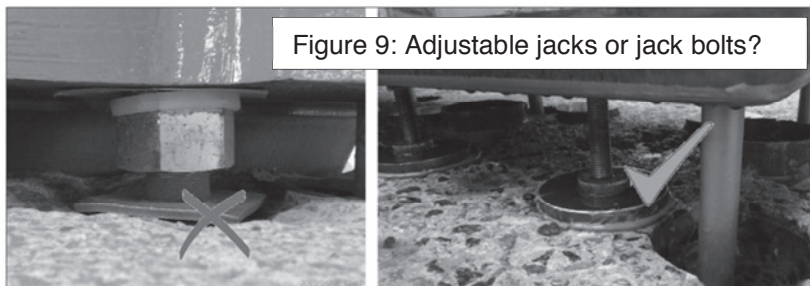


Figure 9: Adjustable jacks or jack bolts?

are subjected to corrosion which jeopardizes the alignment. Leaving (adjustable) alignment tools in place is strongly dis-advised. (API RP 686). [3]

The only correct solution is to use jack-bolts. They are easy to apply in soleplates, skids or

frames. The bolts are removed after full cure of the grout, followed by proper torqueing of the anchors. Jack bolts should be engineered to carry full weight of the machine skid under all conditions expected during skid levelling.

On the concrete foundation, a round metal landing pad should be placed to carry the jacking screw. The design of the pad is stainless steel with rounded edges and can be found in the API RP 686.

### 4.4 Anchoring

Anchor pockets are to be drilled according to the calculated anchor data. Besides the fact that the adhesive surface of the pocket is determinative, the diameter to be drilled is also to be chosen based on the existing situation of the old anchor. Is it only the anchor that is to be removed, or is there also a metal sleeve or a hammerhead construction that is to be removed?



Figure 10: Installation of compressor with anchors hanging free

Best practice for anchor bolt installation is to have the anchors hanging free, and centered, from the machine feet into the pockets before grouting them. This method guarantees correct height and position, without touching the concrete. An equal space between anchor and machine-foot-hole is obtained which makes the necessary alignment possible.

A group of anchors, such as installed in the frame, should perform all as equal as possible. It should be avoided to have 1 or 2 anchors apply excessively more or less load than the others; a deviation of less than 10% is best practice. For this reason it is to be avoided to replace one or two anchors only, leaving the others in place.



## 4.5. Grouting

According to API RP 686 and other recommendations, epoxy-grouts are always best practice for reciprocating compressor systems.

Epoxy grout has many advantages over cement grout, however there are also some issues. If the application is done by a certified and experienced company, these difficulties will have no negative influence. Inexperienced applicators will face some unexpected situations what will lead to problems. Some examples of essential concerns:

- Creep calculation;
- Temperature limitations;
- Mixing techniques;
- Usage of expansion joints;
- Edge lifting;
- Temperature during application;

## 4.6. Injection of cracks

As explained in chapters 2.1.5 and 2.1.7, there is a big difference in cracks in grouting and cracks or cold joints in the concrete foundation.

### Cracks in the cement grout layer

Although in the past attempts have been made to inject cracks in grouting with low viscosity epoxy, the results are generally very disappointing due to the poor quality of the cementitious grout. Replacing the grout layer with epoxy-grout is the best option.

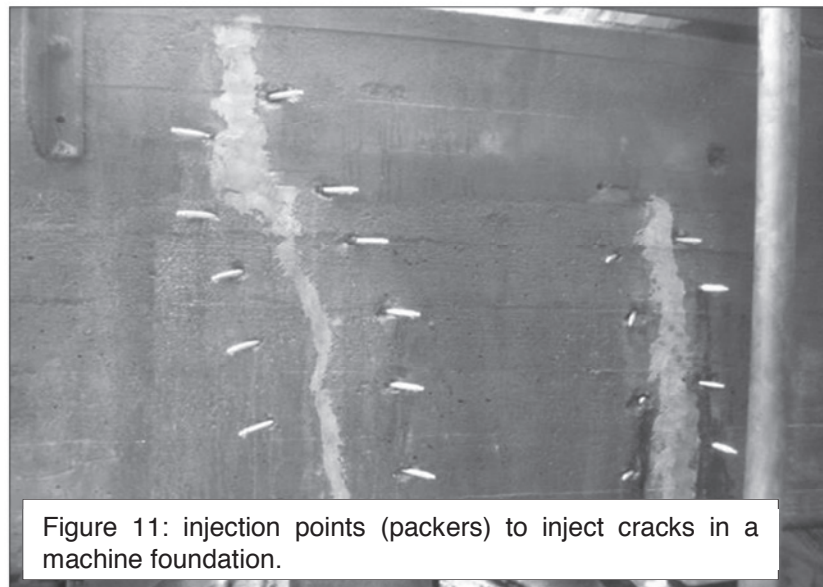


Figure 11: injection points (packers) to inject cracks in a machine foundation.

### Cracks in the foundation

Vertical cracks running in corners and along the sump are easily to be injected with low viscosity epoxy. Low pressure pumping in a slow rate will push the majority of oil and water out.

Special epoxies absorb a considerable amount of oil and water as well. Stone pockets will be filled.

Horizontal cracks or cold joints reduce the possibility to transmit vibrations into the mat (ref. 2.1.7). Due to the on-going vibrations, a clearance at this plane is created in the foundation. This creates two 'separated' parts in the foundation. Injection of these cracks with an epoxy will not be satisfactory since these horizontal disconnections require additional compressive strength in order to bring the 'separated parts together again'. Therefore, long anchors (pull anchors, see figure 6) are to be installed across the cold joint making the foundation monolithic again.



## Epilogue

We hope that this paper will give some guidance in a situation where problems with foundation or anchoring of a reciprocating compressor system are suspected. For ease of understanding, more extensive data and details are avoided, but these can be found in the applicable guidelines.

Several international standards, guidelines and best practices on the design of foundations, anchors and grouting of reciprocating compressor systems have been developed. Unfortunately, most of this material is not available for everybody, is too extended or not directly applicable.

For that reason an EFRC project was started entitled: "Summary of international guidelines, standards and best practices of foundations, anchors and grouting of reciprocating compressor systems". This study gives a comprehensive summary of international guidelines, standards and best practices of foundations, anchors and grouting of reciprocating compressor systems.

This document is intended to be used by rotating equipment and civil engineers of end users, packagers, EPC contractors, grouting companies and reciprocating compressor OEM's. The document can be downloaded from the EFRC website ([www.recip.org](http://www.recip.org)) at the end of 2016. [1]

In addition to this a "Best Practices in Compressor mounting" A thorough study has been presented by Jim Kuly at the 7th EFRC Conference in 2010, Florence. [2]

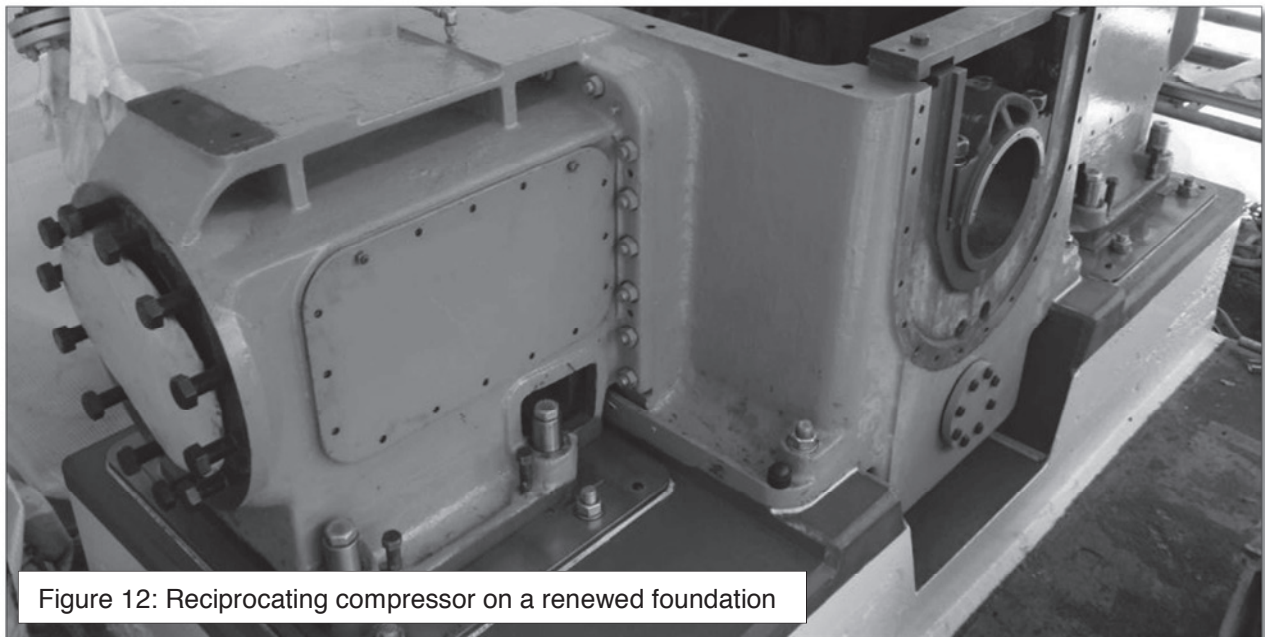


Figure 12: Reciprocating compressor on a renewed foundation



## References

- [1] EFRC project: "Summary of international guidelines, standards and best practices of foundations, anchors and grouting of reciprocating compressor systems" ([www.recip.org](http://www.recip.org))
- [2] EFRC paper "Best Practices in Compressor Mounting"  
James A.Kuly, October 2010 Florence, Italy  
ITW/ Polymer Technologies, USA, at the occasion of the 7th EFRC Conference,
- [3] "Recommended Practice for Machinery Installation and Installation Design "  
API Recommended Practice 686 second edition, December 2009  
Ref 5.4.2
- [4] GMRC Technical Report "Foundation Guidelines"  
A. J. Smalley P. J. Pantermuehl, January 1997  
Mechanical and Fluids Engineering Division Southwest Research Institute  
Report No. TR-97-2
- [5] GMRC Guideline For High-Speed Reciprocating Compressor Packages For Natural Gas Transmission & Storage Applications, October 7, 2013 Gas Machinery Research Council ACI Services Inc.
- [6] "Experimental and numerical investigation of dynamic rocking foundation behavior"  
Phipps, Jacob Nathan (2013). Graduate Theses and Dissertations.  
Paper 13615
- [7] EFRC project: "Guidelines for Vibrations in Reciprocating Compressor systems"  
European Forum Reciprocating Compressors (EFRC), November 2009
- [8] "Sulfate attack in concrete and mortar"  
An abstract from the book 'Understanding Cement' ISBN-13: 978-0-9571045-2-5
- [9] "Polymers in Concrete", 1994  
Satish Chandra, Yoshihiko Ohama  
ISBN-13: 978-0849348150
- [10] "Effect of Crude Oil Spill on Compressive Strength of Concrete Materials"  
Ejeh, S.P. and Uche. Journal of Applied Sciences  
Research: 1756-1761.2009
- [11] "Mechanical vibration - Evaluation of machine vibration by measurements on non-rotating parts" Part 8: Reciprocating compressor systems'  
BS ISO 10816-8:2014
- [12] EFRC paper "Reciprocating Compressor Foundations They do not last forever"  
R. van Lienen, H.Lankenau, 5th EFRC Conference March 2007, Prague.  
NEAC compressor service GmbH
- [13] "Mechanical vibration - Evaluation of machine vibration by measurements on non-rotating parts" Part 8: Reciprocating compressor systems  
ISO 10816-8:2014







# Technical Paper

**Session: 45-2**

**Session Name: Foundation**

## **Dynamic analysis of a compressor foundation and validation with respect to experimental data**

**Author:**

**Alberto Callerio  
Studio Geotecnico Italiano srl  
20141 Milano, Italy**

**Co-Author:**

**Alfio Bisighini  
Studio Geotecnico Italiano srl  
20141 Milano, Italy**

## Summary

Air Liquide Italia decided for the replacement of a vertical reciprocating compressor for oxygen service in its VR plant, located in Castelnuovo del Garda, Italy.

Numerical analyses of the dynamic response of the compressor rigid block foundation were carried out by means of the computer code DYNA5™ (Novak, 1999) for verification with respect to Standards and vendor requirements.

Potential resonance effects were investigated on the basis of calculation by sensitivity analysis on soil parameters. Being an analysis of the dynamic response of the foundation of vibrating machines frequently affected in practice by the lack of knowledge on input parameters, advantage has been taken, for benchmarking of the numerical model, by the presence of a full functional compressor located nearby, similar to the new unit to be installed. Furthermore, to verify the presence of resonance effects, the dynamic characterization of foundation response was carried out by inducing forced vibration with an electro-mechanical generator, connected to the foundation block of the replaced compressor.

On the basis of the results obtained, the new compressor will be installed by modifying the geometry of the existing foundation without any change to foundation type or compressor room.



## Introduction

The Air Liquide VR plant located in Castelnuovo del Garda (Italy) is an ASU (Air Separation Unit) used for the production of air gases (oxygen, nitrogen, argon). The gaseous oxygen is produced at about 30 bar and compressed up to about 60 bar by two reciprocating compressors, in order to feed the AL oxygen pipeline network, providing oxygen to several customers, mainly represented by ironwork factories.

Originally, two identical vertical reciprocating compressors (named C40-1 and C40-2, two cranks, single stage) were installed inside the same heavy concrete building. The two compressors are directly anchored to two separated concrete foundation blocks, each of them isolated from the footings of the surrounding blast-proof building.

The new compressor (C40-3) is rather similar to the one to be substituted (C40-1), with some differences: maximum discharge pressure increased from 60 bar up to about 70 bar, speed reduced from 595 rpm down to 498 rpm, single acting instead of double acting; capacity and power (1 MW) remain the same. A requirement was to fit the new compressor on the same foundation block, by limiting additional construction works.

Regarding vibration limits, the compressor Vendor specified a vibration velocity threshold at foundation top edge of 2 mm/s r.m.s. (1st - 4th harmonic of compressor speed) as reference for civil design of foundations.

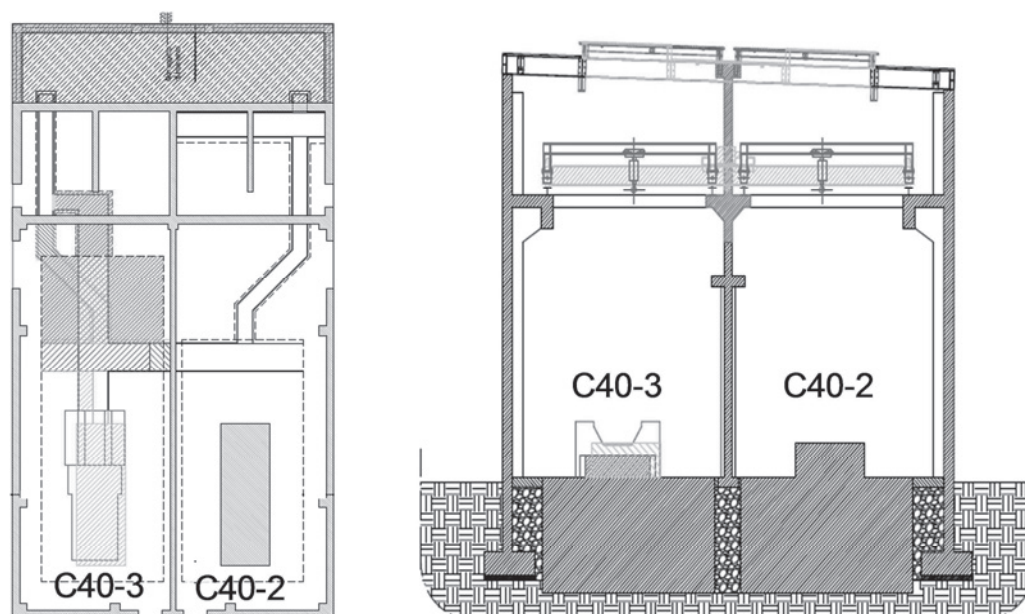


Figure 1: Compressors location. Left: plan view. Right: vertical cross section.

The first step consisted of a detailed analysis of the foundation, in order to assess:

- if the existing foundation was suitable also for the new machine,
- on the contrary, if the existing foundation was to be extended or modified.

In case some modifications would have been required, the operator was interested in evaluating a solution that would not require any modification to the building structure as extension of the existing foundation, installation of micropiles, soil improvement by jet grouting, etc.

## Analysis method

The foundations of vibrating machines are subjected to static and dynamic loads, the latter mainly generated by the rotating/reciprocating masses during functioning. These loads are

characterized by a quasi-harmonic variation of their amplitude with time. In principle, all the load components (6) may vary with different amplitude and phase shift, so the analysis of the foundation response shall take these into account, in order to return the six components of displacement and velocity of the foundation (3 displacement components along the horizontal and vertical axes, plus rotations), generally considered as a rigid block.

In the preliminary phases of design, machine foundations are defined by rules-of-thumb. As an example of these rules, Indian Standard 2974-3 (1992) states that the mass of the foundation shall be greater than that of the machine, eccentricity of loads shall not exceed 5% along each axis, centre of gravity should be below the machine, plus additional requirements on the location of shaft and stability. Another criterion, cited as reference by Gazetas (1983) and ACI-351-3R-04 Standard, states that a massive concrete foundation shall have a total weight equal to at least three to five times the weight of the supported machine. According to P. Srinivasulu et al. (1976) the principal design criteria for a foundation subjected to variable forces is based on natural frequency evaluation (at least 30% away from machine operating speed), amplitude of displacement during functioning ( $< 0.2$  mm), stress (static + dynamic) under the permissible value (in the range of 0.4 times the bearing capacity).

Afterwards, during the detailed design phase, numerical analyses are generally performed to verify the foundation dynamic response in terms of expected vibration amplitudes.

For the case under examination, considering that the foundation block was already present, a verification was carried out by means of the computer code DYNA5™ (Novak, 1999), which returns the response of rigid and potentially flexible foundations to various types of dynamic loads. The stiffness and damping constants of the foundation-soil system are evaluated by the DYNA code for the case of shallow foundations considering the six degrees of freedom as coupled (fully populated stiffness and damping matrices). The halfspace or layered soil media stiffness and damping constants are frequency dependent and evaluated by DYNA using the theory of Veletsos et al. (1971, 1973 and 1974) with soil material damping (viscosity).

The effects of the embedment of the compressor footing (see Figure 1), potentially acting toward a reduction of the induced motion due to lateral confinement, have not been considered in the analyses. In fact, the presence of an isolating foam layer was detected all around the foundation block and the lack of information regarding the effective excavation phases or compaction carried out during construction of machine foundations and building, led us to exclude any potential embedment effect not sufficiently supported by evidence.





## Soil data

A fundamental step in the analysis of vibrating machine foundations consists in the definition of soil dynamic properties. In the analyses carried out, the compressor footing was considered to rest on the surface of a deep homogeneous deposit modelled as either a homogeneous or layered halfspace. The case of layered media has been considered as well, in order to investigate potential resonance effects induced by a soft shallow layer resting on a stiffer formation located below (partially evidenced by the site investigation results). For the purposes of this study, the main soil parameters of interest are:

- The shear modulus  $G_0$  (Pa) for small shear strains ( $\gamma \sim 1E-4 \%$ ), directly related to the apparent velocity of propagation of elastic shear waves  $V_S$  (m/s) by the relationship:

$$G_0 = \rho V_S^2$$

where  $\rho$  ( $\text{Kg/m}^3$ ) represents the mass density.

- The intrinsic damping, generally defined in terms of damping ratio  $\zeta$  (with respect to the critical).

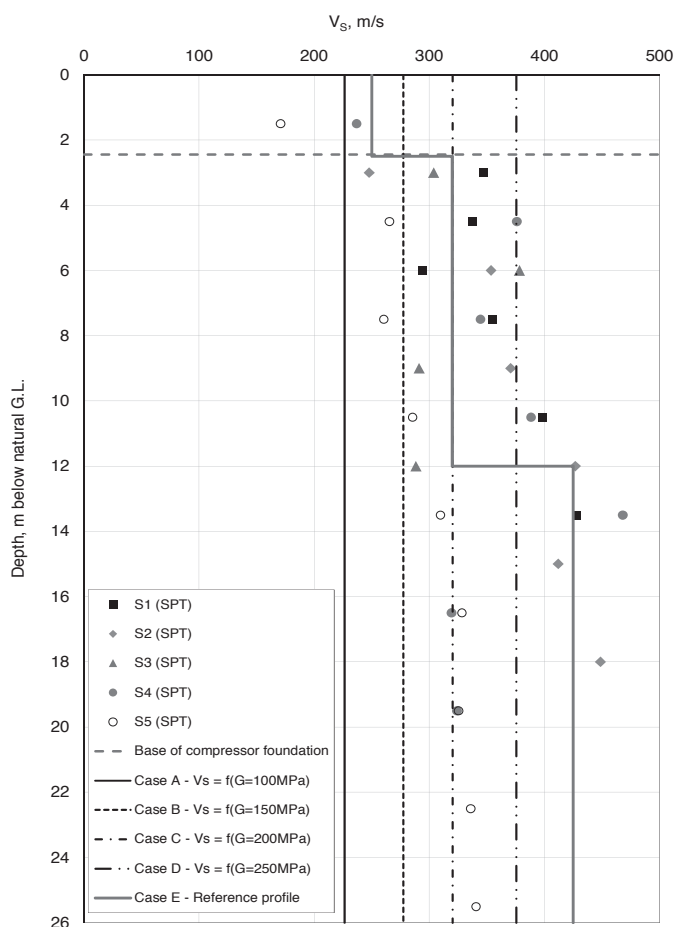


Figure 2: Shear wave profiles and geotechnical data interpretation.

Regarding soil stiffness, only standard geotechnical tests (Standard Penetration Tests, SPT) were performed during the soil investigation campaign conducted in the plant area; ground is characterised by the presence of relatively stiff granular formations. Soil stiffness was estimated on the basis of literature correlations (Ohta & Goto, 1978) on SPTs carried out within a borehole located in the area of the compressor building. The result of the procedure is shown in Figure 2, where a series of reference profiles considered in the analyses are superimposed to SPT correlated data; below the foundation base (-2.5 m with respect to actual ground level)  $V_S$  values resulted in the range of 250 – 450 m/s, with an increasing trend with depth. Considering the uncertainties, a set of values of shear modulus at small strains have been defined as representative within the first 25-30 m of depth, to investigate the sensitivity of foundation response to this parameter:  $G_0 = 100$  (case A, lower bound), 150, 200 (case B and C, best estimate) and 275 MPa (case D, upper bound). An additional case E has been included in the analyses by considering a layered soil with increasing of the stiffness with depth (see reference profile of Figure 2), to investigate potential resonance effects induced by a step variation of stiffness below the compressor.

Concerning the intrinsic damping ratio  $\zeta$  related to energy losses in the soil material, the measurements are generally conducted in laboratory as an example by performing a Resonant Col-

umn Test (RCT) on soil samples. Some attempts have been made to obtain an estimate of the damping ratio from Cross-Hole tests raw data (Lai et al., 2015), although the procedure is still in its initial phases. In this study, reference to literature data was made ([9], [17]): considering the small amplitude of induced shear strains in soil, within the quasi-elastic domain of soil response, it has been assumed a rounded value of  $\zeta=0.01$  (1% with respect to critical). Radiation damping, related to the geometric dissipation of waves due to spreading, is modelled internally by the code itself, considering the prevailing propagation modes, foundation geometry and mass.

### Compressor foundation geometry

The simplified geometry of the foundation input in DYNA is shown in *Figure 3* for both cases considered, i.e. (a) actual geometry and (b) elongated profile aimed at increasing the inertial effects (+50% of mass) according to geometry constraints. The location of the verification points, where the displacement/velocity of the rigid footing were post-processed are also depicted in *Figure 3*. In Table 1, the coordinates of the center of the load system are listed: the crank axis does not contain the centre of mass of the foundation, and therefore a system of additional moments have been input in the analyses.

*Table 1: Coordinates of the centre of the load system with respect to the foundation centre of mass (C.M.).*

	Actual foundation	Elongated
$x_L$	-0.15 m	1.04 m
$y_L$	0.00 m	0.00 m
$z_L$	2.47 m	1.41 m

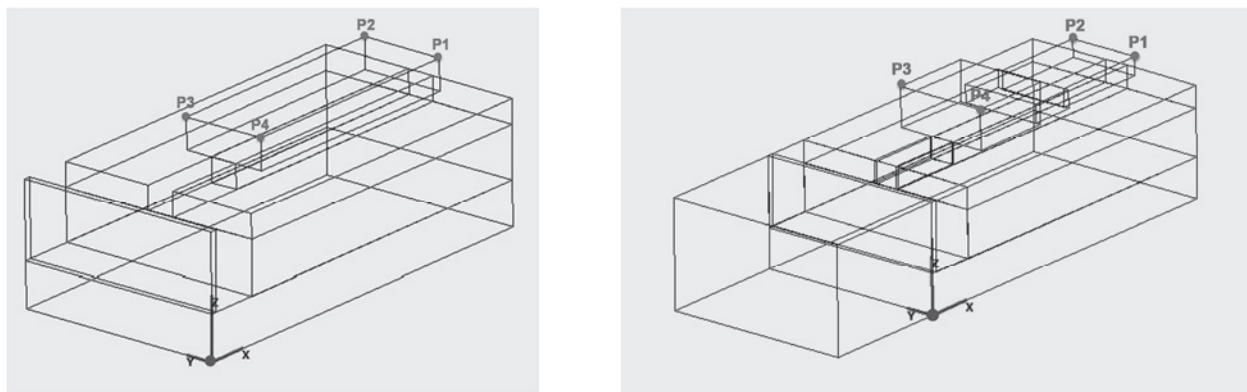


*Figure 3: Geometry of the actual and elongated foundations as input to DYNA. In red the verification points.*

### Load system and analysis cases

Harmonic loading is caused by unbalanced masses of reciprocating machines such as compressors. For each direction of motion, this excitation may have one or more harmonic components (as the case). The harmonic load  $f_i(t)$  acting along the degree of freedom  $i$  can be expressed as function of time  $t$ :

$$f_i(t) = c_0 + \sum_{k=1}^n c_k \cdot \cos(k\omega_i t + \phi_k)$$

where:

- $c_0$  amplitude at time  $t = 0$ ;
- $c_k$  amplitude of the harmonic  $k$ ;
- $\omega_i$  circular frequency of excitation;
- $\phi_k$  angular phase of excitation.
- $n$  number of harmonics.

Amplitude and phases of input loads are listed in Table 2, according to the reference system of Figure 4. The harmonic loads were pre-processed in amplitude and phase for each direction of motion, including rotations and input to DYNA as load time history. The two compressors have different speed, i.e. 585 rpm (C40-2) and 498 rpm (C40-3), equivalent respectively to 9,75 Hz and 8,3 Hz.

The acting loads do not include the contribution of forces arising from pressure pulsations inside the compressor, suction and discharge dampers and piping (anchored to the compressor foundation block through a steel structure). These forces were unknown at the time of this study, since results of pulsation study came only later. As suggested also by the compressor vendor, they were considered as negligible.

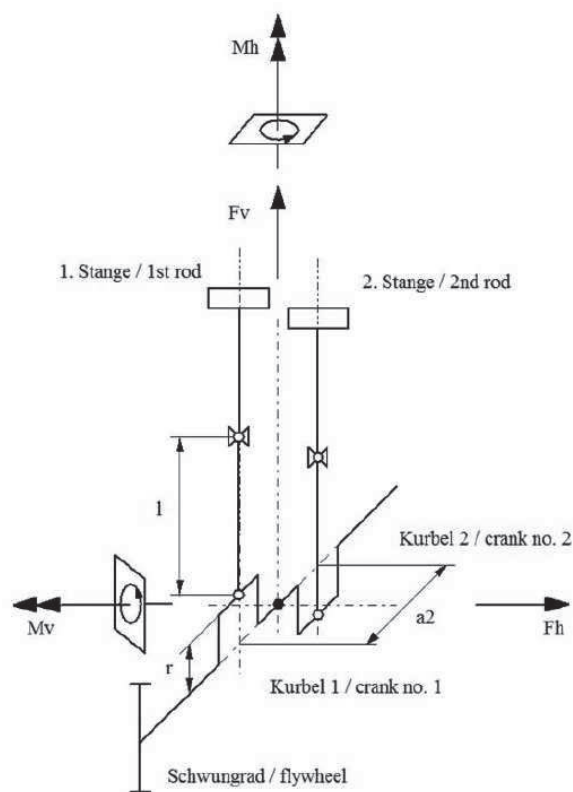


Figure 4: reference system for the load definition

In relation to the characteristic of loads and footing, the following cases were analyzed:

CASE 1: Compressor C40-2, currently in operation (reference case)

CASE 2: Compressor C40-3 under design, and actual geometry of the foundation block.

CASE 3: Compressor C40-3 under design, considering an elongated foundation block.

For each of the above cases, five soil stiffness value/profiles have been investigated (cases A, B, C, D, E, see Section "Soil data" above).

Table 2: Harmonic loads amplitude and phase for compressors C40-2 and C40-3.

Load Component	C40-2 - speed 585 rpm				C40-3 - speed 498 rpm			
	$k = 1$		$k = 2$		$k = 1$		$k = 2$	
	$C$ KN, KNm	$\varphi$ °	$C$ KN, KNm	$\varphi$ °	$C$ KN, KNm	$\varphi$ °	$C$ KN, KNm	$\varphi$ °
Fv	0.00	-	47.84	180.00	0.00	-	59.04	180.00
Mh	30.11	0.00	0.00	-	4.32	180.00	0.00	-
Mv	148.51	90.00	0.00	-	114.99	90.00	0.00	-

Note:  $k$  is the number of harmonic.  $F_h = 0$ .

### Results of the numerical analyses

The results returned by DYNA at the centre of mass of the foundation were post-processed at control points indicated in *Figure 3* under the hypothesis of rigid body motion. A summary of the results obtained from the analyses conducted is listed in Table 3 in terms of peak and r.m.s. (root-mean-square) velocity ranges. In the absence of a preliminary indication of prevalent component of motion, the peak and r.m.s. values of velocity have been calculated on (a) the 3 component of motion separately and (b) the displacement vector. The r.m.s. velocity values obtained were compared to the reference limit in terms of effective velocity of 2 mm/s specified by compressor vendor and DIN 4024 norm, and the following comments apply:

- The r.m.s. (effective) values obtained from the analyses are always within the limit of 2 mm/s, in all the cases examined. In particular, for the existing C40-2 compressor, the calculated r.m.s. velocity lies within 0.72, while for the C40-3 compressor case it is within 1.46 mm/s.
- The peak values occasionally exceed the limit of 2 mm/s for the softest soil profile case, introduced only for comparison purposes but not supported by soil data.
- Velocity at the base of the compressor tends to decrease with increasing soil stiffness; considering the case of  $G_0 = 200$  MPa as the most representative, the C40-3 compressor r.m.s velocity is  $< 1$  mm/s.
- The new compressor C40-3 induced velocities greater by 15-25% with respect to those of the one currently in operation (C40-2). This may be due to the different amplitudes of the rotational load components and, although with less impact, to the different speed of rotation.
- No significant resonance effects are expected in the frequency range from 1 to 30 Hz, even for the case layer media, as confirmed by the measurements conducted (see below).
- Although the r.m.s velocity values calculated for the new compressor are within 50% of the limit for the existent foundation geometry, the elongation of the footing will give a noticeable additional safety margin which was considered worth of attention, considering that in the analyses the potential load due to pressure pulsations has not been taken into account and were unknown at the time of the study.



Table 3: Summary of the numerical results. Ranges of r.m.s and peak velocity.

Velocity, mm/s	CASE 1 Compressor C40-2	CASE 2 Compressor C40-3. Original foundation geometry.	CASE 3 Compressor C40-3. Elongated founda- tion.
r.m.s. (single component)	0.72 - 1.27	0.87 – 1.50	0.71 – 1.08
r.m.s. (vector)	0.74 - 1.46	0.88 – 1.58	0.72 – 1.11
Peak (single component)	1.07 - 1.99	1.27 – 2.30	1.01 – 1.58
Peak (vector)	1.07 - 2.17	1.27 – 2.31	1.04 – 1.61

### Measurements

A campaign of vibration surveys and forced dynamic test was carried out as additional control/verification of the dynamic response of the foundation of compressors C40-2 and C40-3. In particular, the following measurements were carried out at the two compressor locations (C40-2 and C40-3):

- Survey of vibration induced at C40-2 foundation level and ancillary elements during a series of test activations of the compressor, aimed (among the objectives) at verifying the numerical calculation carried out to assess the response of the foundation. These measurements were carried out with compressor unloaded, in order to reduce the effects of pressure pulsations (not considered in the numerical model). The following is noted:
  - The r.m.s. velocity lay within the 0.3-1.1 mm/s range, with a mean value and standard deviation of  $0.475 \pm 0.24$ , in line with the results obtained from the calculations which can be considered as validated by measurements.
  - The above can be considered also as a validation of the calculation carried out for compressor C40-3, currently under installation. After the C40-3 compressor has entered into operation, the execution of a specific measurements survey will permit to validate furthermore the calculation made.
  - The peaks of the measured foundation velocities are generally higher than those estimated through calculation by a factor of 2 at maximum. This is not unexpected, considering the difficulties of calculating a peak quantity which is generally governed by higher frequency component (not investigated by the numerical analyses which, according to requirements, topped at 4th harmonic freq. of load, i.e. < 40 Hz).
- The existing foundation block at C40-3 envisaged location was characterized in terms of dynamic response by means of an electro-mechanical generator of vibration (i.e. “vibrodyne”) capable to generate a system of sinusoidal forces in the frequency range of 1-40 Hz, with adequate amplitude (see Figure 5). On the basis of the results obtained, it was possible to assess the dynamic response of the foundation in terms of fundamental frequencies. In particular, this test was aimed at exploiting potential resonance effects within the investigated range of frequencies of interest (from 0 to 40 Hz) by measuring the variation in phase and amplitude with frequency of the transfer function between load and acceleration component of interest. The main aspects of interest of the method and results obtained are the following:
  - Location of controlling points during test was quite similar to those of the measurements carried out at compressor C40-2. This permitted to put in relation the solution obtained in terms of response of the foundation block, calculation and monitoring (of C40-2 compressor).



- The frequency of the load components (2nd harmonic of vertical load, and 1st harmonic of the rotational component) are generally lower than those of the soil-foundation system determined by means of the forced vibration test (in bold below), i.e.:
  - Fz freq. (k=2) = 16.6 Hz < **21 Hz**
  - My freq. (k=1) = 8.3 Hz < **34-36 Hz**
  - Mz freq. (k=1) = 8.3 Hz < **40 Hz**
- The observed response of the foundation system has been classified as highly damped due to inertial and radiation effects.
- Considering the above, it has been concluded that significant amplification effects due to resonance should not be expected for the case of the new compressor, within the load frequency range of interest.

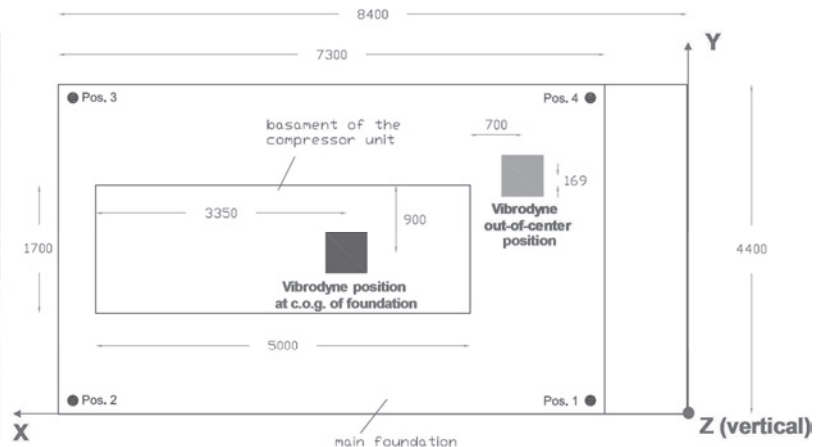
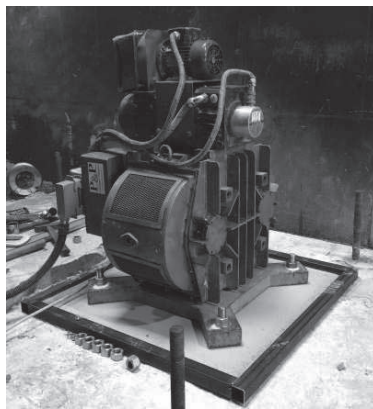


Figure 5: Forced vibration test. Left: dynamic exciter (vibrodyne). Right: layout of measurements.

## Conclusion

The replacement of a vertical compressor demanded for the execution of detailed analysis of the foundation response. The calculation was carried out by taking into account the uncertainties related to soil properties by means of a sensitivity analysis over the soil stiffness parameters of interest.

The presence of a similar adjacent compressor permitted to validate the calculation with respect to the results of experimental measurements. The results obtained from the survey carried out, which comprised the dynamic characterization of foundation block, permitted to conclude that (a) the calculation carried were confirmed and (b) no significant amplification effects due to resonance need to be reasonably expected.

Thanks to the analysis performed, operator had the chance of deciding, with a good confidence, to simply modify the geometry of the existing foundation without any modification to the compressor room, installation of pile or execution of soil improvement which may cause delay to service.



## Bibliography

- [1] ACI Committee 351, ID 351.3R-04, Foundations for Dynamic Equipment, published in 2004, reapproved in 2011.
- [2] Air Liquide, Engineering Practice, Design Criteria for Vibrating Machine Foundation, Ref. G-EP-1-3-2, Rev. 0., July 16<sup>th</sup> 2013.
- [3] Beredugo, Y.O. and Novak, M. (1972b) - "coupled Horizontal and Rocking Vibration of Embedded Footings," Canadian Geotechnical Journal, Vol. 9, No. 4, pp. 477-97.
- [4] DIN 4024, Part 2, Machine foundations – Rigid foundations for machinery subject to periodic vibrations, April 1991.
- [5] EFRC, Guidelines for Vibrations in Reciprocating Compressor Systems, European Forum Reciprocating Compressors, 2009.
- [6] Gazetas, G., Analysis of machine foundation vibrations: state of the art, Soil Dynamics and Earthquake Engineering, 1983, Vol. 2, No. 1.
- [7] Gazetas G., "Formulae & Charts for Impedance Function of Surface and Embedded Foundations", Journal of Geotechnical Engineering, ASCE, Vol.117, No 9, pp.1363-1381, 1991a.
- [8] Gazetas G., "Foundation Vibration", in Foundation Engineering Handbook, Second Edition, Ch. 15, pp. 553-593, 1991b.
- [9] Idriss, I. M., (1990) "Response of Soft Soil Sites during Earthquakes" Proceedings of the Memorial Symposium to honour Professor Harry Bolton Seed, Berkeley, California, Vol. II, May (as cited in the EERA Manual, Bardet et al., 2000).
- [10] Indian standard, code of practice for design and construction of machine foundations part 1 foundation for reciprocating type machines (second revision), November 2007.
- [11] Lai, C.G. and Özcebe, A. G. (2015), Non-Conventional Methods for Measuring Low-Strain Dynamic Properties of Geomaterials, Proc. of 6<sup>th</sup> International Conference on Earthquake Geotechnical Engineering, 1-4 Nov. 2015, Christchurch (NZ).
- [12] Novak, M. And Sachs, K. (1973) - "Torsional and Coupled Vibrations of Embedded Footings," Inter. J. Earthquake Engrg. And Struct. Dyn., Vol.2 No.11, p.33.
- [13] Novak, M. (1974) - "Effect of Soil on Structural Response to Wind and Earthquake," Inter. J. Earthquake Engineering and Struct. Dyn., Vol. 3, No.1, pp. 79-96.
- [14] Novak, M., DYNA 5 – Dynamic Analysis of Foundations for the Effects of Harmonic and Impact Loadings, University of Western Ontario, 1999.
- [15] Ohta Y., Goto N. (1978). Empirical shear wave velocity equations in terms of characteristic soil indexes, Earthquake Engineering and Structural Dynamics, Vol. 6, pp. 167-187.
- [16] Srinivasulu, P., Vaidyanathan, C. V., Handbook of Machine Foundations, McGraw-Hill, 1976.
- [17] Seed, H. B., Idriss, I. M. (1970) "Soil Moduli and Damping Factors for Dynamic Response Analysis", Report No. UCB/EERC-70/10, Earthquake Engineering Research Center, University of California, Berkeley, December, 48 p. (as cited in the EERA Manual, Bardet et al., 2000).
- [18] Veletsos, A.S. and Wei, Y.T. (1971) - "Lateral and Rocking Vibration of Footings," J. Soil Mech. And Found. Div., ASCE, SM9, September, pp. 1227-1248.
- [19] Veletsos, A.S. and Verbic, B. (1973) - "Vibration of Viscoelastic Foundation," J. Earthquake Engrg. And Struct. Dyn., Vol. 2, pp. 87-102.
- [20] Veletsos, A.S. and Nair, V. V. D. (1974) - "Torsional of Vibration of Viscoelastic Foundation," J. Geotech. Div., ASCE, Vol. 100, No. GT3, March, pp. 225-246.





# Technical Paper

**Session: 46-1**

**Session Name: Pulsation / Vibration 2**

## **Non-traditional vibration mitigation methods for reciprocating compressor systems**

**Author:**

**André Eijk**  
TNO  
Heat Transfer and Fluid Dynamics  
2628CA Delft, Netherlands

Co-Author 1:

Dorus de Lange  
TNO  
Heat Transfer and Fluid Dynamics  
2628CA Delft, Netherlands

Co-Author 2:

Jan de Vreugd  
TNO  
Heat Transfer and Fluid Dynamics  
2628CA Delft, Netherlands

Co-Author 3:

Erik Slis  
TNO  
Heat Transfer and Fluid Dynamics  
2628CA Delft, Netherlands

## Summary

Reciprocating compressors generate vibrations caused by pulsation-induced forces, mechanical (unbalanced) free forces and moments, crosshead guide forces and cylinder stretch forces. The traditional way of mitigating the vibration and cyclic stress levels to avoid fatigue failure of parts of the reciprocating compressor system (piping, separators, dampers, and compressor) is to stiffen the structures by e.g. the installation of additional pipe supports or steel structures. This is becoming more and more challenging because compressor speeds are increased, resulting in higher frequencies to be mitigated. Higher frequencies require stiffer structures which is often not possible because the available space and the absence of stiff structures in the vicinity is limited. This is especially the case for high elevated pipe systems, e.g. the pipe between the separator and suction damper.

At mechanical resonance, the damping ratio determines the amplitude of the vibration: more damping decreases the vibration and cyclic stress amplitude leading to lower fatigue failures. Mitigating vibrations of rather low damped systems is possible by applying the concept of constrained layer damping (CLD). The technique has been used for decades in other industries such as the space and automotive industry, but is not often (if at all) used in reciprocating compressor systems up to now.

Another way of mitigating vibrations is the application of a tuned mass damper (TMD) system which is often used in ships, building and bridges. The disadvantage of TMD systems is that fatigue failure of the TMD can occur if not damped sufficiently.

This paper presents the investigative work performed on the potential of using CLD and a TMD for a U-pipe configuration and a pulsation damper. The application of CLD to increase the damping of the TMD to avoid fatigue failure of the TMD is also discussed into detail.

Detailed, material characterization, FE calculations and design optimization has been performed, followed by experiments. By means of measurements it is shown that a large reduction in vibration and cyclic stress levels can be achieved. Reduction factors between 13 and 42 have been achieved with a TMD system and 20 for a CLD application. This paper explains the principle and optimized design of a CLD and damped TMD systems and will show the effectiveness for two different parts of existing reciprocating compressor systems.

## 1. Introduction

Reciprocating compressors are used in the field of oil refining, chemical and petrochemical industries, air separation as well as gas transport and storage. The reciprocating compressor's flexibility to handle wide flow variations, and to generate high head, independent of density make it a vital component in today's energy markets, upstream, midstream, and downstream. Flow variation in time and space make the reciprocating compressor and its responsive piping an intimately connected system, and demand effective system design with respect to vibrations. If mismanaged the pulsed energy input can cause pipe failures, inefficiency, and capacity limitations.

Because the reciprocating compressor system is the heart of an installation it shall therefore operate reliably for the long term operation.

There is a trend in the market to go to higher flows, pressures and compressors speeds. The experience is that it is becoming more challenging to mitigate unacceptable vibrations in the field for higher frequencies (>50 Hz) which require in general stiffer and heavier structures.





However, this is not always possible because of limits in the available space and the absence of stiff structures in the vicinity.

Experience in several projects has shown that it was very difficult to solve the vibration problems with the traditional mitigation measures. This was the reason to start an R&D project of which the target was to investigate the effectiveness of non-traditional mitigation techniques. This R&D project was focusing on the investigation of the concept of constrained layer damping (CLD) and tuned mass damper systems (TMD) for reciprocating compressor systems. Experience has been built up with TMD and CLD for ships and space applications and the knowledge has been used in this project. The target of the project was to optimize the use of CLD and TMD for reciprocating systems which experienced too large vibration levels in the field.

This paper summarises the investigative work performed on the potential of using CLD and a TMD for two different configurations. The first configuration is a U-pipe which is a typical configuration for a pipe between the separator and suction pulsation damper. The second configuration is a large suction pulsation damper of underground gas storage (UGS) system. For both configurations too high vibrations levels were experienced in the field. These large vibrations levels could not be mitigated in an easy way with the traditional vibration mitigation techniques. Measurements have shown that the reduction in dynamic response (vibration and cyclic stress levels) can be increased significantly for both structures with a damped TMD or CLD.

An explanation of the used abbreviations in this paper are as follows:

- CLD: Constrained Layer Damping
- TMD: Tuned Mass Damper
- FRF: Frequency Response Function
- MNF: Mechanical Natural Frequency
- DMA: Dynamic Mechanical Analyser

## 2. Mechanical Vibrations, Tuned Mass Damper systems and Constrained Layer Damping

### ***Background on mechanical vibrations***

General The basic principles of a complex frequency form of solution for a single degree of freedom system (see left hand side picture of Figure 1) with viscous damping are introduced in this chapter [1]. The equation of motion for forced harmonic excitation may be written as:

$$m\ddot{x} + c\dot{x} + kx = Fe^{j\omega t} \quad (1)$$

, where  $x$  is the displacement;  $\dot{x}$  the velocity,  $\ddot{x}$  the acceleration,  $F$  the excitation force,  $\omega$  the circle frequency ( $\omega$  is  $2\pi$  times the excitation frequency  $f$ );  $m$  the mass;  $c$  the viscous damping and  $k$  the spring stiffness

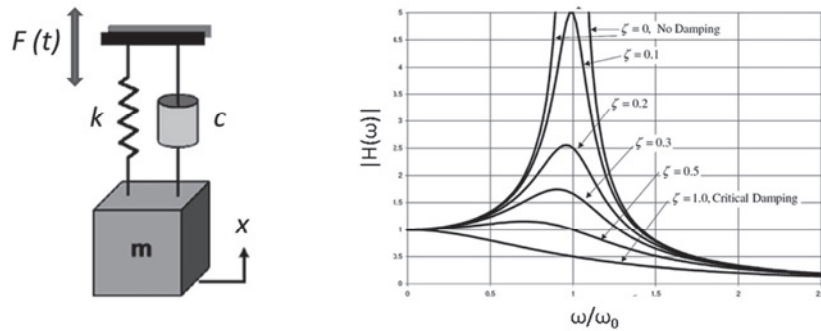


Figure 1 Single degree of freedom system (left picture) and Frequency Response Function (FRF)(right picture)

The right hand side picture of Figure 1 shows the absolute value  $|H(\omega)|$  of the complex frequency response function (FRF) as a function of the dimensionless frequency ratio  $\omega/\omega_0$  for various values of the damping ratio  $\zeta$ .  $\omega$  is the excitation frequency and  $\omega_0$  is the mechanical natural frequency (MNF) and is defined in (2).

If the excitation frequency  $\omega$  equals the mechanical natural frequency ( $\omega=\omega_0$ ), the system is called to be in resonance. At resonance the vibration and cyclic stress levels can be too high leading to fatigue failure. For that reason the resonance shall be avoided or shall be controlled in an adequate way.

The damping ratio  $\zeta$  is defined in (3). Instead of the damping ratio also the loss factor is used which is  $2\zeta$ .

$$\omega_0 = \sqrt{k/m} \quad (2) \quad \zeta = \frac{c}{c_c} = \frac{1}{2} \frac{c}{\sqrt{km}} \quad (3)$$

, where  $m$  is the mass,  $k$  the stiffness,  $c$  the viscous damping ratio and  $c_c$  the critical viscous damping ratio.

It can further be concluded from the FRF of

Figure 1 that increasing the damping ratio  $\zeta$  tends to diminish the amplitudes and to shift the peaks to the left of the vertical through  $\omega/\omega_0 = 1$ . The peaks occur at frequencies given by (4) and the peak value of  $|H(\omega)|$  is given by (5). For light damped systems ( $\zeta < 0.05$ ), which is typically the case for (parts of) compressor systems, the curves are nearly symmetric around the vertical through

$\omega/\omega_0 = 1$  and are given by (6) were  $Q$  is known as the quality or amplification factor.

$$\omega = \omega_0 \sqrt{1 - 2\zeta^2} \quad (4) \quad |H(\omega)| = \frac{1}{2\zeta \sqrt{1 - \zeta^2}} \quad (5) \quad |H(\omega)| \approx \frac{1}{2\zeta} = Q \quad (6)$$



## Background on Constrained Layer Damping (CLD) systems

This chapter only summarizes some basic understanding on constrained layer damping. More detailed explanation can be found in several publications as listed in references [2-13].

For reciprocating compressor systems the damping ratio as discussed in the former section is typically smaller than 5%. A possible method to increase the damping ratio, and consequently also reducing the vibration and cyclic stress levels, can be achieved by the application of a Constrained Layer Damping (CLD). The CLD consists of a “sandwich” which is formed by laminating a damping layer (viscoelastic material) in between two structural constraining base layers, see Figure 2. When the system deforms during vibration, shear strains will be developed in the damping layer and energy is lost through shear deformation of the material.

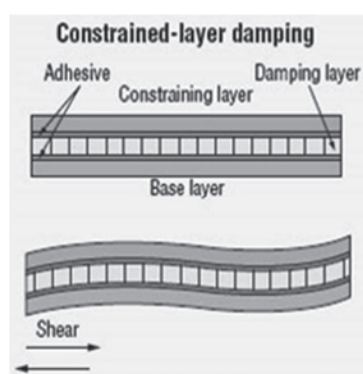


Figure 2 Constrained Layer Damping (CLD)

Viscoelastic material combines the properties of a purely elastic and purely viscous material. For an elastic material the strain and stress response are perfectly in-phase. This results in an elastic energy storage during deformation and all energy is released during relaxation. A viscous material has a 90 degrees phase shift between the strain and stress. This results in all energy being lost in a cycle. A viscoelastic material is somewhere in between the purely elastic and viscous behaviour. The stress strain relation for different materials is shown in Figure 3.

The stress-strain relationship for a linear viscoelastic material under a repeated cyclic loading is for that reason an ellipse, see right hand side picture of Figure 3. The slope of the major axis of the ellipse is a measure of the stiffness and the area is a measure of the damping.

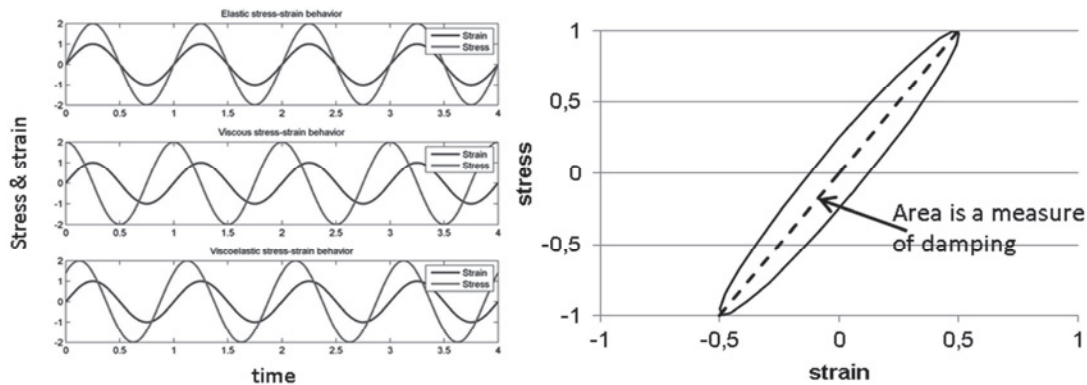


Figure 3 Stress strain relation for different types of materials

The elastic element can be modelled by a linear spring with a stiffness coefficient  $E$  and the viscous element by a dashpot with a coefficient of viscosity  $\eta$ . Hence, viscoelastic models are combinations of linear spring and dashpots. The most common model is the Maxwell model as illustrated in Figure 4.

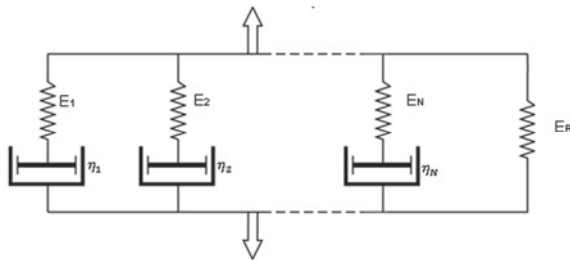


Figure 4 Generalised Maxwell model

The generalized Maxwell modulus is defined in (7) where  $\tau_n$  is the  $n^{th}$  characteristic relaxation time which is defined as  $\tau_n = \eta_n / E_n$ . For the case of a generalized Maxwell element subject to a sinusoidal strain, the (elastic) storage modulus  $E'(\omega)$  and (damping) loss modulus  $E''(\omega)$  take the form as defined in (8) and (9) respectively. The  $\tan(\delta)$  ratio is a measure of material damping. It represents the ability of a material to dissipate mechanical energy by conversion into heat. The  $\tan(\delta)$  ratio is a useful index of material viscoelasticity since it is a ratio of viscous and elastic moduli. The  $\tan(\delta)$  ratio is defined in equation (10).

$$E(t) = E_R \sum_{n=1}^N E_n \exp\left(-\frac{t}{\tau_n}\right) \quad (7) \quad E'(\omega) = E_R + \sum_{n=1}^N \left( \frac{E_n \omega^2 \tau_n^2}{1 + \omega^2 \tau_n^2} \right) \quad (8)$$

$$E''(\omega) = \sum_{n=1}^N \left( \frac{E_n \omega \tau_n}{1 + \omega^2 \tau_n^2} \right) \quad (9) \quad \tan(\delta) = \frac{E''(\omega)}{E'(\omega)} \quad (10)$$

Viscoelastic materials, like polymers and rubbers show large changes in properties with temperature variation.

If well-chosen and used in the right temperature regime, they can possess high damping properties. Prediction of thermal-mechanical stresses and deformations require therefore the input of accurate temperature dependent properties. The damping dependency on temperature is schematically illustrated in Figure



5. At lower temperatures the polymer is in its glassy state, while in the transition region the material possess the highest damping performance and at the high temperatures the polymer behaviour is rubbery like. For these reason the temperature effect of the damping properties shall always be taken into account during the design of a CLD. Figure 6 shows the effect on damping [16] on the application of CLD in space structures.

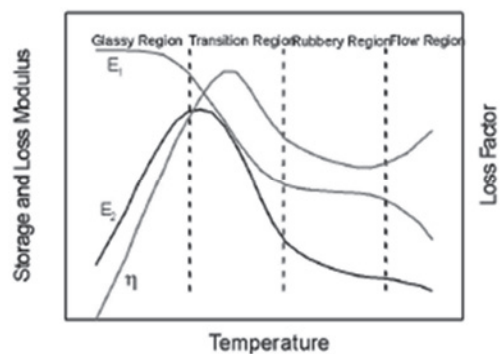


Figure 5 Temperature effect on loss factor

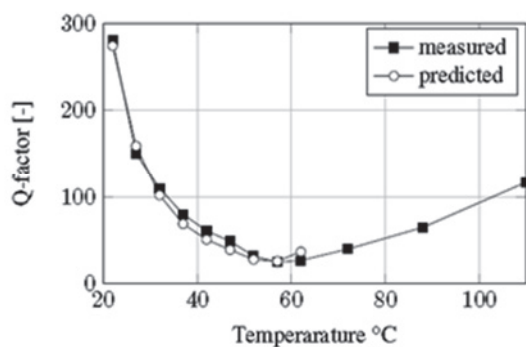


Figure 6 Measured quality factor as a function of temperature for a particular material

The required material data of the viscoelastic material shall be provided by the manufacturer. However, the experience is that the provided data is not always correct or insufficient. It is therefore strongly recommended to measure the required material properties. This is normally done with a Dynamic Mechanical Analyser (DMA).

A DMA [16], also known as dynamic mechanical spectroscopy, is a technique used to study and characterize materials and is very useful for studying the viscoelastic behaviour of polymers. A sinusoidal stress is applied to the sample and the deflection of the specimen is measured, allowing one to determine the material properties such as complex modulus. The measured damping characteristics are implemented in ANSYS [14].



## Background on Tuned Mass Damper (TMD) systems [17-19]

A tuned mass damper (TMD) is a passive device consisting of a mass, a spring, and a damper that is attached to a structure in order to reduce the the vibration and cyclic stress levels of the structure.

The TMD concept was first applied in reducing the rolling motion of ships as well as ship hull vibrations. It is a commonly applied and accepted method in the civil industry for buildings, bridges etc. in general for low frequencies. However, it has not been applied yet for many structures in the oil and gas industry, especially for compressor and pump systems.

The challenge in rotating equipment systems nowadays is the relative high frequency (up to  $\approx 100$  Hz) in comparison with civil structures which can also lead to fatigue failure of the TMD and mounting system. The application of a TMD is for those systems an attractive option in reducing excessive vibrations and the risk of fatigue failures. An example of a TMD is shown in Figure 7 and is typically tuned to the mechanical natural frequency (MNF) of the primary system. The terms  $m_1$ ,  $k_1$ ,  $c_1$ ,  $x_1$  represent respectively the mass, stiffness, damping and displacement of the structure of interest to which the TMD is mounted, while  $m_2$ ,  $k_2$ ,  $c_2$ ,  $x_2$  represent the mass, stiffness, damping and displacement of the TMD and  $F(t)$  represents the excitation force. As the two masses move relative to each other (90 degrees out of phase), the passive damper is stretched and compressed, reducing the vibrations of the structure by increasing its effective damping ratio.

One of the disadvantages of TMD a system is that are typically effective over a narrow frequency band and must be tuned to a particular MNF for that reason. Besides that they are not effective if the structure has several closely spaced MNF's and may even increase the vibration and cyclic stress levels if not tuned well. This can happen if the MNF of the system after the installation of the TMD is shifted to a frequency where the amplitude of the e.g. the pulsation-induced force is larger.

The TMD system shall therefore always be tuned in the field therefore to account for differences between the model and reality. Also the TMD shall always be designed with an adjustable mass and/or spring. If possible, measurement of the MNF's and mode shapes of the structure shall be made which can be used to tune the simulation model.

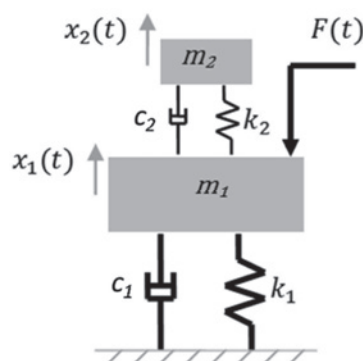


Figure 7 Schematic of a TMD

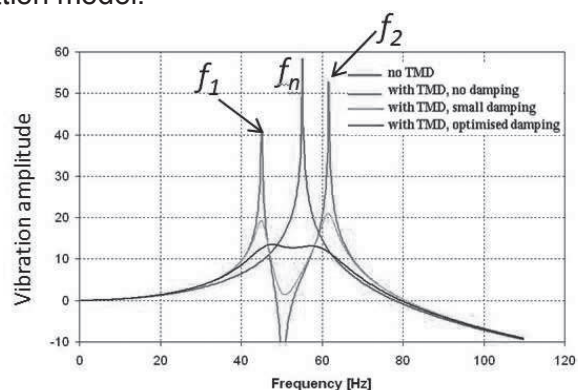


Figure 8 Demonstrating the effectiveness of a TMD

The MNF of the primary system can be split into a lower  $f_1$  and higher  $f_2$  frequency by attaching a spring-mass tuned to the same fundamental natural frequency  $f_n$  of the primary system as shown in Figure 8.



The most significant design variable for the damper is the mass ratio  $\mu$  as defined in (11) where  $m_1$  and  $m_2$  are respectively the mass of the TMD and mass of the structure of interest. When the mass ratio increases, the TMD becomes more effective and robust. In most applications the mass ratio is designed to be in the range of 1-10%. In the design of a TMD, the mechanical natural frequency of the damper  $f_d$  is defined by (12) and, the damping ratio of the damper  $\zeta_{opt}$  can be calculated from (13).

$$\mu = \frac{m_2}{m_1} \quad (11) \quad f_d = \frac{f_n}{1 + \mu} \quad (12) \quad \zeta_{opt} = \sqrt{\frac{3\mu}{8(1 + \mu)^3}} \quad (13)$$

If there is zero damping then resonance occurs at the two undamped resonant frequencies of the combined system  $f_1$  and  $f_2$ . The other extreme case occurs when there is infinite damping, which has the effect of locking the spring  $k_2$ . In this case the system has one degree of freedom with stiffness of  $k_1$  and a mass of  $m_1 + m_2$ .

Using an intermediate value of damping somewhere between these extremes, it is possible to control the vibration of the primary system over a wider frequency range.

The damping of the TMD, which has been investigated in the research program, is achieved by the application of a CLD which is adhesively bonded to the spring, see also Figure 12. The effect of the damped TMD with a CLD will be demonstrated with two examples which will be discussed in the next section.

### 3. Example of a U-pipe configuration

#### *Introduction*

During start-up of a reciprocating compressor system, unallowable vibration levels were experienced in the U-pipe configurations as installed between the separator and suction pulsation damper, see Figure 9. The high vibration levels were measured at 57 Hz perpendicular to the plane of the pipe system. It was measured that the high vibration levels were caused by the excitation of a MNF of 57 Hz by the cylinder stretch displacement of 3 times the compressor speed. This was also calculated during the design of the system but it was not clear why the measured vibration levels were much higher than calculated. From field measurements it was shown that the difference between the calculated and measured vibrations were caused by a much lower damping ratio of 0.8% for both pipes while 2% had been modelled. It was calculated that the high vibrations would lead to fatigue failure. For that reason the system could not be operated up to maximum compressor speed, leading to a loss in production. Acceptable vibration and cyclic stress levels, leading to a safe and reliable system for the long term, can be achieved if the lowest MNF is increased up to 20% above the excitation frequency. This finally lead to a rather stiff structure because of the absence of a stiff structure in close vicinity of the piping, see Figure 10. This was one of the motivations to investigate non-traditional vibration mitigation techniques which are easier and cheaper to install to ensure a reliable, safe and efficient operation for the long term. For that reason the application of a CLD and damped TMD with CLD has been investigated in the research project for such a U-pipe configuration.

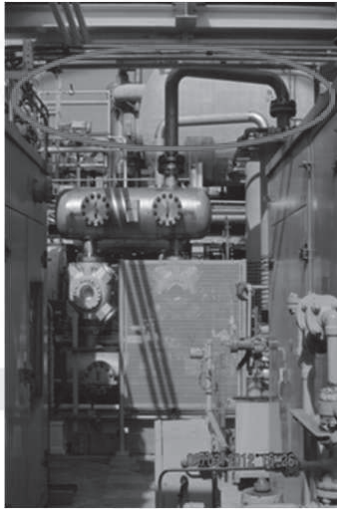


Figure 9 Original as built system      Figure 10 System with additional stiffening

### **Tuned mass damper system (TMD)**

A finite element model of a 6" schedule 40 pipe system has been generated and has been tuned to the measured mode shape. The next step was to design the TMD in such a way that the MNF of 57 Hz of the primary system is split into a lower  $f_1$  and higher  $f_2$  MNF of respectively +20% and -20% around the MNF of 57 Hz. It was calculated that only a very small mass of 2.5 kg (pipe has a weight of  $\approx 65$  kg) was required to achieve this. Moreover a simple leaf spring has been used for the spring and the TMD could be tuned by adjusting the lengthwise position of the of the spring leaf. Because the compressor has a large speed range variation, the two MNF's  $f_1$  and  $f_2$  would always be excited by varying the compressor speed because it was not possible to shift them out of the complete compressor speed range. Without additional damping of the TMD, it was shown that the pipe vibrations would still exceed the allowable level with the TMD installed. Besides that the additional damping was also required to avoid fatigue failure of the TMD itself.

To dampen the vibrations of the pipe and TMD, a CLD was chosen because it has a relative large damping ratio for the complete speed range, is low cost and rather easy to install. The viscoelastic properties of the CLD were measured with the DMA technique [16] and have been implemented in the ANSYS [14] model.

The CLD has been adhesively bonded to both sides of the leaf spring (see also Figure 12) and the dimensions have been further optimised with the ANSYS model. Figure 11 shows the different vibration levels as a function of frequency (FRF: Frequency Response Function) and it can be seen that the TMD is very effective. The ratio of vibration levels of the pipe without (blue line) and with the damped TMD (red dotted line) is approximately a factor of 26. This ratio is based on the fact considering that the frequency  $f_1$  of 45 Hz can also be excited because the compressor can be operated over the entire speed range (worst-case scenario). If the compressor would have a fixed speed, the ratio would be much higher. The vibration and cyclic stress levels will be reduced with the same factor if the pipe is excited with the same force at the frequency  $f_1$  of 45 Hz. Moreover it can be concluded that the ratio in vibration levels with and without the CLD mounted on the TMD is approximately a factor of 3 for the TMD and 2 for the pipe system.

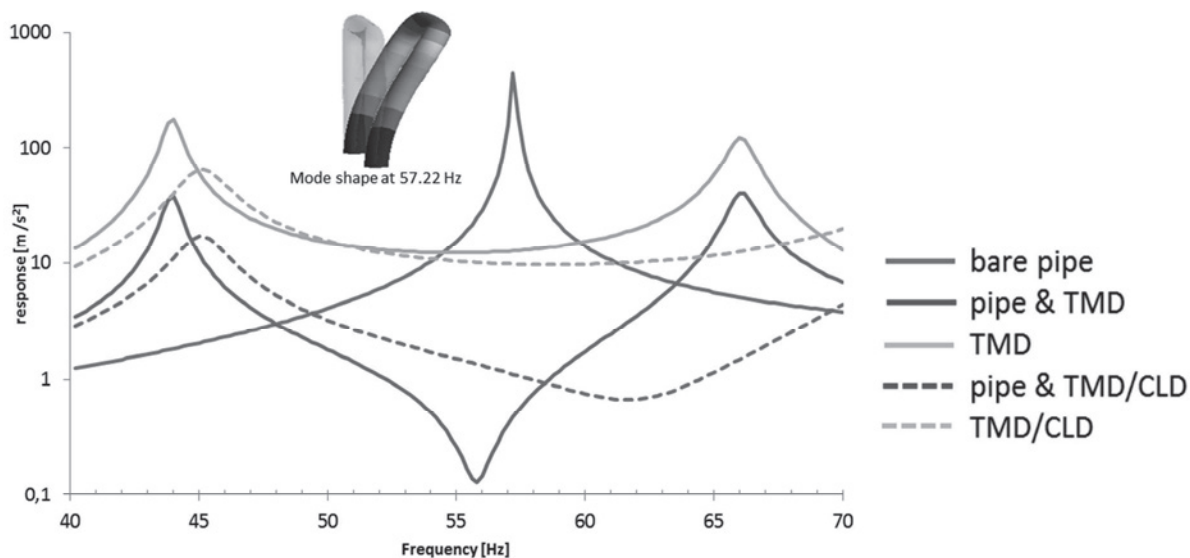


Figure 11 Calculated FRF's for pipe and TMD to tune the mode shape at 57.22 Hz

Measurements have been carried out on the test pipe at the test laboratory with the TMD attached as shown in Figure 12. An impulse hammer excitation method has been used to measure the FRF's. The FRF's of the pipe without and with the TMD are shown in Figure 13. From the FRF's it can be concluded that the measured MNF of the lowest mode shape is 50 Hz instead of the calculated value of 57.22 Hz. This was caused by the flexural flexibility of the mounting plates, causing rotational compliance rather than full fixation. TMD is very effective because the measured ratio in vibration levels with and without the TMD is approximately 42. This is even larger than the calculated value which is probably caused by the flexible mounting plate and means that the model differ from the actual system. Moreover it is noted that the absolute value of the vibration levels from Figure 11 and 13 cannot be compared because the excitation methods are different. So only the ratio of the vibration levels can be compared for that reason.

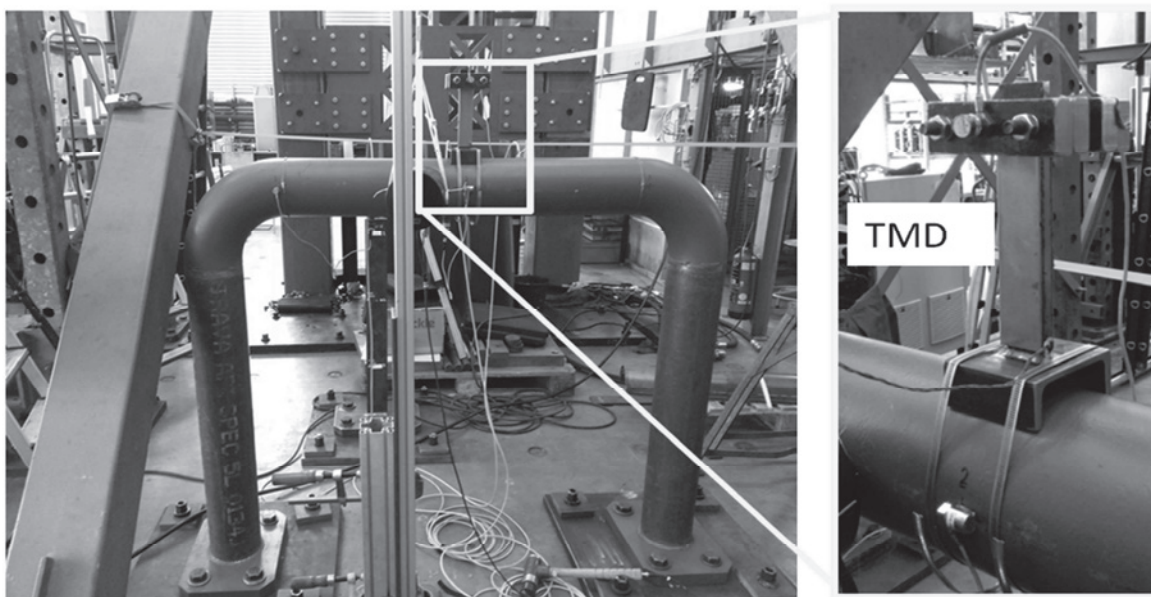




Figure 12 U-pipe with TMD

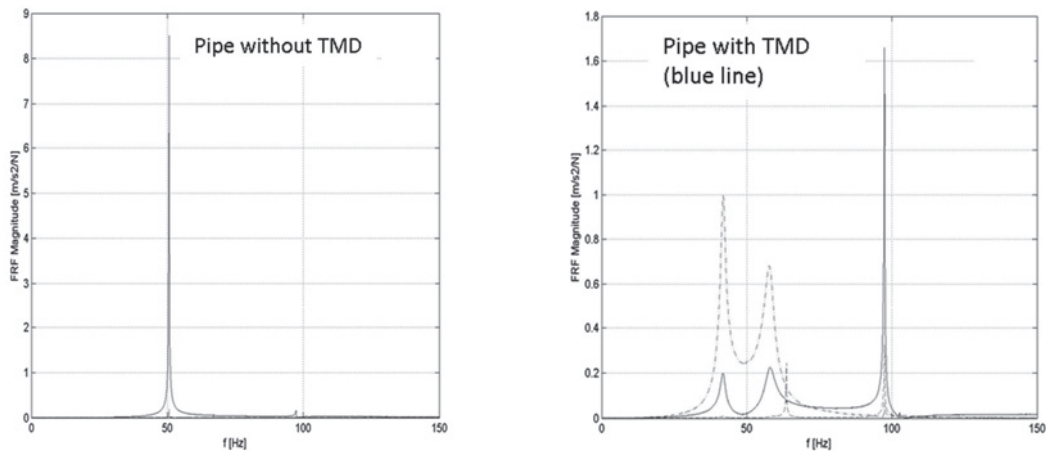


Figure 13 Measured FRF's of bare U-pipe (left) and with TMD (right)

### Constrained layer damping (CLD)

The second method of increasing the damping and so reducing the vibration and cyclic stress levels was the investigation of the effectiveness of CLD added to the pipe. The effectiveness of the CLD is largest when it is mounted on the locations with the largest strain. For the U-pipe the largest strain will occur in the vertical parts at the mounting plates. For that reason the CLD has been mounted on the two vertical straight pipe sections of the U-pipe. The CLD is also very effective because the ratio in vibration levels with and without the CLD is 23 for the mode of interest. This is in the same order of that of the damped TMD, see Figure 11.

Figure 14 shows the test pipe with the CLD adhesively bonded to the vertical parts of the pipe. The measured ratio in vibration levels with and without the CLD is approximately 20 which is in the same order of the calculated value of 26.

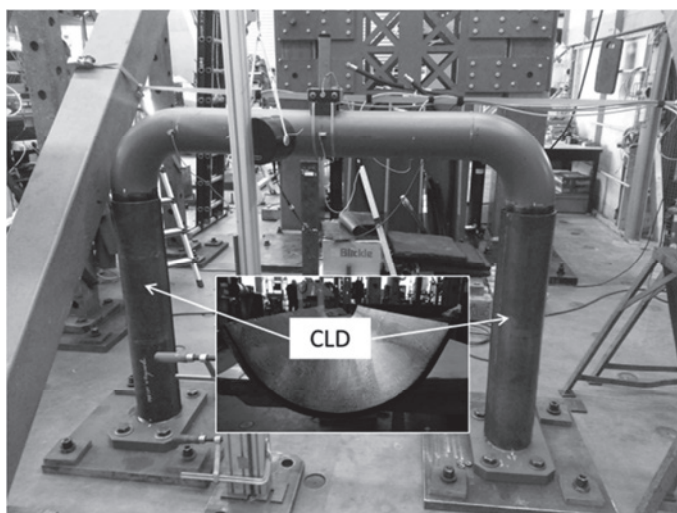


Figure 14 Test pipe including the CLD





#### 4. Example of a large pulsation damper

##### *Introduction*

Inspired by the results of the TMD and CLD of the U-pipe has shown to be very effective the idea was proposed to apply this also for a suction pulsation damper. The reason that a suction damper has been chosen is that severe vibration problems have occurred in several projects with these dampers and it was shown that it is sometimes very difficult to reduce the vibrations in the field to acceptable levels with traditional vibration mitigation measures. Arguably, cylinder stretch is the major source of most of the suction damper vibration problems.

Frequencies between 50-100 Hz have been observed in several projects. In general stiff structures, which support the suction dampers, are applied to shift the MNF far enough from the excitation frequencies. However, because of the rather high frequencies and high elevation of these dampers for large compressors, stiffening is not feasible anymore. For that reason the application of a CLD or a TMD could be a feasible solution to mitigate the vibrations. Unfortunately it was not possible to test this in the field but a spare pulsation damper could be borrowed from RWE for the tests at the laboratory as shown in Figure 15. The damper has a mass of approximately 3000 kg. Preliminary calculations with the application of only CLD attached to the damper have shown that the damping could be increased with a factor of 2 which is much less than the values of the U-pipe. The reduction of vibration levels with a factor of 2 was not enough to achieve acceptable vibration levels. For that reason the focus was on the investigation of applying a damped TMD.



Figure 15 Suction pulsation damper

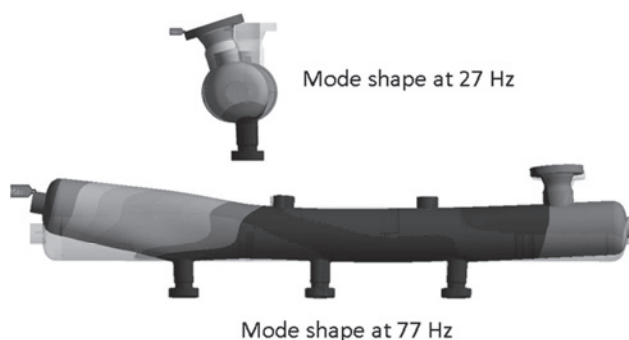


Figure 16 Mode shape at 27 and 77 Hz

A finite element model of the pulsation damper has been generated and two typical mode shapes have been selected for improvement of the system because experience has shown that these modes have exhibited large vibrations problems. The two investigated modes illustrated in Figure 16 are: Rotation of the damper around the cylinder nozzles denoted as mode 1 at 27 Hz; Vertical translation of the overhanging end, denoted as mode 2 at 77 Hz. These are typical modes of such a damper.

Similarly to the TMD of the U-pipe, the first step was to determine the mass of the TMD for the two selected modes. The calculated mass for mode 1 and mode 2 are respectively 75 kg and 20 kg. The target was to apply one TMD system which could be used for both modes. For that reason one geometry was chosen with adjustable masses. The spring of the TMD was a leaf spring with a CLD layer adhesively bonded on both sides. The damping effect of a CLD is largest at the location with the largest strain. This is at the “bottom” of the leaf spring as shown in

Figure 17 and has been achieved by applying a curved geometry at that location. The curved geometry has also the advantage of reducing the cyclic stress in the TMD. A detailed view of the TMD is shown in Figure 17. Figure 18 shows the TMD mounted on the cap of the damper to tune mode 2 (vertical mode). Figure 19 shows the TMD mounted to tune mode 1 (rotation around the nozzles).

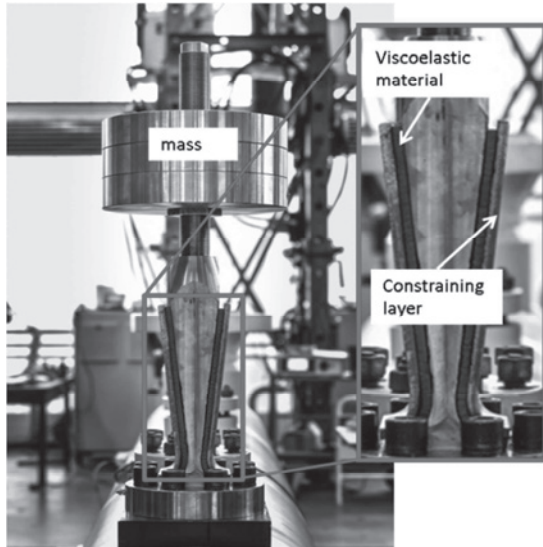


Figure 17 Photo of TMD

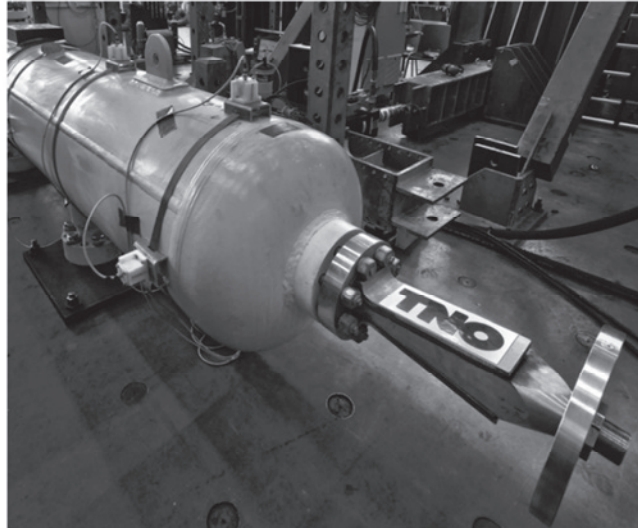


Figure 18 TMD to tune mode 2 (vertical mode)

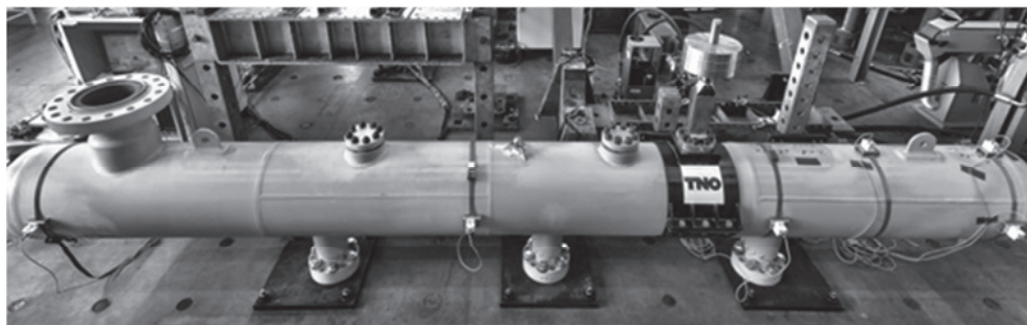


Figure 19 TMD to tuned mode shape 1 (rotation around nozzles)

From the results of the calculations it is shown that the minimum calculated ratio of quality factor of the damper without and with the damped TMD is approximately a factor of 13 for mode 1 and 14 for mode 2.

From the measured FRF's as shown in Figure 20 and Figure 21 it can be concluded that the minimum reduction factor of the vibration levels is 17 for mode 1 ( $f_2$ ) and 13 for mode 2 ( $f_2$ ). This means that the quality of the model is rather good. Moreover it can be concluded from the measurements that the measured frequency of 76 Hz is a local resonance of the baffle choke tube inside the damper. This mode is also damped significantly by the TMD which is a positive side effect and the conclusion is that the application of the damped TMD is very effective. The measured frequencies of mode 1 and mode 2 deviate from the calculated frequencies. As explained for the pipe this is caused by the imperfect clamping of the nozzle end.



After detailed inspection of the TMD it was also concluded that the bonding of the CLD at the foot was not optimal caused by the curvature. The curvature causes a tensile (peel) stress which an adhesive bonding layer cannot handle very well.

It can be concluded that the damping of the TMD with CLD has a very large effect in reducing the vibration and cyclic stress levels. To be able to optimise a TMD it is strongly recommended to measure, if possible, the MNF's in the field.

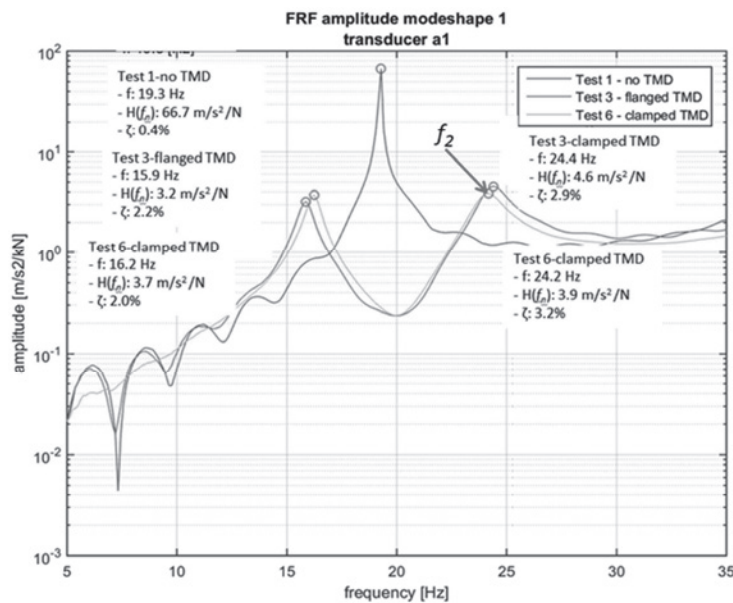


Figure 20 FRF of mode 1 of the pulsation damper

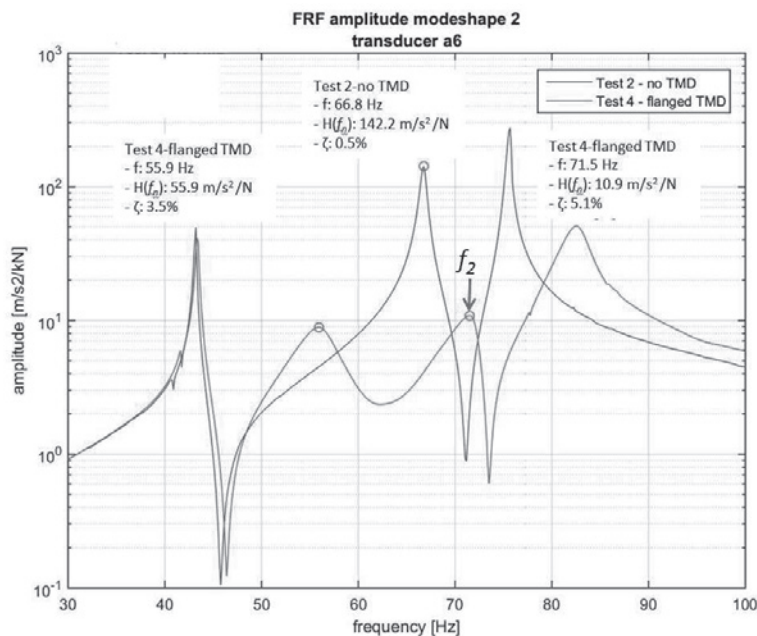


Figure 21 FRF of mode 2 of the pulsation damper

## Conclusions and recommendations

The project has shown that a large reduction in vibration levels of (parts of) reciprocating compressor systems can be achieved with non-traditional vibration mitigation techniques such as CLD and damped TMD's.

The advantages of a CLD are that they are very effective in reducing the risk of fatigue failures at rather low costs. Besides that they are easy to install and are very effective for a large frequency range.

The prediction and optimization of the damping performance after application of CLD can be made by finite element modelling. Such a model requires the input of the viscoelastic properties which shall be measured with a Dynamic Mechanical Analyser. The effect of temperature shall be included in the DMA because the viscoelastic properties are strongly temperature dependent.

Experiments with a U-pipe configuration with CLD have shown a reduction factor of 20. Tests with a damped TMD with CLD, have shown even a larger reduction factor of approximately 42 which is significant.

For larger structures, such as suction pulsation dampers, it is more beneficial to apply a damped TMD instead of a CLD because it is more effective. Moreover, the addition damping of the TMD reduces the risk of fatigue failures of the TMD.

To design the best TMD, the dynamic properties of the system such as mode shape, mechanical natural frequency and damping ratio, must be well known and if possible shall be measured. Moreover the TMD shall be designed in a way that it can be tuned in the field.

Experiments with a large pulsation damper have shown a reduction factor between 13 and 17 depending on the mode of interest for a variable speed compressor. In case of a fixed compressor speed the reduction factor is even much larger and reaches the quality factor at resonance of the original system.

In another research project as carried out recently it was also shown that CLD is a very effective way of mitigation vibrations as experienced in screw and turbo compressor applications where frequencies are generally much higher.

## Acknowledgement

The authors would like to thank RWE Gasspeicher GmbH, for borrowing the pulsation damper.





## References

- [1] Hartog, J. P. D. (1956). Mechanical Vibrations, McGraw-Hill.
- [2] R. Plunkett, C. T. Lee, 1969, Length Optimization for Constrained Viscoelastic Layer Damping.
- [3] Y. LU, 2009, Noise reduction of a refrigerator compressor by applying multiple adjustable constraining bands with damping layers.
- [4] H. Zheng, G.S.H. Pau, G. R. Liu, 2002, Optimization of passive constrained layer damping treatments for vibration control of cylindrical shells.
- [5] Q. Qiu, Z.P. Fang, H.C. Wan, 2006, Transfer function method for frequency response and damping effect of multilayer PCLD on cylindrical shell.
- [6] I. Saidi, A.D. Mohammed, E.F. Gad, J.L. Wilson, N. Haritos, Optimum Design for Passive Tuned Mass Dampers Using Viscoelastic Materials.
- [7] H. Zheng, G.S.H. Pau, G. R. Liu, 2005, Minimizing vibration response of cylindrical shells through layout optimization of passive constrained layer damping treatments..
- [8] J.J. Hollkamp, R.W. Gordon, 1996, An experimental comparison of piezoelectric and constrained layer damping
- [9] E. Balmes, et al, 2010, Constrained viscoelastic damping, test/analysis correlation on an aircraft engine.
- [10] E.M. Kerwin, 1958, Damping of flexural waves by a constrained viscoelastic layer
- [11] D.J. Mead, S. Markus, 1968, The forced vibration of a three-layer, damped sandwich beam with arbitrary boundary conditions.
- [12] R. Taulbee, 2013, Vibro-acoustic analysis of a thin cylindrical shell with minimal passive damping patches.
- [13] C.A. Gallimore, 2008, Passive viscoelastic constrained layer damping application for a small aircraft landing gear system.
- [14] ANSYS reference manual
- [15] J. de Vreugd, D. de Lange, J. Winters, J. Human, F. Kamphues, E. Tabak, "Damping in Space Constructions", Conference on Space Constructions, Materials and Environmental Testing, 2014
- [16] Dynamic Mechanical Analysis: A Practical Introduction, 2nd Edition, Kevin Menard, CRC Press, 2008
- [17] Webster, A.C. and R. Vaicaitis (1992). "Application of Tuned Mass Dampers To Control Vibrations of Composite Floor Systems." Engineering Journal/American Institute of Steel Construction, Q3/1992:116-124
- [18] Al-Hulwah, K. I. (2005). Floor Vibration Control Using Three Degree of Freedom Tuned Mass Dampers. The School of Engineering, University of Dayton. Ph. D. Inman, D. J. (1996). Engineering Vibration, Prentice-Hall, Inc.





[19] Optimum Design for Passive Tuned Mass Dampers Using Viscoelastic Materials Australian Earthquake Engineering Society 2007 Conference (I Saidi<sup>1</sup>, A D Mohammed<sup>2</sup>, E F Gad<sup>1, 3</sup>, J L Wilson<sup>1</sup>, N Haritos<sup>3</sup>).



# Technical Paper

**Session: 46-2**

**Session Name: Pulsation / Vibration 2**

## **Development of a new adaptive pulsation damping device without external energy supply**

**Author:**

**Patrick Tetenborg  
Research Assistant & Project Engineer  
KÖTTER Consulting Engineers GmbH & Co. KG  
48432 Rheine, Germany**

**Co-Author:**

**Andreas Brümmer  
Head of the Chair of Fluidics  
Technische Universität Dortmund  
44227 Dortmund, Germany**

## Summary

In many technical applications or plants the use of reciprocating compressors leads to higher pipeline vibrations, which are often pulsation induced. One typical measure to reduce these pulsations is the installation of orifices or special pulsation damping plates which have the advantage of easy installation in new or existing pipelines. However, the disadvantage of these devices is a significant remaining pressure loss.

With the objective of minimizing this undesirable pressure loss, an adaptive pulsation damper without external energy input (passive) has been developed. This pulsation damper is based on a transient behavior of its pressure loss coefficient. Depending on the pulsations at the inlet side of the new device the flow cross section and therefore the pressure loss coefficient is adapted periodically. The energy required to achieve this periodic motion is taken from the pulsating flow itself. Accordingly, the behavior of the new pulsation damping device only depends on the transient flow, which corresponds to the adaptive characteristics and enables a passive performance.

Within the present paper the working principle of the new pulsation damping device is presented using numerical simulations of an ideal pulsation damping definition. Based on the acquired adaptive principle a first prototype has been designed. This prototype has been built and tested at the closed loop air test rig for pulsating flows at the TU Dortmund. Designing and tuning has been verified by primary investigations of structural dynamic behavior and measured fluid mechanical static operating conditions. Subsequently operating behavior with pulsating flow has been analyzed. Comparisons with a non-damped situation and static damping devices show the advantages of this new development, already signed in as patent.



## 1. Introduction

Reciprocating compressors function by means of a periodical compression process. This periodic behavior leads to high flow and pressure fluctuations during the suction and discharge process. Therefore, acoustic pulsation dampers are usually installed next to the compressor. They achieve an initial significant reduction of induced pulsations to the attached pipe system. The design of these dampers has a massive influence on the achieved attenuation. Large dampers are expensive, which often leads to a compromise between a good damping effect and acceptable costs. This may result in pulsation levels e.g. above the values of the API 618 guideline [1]. In this case further measures are necessary to reduce pulsation.

Various damping principles can be used. An analysis of different reduction measures has shown that dissipative damping is one of the most reliable and effective mechanism [2]. Dissipative installations inside the piping often take the form of orifices, pulsation damper plates [3] or alternatively multi-bore-orifices. The main advantage of this type of device is its low installation complexity and good damping ratio with regard to acoustic resonances. Unfortunately, this pulsation damping principle is associated with a significant remaining pressure loss, which leads to a compromise between acceptable pressure loss and effective pulsation damping. In [4] a variable orifice with changeable loss coefficient has been presented. This makes it possible to change the damping behavior as a function of the current operating point. However, the current damping behavior is no improvement on static devices, and an external energy input is necessary. In 2013 a new research and development project has been initiated between KÖTTER Consulting Engineers and TU Dortmund, aimed at developing a damping device with better operating conditions than state of the art throttle devices. The new device should work adaptively and passively within the oscillation period of the pulsations and without external energy.

## 2. Ideal operating conditions

The damping mechanism of a dissipative damping device is based on the nonlinear dependence between the velocity fluctuation and the pressure drop. To increase the damping ratio stronger throttling is required. The prime disadvantage is the remaining pressure loss as a consequence of the dissipation. This results in a compromise between sufficient damping and acceptable pressure loss. To avoid this compromise advanced damping behavior is required. As a first step towards the new damping device the behavior of an ideal damped pulsation is defined, figure 1.

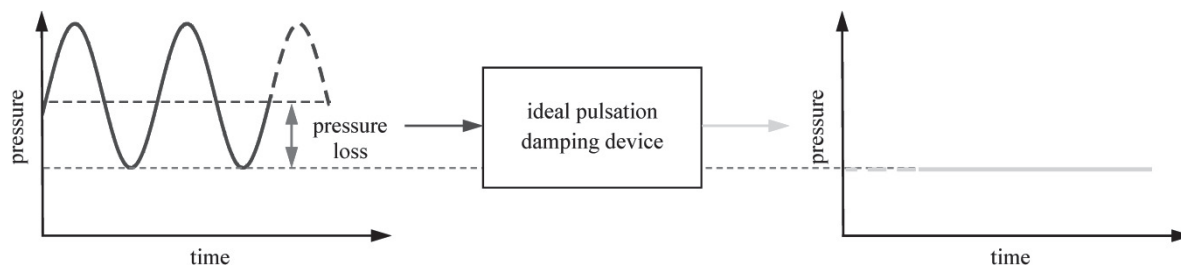


Figure 1: definition of the ideal dissipative pulsation damping behavior

The usage of the word “ideal” here refers to the achievement of a completely steady state condition behind the device. This still includes a remaining pressure loss, because the dissipative damping mechanism is not able to recover lost pressure. This pressure loss is minimized by orientating to the minimal turning point of the upstream pressure fluctuation. This does not mean that pressure pulsations with an amplitude of ten percent of the static pressure result in ten percent static pressure loss. The relevant turning point depends on the new pulsation situation with installed ideal pulsation damping device and therefore with reduced pulsation levels downstream and upstream of the device. Acoustic impedance describes the fundamental correlation between pressure fluctuation and flow fluctuation. Hence the velocity fluctuation behind the pulsation damping device also has to be eliminated.

Due to analytical considerations in case of a non-reflecting boundary condition downstream of the ideal damping device a non-fluctuating pressure just behind the damping device leads to a non-fluctuating velocity too. In the theory of linear acoustics a non-reflected wave is characterized by a constant relationship between pressure and flow fluctuation as a result of acoustic impedance with the fluctuation taking place in phase. Velocity fluctuations will also be eliminated if the existing acoustic power does not traverse the ideal pulsation damping device. Further investigations with a superimposed mean flow are not easy to treat analytically. Therefore, numerical investigations based on the definition of ideal pulsation damping have been carried out in order to acquire an advanced damping behavior. The method of characteristics has been used dealing with the three characteristic equations – continuity equation, momentum conservation and energy conservation. To investigate ideal damping behavior a new interface for the ideal definition of pulsation damping has been developed. This includes a control loop which manipulates the loss coefficient in each time step in order to stabilize the pressure behind the device at a constant level, fig. 2.

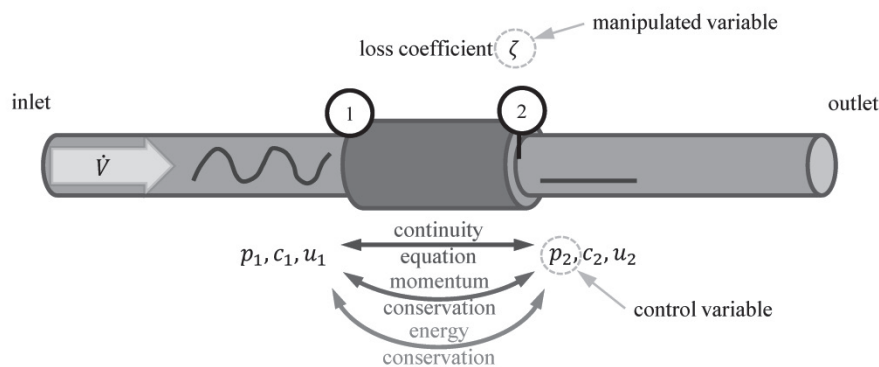


Figure 2: implemented interface in the numerical scheme for analyzing ideal pulsation damping device

The manipulated loss coefficient is part of the momentum conservation employed and has a direct impact on the downstream pressure. The defined reference for the loss coefficient in this implementation is the upstream condition:

$$p_{t,1}(t) - p_{t,2}(t) = \zeta(t) \cdot \rho_1(t) \cdot \frac{c_1(t)^2}{2}$$

To analyze the dynamic behavior in a piping system a one-dimensional model was set up. This includes a pulsation excitation at the inlet of the domain defined by a harmonic pressure fluctuation and a constant velocity at the outlet boundary, fig. 3. The boundary conditions conform to a low-impedance inlet boundary and an acoustically hard boundary at the outlet.





Excellent damping performance is achieved for resonant pulsation problems. Therefore, the length of the model is 17.5 m and the excitation frequency is about 15 Hz. This matches the  $\frac{3}{4} \lambda$  resonance of the system for nearly ambient conditions and medium air characteristics. The simulated pressure and velocity fluctuation for the original system without the ideal damping device are shown by the dashed envelopes in fig. 3. Subsequently the simulation was carried out with the damping device positioned next to the maximum velocity fluctuations. The resulting envelopes confirm the ideal damping behavior desired.

In the next step an adaptation principle had to be found for converting this dynamic damping behavior into a viable construction. This was detected by correlating the periodic static differential pressure and the dynamic loss coefficient along the ideal damping interface, fig. 4.

$$\frac{\Delta p(t)}{\zeta(t)} = \frac{p_1(t) - p_2(t)}{\zeta(t)} \approx const.$$

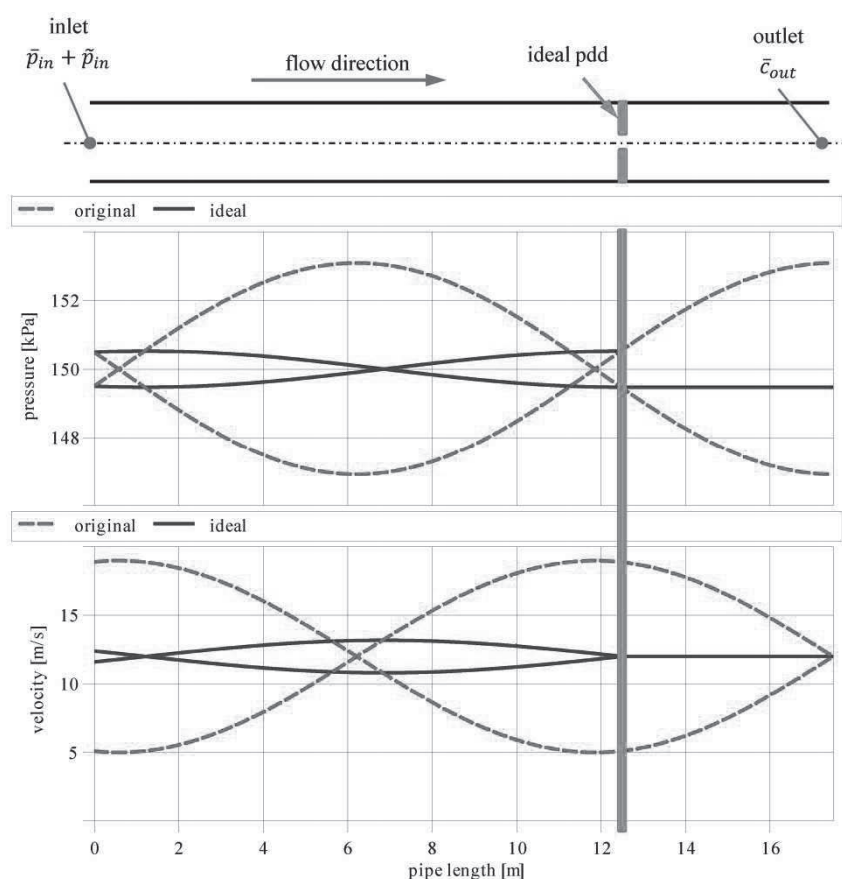


Figure 3: envelopes of the local pressure and velocity fluctuation along a pipe for a harmonic excitation (original  $\triangleq$  without damping device; ideal  $\triangleq$  with installed damping device)

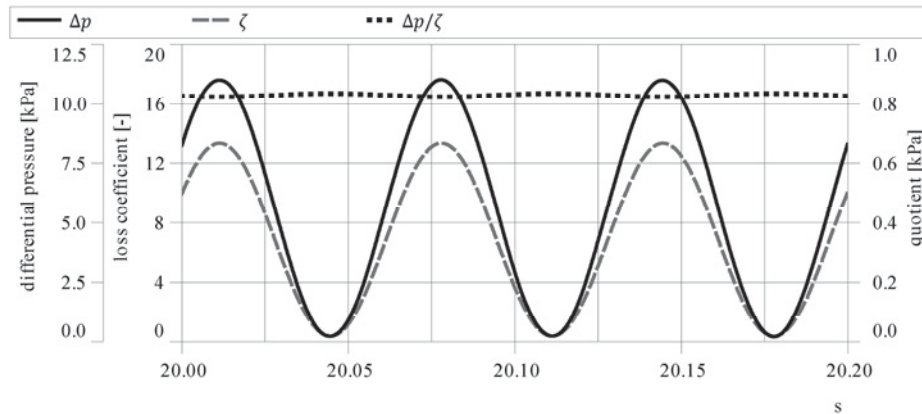


Figure 4: time signal of differential pressure, loss coefficient and their quotient

This adaptation principle results from the fact that the total pressure difference is almost equal to static differential pressure and takes into account the eliminated velocity fluctuations just in front of the ideal pulsation damping device. The ideal damping interface matches to the sound reflection behavior of an acoustically hard boundary. Another result of this behavior is the virtually exact validity of the quotient:

$$\frac{\Delta p(t)}{\zeta(t)} = \frac{1}{2} \cdot \rho_1 \cdot \bar{c}_1^2 = \text{const.}$$

The resulting quotient of the differential pressure and the loss coefficient is also known as dynamic pressure.

### 3. Design of prototype

The derived adaptation principle has to be converted into a functional concept for constructing a corresponding adaptive and passive pulsation damping device, fig. 5. Due to the already described dependencies it makes sense to use the local pressure up- and downstream the pulsation damping device as forces by using adequate areas. These forces can be handled as excitation forces on a moveable structure. The motion of the structure achieves a dynamic loss coefficient. This dynamic coefficient results from a changing flow cross section.

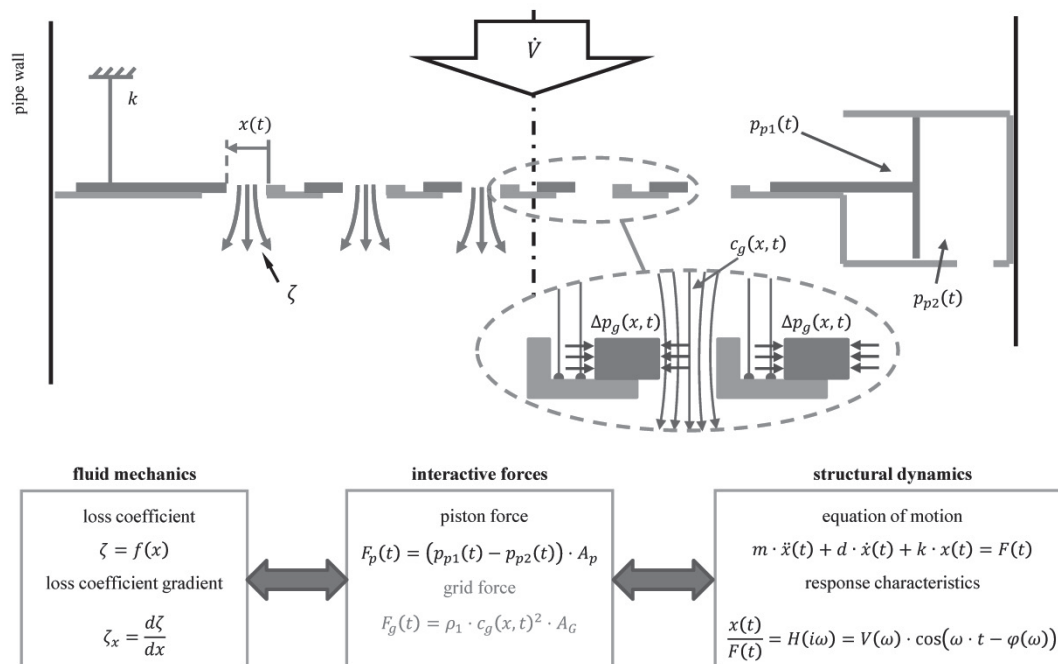


Figure 5: concept for the adaptive and passive pulsation damping device

The damping device consists of a fixed and a moveable part. The fixed part has a fixed piping installation. This consists of a grid with a defined distance between bars and a cylinder. A moveable counterpart of the grid permits a dynamically changing flow cross section. The moveable part is attached to the fixed installation by adjustable leaf springs with spring constant  $k$  and is coupled to a piston which is installed inside the cylinder. The front of the piston is connected to the upstream fluid condition  $p_{p1}$ , while the back is connected to the downstream fluid condition  $p_{p2}$ . This generates the necessary adaptive force for the grid motion. This motion changes the flow cross section and achieves the required dynamic loss coefficient. In general, the piston forces should suffice to achieve adaptive and passive damping behavior. Unfortunately at the available test rig with pressure nearly ambient conditions, they are pretty small. Therefore, additional forces along the grid bars may be used. They relate to the pressure difference between the two sides of the bars, resulting from the stagnation pressure on one side and the reduced static pressure on the other side. This additional force is not part of the analyzed working principle of the device but necessary due to the low static pressure. In general it is quite easy to avoid this force by installation of the moveable grid on the downstream side. The structure has to be tuned to a high eigen frequency to guarantee in-phase movement to the adaptive excitation forces, cf. [5]. This leads to a light-weight structure of the moveable part with minor inertia because of low allowable stiffness regarding the low excitation.

The behavior of the different physical aspects and the adaptive and passive principle must be integrated with each other in order to design a well operating prototype. Therefore, the quotient of differential pressure and loss coefficient is depicted in terms of the fluid mechanical, structural dynamical and interacting behavior of the pulsation damping device shown in figure 5.

$$\frac{\Delta p(t)}{\zeta(t)} = \frac{1}{\zeta_x \cdot A_p \cdot H(i\omega)} = \frac{1}{2} \cdot \rho_1 \cdot \bar{c}_1^2$$

This designing formulation ignored the unwanted grid forces. Two dimensional flow simulations with different deflections of the grid have been realized for the design process of the first

prototype. The results have been used to define the dimensions of the fixed and moveable grid and permit a prediction of loss coefficient gradient. Subsequently the maximal usable size of a piston in the construction was specified. The only missing variable is the response characteristic, knowing the volume flow and the fluid conditions. This has been pre described by an analytical beam model. The accuracy of this analytical model is not vitally important because a large range of free length for the leaf springs has been included in the construction.

#### 4. Prototype

The concept described above enables the realization of a usable adaptive and passive pulsation damping device. The prototype is a special lightweight construction using a moveable carbon grid, a carbon piston and all other moving parts made of aluminum, fig. 6.

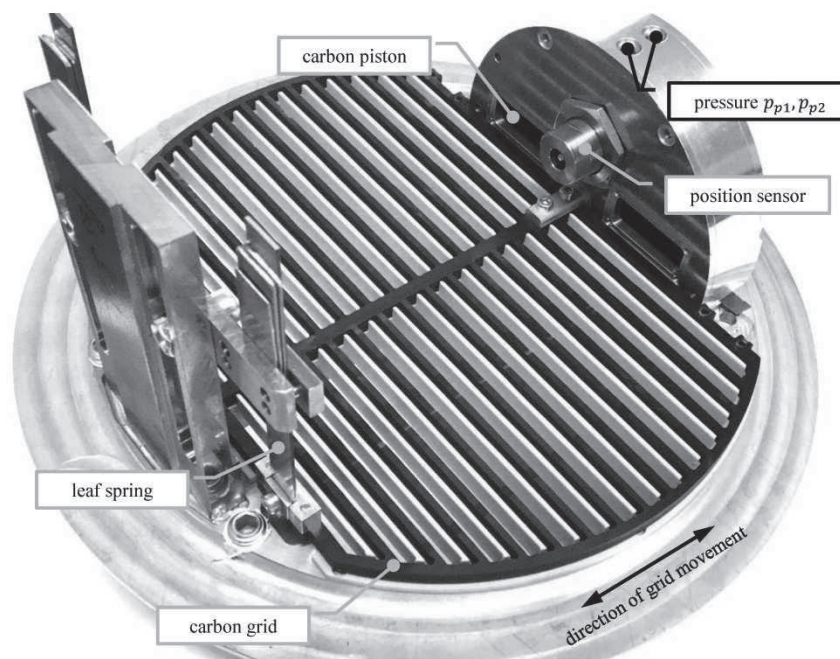


Figure 6: prototype of the adaptive and passive pulsation damping device

This permits the low pressure application with high flexibility and acceptable eigen frequency. The grid possesses 15 slits with a maximum width of 5 mm. The maximum deflection of the dynamic grid is 2 mm, which corresponds with a minimum width of the free flow cross section of 3 mm. This results in an area ratio of:

$$\alpha = \frac{A_{grid}}{A_{pipe}} = 0,230 \dots 0,384$$

The important values for the adaptive forces are the available piston and grid bar areas. The piston has a diameter of 100 mm corresponding to an area of 7850 mm<sup>2</sup>. The current height of the grid bars is 5 mm, corresponding to an area of 12850 mm<sup>2</sup>. A thinner grid with a height about 2 mm corresponding to an area of 5140 mm<sup>2</sup> will be examined shortly. This should make it possible to balance the influence of the grid forces. A further advantage is the lower weight, getting a small beneficial eigen frequency shift. Two pressure sensors are installed inside the cylinder and a position sensor detects the dynamic grid motion in order to provide detailed information about the operating behavior.



## 5. Test rig and experimental setup

Investigations of the new adaptive and passive pulsation damping device are carried out at the closed loop air test rig for pulsating flow at the Chair of Fluidics at the TU Dortmund. The test rig has been built for a number of investigations dealing with steady-state and unsteady phenomena of fluid mechanics.

It is equipped with two positive displacement compressors attached to two vessels – suction and discharge side -, a cooler and a pressure regulator. The installed screw compressor can handle high pressure levels up to eight bar at a low volume flow of 500 m<sup>3</sup>/h. The roots blower does only operate on ambient conditions at the suction side, and can achieve a differential pressure of 800 mbar at a maximum volume flow of 2000 m<sup>3</sup>/h. For measuring the current mean flow a reference measurement section is included in the test rig. The test section has a nominal diameter of DN 200 and can have a very large number of different pressure, velocity and temperature sensors installed along the pipe. A pulsation generator is installed at the inlet of the test section. It permits unsteady flow behavior up to 100 Hz with pulsation indices – defined as ratio between the velocity fluctuation amplitude and the mean velocity – up to one. Figure 7 shows the test section with additionally installed sensors for determining unsteady behavior.

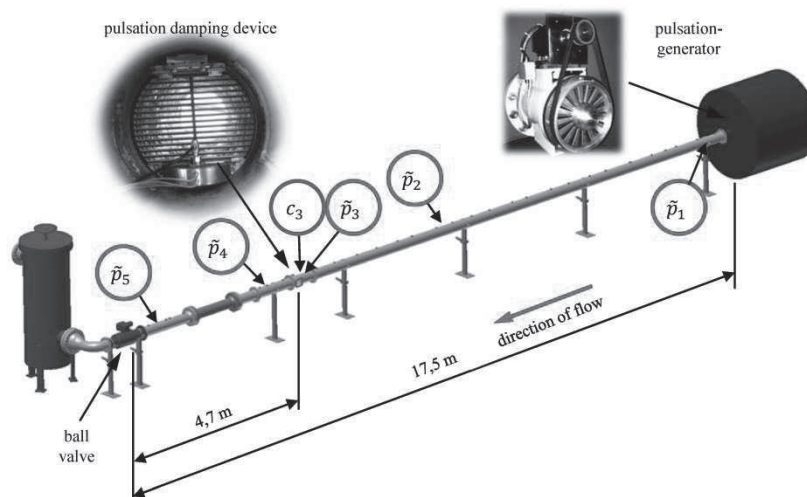


Figure 7: experimental setup

The pulsation generator works with a rotating radial slit panel. Pulsation is induced during the rotation according to the dynamic free flow cross section. The intensity of pulsation can be leveled by an additional bypass. A ball valve is installed at the end of the test section. It is nearly closed for the measurements in order to control the mean pressure in the piping at about 1.5 bar. Because of this strong throttling it can be treated as an acoustically hard ending. Next to the installed sensors at the pulsation damping device, another five piezo-electric sensors for measuring the pressure fluctuations, and a piezo-resistive sensor for the mean pressure loss are also installed. An additional thermal anemometer registers the velocity in the middle of the piping in front of the device. The sampling rate for the sensors is 2 kHz. Further analysis of the unsteady behavior is primarily based on the pressure measurement positions next to the pulsation damping device and at the end of the piping in front of the ball valve.



## 6. Measurement results

Independent analyses of the fluid mechanical and structural behavior were carried out before testing the pulsation damping behavior in pulsating flow. First of all, the device has been installed inside the test rig to acquire information on the pressure loss coefficient dependent on the deflection. The leaf spring was mounted with a high flexibility and measurements with different volume flows were taken. The deflection of the moveable grid increases with rising volume flow as a result of increasing differential pressures on the piston and grid areas. Measurements of the volume flow, static pressure, differential pressure and temperature were taken at nearly ambient conditions, fig. 8. They made it possible to determine the loss coefficient and the consequent loss coefficient gradient, fig. 9.

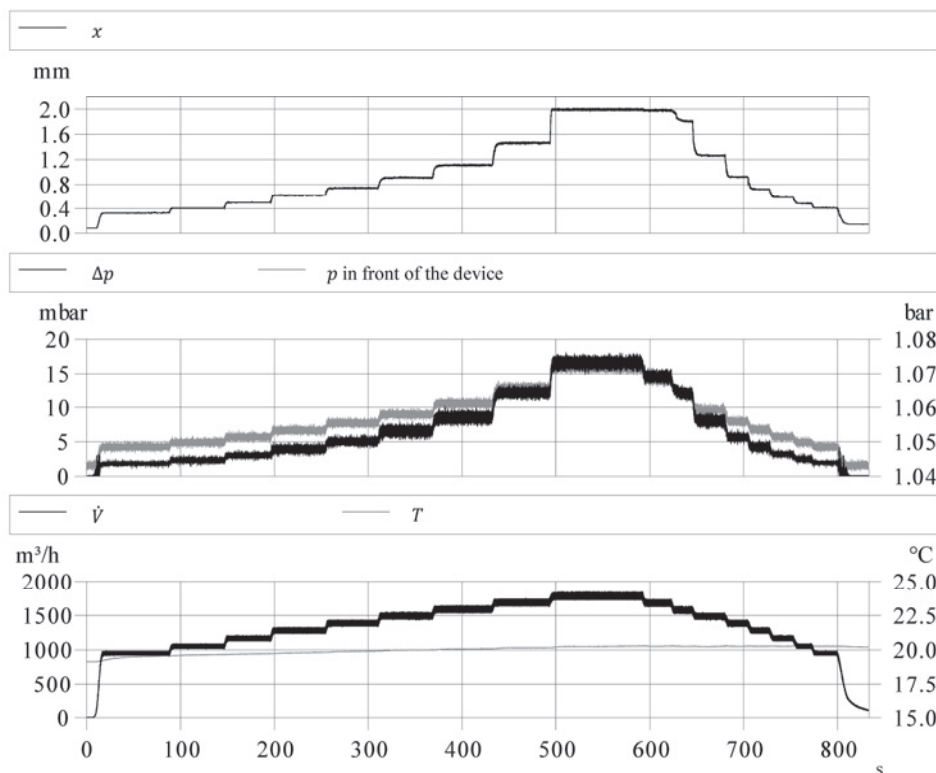


Figure 8: static measurements of the fluid mechanical behavior

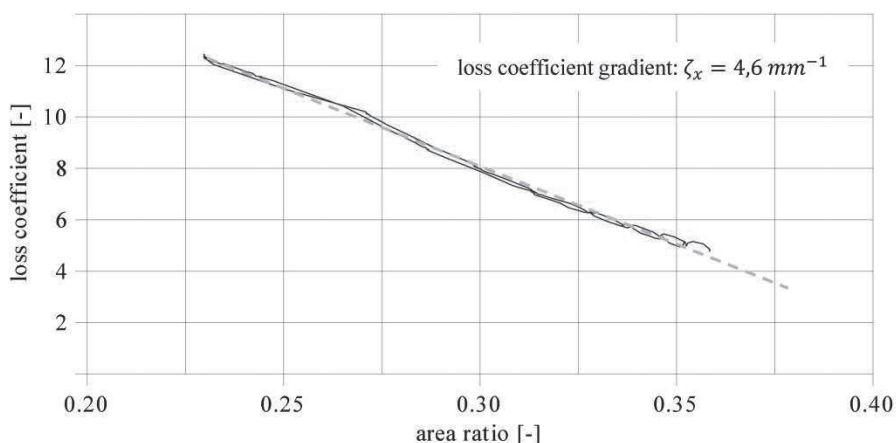


Figure 9: loss coefficient as a function of area ratio



This leads to a desired response factor of  $|H(i\omega)| = 0,28 \text{ mm/N}$  in phase, with reference to the chosen operating conditions (volume flow of  $1250 \text{ m}^3/\text{h}$  and a mean pressure of  $1.5 \text{ bar}$ ), the specified piston area and the designing equation in section 3. Impact approaches have been carried out by using an impact hammer to check the response characteristic of the structure. Different lengths of free moving leaf springs were selected. Figure 10 shows the response characteristics measured using the response factor and the according phase shift between impact and deflection of the structure. The coherence (non-labeled graphs with most values next to 1,0) is also shown as a quality feature for the linear dependency of the impact force and the deflection. A coherence of 1,0 corresponds to an ideal linear dependency.

The eigen frequencies for the measured leaf spring lengths are between 32 and 74 Hz. The response factors show that even the highest flexibility with a eigen frequency of 32 Hz does not achieve the required factor of  $0,28 \text{ mm/N}$  in phase. It seems reasonable to employ highest possible flexibility. Unfortunately no acceptable phase relation can be found with such high flexibility. A compromise has been chosen by taking a medium leaf spring length of 50 mm and additionally using the superfluous grid forces.

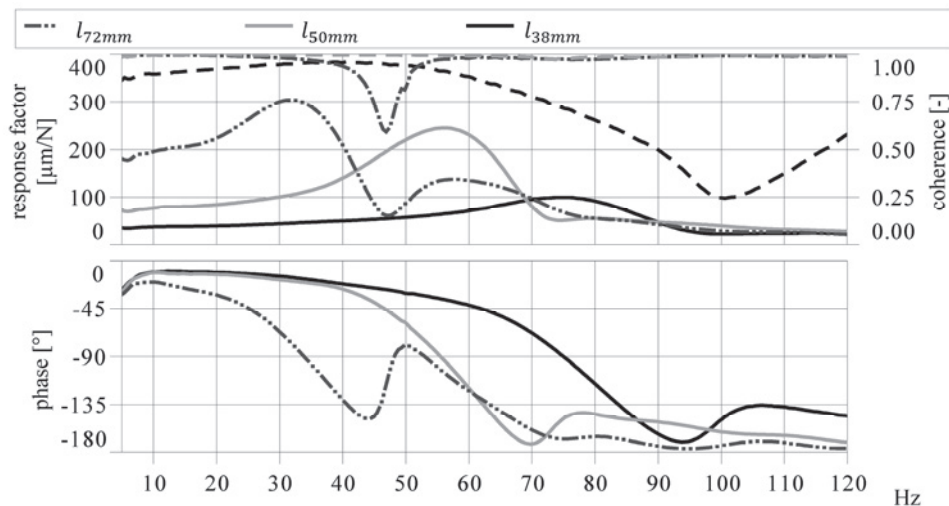


Figure 10: response characteristic  $|H(i\omega)|$  for different free moving leaf spring lengths

Subsequently, the pulsation damping device has been installed in the measurement section. The pulsation generator was used to determine the operating behavior in comparison with static devices by means of frequency sweeps, fig. 11.

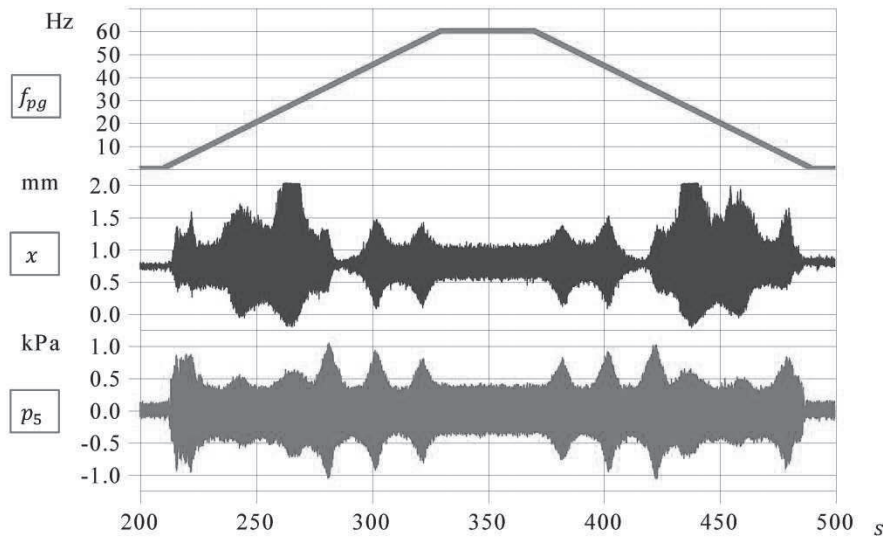


Figure 11: time signal of the excitation frequency, the deflection of the dynamic grid and the pressure pulsations in front of the ball valve

The pulsation amplitudes in front of the ball valve in the original case without any damping device are the reference benchmark for comparing the new adaptive and passive pulsation damping device with static damping devices. Thus a pulsation amplitude ratio can be defined:

$$p_{rel} = \frac{\hat{p}_{damped}}{\hat{p}_{original}}$$

The measurement results for the different setups and the pulsation amplitude ratios are shown in fig. 12. The relative remaining pressure loss

$$\Delta p_{rel} = \frac{\Delta p_{device}}{p_{static}}$$

is also depicted to complete the comparison between the different damping measures (original: pure pipe;  $\zeta=3$ : fixed moveable grid at max. opening (5 mm);  $\zeta=12$ : fixed moveable grid at min. opening (3 mm);  $\zeta(t)$ : operating as pulsation damping device). The spectral pressure pulsations of the original system are characterized by the different resonance frequencies for an acoustic open and closed piping system at 5 Hz, 15 Hz etc. The results for the different damping situations show a distinct effect on the pulsation situation at resonances of 15 Hz and 25 Hz. Other resonance frequencies are not affected by the damping devices because of a positioning next to low velocity fluctuations. In particular, a comparison between the pulsation amplitude ratios for the resonance frequency at 15 Hz shows that the new adaptive and passive pulsation damping device achieves the best damping behavior at reduced remaining pressure losses.

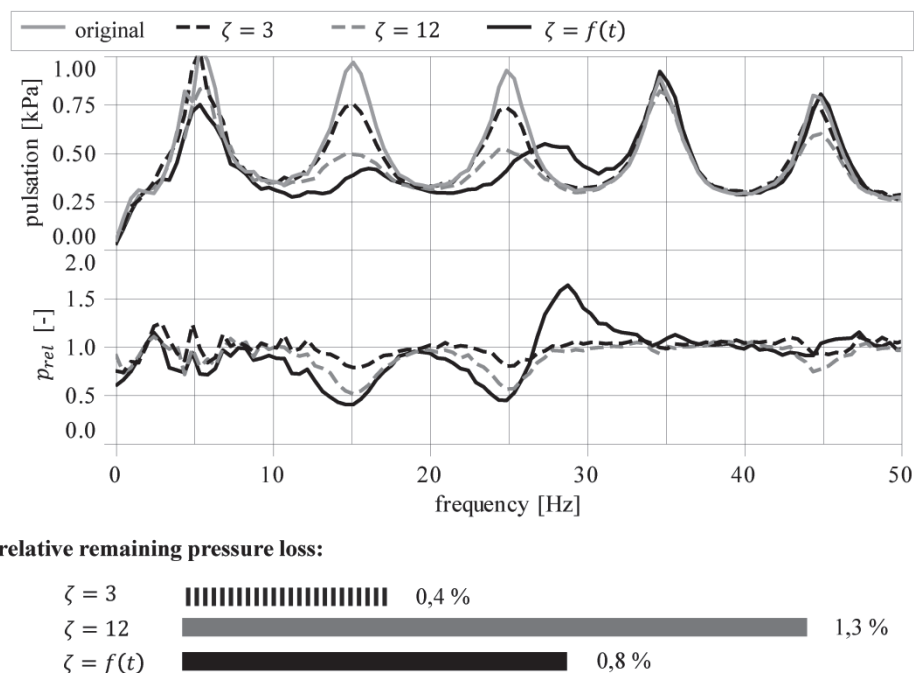


Figure 12: spectral pulsation amplitudes and pulsation amplitude ratios for different damping situations – none, static and dynamic – and relative remaining pressure loss

At higher frequencies the dynamic behavior of the pulsation damping device does not conform to adaptive and passive principle because of the phase shift between the piston forces and the grid movement. This is a result of the low eigen frequency because of low dynamic forces as a result of the nearly ambient conditions. An installation in a plant with higher static pressure levels would enable the device to avoid the use of grid forces, and the dynamic structure could be tuned to higher eigen frequencies.

## 7. Conclusions

A new adaptive and passive pulsation damping device with a dynamic in time behavior has been developed and also signed in as patent. The device works according to the adaptive physical principle, as acquired by analytical considerations and numerical simulations. The adaptive principle uses a constant ratio between the ideal differential pressure and the time depending loss coefficient, which matches the dynamic pressure of the mean upstream flow conditions. The first measurements at the closed loop air test rig at the Chair of Fluidics have been completed successfully. They demonstrated good operating behavior with improved damping behavior and reduced remaining pressure loss compared with a static device. A still better performance is in view, knowing the not perfect configuration of the current prototype. Looking forward to higher acoustic impedances an even better damping behavior is expected. In this case the grid forces could be eliminated out and the phase relationship of incoming pressure pulsation and structure movement would be improved. Higher forces also occur in the case of higher impedances. This would lead to the possibility of using higher leaf spring stiffness, which would raise the eigen frequency. Thus, the response characteristics would achieve a better phase trend at higher operating frequencies.

Further investigations at the closed loop air test rig will be carried out in the near future, using a thinner grid. This will lead to lower grid forces as a result of smaller grid areas in the direction of movement. Another positive effect will be the eigen frequency shift, which may permit more flexible leaf springs. This would be an advantage in terms of piston forces and would permit an increase in the response factor.

### References

- [1] API Standard 618: Reciprocating Compressor for Petroleum, Chemical and Gas Industry Services. 5<sup>th</sup> edition. American Petroleum Institute. Washington D.C.. 2007.
- [2] Hesse, D.: Konstruktionssystematische Erarbeitung adaptiver Dämpfungsmechanismen. Bachelorarbeit. FG Fluidtechnik, TU Dortmund. 2015.
- [3] Kötter, E. W.: Dämpferplatte für den Einbau in Rohrleitungen. Patent, DE19538178C1. 1995.
- [4] Adair, J. W.: Dynamic variable orifice for compressor pulsation control. Patent, US20150204317A1. 2015.
- [5] Den Hartog, J. P.: Mechanische Schwingungen. Springer Verlag, 1952.





# Technical Paper

**Session: 46-3**

**Session Name: Pulsation / Vibration 2**

## **Design change in the motor's bearing pedestal and baseplate in order to solve vibration problem in reciprocating compressor**

**Author:**

**Nikolaos C. Kesimoglou**  
**Rotating Engineer, Elefsis Refinery Maintenance Department**  
**Hellenic Petroleum SA**  
**19200 Elefsis, Greek**

**Co-Author:**

**Konstantinos G. Adamakis, MEng, MSc**  
**Rotating Engineer**  
**Elefsis Refinery Maintenance Department**  
**Hellenic Petroleum SA**  
**9200 Elefsis, Greek**

## Executive Summary

In Elefsis Refinery, during the commissioning of three make-up reciprocating compressors of the Hydrocracker Unit, a major vibrations issue appeared. The trains are identical, a 7 MW motor drives a 4-throw compressor with three compression stages and one dummy stage, which pressurizes H<sub>2</sub> from 24 to 183 bar(a). The capacity is controlled through step-less capacity controllers, achieving a range from 30% to 100%, with 1% step.

On June 2012 the trains started up for the very first time. The vibration limits were set by the motor vendor at 4.5 mm/s rms "alarm" and 7.1 mm/s rms "trip" according to IEC 60034-1 international standard. The compressors had no-load vibrations in NDE motor bearing at 2-3 mm/sec rms. Although, when loaded the vibration levels in motor bearing reached 8-10 mm/sec rms, well above trip limit.

The first action was to reinforce the motor's bearing pedestal by welding pipe supports on both sides. This managed to reduce the vibrations only by 1-2 mm/sec rms. The initial vibration analysis revealed that it was not a process issue, the vibrations did not come from the motor itself and the dominant frequency was close to a local resonance of the motor bearing pedestal of 55-60 Hz.

A FE model of the motor's skid and pedestal was developed in order to act as a basis for the structural modifications to be carried out in order to attenuate vibration levels. The proposed actions were to regrout the train with high quality epoxy, install four more anchorbolts (two in the corners of the motor skid and two under the pedestal) and increase the size of the soleplates in order to reduce the movement of the pedestal. After the completion of grouting and mechanical activities the unit started again on November 2012, but the problem remained.

In order to reach the final solution, the compressor train had been tested for different loads, with and without the reinforcement to the NDE bearing. In total 32 channels had been installed in order to collect reliable data. It was seen that the bearing housing was amplifying the vibrations from the rotor to the bearing housing for some of the orders; 10X-16X with and without reinforcement. The fact that the reinforcing pipes were stiffening the bearing housing in a positive manner indicated that the NDE bearing pedestal was too weak to ensure vibrations levels below the accepted level.

The model of the train became more accurate by introducing the model of the rotor. This helped in order to implement different proposed pedestal solutions in the computational model. The analysis proposed a new pedestal with increased weight by 10 times. Moreover, the baseplate of the skid of the motor had been reinforced by welding thick plates in the corners.

With the new pedestal, there was a clear improvement of the vibration levels: At axial direction they decreased by 82% (shaft line) and 62% in horizontal and vertical directions. The levels were recorded on the outboard bearing at 40% of load. After the successful completion of the first unit on summer of 2013, the second unit followed on September 2013 and the third unit on October 2014. By January 2015 all three units were running without vibration issues.

In the end of the activities it was decided to reevaluate the limits of the motor's bearing according to the vibration levels of the compressor. The new limits were chosen from the EFRC Guidelines for Reciprocating Compressors at 8 mm/sec alarm and 12 mm/sec rms trip. The units were changed in 0-pk levels to 11.5 mm/sec and 17 mm/sec respectively, in order to capture the nature of the reciprocating compressor's vibrations.



## Introduction

### Elefsis Refinery Upgrade Project

Elefsis refinery is located in Athens Greece and is one the three Hellenic Petroleum refineries in the country. A major investment of 1.4 billion € upgraded the refinery from topping to a hydrocracking one. Elefsis Refinery Upgrade Project (ERUP) finished commissioning in 2012 and started a plant of 100 kbpd capacity and a complexity index 11.3 (Nelson) or 13.9 (Solomon), which places it in one of the most complex refineries in Europe. The new plant has a Hydrocracker Unit (39 kbpd) with high requirements of H<sub>2</sub> pressure (180~190 bar) and flow (65,500~72,300 Nm<sup>3</sup>/h). The best solution to deliver the above requirements in a Hydrocracker unit is a reciprocating compressor.

### Reciprocating Make-Up Compressors

There are three make-up reciprocating compressors in Hydrocracker Unit. Two are operating in various capacities and one remains stand-by. The make-up gas compressors combine in single machine the duty of two different services: A certain amount of hydrogen is diverted to the Unionfining Recycle circuit from the discharge of second stage, whereas the remaining throughput is further compressed in a third stage to feed the Unicracking section. The unit cannot operate in full capacity with only one machine running.

The compressor train consists of one 55 TN electric motor of 7.1 MW and speed of 330 rpm with an overhung fan on the Non Drive End (NDE) side of the motor and only one NDE bearing. On the Drive End (DE) side of the motor a 4 TN flywheel is mounted on a stiff coupling, in solid shaft flanged ends, to the compressor crank shaft. The compressor DE bearing also works as DE bearing for the motor. The 104 TN reciprocating compressor consists of 3 active stages and one dummy stage. The inlet pressure to the compressor is approximately 24 bar(a) pure H<sub>2</sub> and at the discharge from stage 3 the pressure reaches approximately 183 bar(a) and 65,500 Nm<sup>3</sup>/h rated capacity. The capacity is controlled through step-less capacity controllers in the suction valves, achieving a range of 30%-100% with 1% step. The layout of the train is illustrated in Figure 1.

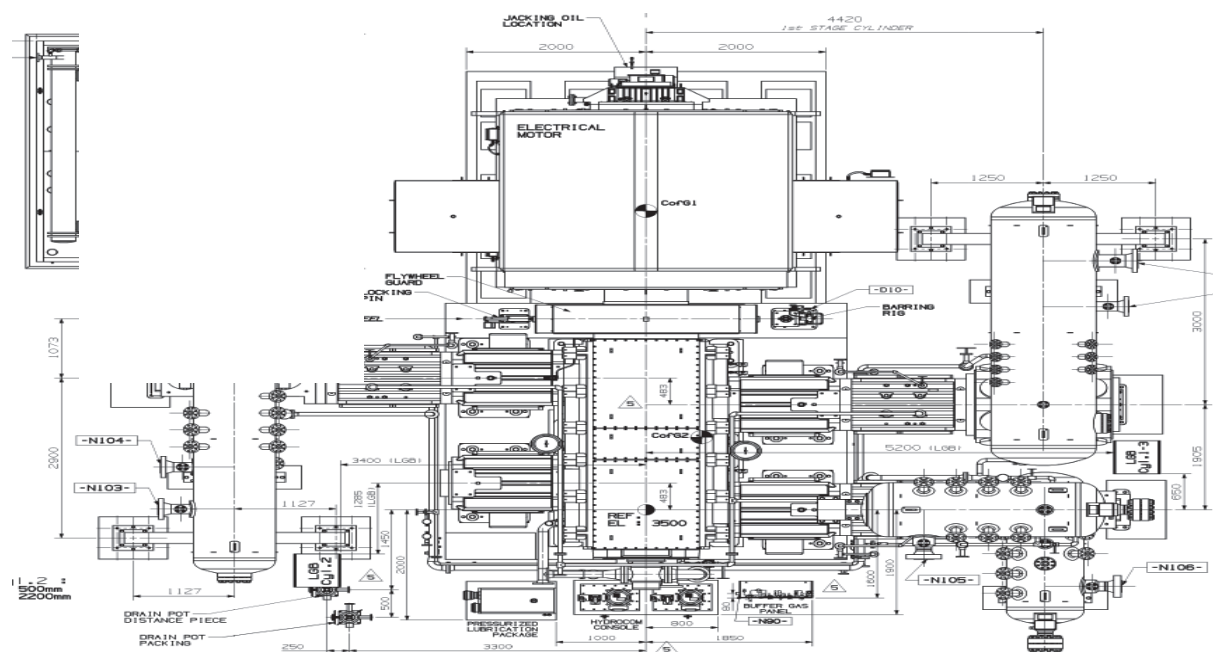


Figure 1: Compressor and Motor layout.

## The problem: Excessive vibrations in the NDE motor's bearing

### Commissioning Activities – Vibration Problem

The reciprocating compressors are fully monitored with internal cylinder pressure, crosshead & frame acceleration, piston rod position and temperature sensors. Additionally, a pair of velomitors is installed at the NDE bearing of the motor. Complementary measures are also carried out by portable measurement instrument at the NDE bearing of the motor.

According to API 618 [1] the electric motor should comply with IEC 60034-1 [2]. Additionally, when there is no specific requirement on the vibration values, the motor is provided to withstand the usual international standards recommendation (indicated also in the ISO 10816-3 [3]). Accordingly, the vibration limits were set by the motor vendor at 4.5 mm/s rms "alarm" and 7.1 mm/s rms "trip" (thresholds for in situ operation). The machines were guaranteed, with comfortable safety margins, to be able to operate for the long term with vibrations inside that limits. The compressor is designed to operate with many different combinations of cylinders running at no, part or full gas load. Each combination will provide some different loading on the unit and a unique vibration level, none of which should normally be excessive.

On June 2012 the commissioning activities were completed and the trains started up for the very first time. The compressors had no-load vibrations in NDE motor bearing of 2-3 mm/sec rms. Although, when loaded the vibration levels in motor bearing reached 8-10 mm/sec rms, well above trip limit of 7.1 mm/sec rms. From 30% to 45% loading 3<sup>rd</sup> stage all the vibrations increased, from 45% to 65% all vibrations decreased slightly and the units were operating close to trip limit (almost 6.5-7 mm/sec rms). From 65% and above, the vibrations increase again over trip limit (max 10 mm/sec rms).

### Initial actions: Motor's bearing reinforcement – Vibration Analysis

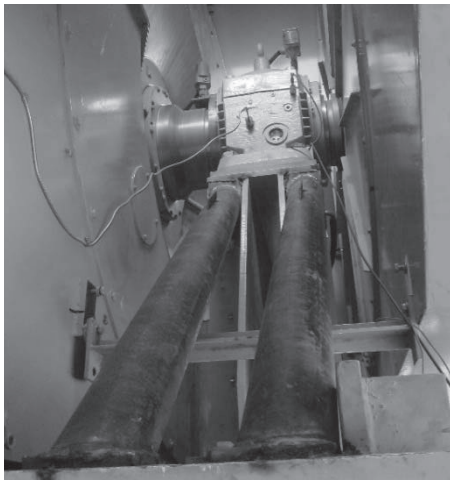


Figure 2: Welded supports in the NDE motor's bearing.

The refinery was under the pressure of the initial startup and there was no room for failure. The units had to start even with a temporary solution and a detail plan was going to be decided afterwards. At this phase, the best proposed solution was to reinforce the motor's bearing pedestal by welding pipe supports on both sides. Two supports were welded in each side, four in total, as shown in Figure 2. This action was going to be very critical for the discovery of the final solution. The main problem was that the vibrations were reduced only by 1-2 mm/sec rms and nobody could tell with confidence if the pipes could stand the forces or the problem had been transferred elsewhere.

On August 2012 an initial detailed vibration analysis was carried out from the available data of the compressor, with the following findings:

- It was not a process issue. The analysis of all PV diagrams and crosshead acceleration did not show abnormal behavior which could explain the high vibration.
- In no load test the vibration level was acceptable and around 2mm/s rms at NDE motor bearing sensors. The high vibration occurred only when the reciprocating compressor was loaded. The causes of the high vibration did not come from the motor itself.
- The compressor displayed vibration levels around 3 mm/sec rms in frame. Frequency analysis revealed that the motor vibrations increased when the loading was increased.



This was caused by an increase in a single frequency component, namely the 10<sup>th</sup> harmonic (10X or 55.5 Hz) of the rotational speed (see Figure 3). The 10<sup>th</sup> harmonic was not a dominating component on any of the compressor vibration signals.

- The level of vibration at the NDE bearing of the motor increased up to 10-11 mm/s rms with the supports installed.
- A likely candidate to cause such high vibrations was the excitation of a (local) structural natural frequency. Bump tests along with operational deflection shape analyses suggested that there was a local resonance of the motor bearing pedestal along 55-60 Hz. There was not an agreement between the predictions of the natural frequency measured during standstill (60 Hz) and during coast down (55 Hz). An explanation for the shift in natural frequency was that there was some, potentially nonlinear, interaction between rotor and bearing pedestal. During standstill the rotor is resting on the bearing and adds mass to the bearing pedestal system. However during operation the rotor is lifted but also interacts by inertia and stiffness contributions from the bearing oil film.
- With the current instrumentation, it was not possible to determine if it was a bearing support movement or a shaft movement.

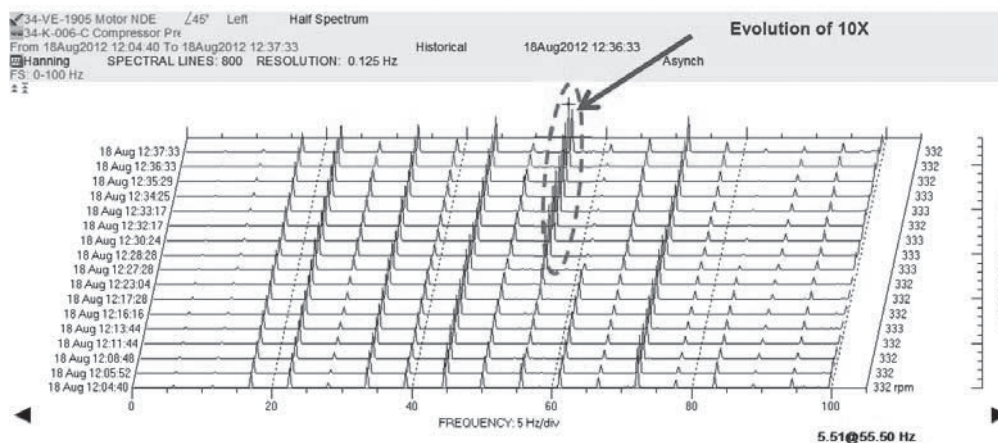


Figure 3: Waterfall of one velomitor sensor in the NDE bearing. Vibration increased from 7 to 10 mm/sec rms as the load increased. Evolution of 10X (55.5Hz) component.

### Motor model creation: Finite Element Analysis

In order to reach a solution and schedule the next actions, the compressor's motor pedestal and skid were modeled using Ansys v14 (Figure 4). The two masses shown represent the stator mass (A) and the bearing housing mass (B). Mass B weighs 780 kg and has the following inertias:  $I_{xx} = I_{yy} = 74.3 \text{ kgm}^2$  and  $I_{zz} = 90.2 \text{ kgm}^2$ . Mass A weighs 30500 kg and has the following inertias:  $I_{xx} = 51850 \text{ kgm}^2$ ,  $I_{yy} = 40680 \text{ kgm}^2$  and  $I_{zz} = 64330 \text{ kgm}^2$ . The inertias for both components were calculated considering a rectangular prism. Both masses are attached to their respective anchor points by means of rigid links. The skid's anchor points are represented by ten different linear springs in all three directions, with a constant value of  $1E10 \text{ N/m}$ . The global coordinate system is defined with Z being the axis of the rotor (positive from the DE to the NDE), X is in the transversal direction and Y in the vertical direction (positive upwards).



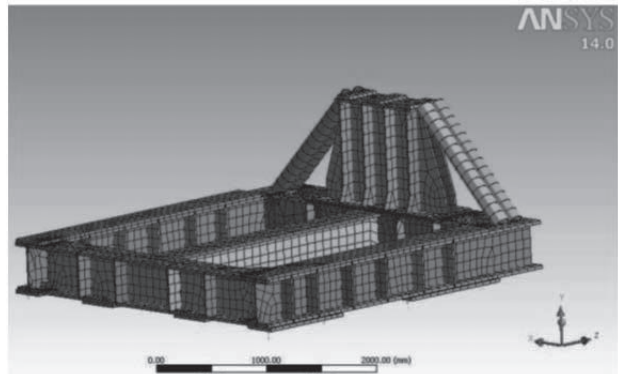
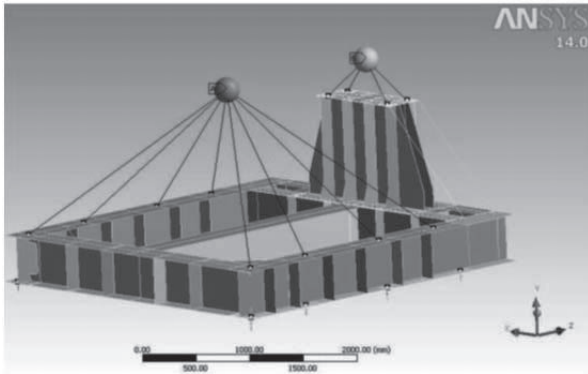
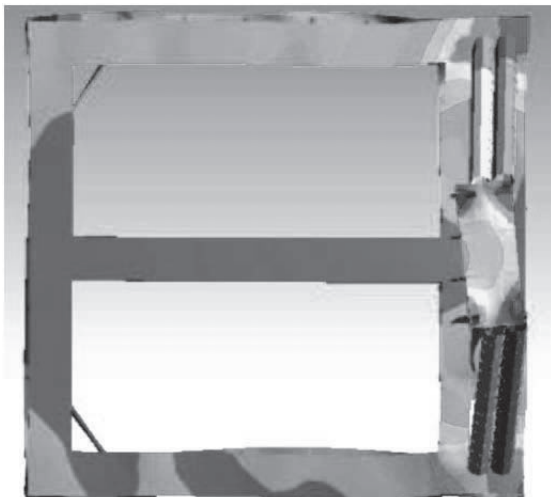


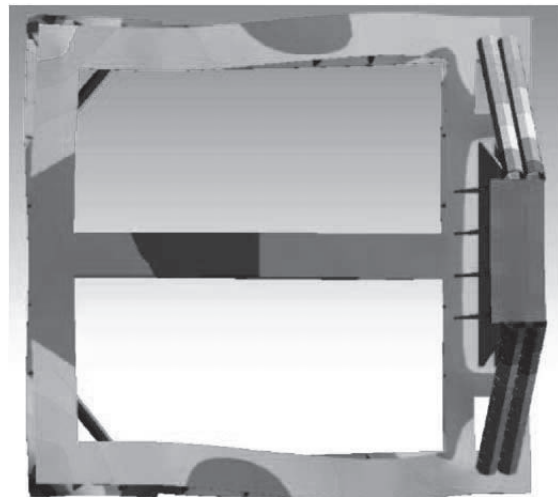
Figure 4: Finite Element Model of the motor's skid with pedestal (left) and meshing (right).

All skid and pedestal elements used in this analysis are plate elements, as presented in Figure 4. The four braces supporting the pedestal to the skid are modeled as beam elements. The cross section of the beam elements corresponds to that of a 6" schedule 80 pipe.

A modal analysis had been carried out, using the FE model, and the first six modes were calculated. Several of these modes correspond to movements of the stator/bearing housing mass and the respective deformation of the skid and/or pedestal (see Figure 5 and Table 1). The dominant mode, with the higher amplitude, is the 5<sup>th</sup> mode, rotation of pedestal about the transversal axis



Mode 1: 22.6 Hz



Mode 2: 29.2 Hz.

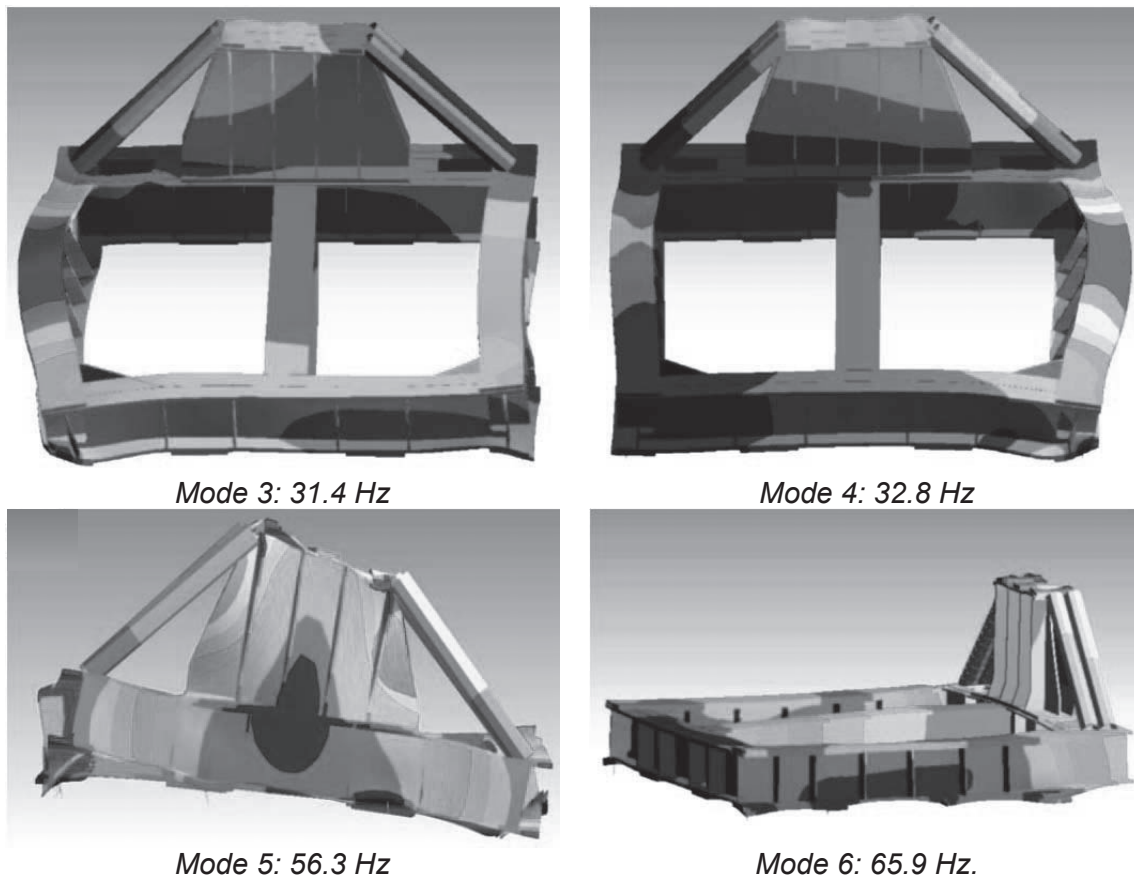


*Figure 5: The 6 first modes. Maximum excitation, close to mode 5: Rotation of pedestal in the transversal & vertical axis.*

The first six modes calculated had been compared to the real data and were found to be in very good agreement. This strengthens the reliability of the model. Furthermore, the impact test showed the existence of a natural frequency at around 60 Hz, when the machine was stopped. Once the machine is en route, the mode is shifted down to circa 55 Hz, which corresponds to mode 5 presented above. The difference between the impact test natural frequency and that given by the FE model relies in the mass and stiffness distribution. Furthermore, modes 1, 3, 4, and 6 are less excitable by the actual forces acting on the unit and then are not observable (as resonance peaks) in the measurements at site.

<b>Mode</b>	<b>Natural Frequency (Hz)</b>	<b>Comment</b>
1	<b>22.6</b>	Rotation of pedestal about the transversal and the vertical axis
2	<b>29.2</b>	Rocking of pedestal about transversal axis
3	<b>31.4</b>	Movement of stator mass-beams in phase
4	<b>32.8</b>	Movement of stator mass-beams out of phase
5	<b>56.3</b>	Rotation of pedestal about the transversal and the vertical axis
6	<b>65.9</b>	Translation of pedestal and skid beams along vertical axis

*Table 1: The 6 first modes of natural frequencies. The 5<sup>th</sup> is the dominant one.*

Taking the above analysis into consideration, the proposed actions, in order to decrease the vibration levels, were to move away from the natural frequencies and namely to the 55-56 Hz which seems to cause the increase. In order to achieve this at site, it was decided (taking also in consideration past experience) to regrout the train with high quality epoxy, install four more anchorbolts (two in the corners of the motor skid and two under the pedestal) and increase the efficiency of the soleplates in order to reduce the movement of the pedestal in mode 5.

### ***Regrouting, motor soleplates and anchoring improvement***

The grouting was in poor condition with big cracks all over the base under compressor and motor skid. The cracks had 2-3 mm height differences and openings (see Figure 6 upper left picture). Also many of the pull down checks of the compressor's anchorbolts were out of limits. The machines were grouted with poor quality epoxy under high temperatures (summer 2011) during the installation phase. This was known from the beginning, but when the vibration problem appeared, it was one of the factors that had to be eliminated.

The actions, which were implemented on August-November 2012 in the first train, were to totally dismantle compressor and motor and perform major mechanical overhaul with new grouting. The soleplates under the motor were optimized in order to increase the contact area of the motor skid and the soleplate (see Figure 6 bottom left picture). The two soleplates under the pedestal were enlarged to support greater area. Furthermore, four extra anchorbolts were installed for better anchoring, two in the corners of the motor's baseplate and two inside, under the pedestal (see Figure 6 upper right picture). The train was grouted with a top quality epoxy, with the appropriate expansions joints and thickness, in order to totally eliminate potential cracks (see Figure 6 bottom right picture). As machining at site was not possible, in the corners of the motor skid, special epoxy grouting acted as two extra soleplates for the two new anchorbolts.

After the proper curing time of the epoxy was passed, the machine was assembled by paying extra attention to strictly follow the procedures. The maintenance activities lasted 2.5 months and many resources and spare parts were used. By the end of the activities, a newly installed reciprocating compressor with its driver with the best possible grouting was ready for commissioning.

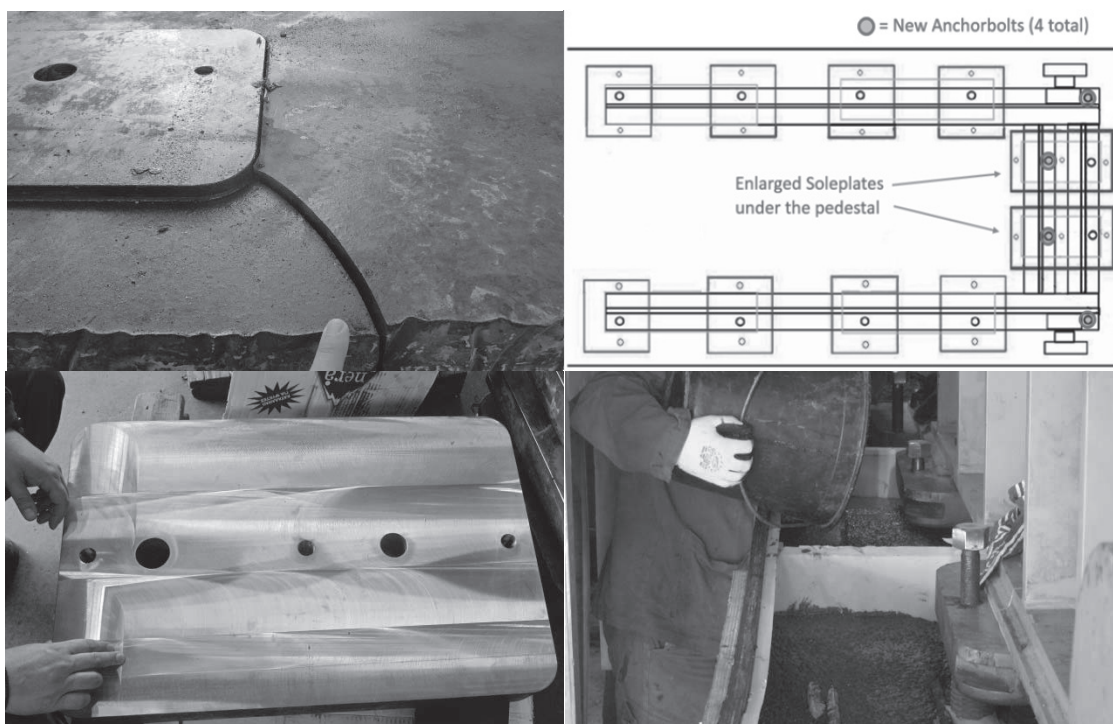


Figure 6: (Upper left) big cracks in the grouting, (upper right) schetch of new enlarged soleplates under the motor and new anchorbolts' positions, (down left) new enlarged soleplate, (down right) new grouting with expansion joints.

### Failure and management support

After the completion of grouting and mechanical activities the unit started again on November 2012, but the problem remained. Without welded supports in the NDE motor's bearing at 30% 3rd stage load the vibrations were 10-12 mm/sec rms (see Figure 7). With welded supports at 32% load the vibrations decreased to 8-9 mm/sec rms. In loadings more than 70% the vibrations slightly decreased. Although, the normal operation of the unit is between 60-65%.

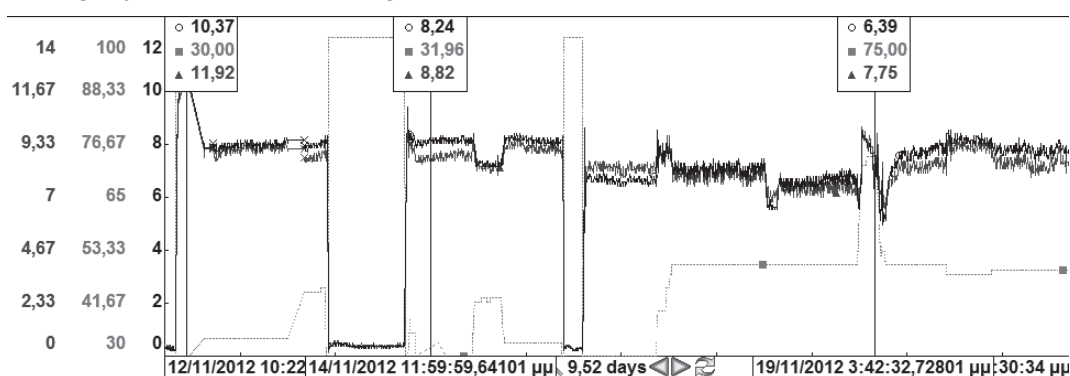


Figure 7: Two velomiters in the NDE motor's bearing (blue, black) and the loading (red) for three loadings: without supports (30%), with supports (32%, 75%).

It was clear that the initial actions, which lasted more than 3 months and used a lot of resources, did not have the expected outcome. The vibration levels remained the same. Some possible causes for the problem had been eliminated, like the grouting and the anchoring of the motor skid, but the vibrations did not decrease at all. At this point it has to be mentioned that the



team, consisted of Hellenic Petroleum, compressor and motor vendor specialists, had the full support of the top management of all three companies. The team stayed united and focused in the next steps which eventually led to the solution.

## Solution

### *Trying to find the root cause: Measurement Campaign*

In order to reach the final solution, a detailed measurement of the whole train was needed. The compressor train had been tested for different loads, with and without the reinforcement to the NDE bearing. During these tests a number of measurements had been carried out. In total 32 channels had been installed in order to collect reliable data. The recorded signals were: Vibration measurements (acceleration) on compressor stage 3 and its foundation, in total 4 channels. Vibration measurements (acceleration) on NDE bearing house, in total 3 channels. Dynamic pressures on the first stage suction, all stages discharge and cylinder pressures for all three cylinders on both sides of the piston (since the compressor is double acting), in total 10 channels. Lateral shaft vibrations for the NDE and DE side relative to the foundation as well as the relative movement between compressor casing and compressor crank shaft between bearing 2 and 3 inside the compressor, in total 6 channels. Axial shaft vibration at the DE side, 1 channel. On the motor, rotor torque and bending in two sections had been recorded with strain gauges connected to a radio transmitter. Similar measurements had also been performed on the fan at the NDE side of the motor, in total 10 channels. Strain measurements on the NDE motor bearing pedestal and on the reinforcing pipes, total 3 channels. Some main channels/instruments are shown in Figure 8.

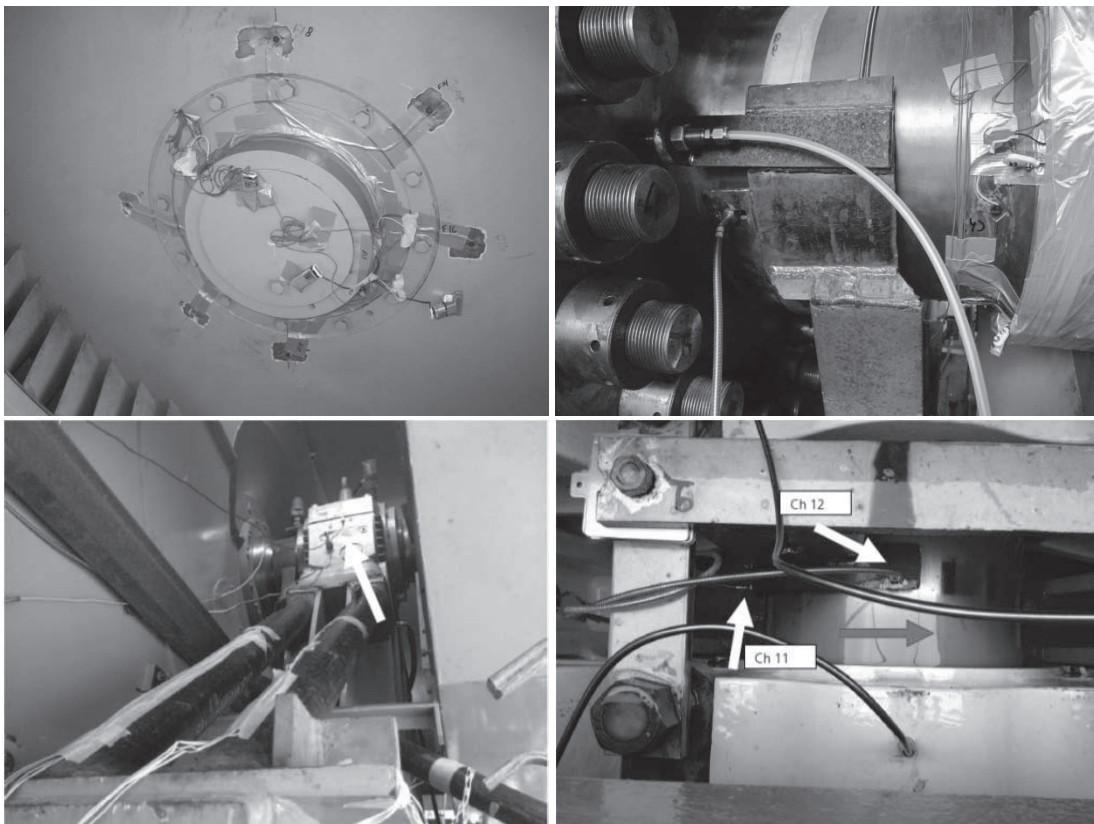


*Figure 8: Various channels on motor's fan, shaft DE, motor pedestal and on compressor's DE bearing.*





From the constant operation at different loads it was shown that the torsional natural frequency is 36.2 Hz and has a viscous damping of 0.3% of critical damping. The torsional natural frequency is somewhat lower than what is calculated by the vendor at 42 Hz. In Figure 9 it is illustrated the compressor's average torque value on rotor with and without supports.

From the bending measurements on the motor shaft it was seen that the 1X component was the dominating order in the frequency spectra. The rotating bending moment is seen to peak when strain gauges are at the top (12 o'clock) and bottom (6 o'clock). The measurements show that stresses were compressive at the top and tension at the bottom indicating that bending stresses in the motor shaft was mainly due to gravitational sag of the rotor between the bearings. Bending strain variations were found to be less than 175 $\mu$ S pk-pk ( $\mu$ S= $\mu$ m/m), which correspond to a stress variation of about 37MPa pk-pk.

The maximum dynamic shear stress variations were measured to 38MPa pk-pk, when operating in load setting 53% - 53% - 30% in manual mode. There was no clear correlation between torsional vibration level and the vibration level measured on the motor NDE bearing.

When comparing the order spectra in velocity for the horizontal proximity probes and the horizontal accelerometer on the NDE bearing, it was seen that the bearing housing was amplifying the vibrations from the rotor to the bearing housing for some of the orders; 10X-16X of rotating speed with and without reinforcement.

Testing could not be performed without the reinforcing pipes; the vibrations and the risk of tripping the machine were increasing rapidly (see Figure 10). This made clear that the pipes with the added stiffness were lowering the vibration levels. From the strain measurements on the pipes it was shown that the pipes were supporting the bearing housing taking up dynamic forces in the range of 56kN pk-pk. The fact that the reinforcing pipes were stiffening the bearing housing in such a positive manner indicated that the NDE bearing pedestal was too weak to ensure vibrations levels below the accepted level.

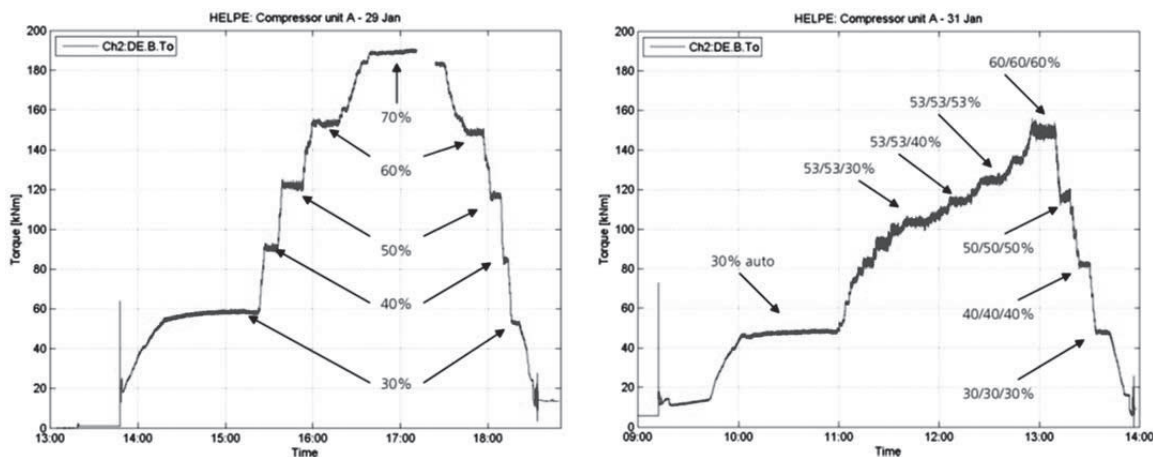


Figure 9: Compressor average torque value on rotor with supports (left) and without supports (right).

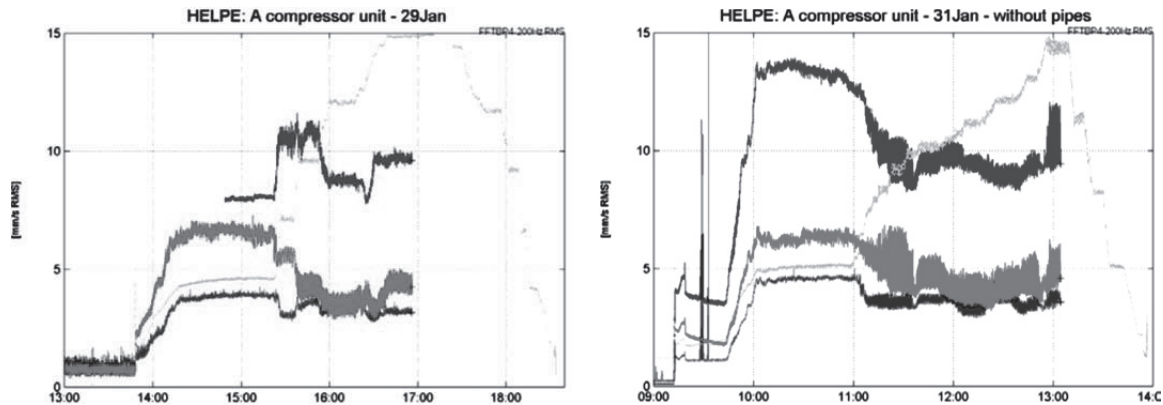


Figure 10: Vibration measurements on motor NDE bearing. Horizontal, Vertical, Axial. With supports (left) and without supports (right).

In the end of the measurement campaign it was decided that the reinforcement in the NDE bearing pedestal should remain, until a permanent solution was found. Moreover, It was advised that the compressor should be operated close to 60% load, since the vibration behavior at the NDE bearing was lowest in this range.

### Model of the rotor and recommended scenarios for solution

The model of the train became more accurate by introducing the model of the rotor, which consisted of 55 stations and 54 elements. This would help in order to implement different proposed solutions in the computational model. The model is illustrated in Figure 11.

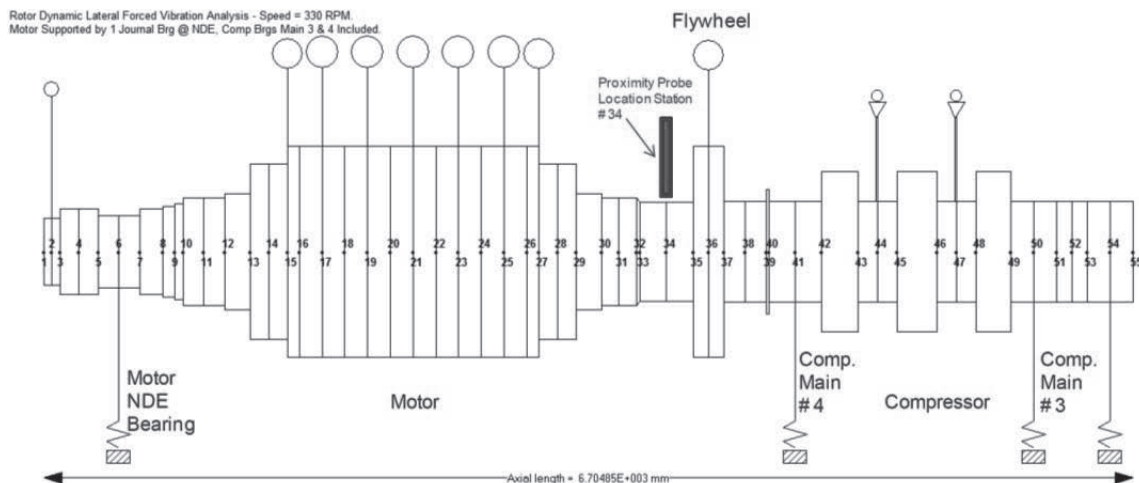
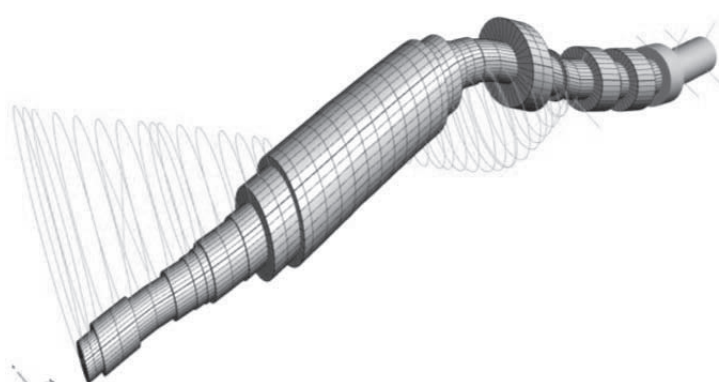


Figure 11: Rotor model representation.

For rotor dynamic simulation of the system, the bearings were introduced to the mathematical model with their dynamic coefficients (stiffness and damping). These bearing characteristics are highly non-linear and they are influenced by such parameters as speed, load and lubricant temperature. Rotor dynamic analyses were performed with the above constructed rotor/bearing models and with consideration to various excitations representing mechanical unbalance force and forced harmonic response applied at compressor throws. The following four different NDE bearing support flexibilities were considered:



- **Model A** – Rigid supports. This will act as model for comparison.
- **Model B** (Base Line) – Motor’s computed support stiffness and mass properties:  $K_h=2.72331E+08$  N/m,  $M_h=844$  kg,  $K_v=6.72314E+08$  N/m,  $M_v=1612$  kg. This model configuration of the support structure was believed to be the as-is existing system in the field.
- **Model C** (Model B x1.5) – Pedestal stiffness and mass properties for the new design:  $K_h=4.29000E+08$  N/m,  $M_h=2299$  kg,  $K_v=1.37760E+09$  N/m,  $M_v=4161$  kg. This configuration of the support structure is examined as the new proposed design to the existing configuration.



- **Model D** (Model B horizontal x2.2, vertical x1.5) – Same as model C however the horizontal pedestal stiffness increased by a factor of 1.40 (total). This resulted in values of  $K_h=6.000E+08$  N/m while all other values remain the same. Similar to model C above, this configuration of the support structure is also examined as possible modification to the existing configuration.

Figure 12: 5<sup>th</sup> mode of the rotor in base line model B.

Based on the analyses performed, it was indicated that the rotor/bearing system with NDE support flexibility considered did introduce system natural frequencies with low levels of damping that were excitable and did slightly amplify the dynamic response characteristics of the drive motor NDE bearing location and its supports (see Table 2 for models comparison). In Figure 12 is the calculated 5<sup>th</sup> mode of the rotor model. Accordingly, displacements and transmitted forces to the drive motor bearing were increased. Modification to the motor NDE bearing support stiffness reflecting model C did reduce pedestal vibrational amplitudes by as much as 30% for 30% loading, 7% for 60% load and 37% for 100% loading. For the recommended support stiffness reflecting model D, the reduced pedestal vibrational amplitudes was 42% for 30% loading, 18% for 60% load and 48% for 100% loading. However, reduction in displacements did not reduce the transmitted dynamic force to the pedestal. The computed transmitted forces had to be utilized in an effort to quantify the fatigue life of the support structure and its welded connections from which a factor of safety had to be established.

Rotating Speed 330 rpm

Model	Mode 1		Mode 2		Mode 3		Mode 4		Mode 5		Mode 6	
	Frequency (Hz)	Critical Damping Ratio	Frequency (Hz)	Critical Damping Ratio	Frequency (Hz)	Critical Damping Ratio	Frequency (Hz)	Critical Damping Ratio	Frequency (Hz)	Critical Damping Ratio	Frequency (Hz)	Critical Damping Ratio
A	4,2	0,84	4,5	0,86	39,8	0,17	42,6	0,02	73,6	0,02	81,0	0,02
B	4,2	0,85	4,6	0,85	24,8	0,08	33,3	0,03	51,2	0,09	58,4	0,03
C	4,2	0,85	4,6	0,86	28,0	0,09	37,5	0,04	51,5	0,08	61,9	0,02
D	4,2	0,85	4,6	0,86	31,1	0,1	37,5	0,04	53,5	0,08	62,1	0,02

Table 2: Natural Frequencies comparison for all models.

The improvement is visible in Figure 13. There is a comparison in pedestal vibrations between the existing model B and the two proposed C and D. Moreover, there is a comparison in shaft vibrations NDE motor bearing between all the models and the measured values at site. Vibrations are in displacement (mm pk-pk) and it is clear that the best results are achieved with model D. Although exact comparison between measured and calculated displacement was not achieved fully, by similarity analysis between models B, C and D the recommendation was to stiffen the support as much as possible and at the level of model D or higher.

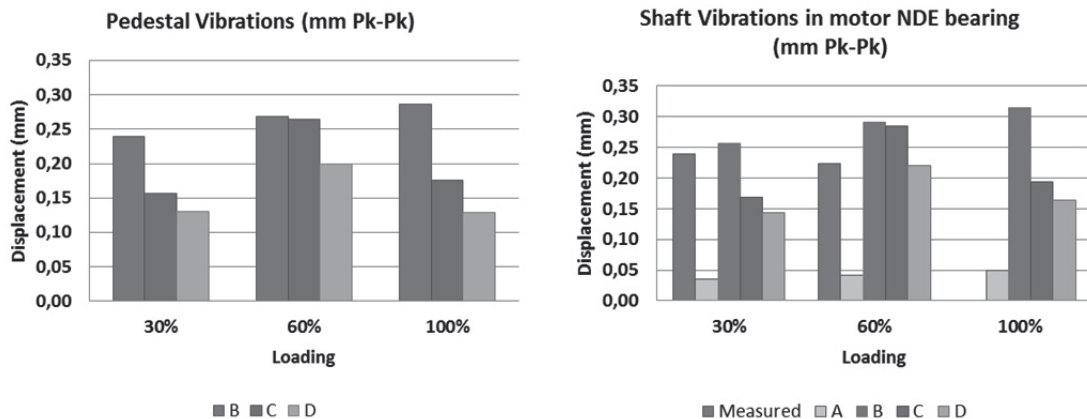


Figure 13: Models comparison - Displacements in the pedestal (left) and in shaft position NDE motor bearing (right) for loadings 30%, 60% and 100%.

### Final Solution: Pedestal Redesign and Baseplate reinforcement

In order to achieve the stiffness increase of model D the solution which was implemented is shown in Figure 14. The new pedestal was completely redesigned and increased its weight by 10 times, almost 4.5 TN. Due to geometrical restrictions the pedestal could not be oversized more. For these reason, the pipe supports were replaced by rigid brackets in order to further increase the stiffness of the system. Moreover, the baseplate of the skid of the motor had been reinforced by welding thick plates in the corners (see details A & B at Figure 14). All these modifications, combined with the new grout, optimized soleplates and the extra anchorbolts were expected to achieve the results of the model D.

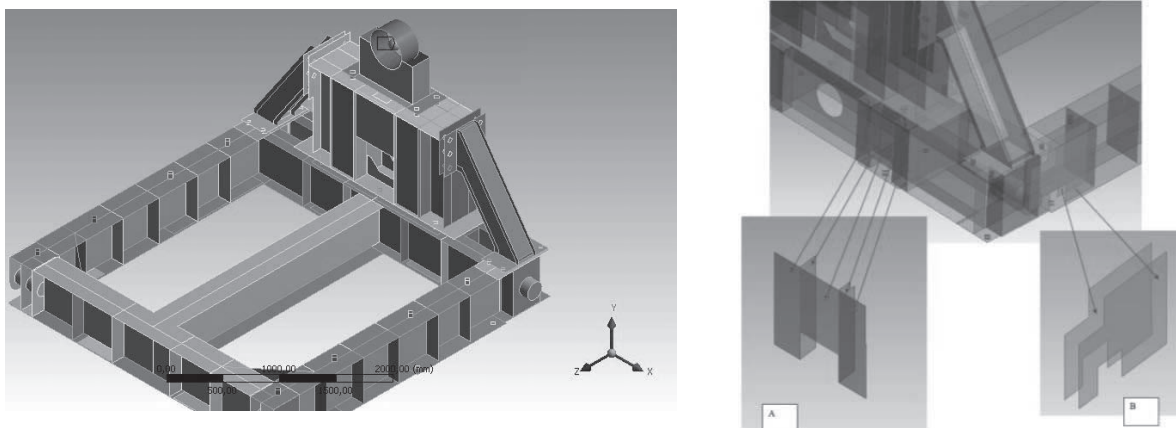


Figure 14: New pedestal with brackets (left) and reinforcement plates A & B in the baseplate (right).





### Implementation of the solution

At June 2013, almost one year after the detection of the problem, the new solution was ready to be implemented at site in the unit with the new grout and the optimized anchoring. The installation lasted two weeks. In the brackets, epoxy grout connected the two metal areas, as machining at site was impossible.

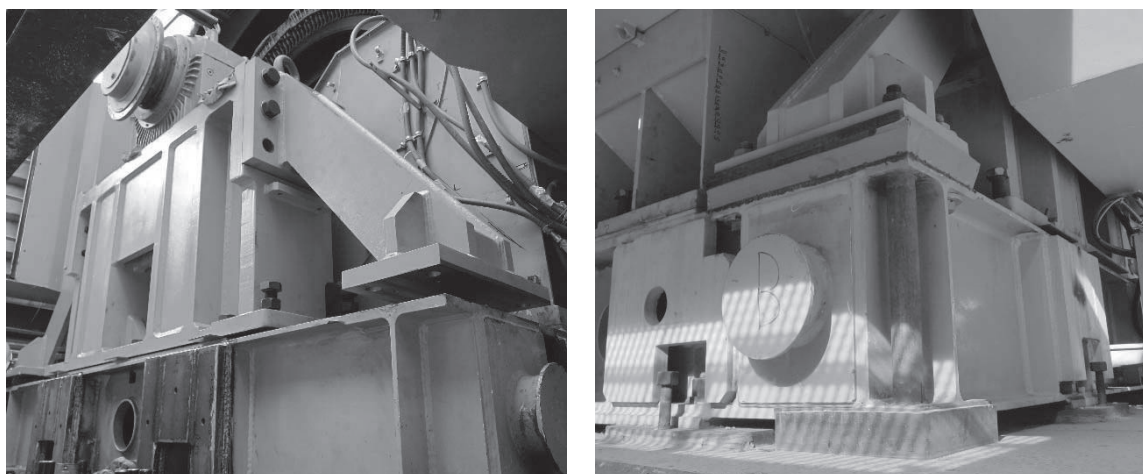


Figure 15: New pedestal and reinforcement plates (left), grout and prolonged anchorbolts (right).

The stiffness of the pedestal had been increased to the maximum. In order to achieve the best results, the only thing that could had been improved, was the damping factor (see Table 2). The proposed solution that was implemented, was to prolong the corner anchorbolts and tight them directly to the brackets of the pedestal (see right picture in Figure 15). This would help to lead the vibrations directly to the grouting.

### Measure the success

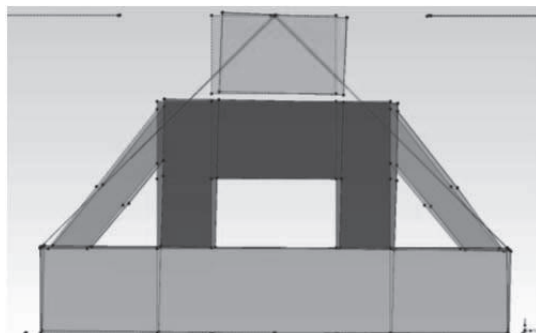


Figure 16: Pedestal's rocking

From the first startup of the redesigned unit the improvement was obvious, but in order to accurately evaluate the new installation and the level of vibrations in all the train, another measurement campaign took place. The new pedestal was modeled as illustrated in Figure 16. With the new pedestal, there was a clear improvement of the vibration levels: At axial direction they decreased 82% (shaft line) and 62% in horizontal and vertical directions. The levels were recorded on the outboard bearing at 40% load in 3<sup>rd</sup> stage.

The highest level of vibration reached 5.18 mm/s RMS in horizontal direction at 70% of load. The general behavior of the motor can be considered as acceptable for unrestricted long time operation. In Figure 17 there is a comparison of the overall velocity level with the old and the new pedestal in all three axes. The actual improvement was better than the prediction of the theoretical model D. This was probably due to the extra field modifications that had not been inserted in the model. The most significant was the prolonged anchorbolts in the corner of the motor skid. This improvement led the vibrations from the rotor directly to the grout and to the cement base of the motor.



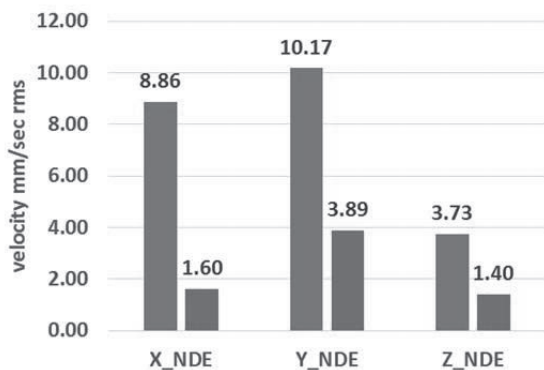


Figure 17: Old and new pedestal's vibrations.

After the successful completion of the first unit, the second unit followed on September 2013 and the third unit on October 2014. A 70 days overhaul was needed in each machine in order to implement the combination of the solutions: the new grouting, the optimized anchoring and the new pedestal. By January 2015 all three units were running without vibration problems.

### **New alarm and trip limits**

During the research of the solution in the vibration problem, it was clear that the limits of 4.5 for alarm and 7.1 for trip mm/sec rms were not suitable for reciprocating machine. Reciprocating machines generate higher vibrations from their operation and the driver should follow these levels. The EFRC Guidelines for vibrations in Reciprocating Compressor Systems [4] is the most complete and reliable source of information in order to evaluate the operation of a machine. In the end of the redesign activities it was decided to reevaluate the vibration limits of the motor according to the levels of the compressor. The new limits were set at 8 mm/sec alarm and 12 mm/sec rms trip according to the EFRC Guidelines. The units were changed in 0-pk levels to 11.5 mm/sec and 17 mm/sec respectively, in order to capture the nature of the reciprocating compressor vibrations. In this way the machines are protected safely and reliably up to today. The above guidelines were introduced in ISO 10816-8 [5] which was released in 2014.

### **Resume**

In this paper, the problem of excess vibrations in the NDE motor bearing in all three make-up reciprocating compressors of the Hydrocracker Unit in Elefsis Refinery is tackled both theoretically and in practice. Supports were welded in the bearing and a detailed analysis was made of the vibrations with the use of FE model. The initial recommendations resulted in new grouting for the whole train, optimization of the motor's soleplates and increase of the anchoring points. The problem insisted and a rigorous measurement campaign revealed that the pedestal of the motor's bearing was too weak. A second more detailed analysis with a dynamic model of the rotor and the comparison of different theoretical models led to a significant increase in the stiffness of the pedestal. The solution was applied in all machines with success and the vibration levels were decreased more than it was expected. The alarm and trips levels were reevaluated according to EFRC Guidelines for Reciprocating Compressors.



## **Bibliography**

1. API Standard 618: Reciprocating Compressors for Petroleum, Chemical, and Gas Industry Services. 5<sup>th</sup> edition December 2007.
2. IEC 60034-1: Rotating Electrical machines. Part 1: Rating and performance, 11<sup>th</sup> edition April 2004.
3. ISO 10816-3: Mechanical vibration - Evaluation of machine vibration by measurements on non-rotating parts. Part 3: Industrial machines with nominal power above 15 kW and nominal speeds between 120 r/min and 15 000 r/min when measured in situ, 1<sup>st</sup> edition May 1998.
4. EFRC Guidelines for vibrations in Reciprocating Compressor Systems. 3<sup>rd</sup> edition May 2012.
5. ISO 10816-8: Mechanical vibration - Evaluation of machine vibration by measurements on non-rotating parts. Part 8: Reciprocating compressor systems. 1<sup>st</sup> edition July 2014.





# Technical Paper

**Session: 47-1**

**Session Name: Calculation 1**

## **Field performance assessments using enhanced simulation modeling for reciprocating compressors**

**Author:**

**H.J.M. Baan MSc.  
Howden Thomassen Compressors BV  
6991 GS Rheden, The Netherlands**

## Summary

The basic thermodynamic and mechanical performance characteristics of a reciprocating compressor can be described using algebraic relations. This method is capable of producing accurate results for general performance predictions; however there are some cases and applications which require a far more accurate simulation of the actual thermodynamic processes occurring in a reciprocating compressor.

In this paper, a compressor performance simulation model is presented which is able to accurately capture transient and time-dependent effects in the compression cycle simulation whilst providing the flexibility to expand the model beyond the compression cycle itself. This is achieved by means of adopting a simulation method in the time domain. Using a novel numerical solution method that uses a variable time step in combination with an explicit and implicit method, a multistage simulation can be performed in just a few seconds on an average computer and can therefore be used for compressor selection, detailed design as well as field performance assessments.





## Introduction

The thermodynamic performance aspects of a reciprocating compressor can be described by using analytical calculation models. The accuracy of this method is however limited by certain factors. The first problem is that gas properties are a function of pressure and temperature, which may change significantly during compression or expansion. Critical events during the compression cycle, such as opening and closing of suction and discharge valves, can have a notable influence on the performance of a reciprocating compressor. Accurate modeling of these events in analytical calculations models is complicated and the accuracy is limited, especially when compressor valve losses are high and the effect on the overall performance becomes significant. When heat transfer between the process gas, cylinder, cooling water and environment, as well as friction losses are taken into account, an analytical model becomes even more complex.

Other factors affecting the compressor performance are related to flow, such as compressor valve losses and pressure losses in cylinder valve ports, passages and orifices in pulsating flows. Accurately capturing these effects without considering the time-dependent flow characteristics is limited to including generalized approximations in the analytical model.

Resorting to a different method is required in order to capture the full complexity of the thermodynamic process without compromising on accuracy. By adopting a numerical simulation method in the time domain, the transient effects and events during the reciprocating compressor operating cycle can be simulated. Instead of using an analytical relation to determine the compressor flow rate, temperature or required torque during one revolution of the crankshaft, this revolution is divided in a large number of small steps. The change in volume due to piston movement is determined for each step, gas pressure and temperature are calculated, and eventual valve opening or closing based on the pressures in the adjacent volumes is simulated. At every step the thermodynamic properties of the gas are calculated, heat transfer as function of the current temperature and friction as function of local velocities are calculated and the mass- and energy fluxes in the system are determined.

## Volume-based simulation model

To simulate the thermodynamic performance of a reciprocating compressor a volume based model is employed. A visual representation of a part of the model is included in *Figure 1*. This model consists of several linked volumes of which the size and relation to other volumes can be changed as a function of time. As an example, the crank-end cylinder volume can initially be an isolated volume with an imposed reduction of size due to the movement of the piston, whilst after opening of the discharge valve a mass flow can be transferred to the cylinder discharge passage volume.

Since the model is flexible and dynamically constructed, specific components can easily be added such as clearance pockets (including clearance pocket valves), a Free Floating Piston, pulsation dampeners, interconnecting piping etc.

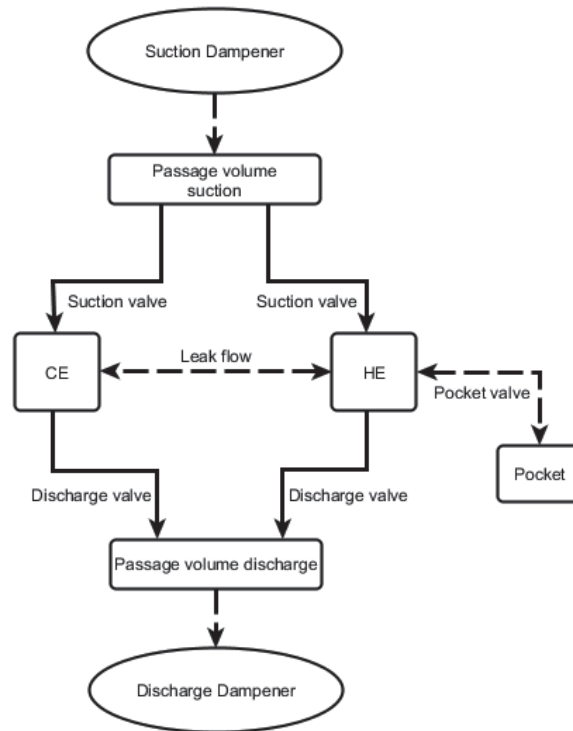


Figure 1: Volume model for a single cylinder

### Equations

The first law of thermodynamics states<sup>1</sup>:

$$dE = dQ - dW \quad (1)$$

while work is given by:

$$\begin{aligned} dW &= pdV \\ W &= \int pdV \end{aligned} \quad (2)$$

The total energy in each volume consists of the internal, kinetic and potential energy, and is given by:

$$dE = dU + d(KE) + d(PE) \quad (3)$$

The principles of mass and energy conservation apply to the system as a whole as well as to the individual volumes, taking any transfer of mass or energy to and from the system into account. Pressure and temperature are assumed to be uniformly distributed within each volume. Kinetic energy is low, and gravitation can be neglected. This assumptions reduce the total energy equation to:



$$\frac{dE}{dt} = \frac{dU}{dt} \quad (4)$$

The specific internal energy is defined as:

$$u \stackrel{\text{def}}{=} U/m \quad (5)$$

The internal energy expressed in specific quantities is given by:

$$\frac{dU}{dt} = d(mu) = udm + mdu \quad (6)$$

Enthalpy and specific enthalpy are given by:

$$H \stackrel{\text{def}}{=} U + PV \quad h = u + Pv \quad (7)$$

Furthermore, the heat capacity at constant volume and constant pressure are given by:

$$C_v = \frac{1}{m} \left( \frac{\partial U}{\partial T} \right)_v = \left( \frac{\partial u}{\partial T} \right)_v \quad (8)$$

$$C_p = \frac{1}{m} \left( \frac{\partial H}{\partial T} \right)_p = \left( \frac{\partial h}{\partial T} \right)_p$$

The law for conservation of mass states that for any system closed to all transfers of matter and energy, the mass of the system must remain constant over time:

$$dm = \sum \dot{m}_i dt \quad (9)$$

Combining equation (1), (4), (6), (7) and (9) yields:

$$dQ + \sum h_i \dot{m}_i - PdV = udm + mdu \quad (10)$$

This equation can further be rewritten by expressing du by as u(T, v):

$$du = \left( \frac{du}{dt} \right)_v dT + \left( \frac{du}{dv} \right)_T dv \quad (11)$$

$$du = C_v dT + \left[ T \left( \frac{dP}{dT} \right)_v - P \right] dv$$

$$mC_v dT = dQ + \sum (h_i - h) \dot{m}_i dt - T \left( \frac{dP}{dT} \right)_v m dv \quad (12)$$

Resulting a differential equation with two variables (m and T):

$$\dot{m} = f(m, T, \dot{T}, t) \quad \dot{T} = g(m, \dot{m}, T, t) \quad (13)$$

The properties of a fluid in a volume as function of pressure and temperature can be described by means of an equation of state<sup>2</sup>. In this paper the Peng Robinson equation is used, but others can be used for specific applications.. These equations are used to determine enthalpy  $h$ , Density  $\rho$ , specific heat constant for constant pressure and constant volume  $C_p$  and  $C_v$ , and the derivative of pressure with respect to temperature at constant volume  $(dP/dT)_V$  as function of pressure and temperature.

This type of equations is known as an initial value problem: an ordinary differential equation together with an initial condition at a given point in time. These values are given by  $T_0$  and  $m_0$  for each volume at  $t = 0$ .

### Challenges in numerical simulations

Initial value problems are in general solved in time using linear multistep methods<sup>3,4,5</sup>, by taking a small step in time ( $h$ ), in which the function value does not change significantly. Now the value of  $m_1 = m_0 + hf(m_0, T_0, \dot{T}_0, t_0)$  and of  $t_1 = t_0 + hg(m_0, \dot{m}_0, T_0, t_0)$ .

This method is called the Forward Euler method, a first order Forward Differentiation Formula [FDF]. The error per step is proportional to the square of the step size. A smaller error can be achieved by decreasing the step size or by using a higher order differential formula, e.g. by taking additional preceding points into account<sup>6</sup>.

The working cycle of a reciprocating compressor features parts which are characterized by quasi-linear dynamics, e.g. compression, as well as highly nonlinear dynamics as encountered during the opening and closing of compressor valves, or when the fluid state is near to a phase transition, in which mass and temperature are highly nonlinear. Results show that an explicit solver is not able to achieve the required stability due to rapid changes of the system. This is demonstrated in *Figure 2*: The explicit scheme requires 500 time steps per degree to obtain a stable solution. A larger time step results in instability.

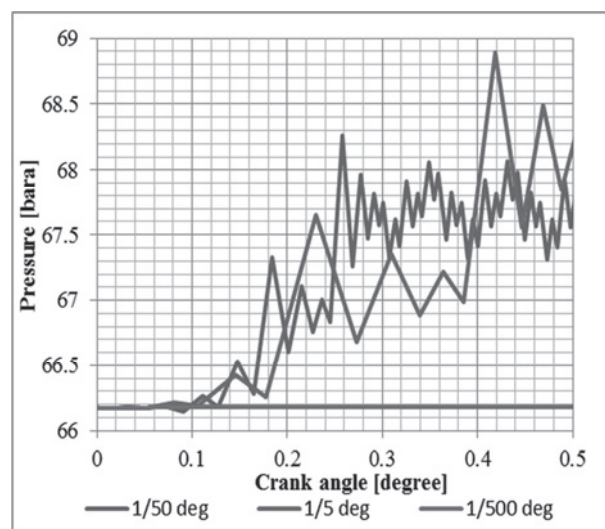


Figure 2: Instability of an explicit scheme at larger time steps.

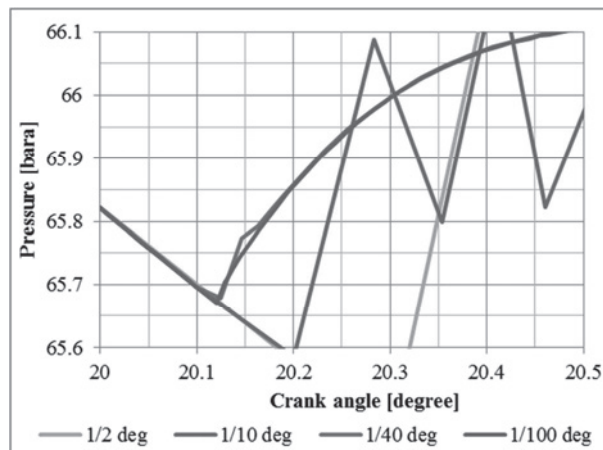


Figure 3: Accuracy of an implicit scheme for different step sizes

Forward Differentiation Formula methods are explicit methods since only data from previous time steps is taken into account. The Backward Differentiation Formula [BDF] however belongs to a family of implicit methods. The Backward Euler method at  $t = 0$  for example is given by  $m_1 = m_0 + hf(m_1, T_1, \dot{T}_1, t_1)$  and of  $t_1 = t_0 + hg(m_1, \dot{m}_1, T_1, t_1)$ . Since this equation is nonlinear, a Quasi-Newton method is used to solve these nonlinear equations.

The advantage over an explicit method is the increased stability, which allows a larger time step. However, at valve opening and closing overshoot does occur when the step size is too large. Figure 3 shows that at least 100 steps per degree are required to describe valve opening and closing; which brings the total to 36,000 calculation steps per single revolution. Due to its complexity this would result in long computation times.

### Optimizing the solution method

A small time step is only required for specific regions. In order to reduce the calculation time a flexible time step scheme is adapted which increases and decreases the time step based on rate in which the variables change over time. Furthermore the order of the scheme is also dynamically adapted. A schematic overview of the working of the scheme is given in Figure 4.

The specific advantages of both the implicit and explicit algorithms can be used to achieve the required level of accuracy and stability without compromising on calculation time.

First mass and temperature are calculated for each volume using the explicit FDF scheme. Afterwards mass and temperature are calculated using an implicit BDF method. The nonlinear BDF equations are solved using a dedicated solver. When the answer provided by the backward scheme is too far off the FDF solution, the calculation point is rejected and the time step is automatically reduced, since this would imply the occurrence of nonlinear effects<sup>7</sup>.

Figure 5 clearly shows the resulting decrease in step size around the closing of a crank-end suction valve. Short before the closing the step size is reduced by a roughly a factor  $10^3$ . In the next time steps the step size is gradually increased again.



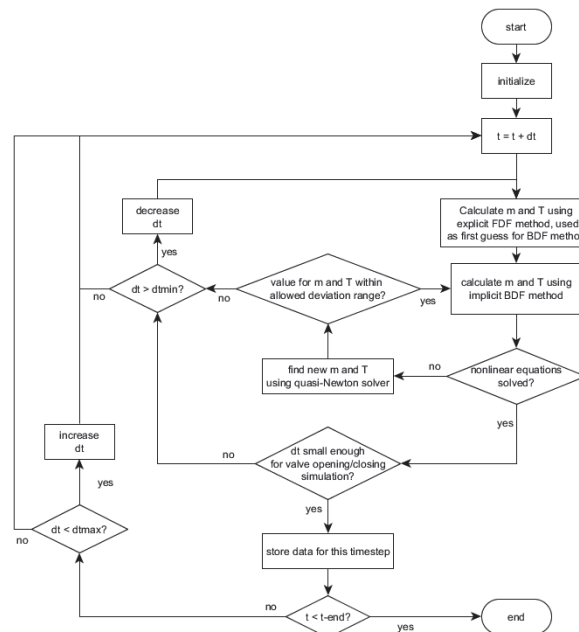


Figure 4: Flow chart time simulation model

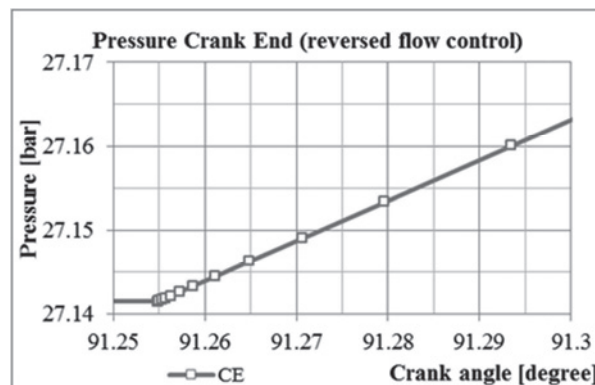


Figure 5: Changing time step during closing of a suction valve

### Modelling improvements

These advanced simulation techniques are used to select appropriate cylinder designs, compressor frames and pulsation dampeners, but are also used to simulate all the operating cases to determine maximum rod and pin load as well as crankshaft torque fluctuations at full and part-load conditions with valve unloading, clearance pockets and reversed flow control.

Due to the fact that all heat transfer to the cooling water and environment, frictional heat and the exact gas properties<sup>8</sup> are known for each single point in time a very accurate prediction of discharge temperature and other performance aspects can be made. Also the temperature rise of the process gas in case of reversed flow capacity control or suction valve unloading can be determined with high accuracy.



Since the calculation is performed in the time domain, it is also possible to simulate transient operating conditions where pressures, temperatures or gas composition are not constant, such as during the start-up and pressurization of a compressor. Furthermore advanced valve motion can be simulated to check valve behavior for every operating condition.

### **Field performance assessments**

The simulation model in the time domain is not only useful for selection and design applications, but can also be applied to verify the performance of compressors in the field. The accuracy is increased significantly compared to conventional calculations models as the simulation model in the time domain is also able to capture the effects of relevant factors external to the compression volume itself, such as gas passage channels, orifices, nozzles and pulsation vessels. This enables correct assessment and identification of compressor performance issues, allowing attributing specific effects witnessed in field measurements to the correct cause. In addition simulation data can be used to compare field measurement data with simulation results in order to verify the compressor performance. Ideally the measurement data should closely resemble the simulation results. If any discrepancies are identified, several performance aspects can be modified to assess the effect on the performance. For example:

- Valve leakage
- Obstruction in pipe section
- Wrong (installed) orifice
- Increased leak flows
- Changes in gas composition
- Condensation of process gas

### **Case study**

<i>Case 1: 3-stage combined heat/power compressor, 495rpm</i>			
Stage 1	Stage 2	Stage 3	
3.3 – 9.6	9.3 – 26.9	26.4 – 72.4	bar(a)
60% H2		15% C2	
15% C1		10% C3+, others	

An increase in crosshead guide vibration levels of the 3rd stage cylinder of a reciprocating compressor was measured in the field. In order to verify that the cylinder itself was performing as expected, a pressure volume measurement was analyzed. Figure 6 shows the measurement and the simulation data of the crank-end side of subject cylinder. The results from the measurements provide a good match with the simulation data, except for the cylinder pressure pulsations which are outside the scope of the used model since no relevant valve data was available. The dominant frequencies in the pulsations are found to be different from the observed vibrations on the crosshead guide, therefore it can be concluded that the actual compressor performance is corresponding with the theoretical model and there is no apparent relationship between the pressure pulsations and witnessed vibrations.

<i>Case 2: 1-stage refinery compressor, 425rpm</i>	
Stage 1	
~ 67 – 81	bar(a)
55% H2 40% C1 5% C2+	

A single stage, double-acting reciprocating compressor operating in a refinery was known to operate at conditions deviating from the original design; especially the process gas composition changed significantly over time. Pressure-volume measurements were performed to validate the performance and loading of the compressor. The measured cylinder pressures were found to be considerably different from the compressor design values. As a first step, the simulation model of this specific compressor was generated, using the original design and actual gas composition, measured suction and discharge pressures as well as the actual compressor valves.

The simulation based on the original gas composition predicts a lower cylinder pressure differential than measured. Since the actual gas composition has changed over time and the molecular weight is increased, a second simulation is performed with the actual gas composition. The discharge side pressure profile does match with the simulation results, but on suction side there is still a discrepancy between the measurement and the simulation results.

After analyzing the first results, it became apparent that the compressor installation had been modified in the past and restriction orifices were added between the cylinder flange and suction and discharge pulsation dampeners. The effect of subject orifices on the compressor performance in terms of flow and loading was never considered. The difference due to the changed gas composition had a less pronounced effect on the cylinder pressures and loading of the compressor.

The model was subsequently expanded to include the orifices as well as pulsation dampeners. *Figure 7* and *Figure 8* clearly indicate the effect of the addition of the orifices to the system. *Figure 7* depicts the measurements and simulation results with a only the discharge orifice, while *Figure 8* shows the effect of the added suction orifice to the cylinder pressures. The root cause of the deviating cylinder pressures could therefore correctly be attributed to the orifices and a correct assessment of the current loading condition of the compressor could be made.

The numerical simulation method is therefore able to accurately model and include the effects of time- and flow dependent elements such as restriction orifices on the overall performance of the compressor.

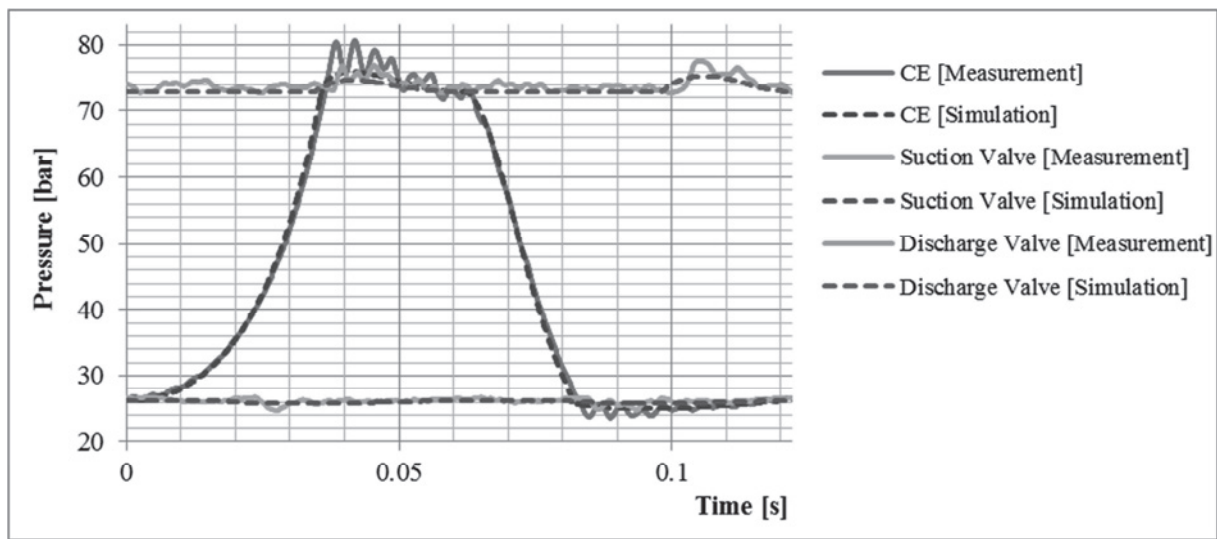


Figure 6: *pV*-measurement and simulated *pV*-diagram

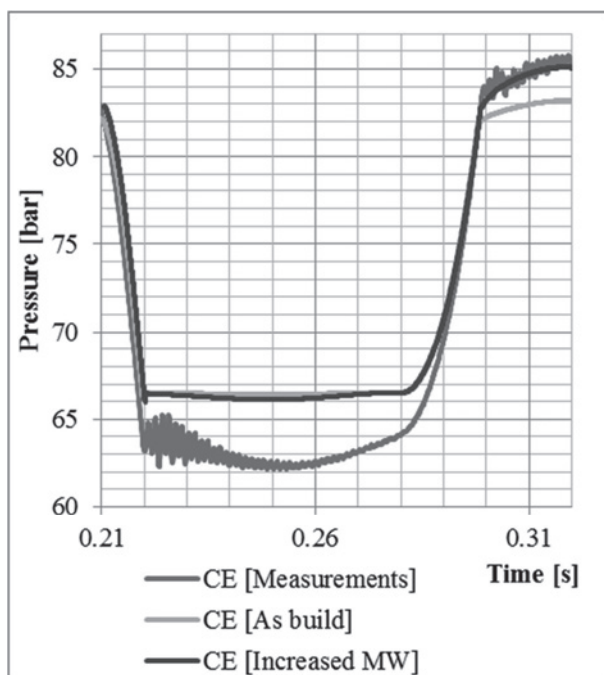


Figure 7: Measurements and simulations results (as build and increased mole weight)

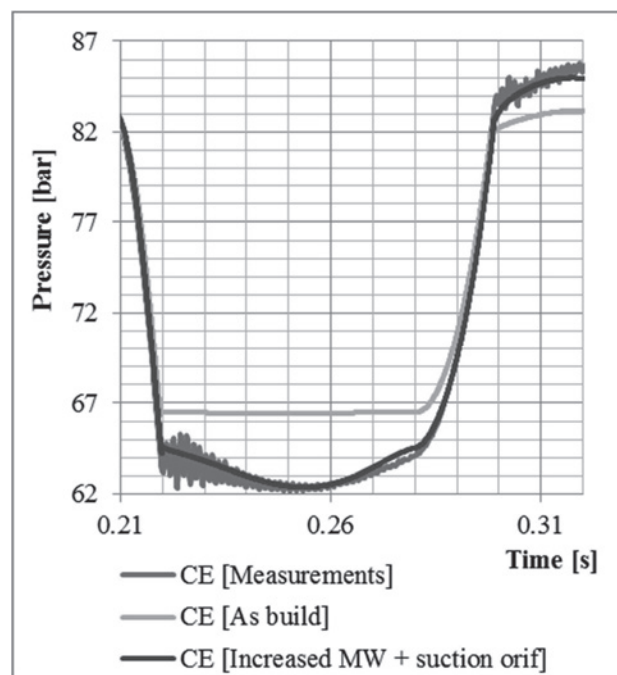


Figure 8: Measurements and simulations results (as build and increased mole weight + suction orifice)

## **Conclusion**

Simulating the thermodynamic performance of a reciprocating compressor in the time domain brings numerous advantages, but also difficulties due to the complexity of the model and rapidly changing conditions. A significant number of factors which have an effect on the performance of the compressor and are time- or flow-dependent, such as opening and closing of valves, heat transfer to cooling water, frictional losses and the effect of flow restrictions, can be simulated more accurately compared to using analytical models. The inherent challenges associated with a numerical simulation model can be overcome by using a high order numerical scheme which uses a combination of an explicit and implicit scheme. This approach enables the application of an adjustable time step to keep computation times low which is required for compressor design selections, without compromising on accuracy. The results of the simulation can be used to provide a better temperature prediction and accurate flow calculations. Furthermore the simulation model can be used to validate compressor performance in the field and identify the contribution of different components to possible discrepancies between measurements and simulation.

## **References**

1. Kittel, C. Kroemer, H. *Thermal Physics, second edition (1980), ISBN 0-7167-1088-9.*
2. Tuhovcak, J., Hejlik, J. and Jicha, M, *EPJ Web of Conferences. 92, 02100 (2015)*
3. Radhakrishnan, K., Hindmarsh, A.C. (1993), *NASA, 1327.*
4. Hanke, M. (2001), *Uppsala University, 01.*
5. Kurganov, A., Tadmor, E. (1999), *J. Comp. Phys., 160: 241-282.*
6. Hairer, E., Wanner, G. (2010), *Scholarpedia, 5(4):4591.*
7. Wang, D., Ruuth, S.J. (2008), *J. Comp. Math., 26(6):838-855.*
8. Edmister, W.C., Lee, B.I., *Applied Hydrocarbon Thermodynamics vol.1. (1983), ISBN 0-87201-855-5*





# Technical Paper

**Session: 47-2**

**Session Name: Calculation 1**

## Large size reciprocating compressor analysis with a finite volume 1D model

**Author:**

**Isacco Stiaccini**  
Research Fellow  
University of Florence  
50139, Italy

**Co-Author 1:**

Niccolò Fiorini,  
PhD Student,  
University of Florence,  
50139 Florence, Italy

**Co-Author 2:**

Francesco Balduzzi  
Research Fellow  
University of Florence  
50139 Florence, Italy

**Co-Author 3:**

Giovanni Ferrara  
Associate Professor  
University of Florence  
50139 Florence, Italy

**Co-Author 4:**

Alberto Babbini  
Lead Engineer  
GE Oil & Gas – Nuovo Pignone  
50127 Florence, Italy

**Co-Author 5:**

Gianni Orsi  
Lead Engineer  
GE Oil & Gas – Nuovo Pignone  
50127 Florence, Italy

## Summary

In the reciprocating compressor design process, the performance predictability plays a key role since the early stages. Performance of reciprocating compressors are often calculated by means of lumped parameter numerical model, neglecting the presence of unsteady phenomena such as pressure waves travelling inside cylinder bore and suction/discharge gas chambers. Dealing with a large size compressor, it can be observed that the time needed for the pressure waves to travel the whole cylinder bore is comparable with the duration of the physical phenomena of the thermodynamic cycle. This affects the gas transfer process inside the cylinder chamber, mostly during the suction and discharge phases, and thus the compressor performance. The authors inferred that a spatial discretization of the compression chamber domain could be useful in order to more accurately predict the indicated power and mass flow rate. In this case, the accuracy of lumped parameter models in predicting the compressor performance demonstrated to be improvable. In fact, the modelling of the compression chamber domain by using one only lumped element does not allow to simulate the gas motion inside the cylinder. Therefore, a more realistic way to simulate the mass flow inside the chamber is to increase the spatial dimension of the fluid domain representation. This leads to a numerical model that includes a spatial definition of the cylinder chamber, in order to account for the fluid inertial effects.

In order to meet this need and to increase the accuracy of the thermodynamic cycle simulation, the authors developed a one-dimensional compressor model that solves the fluid dynamic equations by applying the finite volume method (FVM). At first, the FVM model was validated on a simplified test case simulated with transient CFD. Then, a real large size reciprocating compressor was tested both with the FVM model and a lumped parameter model. The compressor performance was monitored and the numerical results were compared with experimental measurements collected on a dedicated test bench. The FVM model showed a better agreement with the experimental data with respect to the results of the lumped parameter model. The comparison between the numerical results and the experimental data was useful to assess the influence of the fluid distribution in the cylinder chamber on the compressor performance predictability. The importance of simulating the cylinder chamber with a good spatial discretization showed to be crucial to match the experimental data.

## Introduction

The performance predictability of reciprocating compressors has a key role since the early stages of the design. The proper knowledge of the compressor performance with a given set of geometrical and thermodynamic parameters is useful to reduce both time and costs of the design.

Numerical models that simulate the thermodynamic cycle of the compressor are widely used with the aim of analyzing the phenomena involved in the thermodynamic cycle and predicting the compressor performance. In the first phases of the design, lumped parameter models are widely used for preliminary analysis because of the low computational cost. These models simulate the cylinder chamber as a lumped element, whose volume varies with time. The thermodynamic properties (i.e. pressure, temperature and density) are uniform in the whole fluid domain that the volume represents and the change of state in the cylinder chamber follows quasi-static transformations.

The first lumped parameter model of a reciprocating compressor was developed by Costagliola<sup>1</sup>. In this model the valve dynamics was also included, and the valve motion depends on the pressure difference across the valve. In the following years, this kind of model found a wide application for both research activity and industrial design. Concerning the reciprocating compressor study, Winandy<sup>2</sup> used a similar numerical model for the estimation of compressor perfor-



mance. The same model was applied by Elhajj<sup>3</sup> to develop a condition monitoring strategy for a two-stage reciprocating compressor. A comprehensive simulation model for a semi-hermetic CO<sub>2</sub> reciprocating compressor in which the leakage and frictions are considered was developed by Yang<sup>4</sup>. A natural gas reciprocating compressor was simulated by Farzanhed-Gord<sup>5</sup> that integrated the real gas properties in the lumped parameter model of the compressor. In all of these studies, the numerical results were compared with experimental data. The agreement highlights that the model is suitable for preliminary evaluations. Gimeli<sup>6</sup> extended the 0D-1D thermos-fluid dynamic simulation approach to describe the phenomena internal to the volumetric machines, reproducing pressure waves' propagation in the ducts. Lang<sup>7</sup> coupled the 0-, 1- and 3D tools for the simulation of the suction line of a reciprocating compressor.

Dealing with large size reciprocating compressors, the authors found that the performance predictability of the lumped parameter models has limits that cannot be neglected. This was addressed to the inability of such models in simulating the pressure wave propagation phenomena that affects the thermodynamic cycle. For this reason, an upgrade of the fluid domain discretization is needed. A first insight of the effect of waves and unsteady flow inside the cylinder was given by E. Machu<sup>8</sup>, who calculated simple waves by using the method of characteristics. Later G. Machu<sup>9,10</sup> described a numerical model based on the one dimensional Euler equations: the model was able to describe also laterally running waves moving inside the compressor chamber. Then, Aigner<sup>11</sup> and Steinrück<sup>12</sup> presented a compressor model focusing on the evaluation of a compressor performance with improved description of the physical phenomena involved in the compressor thermodynamic cycle. A spatial discretization was considered both inside the cylinder chamber and the compressor plena.

The above mentioned models inspired the authors to carry out the activity presented in this paper. In this work, the authors developed a FVM numerical model based on the F-wave solution method of the Euler equation in the fluid domain of the compressor chamber. The model has a 1D spatial distribution: the cylinder chamber is discretized in a finite number of volumes that change size during the simulation as a consequence of the piston movement during the compressor operation. In case of multi-valve configurations, in the FVM model a single valve with an equivalent section represents the three valves. Suction and discharge valves are then facing one each other in the cylinder. Moreover, the numerical accuracy of the model was increased by using flow coefficients computed with stationary CFD simulations.

In a preliminary phase of the model development, two test cases on simplified cylinder geometries were simulated and the results were compared with ad hoc unsteady CFD simulations. In this way, a preliminary validation of the numerical model was achieved. Then, the model was used to simulate a real compressor and the results were compared with the measurements collected during an experimental activity. The compressor simulations were carried out also with a simplified lumped parameter model that does not take into account any corrective terms. In each numerical model, the valve flow coefficients were obtained from experimental flow characterizations on a dedicated test bench.

By comparing the numerical results with experimental measurements, the advantages in terms of performance predictability of the FVM model were assessed.

### **FVM Numerical model**

Dealing with large size reciprocating compressors, lumped models are not reliable to fully predict the performances of the machinery due to the simplified discretization of the in-cylinder fluid domain. To improve the predictability, a one-dimensional numerical model was developed by taking into account the fluid domain geometry of the compression chamber (*Figure 1*) and thus

the pressure wave propagation and mass flow of gas inside the cylinder. The cylinder was modelled by choosing the diametrical axis connecting suction and discharge central valves. The computational domain also includes a simplified configuration of the cylinder gas chambers to take into account the pressure variations in the volumes upstream and downstream of the valves during the suction and discharge phases.

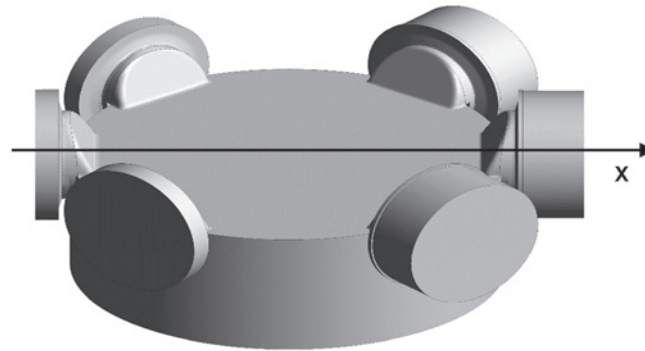


Figure 1 – CAD of the in-cylinder fluid domain.

### Mathematical model

The one-dimensional governing equations for the gas flow are obtained by taking the mass, momentum and energy balance over a cross section:

$$\frac{\partial}{\partial t}(\rho A) + \frac{\partial}{\partial x}(\rho u A) = 0, \quad (1)$$

$$\frac{\partial}{\partial t}(\rho u A) + \frac{\partial}{\partial x}(\rho u^2 A + p A) = p \frac{\partial A}{\partial x}, \quad (2)$$

$$\frac{\partial}{\partial t} \left[ \rho A \left( C_v T + \frac{u^2}{2} \right) \right] + \frac{\partial}{\partial x} \left[ \rho u A \left( C_v T + \frac{u^2}{2} \right) + u A p \right] = 0. \quad (3)$$

Assuming isentropic conditions ( $s = \text{const.}$ ), pressure can be expressed in terms of density and entropy:

$$p = p(\rho, s). \quad (4)$$

In order to solve conservation laws that describe the fluid motion, the system of hyperbolic equations can be written in conservative form as:

$$\frac{\partial \mathbf{q}}{\partial t} + \frac{\partial \mathbf{f}(\mathbf{q}, x)}{\partial x} = 0. \quad (5)$$

Where the state vector  $\mathbf{q}$  and the flux function  $\mathbf{f}(\mathbf{q}, x)$  are defined as follows:



$$\mathbf{q} = \begin{Bmatrix} R \\ u \end{Bmatrix}, \quad f(\mathbf{q}) = \left\{ \frac{Ru}{2} \frac{p_0}{\rho_0^{\gamma}} \left( \frac{R}{A} \right)^{\gamma-1} \right\}. \quad (6)$$

Where  $R=\rho A$ . In the Finite Volume Method, the computational domain is divided into cells and the unknown quantity that is numerically computed is the cell average of  $\mathbf{q}$  on each cell. The authors followed the F-wave approach<sup>10</sup> as suggested by Aigner<sup>11</sup> to reduce the system (6) to the form:

$$\mathbf{Q}_i^{n+1} = \mathbf{Q}_i^n - \frac{\Delta t}{\Delta x} \left( \mathbf{z}_{i+\frac{1}{2}}^1 + \mathbf{z}_{i-\frac{1}{2}}^2 \right). \quad (7)$$

The interaction between two cells is done through the cell interface, which separates the two different states at the left and at the right side. This interaction can be exactly solved since the initial conditions at time  $t=n \cdot \Delta t$  correspond to the Riemann problem, determining the local wave structure<sup>13,14,15,16,17</sup>.

In the 1D model the diameter that links the suction and discharge central valves has been chosen as the main direction of mass flow rate inside the cylinder (x axis). The equations of motion (Euler equations) are integrated over a cross section  $A(x,t)$  perpendicular to the x axis. The cross section areas vary with time due to the piston motion. The computational domain consists of the interior of the compressor, including the cylinder, the valve pockets and the pressure chambers. Cylinder, suction and discharge pressure chambers are considered as three different domain linked at the same compressor boundary through which the communication is done with the mass flow rate. In *Figure 2* a schematic representation of the fluid volume discretization of cylinder with pocket volumes and gas chambers is shown. The pocket volumes are split into two volumes: one that is located in the cylinder head (head pocket) and the other is facing the valve (valve pocket). This configuration allows taking into account the whole length of propagation of the pressure waves (valve to valve) inside the cylinder.

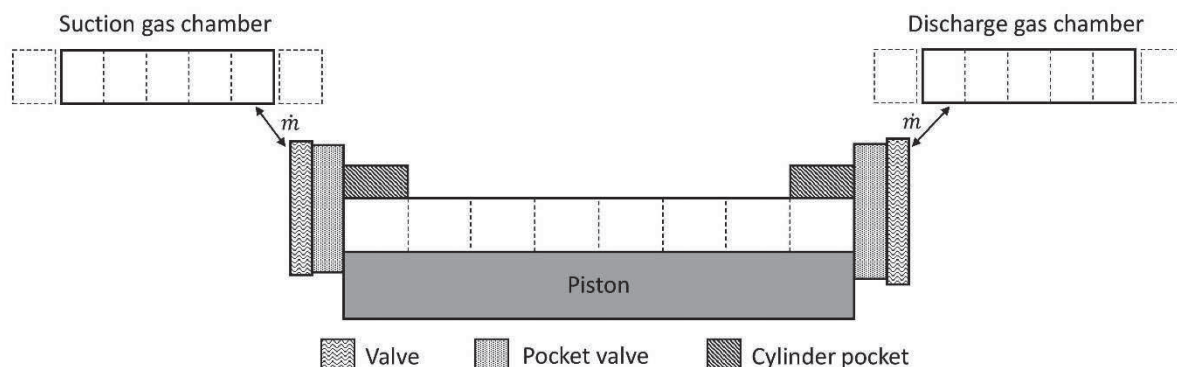


Figure 2 - Discretization scheme of the fluid domain.



### Boundary conditions

In order to obtain a good predictability of the FVM model, the choice of boundary conditions is of primary relevance. The state variables values at the boundary of the fluid domain are set by imposing the proper  $\mathbf{Q}$  value in the ghost cells. In other words, the values of  $\mathbf{Q}$  in the ghost cells are set in order to obtain specific state variable values at the boundaries. During compression and expansion phases, a rigid wall boundary condition is imposed in the cylinder domain. In this case the values of variables of the ghost cell are set to ensure a zero speed at the wall:

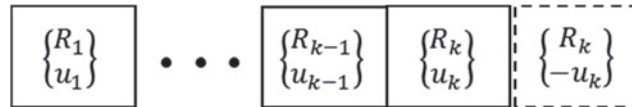


Figure 3 - Subdivision of the computational domain into grid cells. Dashed line represents the ghost cell at the right boundary.

$$\mathbf{Q}_{k+1} = \begin{Bmatrix} R_k \\ -u_k \end{Bmatrix}. \quad (8)$$

When the valves are open, mass flow rate is computed at the interface between cylinder and pressure chamber (Figure 2). It is done by considering the flow through the valve as the (stationary) outflow of a gas from a pressurized container through a convergent nozzle:

$$\dot{m}_{ideal} = \frac{p_0 A_{ref}}{\sqrt{RT_0}} \sqrt{\frac{2\gamma}{\gamma-1} \left(\frac{p}{p_0}\right)^{\frac{2}{\gamma}} \left(1 - \left(\frac{p}{p_0}\right)^{\frac{\gamma}{\gamma-1}}\right)}. \quad (9)$$

$A_{ref}$  is the geometrical area of the valve used as a reference, and  $K_s$  is the flow coefficient that is defined as follows:

$$K_s = \frac{\dot{m}_{real}}{\dot{m}_{ideal}}, \quad (10)$$

where  $\dot{m}_{real}$  can be numerically or experimentally determined. By taking advantage of the flow coefficient  $K_s$ , it is possible to compute the mass flow rate in the FVM model and the boundary values are so set:

$$\mathbf{Q}_k = \begin{Bmatrix} R_k \\ \dot{m}_{out} \\ R_k \end{Bmatrix}. \quad (11)$$

Non-reflecting condition has been used at the external boundaries of gas chambers.

$$\mathbf{Q}_{k+1} = \mathbf{Q}_k \quad , \quad \mathbf{Q}_0 = \mathbf{Q}_1. \quad (12)$$



### Numerical test cases

The FVM numerical model reliability was preliminary evaluated by taking advantage of a direct comparison with CFD simulations. Two simplified numerical test cases were defined and simulated both with the FVM model and CFD. The two configurations are shown in *Figure 4* and are named “Oval” (*Figure 4.a*) and “3Valves” (*Figure 4.b*). The “Oval” configuration is defined by a single suction duct (in blue) and a single discharge duct (in red), which have a cross-section equivalent to the sum of the cross-sections of the three ducts of the “3Valves” configuration.

Unsteady CFD simulations of the working cycle of both simplified compressor configurations were performed by making use of the porous approach for the valve representation, presented by some of the authors in previous works<sup>18,19</sup>. The method is based on the assumption of mutual independence between the distinct sources of losses (so-called superposition of effects principle) and consists of substituting, in the CFD model, the actual valve geometry with an equivalent porous region. Porous regions are zones of the fluid domain for which, in the CFD solver, a sink term is added to the standard Reynolds-Averaged Navier-Stokes equation, thus generating a localized pressure drop equivalent to the pressure drop produced by a valve, together with a straightening of the flow. Additional details can be found in the aforementioned papers.

Numerical CFD simulations have been carried out with the commercial code ANSYS® Fluent®. The equations for a compressible, non-steady, three-dimensional turbulent flow are solved by means of the U-RANS (Unsteady Reynolds-Averaged Navier-Stokes) approach by adopting the standard  $k-\varepsilon$  turbulence model along with wall functions for the near wall treatment. The piston motion is handled by adding/removing the cylinder cells while they are stretched/compressed (*layering* method). The overlapping between liner and pockets during the piston masking phase is handled by means of *sliding interfaces*: the faces that aren't overlapping are defined as wall boundary while the overlapping faces are replaced by a set of faces internal to the mesh. The PISO algorithm is employed to solve the pressure-velocity coupling and the second order upwind scheme is used for spatial discretization of the whole set of RANS and turbulence equations. Two complete cycles with an angular timestep of  $0.1^\circ$  were necessary to correctly initialize the flow field and to achieve a periodic solution.

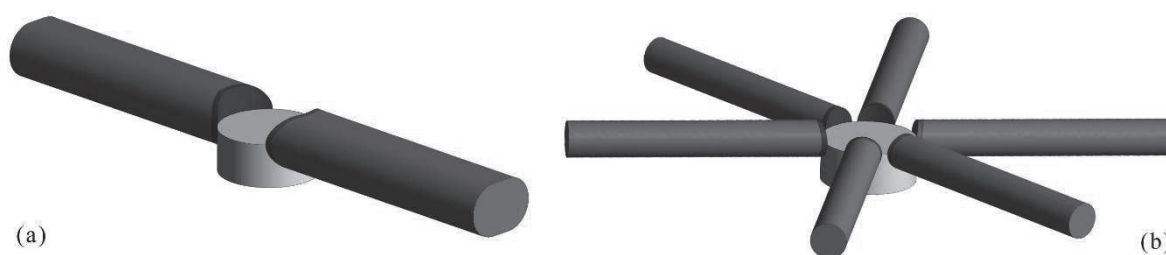


*Figure 4 - The two test cases simulated with both the FVM and the CFD, Oval (a) and 3Valves (b).*

The geometrical and thermodynamic data of the two test cases are the same of the experimental test case shown in the next paragraph. The valve opening angles were imposed and chosen on the basis of suction and discharge design pressure.

The test case geometries were defined with the aim of determining the influence of tridimensional wave propagation on the thermodynamic cycle. Moreover, particular attention was paid to define the FVM model reliability on simulating geometries with different valves distribution.

Both cases were fluid-dynamically characterized with CFD steady-state simulations that allowed computing the suction and discharge flow coefficients needed by the FVM model (*Figure 5*). It can be noticed how the coefficients start to vary from a specific piston position, corresponding to the piston masking beginning, due to the reduction of the flow area of the valve pocket.

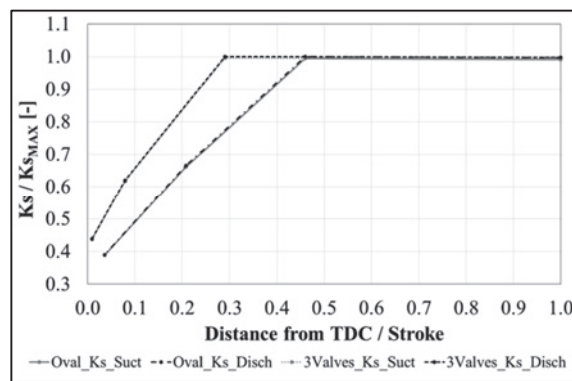


*Figure 5 - Flow coefficients of the two test cases. The values were computed by processing CFD steady-state simulations with different piston positions.*

The working cycle of both test cases was simulated also with a lumped parameter model, in order to highlight the difference in the prediction capability of the FVM model with respect to a 0-D model. In *Figure 6.a* and *Figure 6.b* the Clapeyron diagrams of the two test cases (“Oval” and “3Valves” respectively) are shown. It can be noticed how the FVM model is in good agreement with the CFD results in both cases, while the lumped parameter model (“0D”) underestimates the cycle absorbed power. This effect is due to the pressure wave propagation influence that is not considered by the lumped element discretization of the numerical model. On the other hand, the FVM model allows considering such phenomena and their influence on the thermodynamic cycle. It follows that the performance predictability of the FVM model shows to be higher than the lumped parameter one.

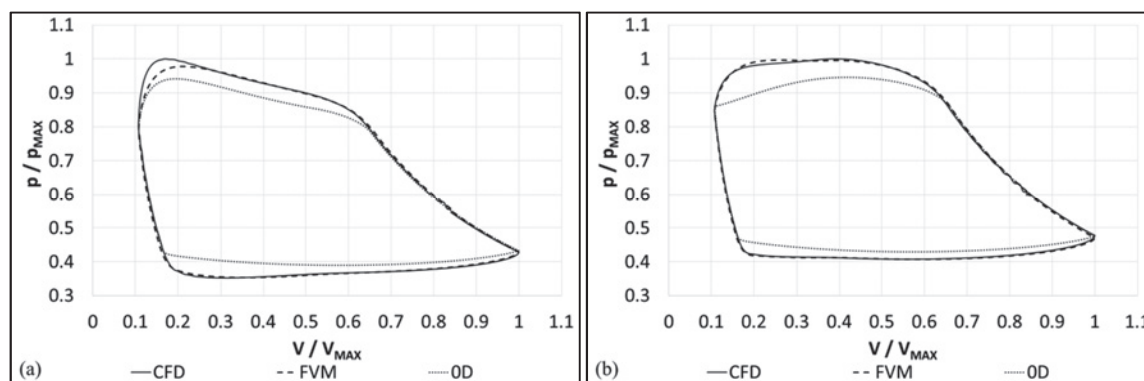


Figure 6 - In-cylinder pressure of “Oval” (a) and “3Valves” (b) test case.

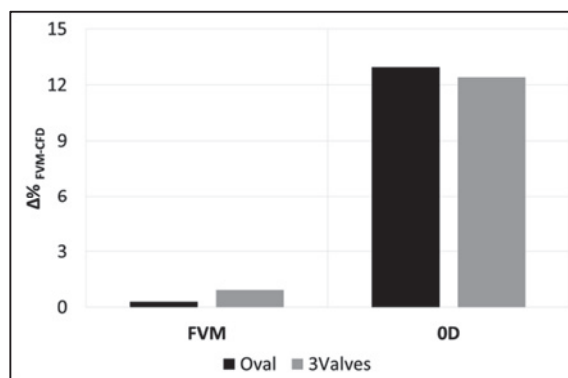


Figure 7 - Indicated absorbed power percentage difference between the CFD simulation results and the numerical model ones.

In Figure 7 the percentage difference between the numerical simulations and CFD results is shown in terms of indicated absorbed power, as defined in (13). It is important to notice how the FVM reliability in performance prediction overcomes the one of the lumped parameter model.

$$\Delta\%_{FVM-CFD} = \frac{W_{FVM} - W_{CFD}}{W_{CFD}}. \quad (13)$$

### Experimental test cases

The FVM numerical model was used to simulate the working cycle of a real compressor, whose data are summarized in Table 1. Numerical results were compared with measurements collected at the test bench during an experimental campaign on the compressor. The compressor was simulated also by taking advantage of a lumped parameter model.

Both numerical models require the knowledge of the flow coefficients for the evaluation of the pressure losses along the suction and discharge flow paths. These were computed with CFD steady-state RANS simulations by adopting the same turbulence model and numerical algorithm of the unsteady calculations on the simplified test cases. The computational domain was defined by the whole cylinder geometry, including valves, plenums, cages, pockets, etc. Simula-

tions were carried out by imposing the pressure at the cylinder flanges and the velocity of the piston for different piston positions. This allowed taking into account the pocket-valve, valve and plenum losses of the compressor and the piston-masking effect was also considered in the numerical simulations. In *Figure 8* the suction and discharge flow coefficient derived with the CFD simulations are shown for various piston positions.

Compressor data		
Rotating speed	[rpm]	375
Bore	[m]	0.77
Stroke	[m]	0.36
Number of valves	[-]	3+3

Table 1 - Design parameter of the reciprocating compressor simulated and experimentally tested.

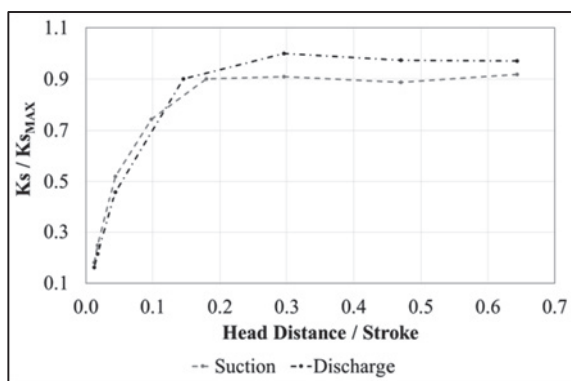


Figure 8 - Flow coefficients of the real compressor. The values were computed by processing CFD steady-state simulations with different piston positions.

The comparison was carried out in terms of in-cylinder pressure and absorbed power. In *Figure 9.a* it can be observed how the FVM model predictability of the thermodynamic cycle overcomes the one of the lumped parameter model. The main difference between the two numerical models can be observed in the suction and discharge phases, the ones that are mostly affected by the pressure wave propagation inside the cylinder chamber.



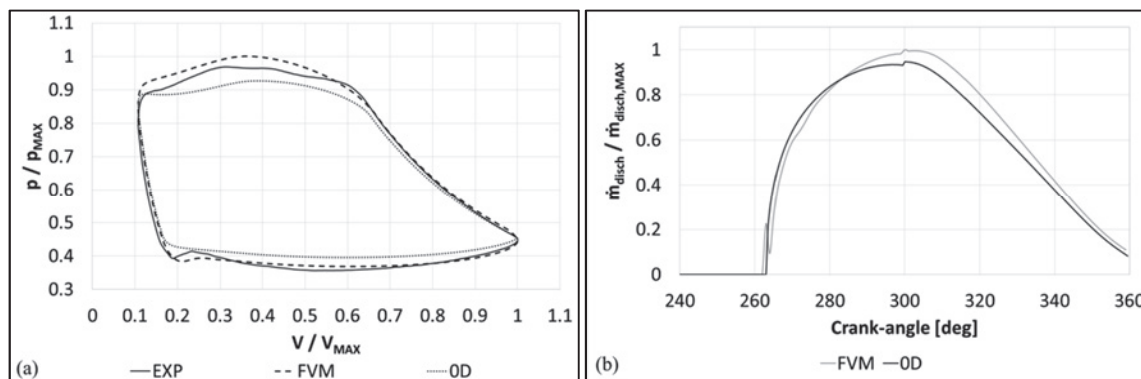


Figure 9 – Comparison in terms of in-cylinder pressure compressor (a) and discharge mass flow rate (b).

In more detail, the lumped parameter model underestimates the pressure losses when the valves are open, since the pressure in the compression chamber is greater than the experimental pressure during the suction phase and lower during the discharge phase. On the contrary, the FVM is able to correctly reproduce the pressure increase after the discharge valve opening and the pressure reduction after the suction valve opening. This capability is directly related to the inertia effect of the gas, which can be modeled only with a one-dimensional approach. After the discharge valve opening, only a small portion of the compression chamber close to the discharge valve actually starts the discharge phase, while the remaining volume of the compression chamber is not yet influenced and keeps compressing the gas. The delay due to the time needed for the pressure wave propagation determines the further increase of the global pressure and the inertial effect of the mass flowing out from the discharge valve. This can be shown in *Figure 9.b*, where the inertial effect of the flow in the FVM model can be noticed because of the lower mass flow rate in the first phase of the discharge respect to the one computed by lumped parameter model, despite the FVM discharge begins a few degree earlier.

The reliability of the numerical models was finally assessed by comparing the compressor performance expressed in terms of indicated absorbed power. The percentage absorbed power difference between the numerical models and the experimental measurements is computed as defined in (14). The values are shown in *Figure 10*.

$$\Delta\%_{NUM-EXP} = \frac{W_{NUM} - W_{EXP}}{W_{EXP}} \quad (14)$$

It can be observed how the predictability of the FVM model is higher than the lumped parameter model and allows to compute the compressor performance with higher accuracy.

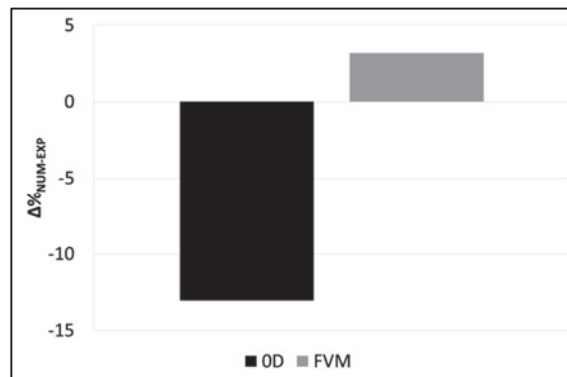


Figure 10 - Indicated absorbed power percentage difference between the experimental measurements and the numerical model ones.

### Conclusions

The performance predictability plays a key role in the reciprocating compressors design. Since the early stages of the process, a numerical model with high reliability in simulating the compressor thermodynamic cycle can lead to great advantages. Dealing with large size reciprocating compressors it was noticed that the time needed for the pressure waves to travel the whole cylinder bore was comparable with the physical phenomena involved in the thermodynamic cycle. It was inferred by the authors that the spatial discretization of the cylinder chamber could be useful to improve the performance predictability.

The numerical models commonly used are the lumped parameter ones, whose accuracy in predicting the large size compressor performance demonstrated to be improvable, due to their inability of simulating the gas motion inside the cylinder chamber. In order to increase the accuracy of the thermodynamic cycle simulation, an increased spatial dimension of the fluid domain discretization is needed.

In this work, a 1D numerical model was developed. The model is based on the Finite Volume Method (FVM) and the F-wave method is used to solve the equations that describe the fluid domain.

The FVM model at first was used to simulate two numerical test cases: the results were compared with the ones of CFD simulations. The same test cases were simulated with a lumped parameter model too. Then, the FVM and lumped parameter models were compared on a real test case. Experimental measurements were used as term of comparison for the assessment of the numerical model reliability.

In both the test and experimental case the FMV model showed higher cycle simulation reliability and performance predictability than the lumped parameter model, increasing the accuracy in the performance computation.



## References

- <sup>1</sup> Costagliola, M, 1950. The theory of spring-loaded valves for reciprocating compressors. *Journal of Applied Mechanics*, 415-420.
- <sup>2</sup> Winandy, E., Saavedra, C., Lebrun, J., 2002. Simplified modeling of an open-type reciprocating compressor. *Int. J. Therm. Sci.* 41, 183-192.
- <sup>3</sup> Elhaj, M., Gu, F., Ball, A.D., Albarbar, A., Al-Qattan, M., Naid, A., 2008. Numerical simulation and experimental study of a two-stage reciprocating compressor for condition monitoring. *Mechanical Systems and Signal Processing* 22, 374-389.
- <sup>4</sup> Yang, B., Bradshaw, C.R., Groll, A.A., 2013. Modeling of a semi-hermetic CO<sub>2</sub> reciprocating compressor including lubrication submodels for piston rings and bearings. *Int. J. Refrigeration* 36, 1925-1937.
- <sup>5</sup> Farzaneh-Gord, M., Niazmand, A., Deymi-Dashtebayaz M., Rahbari, H.R., 2015. Thermodynamic analysis of natural gas reciprocating compressors based on real and ideal gas models. *Int. J. Refrigeration* 56, 186-197.
- <sup>6</sup> A. Gimelli, A. Rapicano, F. Barba and O. Pennacchia, Reciprocating compressor 1D thermofluid dynamic simulation: problems and comparison with experimental data, *International Journal of Rotating Machinery* Volume 2012 (2012), Article ID 564275.
- <sup>7</sup> W. Lang, R. Alambauer, A. Burgstaller, D. Nagy, Coupling of 0-, 1- and 3-d tool for the simulation of the suction line of a hermetic reciprocating compressor, *Internal Compressor Engineering Conference*, 2008.
- <sup>8</sup> Machu, E. (1998): Problems with modern high speed short stroke reciprocating compressors: Increased power requirement due to pocket losses, piston masking and gas inertia, eccentric gas load on the piston. *Proceedings of Gas machinery conference USA*.
- <sup>9</sup> Machu, G. (2004): Calculating reliable impact valve velocity by mapping instantaneous flow in a reciprocating compressor. *Proceedings of gas machinery conference GMRC USA*.
- <sup>10</sup> Machu, G. (2005): Pulsationen im Verdichtungsraum - eine potentielle Schadensursache. *Industriepumpen und Kompressoren Heft 2/2005* Vulkann Verlag Essen, Mai 2005.
- <sup>11</sup> Aigner, R., 2007. Internal flow and valve dynamics in a reciprocating compressor. PhD Thesis, Wien.
- <sup>12</sup> H. Steinrück, R. Aigner, G. Machu: "Transversal waves in a reciprocating compressor", *Acta Mechanica (eigenladent)*, 201 (2008), 1-4, S. 231-248.
- <sup>13</sup> R. J. LeVeque, *Finite Volume Methods for Hyperbolic Problems*, Cambridge test in applied mathematics, 2004

- <sup>14</sup> A. Mazzia, Numerical Methods for the solution of Hyperbolic Conservation Laws
- <sup>15</sup> A.C. Berkenbosch, E.F. Kaasschieter, J.H.M. ten Thije Boonkkamp, Finite-Difference Methods for One-Dimensional Hyperbolic Conservation Laws, Numerical Methods for Partial Differential Equations, 8, 267-276, (1992)
- <sup>16</sup> E. Godlewski, P.A. Raviart, Hyperbolic systems of conservation laws, Mathematiques et Applications, Ellipses, Paris (1991).
- <sup>17</sup> R.J. LeVeque, Numerical Methods for Conservation Laws, Lectures in Mathematics, Birkh"auser, Verlag, Basel, (1990).
- <sup>18</sup> G. Pratelli, A. Babbini, F. Balduzzi, G. Ferrara, R. Maleci e L. Romani, 2012, CFD Evaluation of Pressure Losses on Reciprocating Compressor Components, 8th Conference of the EFRC, Dusseldorf
- <sup>19</sup> Balduzzi, F., Ferrara, G., Maleci, R., Babbini, A. and Pratelli, G., 2015, A Parametric Computational Fluid Dynamics Analysis of the Valve Pocket Losses in Reciprocating Compressors, Journal of Pressure Vessels Technology, 137(1), pp. 1-10



# Technical Paper

**Session: 47-3**

**Session Name: Calculation 1**

## Vibration analysis in reciprocating compressors

**Author:**

**Vasillaq Kacani**  
**Leobersdorfer Maschinenfabrik GmbH**  
**2544 Leobersdorf, Austria**

**Co-Author:**

**Ernst Huttar**  
**Leobersdorfer Maschinenfabrik GmbH**  
**2544 Leobersdorf, Austria**



## Summary

During start-ups, continuous operation, and shutdowns, reciprocating compressors generate high dynamic loads. Especially, during passing of the resonance or near the critical speeds the loads are at their maximum. The main sources of these loads are: (i) the shaking forces due to pressure pulsation, (ii) inertia forces and gas forces, and (iii) torsion, forces caused by torsional vibrations of the drive. These loads lead to vibration in components of the compressor. Different standards and guidelines specify several dynamic analyses that mitigate such vibrations in order to avoid the overload of structures. Generally, the modelling criteria and/or the required parameters of compressors such as stiffness, damping, adequate boundary system limits etc. are not clearly defined or are missing. For example, the modeling criteria as well as the prestressed effects of the structures arising from internal pressure, temperature and the misalignments during the assembly of the components, are of importance for the calculation of natural mechanical frequencies and the system's mechanical response under dynamic loads. Moreover, modelling of the structure, modelling of the crank gear, the damping factors, and the damping ratio of the mechanical structure are critical for the dynamic behavior of the drive train and for the design of other mechanical components

This paper presents the influence of modelling on the mechanical natural frequencies and the effect of inertia loads on the structure vibration and it also describes the impact of the crank gear damping on the speed fluctuation to ensure a safe operation and increasing the reliability of reciprocating compressors.

In this paper it is shown, that conventional way of modelling is not sufficient. For best results is required to include the whole system (bare block, frame, coupling, main driver, vessels, pipe work, etc.) in the model (see results in table 1).



## 1. Introduction

The main dynamic loads on reciprocating compressors are: the shaking forces due to pressure pulsation, inertia forces and gas forces, and additional forces due to the torsion vibration of drive train. The shaking forces occur typically when there is a change in pipe direction or area, at cylinder passages, on the ends of the pulsation dampers, on elbows, on reducers, on orifices, on tee pieces and on other pipe components. The inertia forces are caused by oscillating of reciprocating masses. The inertia forces act through the cross head on the structures and on the main bearing of crankshaft. The cylinder gas forces are generated within the cylinder during the working cycle: suction, compression, discharge and expansion. The gas forces are generally the highest one. They also act on cylinder covers and through the crank mechanism. They also act on crosshead guide and on crankshaft main bearing. These loads lead to vibration of the compressor components. Modeling has a direct impact on the modal analysis and the calculation of the forced vibration. The modeling criteria as well as the pre-stressed effects of the structures due to internal pressure, temperature and the misalignments during the assembly of the components, are of importance for the calculation of natural mechanical frequencies and the system's response under dynamic loads. Moreover, modelling of the structure, modelling of the crank gear, the damping factors, and the damping ratio of the mechanical structure are decisive for the dynamic behavior of the drive train and also for the design of other mechanical components.

The influence of inertia and cylinder gas forces, in addition to the pulsation shaking forces, is included in the forced-mechanical-response analysis of the compressor mechanical model. This requires an adequate finite element model of reciprocating compressors, specifically of the crankshaft, of the crankcase, of the distance pieces and of the pulsation suppression devices. For this components a 2D and 3D-modeling is used. This model also enables an undertaking of the lateral dynamic analysis of the crankshaft and the stress evaluation under torsion and bending [3], [11]. The calculation of the torsional/lateral vibration mode shapes and the mechanical natural frequencies of crankshaft with flywheel will be performed with a separate 3D-model.

## 2. Vibration analysis of the complete compressor unit

The compressor unit consists of all in-skid components such as compressor manifold, piping system, e-motor / engine, pipe, base frame, pipe/vessel supports, anti-vibration mounts etc. The skid is connected on its termination points to the off-skid piping system. In different regulations and standards [2], [3], [11] are included recommendations and proposal regarding the scope of supply, limits of the system as well as the exciting loads for the vibration analysis of the compressor mechanical model. For many reciprocation compressor units, such as off-shore applications or compressors mounted on a skid, the recommended limits of the system should be extended, at least, up to base frame - foundation interface. If available the anti-vibration mounts should be included in the analysis. Not only the cylinder gas forces but also the inertia loads must be taken into consideration while performing the mechanical response analysis of the reciprocating compressor systems. The goal of vibration analysis is the determination of the dynamic load on all components of compressor unit and the comparison with the maximum allowable values [2],[11]. This requires an accurate modeling of all parts and adequate definition of the connecting zones (interfaces) between all components involved.

## 2.1. Modeling

The modeling of reciprocating compressors requires much experience and represents a balancing act. On the one hand, the model should be as simple as possible to reduce calculation time and on the other hand as fine as necessary to get the correct technical solutions. The preprocessing is the most time consuming step while undertaking vibration analysis. In this paper an automatic parametric modeling of the components of the reciprocating compressor is shown. The script language APDL [5] (ANSYS Parametric Design Language) is used for modelling of all components. Special interfaces are defined to get the dynamic force member on bolts or contact areas/zones for all connecting parts. Generally, the crankcase is rarely modelled. The modelling effort for the crankcase may be expensive but it is absolutely necessary for the vibration analysis. Using the parametric design language, the modeling effort can be considerably reduced. The correct influence of cylinder gas forces and crank gear mass forces on vibrations of the machine can only be achieved by an adequate modelling of the crankcase, cross head, distance piece, and pulsation suppression devices. The use of 1D pipe or beam elements is only for some components such as pipes, tee-pieces support beams [6] admissible. Crankcase, distance piece, base frame and pulsation suppression devices should be modeled at least with 2D shell-elements. The recommended system limits, specified in the API 618 [11], needs to be expanded with all components up to the base frame, including if available the anti-vibration mounts. The following figures shows the finite element models for crankcase, crankshaft, flywheel, cylinder, cylinder supports, piping systems, pulsation suppression device, e-motor, base frame, piping and vessel supports. The bolts are modeled with pretension elements and are connected to the structure via spider with MPC-elements. Figure 1 shows the finite element model of the base frame, including the pedestal for the reciprocating compressor and e-motor as well as the base plates for the vertical separators: *a)* on-shore application, the skid is connected with bolts to the concrete fundament *b)* off-shore application, the skid is isolated, supported on anti-vibration mounts (AVM). The bolts and AVM are part of base frame model. Figure 2 shows the crankcase manifold including the crankshaft, flywheel and the distance piece. The presented model is also suitable for the dynamic lateral analysis of the crankshaft. For the crankshaft main bearings, spring elements with appropriate stiffness and damping were used.

*Figure 1. FE-Model of base frame and pedestal: a) onshore-application b) offshore- application.*





Figure 2. Crankcase, flywheel, crankshaft, main bearing

Based on the parametric technique described above, Figure 3 shows the finite element model of the two stage balanced opposed B154 with a power of 1MW, 720 rpm, 45t weight, offshore reciprocating compressor unit with crankcase, crankshaft, flywheel, double compartment distance pieces, cylinders, cylinder supports, e-motor, pulsation suppression devices, coolers, separators, piping system, base frame including pedestal, anti-vibrating mounts and all corresponding supports.

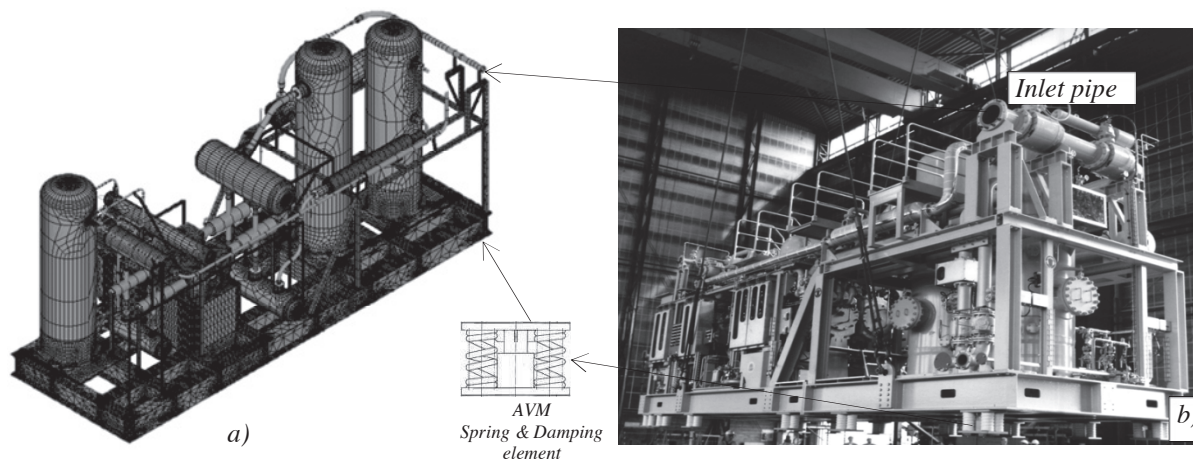


Figure 3 a) FEM of compressor unit, b) photograph of the offshore application with anti-vibrating mounts.

## 2.2. Modal analysis

After the modeling of the compressor, the modal analysis can be performed. The effect of pre-stressed conditions – temperature, internal pressure, misalignment - on the natural mechanical frequencies (NMF's) is described in [7], [10]. Under pre-stressed conditions the mechanical system is stiffer and so the natural mechanical frequencies were higher. Figure 4 shows the circumferential mode of vibration and the corresponding natural frequency of a vertical vessel – length  $L=3000\text{mm}$ , Diameter  $OD=609\text{mm}$ , shell thickness  $t=15\text{mm}$  – depending on the internal pressure. The curve in figure 4 c) represents the ration of the frequency  $f(p)$  under internal pressure  $p$  to the frequency  $f_0$  at pressure zero. The difference between the two natural frequencies  $f_{(p)}$  and  $f_0$  is up to 25%, and depends on internal pressure.

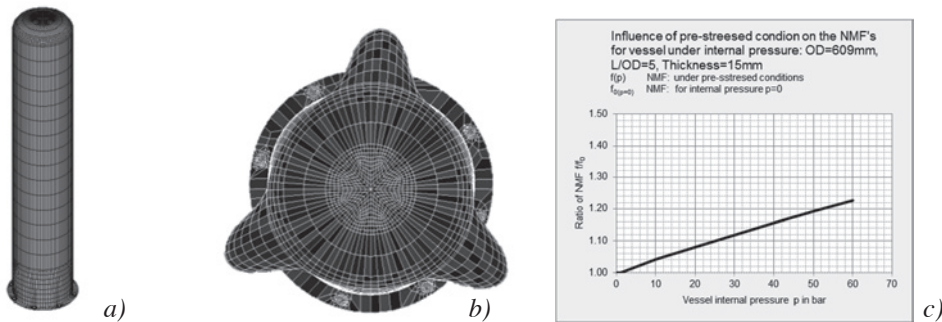


Figure 4. a) Vertical separator L/D=5, D=609mm, t=15mm, b) vibration mode, c) frequency ratio  $f_{(p)}/f_0$ .

Further the system modelling limits has a major influence on the natural mechanical frequencies (NMF's) of compressor units. In figure 5 three different models of a compressor unit are shown: a) pulsation suppression devices and piping system, b) crankcase manifold, piping system, cylinder and cylinder support and c) complete compressor unit including e-motor, base-frame with anchor bolts on concrete foundation. The figures 5a) and 5b) represent a simplified model that is commonly used to carry out pulsation studies in reciprocating compressors. The third model is closer to the real system. This model must be used for simulation calculation.

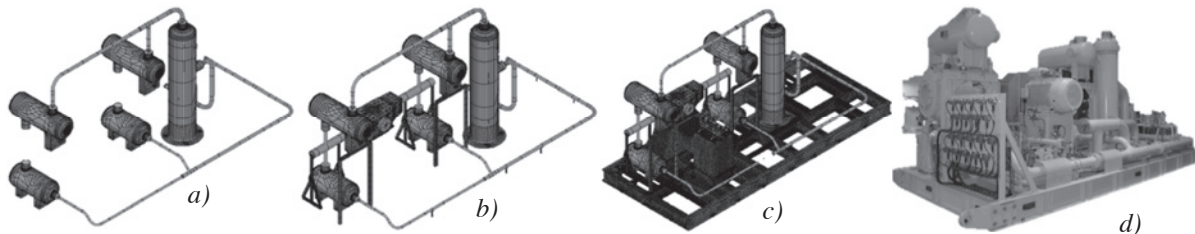


Figure 5. Three different models for the same compressor unit: a), b,) c) and photograph d), on-shore application.





The following table contains the first 10 MNF's, calculated for the three above models. The differences between the natural frequencies are more than 100%. The first models are practically unsuitable for conducting vibration analysis. Only the third model can provide useful results. With this model both the dynamic response analysis and the thermal study can be performed immediately one after another. So, quickly and easy an optimal solution can be found, as the pipe thermal stress analysis is in conflict with the goals of the mechanical dynamic design.

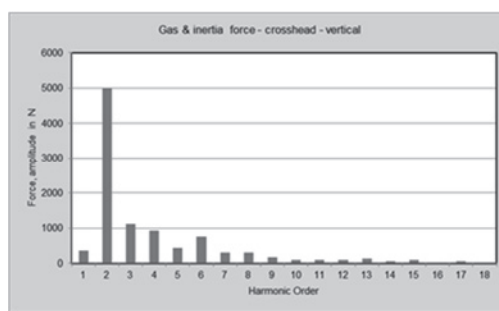
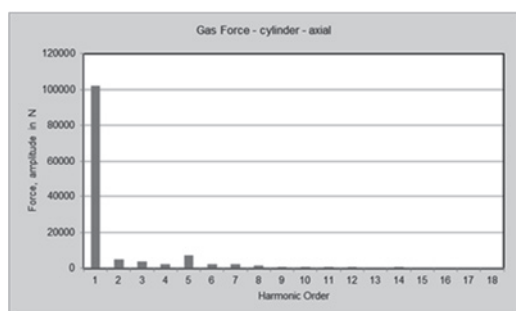
Table 1

NMF's: Natural mechanical frequencies			
Number	Model a)	Model b)	Model c)
[-]	[Hz]	[Hz]	[Hz]
1	28.5	27.7	16.2
2	29.6	28.2	17.9
3	40.4	29.4	22.1
4	59.6	40.4	25.5
5	63.1	41.9	26.3
6	67.0	43.1	31.0
7	74.8	60.8	34.5
8	84.7	61.1	35.2
9	86.7	63.0	38.0
10	92.7	63.9	39.0

The difference between the NMF's ~75%

### 2.3. Forced mechanical response analysis

Next, the forced response analysis shall be performed. The exciter forces on the structure are the inertia (mass) forces, gas (stretching) forces in cylinders as well as the shaking forces on valve passages, cylinder passage, heads of the pressure pulsation devices, separators, coolers, pipe work components such as elbows, tee's, reducers, safety valves, etc. Figure 6 shows harmonic amplitudes of the cylinder gas force  $F_{Gas,axial}$  acting in cylinder in axial direction (cylinder axis), gas and mass force  $F_{crosshead\_vertical}$  acting on the crosshead guide in vertical direction (vertical to cylinder axis), gas and mass force  $F_{Crank\_pin\_vertical}$ ,  $F_{Crank\_pin\_axial}$  acting on the crank pin in normal and axial direction. Thus there are four different dynamic exciter forces for each axis of the reciprocating compressor. Further, additional forces, resulting from the torsion should also be considered. The exciter forces must be determined for all operating conditions of the reciprocating compressor. For unloaded start-up and shut-down, only the mass forces of oscillated and rotated parts are acting on the compressor components.



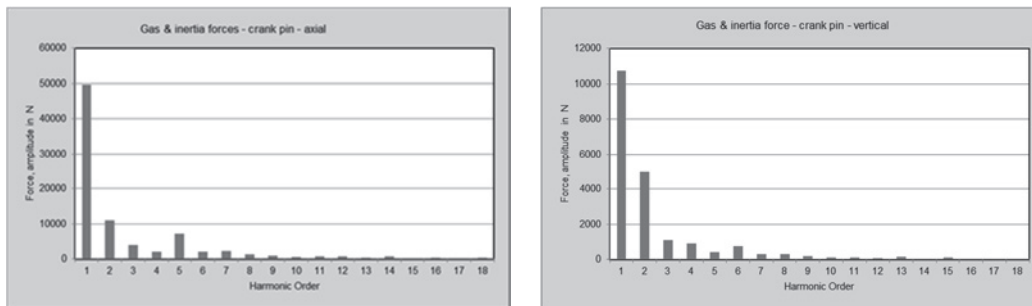


Figure 6. Exciting forces of reciprocating compressor:  $F_{Gas,axial}$ ,  $F_{crosshead\_vertical}$ ,  $F_{Crank\_pin\_vertical}$ ,  $F_{Crank\_pin\_axial}$

In figure 7 the results of the simulations during the unloaded start-up under inertia forces are shown. The results are for the offshore application shown in figure 3. To continue figure 7 a) shows the dynamic loads on the anti-vibrating mount (AVM) in three directions: axial  $F_x$ , vertical  $F_y$  and horizontal  $F_z$ . Figure 7 b) contains the vibration velocity at inlet pipe, at cylinder 1, and at cylinder 2. Figure 8 shows the results for the onshore application: a) crankcase bolt forces and b) vibration velocities. The investigation can be done for all specified operating condition of reciprocating compressor. The last step is the thermal stress analysis which can be performed with the same model. The simulation steps - modeling, modal analysis, dynamic analysis, thermal analysis - can be repeated until the required specified criteria are met. During the simulation process also different standards, regulations and specifications [1], [2], [3], [4], [11], [12] must be considered.

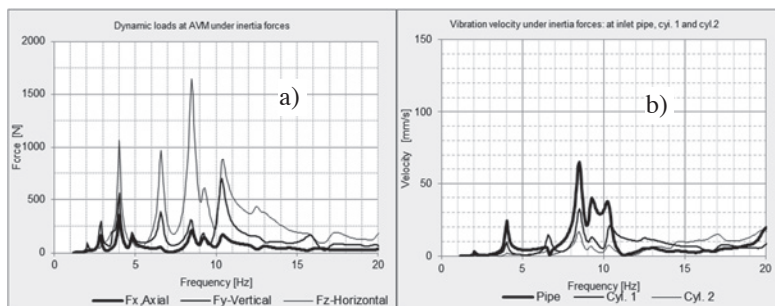


Figure 7. a) Dynamic loads on AVM  
b) vibration velocities at inlet pipe, cylinder 1, and cylinder 2 for the offshore application in Figure 3.

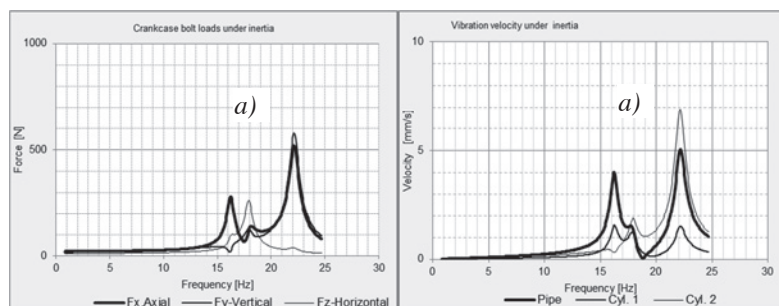
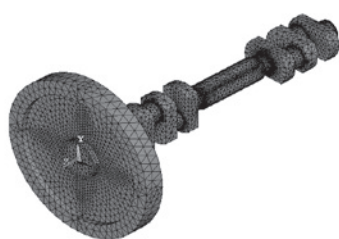


Figure 8. a) Dynamic loads on crankcase bolt b) vibration velocities at inlet pipe, cylinder 1, and cylinder 2 for the onshore application in Figure 5.

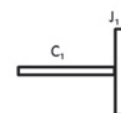
### 3. Torsional vibration

The reciprocating compressors have an extensive drive train. There are very complex components as, crankshaft, flywheel, electric machine, turbine, engine, fan, screw compressor, blower, viscous damper, coupling, gear unit, V-belt etc. The correct determination of all necessary data and parameters for the torsional vibration analysis (TVA) is very important. This has very high impact on the quality of the calculation, on the reliability and the availability of reciprocating machine train. The main parameters of the components are the torsional stiffness, the damping factors and the excitations. The calculation of stiffness of the crankshaft of reciprocating compressors is described in detail in [8], [9]. The figure 8 shows the finite element (FE) model of the crankshaft and flywheel of a four cylinder 3MW horizontal compressor. The calculated 1<sup>st</sup> and 2<sup>nd</sup> natural torsional frequencies (NTF) are  $f_1=114$  and  $f_2=323$ Hz. The mass moment of inertia  $J$  of the crankshaft is  $\sim 25\text{kgm}^2$ . The stiffness  $C_1$  and  $C_2$  for one or two mass spring torsional system for the crank shaft – figure 8 - can be determined from previously calculated NTF's and  $J$ 's based on the corresponding frequency equations (Eq. 1), (Eq. 2) and (Eq. 3) below [13]. For two mass spring model - with  $J_1=J_2=\sim J/2=12.5\text{kgm}^2$  -the calculated torsional stiffness are (from Eq. 2 and Eq. 3)  $C_1=21138976\text{Nm/rad}$ ,  $C_2=15619613\text{Nm/rad}$ .



Single mass – spring system :

$$4\pi^2 \cdot f_1^2 = \frac{C_1}{J_1} \quad (\text{Eq. 1})$$



Two mass – spring System :

$$4\pi^2 \cdot f_1^2 = \frac{1}{2} \cdot \left[ \left( \frac{C_1 + C_2}{J_2} + \frac{C_1}{J_1} \right) - \sqrt{\left( \frac{C_1 + C_2}{J_2} + \frac{C_1}{J_1} \right)^2 - \frac{4 \cdot C_1 \cdot C_2}{J_1 \cdot J_2}} \right] \quad (\text{Eq. 2})$$

$$4\pi^2 \cdot f_2^2 = \frac{1}{2} \cdot \left[ \left( \frac{C_1 + C_2}{J_2} + \frac{C_1}{J_1} \right) + \sqrt{\left( \frac{C_1 + C_2}{J_2} + \frac{C_1}{J_1} \right)^2 - \frac{4 \cdot C_1 \cdot C_2}{J_1 \cdot J_2}} \right] \quad (\text{Eq. 3})$$

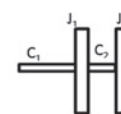


Figure 8 Crankshaft torsional model

The relative shaft damping coefficient  $k_i$  (various couplings or shaft damping) depends on the Lehr's damping factor and the corresponding natural torsional frequency [14]. For the absolute damping coefficient  $k_a$ , there are data available only for diesel engines [13], [14]. The absolute damping factors depends on piston area  $A$ , crank radius  $r$  and the type of engine represented through coefficient  $\mu$  which are included in the following equation (4):

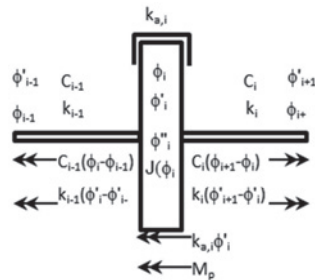
$$k_a = A \cdot r \cdot \mu \quad (\text{Eq. 4})$$

$A$  Piston Area :

$r$  Crank radius

$\mu$  Diesel engine type

The mathematical model of each throw [9] of the crankshaft of reciprocating compressor is (Eq. 5):



$$J(\phi_i) \cdot \phi_i'' + \frac{1}{2} \cdot \frac{dJ(\phi_i)}{d\phi_i} \cdot \phi_i'^2 + k_{a,i} \cdot \phi_i' + k_{i-1} \cdot (\phi_i' - \phi_{i-1}') + C_{i-1} \cdot (\phi_i - \phi_{i-1}) - k_i \cdot (\phi_{i+1}' - \phi_i') + C_i \cdot (\phi_{i+1} - \phi_i) + M_p(\phi_i, \phi_i') = 0 \quad (\text{Eq. 5})$$

Figure 9 Crank gear equation of motion for the throw  $i$ : throw angle  $\phi_i$ , angular velocity  $\phi_i'$ ,

For the simulation under resonance conditions the equation of motions in [8] and [9] should be extended with the equation for connecting rod and oscillating parts (crosshead, piston rod and piston). Therefore the mass, the mass moment of inertia and the center of gravity (C.o.G) location of the connecting rod are required. The equations of motion can then be derived from the kinetic energy of the system. The required torques on the shafts of driven train and the angle velocities on each mass can be obtained from the numerical solution of differential equations [15]. The torsional vibration analysis should be performed for all operation cases of the compressor unit including: continuous operation, part-loads, start-up, shut-down under loaded and unloaded condition, emergency shut-down etc. Generally the emergency shut-down represents a critical case. Furthermore, the operating of the system under resonance condition must be taken into consideration. In this paper the calculation of speed fluctuation of the crankshaft throw, and dynamic torques under the resonance conditions – high frequency resonance with up to ~15th harmonic - of the reciprocating compressor, is described. Near the resonance, high dynamic shaft torques and a high fluctuation of rated speed is expected. This will result to higher rod load and cross head normal force. Furthermore this can affect the cylinder PV-Curve and it can influence the power consumption, capacity, and the pressure pulsation. Since the absolute damping of crank gear has a strong influence on the speed fluctuation, their precise determination is of major importance. The following figures show the results simulation of torsional vibration analysis.

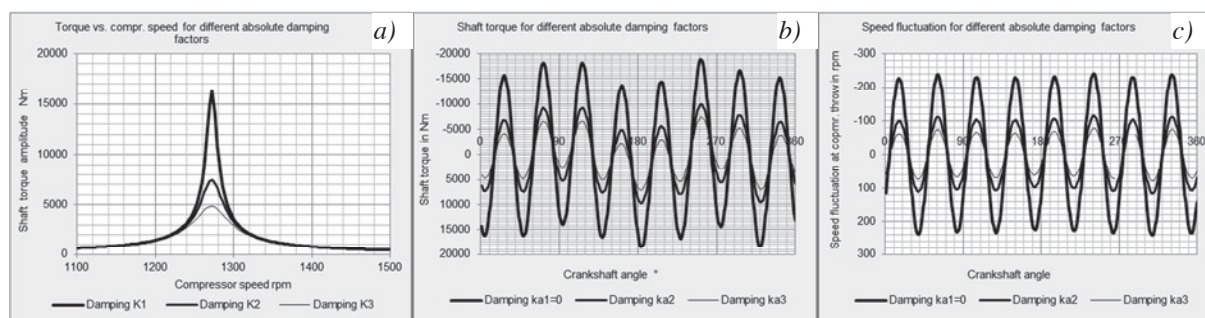


Figure 10 a), b) Torque amplitude, c) Speed fluctuation of crankshaft throw.

Figure 10 a) shows the torque amplitude over compressor speed for three different absolute damping factors  $k_a$  of crank gear. Near the resonance the dynamic torque at the crankshaft, as expected, is very high. To show the influence of the damping the calculation was performed for three different damping coefficients:  $k_{a1}=0$ ,  $k_{a2}=5\text{Nms/rad}$  and  $k_{a3}=10\text{Nms/rad}$ .  $k_{a2}$  corresponds approximately to the above equation (4) for diesel engine. Depends on the calculated torque loads, generally a separation margin from the critical speed is required.

Figure 10 b) and 10 c) shows the dynamic torque amplitude and the speed fluctuation versus crankshaft angle, at resonance condition for different damping coefficients.

#### 4. Summary

- 
- The finite element model of compressor units should include at least the following components: crankcase, crankshaft, distance piece, e-motor, pipe work, pressure pulsation devices and base-frame. A combination of 1D, 2D and 3D elements is required to realize a proper model. The crankcase, the distance piece, the pressure pulsation devices and the base-frame must be modeled with 2D elements. For some local zones 3D elements are required. The modeling methods and the scope of the system should be carefully selected. Depending on the scope of the model, the natural frequencies differ from each other up to 100% and sometimes more.
- The modal analysis as well as the forced mechanical response analysis, must be carried out at pre-stressed condition of the compressor unit. In the pre-stressed state, the system is stiffer, and consequently the natural frequencies are higher. For vessel under internal pressure the NMF's are up to 25% higher compared to the natural mechanical frequencies for the unloaded conditions!
- The forced vibration analysis must be performed, not only under the shaking-forces and cylinder- gas-forces as specified in API 618, but also under inertia-forces.
- With the presented model can be performed successively, the forced response mechanical analysis and the thermal study. So quickly and easy an optimal solution can be found, as the pipe thermal stress analysis is in conflict with the goals of the dynamic mechanical design.
- The presented model allows a lateral dynamic analysis of the crankshaft, under inertia forces, gas forces as well as forces due to torsion.
- The torsional vibration analysis should be performed for all operation cases of the compressor unit including: continuous operation, part-loads, start-up, shut-down



under loaded and unloaded condition, emergency shut-down. The calculation must be carried out also for the expected torsional critical speeds (resonance condition). At the critical speed or near the critical speed the torque amplitude and the speed fluctuation are very high. This causes higher rod load and cross head normal force. This can also affect the cylinder- PV-Curve and so the power consumption, capacity, and the pressure pulsations of the machine.

## 5. References

- [1] VDI 2230 Systematic calculation of high duty bolted joints.
- [2] VDI 3842 Vibration in piping systems
- [3] VDI 2049 Torsional vibration of driveline - Calculation, measurement, reduction
- [4] ISO 10816-8:2014, Mechanical vibration - Evaluation of machine vibration by measurements on non-rotating parts - Part 8: Reciprocating compressor systems
- [5] ANSYS Computer-aided engineering software.
- [6] Kacani V., Huttar E., Stibi H. Torsionsschwingungen in Kolbenkompressoranlagen. Der Kolbenkompressor- eine zeitgemäße Arbeitsmaschine 4.-5. November, 1999, Dresden
- [7] Kacani V., Huttar E., Economical pipe stress analysis using parametric modelling and design standards. 4<sup>th</sup> Conference of the EFRC, 2005, Antwerpen
- [8] Kacani V. Huttar E., Heumesser T. Simulation of Reciprocating Compressor Start-Up. 6<sup>th</sup> Conference of the EFRC 2008, Düsseldorf
- [9] Kacani V. Simulation of Reciprocating Compressor Start-Up and Shut down under Loaded and Unloaded Conditions. International Compressor Engineering Conference at Purdue, July 16-19, 2012
- [10] Kacani V., Huttar H., Ognar, G. State of the Art Design and calculation of Vessels and Piping Systems in Reciprocating Compressors. ICCR, Xi'an, China.
- [11] API Standard 618, Fifth Edition, Reciprocating Compressors for Petroleum, Chemical, and Gas Industry Services.
- [12] FKM Rechnerischer Festigkeitsnachweis für Maschinenbauteile. VDMA Verlag
- [13] Holzweißig F., Dresig H. Lehrbuch der Maschinendynamik. Springer Verlag 1979
- [14] Andreas Laschet. Simulation von Antriebssystemen. Springer Verlag. Springer Verlag 1988
- [15] Julien C. Sprott. Numerical Recipes. Cambridge University Press 1991



# Technical Paper

**Session: 48-1**

**Session Name: Pulsation / Vibration 3**

**How to evaluate the dynamic behaviour of a gas system without all the technical documentation of a compressor?**

**Author:**

**Urszula Warzyńska, née Radziwanowska  
Wrocław University of Technology  
Department of Maintenance and Operation of Logistics,  
Transportation and Hydraulic Systems  
50-371 Wrocław, Poland**

**Co-Author:**

**Piotr Harnatkiewicz  
Wrocław University of Technology  
Department of Maintenance and Operation of Logistics,  
Transportation and Hydraulic Systems  
50-371 Wrocław, Poland**

## Summary

This paper discusses possible method of acoustic simulation based on field measurements. The method is based on measurements of dynamic changes of pressure in the discharge and suction pipe close to the compressor. The whole measurement setup and sensors used are described as well as signal acquisition and conditioning. Then the possible ways of implementing the measured data into the acoustic simulation are discussed. Later, in the paper, a comparison between two acoustic analyses is shown: an analysis with a pressure function based on a pressure signal measured in a field and analysis with full definition of compressor as a boundary condition. All the acoustic simulations are performed in the software dedicated to this type of analysis. The procedure of acoustic simulation and assessment of a dynamic behaviour of the gas system is consistent with the guidelines of API 618 (5<sup>th</sup> Ed.) standard. Comparison of the results is obtained by compilation of general results of pressure peak-to-peak value in relation to limit value in the installation and by checking the pressure peak-to-peak values in selected nodes. For the specified nodes in the system, pressure wave spectrum is plotted for comparison of amplitudes of particular harmonics. During the simulation the results of shaking forces were also obtained, which are shown in the plots of shaking forces frequency spectra. Finally, the advantages and drawbacks of the specified method are discussed and the proposed method is evaluated.

## Introduction

Currently available commercial software for acoustic and mechanical analysis of reciprocating compressor systems usually requires a very detailed technical specification and even a precise internal geometry of compressor cylinder as input data for simulation of piston kinematics and acoustic wave shape. In the case of newly designed system, it is easier to gain the information from the compressor manufacturer. The actual problem occurs in the case of older installations, which require a modification, when the compressor documentation is lost or incomplete and a compressor type is no longer in production. Then the question of how to omit the precise modelling of the compressor and still get accurate analysis results arises. The method described in this paper proposes to use of pressure function as a boundary condition, obtained from the field measurements in real operating conditions.

## Field measurements

The measurements were made in one of the gas compressor stations in Poland during a supervised test operation of reciprocating compressors. Dynamic pressure changes in the system were measured with the use of dedicated measurement equipment, which meets the stringent requirements of operation in the hazardous conditions of zone 2 (the threat does not occur during normal operation and if it occurs, it lasts for a short time), and higher risk zones - zone 1 (threat may occur in normal conditions). The measured signals were recorded on the hard drive of an industrial laptop coupled with the measuring system using dedicated software (Figure 1). The measuring system consisted of:



- four pressure sensors, with following parameters: nominal pressure up to 600bar, over-pressure up to 1000bar, accuracy  $\leq \pm 0.35\%$  FSO, response time  $\leq 10\text{msec}$ ,
- other equipment (shown in Figure 1): laptop (1), signal amplifier with the conditioning system (2, 3), signal separator (4), EX barrier (5), EX cables.

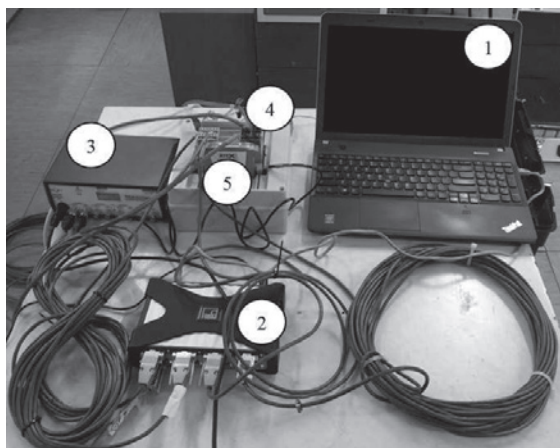


*Figure 1 Measurement equipment*

The pressure sensors were mounted in the specified locations in the system in order to capture pressure wave propagation. Four pressure transmitters were used, from which one was mounted in the suction pipeline, close to the compressor skid, and three sensors were used in the discharge section – in the discharge damper inlet nozzle, in the pipeline section upstream a cooler, and the last one in the downstream pipeline of the cooler. For the current study, the most important information gives the pressure sensor located nearest the compressor, which in this case was in the inlet nozzle of the discharge damper (Figure 2).

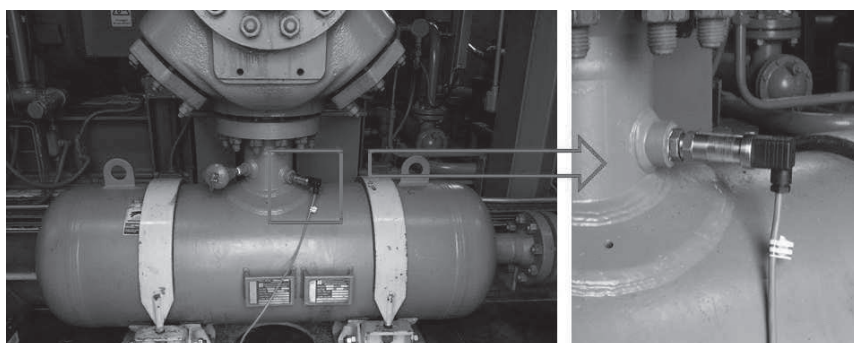


*Figure 2 Location of the pressure transmitter*

Dynamic pressure change was recorded for several different rotational speeds of the compressor in order to capture pressure pulsation in operating conditions of the system. The worst (critical) condition was chosen for the current study. The operating conditions were as follows: suction pressure 33barg, discharge pressure 42barg, suction temperature 7°C and discharge temperature 25°C. The measurements were done in winter conditions.

## Acoustic study

A pressure pulsation analysis was carried out in the commercially available software Bentley Puls whose algorithms are based on the Helmholtz model (lumped parameter method) and one-dimensional plane wave theory. In the software, the numerical model of gas system is prepared by creating nodes-defined system geometry assigned with inter-connecting elements. The elements include components such as pipes, tees, reducers, valves and orifice plates. Element transfer matrices are integrated into an overall system matrix composed of linear equations with complex coefficients and variables. The variables include RMS values of pulsating pressure and volume flow velocity at each node. Ideally, acoustic analysis is performed at the design stage in order to prevent pulsation problems after system startup. However, the program can also be used to determine modifications required to existing systems where there is a pulsation problem and this is the case in this study [2].

The geometry of gas compressor station, in which the measurements were carried out, was prepared based on the detailed technical drawings, pipelines isometrics and P&ID. For current purposes, only discharge part of the system was analysed. In general, the same procedure may be taken for the suction side as well.

The gas installation on the discharge side consists of two 2-cylinder reciprocating compressors with discharge dampers for each cylinder, two coolers for each of the compressors, an oil separator and additional armature. The geometry of the analysed installation is depicted in Figure 3.

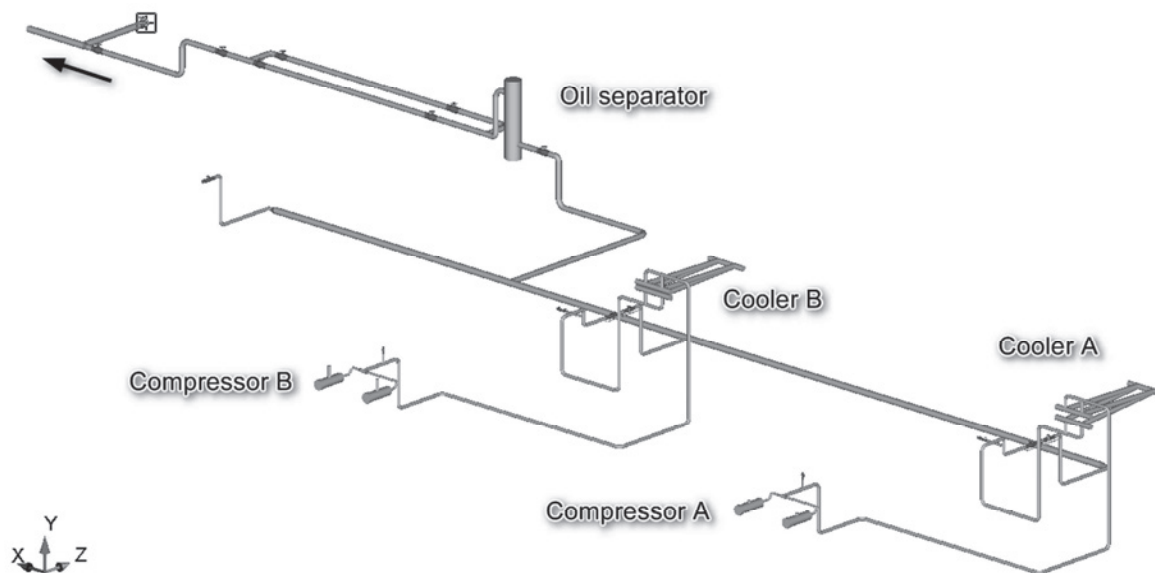


Figure 3 Gas installation model – discharge side

The geometrical model was a base for two acoustic simulations differing in the boundary condition. In the first simulation, the variable pressure function was applied as a pulsation source, while in the second one - reciprocating compressor node was a pulsation source. All the other boundary conditions were exactly the same in both computations. In the analysis, compressor A





was loaded and compressor B was unloaded. The discharge and suction pressures and temperatures were applied according to the operating conditions during the measurements.

### Model with pressure function

The dynamic pressure signal in the time domain was processed and Fourier transform was applied in order to achieve amplitude and phase spectrum. After analysis of amplitude spectrum of the signal, it was noted, that the highest amplitudes occur for the first, second and sixth harmonics. Above tenth harmonic, pressure pulsation amplitudes were negligibly small. In Table 1, the values of pressure amplitude (A), frequency (f) and phase ( $\phi$ ) of each of ten first harmonics of the pressure signal are shown.

No.	A [kPa]	f [Hz]	$\phi$ [rad]
1	5.68	13.48	-0.0292
2	14.89	27.54	-0.0261
3	0.46	41.02	0.0933
4	2.92	54.49	0.0197
5	3.04	68.55	-0.0611
6	5.59	82.03	-0.0676
7	1.59	95.51	-0.1132
8	2.47	109.57	0.0051
9	2.70	123.05	0.0007
10	1.90	136.52	0.0152

Table 1 Pressure wave parameters for the first ten harmonics

From the above data, taking inverse Fourier transform, the simplified variable pressure function was obtained (Figure 4) and used as a boundary condition in the first acoustic simulation.

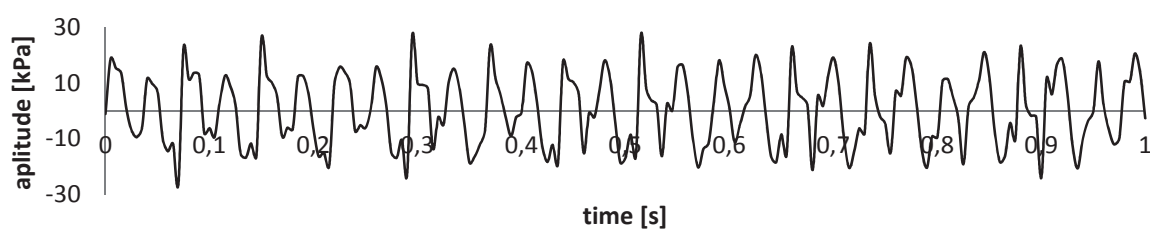


Figure 4 Pressure function versus time used in the simulation

From a numerical point of view, to obtain the result of flow dynamic calculation, the inlet and outlet boundary conditions in the form of pressure or volume flow are needed. The most common approach is to specify the volume flow at the inlet. Pressure and flow are dependent on each other and related by impedance [3]:

$$Z = \frac{P}{Q}$$

where: Z – impedance, P – pressure function in complex notation, Q – volume flow in complex notation.

In the simulation, the four-pole concept of solving the wave equation is used, which means that inlet and outlet conditions of the system are related by the matrix of coefficients or more precisely the multiplication of matrices dependent on system elements (their impedances).

$$\begin{bmatrix} Q_1 \\ P_1 \end{bmatrix} = \begin{bmatrix} \cosh \gamma L & \frac{j\omega S}{\rho c^2 \gamma} \sinh \gamma L \\ \frac{\rho c^2 \gamma}{j\omega S} \sinh \gamma L & \cosh \gamma L \end{bmatrix} \cdot \begin{bmatrix} Q_2 \\ P_2 \end{bmatrix}$$

where: c – speed of sound [m/s], ρ - gas density [kg/m<sup>3</sup>], L – effective length [m], S – cross-sectional area [m<sup>2</sup>], j – imaginary unit,  $\gamma = a + jk$ ,  $k = \omega/c$ , a – fluid damping constant.

The above equation may be written as:

$$\begin{bmatrix} Q_1 \\ P_1 \end{bmatrix} = \begin{bmatrix} A & B \\ C & D \end{bmatrix} \cdot \begin{bmatrix} Q_2 \\ P_2 \end{bmatrix}$$

and for the whole system:

$$\begin{bmatrix} Q_1 \\ P_1 \end{bmatrix} = \begin{bmatrix} A_1 & B_1 \\ C_1 & D_1 \end{bmatrix} \begin{bmatrix} A_i & B_i \\ C_i & D_i \end{bmatrix} \cdots \begin{bmatrix} A_n & B_n \\ C_n & D_n \end{bmatrix} \begin{bmatrix} Q_{n+1} \\ P_{n+1} \end{bmatrix}$$

In fact, in a pulsation study in this particular software, there are two possible pipeline terminations which allow us to solve the equation: anechoic end - the impedance is equal to 0 (Z=0), which means no reflections and therefore P=0 at the outlet, or closed end (Z=∞), which relates to full reflection, and Q=0 at the outlet.

The most important condition, when specifying pressure function as an inlet boundary condition, it that the pressure signal was measured as close as possible to the compressor cylinder. In the other way, the pressure function measured in some distance from the compressor may be deformed by the wave reflections in the system.

### Model with a full compressor definition

In order to model the reciprocating compressor as a pulsation source in the system, several important parameters are needed, and above all, the most accurate geometry of the cylinder internals and connectors. The compressor's internal diameters and lengths as well as valve volumes were modelled based on detailed manufacturer cylinder drawings. Aside from pressure and temperature conditions both on the suction and discharge side of the system, the geometry data had to be given, in particular – crank radius, connecting rod length, piston diameter, rod diameter (in crank end cylinder side), clearance volume, phase angle and also rated valve loss.



Based on this input, the inlet flow rate function might be calculated. As modelling reciprocating compressor as a pulsation source is a standard procedure, it will not be further described in this section.

### Comparison of the results

In this section, the acoustic analysis results obtained in two simulations are compared. Before analysing and comparing the results of both simulations, it should be noted that pressure and flow boundary conditions were not in the same node of the model. The pressure boundary condition was introduced in a node referring to pressure transducer location during the measurements. In the simulation with flow boundary condition, additionally the cylinder internals were modelled. In Figures 5 and 6, the general results are displayed in the form of colour contour map depicting pressure peak-to-peak values to API618 limit values ratio [1]. The red sections mean that the pressure pulsation exceeded API618 level, colours from green to orange indicate sections, where pressure pulsation is within the acceptable range.

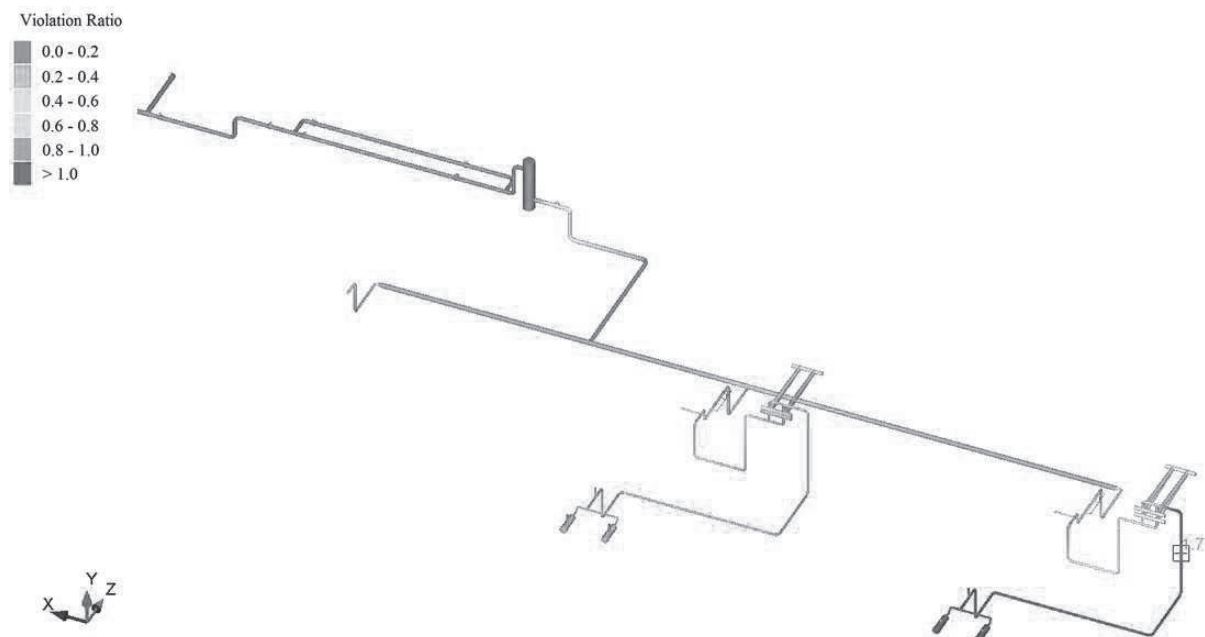


Figure 5 Pressure pulsation violation ratio contour plot – simulation with pressure source

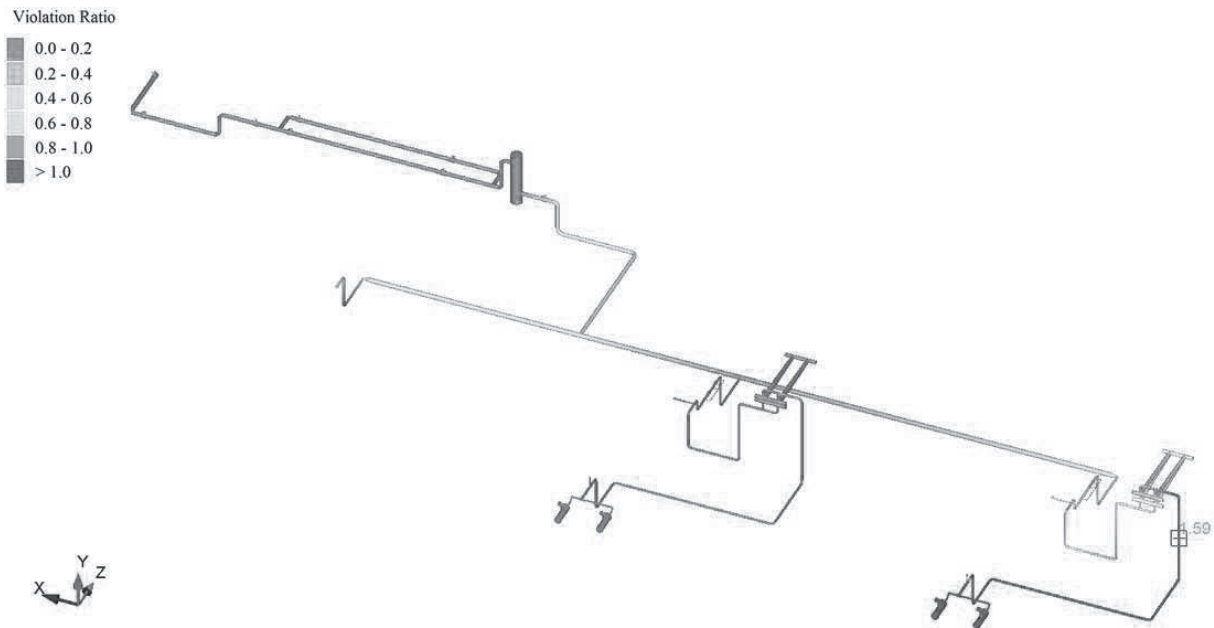


Figure 6 Pressure pulsation violation ratio contour plot – simulation with compressor boundary condition

The highest pressure pulsation amplitudes occur in the pipeline between the compressor A and cooler A. In the later pipeline, behind the cooler, pressure pulsation is attenuated and does not exceed API618 limit values. For the comparison of the results and further analysis, four nodes were chosen in that section (Figure 7).

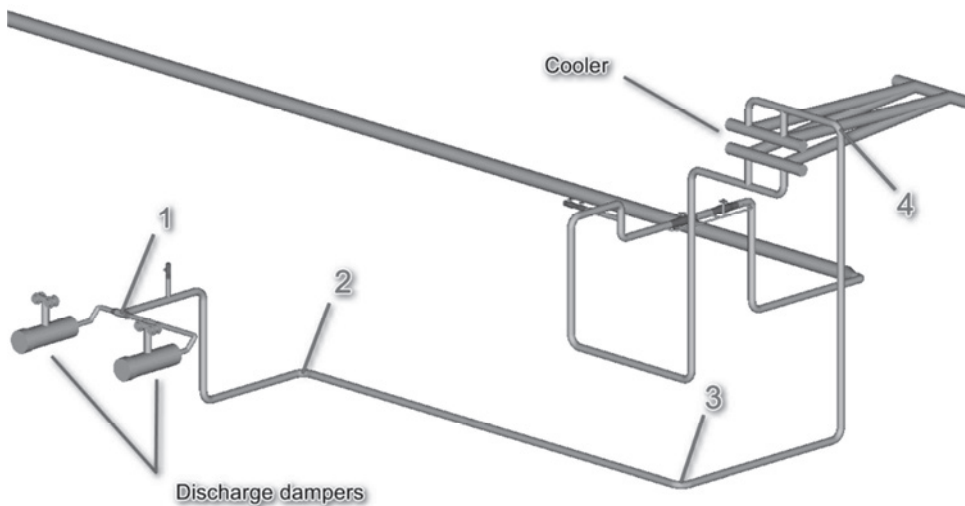


Figure 7 The comparative nodes of the system

In Figure 8, for the specified nodes in the system, pressure amplitude spectra are displayed, resulting from the simulation with pressure source (blue line) and compressor boundary condi-



tion (green line). Additionally, the API618 5<sup>th</sup> curve specifying limit values for the pipeline is included in the plots. The plots represent peak-to-peak pressure pulsation in [kPa] versus frequency in [Hz].

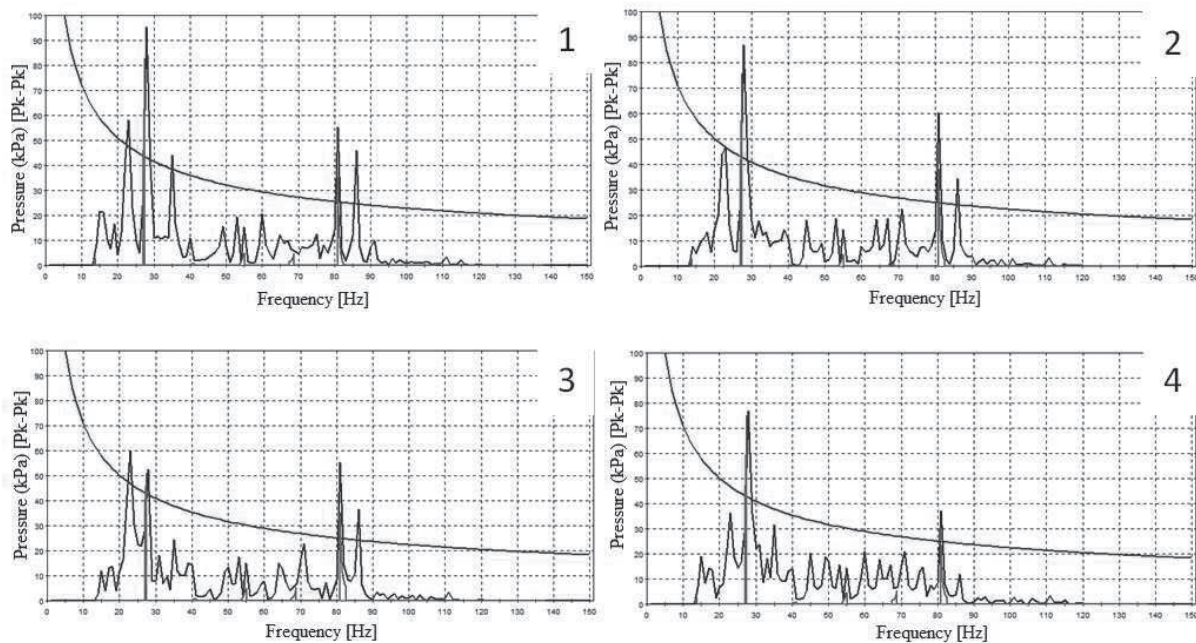


Figure 8 Comparison of amplitude spectra obtained in both simulations: variable pressure source (blue curve), compressor source (green curve), API618 (red curve)

The first observation is that both simulations indicate excessive pressure pulsation in analysed pipeline, exceeding API618 limit values. The highest peak-to-peak pressure value occur for the second harmonic, which corresponds to the frequency of about 27Hz. Also the sixth harmonic (about 82Hz) reveals pressure peak. The plots of first analysis results (pressure function analysis) are much more diverse than the second one. Additionally, pressure peaks in the amplitude spectra may be seen. It is due to the measured pressure signal, which already contained additional distortions resulting from i.e. valves operation and wave reflections from a damper. While the simulated compressor flow function is “clear”, similar to sinusoidal function. In Table 2, the values of pressure pulsation for the second harmonic are compared for both simulations and the percentage difference in obtained results.

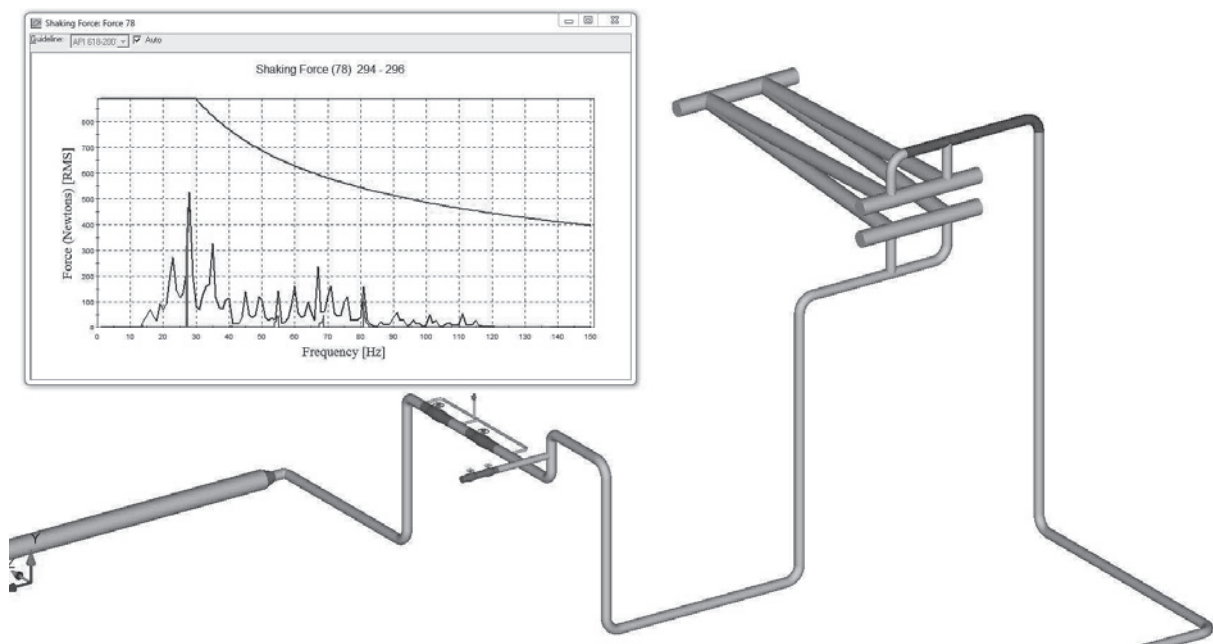
Node No.	Compressor source $p_{pk-pk}$ [kPa]	Pressure function $p_{pk-pk}$ [kPa]	Results difference [%]
1	82.8	95.4	13.2
2	75.8	87.0	12.9
3	51.0	52.5	2.9
4	75.0	76.8	2.3

Table 2 Comparison of pressure pulsation values in the second harmonic and results difference



In all of the four specified nodes, pressure pulsation peak-to-peak values in second harmonic are higher in the simulation with pressure function than in the simulation with compressor source. The more noticeable difference in results refer to nodes closer to the compressor (less than 15% difference in results). For nodes closer to the cooler, the difference in results in both simulation are less than 3% for the second harmonic.

As a result of performed simulations, shaking forces plots were also obtained. In Figure 9, the shaking forces plot in frequency domain is shown, in the pipeline section upstream the cooler. Similarly to the pressure pulsation plots, the highest shaking force appear in the second harmonic, in both simulations. In this case, the shaking force levels are much below the API618 curve.



*Figure 9 Comparison of shaking force plot in exemplary location in the system – cooler inlet piping*

The results of the analyses may be further processed by exporting shaking forces into Auto-Pipe, in order to create forced harmonic load for stress analysis of pipelines.



## Pros and cons

The first and most important advantage of proposed method to perform acoustic study by the use of pressure function as a source is that there is no need to obtain the details of compressor cylinders, in particular the detailed geometry of the internals. This may save time, while waiting for the detailed data to start calculations, which at the end may be incomplete.

Secondly, the results obtained by both simulations, in general give similar results as shown in pressure violation ratio contour maps. Pressure function as a boundary condition impose more conservative results than a compressor boundary condition.

Moreover, the obtained in both simulations results are similar, and the highest pressure peaks occur for the same frequencies. The values differ in less than 15%.

The disadvantage of the proposed method is that the measured signal does not refer to clear pressure pulsation generated by compressor, but already includes wave reflections. Therefore, the simulation is vitiated by an error at the beginning. To minimize the error, the location of pressure transducer should be as close as possible to the compressor, to avoid interference of pressure waves.

Furthermore, the simulation with the pressure function is calculated only for the specified rotational speed referring to the measured signal. It is possible to measure dynamic pressure changes for a few rotational speeds of the compressor or the whole range of speeds, and then to make a number of acoustic simulations with different pressure functions. However, this requires some effort and is time-consuming.

## Conclusions

In the paper, the method of simulation of pressure pulsation in a gas system without detailed specification of a reciprocating compressor is described. The method involves pressure function as a pulsation source, which is defined by measured dynamic pressure change in the real system. The proposed method is not intended to replace algorithms of compressor source in the acoustic simulation, but may be an alternative opportunity for the evaluation of pressure dynamic phenomena in gas system without all the required compressor data, which may save the time needed to complete an acoustic simulation study.

## References

1. API 618 Reciprocating compressors for petroleum, chemical, and gas industry services, Fifth Edition, American Petroleum Institute.
2. Kollek W., Harnatkiewicz P., Lubecki Sz., Osiński P., Radziwanowska U., Metody analizy pulsacji ciśnienia oraz drgań w sieci przemysłowej do przesyłu gazu. Inżynieria Maszyn, 2014, R. 19, z.2.
3. Soedel W., Sound and vibrations of positive displacement compressors, Taylor & Francis, Inc., 2007.





# Technical Paper

**Session: 48-2**

**Session Name: Pulsation / Vibration 3**

## **Vibration assurance of vertical scrubbers for reciprocating compressor packages**

**Author:**

**Kelly Eberle, BSc, PEng  
BETA Machinery Analysis (Wood Group Vibration, Dynamics & Noise)  
118, 4242 7th Street SE  
Calgary, AB T2G 2Y8, Canada**

## Summary

Compressor packagers, OEMs, end users, engineering companies and industry organizations have long recognized the risks of liquids in reciprocating compressor systems. API 618 and EFRC have guidelines for the design of devices to remove liquids from gas streams for reciprocating compressors. These devices may be required on reciprocating compressor package on the inlet gas stream and after every cooler where there is concern of excess liquids in the gas stream. These devices are generically referred to as separators or scrubbers.

While there are comprehensive guidelines and best practices for removing liquids and handling liquid disposals, there is no complete reference for managing vibration and fatigue failures of scrubbers. Scrubbers are at a significant risk for vibration in reciprocating compressor applications. Normal operation of the reciprocating compressor generates significant steady-state dynamic loads. High vibration can result if design measures are not taken to minimize dynamic loads or minimize the scrubber dynamic flexibility. Also, the scrubber design considerations for liquid separation, minimizing fabrication costs and vibration assurance are often at odds. A balanced design approach considering all these requirements is necessary to assure reliability and safety of the reciprocating compressor package.

This paper will outline factors affecting the scrubber design with respect to vibration control. Best practices for the design, installation and field testing of the scrubber and attached instrumentation will be presented. The goal of the paper is to educate designers and purchasers of scrubbers to consider vibration control early in the project. This approach will significantly reduce vibration levels and costs in the asset's life cycle.





## 1. Introduction

The EFRC has published a guideline document outlining design practices and theory involved in avoiding liquid problems for reciprocating compressor systems [1]. The guideline is an excellent resource to ensure the device for separating liquids from the gas is properly designed from a process perspective. Safe and reliable operation of the reciprocating compressor from a process standpoint is assured by following this guideline.

A significant risk factor in a reciprocating compressor installation design is fatigue failures due to vibration. Separation devices are frequently found to be a concern for fatigue failure. The EFRC guideline does not address this issue. API 618 5<sup>th</sup> Edition gives some general guidance for avoiding mechanical resonance that can lead to fatigue failures. The GMRC guideline for high speed reciprocating compressors [2] has some additional measures for minimizing vibration for components on compressor packages. There remains a knowledge gap in the reciprocating compressor industry in the design of separation devices to assure reliability and safe operation with respect to fatigue failures from vibration. The goal of this paper is to present some of the measures to fill these gaps and their technical basis.

The EFRC guideline refers to a range of separation devices such as separators, knockout drums, cyclones, coalescers and scrubbers. The word “scrubber” will be used as a general term to refer to all of these devices as a matter of convenience for the remainder of this discussion. A “scrubber” is any vertical vessel that is used for separation of liquid or solids from a gas stream that is supplied to or discharged from a reciprocating compressor.

This paper outlines:

- Fundamentals of vibration: an overview of dynamic forces and dynamic flexibility.
- Design goals to minimize vibration: a description of the API618 approach to avoid or manage vibration.
- Industry best practices, consists of topics relating to the design process, scrubber base and shell designs, instrumentation and field testing.

## 2. Fundamentals of Vibration

The typical approach for discussing the fundamentals of vibration starts with consideration of a single degree-of-freedom mechanical system as shown in Figure 1. The mechanical system is comprised of a mass ( $m$ ), spring ( $k$ ), and damper ( $c$ ).

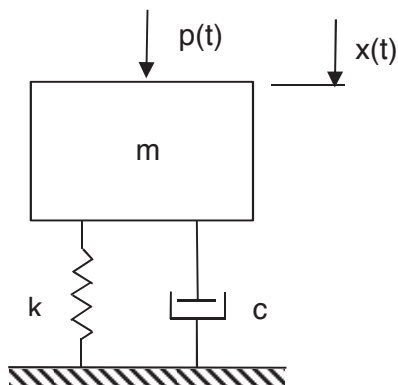


Figure 1: Model for the single degree-of-freedom mechanical system

A time varying force ( $p(t)$ ) acting on the mass results a time varying displacement ( $x(t)$ ) or vibration of the mass. Equation 1 shows the relationship between the force and the motion of the mass.

$$m\ddot{x} + c\dot{x} + kx = p(t) \quad (1)$$

The term  $\ddot{x}$ ,  $\dot{x}$ , and  $x$  represent the acceleration, velocity and displacement of the mass. Equation 1 accurately represents the physics of the mass motion in precise mathematical format. A less rigorous form but more intuitive form of Equation 1 in terms of understanding vibration is given by the following expression.

$$V = P_D \times F_D \quad (2)$$

Where  $V$  is the vibration,  $P_D$  is the dynamic force and  $F_D$  is the dynamic flexibility. Minimizing vibration requires minimizing the dynamic force or the dynamic flexibility. Underlying this simple equation are many details that must be considered for scrubbers in a reciprocating compressor application. Reciprocating compressors generate many dynamic forces at many frequencies. The dynamic flexibility is a function of the static stiffness, mass and damping of the structure. A thorough discussion of these factors is presented in Appendix A. The important concept to consider in designing scrubbers are concisely summarized in Equation and referenced in the remainder of the paper.

### 3. Design Goals to Minimize Vibration

The approach to minimize vibration is to reduce the dynamic forces, reduce the dynamic flexibility or both as shown in Equation 1. API 618 and API RP 688 include guidelines for both reducing the dynamic loads and dynamic flexibility. Pulsation shaking force guidelines are given for pulsation bottles (manifolds) and piping however there is no guideline for pulsation shaking forces in scrubbers. Some companies have developed their own guidelines for scrubber pulsation shaking forces. These approaches will help to minimize vibration however there are many other dynamic loads that can cause high scrubber vibration.

One approach to minimize the dynamic loads that act on the scrubber is to remotely locate the scrubber from the reciprocating compressor. The definition of “remotely located” is difficult to quantify but in general means that the scrubber is far enough away from the reciprocating compressor that the local forces and moments generated by the reciprocating compressor are not transmitted through the piping, skid structure or foundation to the scrubber. One reference [3] states that a component can be considered “remote” when the component has at least 6m (20 ft) of piping between it and the bottle flange. This length is a reasonable criterion if the scrubber is located on a skid and foundation that is independent from the reciprocating compressor.

Most high speed reciprocating compressor packages have a layout where the scrubber is close-coupled, that is a short section of pipe directly connects the scrubber to the suction bottle installed on the reciprocating compressor cylinders. Reducing all the dynamic loads to low levels is not possible as explained in Appendix A. Minimizing scrubber vibration can only be done by evaluating the dynamic flexibility. The general approach for minimizing the scrubber vibration is to ensure the mechanical natural frequency of the scrubber is at least 2.4 times compressor speed. A high speed reciprocating compressor that is operating at 1200 rpm results in a mechanical natural frequency guideline of  $1200 \times 2.4 = 2880$  cpm. This approach is illustrated



by the “overtuned” curve shown in *Figure 2*. The scrubber mechanical natural frequency is adjusted or “tuned” above the second order of compressor speed.

A 20% separation margin, or difference between the natural frequency and the frequency at which the compressor force occurs, is specified for two reasons. First, the shape of the resonance curve will result in dynamic flexibility that is greater than the static flexibility even when the mechanical natural frequency is greater than the excitation frequency. Second, there will be small differences between the construction and installation of scrubber and compressor package that will result in the scrubber mechanical natural frequency calculated at the design stage being different from the actual mechanical natural frequency. Over-tuning the scrubber mechanical natural frequency to meet the minimum guideline of 2.4x compressor speed will generally result in acceptable scrubber vibration.

Over-tuning the scrubber mechanical natural frequency is not necessary for all applications. A 20% separation margin is also possible for a fixed speed compressor operating at 1200 rpm as shown in *Figure 2*. A scrubber mechanical natural frequency that is tuned between the fundamental and second order speeds is said to be inter-tuned. A scrubber mechanical natural frequency that is tuned below the fundamental speed is said to be detuned. The scrubber dynamic flexibility and vibration may be acceptable for an inter-tuned or detuned design. The risk with the inter-tuned scrubber design is that the static flexibility may be too low resulting in unacceptable vibration due to normal dynamic loads. The risk with the detuned design is that there may be a second scrubber mechanical natural frequency that is lowered and is now resonant at the second order. The example shown in *Figure 2* demonstrates a single mechanical natural frequency. Scrubber, and any other real system, will have multiple mechanical natural frequencies.

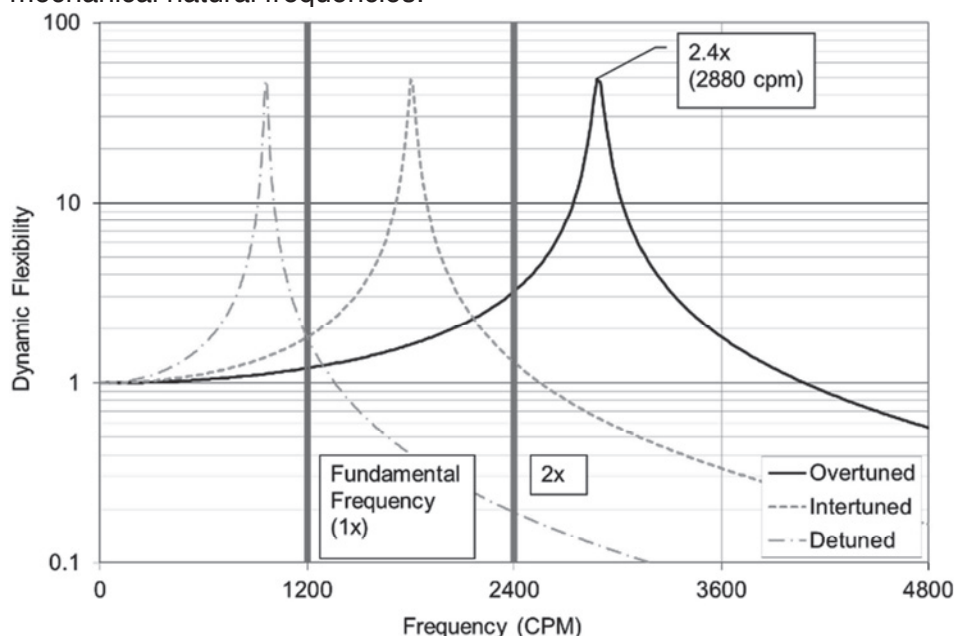


*Figure 2: Scrubber Mechanical Natural Frequency Tuning*

Ensuring a 20% separation margin is more difficult, and often not practical, for variable speed reciprocating compressors. Consider a case where the compressor has an electric motor VFD operating from 600 to 1200 rpm. The fundamental frequency range is 600-1200 cpm and the second order frequency range is 1200-2400 cpm. There is no frequency between the fundamental and second order frequency where the scrubber mechanical natural frequency can be inter-tuned as shown in *Figure 3*.

Figure 3 It is still possible to detune the scrubber but the frequency will be very low resulting in either a very high static flexibility or an increased risk of a second mechanical natural frequency being lowered into a resonance condition. Designing scrubbers to minimize vibration in a variable speed application are a significant challenge.

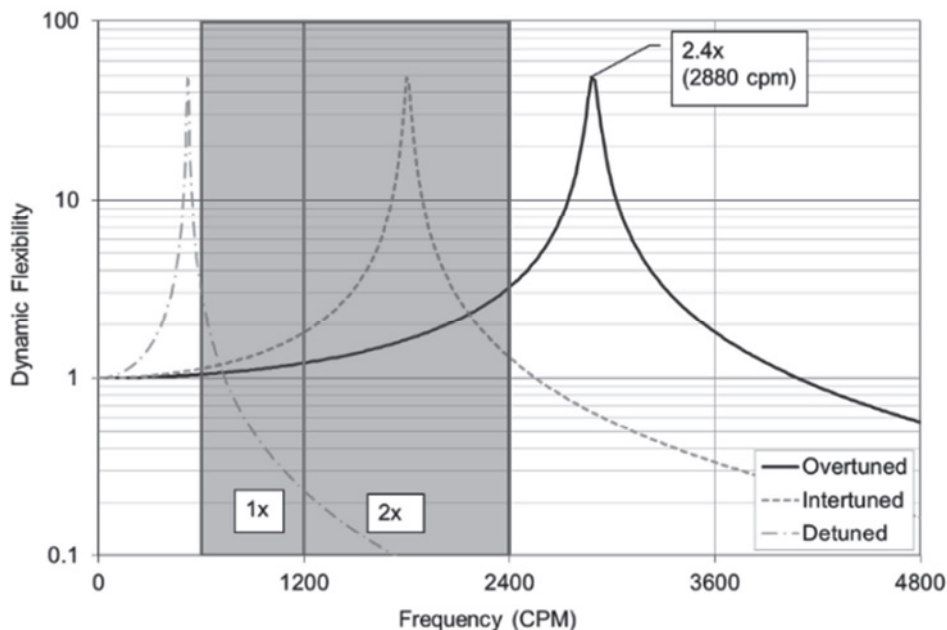


Figure 3: Variable Speed Compressor

The previous comments on frequency avoidance and tuning the scrubber mechanical natural frequency relates to the dynamic flexibility of the scrubber as a single body vibrating as a cantilever beam would vibrate. Another significant risk for fatigue failure on a scrubber includes the instrumentation and other small diameter nozzles that are included on the scrubber as part of its normal operating requirements. These connections may include

- nozzles with blinds that are used for inspection,
- liquid level sight glasses or gauges, liquid level sensors,
- relief valve connections,
- temperature gauges, and
- liquid drains.

Figure 4 shows an example of the attachments that may be installed on a scrubber mounted on a reciprocating compressor package. These attachments can have excessive vibration at frequencies that are above the 2.4x frequency guideline. The main dynamic forces that causes vibration of the scrubber attachments are pulsation shaking forces and compressor cylinder gas forces. The pulsation shaking forces can be reduced with proper pulsation design practices however the cylinder gas forces cannot be changed. The cylinder gas forces occur at all orders of compressor speed so frequency avoidance is not practical, particularly for variable speed compressors.



Figure 4: Example of Scrubber Attachments

Figure 5 shows an example of the cylinder gas forces for orders 1x to 5x for a range of operating points. An operating point represents a particular pressure ratio, suction temperature, gas composition and cylinder load step. The cylinder gas forces are high at 2x, 3x and 4x compressor speed. The dynamic flexibility of the scrubber attachments must be changed to avoid resonance at these orders. It is also important to note how these forces change depending on the operating point. A scrubber attachment that is resonant at 3x compressor speed may have acceptable vibration when operating at point 10. The cylinder gas forces at 3x will be much higher for operating point 1. Vibrations will increase and may be excessive when operating at point 1. This change in cylinder gas forces must be considered when assessing vibrations on reciprocating compressor packages.

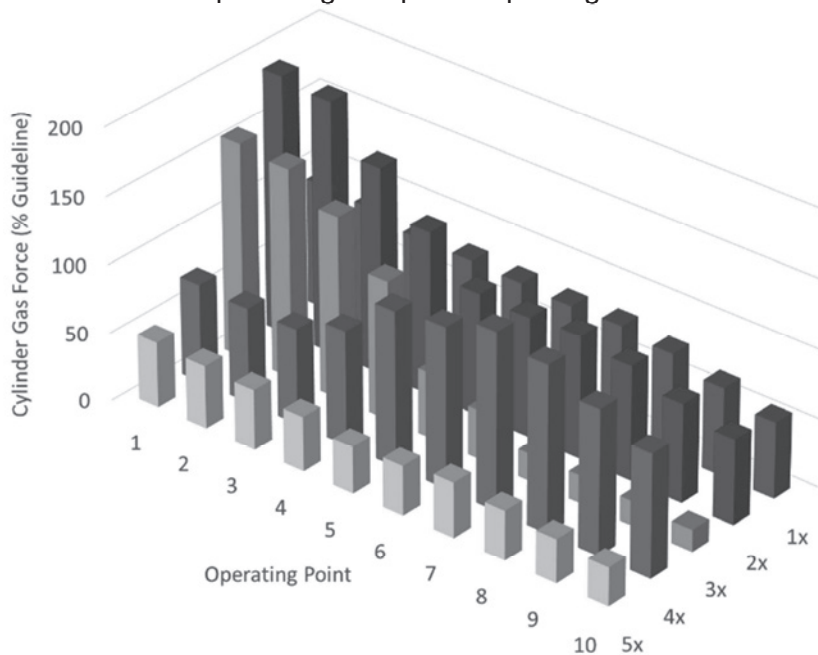


Figure 5: Compressor Cylinder Gas Force



The challenge to avoid fatigue failures on scrubber attachments is to reduce the dynamic flexibility of these attachments so that the mechanical natural frequencies are higher than orders where the response due to cylinder gas forces is significant. The scrubber connections may include heavy flanged valves or include redundant valves and instrumentation that have a long projection from the vessel shell. The combination of the large weight and long projection results in significant dynamic flexibility. There are many best practices that will reduce the likelihood of failure on the scrubber attachments that will be outlined in the following sections.

#### 4. Industry Best Practices

The sections that follow summarize some of the most important design procedures and best practices for minimizing vibration on scrubbers.

##### 4.1 Pre-Selection of Scrubbers

Section 4.2 of EFRC guideline [1] has a section describing a process of pre-selection of scrubbers for handling liquids in the gas stream. The pre-selection of the scrubber design and general vessel size should also consider factors that will minimize vibration. Earlier sections of this paper described the impact of having a scrubber close-coupled to the reciprocating compressor versus remotely located as well as installing the scrubber in an application that is fixed speed versus variable. These and other factors need to be considered in the pre-selection of the scrubber. The factors controlling the scrubber's vibration are complex so consultation with an engineering specialist company is recommended early in the design process.

A typical project timeline is shown in *Figure 6*. A project begins with a planning or FEED (Front End Engineering and Design) stage where the initial specification and general equipment selections are done. The pre-selection of the scrubber design is often done in this phase.

The detailed design phase is then started if approval is given. Equipment suppliers and packagers will be awarded contracts and begin their detailed design. These suppliers will hire vibration consultants and other engineering specialist to help with the detailed engineering. It is normally at this point where vibration problems with the scrubber are identified. However the equipment package design has progressed and budgets have been set so making a significant change in the scrubber design to avoid a vibration problem is difficult. Remedial measures to control vibration may result in a less than desirable final design. For example, large braces may be needed to minimize scrubber vibration. The braces can restrict access for maintenance and pose safety hazards.

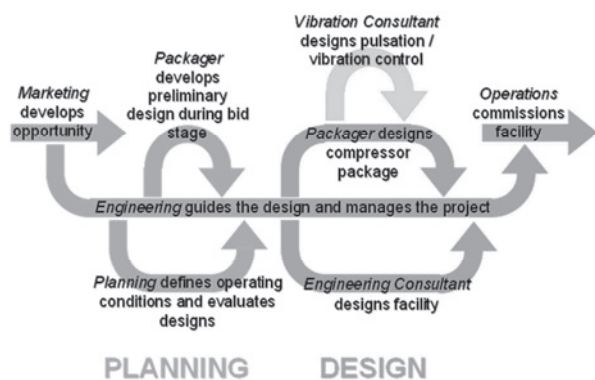


Figure 6: Typical Project Timeline

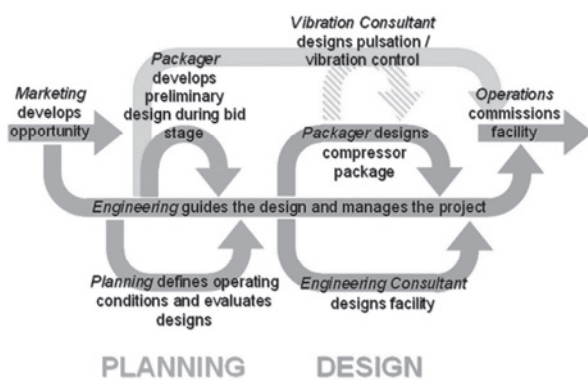


Figure 7: Recommended Project Timeline



The recommended timeline for involvement of the vibration consultant is illustrated in Figure 7. The vibration consultant should have input very early in the project planning stage. Pre-selection of the scrubber design with consideration for vibration control will avoid costly delays and redesign later in the project.

A second factor that must be considered in the pre-selection of the scrubber is achieving a balance of roles and responsibilities. The equipment packager is responsible for delivery the equipment within a certain time for an agreed upon price. Their responsibility may include initial commissioning and a limited warranty period. The project owner will be responsible for the design, construction and long term operation of the asset. The goals of the equipment packager and project owner are not necessarily aligned. For example, an equipment packager may choose a scrubber design that includes a shell size of DN500 and 3.5m seam-to-seam length. The vibration consultant working for the equipment packager may identify this scrubber as a risk for high vibration and recommend a DN600 and 2.5m seam-to-seam length. An alternative to the larger diameter scrubber is to keep the original shell size and install two DN150 pipe braces on the scrubber. The equipment packager may choose the scrubber design with the brace as the scrubber material costs and fabrication costs are lower. The project owner may be willing to forego the extra cost for the larger diameter scrubber to avoid the maintenance and safety concerns with adding braces on the smaller diameter scrubber. Involvement of the owner throughout the design process is important to ensure overall project goals are met.

#### 4.2 Scrubber Base Design

The design of the base for the scrubber is one key to over-tuning the scrubber mechanical natural frequency. Scrubbers may be mounted directly to a concrete foundation or steel skid. Figure 8 and

Figure 9 show typical base design details that maximize the base stiffness when a bolted base connection is used.

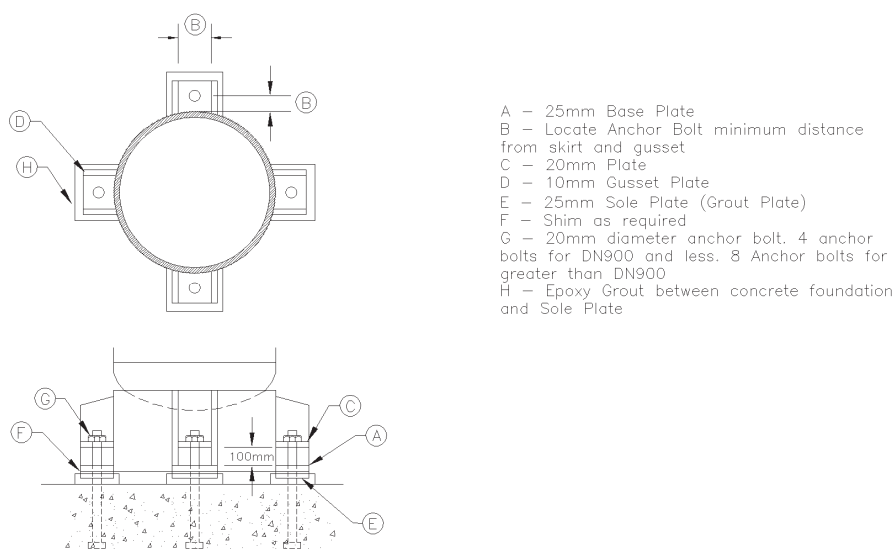


Figure 8: Scrubber Base for Mounting on a Concrete Foundation

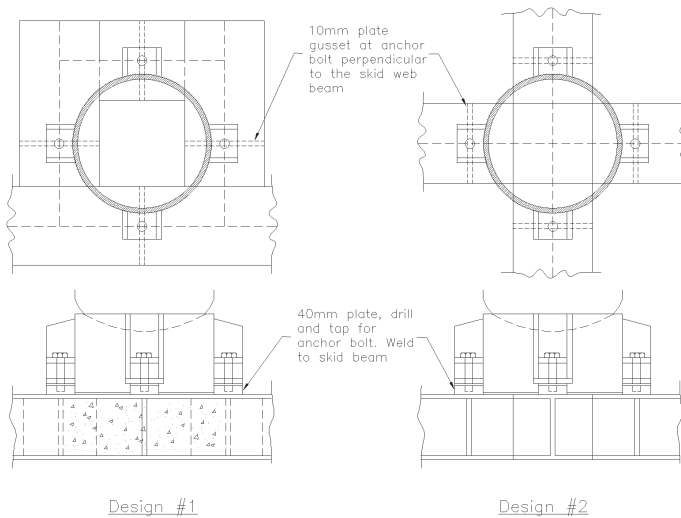


Figure 9: Scrubber Base for Mounting on a Steel Skid

Two important features of this design are

1. Shims are recommended between the base plate and the sole plate attached to the foundation or skid. The shims are necessary to ensure there is full contact and transfer of stiffness between foundation and the scrubber.
2. A minimum bolt stretch length of 8 diameters is recommended to minimize vibratory loosening of the bolt.

If the scrubber is to be mounted on a steel skid, it is preferred to weld the scrubber skirt directly to the skid beams rather than bolts as shown in Figure 9. Welding the skirt to the skid beams ensures a direct transfer of stiffness. Welding the skirt to the skid is not always possible due to requirements for shipping or maintenance.

The arrangement of the beams below the scrubber is important in the base stiffness. An arrangement as shown in Design #2 is acceptable for cases where the scrubber skirt is welded to the skid beams. The weld will directly connect the web of the skid beam to the skirt. Alternatively a “box” arrangement of beams can be used as shown in Figure 10. The skid beam webs should be spaced at approximately 90% of the outside diameter (OD) of the scrubber to maximize the skid stiffness.

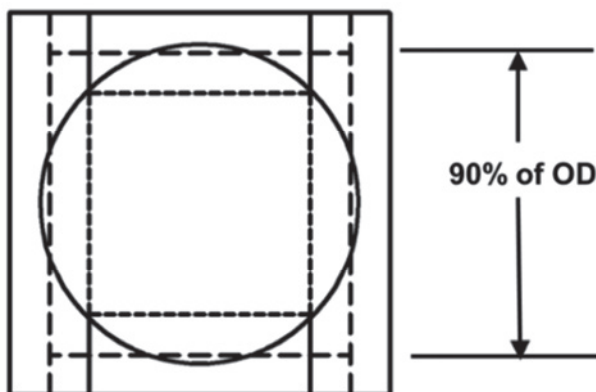
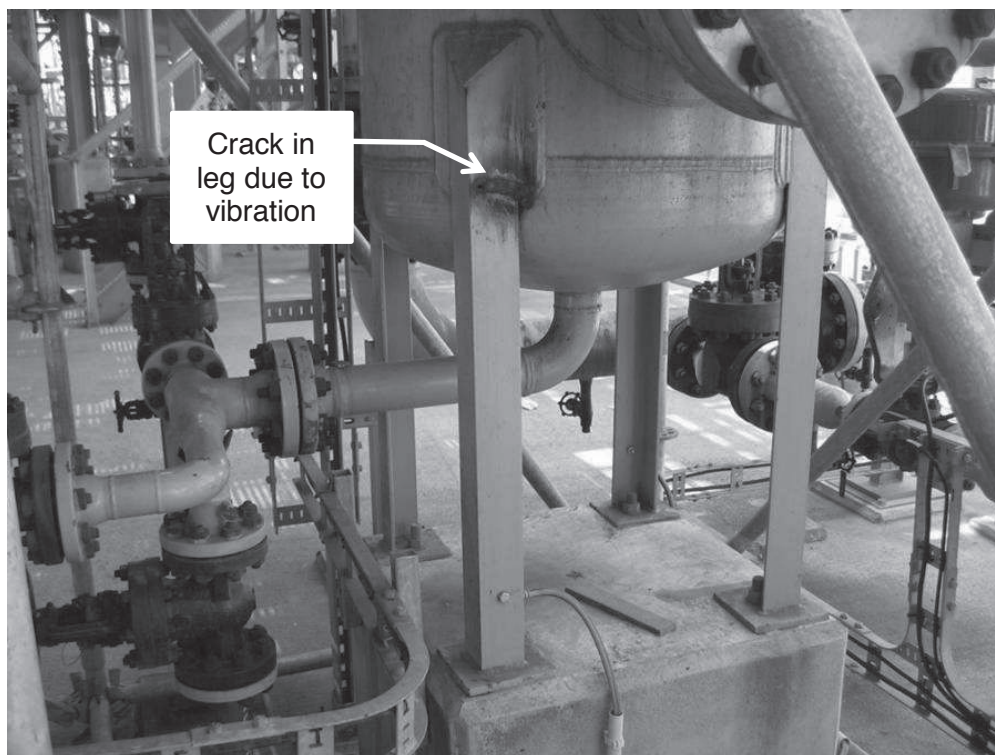


Figure 10: Skid Beam Arrangement



A skirt is the preferred method of supporting a scrubber in a reciprocating compressor application. Typically the skirt outside diameter and wall thickness should be the same as the main vessel. One exception is for high pressure service where a very thick wall vessel is required in which case a 25mm wall thickness skirt is generally sufficient. A scrubber base fabricated from structural angle sections, commonly called legs, is not recommended for reciprocating compressor service. The legs are often too flexible resulting in high vibration that can lead to cracking of the structural section as shown in *Figure 11*.



*Figure 11: Scrubber Base with Leg Supports*

There are many factors to consider in the design of a scrubber base. The proposed base design shall be evaluated during the detailed design stage to ensure it will be acceptable. A finite element model of the scrubber base including the skirt, base plate and skid which uses shell or solid elements is required as shown in *Figure 12*.

A design study that assumes the scrubber base is rigid or anchored is not sufficient and puts the scrubber design at risk of high vibration.

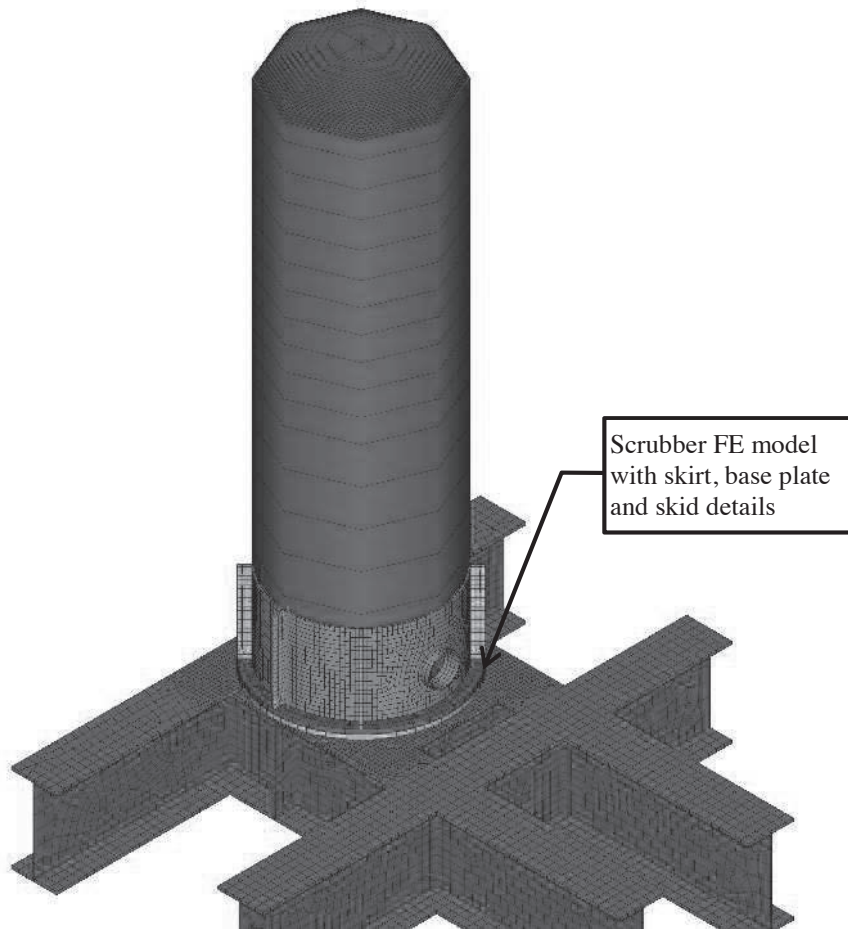


Figure 12: Scrubber Base Finite Element Model

#### 4.3 Scrubber Shell Sizing

An important factor in determining if the scrubber will be over-tuned is its height and diameter. The scrubber mechanical natural frequency,  $MNF$ , is proportional to the square of the diameter,  $OD$ , divided by the height,  $h$ , ignoring the effect of wall thickness, as represented in Equation 3.

$$MNF \propto \left( \frac{OD}{h} \right)^2 \quad (3)$$

Small changes in the diameter and height can have a significant impact. Scrubbers on high speed reciprocating compressor packages are often at risk of not being over-tuned as meeting the over-tuning criterion of 2.4x is a challenge. Typically a ratio of diameter to height of more than 0.2 to 0.25 will result in an over-tuned scrubber for runs speeds to 1,000 to 1,200 rpm. The diameter to height ratio of 0.12 may be acceptable for low speed reciprocating compressors (300-360 rpm). Note the previously stated ratio as based on the assumption that the scrubber does not include a large manway, access flange and blind to changing vessel internals and that the scrubber has a suitable base as described in the previous sections. A larger diameter to height ratio may be required for installations that do not meet good design practices for vibration control in other areas.





Scrubbers are most commonly installed on the suction side of the reciprocating compressor. The suction pressure may be low which can result in a relatively thin wall thickness to meet the pressure code requirements. Thin wall vessels are a risk for high frequency vibration of the shell or attachments on the shell. A minimum shell thickness of 13mm has been adopted by several operating companies as a standard requirement [2]. The minimum 13 mm wall thickness requirement is also applied to stainless steel shell material where the pressure code requirement would be much less.

#### 4.4 Service Considerations

Some scrubber designs require inspection or maintenance of the internal components. Typically access to the internal components is by a blind flange or flange set located at the top of the vessel. The flange set can be very heavy. The combination of the large mass and location at the top of the scrubber results in a very low mechanical natural frequency. Selecting a different scrubber design that does not require inspection or maintenance of the internal components should be considered if the application will allow. Another alternative is to remotely locate the scrubber from the reciprocating compressor so that the dynamic forces that cause vibration will be minimized. One option to consider is to lower the flange set as shown in *Figure 13*.

Lowering the flange set will significantly reduce the dynamic flexibility. The scrubber shell OD/h ratio could also be increased beyond what is normally required when a flange for access is required.

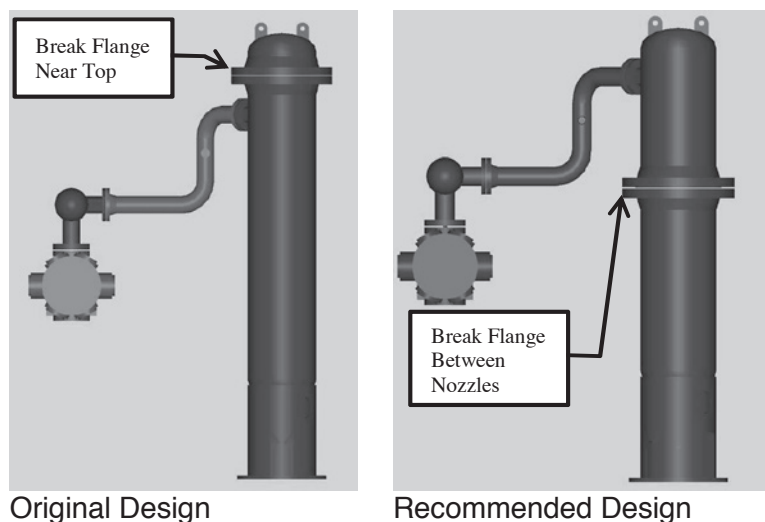


*Figure 13: Scrubber Break Flange Locations*

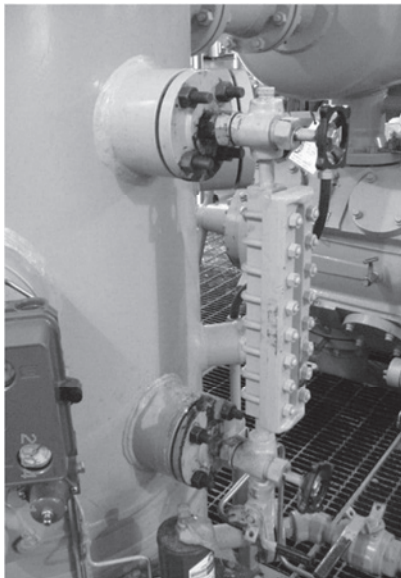
#### 4.5 Instrumentation

The most common components that experience fatigue failures on scrubbers are the small diameter attachments, that is, the sight glass, bridle, drip pot, temperature gauge and level transmitters. Generally these components are most at risk when the scrubber is closely coupled to the compressor. Vibration is caused by a combination of high dynamic flexibility and significant levels of cylinder gas forces at orders above the second order of compressor speed. The high dynamic flexibility is typically the result of a large suspended mass extending a significant distance away from the vessel. The Energy Institute [4] and Gas Machinery Research Council [3] have published design guidelines for design and evaluation of small diameter connections that can reduce failures of scrubber attachments. Following are general recommendations that will minimize the potential for high vibrations and failures:

1. Minimize the projection of the nozzle from the shell by using studding outlets or RFLWN (raised face long weld neck) flanges trimmed to a minimum length rather than RFWN (raised face weld neck) flanges.
2. Eliminate isolation valves between the nozzle and the attachment. If the attachment must be isolated, use either:
  - a. monoflange valves or
  - b. mount the attachment directly on the scrubber shell or on a separate support column. Install a small male/female threaded, full port needle valve on nozzle. Use tubing or braided hose from the valve to the remotely located attachment.
3. Install a repad and gussets in two planes for RFWN nozzles. The nozzle must be stress relieved after welding.
4. Orientating the nozzle and attachments parallel to the direction of piston motion. Install poison pads (welding pads) on the scrubber to allow for field braces should they be required.

The sight glasses or level gauge for visually checking the liquid level in scrubber is perhaps the component with the most vibration problems.

Figure 14 shows two acceptable arrangements. The sight glass should be mounted as close to the scrubber as possible as shown by the studding outlet arrangement on the left. Some scrubber designs include a special mounting bracket on the scrubber shell and tubing or steel braid flex hose between the nozzle and sight glass. A remote mounted sight glass design is shown on the right. Note the relatively short and lightweight ball valves used on the scrubber for isolation.



Studding Outlet



Remote Mount with Small Valves

Figure 14: Scrubber Sight Glass Layout Options

#### **4.6 Field Testing and Field Vibration Solutions (Dealing with an Existing Design)**

Evaluating vibrations of the scrubber during start-up and commissioning is a key part of assuring safe operation of the reciprocating compressor asset. Vibrations on the scrubber and attachments must be measured over the entire compressor operating speed range. Vibrations must be checked whenever there are significant changes to reciprocating compressor operation



such as a change in load step, compression ratio, temperature, or gas composition. ISO 10816-8 does not specify a vibration guideline for scrubbers. It is suggested that the vibration levels for the pulsation bottles be applied to the scrubbers. The vibrations should be measured on the scrubber at a height of approximately 2m above the base. Measurements must be taken in the horizontal plane in the directions parallel and perpendicular to the reciprocating compressor crankshaft axis.

If vibrations are high, additional testing and analysis is required. The dynamic forces and dynamic flexibility must be assessed. Dynamic forces can be evaluated with measurements for reciprocating cylinder unbalance, compressor cylinder pressure-time signatures and evaluating pressure pulsations in the piping into and out of the scrubber. Dynamic flexibility can be measured with impact testing or shaker tests. The usual case is that the dynamic forces have been controlled by the design study and dynamic forces are not the cause of the high vibration. The most common cause of the high scrubber vibration is the dynamic flexibility for the field installation is different from that determined during the design study. Problems encountered during either construction or installation typically result in differences in the dynamic flexibility. Eliminating the vibration problem then comes down to a decision as to how to change the dynamic flexibility by a practical method for the existing scrubber and field installation.

As demonstrated by *Figure 2*, the scrubber may be under-tuned, inter-tuned or over-tuned to achieve an acceptable dynamic flexibility to minimize vibration. Tuning can be done by changing the stiffness or mass. A common approach to increasing the stiffness is to add braces to the scrubber as shown in *Figure 15*. The braces can be connected to the scrubber by a flat bar band or clamp around the shell. Braces can be effective but take up a lot of space which can be a concern for maintenance and safety hazard for tripping or head injury.

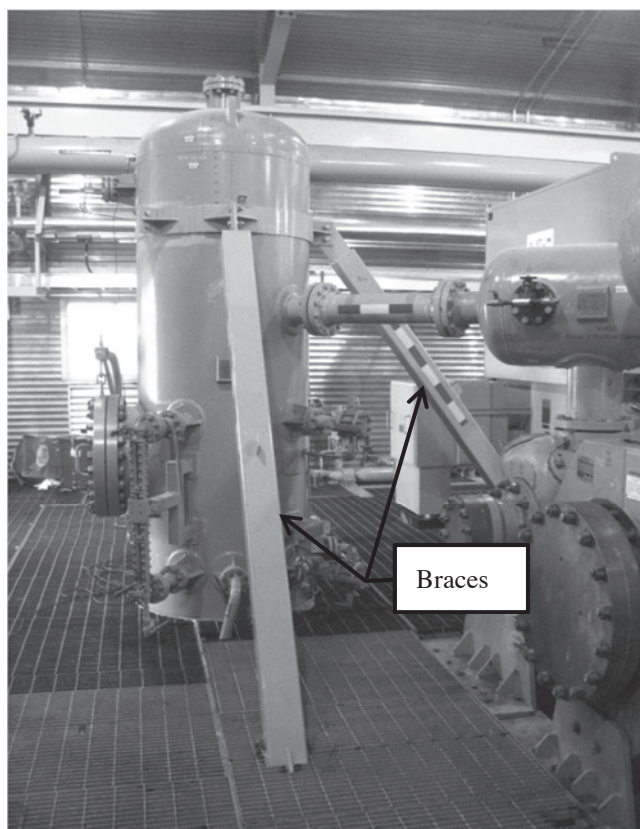


*Figure 15: Scrubber Braces in Two Directions*

Detailed measurements of the scrubber mode shape and operating deflection shape may point to excess flexibility in the base connection or skid below the base. Gussets on the skirt, base plate or skid may be necessary. Adding epoxy grout to the void in the skid under the scrubber or adding more anchor bolts from the skid to the foundation may also reduce the dynamic flexibility of the base to over-tune the scrubber.

Inter-tuning the scrubber resonance by introducing flexibility is sometimes a solution to high scrubber vibration. If the scrubber base includes anchor bolts as shown in *Figure 8* and *Figure 9*, loosening one or more of the anchor bolts may be sufficient. Another approach to add flexibility is to increase the size of the cut-out (hole) in the skirt. One or more cut-outs are often required in the skirt for access to the drain connection. The usual approach is to minimize the cut-out size to over-tune the scrubber. Only a very small portion of the skirt is required to meet the static support requirements. A large portion of the skirt can be removed to increase the flexibility and detune the resonance as shown in *Figure 16*.

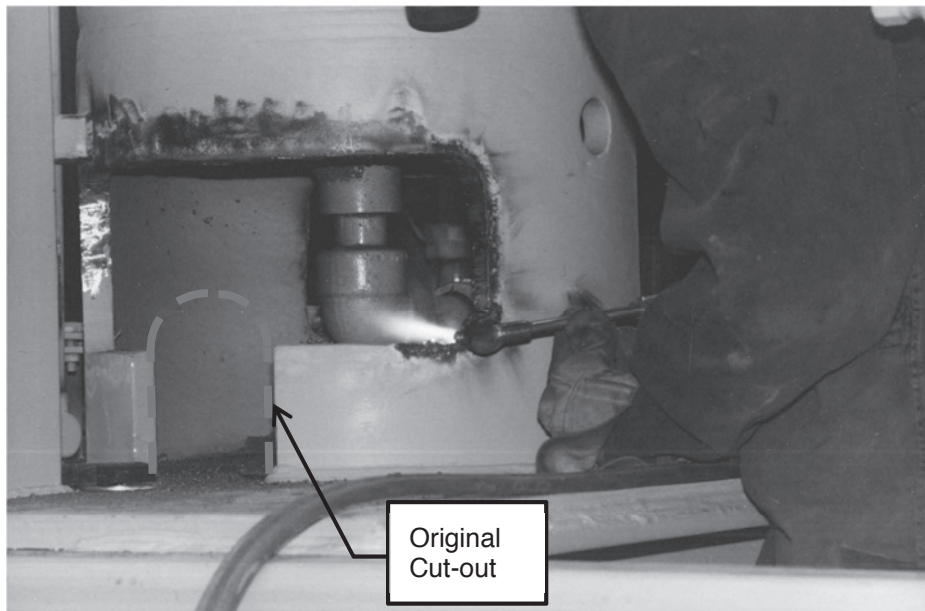


*Figure 16: Scrubber Skirt Cut-out*

Another method to increase the dynamic flexibility is to increase the mass of the scrubber. A mass clamped to the top of the scrubber will generally be the most effective. The mass could be in the order of 50 kg to 250 kg depending on the size of the scrubber and frequency shift that is required.

Figure 17 shows one example of adding a mass near the top of a scrubber by sections of solid steel bars welded to a band clamp. The mass must be firmly attached to the scrubber so that the mass moves or participates with the scrubber vibration. Simply binding of the mass to the scrubber by ropes or cable may not be sufficient.



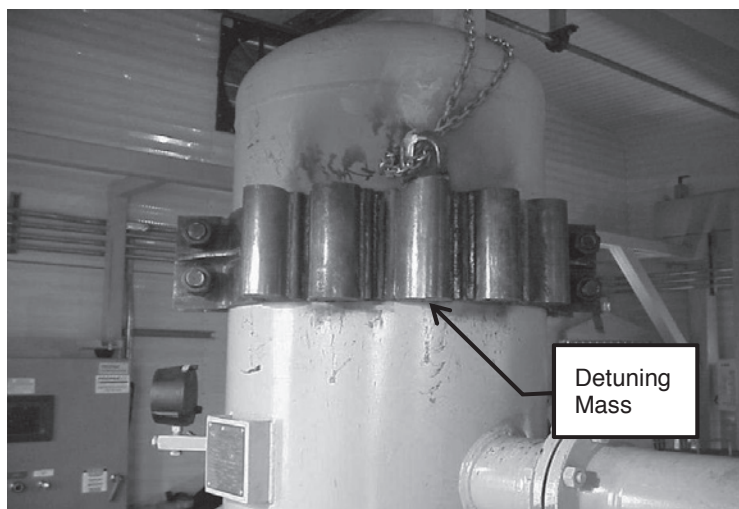
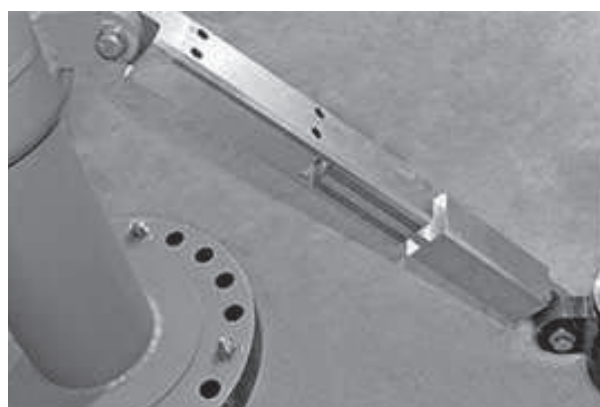


*Figure 17: Mass Added to Scrubber*

Tuning the scrubber resonance by changing the flexibility or mass can be effective solutions to reduce vibration particularly for fixed speed applications or applications with a limited variation in operating conditions. Other solutions to control vibration may be necessary for more challenging applications. As demonstrated in Figure A.3, increasing the damping can significantly reduce vibration at resonance. Adding damping using conventional devices is challenging due to the relatively low amplitude of the vibration and difficulty in calculating the damping properties of material. One method of adding damping is by specially engineering materials in a small brace design as shown in Figure 18. The damper brace is much smaller in size and footprint than a traditional brace. Another option for controlling scrubber vibration is installation of the vibration absorber as shown in the right image of Figure 18. The vibration absorber uses a separate spring-mass system that is attached to the scrubber that transfers the vibration energy from the scrubber to vibration energy in the added spring-mass system. The spring-mass system in the vibration absorber must be a proven and reliable design as the vibration amplitudes of the absorber mass can be high.



Damper Brace



Vibration Absorber

*Figure 18: Other Devices to Control Scrubber Vibrations*



## 5. Conclusions

This paper has presented the analytical basis as to why scrubbers vibrate, the potential risks from high vibration, industry best practices to avoid vibration and fatigue failures and solutions to mitigate vibrations for existing field installations.

## 6. Future Work

It is recommended that the current EFRC guideline regarding avoiding liquid problems [1] be expanded to include reference to this technical paper or include a separate section on vibration control of vertical scrubbers. Proper design of the scrubbers for avoiding liquid problems is an important topic but some decisions about the design for liquid control increase the risk of fatigue failures due to vibration. Failures of scrubbers and in particular scrubber attachments are a common industry problem. A logical extension of this proposed work is compiling similar guidelines or industry best practices for horizontal scrubbers. BETA (Wood Group Vibration, Dynamics & Noise) welcomes the opportunity to participate in developing future version of this guideline.

## 7. Bibliography

- [1] EFRC, "Guideline On How To Avoid Liquid Problems In Reciprocating Compressor Systems," EFRC c/o Technische Universität Dresden, Dresden, 2014.
- [2] GMRC, "Guideline For High-Speed Reciprocating Compressor Packages For Natural Gas Transmission & Storage Applications," GMRC, Dallas, 2013.
- [3] GMRC, "Design Guideline for Small Diameter Branch Connections," GMRC , Dallas, 2011.
- [4] E. Institute, "Guidelines for avoidance of vibration induced fatigue failure in process pipework," Energy Institute, London, 2008.

## 8. Acknowledgements

The paper is a collection of many years of knowledge and experience from industry in general as well as BETA's Field and Design teams. Special thanks goes to Wally Bratek, Chris Harper, Bill Eckert and Brian Howes for their contributions.



## APPENDIX A: Fundamentals of Vibration

Understanding the solutions for minimizing vibrations and fatigue failures on scrubbers requires a basic knowledge of vibration and dynamic response of structures. Before discussing the dynamic, consider the static response of simple cantilever beam as shown in Figure A.1.



Figure A.1 Deflection of a Cantilever Beam due to an applied Force

A force applied at the end of the beam,  $P$ , causes a deflection,  $\delta$ , based on the flexibility,  $F$ , of the beam as described in the Equation 3. The more flexible the beam is, the greater the deflection for a given force.

$$\delta = P \times F \quad (4)$$

This relationship between the applied force and the resulting displacement remains valid as long as the force is constant or applied very slowly. The forces in a reciprocating compressor installation are oscillatory or dynamic in nature, that is, the force varies from a positive to negative amplitude many times a second. The dynamic or oscillatory displacement or vibration,  $V$ , resulting from the dynamic force,  $P_D$ , is a result of the dynamic flexibility,  $F_D$ , as stated by Equation 4.

$$V = P_D \times F_D \quad (5)$$

The core to understanding any vibration problem and measures to mitigate the vibration lies within Equation 4. The source of vibration is the dynamic force. An understanding of the different dynamic forces that are generated by a reciprocating compressor and how they can be minimized will directly address the resulting vibration. Some dynamic forces are inherent in the reciprocating compressor design and cannot be changed. The dynamic flexibility must be reduced to minimize vibration in these cases.

## Dynamic Forces

The dynamic forces, sometimes referred to as loads, for a typical engine drive reciprocating compressor are shown graphically in Figure A.2.

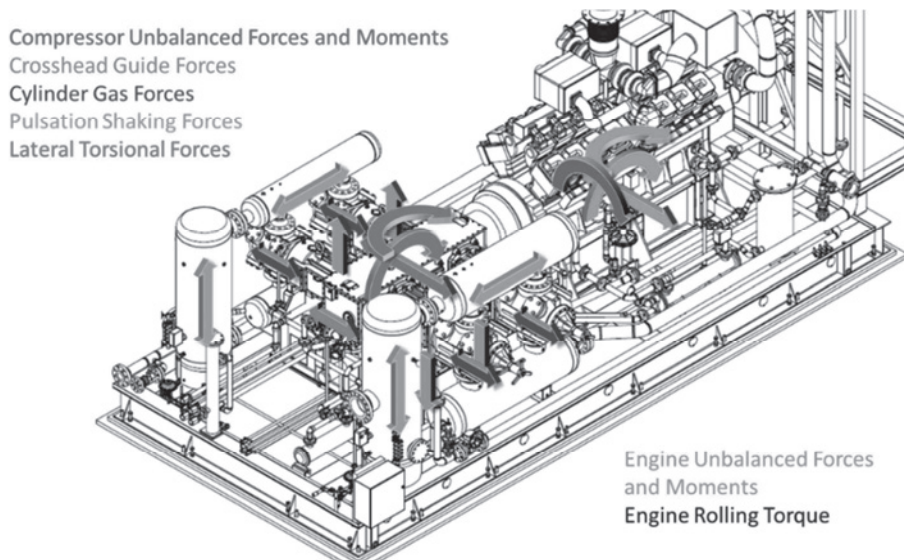


Figure A.2 Dynamic Forces in an Engine Driven Reciprocating Compressor

The dynamic loads include both forces and moments. Dynamic forces and moments from unbalanced reciprocating and rotating inertias are present in reciprocating compressors and engines. These unbalanced forces and moments are often the highest dynamic loads. These loads are the results of the machinery design and the tolerances in the weight of the reciprocating and rotating components. These loads are present even when the compressor is fully unloaded. There is very little that can be done to minimize these loads for a particular compressor design.

Crosshead guide forces and cylinder gas forces are primarily the result of compressing the gas. Operating factors such as the compression ratio, cylinder loading and gas composition impact these forces for a given compressor geometry. These forces occur at all orders of compressor speed and can be significant up to 10x compressor speed and vary greatly in amplitude with changes in the operating factors. It is not always possible to change the operating factors to minimize these dynamic forces as the pressure and flow requirements for the compressor application must be met.

Pulsation shaking forces are the result of pressure pulsations generated by normal operation of the reciprocating compressor. A design study to design the compressor manifolds (also referred to as bottles or dampers), piping and other components can reduce these dynamic forces. However reducing the pulsation shaking forces to zero is not practical. There will be some residual pulsation shaking forces that must be considered in the final design.

All these loads must be considered in the design of scrubbers to minimize vibration. The large forces and moments due to unbalance must be avoided by reducing the overall flexibility of the vessel. The cylinder gas forces and residual pulsation shaking forces can excite vibration on small diameter piping and instrumentation that is connected to the scrubber.



### **Dynamic Flexibility**

The dynamic flexibility is defined by three structural properties; static flexibility, mass and damping.

The static flexibility as noted in Equation 1 is the ratio of the displacement and the static force. It is intuitive that reducing the static flexibility will reduce the dynamic flexibility. Increasing the bending inertia of the beam will reduce the deflection in the example of the cantilever beam. However increasing the bending inertia means that the cross-sectional area of the beam is also increasing. A larger cross-sectional area means the beam has more mass. Generally more mass means an increase in dynamic flexibility. One must consider changes in static stiffness and changes in mass when calculating the dynamic flexibility.

Consider the example of scrubber that is initially designed with a DN500 (20" NPS) schedule 80 shell. The designer may decide to take a conservative approach and opt for a thicker shell material to make sure the scrubber has a low flexibility to avoid vibration problems. A DN500 schedule 160 shell is selected. The moment of inertia for a schedule 160 shell is significantly higher than a schedule 80 shell as shown in Table A.1. The schedule 160 shell is better from a static flexibility perspective. However the mass of the schedule 160 shell is much greater than the schedule 80 shell. The ratio of the shell inertia and mass for the schedule 160 shell is actually lower than the schedule 80 shell, about -9%, meaning it has a higher dynamic flexibility. An alternative design with a thinner shell is shown in Design Option 3. Design Option 3 has a considerably lower moment of inertia as compared to the original design however it's mass is also lower. The ratio of the inertia and mass for Design Option 3 is actually higher than the original design by 7%. It would be advantageous for the designer to choose Design Option 3 rather than Design Option 2 to avoid vibrations due to low frequency forces. This example illustrates the key concept of static flexibility and mass and their impact on dynamic flexibility that is often overlooked by designers experienced in static analysis.

*Table A.1 Example Scrubber Shell Properties*

Design Option	Shell Size	Moment of Inertia (mm <sup>4</sup> x10 <sup>9</sup> )	Mass of Pipe (kg/m)	Inertia/Mass (x10 <sup>3</sup> )	Percent Difference
1	DN500 S80	1.15	312	3.70	
2	DN500 S160	1.91	565	3.38	-9%
3	DN500 S20	0.46	117	3.94	7%

### **Damping at Resonance**

The third property or factor in the dynamic flexibility is damping. Damping is the property that absorbs and dissipates the vibration energy in a structure. A component with high damping is said to have low dynamic flexibility. Damping is only significant in controlling the vibration and dynamic flexibility for frequencies very close to the mechanical natural frequency of a structure. The mechanical natural frequency is defined as the vibration frequency when not subjected to a periodic force. An alternate definition for the mechanical natural frequency is the frequency at which the dynamic flexibility of a component is a maximum. The effect of damping on the dynamic flexibility is clearly shown in Figure A.3. The dynamic flexibility is identical for 1% and 2% damping except for frequencies that are very close the mechanical natural frequency (ie, frequency ratio close to 1). The damping for scrubbers in reciprocating compressor applications are typically around 1% ±0.5%.

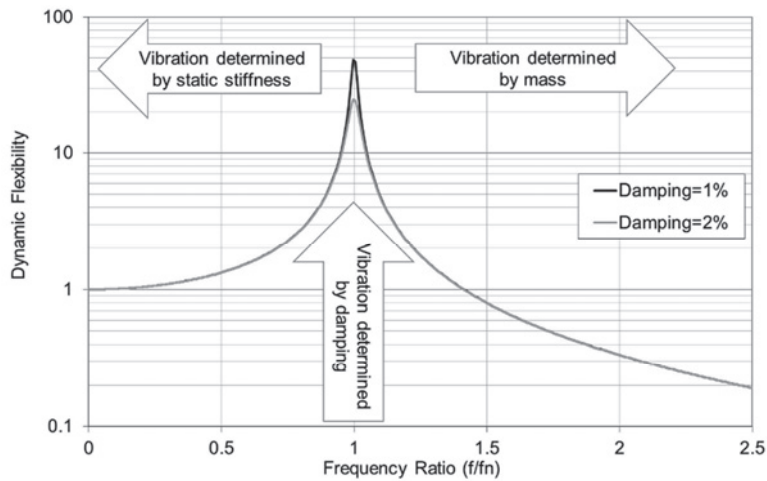


Figure A.3 Typical Frequency Response Function

Figure A.3 also demonstrates other key point about the dynamic flexibility. The static flexibility is represented by the value of the dynamic flexibility at low frequency ratios. As the frequency of the applied force increases towards the mechanical natural frequency, the dynamic flexibility increases. The dynamic flexibility at the natural frequency can be 20x to 50x higher than the static flexibility depending on the damping. A very small static force would result in low static displacement but the same amplitude force applied as a dynamic force at the natural frequency will result in very high vibrations. As the frequency of the applied force increases above the mechanical natural frequency, the dynamic flexibility decreases. This latter part of the response curve is where the mass of structure determines the dynamic flexibility and vibration.

An understanding of dynamic flexibility in the design of scrubbers is key to assuring acceptable vibration. The scrubber must be designed to avoid the high dynamic flexibility that occurs at the mechanical natural frequency. Deciding upon the most appropriate design modifications such as changes to stiffness, mass and/or damping requires knowledge of the dynamic flexibility.





# Technical Paper

**Session: 49-1**

**Session Name: Calculation 2**

**Using OEM performance software to assist with troubleshooting a crosshead failure**

**Author:**

**Benjamin F. Williams**  
**Process Application and Account Manager**  
**Ariel Corporation**  
**Mount Vernon, Ohio USA**

**Co-Author :**

**Jillian T. Toussaint**  
**Senior Machinery Engineer**  
**Air Products and Chemicals, Inc.**  
**Botlek, Netherlands**

## Summary

This paper will be a case study regarding a crosshead failure that occurred in one of four short stroke moderate speed compressors operating in a hydrogen plant in Europe. The paper will describe how the problem was found and the determination of the root cause. The analysis included visual inspection, data trend analysis and the use of OEM compressor performance software to calculate the effect that changes in operating conditions had on the unit. As the process the compressors are used in is proprietary, only general terms will be discussed and actual operating conditions will not be provided.

## Introduction

The hydrogen plant is located in Botlek, Netherlands in the Rotterdam area. It is owned and operated by one of the world's largest suppliers of hydrogen for the refinery and petrochemical industries. The Botlek facility (designated as HYCO 4), began producing hydrogen in December 2011. The facility is designed to produce in excess of 300 tons of hydrogen per day. The hydrogen plant uses four short stroke moderate speed compressors, two in hydrogen product service (Tag numbers K601A/B) and two in refinery fuel gas (RFG) service (Tag numbers K111A/B). The RFG is blended with natural gas and used as feedstock for the hydrogen production process.

Each compressor is packaged on a structural steel skid, along with their auxiliary systems and electric motor drivers. The compressors are driven at 743 RPM and are sized to deliver 100% of the capacity required for their respective service. The focus of this paper is a crosshead failure that occurred with unit K111A.

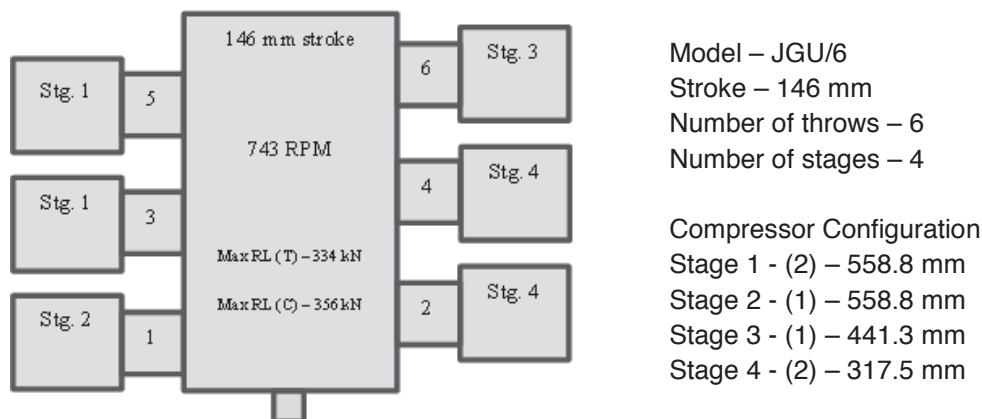


Figure 1 – K111A/B Compressor Description

## Operation

The K111A/B compressors are designed to compress RFG from 3 to 24 bara in three stages of compression. Between stages 3 and 4, additional RFG is added and then compressed to approximately 45 bara. Stage 4 suction and discharge pressures are maintained by a recycle line around the stage.

Each compressor includes head end (HE) suction valve unloaders on all cylinders for capacity control. These unloaders are the valve depressor (finger) type and are used to deactivate the HE of the cylinder by holding the suction valves open. Operating in this mode makes the cylinder single acting crank end (SACE). The normal operating philosophy is to run both compressors at 50% load (all cylinders SACE) and in the event a problem is noted with one compressor, the second compressor would be switched to its 100% load step in order to keep the plant in operation.



## Background

In September 2013, with over 18,000 hours of operation, compressor K111A experienced a crosshead failure on throw 4. The following describes the events leading up to the failure and the determination of the cause.

The compressor was operating in its normal mode with all cylinders SACE. Stage 4 suction and discharge pressures were being maintained by the recycle line. The recycle valve began operating erratically, opening and closing regardless of the actual suction or discharge pressures. When the recycle valve closed, suction pressure dropped significantly below its design value and when the valve opened all the way, suction pressure increased and the discharge pressure dropped due to the decreased flow. Instead of the design 20 bar differential pressure across the 4th stage, the differential pressure actually ranged from 2 – 27 bar. The operator took manual control of the recycle valve to bring pressures back to their normal ranges. The compressor continued to operate.

The following day while troubleshooting the recycle valve, the compressor shut down on high vibration. The compressor was inspected to determine the cause of the shutdown.

## Inspection Results

The initial visual inspection showed smeared babbitt from the crosshead and in the crosshead guide for throw 4. (Figure 2). No damage was noted on throw 2, the other 4<sup>th</sup> stage cylinder.

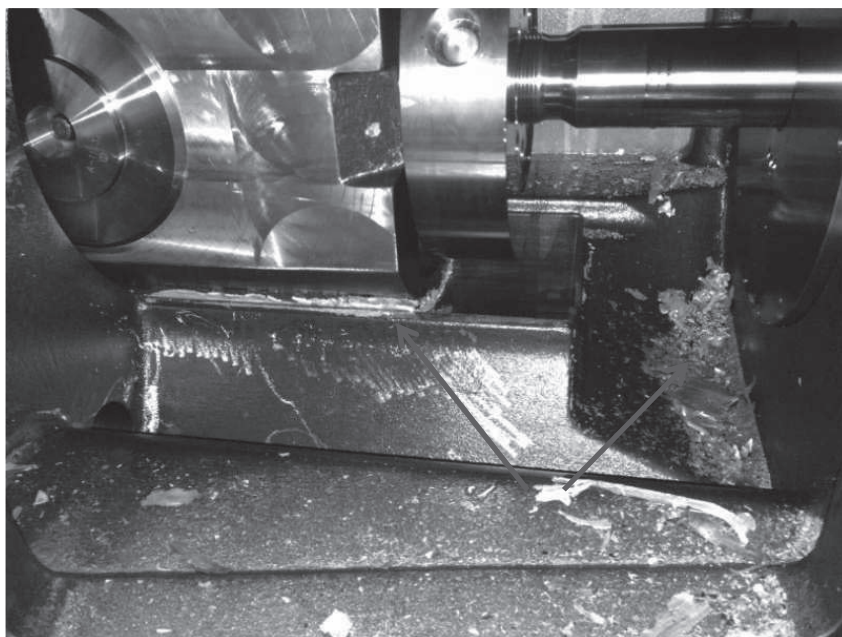


Figure 2: K111A – Throw 4 Crosshead Guide (arrows indicate smeared babbitt).

The compressor valves were removed and visually inspected. The discharge valves were very dirty. After the damage to the crosshead on throw 4 was discovered, the 4<sup>th</sup> stage valves were liquid leak tested.

Cylinder 4 crank end (CE) suction valves showed no leakage. One head end (HE) discharge valve showed slight leakage but both CE discharge valves leaked excessively. There was only slight leakage noted from the valves in cylinder 2.

The throw 4 CE discharge valves were then disassembled for inspection. No rings were broken but there was a thick, tar-like build-up on the sealing areas. It was unknown if this was burnt oil or debris from the gas stream.

Further inspection of the throw 4 crosshead showed the crosshead pin was seized in the crosshead bushings and the crosshead bushings had rotated in the connecting rod. This caused irreparable damage to the connecting rod. The crosshead, connecting rod and crosshead pin and all bushings required replacement. The connecting rod bearing showed very little wear but since the bearing shells had been removed for inspection, the decision was made to replace them.

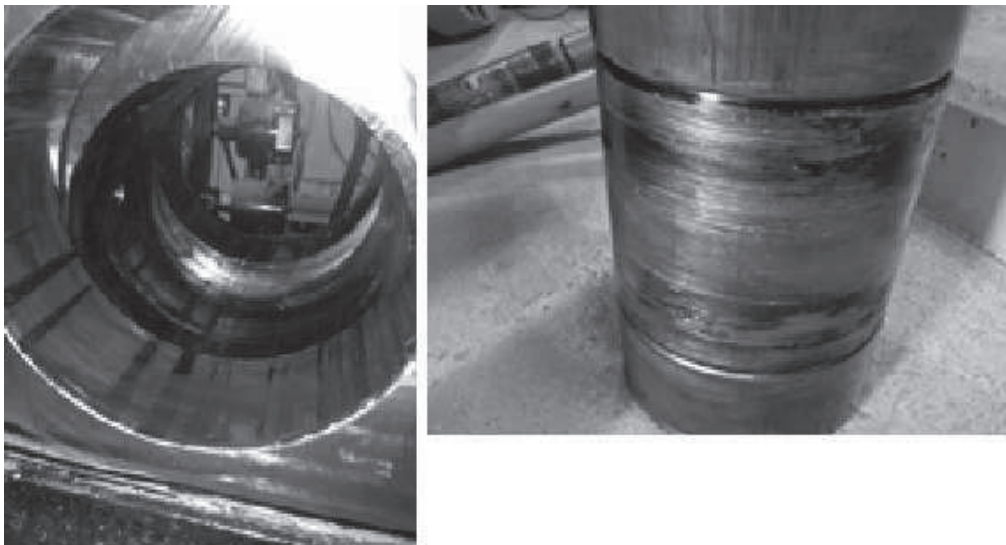


*Figure 3: K111A – Throw 4 Crosshead and Crosshead Pin*

The crosshead guide was cleaned by hand and dye-penetrant inspected. No cracks were found and all crosshead guide bore measurements were within specification.

### **Failure Root Cause Analysis**

The inspection of the compressor determined that a crosshead pin non-reversal failure had occurred. The following section describes what crosshead pin reversal is and describes the two issues that led to the failure.

The initial inspection showed that the CE discharge valves in cylinder 4 leaked excessively. It was also discovered that during troubleshooting of the recycle valve, the compressor experienced high rod loads due to cylinder differential pressure.

### **Crosshead Pin Reversal**

Crosshead pin reversal is the reversal of compression and tension loads at the crosshead pin to connecting rod bushing. Insufficient crosshead pin reversal can lead to inadequate lubrication of the crosshead pin and bushing.

Crosshead pin reversal is measured in the duration of the reversal (degrees of crankshaft rotation) and the magnitude (in percent) of reversal. The percent magnitude is the smaller of the compression or tension forces divided by the larger of the two. The combined inertia and gas loads are used in determining crosshead pin reversal. The inertia component includes the weights of the piston and rod assembly, crosshead, bushings and balance nuts.



The OEM limits for crosshead pin reversal are 30 degrees of crank rotation and 25% magnitude.

The following rod load graphs (Figures 4 and 5) show the gas forces, inertia forces and the crosshead pin force, which is the algebraic sum of the two.

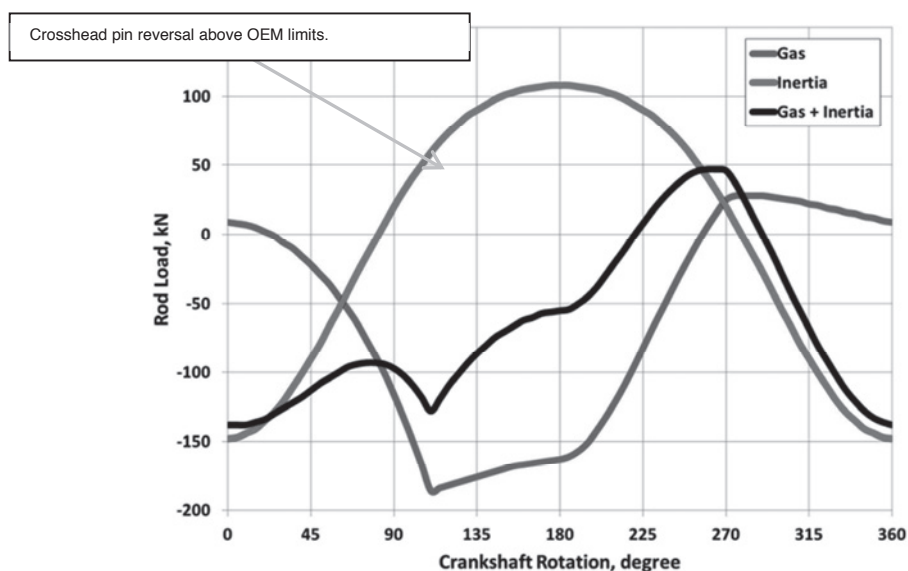


Figure 4: Rod load chart showing sufficient crosshead pin reversal.

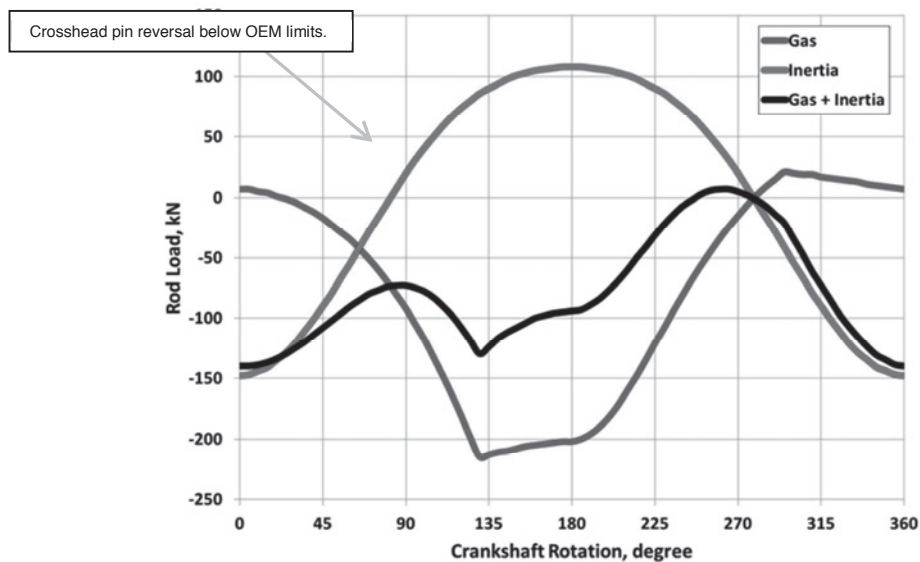


Figure 5: Rod load chart showing insufficient crosshead pin reversal.

### Leaking CE Discharge Valves

The leaking CE discharge valves on throw 4 were the initial focus of the failure analysis. The leaking discharge valves caused an increased pressure in the crank end of that cylinder.

Figure 6 shows the effect of leaking discharge valves on the P-V diagram.



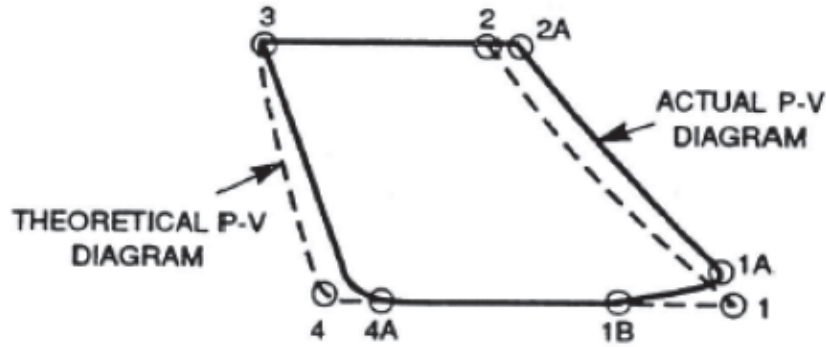


Figure 6: Pressure-Volume diagram showing the effects of a leaking discharge valve.

Figure 6 shows that with leaking discharge valves, the suction valves open late (Point 4A instead of Point 4) and close early (Point 1B instead of Point 1). Leaking discharge valves also cause the cylinder pressure to increase, even though both suction and discharge valves are closed (Points 1A to 1B). This increased discharge pressure will cause the discharge valves to open early (Point 2A instead of Point 2).

Discharge valve failures may or may not cause crosshead pin non-reversal; it depends on the severity of the failure. A significant failure could cause the affected cylinder end to be at discharge pressure all the time and the suction valves will not open. Compression will therefore not occur.

### The Effect on Crosshead Pin Reversal of Leaking CE Discharge Valves

Since all cylinders on K111A were operating SACE, the leaking discharge valve on throw 4 made it more susceptible to a crosshead pin non-reversal problem. This was due to the increased crank end cylinder pressure. Although cylinders 2 and 4 were operating at the same conditions, the increased valve leakage on cylinder 4 made the crosshead pin non-reversal worse on that throw, because the cylinder internal pressure throughout the compressor stroke was higher than that of cylinder 2.

To visually explain crosshead pin reversal with a cylinder that is SACE, please see Figures 7, 8 and 9. When a cylinder is SACE, the piston rod is in tension during compression (Figure 7). The net force on the piston pulls the crosshead away from the crankshaft and the crosshead pin is pulled toward the crankshaft. This opens clearance between the crosshead pin and the cylinder side of the crosshead bushing allowing oil to fill the space.

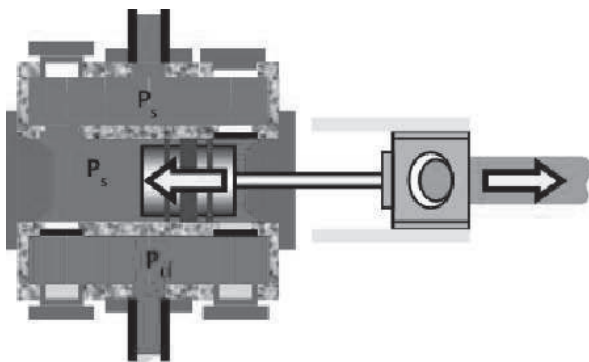


Figure 7: Expansion process begins

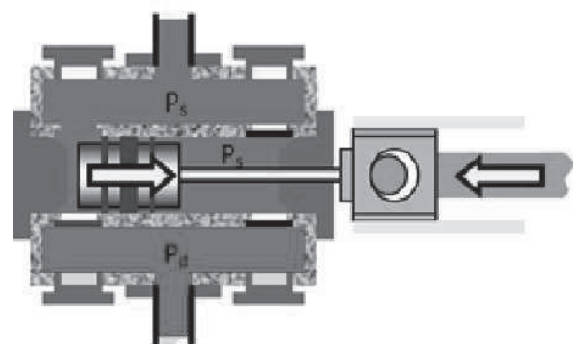


Figure 8: Compression process begins – crosshead pin reversal has occurred.



When the piston changes direction (Figure 8), the piston rod is in compression because even though the cylinder is SACE, the gas force on the HE of the piston is greater than that on the CE because both ends are exposed to suction pressure. This forces the crosshead toward the crankshaft and the crosshead pin is pushed toward the cylinder opening clearance between the pin and the crosshead bushing on the crankshaft side. The changing position of the crosshead pin relative to the crosshead is crosshead pin reversal.

In the case of K111A, the leaking CE discharge valves increased the crank end cylinder pressure, resulting in decreased crosshead pin reversal. (See Figure 9)

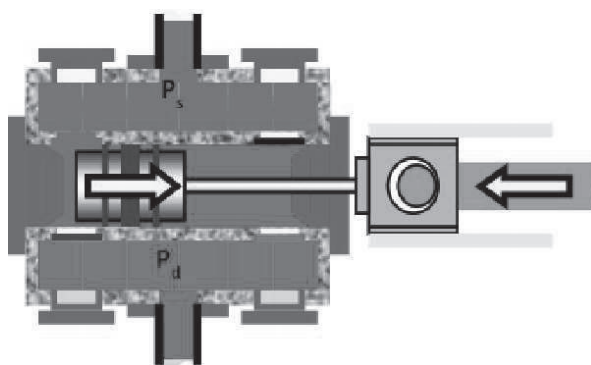


Figure 9: Compression process begins with leaking CE discharge valves. CE cylinder pressure is at or near discharge pressure – crosshead pin reversal has not occurred

### Increased Cylinder Differential Pressure

The normal differential pressure across the 4<sup>th</sup> stage cylinders is approximately 20 bar. It was determined that during the erratic recycle valve operation the cylinder differential pressure varied from 2 to 27 bar.

The following day, during the troubleshooting of the recycle valve, the cylinder differential pressures also varied from the design conditions. It was during the troubleshooting of the recycle valve that the high vibration shutdown occurred.

The increased differential pressure in the 4<sup>th</sup> stage not only impacted crosshead pin reversal, it also caused rod loads to change. In order to determine how much each changed, the OEM software was used to model the compressor operation.

### Using OEM Software to Troubleshoot

In addition to the inspections of the compressor and valves, the compressor OEM performance software was used in the troubleshooting efforts. The OEM performance software is used to select the compressor based on operating conditions and customer requirements. It can also be used as a troubleshooting tool by comparing existing operating conditions to the original design compressor performance calculations, as was done in this case.

The first operating case for comparison noted that for a period of time prior to the failure, the compressor had been running with suction pressure 6 bar lower than design as a means of reducing plant power consumption. Discharge pressure was at the design condition.

This increased differential pressure increased the rod load on the compressor, as expected, but it was also discovered that the crosshead pin reversal calculated by the program was less than the OEM allowable limits. However, the compressor was operating below the associated alarm and shutdown settings used for rod load protection.

The following graphs, generated by the software, compare the dynamic forces for cylinder 4 at the Design operating conditions (Figure 10) and at the reduced suction pressure case that the unit was operating prior to the incident with the recycle valve (Figure 11).

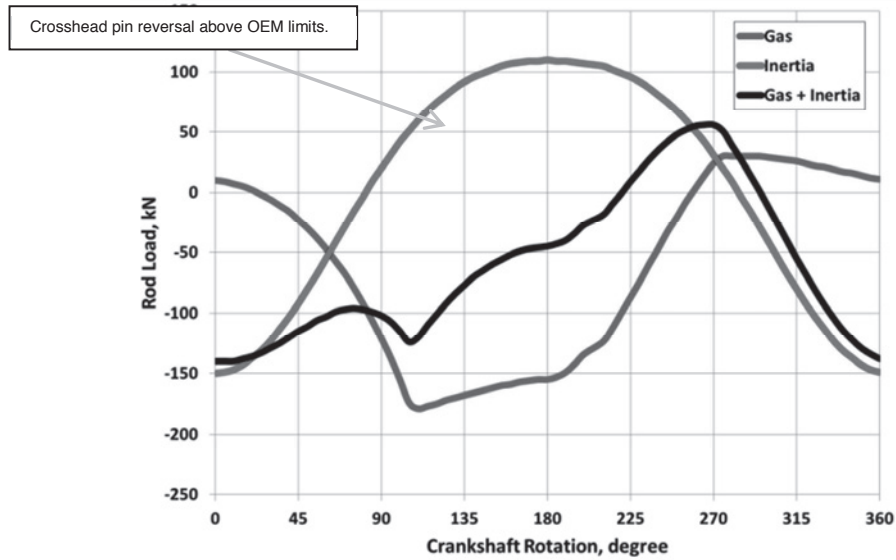


Figure 10: Crosshead pin reversal at design conditions.

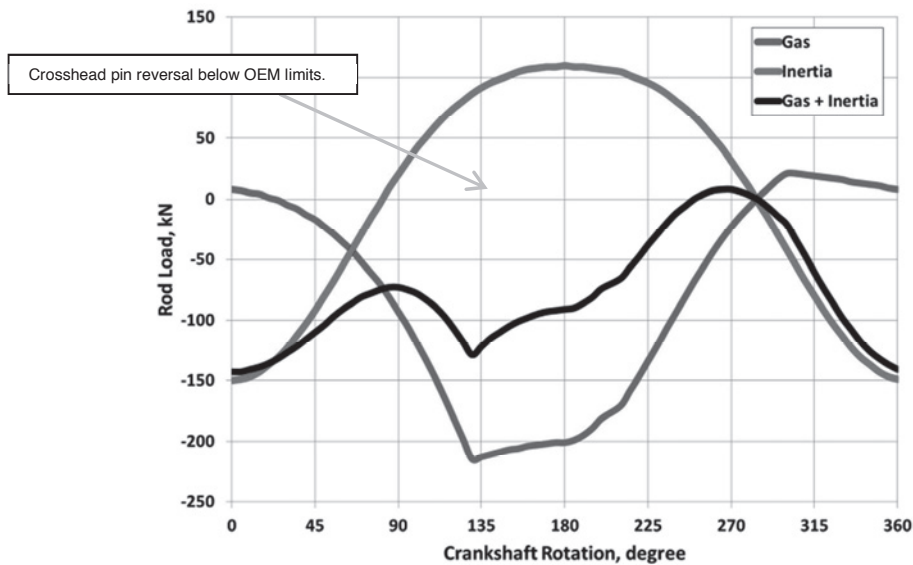


Figure 11: Crosshead pin reversal at time of incident.

The effect on crosshead pin reversal due to the erratic operation of the recycle valve is shown in Figure 12. This graph was generated, using data calculated by the software.

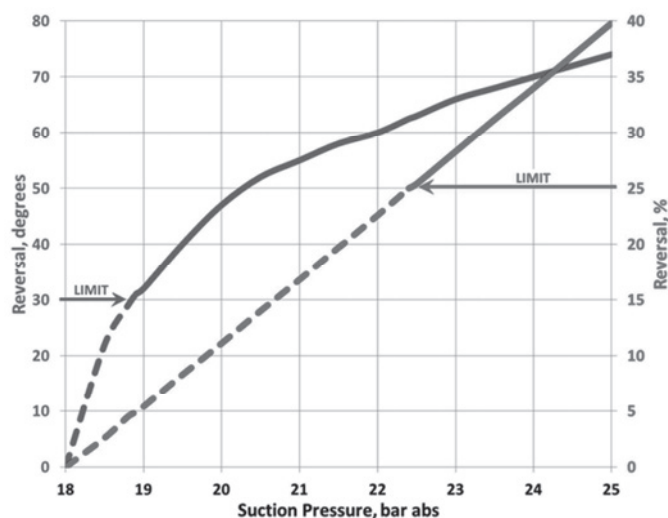


Figure 12: Crosshead pin reversal at varied suction pressures and a constant discharge pressure. OEM limits are highlighted.

While analysing the compressor at various suction and discharge pressures, it was determined that during the recycle valve troubleshooting, the compressor had operated for a period of 13 minutes with a predicted crosshead pin reversal magnitude of 0%.

The multi-run feature of the performance software was then used to analyse all of the compressor stages to ensure adequate crosshead pin reversal through a wide range of operating conditions and compressor load steps. This enabled operators to determine whether rod load or crosshead pin reversal limits were exceeded first.

Based on the information gathered during this analysis, the existing alarm and shutdown setpoints were revised to ensure the compressor was protected in any off-design operating cases where crosshead pin reversal dropped below allowable OEM limits.

## Conclusion

Troubleshooting the crosshead failure involved both physical inspection and the use of OEM software. It was determined that a number of causes led to the crosshead failure. The following will summarize the root causes of the failure and the corrective action taken to address them.

Leaking 4<sup>th</sup> stage CE discharge valves resulted in reduced crosshead pin reversal. As a preventive measure, a more frequent valve temperature monitoring policy was instituted. The temperatures are recorded in a log by the plant operators and in the event of an increased temperature, corrective action is taken. Additionally, monitoring the calculated deviation between actual and adiabatic discharge temperatures was added to the DCS (Distributed Control System) logic. This deviation alarm has proven to be very effective in identifying valve degradation. Since the high deviation alarm has been implemented, a crank end valve failure recently was found that allowed a controlled shutdown before damage could occur to the compressor.

It should be noted that in a double acting cylinder, leaking discharge valves may or may not cause crosshead pin non-reversal since there is gas force on both sides of the piston. Operating a cylinder double acting may make it less susceptible to crosshead pin non-reversal.

Due to plant requirements, the compressor was required to operate in conditions not originally identified. The compressor was able to operate in these off-design conditions, however these operating cases combined with the leaking discharge valves, caused crosshead pin reversal to be significantly reduced. The erratic operation and subsequent troubleshooting of

the recycle valve decreased the crosshead pin reversal even further and ultimately, the crosshead failed.

Calculations made with the OEM software have provided a clear operating map showing the effect on rod loads, discharge temperatures and crosshead pin reversal at the changing conditions. Using data generated by the performance software, alarm and shutdown setpoints were adjusted to allow operation in these areas without damaging the compressor.

It is very important to review off-design operating points to identify those conditions in which compressor limits are exceeded. This can easily be done with OEM software. In the event a failure occurs, it is crucial to know the operating conditions at the time of the failure. This information can be used with the OEM software to assist with troubleshooting the cause.

### **References**

End User operating records and Root Cause Analysis (RCA) data

OEM Software

OEM Training Presentations





# Technical Paper

**Session: 49-2**

**Session Name: Calculation 2**

**Interactions between valve flow characteristics, valve pocket geometry and compressor performance**

**Author:**

**Dr.-Ing. Reiner Schulz  
Research and Development  
Burckhardt Compression AG  
8404 Winterthur, Switzerland**

## Summary

The need to reduce overall pressure losses is one of the most important challenges in meeting the increasing demand for high-efficiency reciprocating compressors. Although in most compressor designs valve losses amount to a bit less than half of the overall pressure losses, the contribution of the valve pockets to the overall losses may be higher than the valve losses in some cases. Therefore pocket losses are far from being insignificant. The losses of both valve and valve pocket are dependent on the pocket geometry since the valve pocket affects the flow in the valve and vice versa.

To improve efficiency, both the evenness of flow through the valves as well as the clearance volume must be optimized. Due to the limitations of the mutually exclusive objectives of low clearance volume and evenness of flow in the usual configuration (cone with slot shaped passage), other arrangements are also taken into consideration for comparison. A double acting cylinder equipped with a new design of a poppet valve has been investigated using moving mesh CFD simulations, taking fluid structure interaction into account. To improve the accuracy of compressor performance analysis, including the prediction of absorbed power, correction factors for both valve and pocket pressure loss coefficients have been derived, however, only an illustrative example is presented within this paper.

**Keywords:** Reciprocating compressor, Valve pocket, Valve losses, Computational Fluid Dynamics (CFD), Moving mesh



## 1. Introduction

Pressure losses in valve pockets can easily be determined for common geometries [1]. They may be expressed by a “pocket factor” based on valve losses. The impact of flow uniformity is neglected. This may be acceptable as long as only valves of similar types (e.g. plate valves of common proportions) are compared. However, the more valve losses are reduced, the more the flow is becoming unevenly distributed - in some cases even giving rise to recirculation through valves. Therefore, if valve types causing different flow distributions have to be compared, the accuracy of the traditional approach is limited. The modern approach based on CFD simulations, as described in many publications [2-9], is computationally too expensive to replace the tools for compressor / valve dimensioning which are based on zero or one- dimensional modeling. Therefore detailed CFD simulations should provide correction factors, which are applied easily to dimensioning tools.

In the first part of the paper steady state flow is assumed throughout. To illustrate the effect of non-uniform flow (or backpressure) on pocket pressure loss, different types of valve pockets have been investigated and the variations of valve pocket shapes are illustrated. The pressure loss of an arbitrary valve is approximated by an axisymmetric distribution of effective flow resistance (or porosity), taking into account non-permeable walls (e.g. centre bolt area). Radial flow in the valve is neglected for simplicity. Pressure loss coefficients for valve and compressor have been determined for different distributions of porosity. Inlet losses, caused by the redirection of flow entering the valve, are an additional important factor (however, they are not considered in this paper). By comparing these loss coefficients to the loss coefficients obtained for even flow (i.e. valve in a wind tunnel), the contribution of the unevenness of the flow to the pressure loss is obtained, i.e. additional loss coefficients due to the interaction of the parts are determined.

Steady state investigations will always be limited due to effects such as:

- Piston masking and squeezing effects near top dead centre;
- Pulsations and effects of gas inertia;
- Detailed flow in valve.

More complex transient flow, fluid structure interaction and moving mesh simulations provide valuable additional information such as gas forces acting on internal valve components and their (in some cases individual) opening and closing times. In the second part of the paper some transient, moving mesh simulations are summarized.

All simulations use air (i.e. ideal gas) as fluid. In order to minimize effects of numerical viscosity, the Monotone Advection and Reconstruction discretisation Scheme [10] is applied throughout. This scheme shows least sensitivity of solution accuracy to mesh structure and skewness. Turbulence is modelled by the standard high Reynolds Number k-ε model with non-equilibrium wall functions.

## 2. Simulations of Steady State Flow

### 2.1 Valve optimisation

Valves are always subject to improvement; a common task is to reduce pressure losses for a given valve type and valve size. A modified design of a poppet valve had been proposed. The pressure loss of the proposed design was compared to the standard design. Two different arrangements were used as shown in Figure 2.1: The valve in a tube (as in a wind tunnel) and the valve between a valve cage dummy and a generic valve pocket representative of many compressor designs. The comparison of the two different models revealed that although the proposed new design performed more or less identically in a wind tunnel measurement, the performance in a compressor is worse than the standard design. Diagram 2.1 shows the comparison of the loss coefficients (static pressure differential divided by dynamic pressure) of the valves. To obtain more realistic data, all pressure loss assessments of valves are performed both in a generic cylinder and in a wind tunnel arrangement. The results also led to further design modifications and finally to the development of a slightly modified poppet valve with pressure losses reduced to 73% in comparison to the standard design in a valve pocket of a standard compressor (Figure 2.2).

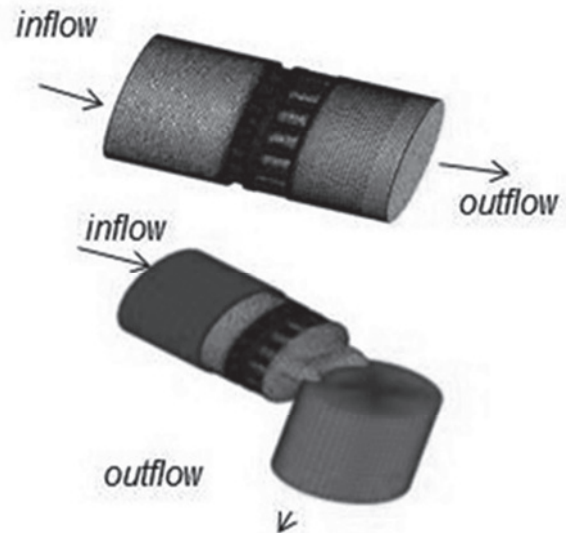


Figure 2.1: Models used for investigations: Wind tunnel type (top), cylinder with valve pocket (bottom)

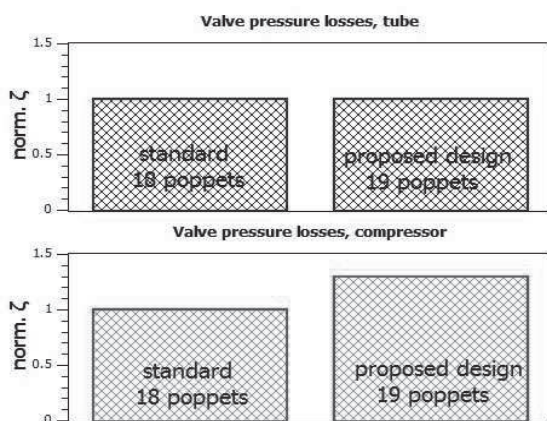


Diagram 2.1: Comparison of normalized pressure loss coefficient of two poppet valve designs. Loss coefficient of valve placed between valve pocket and valve cage (top) and in a wind tunnel arrangement (bottom)

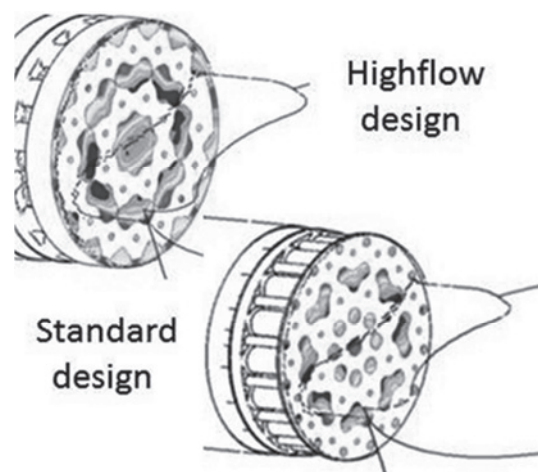


Figure 2.2: Velocity plots, section at valve outlet. Highflow design with pressure loss reduced to 73 % (top) in comparison to standard execution (bottom)



## 2.2 Variation of pocket geometry

Systematic series of valve pocket geometry variations have been investigated. The series have been simulated in order to quantify the effects of interdependency between valve pressure loss characteristics (i.e. not only the overall, averaged pressure loss as determined in a wind tunnel

arrangement but especially the impact of the distribution of flow resistance) and valve pockets of different shapes. At the moment, the parameter variations are limited to geometries with one suction / discharge valve per cylinder. The series uses a conventional arrangement with a right angle between cylinder and valve axis (Figure 2.3). Different shapes of the passage between cylinder and valve pocket are compared.

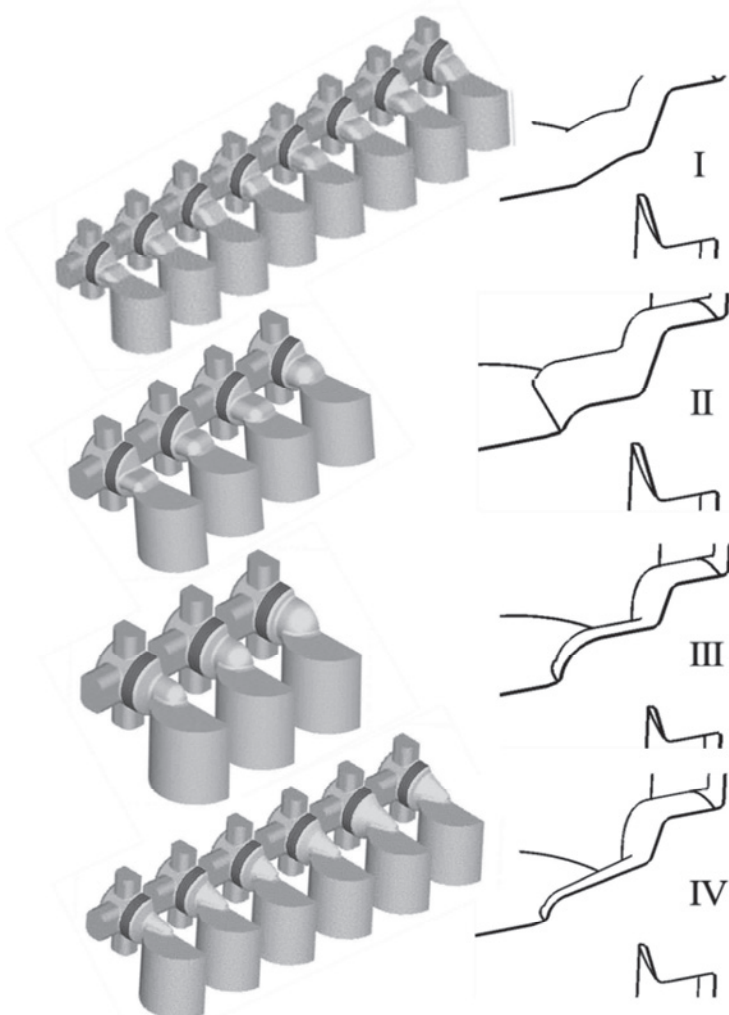


Figure 2.3: Geometry variations of conventional valve pocket arrangement: Type I (combination of wedge and cone), Type II (combination of block and cone), Type III (combination of cylinder and cone) and Type IV (combination of two cones; from top to bottom)

In Figure 2.4 velocity plots are compared. The shape of the passage between the cylinder and the cone adjacent to the valve is clearly visible as a velocity distribution at the section at the valve inlet. In this simulation, the valve pressure loss amounted to half the pressure loss of the valve pocket. The lower the pressure loss of the valve, the higher becomes the unevenness of the flow. In order to describe the pressure loss coefficients of the generic valve pockets, the following approach will be applied: The pressure loss coefficients are tabulated for each design dependent on several

distributions of local pressure resistance of the valve, the shape of the designs are described by parameters of characteristic dimensions (form factors), and the pressure loss coefficient is approximated dependent on these parameters as well as the distribution of the resistance in the valve by least square methods (i.e. curve fitting).

As a result, the pressure loss of the valve pocket can be calculated dependent on dimensions and the pressure loss of the valve and the distribution of flow resistance.



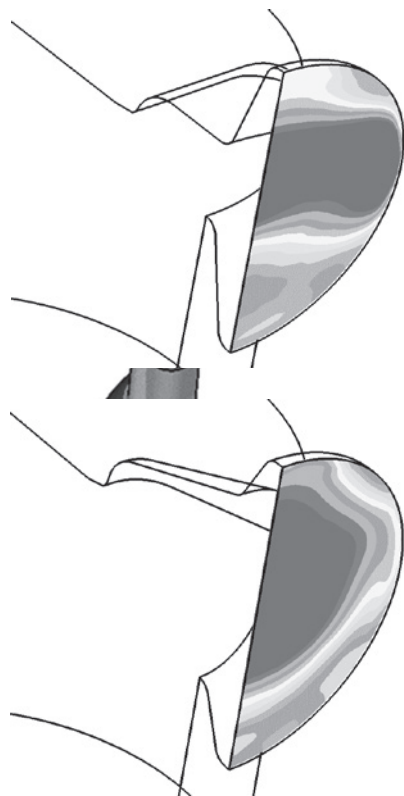


Figure 2.4: Velocity plots of selected valve pockets. Type II (combination of block and cone, top) and Type IV (combination of two cones, from top to bottom)

As the resistance distribution of the valve can be calculated or estimated from the geometry, the impact of different valve types on the main pressure losses in a compressor can be taken into account, e.g. in zero dimensional codes used for compressor dimensioning.

### 2.3 Results: Interaction between pressure losses of valve pocket and valve

Within this paper, the impact of the distribution of flow resistance in the valve on pressure loss coefficients is illustrated for a single design and a small number of idealized distributions only. The valve is approximated by porous cells; within these cells flow is possible only in the direction of the valve axis. The radial distributions of flow resistance applied are plotted in Diagram 2.2 over the normalized radius.

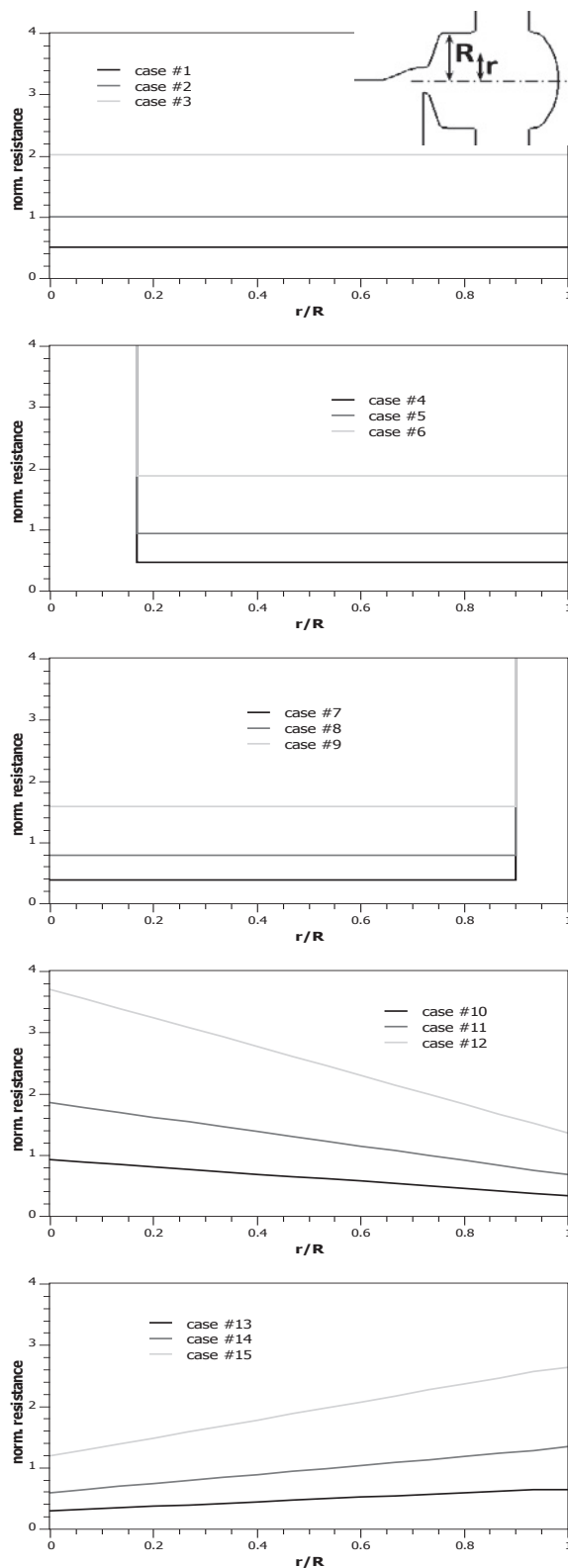
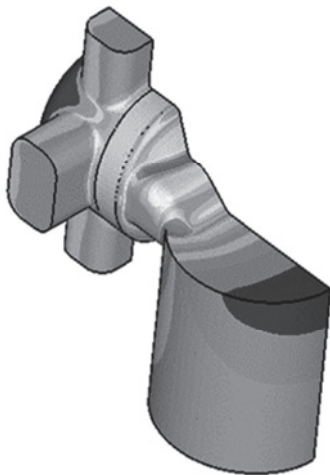


Diagram 2.2: Radial distributions of flow resistance in valve. Constant resistance, constant with central bolt, constant with rim, linear with high resistance in centre, linear with low resistance in centre (top to bottom)



Three levels of flow resistance of the valve are applied to an incompressible flow with a Reynolds Number of 5.0E4 (based on nominal valve diameter and averaged velocity). In a wind tunnel arrangement, all the distributions plotted in the same colour in Diagram 2.2 have the same pressure loss of the valve.

However, if the same valve is investigated in a model with cylinder, valve pocket and valve cage (Figure 2.5), the different distributions result in different pressure losses of the whole combination. The pressure losses are usually described as ratio of static pressure differential divided by dynamic pressure (i.e. total minus static pressure); in this way a pressure loss coefficient is obtained for the valve. We define the pressure loss coefficient for steady flow through a valve with equal cross sectional area of the in – and outlet as:



$$\zeta = \frac{\iint \rho v p_s dA_{in} - \iint \rho v p_s dA_{out}}{\iint \rho v (p_t - p_s) dA_{in}}$$

The same approach may be applied to the parts up- and downstream of the valve (another approach is to calculate the ratio of the area of an orifice required for the mass flow under isentropic conditions to the actual section).

Figure 2.5 Geometry of example valve

pocket

As mentioned before, the pressure loss coefficients are not only dependent on the geometry, but to a smaller portion also on the combination of valve pocket, valve and valve cage. If we denote the pressure loss coefficient of the valve in a wind tunnel arrangement as  $\zeta_{v0}$  and in the valve pocket as  $\zeta_{v1}$ , the pressure loss coefficient of the pocket with inlet - outlet boundary conditions as  $\zeta_{p0}$  and combined with a valve  $\zeta_{p1}$ , the pressure loss coefficient of the valve cage with inlet - outlet conditions  $\zeta_{vc0}$  and combined with a valve  $\zeta_{vc1}$ , then the effects of a combined pocket – valve – valve cage assembly in comparison to the separate parts on pressure loss may be expressed by a factor

$$f_i = \frac{\zeta_{i1} - \zeta_{i0}}{\zeta_{i0}}, i = v, p, vc$$

In Diagram 2.3, these factors are plotted for the design as shown in Figure 2.5 and the 15 distributions of flow resistance of the valve from Diagram 2.2. As can be seen from Diagram 2.3, these factors may exceed the 10% range for pocket and valve, and hence are not negligible. For the valve cage the effect is much higher, however, the contribution of this component to the overall pressure losses is usually very small. When valves of different types (e.g valves with few straight-through modules or an optimized poppet valve) are interchanged with standard valves of common proportions, or between each other, then the compressor performance may behave in an unexpected manner because the change in valve pocket pressure loss may well overcompensate the nominal performance differential of the valves.

The effects illustrated are negligible when, and only when, similar valves (i.e. plate valves of similar proportions of the central bolt etc.) are compared.

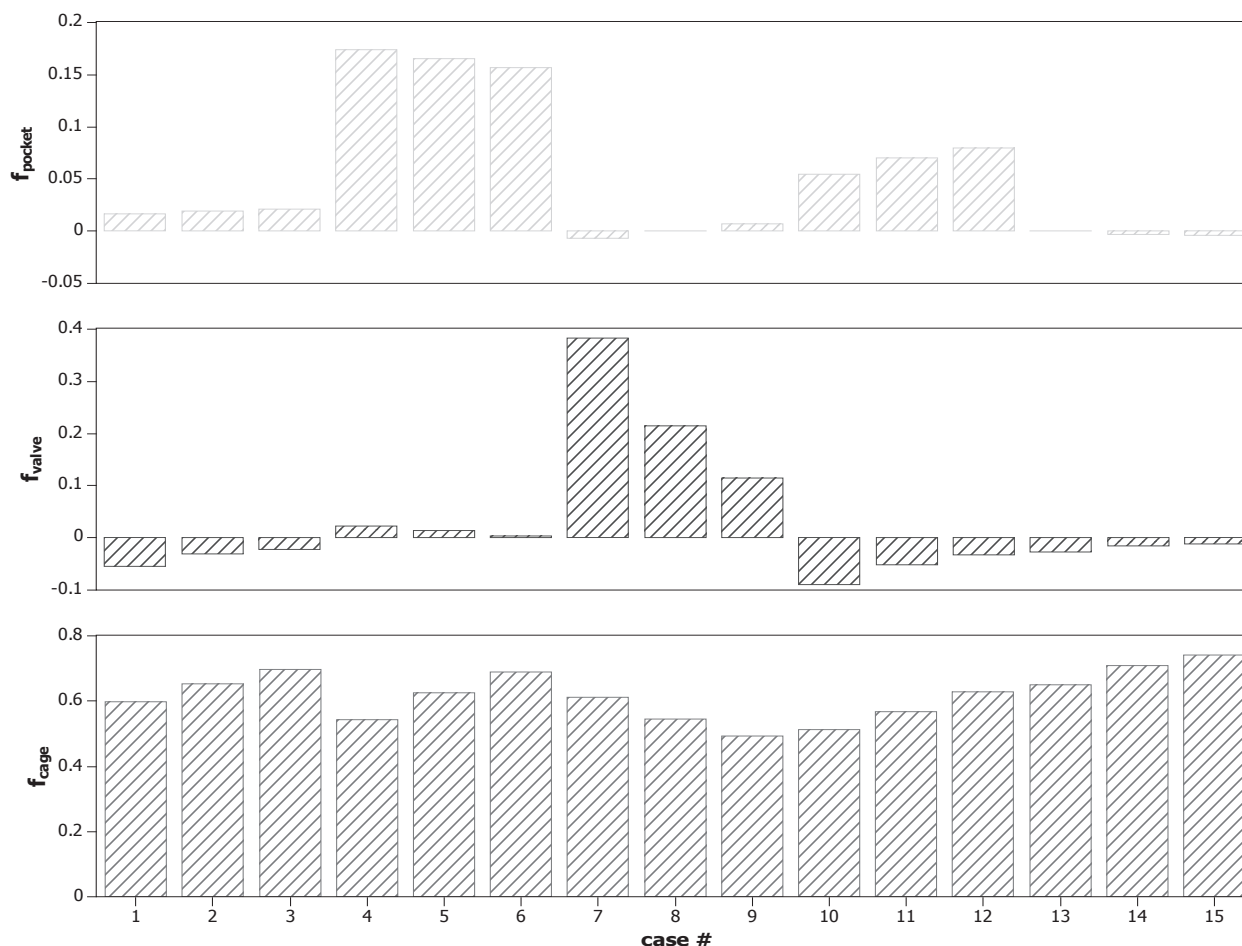


Diagram 2.3: Pressure loss correction factors caused by the interaction of valve pocket, valve and valve cage for the geometry in Figure 2.5 and the distributions plotted in Diagram 2.2 for pocket, valve and valve cage (from top to bottom)

### 3. Moving mesh simulations

#### 3.1 Moving mesh simulations with prescribed motion

A simple model of a compressor cylinder is depicted in Figure 3.1 (left), comprising the cylinder, an inlet and discharge valve pocket, two simple valves, valve cages and collectors. A velocity plot is shown in a cut plane, the piston is at the bottom dead centre.

The geometry of the parts located up and downstream of the compressor cylinder is taken into account by boundary conditions derived from a one-dimensional model. In this model, the valves are a crude approximation of the real geometry, and the opening and closing is prescribed depending on crank angle. The valves are simply switched on or off by coupling or de-coupling the mesh parts. Although such a simple geometry does not give flow details within the valve itself, the resulting time dependent flow in the compressor parts is an useful input for subsequent investigations with a model of higher resolution. By mapping the results of the



simple model onto a refined model as initial condition, computational efforts are reduced to a minimum.

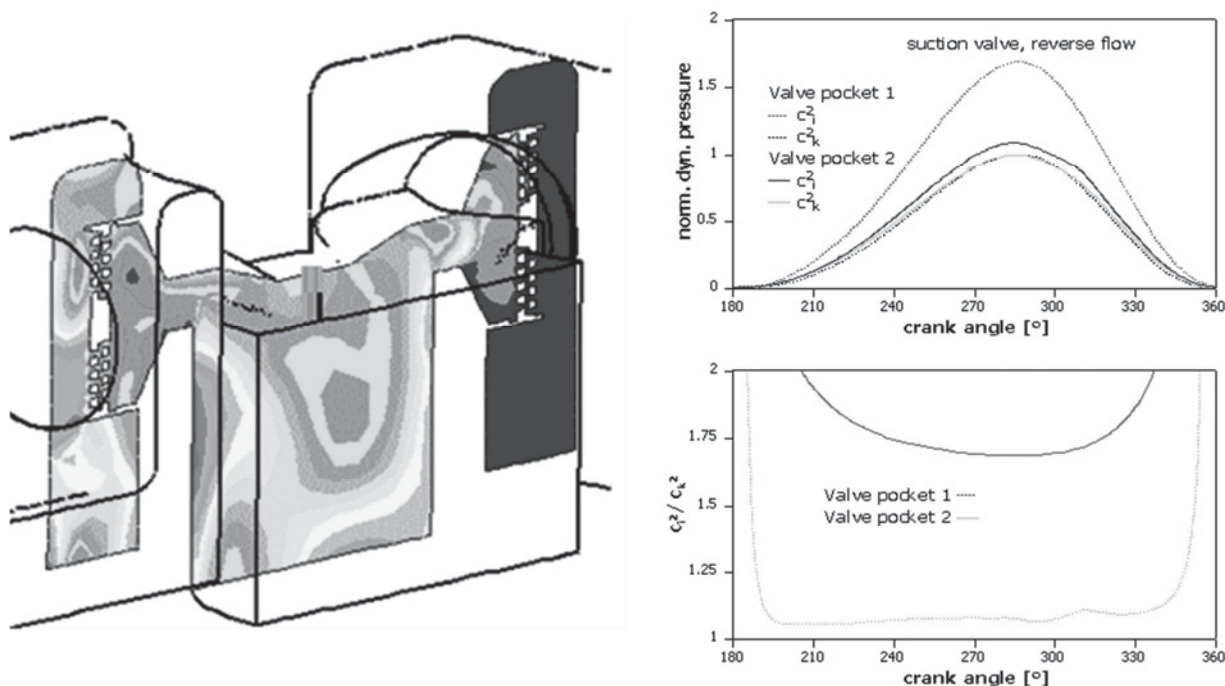


Figure 3.1: Compressor cylinder moving mesh model(left), and comparison of dynamic pressures (diagrams right): Pressures calculated from continuity or integration of the momentum equation at suction valve outlet for two different valve pocket geometries (top), ratio of pressures dependent on crank angle (bottom)

The purpose of the investigations was to determine forces and torques acting on a reverse flow control system. Due to the geometry of the valve pocket the unloader is not only pushed back but parts of the unloader mechanism are also subjected to torque. As a first indication, the momentum flux into the suction valve during reverse flow conditions derived from the model has been plotted vs. the crank angle (Figure 3.1, right).

As can be seen from the diagram, the dynamic pressure calculated from the continuity equation does not necessarily give a good estimation of the momentum flux. The ratio of dynamic pressure, as determined from a mass flow averaged integration of momentum flux, to the dynamic pressure, calculated from the velocity based on the continuity equation, is dependent on the valve pocket geometry as well as the crank angle. In order to obtain the averaged dynamic pressure relevant for the estimation of forces, the velocity determined from continuity must be corrected adequately, the dynamic pressure from momentum is nearly two times higher than the value calculated with the help of the continuity equation.

In a subsequent investigation of flow through a highly detailed model of a ring type suction valve closing with a prescribed motion, the initial and boundary conditions derived from the model described above have been applied.

Figure 3.2 (left) gives an impression of the valve quarter model showing recirculation zones inside the valve caused by the sharp redirection of flow. These recirculation zones block a

significant portion of the flow section of plate or ring valves, not only in under reverse flow conditions. The valve quarter model has been mirrored and a cylinder has been added to investigate the forces acting on the rings during closing in reverse flow (Figure 3.2, right).

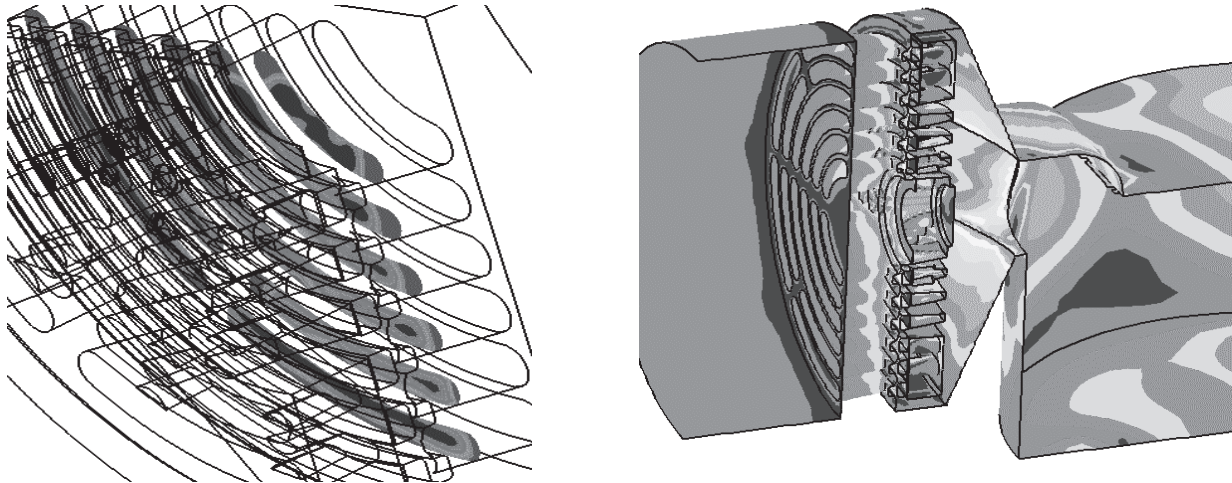


Figure 3.2: Recirculation in a suction valve of ring type, reverse flow condition (compression stroke). Section plot of axial velocity (backflow in regions coloured red, right), internal view (i.e. velocities projected onto the wall, left)

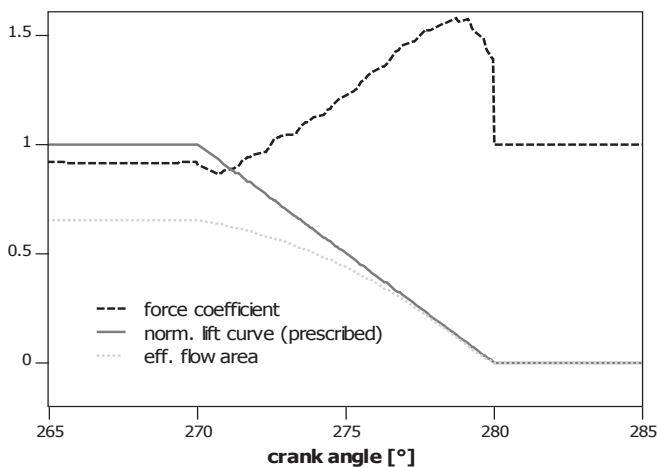


Diagram 3.2: Normalized lift curve, resulting effective flow area and force coefficient dependent on crank angle.

Note that the unloader bell is omitted in this model. The simulated force coefficient, the normalized valve lift curve and the effective flow section of the valve dependent on crank angle are shown in Diagram 3.2. The force coefficient is defined as force divided by the area effective in a closed position, and by the pressure loss of the valve. The normalized effective flow area is derived from the isentropic flow through an orifice.

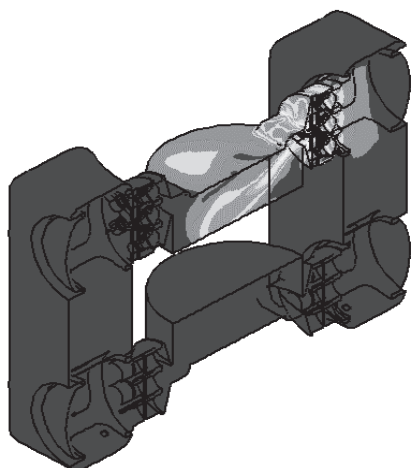
### 3.2 Moving mesh simulation with fluid structure interaction: Double acting compressor cylinder with poppet valves

The third moving mesh model described within this paper comprises a double acting cylinder, two poppet valves of a new design, and the compressor parts up- and downstream of the valves. Figure 3.3 gives an idea of the whole model. The poppet valves are located in the top compression chamber, the bottom chamber is equipped with simple valve dummies (i.e. valves switching on or off as described above). In the CFD simulation poppet valves with seven poppets are investigated, one poppet located centrally and six poppets in a circle around. A new design of the poppet valve results in a very high flow section, especially in the valve guard, and hence the pressure loss in this part of the valve is reduced. In this CFD model, in contrast to the





models described before, the motion of the valve bodies is not anymore prescribed as a function of the crank angle, but by solving the equations of motion for each individual poppet.



A multi cycle simulation was performed and the individual movement was simulated from the second simulated cycle onwards. In Diagram 3.3 the normalized lift dependent on crank angle is shown for two cases. On the left, the poppets are equipped with a spring causing premature closing of the suction valve. As can be seen from the diagram, the poppets at the top and bottom position close faster at the beginning, but are then the ones remaining open for the longest duration. The spring force at maximum lift,  $F_{sm}$ , is equal to 1.0 for this model. In the Diagram at the right, even stronger springs are used ( $F_{sm} \sim 8.0$ ), resulting in an oscillation of the poppets. As a main result of the investigations, not only the individual lift curves are calculated but also the friction work is determined.

Figure 3.3: Moving mesh compressor model with poppet valves in top compression chamber

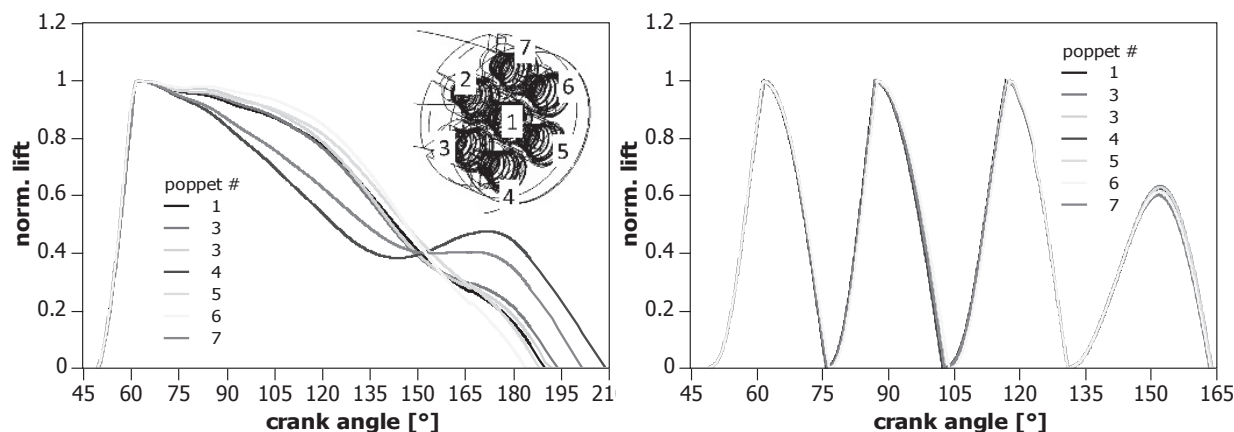


Diagram 3.3: Individual lift curves of poppet valve bodies as simulated in CFD model. Springs ( $F_{sm}=1$ ) resulting in poppets closing prematurely (left) and stronger springs ( $F_{sm}=8$ ) resulting in synchronous oscillation (right)

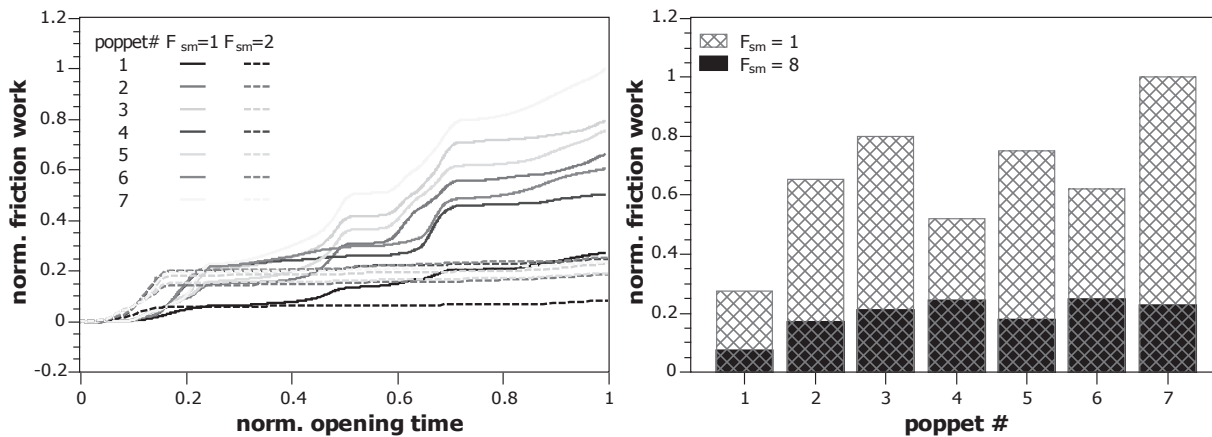


Diagram 3.4: Friction work in poppet guide determined from lateral forces acting on poppets (left) over time and comparison of total friction work per cycle (right)

The friction work is calculated as integral of the lateral forces times the poppet displacement and is plotted as function of the crank angle in Diagram 3.4. Not surprisingly, the friction work of the oscillating poppets is much higher than the friction work of the poppets equipped with a weaker spring. In both cases, the centrally located poppet renders the lowest friction. The determination of the time-dependent flow and valve motion is relevant both for the flow characteristics of the valve as well as for an assessment of the wear to be expected during operation. Due to the asynchronous movement of the valve bodies the effective flow area is dependent on time, both during opening and closing phases, and hence differs from the assumptions used for zero- or one-dimensional compressor performance or valve selector simulation tools.

#### 4. Conclusion

Investigations aiming at reducing pressure losses of small sized poppet valves resulted in an improved valve design and triggered subsequent investigations of flow through the cylinder, valve pocket, valve and valve cage. Not surprisingly, if the overall pressure losses in a reciprocating compressor have to be minimized, the valve pocket geometry has to be taken into account. Not only is the pressure loss in the valve pocket significant, and in some cases even higher than the pressure loss of the valve itself, but also valve and valve pocket are influencing each other as the resulting flow is dependent on both the distribution of flow resistance in the valve and the pocket shape. If valve performance is rated on the basis of a wind tunnel arrangement (instead of a cylinder – valve pocket – valve arrangement) only, misleading results may be obtained. The impact of the design of the valve pocket on compressor performance cannot be over-emphasized. In order to be able to better predict the effects of valve pocket design on valve performance, two sets of half models – in total 28 different geometries – have been simulated so far.

The pressure loss coefficients of the pocket, valve and valve cage are usually treated as constants, however, as illustrated by a simple example, are also slightly dependent on the distribution of flow resistance in the valve, which can be calculated or estimated from the geometry. By introducing the distribution of flow resistance of the valve (described by additional



parameters) the usual approach of pressure loss calculation required for compressor dimensioning and implemented in zero-dimensional codes is preserved, but with improved predictive capabilities—the conventional method is correct only if similar valves (e.g. plate valves with identical centre bolt diameter etc.) are compared among each other.

Steady flow investigations can only give an approximation of flow in a reciprocating compressor. Time-dependent motion effects like piston masking the valve etc. have to be included, and additional effects of transient flow like pulsations have to be taken into account. Moving mesh in-cylinder simulations are a tool common in internal combustion engine development; due to the close relatedness of reciprocating compressors and internal combustion engines a proven methodology has been applied.

Fluid structure simulations of moving valve internals create a deeper insight into valve dynamics and are a prerequisite for wear prediction. In order to predict valve wear, not only the forces acting on the valve internals need to be known but—since a guide does not wear as long as the valve does not move – the temporal evolution of forces, torques and velocities has to be determined and input into a wear model.

More cases need to be studied in detail. However, the investigations presented in this paper demonstrate how advanced modelling used in CFD today can contribute to increasing the reliability of compressor and valve performance predictions.

### Acknowledgments

I want to thank all colleagues from Burckhardt Compression for the fruitful discussions and many suggestions, in particular Luzi Valär from Research and Development as well as Roland Aigner from the Design department. Furthermore, the contribution from external computing resources, in particular Mr. Gropp from CPU24/7, must not be forgotten.

### Bibliographic details

[1] Bauer, F.: *Valve losses in Reciprocating Compressors*, 1988 International Compressor Engineering Conference at Purdue University, July 1988, West Lafayette, Indiana, USA

[3] Balduzzi, F., Ferrara G., Maleci, R., Babbini, A. and Pratelli, G.: *A Parametric CFD Analysis of the Valve Pocket Losses in Reciprocating Compressors*, paper no. PVP2013-97929, ASME 2013 Pressure Vessels and Piping Conference

[4] Pratelli, G., Babbini, A., Balduzzi, F., Ferrara, G., Maleci, R., Romani, L.: *CFD Evaluation of Pressure Losses on Reciprocating Compressor Components*, 8th Conference of the EFRC, Düsseldorf, September 2012

[5] Traversari, R., Faretra, M., Bucci, D., Bassini, S.: *Thermo-fluid-dynamic design of Reciprocating Compressor Cylinders by Fluid Structure Interaction Software simulation*, 7th Conference of the EFRC, Florence, October 2010

[6] Schiavone, M., Manfrone, F., Giacomelli, E.: *Evaluation of the Coefficients used for simulation for Cylinder Valves for Reciprocating Compressors*, 5th Conference of the EFRC, Prague, March 2007

- [7] Manfrone, F., Raggi A.: *Analysis of the Movements of the Valve Sealing Elements*, 8th Conference of the EFRC, Düsseldorf, September 2012
- [8] Aigner R., Meyer G., Steinrück H.: *Valve Dynamic and Internal Waves in a Reciprocating Compressor*, 4th Conference of the EFRC, Antwerp, June 2005
- [9] Meyer G.: *Simulation der Strömung in einem Kolbenverdichter*, Diplomarbeit, TU Wien, 2005
- [10] CD-adapco: *Methodology Manual, StarCD*, 2015

## Promoter



EUROPEAN FORUM  
for RECIPROCATING  
COMPRESSORS  
10<sup>th</sup> EFRC Conference 2016

### **EUROPEAN FORUM for RECIPROCATING COMPRESSORS**

c/o Technische Universität Dresden  
01062 Dresden  
Germany

Phone +49 351 463 32815  
Fax +49 351 463 37247  
E-Mail [contact@recip.org](mailto:contact@recip.org)  
Internet [www.recip.org](http://www.recip.org)

#### **Chairman:**

Dr. René Peters

#### **Organiser:**

Maschinenbau-Institut GmbH  
Frankfurt am Main

ISBN 978-3-8163-0699-3